

**MATERIALS RESEARCH SOCIETY  
SYMPOSIUM PROCEEDINGS VOLUME 422**

# **Rare Earth Doped Semiconductors II**

Symposium held April 8-10, 1996, San Francisco, California, U.S.A.

**EDITORS:**

**Salvatore Coffa**

*CNR-IMETEM  
Catania, Italy*

**Albert Polman**

*FOM-Institute AMOLF  
Amsterdam, The Netherlands*

**Robert N. Schwartz**

*Hughes Research Laboratories  
Malibu, California, U.S.A.*

This document has been approved  
for public release and sale; its  
distribution is unlimited.



**PITTSBURGH, PENNSYLVANIA**

**DTIC QUALITY INSPECTED 3**

1996 1125 130

This work was supported in part by the Army Research Office under Grant Number ARO: DAAH04-96-1-0084. The views, opinions, and/or findings contained in this report are those of the author(s) and should not be construed as an official Department of the Army position, policy, or decision, unless so designated by other documentation.

Single article reprints from this publication are available through University Microfilms Inc., 300 North Zeeb Road, Ann Arbor, Michigan 48106

CODEN: MRSPDH

Copyright 1996 by Materials Research Society.  
All rights reserved.

This book has been registered with Copyright Clearance Center, Inc. For further information, please contact the Copyright Clearance Center, Salem, Massachusetts.

Published by:

Materials Research Society  
9800 McKnight Road  
Pittsburgh, Pennsylvania 15237  
Telephone (412) 367-3003  
Fax (412) 367-4373  
Website: <http://www.mrs.org/>

#### Library of Congress Cataloging in Publication Data

Rare earth doped semiconductors II : symposium held April 8-10, 1996, San Francisco, California, U.S.A. / editors, Salvatore Coffa, Albert Polman, Robert N. Schwartz  
p. cm—(Materials Research Society symposium proceedings ; v. 422)  
Includes bibliographical references and indexes.  
ISBN 1-55899-325-8 (alk. paper)  
1. Semiconductors—Congresses. 2. Rare earth metals—Surfaces—Congresses. I. Coffa, Salvatore II. Polman, Albert III. Schwartz, Robert N.  
IV. Series: Materials Research Society symposium proceedings ; v. 422.  
QC611.8.R37R372 1996 96-9886  
537.6'223—dc20 CIP

Manufactured in the United States of America

<b>REPORT DOCUMENTATION PAGE</b>			Form Approved OMB NO. 0704-0188	
Public reporting burden for this collection of information is estimated to average 1 hour per response, including the time for reviewing instructions, searching existing data sources, gathering and maintaining the data needed, and completing and reviewing the collection of information. Send comment regarding this burden estimates or any other aspect of this collection of information, including suggestions for reducing this burden, to Washington Headquarters Services, Directorate for Information Operations and Reports, 1215 Jefferson Davis Highway, Suite 1204, Arlington, VA 22202-4302, and to the Office of Management and Budget, Paperwork Reduction Project (0704-0188), Washington, DC 20503.				
1. AGENCY USE ONLY (Leave blank)		2. REPORT DATE Nov 96		3. REPORT TYPE AND DATES COVERED Final 1 April 96 - 31 Mar 97
4. TITLE AND SUBTITLE Rare Earth Doped Semiconductors II			5. FUNDING NUMBERS  DAAH04-96-1-0084	
6. AUTHOR(S)  Robert H. Pachavis (Principal investigator)				
7. PERFORMING ORGANIZATION NAMES(S) AND ADDRESS(ES)  Materials Research Society Pittsburgh, PA 15237			8. PERFORMING ORGANIZATION REPORT NUMBER	
9. SPONSORING / MONITORING AGENCY NAME(S) AND ADDRESS(ES)  U.S. Army Research Office P.O. Box 12211 Research Triangle Park,, NC 27709-2211			10. SPONSORING / MONITORING AGENCY REPORT NUMBER  ARO 35710.2-MS-CF	
11. SUPPLEMENTARY NOTES  The views, opinions and/or findings contained in this report are those of the author(s) and should not be construed as an official Department of the Army position, policy or decision, unless so designated by other documentation.				
12a. DISTRIBUTION / AVAILABILITY STATEMENT  Approved for public release; distribution unlimited.			12 b. DISTRIBUTION CODE	
13. ABSTRACT (Maximum 200 words)  The second MRS symposium on "Rare Earth Doped Semiconductors", held three years after the first one, was a truly international meeting with 51 contributions from 14 different countries. Research on rare earth doped semiconductors is mostly motivated by the fact that internal transitions in the rare-earth ions can be used to obtain well defined and temperature independent optical emission from these semiconductors. Recent advances in this research area motivated us to organize this symposium, with the aim to discuss the state of the art in this field, highlight new developments, identify the potential for optoelectronic applications, and to provide a forum  (continued on reverse side)				
14. SUBJECT TERMS			15. NUMBER IF PAGES	
			16. PRICE CODE	
17. SECURITY CLASSIFICATION OR REPORT UNCLASSIFIED	18. SECURITY CLASSIFICATION OF THIS PAGE UNCLASSIFIED	19. SECURITY CLASSIFICATION OF ABSTRACT UNCLASSIFIED	20. LIMITATION OF ABSTRACT  UL	

for making new contacts. Indeed, over 200 papers on rare earth doped semiconductors have been published in the international literature over the past three years, indicating how lively this research area is. While the previous symposium on this topic in 1993 was mostly devoted to papers on rare earth doped II-VI and III-V semiconductors, clearly a shift was seen in the present symposium, as more than half of the presentations were devoted to rare earth doped silicon. This indicates that rare-earth doping of silicon is now seriously considered as a means to achieve silicon-based opto-electronic devices. In addition, several new reports on rare earth doped III-nitrides were presented.



# DISCLAIMER NOTICE



**THIS DOCUMENT IS BEST  
QUALITY AVAILABLE. THE  
COPY FURNISHED TO DTIC  
CONTAINED A SIGNIFICANT  
NUMBER OF PAGES WHICH DO  
NOT REPRODUCE LEGIBLY.**

## CONTENTS

Preface .....	xi
Acknowledgments .....	xiii
Materials Research Society Symposium Proceedings .....	xiv

### PART I: INCORPORATION METHODS AND PROPERTIES

<b>*Ion Beam Epitaxy of <i>In-Situ</i> Er-O Co-Doped Silicon Films</b> .....	3
<i>Morito Matsuoka and Shun-ichi Tohno</i>	
<b>Growth Conditions of Erbium-Oxygen-Doped Silicon Grown by MBE</b> .....	15
<i>J. Stimmer, A. Reittinger, G. Abstreiter, H. Holzbrecher, and Ch. Buchal</i>	
<b>Segregation and Trapping of Erbium in Silicon at a Crystal-Amorphous or Crystal-Vacuum Interface</b> .....	21
<i>A. Polman, R. Serna, J.S. Custer, and M. Lohmeier</i>	
<b>Self Organized Growth in Thulium Doped GaAs Using MBE</b> .....	29
<i>M.R. Bennett, K.E. Singer, A.C. Wright, and Z.H. Jafri</i>	
<b>Properties and Growth of MBE Grown Erbium Doped Gallium Arsenide Co-Doped with Selenium</b> .....	35
<i>P. Rutter, K.E. Singer, A.R. Peaker, and A.C. Wright</i>	
<b>Properties of Ion Implanted and UHV-CVD Grown Si:Er</b> .....	41
<i>M. Morse, B. Zheng, J. Palm, X. Duan, and L.C. Kimerling</i>	
<b>*Er-Doping of GaN and Related Alloys</b> .....	47
<i>S.J. Pearton, C.R. Abernathy, J.D. MacKenzie, R.N. Schwartz, R.G. Wilson, J.M. Zavada, and R.J. Shul</i>	
<b>Low-Temperature Growth of Si:Er by Electron Cyclotron Resonance PECVD Using Metal Organics</b> .....	57
<i>P.S. Andry, W.J. Varhue, E. Adams, M. Lavoie, P.B. Klein, R. Hengehold, and J. Hunter</i>	
<b>Erbium Doped GaAs by MOCVD</b> .....	63
<i>A.C. Greenwald, K.J. Linden, W.S. Rees, Jr., O. Just, N.M. Haegel, and S. Donder</i>	
<b>Neodymium and Erbium Implanted GaN</b> .....	69
<i>E. Silkowski, Y.K. Yeo, R.L. Hengehold, B. Goldenberg, and G.S. Pomrenke</i>	

\*Invited Paper

<b>Optical Centers Related to Laser-Doped Erbium in Silicon .....</b>	<b>75</b>
<i>K. Nakashima, O. Eryu, O. Iioka, H. Minami, and M. Watanabe</i>	
<b>Photoluminescence of Erbium-Diffused Silicon .....</b>	<b>81</b>
<i>H. Horiguchi, T. Kinone, R. Saito, T. Kimura, and T. Ikoma</i>	
<b>About the Electrical and Structural Properties of Erbium Thermally Diffused in Single Crystal Silicon .....</b>	<b>87</b>
<i>S. Binetti, M. Acciarri, I. Gelmi, and S. Pizzini</i>	
<b>Incorporation of High Concentration Luminescent Er Centers in Si and Porous Si by Electroplating .....</b>	<b>93</b>
<i>Chi Sheng, Yongming Cai, Dawei Gong, Daming Huang, Xiaohan Liu, and Xun Wang</i>	

## **PART II: STRUCTURAL, ELECTRICAL, AND OPTICAL PROPERTIES**

<b>*Factors Governing the Photoluminescence Yield of Erbium Implanted Silicon .....</b>	<b>101</b>
<i>W. Jantsch, H. Przybylinska, C. Skierbiszewski, S. Lanzerstorfer, and L. Palmetshofer</i>	
<b>The Effects of Impurity Co-Doping on the Electrical Properties of Erbium Ions in Crystalline Silicon .....</b>	<b>113</b>
<i>S. Libertino, S. Coffa, R. Mosca, and E. Gombia</i>	
<b>Luminescence Decay of the 1.54 <math>\mu\text{m}</math> Emission from Erbium in Silicon .....</b>	<b>119</b>
<i>J. Hartung, J.H. Evans, P. Dawson, A.P. Scholes, T. Taskin, M.Q. Huda, C. Jeynes, and A.R. Peaker</i>	
<b>Defect Engineering in Si:Er Technology .....</b>	<b>125</b>
<i>N.A. Sobolev, O.V. Alexandrov, M.S. Bresler, V.V. Emtsev, O.B. Gusev, D.S. Poloskin, and E.I. Shek</i>	
<b>Photoluminescence of Erbium Implanted in SiGe .....</b>	<b>131</b>
<i>S.J. Chang, D.K. Nayak, and Y. Shiraki</i>	
<b>Characterization of Visible and Infrared (1.54 <math>\mu\text{m}</math>) Luminescence from Er-Doped Porous Si .....</b>	<b>137</b>
<i>R. White, X. Wu, U. H��mmerich, F. Namavar, and A.M. Cremins-Costa</i>	
<b>To Probe the Absorption Edge of Porous Silicon by Erbium .....</b>	<b>143</b>
<i>Xinwei Zhao, Shuji Komuro, Shinya Maruyama, Hideo Isshiki, Yoshinobu Aoyagi, and Takuo Sugano</i>	
<b>Luminescence of Rare Earth Doped Porous Silicon .....</b>	<b>149</b>
<i>T. Kimura, I. Hosokawa, Y. Nishida, T. Dejima, R. Saito, and T. Ikoma</i>	

\*Invited Paper

<b>EXAFS and X-ray CTR Scattering Characterization of Er Doped in InP by OMVPE .....</b>	<b>155</b>
<i>M. Tabuchi, D. Kawamura, K. Fujita, N. Matsubara, N. Yamada, H. Ofuchi, S. Ichiki, Y. Fujiwara, and Y. Takeda</i>	
<b>The 4f Intrashell Transitions of Ytterbium in Indium Phosphide .....</b>	<b>161</b>
<i>Ingrid de Maat-Gersdorf, T. Gregorkiewicz, C.A.J. Ammerlaan, P.C.M. Christianen, and J.C. Maan</i>	
<b>Optical Anisotropy of Er Centers in GaAs:Er,O .....</b>	<b>167</b>
<i>R.A. Hogg, K. Takahel, A. Taguchi, and Y. Horikoshi</i>	
<b>Rutherford Backscattering and Photoluminescence Studies of Erbium Implanted GaAs .....</b>	<b>173</b>
<i>S.E. Daly, M.O. Henry, E. Alves, J.C. Soares, R. Gwilliam, B.J. Sealy, K. Freitag, R. Vianden, and D. Stievenard</i>	
<b>Study of the Zeeman Effect of Er<sup>3+</sup> in GaAs:Er,O .....</b>	<b>179</b>
<i>Dieter Haase, Achim Dörnen, Kenichiro Takahel, and Akihito Taguchi</i>	
<b>Activation of Yb Luminescence in GaAs by Group VI Elements Co-Doping .....</b>	<b>187</b>
<i>V.M. Konnov, T.V. Larikova, N.N. Loyko, V.A. Dravin, V.V. Ushakov, and A.A. Gippius</i>	
<b>Characterization of Er-Doped III-V Nitride Epilayers Prepared by MOMBE .....</b>	<b>193</b>
<i>J.M. Zavada, R.G. Wilson, R.N. Schwartz, J.D. MacKenzie, C.R. Abernathy, S.J. Pearton, X. Wu, and U. Hömmerich</i>	
<b>Annealing Study of Erbium and Oxygen Implanted Gallium Nitride .....</b>	<b>199</b>
<i>John T. Torvik, Robert J. Feuerstein, Chang H. Qiu, Moeljanto W. Leksono, Jacques I. Pankove, and Fereydoon Namavar</i>	

### **PART III: EXCITATION MECHANISMS**

<b>*Excitation and De-excitation of Yb<sup>3+</sup> in InP and Er<sup>3+</sup> in Si: Photoluminescence and Impact Ionization Studies .....</b>	<b>207</b>
<i>T. Gregorkiewicz, I. Tsimperidis, C.A.J. Ammerlaan, F.P. Widdershoven, and N.A. Sobolev</i>	
<b>Incorporation, Excitation and De-excitation of Erbium in Crystal Silicon .....</b>	<b>219</b>
<i>M.J.A. de Dood, P.G. Kik, J.H. Shin, and A. Polman</i>	
<b>*The Possible Mechanism of Excitation of the f - f Emission from Er-O Clusters in Silicon .....</b>	<b>227</b>
<i>V.F. Masterov and L.G. Gerchikov</i>	

\*Invited Paper

<b>Luminescence Quenching in Erbium-Doped Hydrogenated Amorphous Silicon</b> .....	<b>239</b>
<i>A. Polman, Jung H. Shin, R. Serna, G.N. van den Hoven, W.G.J.H.M. van Sark, A.M. Vredenberg, S. Lombardo, and S.U. Campisano</i>	
<b>*Rare-Earth Doped Epitaxial InGaP and its Optical Properties</b> .....	<b>247</b>
<i>B.W. Wessels</i>	
<b>*On the Excitation Mechanism of Erbium and Ytterbium in the Quaternary Compounds InGaAsP</b> .....	<b>255</b>
<i>Peter Wellmann, Albrecht Winnacker, and Gerhard Pensl</i>	
<b>*Energy-Transfer Processes in Oxygen-CoDoped GaAs:Er</b> .....	<b>267</b>
<i>K. Takahel, R.A. Hogg, and A. Taguchi</i>	
<b>Excitation Properties of Er-Doped GaP from Photoluminescence and High Pressure Studies</b> .....	<b>279</b>
<i>T.D. Culp, X.Z. Wang, T.F. Kuech, B.W. Wessels, and K.L. Bray</i>	
<b>Photoluminescence Kinetics Model of P-Type GaAs:Nd</b> .....	<b>285</b>
<i>U.K. Saha and H.J. Lozykowski</i>	
<b>*Excitation and Recombination Processes in Rare Earth Doped II-VI Semiconductors</b> .....	<b>291</b>
<i>M. Godlewski</i>	

#### **PART IV: ELECTROLUMINESCENCE AND INTEGRATION**

<b>*Excitation Mechanisms and Light Emitting Device Performances in Er-Doped Crystalline Si</b> .....	<b>305</b>
<i>F. Priolo, S. Coffa, G. Franzo, and A. Polman</i>	
<b>*Erbium Doped Silicon for Light Emitting Devices</b> .....	<b>317</b>
<i>J. Michel, B. Zheng, J. Palm, E. Ouellette, F. Gan, and L.C. Kimerling</i>	
<b>Photo- and Electroluminescence Study of Excitation Mechanism of Er Luminescence in <math>\alpha</math>-Si:H(Er)</b> .....	<b>325</b>
<i>I.N. Yassievich, O.B. Gusev, M.S. Bresler, W. Fuhs, A.N. Kuznetsov, V.F. Masterov, E.I. Terukov, and B.P. Zakharchenya</i>	
<b>Electroluminescence of Erbium in Oxygen Doped Silicon</b> .....	<b>333</b>
<i>S. Lombardo, S.U. Campisano, G.N. van den Hoven, and A. Polman</i>	
<b>1.54 <math>\mu</math>m Photoluminescence and Electroluminescence in Erbium Implanted 6H SiC</b> .....	<b>339</b>
<i>M. Yoganathan, W.J. Choyke, R.P. Devaty, G. Pensl, and J.A. Edmond</i>	

\*Invited Paper

<b>1.54 <math>\mu\text{m}</math> Electroluminescence from Erbium Doped Gallium Phosphide Diodes .....</b>	<b>345</b>
<i>G.M. Ford and B.W. Wessels</i>	
<b>Neodymium-Doped GaAs Light-Emitting Diodes .....</b>	<b>351</b>
<i>S.J. Chang</i>	
<b>Increased Refractive Indices in Rare Earth Doped InP and In<sub>0.53</sub>Ga<sub>0.47</sub>As Thin Films .....</b>	<b>357</b>
<i>B.J.H. Stadler and J.P. Lorenzo</i>	
<b>Author Index .....</b>	<b>363</b>
<b>Subject Index .....</b>	<b>365</b>

## PREFACE

The second MRS symposium on "Rare Earth Doped Semiconductors", held three years after the first one, was a truly international meeting with 51 contributions from 14 different countries. Research on rare earth doped semiconductors is mostly motivated by the fact that internal transitions in the rare-earth ions can be used to obtain well defined and temperature independent optical emission from these semiconductors. Recent advances in this research area motivated us to organize this symposium, with the aim to discuss the state of the art in this field, highlight new developments, identify the potential for optoelectronic applications, and to provide a forum for making new contacts. Indeed, over 200 papers on rare earth doped semiconductors have been published in the international literature over the past three years, indicating how lively this research area is. While the previous symposium on this topic in 1993 was mostly devoted to papers on rare earth doped II-VI and III-V semiconductors, clearly a shift was seen in the present symposium, as more than half of the presentations were devoted to rare earth doped silicon. This indicates that rare-earth doping of silicon is now seriously considered as a means to achieve silicon-based opto-electronic devices. In addition, several new reports on rare earth doped III-nitrides were presented.

The symposium topics included growth mechanisms, structural, electrical and optical properties, and excitation mechanisms, as well as electroluminescence and integration. Reports on rare-earth doping using MBE, CVD, ion implantation, and ion-assisted deposition indicated that sufficiently high concentrations can now be incorporated in Si as well as III-V semiconductors. The challenge is to optically activate these ions, to excite them efficiently, and to reduce the nonradiative processes that quench the luminescence at high temperatures. Co-doping with impurities such as oxygen, fluorine, nitrogen, and hydrogen has been shown to be essential in achieving this. A lively discussion session was held in which an attempt was made to put all reports on impurity-related effects in a coherent perspective. Some of the most striking conclusions were:

- the formation of rare earth-impurity complexes serves to increase the effective solubility and reduces the mobility of the rare-earth dopants, thus preventing precipitation and segregation.
- the strong interaction between the impurity and the rare-earth ions changes their chemical environment, and thus affects the position of the rare-earth-related defect levels in the bandgap. Therefore, the presence of impurities influences: 1) the energy transfer rate from electron-hole pairs to the rare-earth 4f shell, and 2) the nonradiative backtransfer rate from excited rare-earth ions to the semiconductor electronic system. Other nonradiative processes which decrease the luminescence efficiency may also be affected by the presence of impurities.

- impurities can improve the electrical quality of the material by passivating defects, thus removing alternative carrier recombination routes. As a result, the rare earth excitation efficiency increases. Hydrogen is an interesting candidate for passivation, as indicated by new results on e.g. Er-doped hydrogenated amorphous and porous Si.
- some rare earth-impurity complexes (e.g. Er-O in Si) are not isoelectronic to the host, and as a result will cause doping. At high doping concentration, Auger effects involving free carriers may reduce the luminescence efficiency. Therefore, in rare earth doped p-n diode structures both the electrical and optical properties of the rare earth-impurity complex must be engineered.

Electroluminescence and integration issues were addressed in several presentations. Optimized Si and GaP diodes that were presented have an internal quantum efficiency in the  $10^{-4}$  range. Several new ideas were presented which may help to achieve a further 100-fold increase in the efficiency that is required for most practical applications of rare earth doped semiconductors.

Nearly all presentations given at the meeting are represented by papers in this book. They are grouped together into four sections:

- I. Incorporation methods and properties
- II. Structural, electrical and optical properties
- III. Excitation mechanisms
- IV. Electroluminescence and integration.

We hope that this proceedings, with all contributions put together, will serve as a handbook for all of those active in the field of rare earth doped semiconductors, and will stimulate new insights and new ideas that will lead to practical application of these materials.

Salvatore Coffa  
Albert Polman  
Robert N. Schwartz

June 1996



## ACKNOWLEDGMENTS

The symposium organizers wish to express their appreciation to High Voltage Engineering Europa B.V., the Italian National Research Council (CNR), SGS-Thomson, and the Army Research Office (ARO), for sponsoring this meeting.

Many thanks are due to the invited speakers who gave excellent reviews of their work: S.J. Pearton, B.W. Wessels, K. Takahei, M. Matsuoka, W. Jantsch, T. Gregorkiewicz, V.F. Masterov, P. Wellmann, M. Godlewski, F. Priolo, and J. Michel. We would also like to thank the session chairs who did an excellent job in running their sessions: M. Morse, J. Michel, K. Takahei, F. Priolo, W. Jantsch, S.J. Pearton, T. Gregorkiewicz, and J.M. Zavada.

Finally, we acknowledge the invaluable assistance of the MRS headquarters staff in organizing this meeting and publishing the proceedings.

## MATERIALS RESEARCH SOCIETY SYMPOSIUM PROCEEDINGS

- Volume 395— Gallium Nitride and Related Materials, F.A. Ponce, R.D. Dupuis, S.J. Nakamura, J.A. Edmond, 1996, ISBN: 1-55899-298-7
- Volume 396— Ion-Solid Interactions for Materials Modification and Processing, D.B. Poker, D. Ila, Y-T. Cheng, L.R. Harriott, T.W. Sigmon, 1996, ISBN: 1-55899-299-5
- Volume 397— Advanced Laser Processing of Materials—Fundamentals and Applications, R. Singh, D. Norton, L. Laude, J. Narayan, J. Cheung, 1996, ISBN: 1-55899-300-2
- Volume 398— Thermodynamics and Kinetics of Phase Transformations, J.S. Im, B. Park, A.L. Greer, G.B. Stephenson, 1996, ISBN: 1-55899-301-0
- Volume 399— Evolution of Epitaxial Structure and Morphology, A. Zangwill, D. Jesson, D. Chambliss, R. Clarke, 1996, ISBN: 1-55899-302-9
- Volume 400— Metastable Phases and Microstructures, R. Bormann, G. Mazzone, R.D. Shull, R.S. Averback, R.F. Ziolo, 1996 ISBN: 1-55899-303-7
- Volume 401— Epitaxial Oxide Thin Films II, J.S. Speck, D.K. Fork, R.M. Wolf, T. Shiosaki, 1996, ISBN: 1-55899-304-5
- Volume 402— Silicide Thin Films—Fabrication, Properties, and Applications, R. Tung, K. Maex, P.W. Pellegrini, L.H. Allen, 1996, ISBN: 1-55899-305-3
- Volume 403— Polycrystalline Thin Films: Structure, Texture, Properties, and Applications II, H.J. Frost, M.A. Parker, C.A. Ross, E.A. Holm, 1996, ISBN: 1-55899-306-1
- Volume 404— *In Situ* Electron and Tunneling Microscopy of Dynamic Processes, R. Sharma, P.L. Gai, M. Gajdardziska-Josifovska, R. Sinclair, L.J. Whitman, 1996, ISBN: 1-55899-307-X
- Volume 405— Surface/Interface and Stress Effects in Electronic Materials Nanostructures, S.M. Prokes, R.C. Cammarata, K.L. Wang, A. Christou, 1996, ISBN: 1-55899-308-8
- Volume 406— Diagnostic Techniques for Semiconductor Materials Processing II, S.W. Pang, O.J. Glembocki, F.H. Pollack, F.G. Celli, C.M. Sotomayor Torres, 1996, ISBN 1-55899-309-6
- Volume 407— Disordered Materials and Interfaces, H.Z. Cummins, D.J. Durian, D.L. Johnson, H.E. Stanley, 1996, ISBN: 1-55899-310-X
- Volume 408— Materials Theory, Simulations, and Parallel Algorithms, E. Kaxiras, J. Joannopoulos, P. Vashishta, R.K. Kalia, 1996, ISBN: 1-55899-311-8
- Volume 409— Fracture—Instability Dynamics, Scaling, and Ductile/Brittle Behavior, R.L. Blumberg Selinger, J.J. Mecholsky, A.E. Carlsson, E.R. Fuller, Jr., 1996, ISBN: 1-55899-312-6
- Volume 410— Covalent Ceramics III—Science and Technology of Non-Oxides, A.F. Hepp, P.N. Kumta, J.J. Sullivan, G.S. Fischman, A.E. Kaloyeros, 1996, ISBN: 1-55899-313-4
- Volume 411— Electrically Based Microstructural Characterization, R.A. Gerhardt, S.R. Taylor, E.J. Garboczi, 1996, ISBN: 155899-314-2
- Volume 412— Scientific Basis for Nuclear Waste Management XIX, W.M. Murphy, D.A. Knecht, 1996, ISBN: 1-55899-315-0
- Volume 413— Electrical, Optical, and Magnetic Properties of Organic Solid State Materials III, A.K-Y. Jen, C.Y-C. Lee, L.R. Dalton, M.F. Rubner, G.E. Wnek, L.Y. Chiang, 1996, ISBN: 1-55899-316-9
- Volume 414— Thin Films and Surfaces for Bioactivity and Biomedical Applications, C.M. Cotell, A.E. Meyer, S.M. Gorbalkin, G.L. Grobe, III, 1996, ISBN: 1-55899-317-7
- Volume 415— Metal-Organic Chemical Vapor Deposition of Electronic Ceramics II, S.B. Desu, D.B. Beach, P.C. Van Buskirk, 1996, ISBN: 1-55899-318-5

## MATERIALS RESEARCH SOCIETY SYMPOSIUM PROCEEDINGS

- Volume 416—Diamond for Electronic Applications, D. Dreifus, A. Collins, T. Humphreys, K. Das, P. Pehrsson, 1996, ISBN: 1-55899-319-3
- Volume 417—Optoelectronic Materials: Ordering, Composition Modulation, and Self-Assembled Structures, E.D. Jones, A. Mascarenhas, P. Petroff, R. Bhat, 1996, ISBN: 1-55899-320-7
- Volume 418—Decomposition, Combustion, and Detonation Chemistry of Energetic Materials, T.B. Brill, T.P. Russell, W.C. Tao, R.B. Wardle, 1996 ISBN: 1-55899-321-5
- Volume 420—Amorphous Silicon Technology—1996, M. Hack, E.A. Schiff, S. Wagner, R. Schropp, M. Matsuda, 1996, ISBN: 1-55899-323-1
- Volume 421—Compound Semiconductor Electronics and Photonics, R.J. Shul, S.J. Pearton, F. Ren, C.-S. Wu, 1996, ISBN: 1-55899-324-X
- Volume 422—Rare Earth Doped Semiconductors II, S. Coffa, A. Polman, R.N. Schwartz, 1996, ISBN: 1-55899-325-8
- Volume 423—III-Nitride, SiC, and Diamond Materials for Electronic Devices, D.K. Gaskill, C. Brandt, R.J. Nemanich, 1996, ISBN: 1-55899-326-6
- Volume 424—Flat Panel Display Materials II, M. Hatalis, J. Kanicki, C.J. Summers, F. Funada, 1996, ISBN: 1-55899-327-4
- Volume 425—Liquid Crystals for Advanced Technologies, T.J. Bunning, S.H. Chen, W. Hawthorne, N. Koide, T. Kajiyama, 1996, ISBN: 1-55899-328-2
- Volume 426—Thin Films for Photovoltaic and Related Device Applications, D. Ginley, A. Catalano, H.W. Schock, C. Eberspacher, T.M. Peterson, T. Wada, 1996, ISBN: 1-55899-329-0
- Volume 427—Advanced Metallization for Future ULSI, K.N. Tu, J.W. Mayer, J.M. Poate, L.J. Chen, 1996, ISBN: 1-5899-330-4
- Volume 428—Materials Reliability in Microelectronics VI, W.F. Filter, J.J. Clement, A.S. Oates, R. Rosenberg, P.M. Lenahan, 1996, ISBN: 1-55899-331-2
- Volume 429—Rapid Thermal and Integrated Processing V, J.C. Gelpey, M. Öztürk, R.P.S. Thakur, A.T. Fiory, F. Roozeboom, 1996, ISBN: 1-55899-332-0
- Volume 430—Microwave Processing of Materials V, M.F. Iskander, J.O. Kiggans, E.R. Peterson, J.Ch. Bolomey, 1996, ISBN: 1-55899-333-9
- Volume 431—Microporous and Macroporous Materials, R.F. Lobo, J.S. Beck, S. Sulb, D.R. Corbin, M.E. Davis, L.E. Iton, S.I. Zones, 1996, ISBN: 1-55899-334-7
- Volume 432—Aqueous Chemistry and Geochemistry of Oxides, Oxyhydroxides, and Related Materials J.A. Voight, B.C. Bunker, W.H. Casey, T.E. Wood, L.J. Crossey, 1996, ISBN: 1-55899-335-5
- Volume 433—Ferroelectric Thin Films V, S.B. Desu, R. Ramesh, B.A. Tuttle, R.E. Jones, I.K. Yoo, 1996, ISBN: 1-55899-336-3
- Volume 434—Layered Materials for Structural Applications, J.J. Lewandowski, C.H. Ward, W.H. Hunt, Jr., M.R. Jackson, 1996, ISBN: 1-55899-337-1
- Volume 435—Better Ceramics Through Chemistry VII—Organic/Inorganic Hybrid Materials, B. Coltrain, C. Sanchez, D.W. Schaefer, G.L. Wilkes, 1996, ISBN: 1-55899-338-X
- Volume 436—Thin Films: Stresses and Mechanical Properties VI, W.W. Gerberich, H. Gao, J-E. Sundgren, S.P. Baker 1996, ISBN: 1-55899-339-8
- Volume 437—Applications of Synchrotron Radiation to Materials Science III, L. Terminello, S. Mini, D.L. Perry, H. Ade, 1996, ISBN: 1-55899-340-1

---

**Part I**  
**Incorporation Methods and Properties**

## ION BEAM EPITAXY OF *in-situ* Er-O CO-DOPED SILICON FILMS

Morito MATSUOKA and Shun-ichi TOHNO

NTT Opto-electronics Laboratories, Tokai, Ibaraki 319-11, Japan.

e-mail: mmatuoka@iba.iecl.ntt.jp

### ABSTRACT

Erbium-doped silicon films are grown by ion beam epitaxy (IBE) using an electric-mirror sputtering-type metal ion source in ultrahigh vacuum. *In-situ* erbium doping with concentrations ranging from  $1 \times 10^{16}$  to  $6 \times 10^{20} \text{ cm}^{-3}$  is achieved by sputtering the erbium metal pellet with ions extracted from the silicon metal ion source. The oxygen concentration in the films is also controlled *in-situ* over the range from below  $1 \times 10^{18}$  to  $2 \times 10^{20} \text{ cm}^{-3}$  by using argon gases containing 1 ppb to 100 ppm of oxygen impurities. The erbium incorporation probability drastically increases (by two or more orders of magnitude) when oxygen is contained in the argon gas during film growth. Erbium is selectively oxidized in the Si host. Erbium segregation and precipitation formation are well suppressed by the oxidation. Sharp and well-split photoluminescence is clearly observed in as-deposited films grown typically at  $480^\circ\text{C}$  with oxygen co-doping.

### INTRODUCTION

Considerable interest has been shown in fabricating rare-earth-doped semiconductor films for optically active layers[1], because rare-earth ions produce characteristic intra-4f luminescence emissions that have little dependence on the host material or temperature. Of particular interest is rare-earth-doped silicon[2-7], which offers the possibility of simple opto-electronic integrated circuits (OEIC) with ultralarge scale integrated circuits (ULSI) silicon devices. Erbium-doped silicon is one of the most important materials, in view of its application to  $1.54\text{-}\mu\text{m}$  wavelength devices for optical communications.

Erbium-doped silicon layers are usually fabricated by sequential annealing at high temperature ( $\sim 900^\circ\text{C}$ ) after erbium implantation in Czochralski (CZ) or floating zone (FZ) silicon crystals[2,4,5,7]. Erbium atoms doped in the host silicon tend to react with the silicon atoms and  $\text{ErSi}_2$  compounds are formed at temperatures around  $900^\circ\text{C}$ [5,6]. These phenomena worsen the light-emission efficiency of the erbium-doped silicon. To improve the performance of erbium-doped silicon, chemical reactions between erbium and silicon and the segregation of erbium must be suppressed as much as possible to achieve precise and steep erbium profile control and to increase the erbium doping level. The keys to overcoming these problems are decreasing the film growth temperature and conducting erbium doping *in-situ* at low temperatures without degrading the host silicon film quality.

Furthermore, oxygen co-doping in erbium-doped silicon is also an important factor[4,7] in effectively activating the erbium atoms incorporated in the host silicon. To improve their light-emission efficiency, the erbium atoms should be selectively oxidized in the host silicon. At the same time, the host silicon should not be oxidized so as to avoid degrading its crystallinity. In III-V semiconductor hosts, erbium atoms should be oxidized to activate well and to increase the luminescence efficiency[8].

Molecular-beam epitaxy (MBE) utilizing erbium and oxygen doping is one of the most promising candidates for low-temperature growth of erbium-doped silicon films[3,6]. However, high temperature ( $>600^{\circ}\text{C}$ ) post annealing is still required to improve the crystallinity and to effectively activate the erbium. Consequently, ideal erbium activation is probably still difficult to achieve using this MBE technique. Consequently, the luminescence spectra of MBE films are still diffusive and the peaks are not split well.

Ultrahigh vacuum (UHV) ion beam processes should enable the low-temperature synthesis of bulk-grade silicon films[9]. With these processes, it should be possible to dynamically control the erbium and oxygen doping levels *in-situ* and to perform selective *in situ* oxidation by low-pressure ion processes in an argon gas atmosphere containing oxygen.

In this study, we investigate the low-temperature epitaxial growth of high-quality erbium-doped silicon films *in-situ*. In our previous papers, the silicon films and erbium-doped silicon films were grown by ion-beam epitaxy (IBE)[9] using our newly developed electric-mirror sputtering-type metal ion source[9-12] and by combining the ion-beam sputtering technique with an erbium-metal source in an oxygen-containing plasma beam. Metal ions - even those with a high melting point, such as silicon and erbium - can be extracted from this ion source with high current density ( $>0.1\text{ mA/cm}^2$ ) and low energy (5-150 eV). The impurity level was suppressed below the detection limit of SIMS[9]. As a result, defect-free silicon films were grown on low-temperature substrates (as low as  $400^{\circ}\text{C}$ )[9] and stable IBE of erbium and oxygen co-doped silicon films with strict dopant control and a steep interface was achieved *in-situ* at low temperatures[13].

In this paper, we discuss in-detail the effects of oxygen on the incorporation and segregation of erbium, and on the crystallinity of erbium-oxygen *in-situ* co-doped silicon films. By adding oxygen gases during film growth *in-situ*, erbium atoms are selectively oxidized and the segregation is remarkably suppressed. The erbium incorporation efficiency is dramatically increased (by two or more orders of magnitude) by oxygen incorporation. As a result, the erbium dopant level was strictly controlled over a wide range ( $10^{16}$ - $10^{21}\text{ cm}^{-3}$ ). Oxygen-erbium co-doped silicon films grown in this way exhibit sharp photoluminescence at  $1.54\text{ }\mu\text{m}$  wavelength, corresponding to  $\text{Er}^{3+}$  excitation in the host silicon.

#### UHV SYSTEM AND ION SOURCE CONFIGURATION

The system consists of a process chamber, an analysis chamber, and a load-lock chamber[9]. The process chamber is evacuated by a turbo-molecular pump

backed up by a mechanical booster pump and a rotary pump in series. The analysis chamber is evacuated by an ion pump. The load-lock chamber is evacuated by a turbo-molecular pump backed up by a rotary pump. The system is baked at 150°C before operation. The background pressures of the process, analysis, and load-lock chambers reach  $2 \times 10^{-8}$  Pa,  $1 \times 10^{-8}$  Pa, and  $5 \times 10^{-7}$  Pa, respectively. The system construction was detailed in a previous paper[9].

The electric-mirror sputtering-type metal ion source (referred to as EM-ion source hereafter) was mounted in the IBE process chamber. Figure 1 schematically illustrates the metal ion source and the erbium solid source used in UHV. The ion source consists of a pair of planar and cylindrical silicon targets made from a single-crystal silicon ingot, a cylindrical anode, and a magnetic coil surrounding the planar target.

The silicon targets (a 40-mm-high cylinder with an inner diameter of 100-mm and 5-mm-thick plate with a diameter of 80 mm) were made of B-doped or non-doped Czochralski (CZ) silicon. The oxygen and carbon impurity levels in the target materials were  $2 \times 10^{18} \text{ cm}^{-3}$ , and below  $1 \times 10^{17} \text{ cm}^{-3}$  respectively. The coil generates a magnetic flux whose density reaches about 500 G at the cylindrical target center and penetrates both target surfaces. Negative voltages were applied to the targets.

High-energy secondary electrons emitted from the target surfaces (so-called  $\gamma$ -electrons) oscillate between the targets as a result of E//B confinement[11]. Consequently, dense plasma is generated at pressures ranging from 0.01 to 1 Pa through the beam-plasma interaction[11]. The magnetic field profile flares out from the plasma source toward the substrate and accelerates the plasma towards the substrate. The plasma potential is controlled by adjusting the voltage applied to the cylindrical anode located between the targets. This enables the ion energy to be well controlled between 5 and 150 eV. The ionization ratio reaches about 30% for the ion source either with an extraction grid[11] or without[12]. This EM source works as an ion source at low energy levels even without the extraction grid because the ionization ratio is high enough for IBE and a high ion current can be extracted without space charge limitation during ion propagation onto the substrate surface.

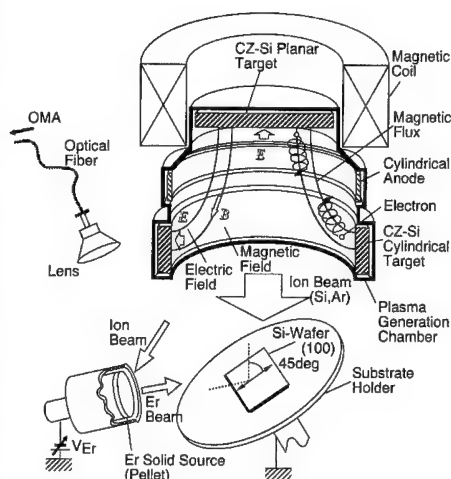


FIG. 1. Schematic illustration of the electric-mirror sputtering-type ion source, the erbium solid source, and the substrate plate mounted to the UHV system.

In this study, we used an ion source without an extraction grid for the silicon IBE because high-density metal ions with energies below 100 eV need to be extracted to grow high-quality silicon films at low temperatures. Typically, in this experiment, 10 eV ions were used for IBE of defect-free silicon films at low temperatures[9].

A solid-source erbium pellet (25 mm in diameter, 99.9% purity) was inserted into the process chamber as shown in Fig. 1 and negative voltages between -30 and -1200 V were applied to it. The ions extracted from the metal ion source were accelerated onto the erbium pellet. Some of the erbium atoms sputtered from the pellet were ionized in the plasma stream and accelerated toward the substrate through the plasma potential in the same way as low-energy silicon ions ( $\sim 10$  eV).

## EXPERIMENT

Silicon (100) wafers (25x25 mm) grown by the Czochralski (CZ) or floating zone (FZ) method were used as the substrates. After 3 cycles of sequential dipping in boiled  $\text{HNO}_3$  and in 3% HF, the wafers were then treated by 3 cycles of sequential dipping in  $\text{HCl}:\text{H}_2\text{O}_2:\text{H}_2\text{O}$  (3:1:1) solvent and in 3% HF. Next, the wafers were treated in  $\text{HCl}:\text{H}_2\text{O}_2:\text{H}_2\text{O}$  (3:1:1) solvent and rinsed in pure water before being loaded into the chamber. The pre-treated wafers, which surfaces are weakly oxidized, were heated at  $830^\circ\text{C}$  for five minutes in a UHV. After a  $2\times 1$  reconstructed surface structure was observed by reflection high energy electron diffraction (RHEED), erbium-doped silicon films were grown at temperatures ranging from 70 to  $700^\circ\text{C}$  (typically  $480^\circ\text{C}$ , at argon pressures ranging from 0.03 to 3 Pa (typically 0.3 Pa) with oxygen impurities of 1 ppb to 100 ppm. The oxygen concentration was controlled by mixing the gases from two lines; one containing 8N-purity argon and the other containing argon and 100 ppm of oxygen[13]. The sputtering power was maintained at 300 W, corresponding to a film growth rate of 0.05 nm/sec.

The crystallographic properties were characterized by transmission electron microscopy (TEM) and Rutherford back-scattering spectroscopy (RBS). The film defect density was estimated by TEM and scanning electron microscopy (SEM) after etching with Wright solvent[9]. The impurity levels, including O, C, N, Ar, Cu, Fe, Co, Cr, Al, B, As, and Er, were measured by secondary ion mass spectroscopy (SIMS). The erbium doping level was calibrated with heavily-erbium-doped silicon films (above  $10^{20}\text{ cm}^{-3}$ ) by using x-ray fluorescence analysis (XFA). The surface crystallinity of the films and substrates were characterized with RHEED analysis. The optical emission of the erbium particles ejected from the erbium pellet was observed by optical multi-channel analysis (OMA). The optical properties of the IBE silicon films were characterized at 4K and 300K by their photoluminescence emission when excited by an Ar ion laser (wavelength  $\lambda$ :  $0.588\text{ }\mu\text{m}$ ) or He-Ne laser (wavelength  $\lambda$ :  $0.633\text{ }\mu\text{m}$ ) at a power of 50 mW.



## RESULTS AND DISCUSSION

### IBE of silicon films on (100) silicon

At growth temperatures above 400°C, the contamination levels were suppressed below the SIMS and XFA detection limits, that is,  $O < 1 \times 10^{18} \text{ cm}^{-3}$ ,  $C < 1 \times 10^{17} \text{ cm}^{-3}$ ,  $N < 1 \times 10^{17} \text{ cm}^{-3}$ ,  $\text{Cu} < 1 \times 10^{16} \text{ cm}^{-3}$ ,  $\text{Mn} < 7 \times 10^{15} \text{ cm}^{-3}$ ,  $\text{Fe} < 1 \times 10^{16} \text{ cm}^{-3}$ ,  $\text{Cr} < 5 \times 10^{14} \text{ cm}^{-3}$ ,  $\text{Al} < 5 \times 10^{14} \text{ cm}^{-3}$ , and  $\text{Co} < 1 \times 10^{16} \text{ cm}^{-3}$ , as published in our previous report[9]. Such low levels of oxygen and carbon contamination are obtained as a result of growing the film in a UHV, using 8-N purity argon gas without oxygen[9].

In the EM-ion source, the high-density plasma was well confined between the targets and the plasma potential was well controlled. As a result, the metal impurities from the chamber wall and shield plates were suppressed below the SIMS detection limit. No pile-up of the contamination was also observed at the film-substrate interface. Although the target we used included  $2 \times 10^{18} \text{ cm}^{-3}$  of oxygen impurity, the oxygen level trapped in the film was much lower than  $1 \times 10^{18}$  (below the SIMS detection limit). In the IBE silicon films grown with 10 eV energy ions, SIMS and XFA measurements also failed to detect argon impurities, which often occur in plasma processes using argon gas[9]. This is because the plasma potential was well controlled and the high-energy reflected argon particles impinging onto the substrate surface were well suppressed during film deposition.

Epitaxial films grow at temperatures above 320°C (film thickness=0.5  $\mu\text{m}$ ), and high-purity silicon films grow at temperature above 400°C. Low-energy ions (~ 10 eV) are best suited for growing epitaxial silicon films with the same level of crystallinity as bulk single-crystal silicon[9]. Defects and penetrating dislocations were not observed by TEM or etch-pit observation by SEM in the IBE silicon films. The minimum RBS yield reached the same level as for bulk single-crystal silicon. Impurities doped *in-situ*, including B and As, were ideally activated in the host silicon films at temperatures below 400°C. In this study, the erbium-doped silicon films were typically grown at 320-700°C with 10 eV ions in the experiments described below.

### Erbium doping control

Figure 2 shows the typical relationships between the voltage applied to the erbium pellet (i.e., the primary ion energy impinging on the erbium pellet), the erbium concentration in the IBE silicon films ( $N_{\text{Er}}$ ), the optical emission at 582.7 nm wavelength (corresponding to Er-atom emission) on the erbium pellet surface ( $I_{\text{Er}5827}$ ), and the primary ion current extracted onto the erbium pellet ( $I_{\text{Er}}$ ). Here, the oxygen concentration in the argon gas was maintained at 10 ppm during film growth. The effect of oxygen addition on erbium incorporation is described in detail in the next section. All these levels monotonically increase with applied

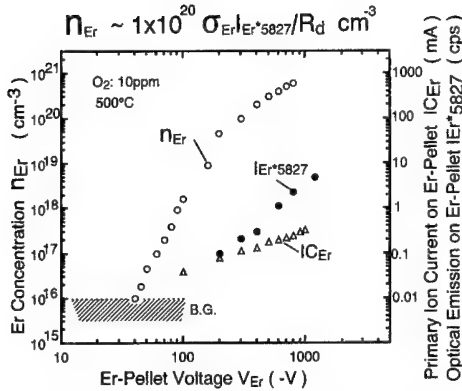


FIG. 2. Relationships between the acceleration energy of primary ions impinging onto the erbium pellet and the erbium concentration doped in IBE silicon films, the optical emission intensity, and the primary ion current accelerated onto the erbium pellet. Here the film growth rate  $R_d$  is maintained at constant (0.05 nm/sec). The Er flux density can be monitored by the optical emission and thereby the Er density was strictly feedback controlled.

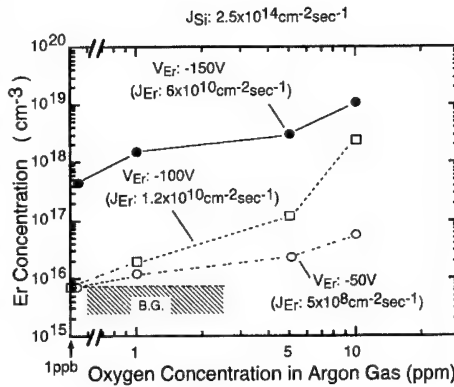


FIG. 3. Relationship between the erbium concentration incorporated in IBE silicon films and the oxygen concentration in the supplied argon gases, where the erbium flux is kept constant.

voltage. As shown in this figure, the erbium concentrations were precisely controlled by adjusting the applied voltage from  $1 \times 10^{16} \text{ cm}^{-3}$  at -50 V to  $6 \times 10^{20} \text{ cm}^{-3}$  at -1000 V.

The erbium concentration is well controlled *in-situ* not only by adjusting the applied voltage (or the primary ion current) but also by moving the erbium pellet relative to the substrate surface and EM ion source, and the erbium flux was accurately monitored by the erbium emission intensity at a wavelength of 582.7 nm  $I_{\text{Er}^*5827}$ , corresponding to electron excitation of outer shell ( $\text{Er}^0\text{-Er}^*$ ). In this experiment, the erbium pellet location was fixed. Therefore, the erbium flux was changed only by the pellet voltage with feedback control of the optical emission  $I_{\text{Er}^*5827}$ .

The optical intensity  $I_{\text{Er}^*5827}$  changes linearly with the erbium flux density in this case, because the electron temperature in plasma does not change much with the erbium pellet voltage, and thus the excitation efficiency of erbium in plasma is almost constant. When the incorporation probability of erbium ( $\sigma_{\text{Er}}$ ) is known, the incorporated erbium density ( $n_{\text{Er}}$ ) in the silicon films can easily be estimated from the  $I_{\text{Er}^*5827}$  value alone. At an oxygen concentration of 10 ppm in the argon during film growth, the erbium incorporation density changes linearly with the intensity  $I_{\text{Er}^*5827}$  and the erbium incorporation efficiency (or sticking efficiency) reaches almost 1 at this condition ( $\text{O}_2$ : 10 ppm,  $500^\circ\text{C}$ ).

Below an absolute voltage of 50 V, optical emission at the erbium pellet was not observed and the erbium atoms were not doped. This is consistent with the sputtering threshold of erbium.

#### Effect of oxygen co-doping on erbium incorporation and segregation

The erbium incorporation efficiency was strongly affected by the oxygen concentration in the argon gas introduced during film growth. The relationship between the oxygen concentrations in the argon during film growth and erbium density incorporated in the films are summarized in Fig.3. As shown in the figure, the erbium incorporation efficiency  $\sigma_{Er}$  dramatically increases as the oxygen concentration in argon gas increases.

At the same erbium pellet voltage (at the same impinging density of erbium), the erbium flux remains almost constant because the oxygen concentration (or surface contamination ratio on the erbium pellet) is much lower than the etching speed in this case. Also, the optical emission measurement by OMA shows that the ejection ratio is constant at the same acceleration voltage on the erbium pellet. Therefore, the change in the incorporated erbium concentration with oxygen concentration in the argon gas during film growth depends on the incorporation efficiency of erbium  $\sigma_{Er}$  in silicon films.

As shown in Fig. 3, the erbium incorporation efficiency  $\sigma_{Er}$  increases by two or more orders of magnitude when oxygen is added to the argon gas. The erbium incorporation efficiency  $\sigma_{Er}$  reaches 1 (ideally incorporated) at an oxygen concentration of 10 ppm and at 500°C. This suggests that the erbium segregation is well suppressed and the sticking efficiency dramatically increases when oxygen is added during film growth. The suppression of erbium segregation by oxygen on Si(100) has also been observed in other forms of MBE growth[14].

The incorporation efficiency depends little on the oxygen incorporation above an erbium concentration of  $1 \times 10^{20} \text{ cm}^{-3}$ . This suggests that the segregation constant does not depend on the oxygen incorporation when the erbium density reaches above  $1 \times 10^{20} \text{ cm}^{-3}$  level.

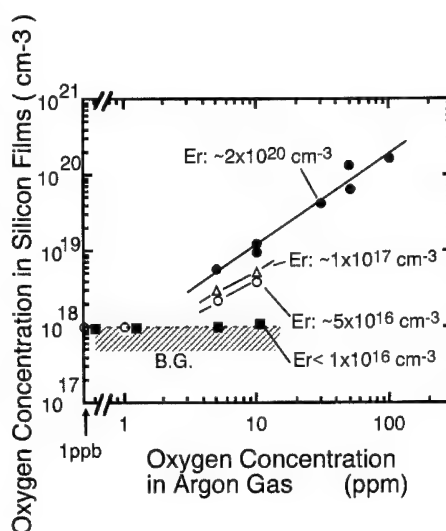


FIG. 4. Relationship between the oxygen concentrations in IBE silicon films and the oxygen concentration in the argon gas during film growth at different Er concentration.

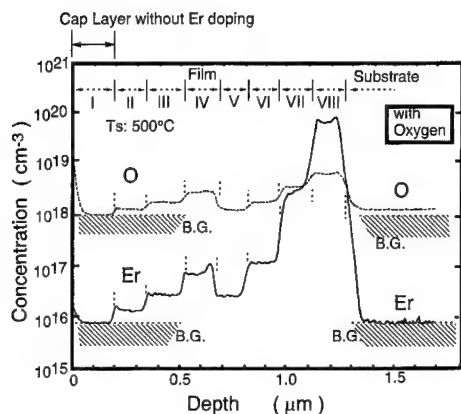


FIG. 5. Typical depth profile of SIMS of erbium and oxygen modulation doped silicon films grown at 500°C with 10 eV ions, where the oxygen concentration in the argon gas ( $BG_O$ ) and the Er pellet voltage ( $V_{Er}$ ) were varied. Each layer was grown at different conditions.

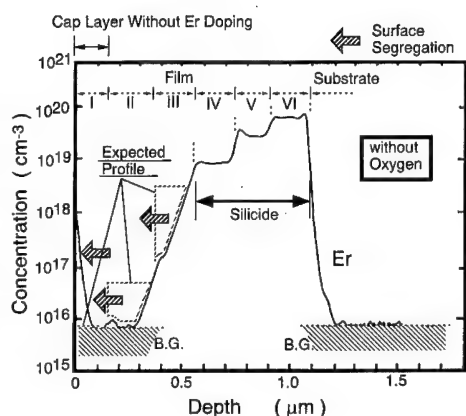


FIG. 6. Typical SIMS depth profile of erbium modulation doped silicon films grown at 500°C with 10-eV ions without adding oxygen in the argon gas during film growth, where the Er pellet voltage ( $V_{Er}$ ) were varied. Each layer was grown at different conditions.

Figure 4 shows the relationship between the oxygen concentration in the IBE silicon films and the oxygen impurity level in the argon gas. The parameter is the incorporated erbium density. The incorporated oxygen concentration monotonically increases with the oxygen impurity level in the argon gas as shown in the figure. The oxygen doping level in the IBE silicon films changes from below  $1 \times 10^{18} \text{ cm}^{-3}$  (SIMS detection limit) at 1 ppm to  $2 \times 10^{20} \text{ cm}^{-3}$  at 100 ppm with an argon pressure of 0.3 Pa. It strongly depends on the incorporated erbium concentration; the higher the erbium concentration, the higher the level of oxygen incorporated in the silicon film. The incorporated probabilities of erbium and oxygen are closely related to each other. This clearly indicates that erbium atoms are selectively oxidized in IBE silicon films. This is a key element of the IBE technique for fabricating erbium-doped silicon films.

These results strongly suggest that the erbium atoms are selectively oxidized in the films. Consequently, precise and steep dopant control is easily achieved by using IBE with oxygen addition during film growth, as shown in Fig. 5. On the other hand, without oxygen co-doping, concentrations of below  $1 \times 10^{19} \text{ cm}^{-3}$  cannot be controlled well. This is mainly because erbium segregation occurs without oxygen co-doping. As clearly shown in Fig. 6, heavy surface and interlayer segregations are observed in the SIMS profile (as shown by arrows in the figure) for erbium doped silicon films without oxygen co-doping. Even in cap

layer without Er doping, high-density Er is detected. As a result, steep and precise control cannot be achieved without oxygen co-doping during film growth.

Above  $1 \times 10^{20} \text{ cm}^{-3}$ , segregation is not observed in the SIMS profile even without oxygen as shown in Fig. 6. This is probably because the segregation coefficient does not change with the oxygen incorporation when Er atoms are heavily doped above the level, as mentioned above. The erbium incorporation efficiency also saturates with oxygen incorporation as shown in Fig. 3. This suggests the existence of a segregation trapping mechanism like a surfactant [15].

The oxidation affinity of erbium is much higher than that of silicon. This also clarifies why oxygen cannot be incorporated in silicon without erbium incorporation at the same time. We should take the segregation coefficient for the collective segregation behavior of oxygen and erbium in silicon. Therefore, oxygen acts as a surfactant (or segregation killer) in silicon. At higher dose levels, the defects or precipitation can suppress the surface segregation of erbium. From the RHEED analysis, it is clarified that the crystallinity worsens as the doping level reaches  $1 \times 10^{20} \text{ cm}^{-3}$ . Consequently, in this case, the worsening of the host-silicon's crystallinity is the main origin of the decrease in the effect of oxygen co-doping on the erbium incorporation efficiency. The defects and dislocations can act as segregation killers, or the formation of the precipitation can also suppress the surface segregation of erbium.

Next, the segregation phenomenon is discussed more in detail. Figure 7 shows the relationship between the film growth temperature and erbium incorporation probability. With low oxygen level below 10ppm, erbium incorporation probability monotonically decreases with the growth temperature below  $500^\circ\text{C}$ , and drastically increases with the growth temperature above  $500^\circ\text{C}$ . On the other hand, with high oxygen level above 50 ppm, the incorporation efficiency does not change with the growth temperature. These results indicate that the erbium incorporation probability reaches 1 with enough oxygen incorporation. Also from the RHEED analysis, it was estimated that the silicide (precipitation) was formed at conditions with low oxygen and at high temperature range. This is why the incorporation probability drastically increases when growth temperature increases above  $500^\circ\text{C}$  with lower oxygen concentration. The silicide formation is suppressed

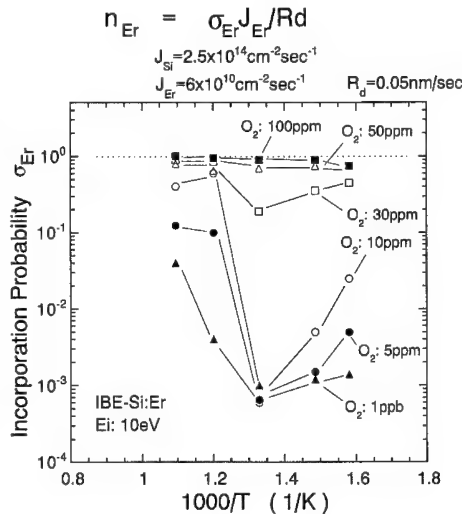


FIG. 7. Relationship between growth temperature and erbium incorporation probability at several oxygen concentrations in argon gas. Here, flux density (impinging density) on the substrate surface of Si ( $J_{\text{Si}}$ ) and Er ( $J_{\text{Er}}$ ) are kept constant. The film growth rate  $R_d$  is also kept constant.

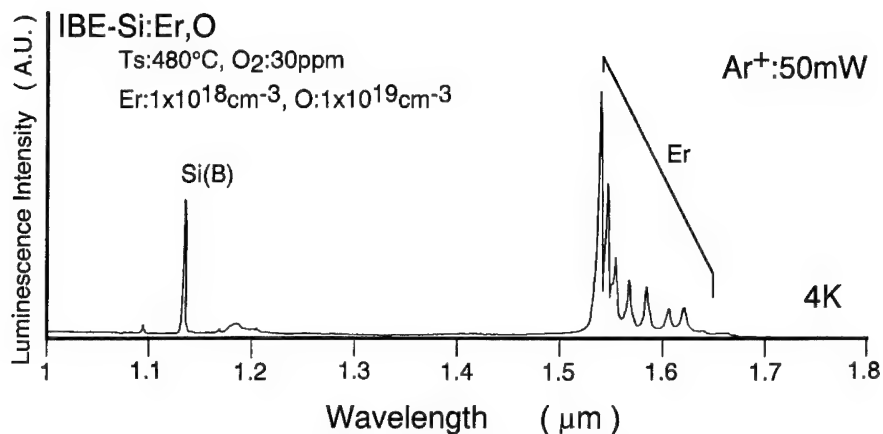


FIG. 8. Typical photo-luminescence spectrum from *in-situ* oxygen-erbium co-doped silicon films as-grown at 500°C with 10-eV ions.

even at high temperature with higher oxygen concentration.

#### Photoluminescence characteristics

Figure 8 shows a typical photoluminescence spectrum from *in-situ* erbium-oxygen co-doped ( $O: 1 \times 10^{19} \text{ cm}^{-3}$ ,  $Er: 1 \times 10^{18} \text{ cm}^{-3}$ ) silicon films as-grown at 480°C with 10-eV ions measured at 4K. Sharp and well-split spectrum with 7 peaks is observed, which indicates that most Er ions are located at the substitutional sites with oxygen in silicon host lattice. Figure 9 shows the relationship between erbium concentration and photoluminescence intensity of oxygen co-doped films and oxygen-free silicon. Light emission at a 1.54- $\mu\text{m}$  wavelength, corresponding to  $Er^{3+}$  ions in the host silicon, is clearly observed for oxygen co-doped silicon films. The photoluminescence of oxygen-free films is much weaker (by an order of magnitude) than oxygen co-doped silicon films. This indicates that erbium atoms in the host silicon are

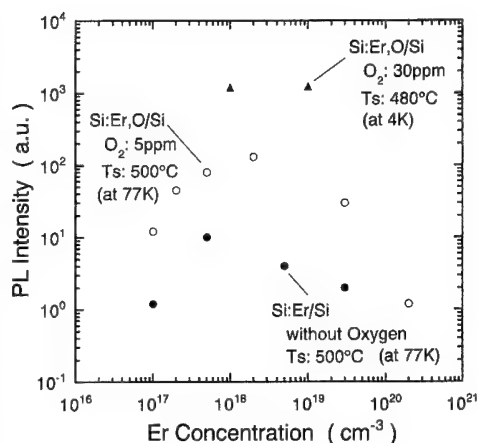


FIG. 9. Relationship between erbium concentration and photo-luminescence intensity of erbium, oxygen co-doped IBE films and oxygen non-doped films at 4 K (30ppm) and at 77K(5ppm, without oxygen).

effectively activated by co-doped oxygen atoms, as achieved in other reports[4-7]. The luminescence intensity monotonically increases as the erbium concentration increases up to  $2 \times 10^{18} \text{ cm}^{-3}$  in the case of 5 ppm and up to  $1 \times 10^{19} \text{ cm}^{-3}$  in the case of 30 ppm. The decrease in the luminescence intensity at higher erbium concentration corresponds to the degradation of crystallinity or precipitation. The balance of the erbium and oxygen concentration is important to keep host crystallinity and thereby effective photoluminescence.

The photoluminescence was also observed at 300 K from *in-situ* erbium-oxygen co-doped (O:  $1 \times 10^{19} \text{ cm}^{-3}$ , Er:  $1 \times 10^{18} \text{ cm}^{-3}$ ) silicon films.

## CONCLUSIONS

Erbium-doped silicon films have been grown by ion beam epitaxy (IBE) using an electric-mirror sputtering-type metal ion source in a UHV. Precise and steep erbium-profile control was achieved *in-situ* by sputtering pure erbium metal pellet with ions extracted from the silicon metal ion source. The erbium-dopant level changed from  $1 \times 10^{16}$  to  $6 \times 10^{20} \text{ cm}^{-3}$ . The oxygen concentration doped in the films was also controlled *in-situ* over the range from below  $1 \times 10^{18}$  to  $2 \times 10^{20} \text{ cm}^{-3}$  by using argon gas containing oxygen impurities ranging from 1 ppb to 100 ppm.

The incorporation efficiencies of erbium and oxygen are closely related to each other. The erbium incorporation efficiency dramatically increases (by two or more orders of magnitude) as the oxygen concentration increases in the argon gas used during film growth. The oxygen concentration level in the IBE films also strongly depends on the erbium concentration in the films. This indicates that erbium atoms are selectively oxidized in IBE silicon films. Moreover, erbium segregation is well suppressed by the addition of oxygen to the argon gas during film growth.

Without oxygen incorporation, the photoluminescence intensity is not clearly observed. On the other hand, the photo-luminescence of  $1.54\text{-}\mu\text{m}$  wavelength light, which corresponds to  $\text{Er}^{3+}$  ions in the host silicon, was clearly observed for oxygen co-doped as-deposited films grown *in-situ* at typically  $480^\circ\text{C}$ .

The IBE system developed in this study is a good candidate for low-temperature *in-situ* fabrication of erbium-oxygen co-doped silicon films with high erbium concentration and high emission efficiency.

## ACKNOWLEDGMENTS

We would like to thank Dr. Hiroaki Hiratsuka of NTT Laboratories for his encouragement and valuable discussions during this study. We would also like to thank Dr. Ken'ichiro Takahei of the NTT Basic Research Laboratories for his valuable suggestions and discussion of Er-doped semiconductors and the characterization of the optical properties of IBE films and Dr. Yoshikazu Honma

of NTT Interdisciplinary Research Laboratories for his suggestions and help with the film analysis.

## REFERENCES

1. For example, "*Rare earth doped semiconductors*", Mat. Res. Soc. Symp. Proc. **301** (1993).
2. H. Ennen, J. Schneider, G. Pomrenke, and A. Axmann, Appl. Phys. Lett., **43**, 943 (1983).
3. H. Ennen, G. Pomrenke, A. Axmann, K. Eisele, W. Haydl, and J. Schneider, Appl. Phys. Lett., **46**, 381 (1985).
4. P. N. Favennec, H. L'Haridon, D. Moutonnet, M. Salvi, and M. Gauneau, Jap. J. Appl. Phys., **29**, L524 (1990).
5. D. J. Eaglesham, J. Michel, E. A. Fitzgerald, D. C. Jacobson, J. M. Poate, J. L. Benton, A. Polman, Y. -H. Xie, and L. C. Kimerling, Appl. Phys. Lett., **58**, 2797 (1991).
6. H. Efeoglu, J. H. Evans, T. E. Jackman, B. Hamilton, D. C. Houghton, J. M. Langer, A. R. Peaker, D. Perovic, I. Poole, N. Ravel, P. Hemment, and C. W. Chan, Semicond. Sci. & Technol., **8**, 236 (1993).
7. F. Priolo, S. Coffa, G. Franzo, C. Spinella, A. Carnera, and Y. Bottoni, J. Appl. Phys., **74**, 4936 (1993).
8. K. Takahei, A. Taguchi, Y. Horikoshi, and J. Nakata, J. Appl. Phys., **76**, 4332 (1994).
9. M. Matsuoka and S. Tohno, J. Vac. Sci. & Technol., **A13**, 305 (1995).
10. M. Matsuoka and S. Tohno, Appl. Phys. Lett., **66**, 1862 (1995).
11. M. Matsuoka and K. Ono, J. Vac. Sci. & Technol., **A8**, 1840 (1990).
12. M. Matsuoka and K. Ono, J. Vac. Sci. & Technol., **A7**, 2652 (1989).
13. M. Matsuoka and S. Tohno, J. Appl. Phys., **78**, 2757 (1995).
14. S. Serna, M. Lohmeier, P. M. Zagwijn, E. Vlieg, and A. Polman, Appl. Phys. Lett., **66**, 1385 (1995).
15. M. Copel, M. C. Reuter, M. H. von Hoegen, R. M. Trump, Phys. Rev., **B-42**, 16829 (1990).



## GROWTH CONDITIONS OF ERBIUM-OXYGEN-DOPED SILICON GROWN BY MBE

J. STIMMER<sup>1</sup>, A. REITTINGER<sup>1</sup>, G. ABSTREITER<sup>1</sup>, H. HOLZBRECHER<sup>2</sup>,  
Ch. BUCHAL<sup>3</sup>

<sup>1</sup> Walter Schottky Institut, Techn. Univ. Munich, D-85748 Garching, Germany,  
email: jstimmer@physik.tu-muenchen.de

<sup>2</sup> ZCH, Forschungszentrum Jülich GmbH, D-52425 Jülich, Germany

<sup>3</sup> ISI 2, Forschungszentrum Jülich GmbH, D-52425 Jülich, Germany

### ABSTRACT

We report on a systematic study of the growth parameters of erbium-oxygen-doped silicon grown by molecular beam epitaxy. The surface quality of the grown layers was measured in situ by RHEED. The samples were characterized by photoluminescence measurements and SIMS. An Er-O-doped Si light emitting diode grown with the optimized parameters is presented.

### INTRODUCTION

The rare earth erbium in its trivalent state is well known to emit photons at  $\lambda = 1.54$   $\mu\text{m}$  after excitation. This wavelength coincides with the absorption minimum of silica-based fibers. Therefore, erbium-doped emitters or amplifiers are of high interest. Since Ennen *et al.* [1] reported the first observation of electroluminescence at 1.54  $\mu\text{m}$  of an erbium-doped silicon light emitting diode, strong efforts have been made to understand the mechanisms of excitation and relaxation of erbium in silicon and to obtain erbium-related luminescence at room-temperature [2,3]. Only very recently room-temperature electroluminescence of erbium-doped silicon LEDs could be observed [4-6].

The usual way of incorporating the rare earth ions and the codopant oxygen is via ion implantation [2-6]. Energies in the range of MeV are needed for erbium. This leads to a high density of defects, even after thermal annealing of the samples. For high erbium concentrations precipitation during annealing causes further problems. To overcome these problems, epitaxial techniques with in situ doping of erbium and the codopant oxygen seem to be a promising alternative.

We present a systematic study of the growth parameters for erbium-oxygen-doped silicon grown by molecular beam epitaxy and an Er-Si LED grown with the optimized parameters.

### EXPERIMENT

A converted Riber molecular beam epitaxy 32 P machine was used for growing the

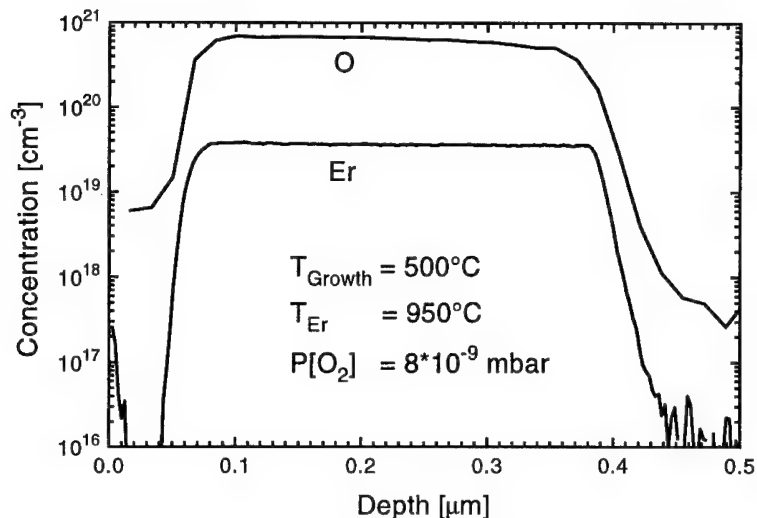


Fig. 1: Secondary ion mass spectroscopy of a MBE grown sample.

erbium-oxygen-doped silicon layers. The pumping system consists of a large turbomolecular pump, a liquid nitrogen cooled shroud with a titanium sublimation pump and a cryo-pump. Base pressure in the chamber is below  $10^{-10}$  mbar. The large turbomolecular pumping system ensures ultra high vacuum conditions despite the inlet of high amount of high purity oxygen introduced from a commercially Riber OPS 2000 plasma source. The oxygen flow rate is controlled with a hand operated UHV valve. The UHV part of the plasma source consists of a thin U-shaped quartz glass tube. A nozzle at the end of this tube is directed towards the manipulator carrying the silicon substrate. Silicon is evaporated from an e-beam source at a constant flux of  $0.3 \text{ \AA/sec}$ . For erbium a standard effusion cell is used.

The samples for photoluminescence measurements were grown on chemically untreated, undoped (100)-oriented float zone silicon substrates. In order to remove the native oxide prior to the growth process, the substrate was heated to  $1000^\circ\text{C}$  for 15 minutes in the chamber. Substrate temperatures during growth were varied between  $400^\circ\text{C}$  and  $800^\circ\text{C}$ . The erbium-oxygen-doped silicon layers were grown by simultaneously evaporating silicon and erbium and providing a suitable flow of gaseous oxygen onto the substrate. The oxygen partial pressure during growth was varied to a maximum of approximately  $10^{-6}$  mbar. The surface of the grown layers were measured in situ by reflection high energy electron diffraction (RHEED).

For the optical measurements, a single grating monochromator and a liquid nitrogen cooled germanium detector were used. Photoluminescence was excited with the 458 nm line of an argon laser, chopped at 20 Hz and detected with standard lock-in techniques.

## RESULTS

In Fig. 1 a secondary ion mass spectroscopy profile of a sample grown by MBE is shown. The substrate temperature was kept at  $500^\circ\text{C}$ . A 50 nm thick silicon buffer layer

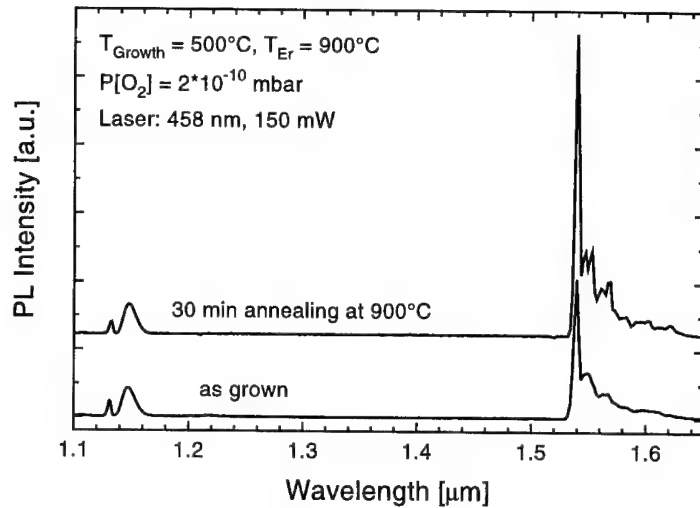


**Fig. 2:** 4 K photoluminescence of an as grown sample and after an additional annealing.

is followed by the 400 nm thick active region. The erbium cell was kept at 950°C and the oxygen partial pressure during growth was approximately  $8 \times 10^{-9}$  mbar. The sample is finished by a 50 nm top silicon cladding layer. Erbium is incorporated at a concentration of  $4 \times 10^{19} \text{ cm}^{-3}$ . The oxygen concentration is more than one order of magnitude higher. Due to the high amount of oxygen provided during growth, no segregation occurred. As will be presented in Fig. 4 due to such high oxygen pressures three dimensional growth occurs.

Low temperature photoluminescence spectra of MBE grown samples are shown in Fig. 2. For this sample the erbium cell temperature was 900°C and the oxygen pressure fixed at  $2 \times 10^{-10}$  mbar. The resulting erbium and oxygen concentrations in the sample are both  $10^{19} \text{ cm}^{-3}$ . The lower spectrum was taken from the as grown sample, whereas the upper spectrum (shifted vertically for clarity) shows the photoluminescence spectrum after an additional annealing step (30 min, 900°C, vacuum). The annealing only results in a slight increase of the erbium peak intensity and a sharpening of the erbium peaks. In both samples, no luminescence originating from defects is observable [8].

A set of samples was grown with the substrate temperature ranging from 400 to 800°C. Since erbium segregation is believed to be also dependent on the oxygen partial pressure, both parameters were investigated simultaneously. Fig. 3 summarizes the results. In all cases, a growth temperature of 500°C gives maximum PL intensity.

By varying the erbium cell temperature which determines the erbium flux, it was found that keeping the erbium cell at 950°C (resulting  $[\text{Er}]$ :  $4 \times 10^{19} \text{ cm}^{-3}$ ) leads to best results in photoluminescence intensity.

Fig. 4 shows the dependence of the PL intensity on the oxygen partial pressure, keeping the substrate temperature and the erbium cell at the optimized values i.e. the erbium cell at 950°C instead of 900°C. According to the RHEED pattern of the surface, three-dimensional growth occurs above  $10^{-9}$  mbar oxygen. This level also limits the

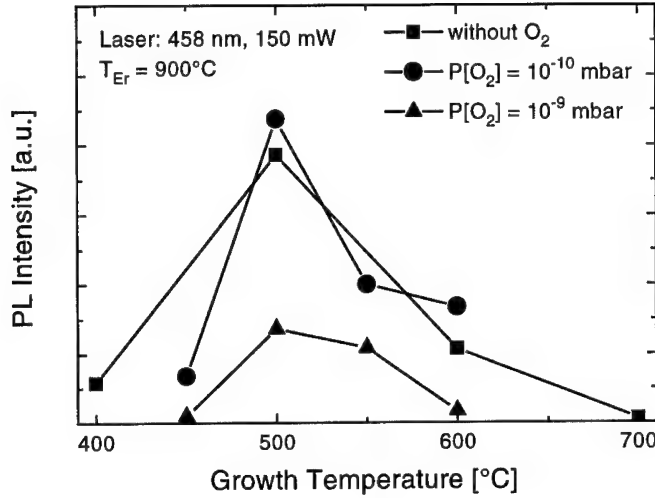


**Fig. 3:** Erbium photoluminescence intensity as measured at 4 K as a function of the growth temperature for different partial pressures of oxygen.

maximum photoluminescence intensity of erbium. In order to get information of the activation of the incorporated erbium the influence of an additional annealing step was investigated for each sample. The erbium PL intensity of the annealed samples is nearly always increased by a factor of four. A similar behaviour is also observed of samples grown at different substrate temperatures. This fact indicates that erbium needs to be activated during the growth process. If the growth parameters are not adequate even additional annealing will not lead to improved results.

With the optimized growth parameters, an erbium-silicon light emitting diode was grown. The  $p^+$  part of the diode is a highly boron doped (100) oriented Si wafer (Cz) with a resistivity of 0.025  $\Omega\text{cm}$ . After the 500 nm active region a 100 nm n-type layer was grown using a highly phosphorus doped silicon sublimation cell.

For diode fabrication, the samples were thinned from the back to a thickness of approximately 150  $\mu\text{m}$ . TiAu contacts were evaporated onto the back side and annealed at 390°C for 60 seconds in vacuum. Mesas with dimensions of 300×400  $\mu\text{m}^2$  and top TiAu contact layers were defined photolithographically. A 200×200  $\mu\text{m}^2$  window was kept uncovered for the exit of the light. Electroluminescence was measured during a square pulse excitation at 39 Hz.

Fig. 5 shows electroluminescence spectra of the Er-Si LED. The spectra were recorded by applying the voltage in reverse bias. The current density was 42 A/cm<sup>2</sup>. The strong signal at  $\lambda = 1.54 \mu\text{m}$  from the intra-4f transition of erbium is observed over the whole temperature range. The spectrum measured at 300 K is offset vertically by three units for clarity. The erbium peak shows no shift and only a decrease in intensity of less than two between 5 K and room-temperature. A weak broadening of the erbium peak is observed with increasing temperature. No luminescence related to the Si band gap is

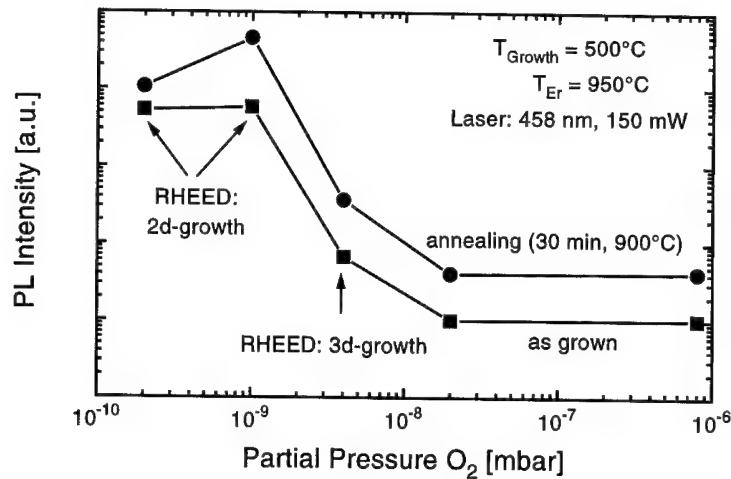


Fig. 4: 4 K erbium PL intensity as a function of the partial pressure of oxygen during growth.

detected. There is, however, a weak continuous background starting at approximately 1.05  $\mu\text{m}$ . Under forward bias the erbium intensity is reduced by a factor of 30 at 5 K and shows a temperature quenching by a factor of ten when going to room-temperature. The shapes of the spectra are not affected. Additional annealing of the diode structure before processing leads to an increase of the electroluminescence by a factor of two under both biasing conditions and over the whole temperature range. A more detailed discussion of the Er-Si-LED can be found in ref. [7].

## CONCLUSIONS

We demonstrated that erbium-oxygen-doped silicon can be grown by molecular beam epitaxy by simultaneously evaporating erbium and silicon and providing a suitable background pressure of oxygen. Up to oxygen partial pressures of  $10^{-9}$  mbar two-dimensional growth occurs. Erbium can be incorporated into a high quality crystal up to concentrations of at least  $4 \times 10^{19} \text{ cm}^{-3}$ . Under reverse bias Er-O-Si LEDs fabricated with optimized growth parameters show intense erbium electroluminescence without pronounced temperature quenching. Under forward bias the electroluminescence is reduced by a factor of ten between 5 K and room-temperature.

## ACKNOWLEDGEMENTS

The erbium-oxygen-doped silicon diodes were grown in a converted Riber MBE 32 P system which was provided to us by Prof. H. Kurz of RWTH Aachen, Germany. The project is supported financially by the Volkswagen Stiftung via Photonik programme and by the Bayerische Forschungsförderung via FOROPTO.

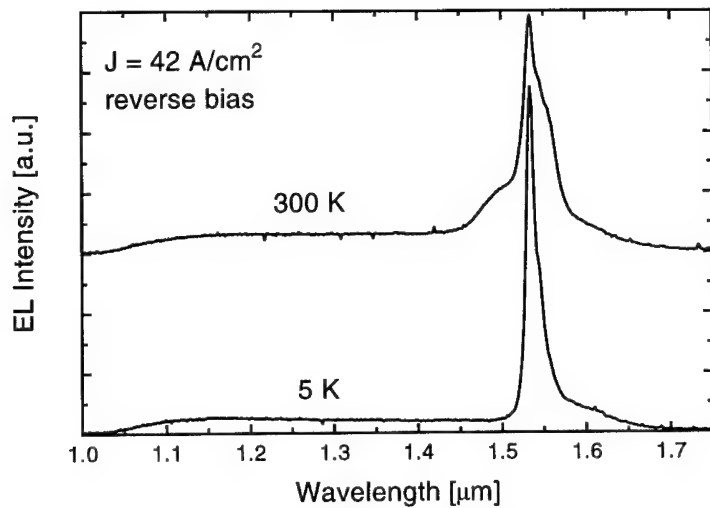


**Fig. 5:** Electroluminescence at 5 K and room-temperature of an Er-O-Si LED grown by MBE. Note that the spectra are recorded under reverse bias conditions.

## REFERENCES

1. H. Ennen, G. Pomrenke, A. Axmann, K. Eisele, W. Haydl, and J. Schneider, *Appl. Phys. Lett.* **46**, 381 (1985).
2. J. Michel, L.J. Benton, R.F. Ferrante, D.C. Jacobson, D.J. Eaglesham, E.A. Fitzgerald, Y.-H. Xie, J.M. Poate, and L.C. Kimerling, *J. Appl. Phys.* **70** 2672 (1991).
3. F. Priolo, G. Franzò, S. Coffa, A. Polman, S. Libertino, R. Barklie, and D. Carey, *J. Appl. Phys.* **78** 3874 (1995).
4. G. Franzò, F. Priolo, S. Coffa, A. Polman, and A. Carnera, *Appl. Phys. Lett.* **64** 2235 (1994).
5. B. Zheng, J. Michel, F.Y.G. Ren, L.C. Kimerling, D.C. Jacobson, and J.M. Poate, *Appl. Phys. Lett.* **64** 2842 (1994).
6. M. Jaumann, J. Stimmer, P. Schittenhelm, J.F. Nützel, G. Abstreiter, E. Neufeld, B. Holländer, and Ch. Buchal, *Appl. Surf. Sci.* (to be published).
7. J. Stimmer, A. Reittinger, J.F. Nützel, G. Abstreiter, H. Holzbrecher, and Ch. Buchal, *Appl. Phys. Lett.* (to be published).
8. R. Sauer, J. Weber, J. Stolz, E.R. Weber, K.-H. Küsters, and H. Alexander, *Appl. Phys. A* **36** 1 (1985).

## SEGREGATION AND TRAPPING OF ERBIUM IN SILICON AT A CRYSTAL-AMORPHOUS OR CRYSTAL-VACUUM INTERFACE

A. POLMAN, R. SERNA, J.S. CUSTER and M. LOHMEIER  
FOM Institute for Atomic and Molecular Physics  
Kruislaan 407, 1098 SJ Amsterdam, The Netherlands, e-mail: polman@amolf.nl

### ABSTRACT

The incorporation of erbium in silicon is studied during solid phase epitaxy (SPE) of Er-implanted amorphous Si on crystalline Si, and during Si molecular beam epitaxy (MBE). Segregation and trapping of Er is observed on Si(100), both during SPE and MBE. The trapping during SPE shows a discontinuous dependence on Er concentration, attributed to the effect of defect trap sites in the amorphous Si near the interface. Trapping during MBE is described by a continuous kinetic growth model. Above a critical Er density (which is lower for MBE than for SPE), growth instabilities occur, attributed to the formation of silicide precipitates. No segregation occurs during MBE on Si(111), attributed to the epitaxial growth of silicide precipitates.

### INTRODUCTION

The optical doping of silicon with erbium has been a very active field of research since its introduction by Ennen *et al.*<sup>1</sup> The erbium ion, when incorporated in Si in the trivalent charge state, shows an intra-4f transition at a wavelength of 1.54  $\mu\text{m}$ , which is important in optical telecommunication technology. The optical doping with erbium is thus an attractive method to obtain light from this important semiconductor. The achievement of high luminescence intensities and quantum efficiencies from Er in Si requires the incorporation of high concentrations of Er in Si. The equilibrium solubility of Er in Si is unknown, but by analogy with the transition elements<sup>2</sup> it is probably in the  $10^{14}$ - $10^{16} \text{ cm}^{-3}$  range, much too low for any practical application.<sup>3</sup> In this paper we use either ion implantation followed by solid phase epitaxial crystallization (SPE), or molecular beam epitaxy (MBE), to fabricate single crystal Si films of several 100 nm thickness, with Er concentrations up to  $10^{20} \text{ cm}^{-3}$ . This is possible by taking advantage of the non-equilibrium nature of the segregation and trapping of Er at a moving crystal-amorphous or crystal-vacuum interface, as is discussed in detail in this paper.

### EXPERIMENTAL

Erbium was implanted into single crystal (c-Si) Czochralski-grown Si(100) at 90 K. Fluences of  $6 \times 10^{13}$ ,  $3 \times 10^{14}$ , and  $9 \times 10^{14} \text{ Er/cm}^2$  were used, at an energy of 250 keV. These doses resulted in full amorphization of a surface layer of  $\approx 140 \text{ nm}$  thickness, with Er profiles confined in the amorphous (a-Si) layer. The Er-doped a-Si layers were recrystallized at 600 °C in a standard vacuum tube furnace at a base pressure of  $10^{-6} \text{ mbar}$ .

Erbium-doped epitaxial Si layers were also grown in an MBE apparatus utilizing an electron beam evaporator for Si and a Knudsen cell for coevaporation of Er. The Si flux was  $1.5 \times 10^{14} \text{ Si/cm}^2\text{s}$ , while the Er flux was either  $3.1 \times 10^{10}$  or  $1.7 \times 10^{11} \text{ Er/cm}^2\text{s}$ , controlled by setting the Knudsen cell temperature at 1030 or 1100 °C. Float zone Si(100) and Si(111) substrates were used at a temperature of 600 °C. The base pressure was  $10^{-11}$

mbar. The native oxide was removed by briefly heating the sample to 1100 °C. After this treatment the surface exhibited a clear 2x1 [Si(100)] or 7x7 [Si(111)] reflection high energy electron diffraction pattern. A 20 nm thick Si buffer layer was first grown before opening the Knudsen cell, to ensure good epitaxy.

All Er-doped Si samples were analyzed using Rutherford backscattering spectrometry (RBS) using 2 MeV He<sup>+</sup> at a scattering angle of 100°. All RBS energy spectra were converted to depth and concentration scales using known stopping powers and cross sections. The depth resolution was 8-10 nm.

#### RESULTS AND DISCUSSION: SPE

Figure 1(a) shows the as-implanted Er depth profiles after  $6 \times 10^{13}$ ,  $3 \times 10^{14}$ , and  $9 \times 10^{14}$  Er/cm<sup>2</sup> implantation at 250 keV. The implantation profiles are Gaussian in shape with a full width at half-maximum of 60 nm and a peak concentration ranging from  $1.0 \times 10^{19}$  to  $1.5 \times 10^{20}$  Er/cm<sup>3</sup>. The depth of the a-Si/c-Si interface (determined from the Si part of channeling spectra) is indicated by the dashed line. Erbium depth profiles after annealing for 15 min. at 600 °C are shown in Fig. 1(b). Channeling data

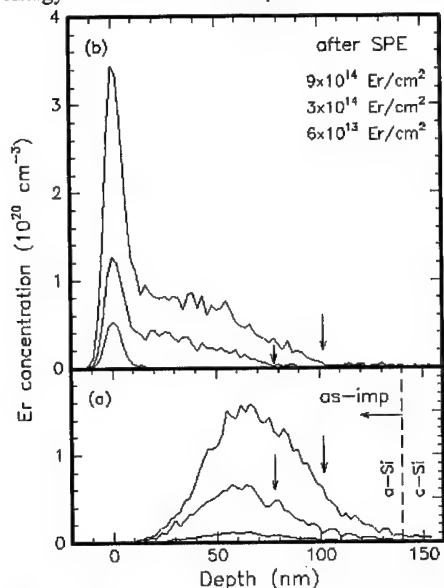


Fig. 1 Erbium concentration depth profiles for  $6 \times 10^{13}$ ,  $3 \times 10^{14}$ , and  $9 \times 10^{14}$  250 keV Er/cm<sup>2</sup>, implanted in Si(100). (a) as-implanted, (b) after SPE at 600 °C.

indicate that in all three cases the amorphous layer has fully recrystallized and good epitaxy is achieved (minimum yield  $\chi_{\min}=3-5\%$ ).

The data in Fig. 1 clearly show that after SPE, Er is segregated towards the surface, with some fraction of the Er being trapped in the crystal. More detailed measurements (using high-resolution RBS) of the Er segregation profile for partially regrown samples indicate that during regrowth the segregated Er piles up in a sharp (several nm wide) segregation spike at the moving interface, while no long range diffusion of Er occurs in the a-Si ahead of the interface.<sup>4,5</sup> Figure 1 shows that the shape of the final trapping profile depends strongly on Er concentration: for the lowest fluence no trapping is observed (as far as can be detected by RBS: secondary ion mass spectrometry measurements show that a low concentration of up to  $3 \times 10^{18}$  Er/cm<sup>3</sup> is actually trapped in the crystal<sup>5</sup>) and all Er is segregated to the surface. For the intermediate fluence no trapping is observed in the region between the original a-Si/c-Si interface and a depth of roughly 80 nm. A gradual increase in the Er concentration is observed from 80 nm depth towards the surface, with a trapped Er concentration just below the surface of  $4 \times 10^{19}$  Er/cm<sup>3</sup>. For the highest fluence, the trapping starts at a depth of 100 nm, and the trapped Er concentration increases up to  $1 \times 10^{20}$  Er/cm<sup>3</sup> just below the surface.



From the data in Fig. 1 it is possible to determine a relation between the Er density in the segregation spike at a certain depth and the Er concentration that is trapped in the crystal at that depth. To do this, the data for the three fluences in Fig. 1 were each analyzed in the following way. The as-implanted Er profile in Fig. 1(a) was first integrated from the initial amorphous-crystal interface depth (140 nm) to a certain depth  $d$  ( $<140$  nm). The same was done for the corresponding Er profile after SPE in Fig. 1(b). The two integrated

values were then subtracted to yield the Er areal density in the segregation spike at the interface after regrowth to a depth  $d$ . This procedure was performed for all depths  $d=20$ -140 nm. As the Er concentration trapped in the crystal is also known for  $d=20$ -140 nm (Fig. 1(b)), a data set could then be derived for the trapped Er concentration as a function of Er interfacial density. This procedure was followed for the three fluences in Fig. 1 and the three data sets are shown in Fig. 2.

The data for the highest fluence implants ( $9 \times 10^{14}$  Er/cm<sup>2</sup>, open circles in Fig. 2) show no trapping for low interface density, but above a threshold of  $\approx 6 \times 10^{13}$  Er/cm<sup>2</sup> at the interface, the trapped Er concentration abruptly increases. The increase is roughly linear with interface density. Data for the  $3 \times 10^{14}$  Er/cm<sup>2</sup> sample are also overlaid (crosses) and show the same behavior, with the same threshold at  $6 \times 10^{13}$  Er/cm<sup>2</sup>. Finally, data for the lowest fluence sample,  $6 \times 10^{13}$  Er/cm<sup>2</sup>, are included (closed circles) and

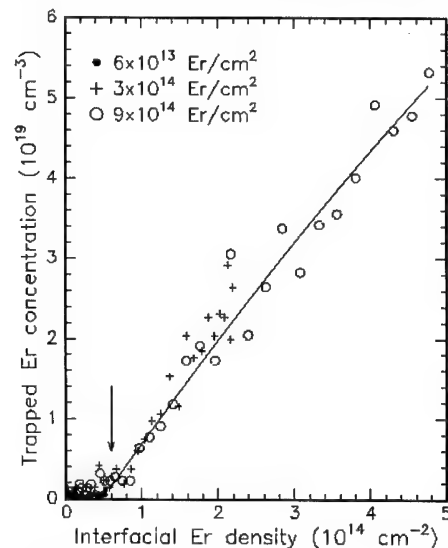


Fig. 2 Trapped Er concentration as a function of Er areal density in the segregation spike at the a-Si/c-Si interface, derived from the data in Fig. 1. Results are shown for  $6 \times 10^{13}$ ,  $3 \times 10^{14}$ , and  $9 \times 10^{14}$  250 keV Er/cm<sup>2</sup> implants. The line serves to guide the eye.

all lie in the left-bottom corner of the figure. Indeed, this implanted Er fluence is lower than the threshold fluence and no trapping was observed. These data consistently indicate that there is a critical Er areal density that can be nearly fully segregated from the growing crystal, but as this limit is exceeded, trapping occurs, at a rate proportional to the interface density. Detailed high-resolution measurements (not shown)<sup>5</sup> of the Er segregation spike during SPE show that in the spike with the critical density of  $6 \times 10^{13}$  Er/cm<sup>2</sup>, the Er peak concentration is  $3 \times 10^{20}$  Er/cm<sup>3</sup>.

The discontinuous incorporation behavior can be explained if the chemical potential of Er in a-Si is a discontinuous function of concentration. This could be understood if defects intrinsic to the a-Si network structure act as traps for the Er. Much work has been devoted to the study of defects in a-Si, and a variety of different techniques have indicated that (possibly vacancy-type) defects can exist in the covalent a-Si random network<sup>6</sup> to a concentration of typically  $5 \times 10^{19}$ - $5 \times 10^{20}$  cm<sup>-3</sup>. Cu and Pd diffusion studies<sup>7,8</sup> in a-Si with

different defect densities have shown that these defects determine the solubility of these impurities in a-Si. Similarly, such defects may determine the solubility of Er in a-Si. This would explain that for low Er concentrations in the segregation spike, the Er nearly completely segregates, as the Er is soluble in a-Si for Er concentrations below the defect density. When the Er density in the segregation spike exceeds the defect density in a-Si, excess Er has to find an alternative site. As the local order in a-Si and c-Si is very similar, the energy associated to this excess configuration may be as high in a-Si as it is in c-Si. At this stage Er can go either in the crystal or stay on the amorphous side, and as a result the trapped Er concentration increases, as is observed.

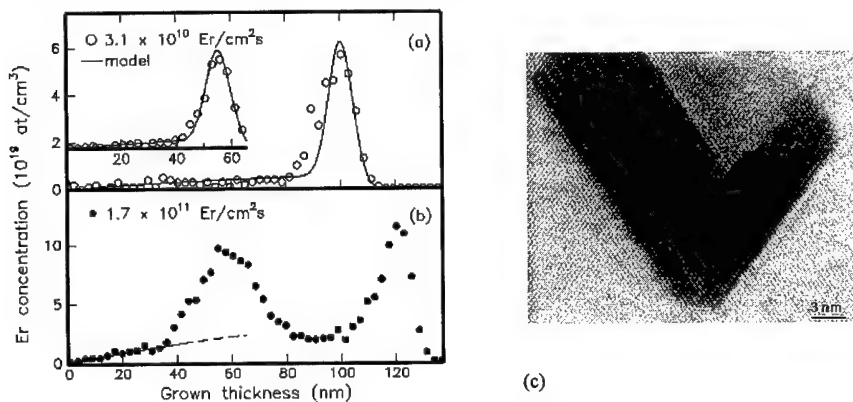


Fig. 3 Er concentration as a function of thickness for MBE grown films on Si(100) at 600 °C. The Er flux was  $3.1 \times 10^{10}$  Er/cm<sup>2</sup>s (a), or  $1.7 \times 10^{11}$  Er/cm<sup>2</sup>s (b). The data for the thin sample in (a) are offset vertically to facilitate comparison. The full lines are calculated profiles according to a kinetic two-dimensional growth model discussed in the text. (c) High resolution cross-section TEM image of the sample in Fig. 3(b), taken at a depth of 60 nm. The MBE growth direction is from bottom to top.

## RESULTS AND DISCUSSION: MBE

Figure 3(a) shows an Er depth profile in a 100 nm thick film grown by MBE at 600 °C at a rate of  $3.1 \times 10^{10}$  Er/cm<sup>2</sup>s. The channeling minimum yield in the Si part of the spectrum is  $\chi_{\min} < 3\%$ , indicating that good epitaxy is achieved. A clear Er surface segregation peak is observed, which accounts for more than 78 % of the total amount of deposited Er. The profile shows a monotonic increase of the Er bulk concentration from the substrate interface towards the surface, up to  $4 \times 10^{18}$  Er/cm<sup>3</sup>. A profile for a 60 nm thick film, grown under the same conditions, is also shown in Fig. 3(a), and shows a similar trend, but with a lower Er density at the surface.

The Er profiles can be well described by a kinetic two-dimensional growth and surface segregation model.<sup>9</sup> Assuming no desorption takes place, the Er bulk concentration  $N_b$  as a function of distance  $z$  from the Si substrate interface may be described by:

$$N_b(z) = F_d / v_g [1 - \exp(-\alpha z / h)],$$

with  $F_d$  the dopant flux,  $v_g$  the growth rate,  $h$  the surface step height, and  $\alpha$  the Er incorporation probability for each growing monolayer. In Fig. 3(a), a calculation

performed with this model is overlaid for the two data sets. The data are convoluted with a depth resolution of 8 nm. Good agreement with the data is obtained in both cases for an incorporation probability  $\alpha=1.5 \times 10^{-3}$ .

Figure 3(b) shows the Er profile for a sample grown at a higher Er flux:  $1.7 \times 10^{11}$  Er/cm<sup>2</sup>s. The same model as described above fits the data, with the same value for  $\alpha$  (drawn line in Fig. 3(b)), until a sharp increase in the bulk concentration takes place at a thickness of around 40 nm. At this point the Er concentration suddenly increases from  $2 \times 10^{19}$  to  $1 \times 10^{20}$  Er/cm<sup>2</sup>. After this maximum, the Er concentration decreases again and finally an Er peak is observed at the surface. Good channeling is observed for the whole film, with  $\chi_{\min}=3\%$ . Fig. 3(c) shows a high resolution cross section TEM image of this sample, taken at a depth of 60 nm, which shows a defect, aligned with (111) planes in the crystal. It is most likely that this is an erbium precipitate as it is known that Er<sub>3</sub>Si<sub>5</sub>(0001) is

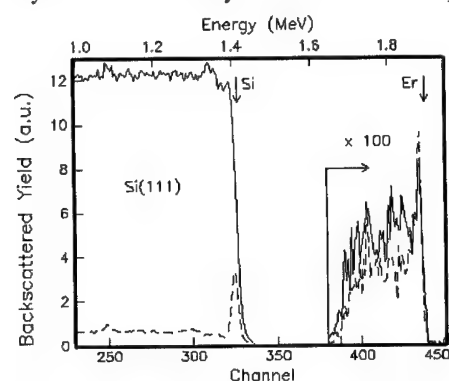


Fig. 4 RBS random (solid line) and channeling (dashed line) spectra for an MBE film grown on Si(111). The Er flux was  $3.1 \times 10^{10}$  Er/cm<sup>2</sup>s. Channeling was performed in the [111] direction. The Er signal is multiplied by a factor 100. The arrows indicate surface channels for Si and Er.

epitaxial on Si(111) with a lattice mismatch of only 1.22 %.<sup>10</sup> Similar precipitates have been observed in other Si-Er MBE experiments, although their origin remained unexplained.<sup>11,12</sup> Precipitation results in incorporation of a large fraction of the segregated Er in the crystal. Upon further growth, the segregation continues, but with a reduced Er surface density and hence lower trapped Er concentration. The data in Fig. 3 indicate that the precipitation phenomena have a kinetic rather than a pure thermodynamic origin. Figure 3(b) shows that the maximum Er concentration that can be incorporated by MBE without precipitation at 600 °C is  $2 \times 10^{19}$  Er/cm<sup>2</sup>. The corresponding areal density (calculated from the model as described above) is  $2 \times 10^{14}$  Er/cm<sup>2</sup>, i.e. a surface coverage of about 30 %. Such a high surface coverage is never reached for the low flux samples (Fig. 3(a)), explaining the continuous growth observed in that case.

Figure 4 shows RBS spectra taken in random and channeling geometries for an MBE film grown on Si(111) under the same conditions as the films on Si(100) in Fig. 3(a). The channeling minimum yield in the [111] direction shows good epitaxial quality ( $\chi_{\min}<3\%$ ). Almost no Er segregation has occurred. The Er yield in the channeling spectrum is 29 % lower than the random yield, indicating that a large fraction of Er atoms is located on ordered positions relative to the [111] direction. This behavior on Si(111) is consistent with the formation of epitaxial silicide precipitates on the surface during growth.

## COMPARISON BETWEEN SPE AND MBE

There are many analogies, as well as characteristic differences between the SPE and MBE experiments. First of all, segregation and trapping is observed during growth at 600 °C for

both the amorphous-crystal and the crystal-vacuum interface. The thermodynamic reason for the segregation lies in the low equilibrium solubility for Er in crystal Si. During SPE, significant trapping in the crystal is observed only when a threshold density in the segregation spike at the interface is exceeded. This is attributed to the presence of defects in the a-Si network, which can act as traps for Er up to a certain concentration. In contrast, continuous trapping in the crystal is observed during MBE, which can be described by a kinetic two-dimensional growth and surface segregation model.

The Er incorporation probability during SPE above the threshold of  $6 \times 10^{13}$  Er/cm<sup>2</sup> (see Fig. 2) is roughly  $10^{19}$  trapped Er/cm<sup>3</sup> per  $10^{14}$  Er/cm<sup>2</sup> in the segregation spike. From the model fit in Fig. 3 we derive for the MBE case an identical incorporation probability:  $10^{19}$  trapped Er/cm<sup>3</sup> per  $10^{14}$  Er/cm<sup>2</sup> floating at the surface. This numerical equality must be purely coincidental since both the thermodynamic and kinetic factors describing the segregation and trapping are quite different for the SPE and MBE cases.

The maximum Er density that can be incorporated during MBE in steady state conditions is around  $2 \times 10^{19}$  Er/cm<sup>3</sup>, corresponding to a surface density of  $2 \times 10^{14}$  Er/cm<sup>2</sup>. The SPE experiments in Fig. 1(b) indicate that up to  $1.0 \times 10^{20}$  Er/cm<sup>3</sup> can be trapped in single crystal Si at 600 °C. Additional experiments,<sup>13</sup> have indicated that above a critical limit of  $1.2 \times 10^{20}$  Er/cm<sup>3</sup> trapped in the crystal (or  $1.2 \times 10^{15}$  Er/cm<sup>2</sup> in the segregation spike), epitaxy breaks down and crystal twins are formed. Comparing MBE and SPE, six times more Er can be incorporated in c-Si by SPE than by MBE at 600 °C. The difference may be due to the larger interfacial Er density that can be stored at the a-Si/c-Si interface before precipitation takes place, compared to that for the c-Si/vacuum interface.

Finally, we note that segregation can be fully avoided, both during SPE and MBE, by using oxygen co-doping. This has been observed for SPE of Er-implanted layers,<sup>4,14</sup> co-implanted with oxygen to a concentration of typically  $10^{20}$  O/cm<sup>3</sup>, as well as for MBE films grown in an oxygen ambient pressure of only  $10^{-10}$  mbar.<sup>15,16</sup> An additional advantage is that oxygen also serves to increase to 1.53  $\mu$ m photoluminescence intensity of Er<sup>3+</sup>.

## CONCLUSION

In conclusion, we have studied the incorporation of Er during SPE of Er-implanted amorphous Si on crystalline Si and during Si MBE. On Si(100), segregation and trapping of Er is observed, both during SPE and MBE. During SPE, nearly full segregation is observed for Er segregation spike densities below  $6 \times 10^{13}$  cm<sup>-2</sup>. Above this threshold, trapping occurs at a rate proportional to the Er density in the segregation spike. The discontinuous behavior is attributed to the effect of defects in the amorphous Si near the interface that can act as traps for Er. The segregation behavior during MBE is described by a continuous kinetic growth model. For high Er fluxes, as the Er surface coverage exceeds  $2 \times 10^{14}$  cm<sup>-2</sup>, MBE Er incorporation breaks down. This is attributed to the formation of silicide precipitates at high Er surface coverages. Data for MBE on Si(111) show no segregation, consistent with the formation of epitaxial silicide precipitates during growth.

## Acknowledgments

René Koper and Henny Zandbergen are gratefully acknowledged for TEM sample preparation and TEM analysis, respectively. This work is part of the research program of FOM, and was made possible by financial support from NWO, IOP-EO and STW. R.S. acknowledges financial support from CSIC, Spain.

## References

- 1 see e.g. Rare Earth Doped Semiconductors, edited by G.S. Pomrenke, P.B. Klein, and D.W. Langer (Mater. Res. Soc. Proc. **301**, Pittsburgh, PA, 1993), and this Proceedings.
- 2 F.A. Trumbore, Bell. Syst. Techn. J. **39**, 205 (1960).
- 3 Y.H. Xie, E.A. Fitzgerald, and Y.J. Mii, J. Appl. Phys. **70**, 3223 (1991).
- 4 J.S. Custer, A. Polman, and H.M. van Pinxteren, J. Appl. Phys. **75**, 2809 (1994).
- 5 A. Polman, J.S. Custer, P.M. Zagwijn, A.M. Molenbroek, and P.F.A. Alkemade, submitted to J. Appl. Phys.
- 6 S. Roorda *et al.*, Phys. Rev. B **44**, 3702 (1991).
- 7 A. Polman *et al.*, Appl. Phys. Lett. **57**, 1230 (1990).
- 8 S. Coffa, J.M. Poate, D.C. Jacobson, and A. Polman, Appl. Phys. Lett. **58**, 2916 (1991).
- 9 S. Andrieu, F. Arnaud d'Avitaya, and J.J. Pfister, J. Appl. Phys. **65**, 2687 (1989).
- 10 J.A. Knapp, and S.T. Picraux, Appl. Phys. Lett. **48**, 466 (1986).
- 11 H. Efeoglu *et al.*, Mater. Res. Soc. Proc. **220**, 367 (1991).
- 12 K. Miyashita, Y. Shiraki, D.C. Houghton, and S. Fukatsu, Appl. Phys. Lett. **67**, 235 (1995).
- 13 A. Polman, J.S. Custer, E. Snoeks, and G.N. van den Hoven, Appl. Phys. Lett. **62**, 507 (1993).
- 14 S. Coffa, F. Priolo, G. Franzò, V. Bellani, A. Carnera, and C. Spinella, Phys. Rev. B **48**, 11782 (1993).
- 15 R. Serna, M. Lohmeier, P.M. Zagwijn, E. Vlieg, and A. Polman, Appl. Phys. Lett. **66**, 1385 (1995).
- 16 M. Matsuoka, and S. Tohno, J. Appl. Phys. **78**, 2751 (1995).

## SELF ORGANIZED GROWTH IN THULIUM DOPED GaAs USING MBE

M.R. BENNETT\*, K.E. SINGER\*, A.C. WRIGHT\*\* AND Z.H. JAFRI\*\*\*

\*Centre for Electronic Materials, UMIST, PO Box 88, Manchester, M60 1QD, UK, [bennett@fs4.ee.umist.ac.uk](mailto:bennett@fs4.ee.umist.ac.uk).

\*\*Advanced Materials Laboratory, NEWI, Deeside, UK.

\*\*\*Department of Electronic and Electrical Engineering, University of Surrey, Surrey, UK.

### ABSTRACT

The growth of epitaxial GaAs doped with the rare earth thulium (Tm) by MBE is reported for the first time. The nature of the incorporation of Tm has been studied using SIMS, RBS, TEM, PL and DCXRD. Sharp doping profiles have been observed by SIMS from samples doped in a staircase structure. Under standard GaAs growth conditions, TEM has revealed a solubility limit of  $\sim 5 \times 10^{19} \text{cm}^{-3}$ , above which Tm precipitates as spherical nano-particles of uniform size (1.3-1.7nm). High resolution TEM has provided no evidence for strain relaxation around these precipitates. Growth at higher substrate temperatures ( $\geq 620^\circ\text{C}$ ) or at As:Ga ratios close to stoichiometry, results in the formation of precipitate wires and/or bifurcated structures ("quantum trees") aligned approximately in the direction of growth. Such behaviour is in common with that of Er in GaAs and suggests that the precipitates result from the self-organised growth of TmAs. Mechanisms for the formation of the quantum wires and trees are suggested. Initial photoluminescence spectra from these samples show two groups of narrow  $\text{Tm}^{3+}$  intra 4f transition lines corresponding to the  $^3\text{H}_5 - ^3\text{H}_6$  ( $\sim 1.01\text{eV}/1.2\mu\text{m}$ ) and  $^3\text{H}_4 - ^3\text{H}_6$  ( $\sim 0.71\text{eV}/1.7\mu\text{m}$ ) transitions. The spectra exhibit an excellent correlation with those obtained from samples grown by MOVPE and also those implanted with Tm by other groups.

### INTRODUCTION

The incorporation of the rare earth erbium in molecular beam epitaxy grown GaAs has already been studied in depth by this group[1,2] amongst others. Under normal GaAs growth conditions a solubility limit of  $8 \times 10^{17} \text{cm}^{-3}$  has been determined, above which the Er forms spherical nano-particles of cubic ErAs of a uniform size which appears to be self limited by the surface migration of erbium during MBE growth. Altering the growth conditions (III-V ratio, growth temperature) allows tailoring of the size of the precipitates and, under certain conditions, wires and even bifurcated structures ("quantum trees") have been obtained. The properties (electrical, optical and magnetic) of these structures have been assessed and a number of interesting phenomena have been observed including magnetoconductance fluctuations[3].

Carrying on from this work, the incorporation of the rare earth thulium (Tm) has been compared with that of Er. TmAs also has a cubic (rock salt) structure, but has a smaller lattice mismatch with respect to GaAs than does ErAs (+1.03% c.f. +1.40%). Another interesting difference lies in the electronic structures of the bulk arsenides. Bulk ErAs is semi-metallic, but quantum size effects for the dimensions of the precipitates studied are predicted to open up a small band gap [4] - although there is no experimental evidence thus far. There is (inconclusive) evidence, however, that bulk TmAs is semiconducting [5] and so the confined TmAs precipitates may exhibit very different electrical and optical properties from those of ErAs. Tm doping of GaAs has not previously been attempted by MBE; although ion implantation and MOVPE doping studies have been reported [6,7].

The incorporation of Tm into MBE grown GaAs has therefore been studied in depth. Several ladder like structures (Tm doped layers interspersed by undoped regions) have been

grown to study first the degree of incorporation of Tm; and second the effect of various growth parameters (growth temperature and As:Ga ratio) on that incorporation. These layers have been assessed using SIMS, RBS, PL and TEM. The results of this investigation appear to indicate that Tm also has a solubility limit in GaAs, above which it is seen to self-organise into TmAs precipitates whose size and shape are again self-limited by the surface migration of Tm during growth. The mechanisms responsible for the growth habits of these precipitates are discussed, as are the implications of the formation of these nano-structures on the electrical and optical properties of Tm doped GaAs.

## EXPERIMENTAL

The layers were grown in a Riber 2300 MBE system. Elemental Ga and As ( $\text{As}_4$ ) sources were used for the matrix elements. A small quantity of Tm sublimate with an estimated purity of ~99.95% was obtained from Ames Laboratory. All layers were grown on nominally on-axis (100) semi-insulating GaAs substrates. Growth rates and constituent fluxes were measured using RHEED oscillations. Sample temperature was measured using an Ircon Modline Series V infrared pyrometer. Secondary ion mass spectrometry (SIMS) was used to calibrate the Tm flux; the SIMS was in turn calibrated using Rutherford backscattering spectroscopy (RBS). Transmission electron microscopy (TEM) was performed using a Philips EM340T electron microscope at 300kV. Details of the techniques used are given elsewhere [8,9]. The photoluminescence (PL) spectra included here were obtained at King's College, London, using a 514nm  $\text{Ar}^+$  laser operating at 400mW. The sample was cooled to 4.2K by immersion in a liquid He bath cryostat. Spectra were obtained using a Nicolet 60SX FTIR spectrometer modified for PL measurements and i) a North Coast Optical liquid nitrogen cooled Ge diode detector to cover the range 0.68-1.18eV; and ii) a Cincinatti Electronics LN2 cooled InSb diode detector to cover the range 0.37-1.11eV. Resolution was of the order of 60-120 $\mu\text{eV}$  (0.5-1.0 $\text{cm}^{-1}$ ).

## RESULTS

The first Tm doped layer grown was a concentration stepped calibration layer (2173) ( $T_g=580^\circ\text{C}$ , As:Ga ~ 3.5 {monolayer growth rate ratio}, Growth Rate ~  $1\mu\text{mhr}^{-1}$ ). A SIMS profile of this layer displayed a sharp dopant profile (Figure 1a) with little evidence of diffusion into the undoped spacer layers, nor for any surface segregation of Tm. RBS analysis of this layer at Surrey University showed a distinct edge from the topmost (highest Tm concentration) layer and thus an estimate of this concentration could be made ( $\sim 1.3 \times 10^{21}\text{cm}^{-3}$ ) against which to calibrate the SIMS data. The relationship between the Tm doping levels and the cell temperature followed an Arrhenius plot up until  $\sim 5 \times 10^{20}\text{cm}^{-3}$ , after which a degree of saturation was seen (Figure 1b), perhaps due to re-evaporation of excess Tm prior to incorporation.

Cross sectional TEM micrographs of this sample revealed the presence of a high density of precipitates in each of the Tm doped layers (Figure 2a). An analysis of the contrast of these precipitates in dark field mode with respect to the GaAs matrix and a comparison with similar micrographs of ErAs precipitates in GaAs [1,2] lead to the conclusion that these precipitates were composed of TmAs in a cubic rock-salt structure. Further TEM micrographs from a second sample (2199) grown with the Tm concentration stepped down from  $5 \times 10^{19}\text{cm}^{-3}$  to  $1 \times 10^{17}\text{cm}^{-3}$  displayed precipitates only in the topmost layer, leading to a figure for the solubility limit of Tm in GaAs of  $1.5 \times 10^{19}\text{cm}^{-3}$ , considerably higher than the equivalent limit for Er in GaAs of  $8 \times 10^{17}\text{cm}^{-3}$  [2]. High resolution micrographs showed that the mean precipitate diameter was of the order of 1.6nm with a uniformity of  $\pm 0.3\text{nm}$ , and also that the precipitates were coherent with the GaAs lattice.

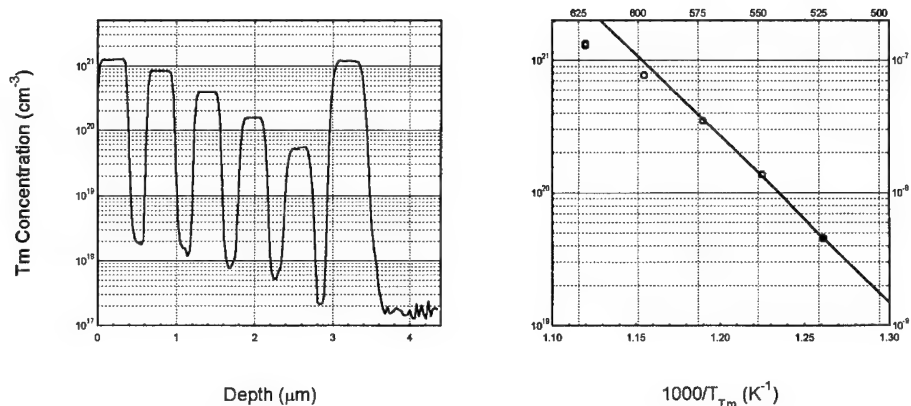


Figure 1 : a) SIMS profile of Tm doped GaAs ladder structure 2173; b) Arrhenius Plot of Tm concentration (peak integral) against reciprocal Tm cell temperature (The solid line represents the Tm vapour pressure curve [10]).

Having demonstrated the self-organised growth of TmAs nano-particles in a GaAs matrix, further Tm doped ladder structures were grown to assess the effect of growth parameters such as substrate temperature and As:Ga ratio on the growth habits of these nano-particles. Cross-sectional TEM micrographs of Tm doped ( $\sim 2 \times 10^{20} \text{ cm}^{-3}$ ) layers grown at various substrate temperatures within the same ladder structure (Sample 2209) showed spherical precipitates over the range 500-600°C. At temperatures above 600°C, however, the precipitates were shown to be elongated into wires oriented in the growth direction (Figure 2b). The precipitate size prior to the formation of wires appears to be controllable between 11 and 20 Å and showed an Arrhenius relationship with substrate temperature (Figure 3), with an estimated activation energy of 0.48 eV.

A further ladder structure (2211) contained five Tm doped layers (again, [Tm]  $\sim 2 \times 10^{20} \text{ cm}^{-3}$ ). For each layer, the As:Ga ratio (monolayer growth rate ratio) was fixed in the range 7.8:1 to 1.25:1 and the fluxes allowed to settle during growth of an un-doped region prior to opening the Tm cell. In common with the behaviour of ErAs precipitates in GaAs, only spherical precipitates were seen for As:Ga ratios of 2.3:1 and above. At ratios close to stoichiometry ( $\sim 1.25:1$ ), however, the precipitate shape changed dramatically to include not only wires aligned in the growth direction, but also multiply bifurcated structures christened 'quantum trees' when seen in Er doped GaAs [2] (Figure 2c and 2d). One interesting aspect of these trees, not investigated before for ErAs, is that they appear to be confined to a particular {110} plane rather than branching randomly in three dimensions as typically seen in dendritic structures. Figure 2c shows the plan view of TmAs quantum trees in a  $\langle 110 \rangle$  direction (yet to be defined), whilst figure 2d shows a similar area in an orthogonal  $\langle 110 \rangle$  direction and shows merely many parallel lines of precipitate material. Such preferential growth in this plane and the added possibility that in branching, the wires may be attempting to grow along specific (possibly  $\langle 111 \rangle$ ) directions, leads to the intriguing prospect of controlling the growth of these precipitates to form uniform wires or plates oriented in well-defined directions and hence greatly improving control of their electrical and/or magnetic properties. We will therefore be investigating this possibility further by growing on alternatively oriented substrates and by attempting to further control the growth by adjustment of growth parameters.



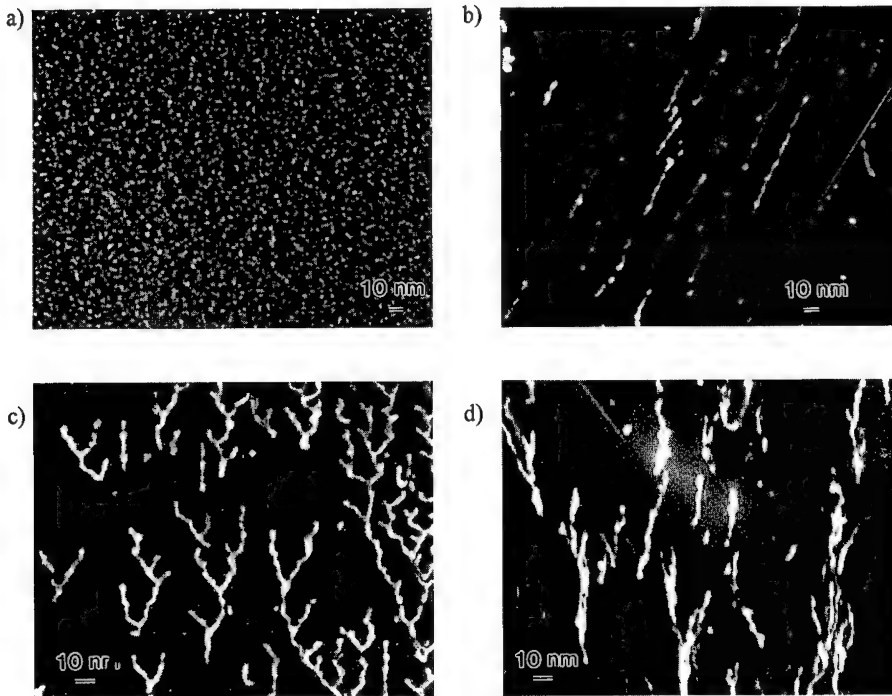


Figure 2 : TEM micrographs of TmAs precipitates in GaAs : a) Spherical precipitates ( $T_g=580^\circ\text{C}$ , As:Ga = 3.5, Growth Rate =  $1\mu\text{mhr}^{-1}$ ), b) TmAs wires oriented in the growth direction ( $T_g = 620^\circ\text{C}$ , As:Ga = 3.5, Growth Rate =  $1\mu\text{mhr}^{-1}$ ), c) TmAs 'quantum trees' (plan view along a  $\langle 110 \rangle$  direction), d) TmAs 'quantum trees' (side view along an orthogonal  $\langle 110 \rangle$  direction) (both :  $T_g=580^\circ\text{C}$ , As:Ga = 1.25, Growth Rate =  $1\mu\text{mhr}^{-1}$ ).

The model proposed to explain the growth habits of ErAs precipitates [1,2], can easily be extended to include TmAs in GaAs. The model states that growth of the precipitates is essentially self-limited by surface diffusion effects (RE arrival rate, RE surface diffusion coefficient, and the effect of Ga and As arrival rates and surface diffusion) rather than by any bulk diffusion. The arrhenius relationship between precipitate size and substrate temperature reflects the increased surface diffusion of Tm at the elevated temperatures, allowing migration over greater distances before arriving at a low energy (TmAs precipitate) site. This therefore means that larger precipitates can grow at higher temperatures before becoming buried under GaAs. It is believed that the calculated activation energy of 0.48eV reflects the activation energy for surface diffusion of Tm. At temperatures of  $620^\circ\text{C}$  and above, it is believed that surface diffusion of Tm is so rapid that the precipitates never actually become buried and so become contiguous through the epilayer.

The change in growth habit with decreasing As:Ga ratio also reflects changes in the surface diffusion of Tm, since very low As overpressures will result in greater Tm migration before becoming captured by As species and hence more opportunity to reach existing TmAs precipitates before becoming buried by GaAs. The reasons for the bifurcation of the wires are unclear at present, but may well be more related to the crystallographic variables discussed above rather than to any aspect of surface kinetics.

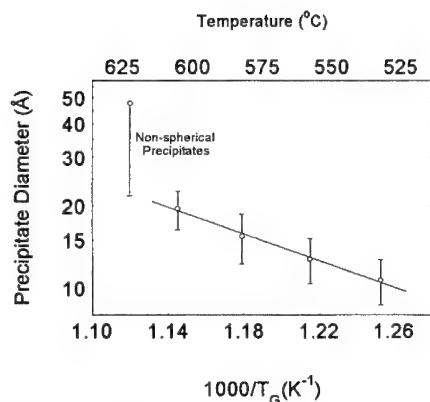


Figure 3 : Arrhenius plot of TmAs precipitate diameter vs. reciprocal substrate temperature in the range 525-600°C (2209).

suggest that the majority of the luminescence is derived primarily from those Tm atoms in solution in the GaAs matrix. Spectra from an epilayer of TmAs grown by MBE at UMIST displayed none of the intra 4f transition peaks. It is to be expected that Tm sited in a TmAs precipitate would give rise to a different set of crystal field split levels than would Tm in a GaAs matrix, but only a more detailed analysis of these spectra will define whether the Tm luminescence derives from either or both of these types of site.

Tm introduced into GaAs by other means (including MOVPE [7] and ion implantation [6]) has resulted in two sets of very sharp photoluminescence lines related to intra 4f transitions associated with the Tm<sup>3+</sup> ion. As can be seen from Figure 4, similar luminescence spectra are seen for samples doped with Tm by MBE. Although the fine structure of these spectra (including details of the many crystal field split peaks) has yet to be elucidated, it is clear that there is broad agreement with spectra obtained from samples doped by other means, particularly for the more often studied <sup>3</sup>H<sub>5</sub>-<sup>3</sup>H<sub>6</sub> transitions based around 1.01eV (1.2μm) (Fig 4b). The spectra shown were obtained from a sample (2199) containing both Tm in precipitate form and Tm in solution up to the solubility limit of 1-5x10<sup>19</sup>cm<sup>-3</sup>. There is evidence to

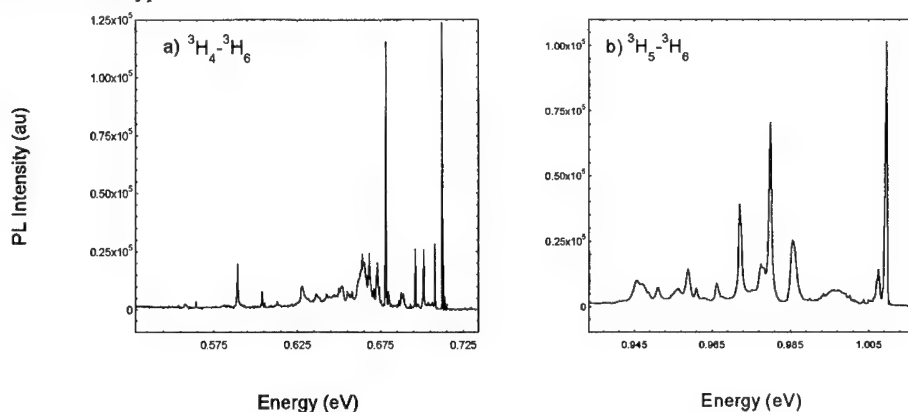


Figure 4 : Photoluminescence Spectra of Intra 4f Tm<sup>3+</sup> related transitions from Tm doped GaAs grown by MBE (Sample 2199) : a) <sup>3</sup>H<sub>4</sub>-<sup>3</sup>H<sub>6</sub> transitions (InSb detector), b) <sup>3</sup>H<sub>5</sub>-<sup>3</sup>H<sub>6</sub> transitions (Ge detector). Power Density ~1.4Wcm<sup>-2</sup> Temperature =4.2K).

The possibility of band edge emissions from the TmAs precipitates has also been investigated. No obvious candidates have as yet been seen, but variable temperature and variable power studies will be initiated to assess any changes in the intensities of the various peaks within the range of the two detectors used. Initial electrical studies (Hall measurements) of the thin (30Å) TmAs layer mentioned above (2216) appear to indicate that it is in fact semi-metallic. If the

TmAs precipitates too are semi-metallic then it is likely that they will tend to quench luminescence from Tm in solution, rather than contributing to it. Further studies of both the electrical and optical properties of TmAs nano-particles and thin films are required before the opening of a band gap due to quantum confinement can be ruled out, however.

## CONCLUSIONS

The epitaxial growth of Tm doped GaAs is reported for the first time. Sharp dopant profiles have been observed by SIMS over the range  $5 \times 10^{19}$  to  $1 \times 10^{21} \text{cm}^{-3}$ , but a degree of saturation was observed above  $5 \times 10^{20} \text{cm}^{-3}$ . Cross sectional TEM micrographs have revealed the presence of TmAs precipitates in all layers doped above a solubility limit of  $1.5 \times 10^{19} \text{cm}^{-3}$ . The size of these precipitates was further seen to be controllable in the range 11-20 Å by adjusting the growth temperature between 500 and 600°C. Growth at higher temperatures and also at As:Ga ratios close to unity leads to the formation of 'quantum wires' oriented approximately in the direction of growth. A high proportion of those wires grown at low As overpressures were seen to branch into 'quantum trees'. The branching took place only in a particular {110} plane, leading to the suggestion that the growth habits of TmAs wires could be controlled precisely by altering factors such as the substrate orientation and the As:Ga flux. It is believed that the growth of the TmAs nano-particles can be described in terms of the surface migration of the RE atom in the same manner as for ErAs in GaAs. PL spectra from MBE grown Tm doped layers show two groups of very sharp lines, related to transitions between the crystal field split levels of the 4f shell of  $\text{Tm}^{3+}$ . These spectra exhibit an excellent correlation with those from GaAs doped with Tm by MOVPE and by ion implantation. It is further believed that the majority of the luminescence seen emanates from Tm in solution in the GaAs, rather than from the TmAs nano-particles. Initial electrical characterisation of thin TmAs epilayers implies that it is semi-metallic and so would be expected to quench luminescence from the intra 4f transitions. No evidence has yet been seen for an optical band gap in the TmAs nano-particles.

## ACKNOWLEDGEMENTS

The authors would like to acknowledge Professor E. Lightowers and colleagues at Kings College London for obtaining the PL spectra and Alan Brown at MATS UK Ltd., Liverpool for performing the SIMS analysis.

## REFERENCES

1. A.R. Peaker, H. Efeoglu, J.M. Langer, A.C. Wright, I. Poole and K.E. Singer, *Mat. Res. Soc. Symp. Proc.*, **301**, 337-345, (1993).
2. K.E. Singer, P. Rutter, A.R. Peaker and A.C. Wright, *Appl. Phys. Lett.*, **64**(6), 707-709 (1994).
3. F. Coppinger, J. Genoe, D.K. Maude, U. Gennser, J.C. Portal, K.E. Singer, P. Rutter, T.Taskin, A.R. Peaker and A.C. Wright, *Phys. Rev. Lett.*, **75**(19), 3513-3516 (1995).
4. V.B. Sandomirskii, *Sov. Phys. JETP*, **25**(1), 101-106 (1967).
5. S.E.R. Hiscocks and J.B. Mullin, *J. Mater. Sci.*, **4**, 962 (1969).
6. G.S. Pomrenke, E. Silkowski, J.E. Colon, D.J. Topp, Y.K. Yeo and R.L. Hengehold, *J. Appl. Phys.*, **71**(4), 1919, (1992).
7. F. Scholz, J. Weber, D. Ottenwalder, K. Pressel, C. Hiller, A. Dornen, K. Locke, F. Cordeddu and D. Wiedmann, *J. Cryst. Growth*, **124**, 470-474 (1992).
8. I. Poole, K.E. Singer, A.R. Peaker and A.C. Wright, *J. Cryst. Growth*, **121**, 121 (1992).
9. J.O. Williams, A.C. Wright and H.M. Yates, *J. Cryst. Growth*, **117**, 441 (1992).
10. R.E. Honig, RCA Publication, Princeton, NJ (1962).

## PROPERTIES AND GROWTH OF MBE GROWN ERBIUM DOPED GALLIUM ARSENIDE CO-DOPED WITH SELENIUM

P. RUTTER \*, K.E. SINGER\*, A.R. PEAKER\*, AND A.C. WRIGHT\*\*

\*Centre for Electronic Materials and Electrical Engineering & Electronics Department, UMIST,  
Manchester, M60 1QD, UK

\*\*Advanced Materials Laboratory, North East Wales Institute, Connah's Quay, Wales, UK

### ABSTRACT

The growth of erbium doped GaAs by molecular beam epitaxy (MBE) can, depending on growth conditions, result in the precipitation of small spherical particles of erbium arsenide. It has been observed that by reducing the V:III (As:Ga) flux ratio to close to stoichiometry wire-like precipitates roughly aligned in the direction of growth are produced. The concentration of erbium incorporated into the GaAs lattice for a constant erbium flux is also affected by the As:Ga flux ratio with an increase in erbium doping being observed with decreasing As:Ga flux ratio.

Electrical measurements have been performed on erbium doped GaAs samples co-doped with selenium, an n-type dopant. Measurements have revealed that when erbium is present, the electron concentration is reduced by an amount approximately equal to 70% of the erbium concentration. DLTS measurements have shown that although large concentrations of deep levels are present in erbium doped material, the measured concentration of these deep levels is not high enough to account for the observed reduction in electron concentration with erbium doping.

### INTRODUCTION

Rare earth impurities in III-V semiconductor materials have attracted much attention with the aim of either producing optical emitters utilizing a  $4f$  transition of the rare earth atom [1], or growing rare earth pnictide/III-V semiconductor multilayers [2]. Erbium has been incorporated into GaAs using a wide variety of techniques such as ion implantation [3], diffusion [4], liquid phase epitaxy [5], metalorganic chemical vapour deposition (MOCVD) [6], and molecular beam epitaxy (MBE) [7]. The solubility limit of erbium in MBE grown GaAs is approximately  $7 \times 10^{17} \text{ cm}^{-3}$ . Above this concentration, near spherical, lattice matched precipitates of ErAs form. The diameter of these precipitates increases from 10 Å to 20 Å with increasing substrate temperature and, at a temperature of 630°C the precipitates become misshapen, roughly in the direction of growth [7]. This paper describes the effect of the As:Ga flux ratio on the incorporation of erbium into MBE grown GaAs. Transmission electron microscopy (TEM) has been employed to examine the structure of the ErAs precipitates whilst secondary ion mass spectrometry (SIMS) has been used to study the concentration of erbium incorporated into the GaAs lattice under various growth conditions.

Electrical measurements on erbium doped GaAs grown by MBE have shown that for erbium doping levels greater than the solubility limit, highly resistive material [8] with carrier lifetimes of the order of picoseconds [9] is produced. These properties have been employed to provide device isolation [10] and to produce high speed metal-semiconductor-metal

photodiodes [11]. In this work, the electrical properties of erbium doped GaAs have been examined by CV and DLTS measurements on n-type material (selenium doped) grown under varying growth conditions.

## EXPERIMENT

The GaAs samples examined in this work were grown in a Riber 2300 MBE system employing conventional thermal effusion cells. Elemental gallium, arsenic, and erbium sources, a Ga<sub>2</sub>Se<sub>3</sub> selenium source, and (100) orientated GaAs substrates were used. The As:Ga flux ratio was determined by measurement of the oscillations in the reflection high energy electron diffraction pattern with the growth temperature ( $T_{\text{sub}}$ ) being measured using an Ircon Modline Series V infra red pyrometer. SIMS was employed to provide compositional analysis of all dopants with two erbium ion implanted GaAs samples providing an erbium calibration of the MBE grown samples accurate to  $\pm 20\%$ . Samples for TEM were examined with a Philips EM430T electron microscope at 300kV. High contrast images of the precipitates were obtained in centred dark field using the {002} reflection. Capacitance-voltage measurements were performed on a HP 4192A LF impedance analyser and used to determine free carrier concentrations. DLTS measurements were performed on a Bio-Rad DL4600 DLTS system connected to a Boonton capacitance meter at temperatures between 14K and 450K.

## RESULTS AND DISCUSSION

### Effect of the As:Ga flux ratio on the growth of erbium doped GaAs

The effect of the As:Ga flux ratio on the formation of ErAs precipitates was investigated by the growth of a GaAs sample at a substrate temperature of 580°C with four 0.5µm thick erbium doped layers grown with As:Ga flux ratios of 7.0, 4.3, 2.3, and 1.3. The erbium flux was identical in each of these layers and chosen to achieve an erbium doping concentration of  $3 \times 10^{19} \text{cm}^{-3}$ . Each erbium doped layer was separated by 0.5µm of undoped GaAs during the growth of which the arsenic flux was changed to the desired value.

Analysis by TEM showed that for the layers grown with the three highest As:Ga flux ratios spherical precipitates of diameter 13Å and identical to those described previously [7] are produced. However, on reducing the flux ratio to 1.3, the growth mode changes dramatically to give wire like precipitates, of average diameter 27Å, and orientated approximately along the growth direction as shown in Figure 1. This phenomena has been explained in terms of the mobility of the surface erbium concentration [12]. Here, as the substrate temperature is increased, the distance erbium atoms can travel before being locked onto a lattice site by the overgrowth of the GaAs increases. If an existing precipitate is a low energy site, then precipitate size will increase with temperature as observed. At some point, the surface erbium will always be able to find an existing precipitate leading to wire like formations as precipitates thread through the growing GaAs layer. This has been observed at both high temperatures and at low As:Ga flux ratios. At a low As:Ga flux ratio the surface mobility of erbium will be effectively increased due to the reduction of excess arsenic on the GaAs surface. The growth of ErAs wires has proved to be reproducible for As:Ga fluxes close to unity and transport measurements on these wires have shown that this system possesses interesting magnetic properties [13].

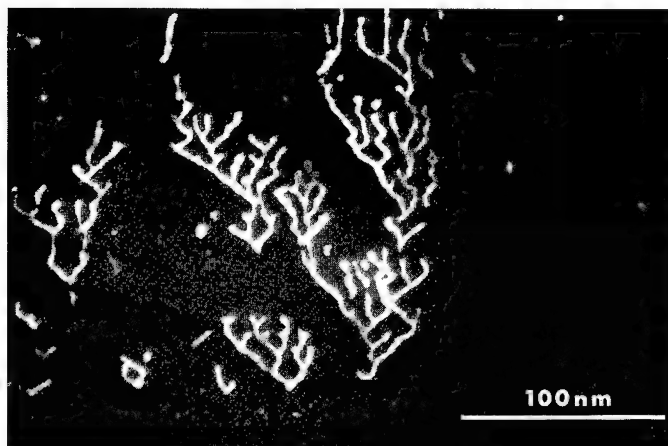


Figure 1: Dark field (002) image of precipitated ErAs wire like structures produced when the As:Ga flux ratio is reduced to close to stoichiometry.

Analysis of this sample by SIMS revealed that although the erbium flux was held constant during the growth of all of the erbium doped layers, the actual incorporated erbium concentration was dependent on the As:Ga flux ratio. An increase in erbium doping by 50% was observed for a decrease in As:Ga flux ratio from 7 to 1.3, see inset of Figure 2. This effect has been observed in a number of different samples for erbium concentrations covering four orders of magnitude, as can be seen in Figure 2. This effect also appears to be enhanced at lower substrate temperatures. It is not as yet clear what mechanism is responsible for this dependence of erbium incorporation with As:Ga flux ratio. This will either be due to increased incorporation at low As:Ga flux ratios (possibly due to an enhanced surface erbium mobility), and/or caused

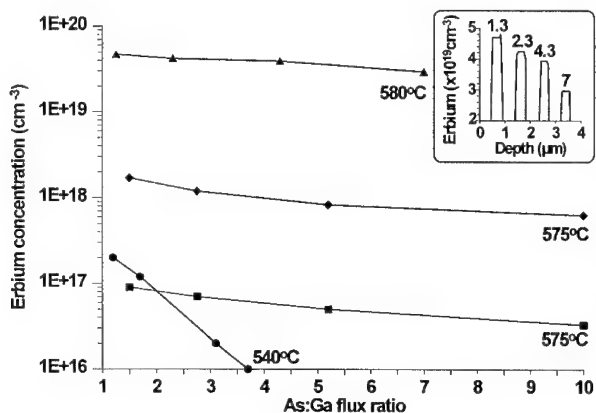


Figure 2: The variation of erbium incorporation with As:Ga flux ratio for a constant erbium flux. The inset shows the SIMS erbium profile for the sample used to provide this data, where the figures above each layer give the As:Ga ratio for that layer.

by increased erbium re-evaporation from the growth surface at high As:Ga flux ratios (possibly due to the production of a volatile Er-As related compound). These issues are discussed in greater depth elsewhere [14][15].

#### The electrical properties of erbium doped gallium arsenide co-doped with selenium

The effect of erbium doping on the electrical properties of GaAs is to reduce the free carrier concentration. This reduction in carrier concentration with erbium doping has been observed and measured in a number of n-type samples grown with varying growth temperature, As:Ga flux ratio, and erbium and selenium concentrations. The results of these measurements are displayed in Figure 3 where the degree of compensation has been quantified as the ratio of carriers removed from the system to the erbium concentration. This value will subsequently be referred to as the compensation ratio. The number of carriers removed from the system is the difference between the intended carrier concentration (determined by CV measurements in an erbium free region, or by the SIMS concentration of the dopant species) and the actual carrier concentration in the erbium doped region. The data in brackets corresponds to the As:Ga flux ratio of a sample followed by its growth temperature in °C. Note that a single p-type (beryllium doped) sample has been examined.

The mean value of compensation ratio for the samples shown in Figure 3 is approximately 0.7, with both n-type and p-type material having been compensated. Assuming that each compensating centre results in the loss of a single electron/hole, this corresponds to 70% of dopant erbium atoms forming compensating centres. This compares with a compensation ratio of unity measured in metalorganic chemical vapor deposition (MOCVD) grown GaAs doped with both silicon and erbium [16]. Although there is a wide spread in the value of compensation ratio for individual samples, there does not appear to be any systematic variation in the level of compensation due to changes in the As:Ga flux ratio for values between 1:1 and 5:1, or by increasing the growth temperature from 540°C to 580°C. The root cause of this compensation for MBE grown erbium doped GaAs has yet to be determined. Possible explanations include the gettering of dopants by the erbium atoms at the epitaxial layer surface during growth (thus preventing them from becoming donors or acceptors) and the production of compensating erbium related electronic states. This later possibility is explored in the following section.

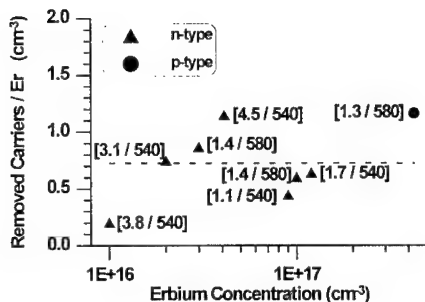


Figure 3: The degree of erbium compensation due to erbium doping in GaAs quantified by the ratio of carriers removed from the system to the erbium concentration. The data in brackets indicates the growth conditions under which each sample was grown, i.e. [As:Ga flux ratio / growth temperature °C].

### DLTS measurements

The DLTS spectra for two erbium doped n-type samples grown under similar conditions except for different substrate temperatures are shown in Figure 4. These spectra show a large increase in deep level concentration with erbium doping. These deep levels have been identified as the M traps, deep levels characteristic of MBE growth [14][17]. It can be seen that the concentration of the M7 level is drastically reduced for growth at the higher growth temperature. The total deep level concentrations of these samples are displayed in Table I, which also shows the concentration of removed majority carriers and the ratio of the deep level concentration to the removed carrier concentration. It can clearly be seen from this table that although high concentrations of deep levels are present in these samples, the measured concentrations of these levels do not exist in high enough concentrations to account for the degree of compensation observed. In the sample grown at 580°C for instance, the deep level concentration accounts for just 7.4% of the removed carrier concentration. These figures also presume that all of the deep levels are acceptors, this is not the case since capture cross-section measurements have shown that levels M1, M4, and M7 are highly likely to be donors, whilst M6 and M2' are probably acceptors[17]. These results do not discount the theory that electronic levels are the cause of the compensation but show that if electronic levels are responsible, then they must be shallow levels and hence invisible to the DLTS measurement.

Table I: The relationship between free carrier compensation and deep level concentration of two erbium doped n-type GaAs samples growth at different substrate temperatures.

Substrate Temperature (°C)	Removed Carrier Concentration (cm <sup>-3</sup> )	Total Deep Level Concentration (cm <sup>-3</sup> )	Deep Level Conc <sup>n</sup> / Removed Carrier Conc <sup>n</sup>
540	4x10 <sup>16</sup>	6.44x10 <sup>15</sup>	0.161
580	2.6x10 <sup>16</sup>	1.92x10 <sup>15</sup>	0.074

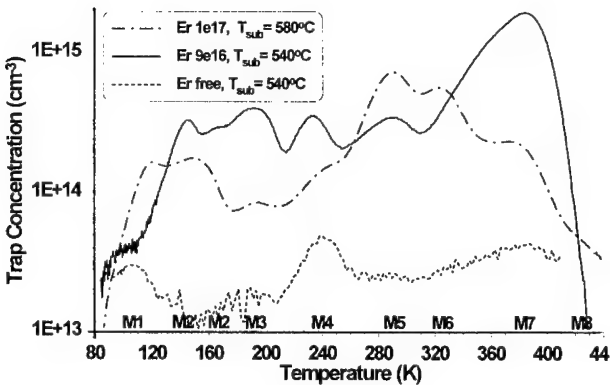


Figure 4: DLTS spectra for erbium doped GaAs taken with a rate window of 200<sup>s</sup>. There is a large increase in the deep level concentration associated with erbium doping. An increase in the growth temperature ( $T_{sub}$ ) has reduced the deep level concentration.



## CONCLUSIONS

The effect of the As:Ga flux ratio on the incorporation of erbium in GaAs grown by MBE has been investigated by a combination of SIMS and TEM measurements. TEM measurements have revealed that for As:Ga flux ratios close to unity, and for erbium doping concentrations above the solubility limit, the form of ErAs precipitates changes from being spherical to being wire-like. SIMS analysis has shown that the As:Ga flux ratio also affects erbium incorporation. Over a wide range of erbium doping concentrations, growth at lower As:Ga flux ratios increases the concentration of erbium incorporated into a sample for a constant erbium flux.

Electrical measurements have demonstrated that the doping of GaAs with erbium by MBE results in the compensation of majority carriers. This reduction in majority carrier concentration corresponds to approximately 70% of the erbium concentration. The possibility that this is due to compensating electronic levels has been investigated using DLTS where it has been shown that although large concentrations of deep levels exist in erbium doped GaAs, these cannot account for the degree of compensation observed.

## ACKNOWLEDGEMENTS

This work has been supported under the European Community ESPRIT Programme (SOLDES Project 7260). P.Rutter also acknowledges the financial support of the EPSRC.

## REFERENCES

1. Rare Earth Doped Semiconductors, edited by G.S.Pomrenke, P.B.Klein, and D.W.Langer (Mater. Res. Soc. Proc. 301., Pittsburgh PA, 1992).
2. C.J.Palmström, S.Mounier, T.G.Finstad, and P.F.Miceli, *Appl.Phys.Lett.* **56**, p. 382 (1990).
3. H.Ennen, J.Schneider, G.S.Pomrenke, and A.Axmann, *Appl.Phys.Lett.* **43**, p. 943 (1983).
4. X.Zhao, K.Hirakawa, and T.Ikoma, *Appl.Phys.Lett.* **54**, p. 712 (1989).
5. F.Bantien, E.Bauser, and J.Weber, *J.Appl.Phys.* **61**, p. 2,803 (1987).
6. K.Uwai, H.Nakagome, and K.Takahei, *J.Crystal Growth* **93**, p. 583 (1988).
7. I.Poole, K.E.Singer, and A.R.Peaker, *J.Crystal Growth* **121**, p. 121 (1992).
8. R.S.Smith, H.D.Müller, H.Ennen, P.Wennekers, and M.Maier, *Appl.Phys.Lett.* **50**, p. 49 (1987).
9. S.Gupta, S.Sethi, and P.K.Bhattacharya, *Appl.Phys.Lett.* **62**, p. 1,128 (1993).
10. H.-P.D.Yang, P.K.Bhattacharya, and Y.-C.Chen, *Electronics Letters* **30**, p. 598 (1994).
11. S.Sethi, T.Brock, P.K.Bhattacharya, J.Kim, S.Williamson, D.Craig, and J.Nees, *IEEE.Electron.Device.Lett.* **16**, p. 106 (1995).
12. K.E.Singer, P.Rutter, and A.R.Peaker, *Appl.Phys.Lett.* **64**, p. 707 (1994).
13. F.Copping, J.Genoe, D.K.Maude, U.Gennser, J.C.Portal, K.E.Singer, P.Rutter, T.Taskin, A.R.Peaker, and A.C.Wright, *Phys.Rev.Lett.* **75**, p. 3513 (1995).
14. P.Rutter, Ph.D.Thesis, University of Manchester Institute of Science and Technology (1995).
15. P.Rutter, K.E.Singer, and A.R.Peaker, *to be submitted to J.Cryst.Growth*.
16. J.M.Redwing, T.F.Kuech, D.C.Gordon, B.A.Vaartstra, and S.S.Lau, *J.Appl.Phys.* **76**, p. 1585 (1994).
17. P.Rutter, K.E.Singer, and A.R.Peaker, *to be submitted to J.Appl.Phys*.

## PROPERTIES OF ION IMPLANTED AND UHV-CVD GROWN Si:Er

M. MORSE, B. ZHENG, J. PALM, X. DUAN, L.C. KIMERLING

Materials Science and Engineering Department, Massachusetts Institute of Technology,  
Cambridge, MA 02139

### ABSTRACT

We have fabricated Si:Er films by ion implantation and ultra-high vacuum chemical vapor deposition (UHV-CVD). The energy of the ion implantation was varied from 200 keV to 4.5 MeV. Oxygen was co-implanted to overlap the erbium profile. At implant energies of 400 keV, we found that the luminescence was optimized at a lower annealing temperature (800° C, 30 minutes) than that needed for the 4.5 MeV implant (900° C, 30 minutes). The light intensity per erbium atom is critically dependent on the implantation energy. However, spreading resistance measurements show that the donor activity of the implanted erbium is independent of energy. We have correlated the donor activity with quantum efficiency by varying the donor spatial distribution and concentration through post implantation heat treatments.

For the UHV-CVD grown Si:Er films, two erbium metallorganic precursors, Er(TMHD)<sub>3</sub> and Er(FOD)<sub>3</sub>, have been used for growths from 550-620° C. The thickness of the erbium layers are similar to that of implanted devices but the Er concentration of  $4 \times 10^{21}/\text{cm}^3$  exceeded the implanted material by two orders of magnitude.

### INTRODUCTION

Erbium-doped silicon has held the promise for silicon based optoelectronics since the first report of Er luminescence in 1983[1]. However, temperature quenching of luminescence is limiting the output power of Er:Si light emitting diodes at room temperature well below that needed for commercial devices [2]. Current research is focusing on two solutions to the problem; improving the processing of erbium-doped single crystalline silicon, or introducing erbium into other types of materials compatible with Si processing. These materials include amorphous Si, oxygen rich poly-Si(SIPOS), Si nanocrystals, and silicon based alloys [3]. This paper will deal exclusively with the single crystalline Si.

There are several points that need to be addressed in any Er-doped single crystal processing. In order to have strong luminescence, large amounts of optically active Er must be incorporated into the silicon lattice. Xie [4] has estimated that  $10^{19}$  Er atoms/cm<sup>3</sup> are needed for device applications, which is approximately two orders of magnitude higher than the solubility limit. Ligands, which have been found to increase luminescence [5], also need to be incorporated around the erbium. This means that low thermal budget processes should be used to avoid precipitation and out diffusion of the ligands [6]. Damage caused by the introduction of the erbium complex must also be minimized to prevent non-radiative recombination pathways which reduce the pumping efficiency.

Several techniques have been used to incorporate Er into silicon [7-10], but ion implantation has, to date, received the most attention due to IC-processing compatibility. Early work employed high energy implantation (~4MeV) to achieve high doses of Er. Anneals at 900° C for 30 minutes after the implant maximized luminescence by healing the implantation damage. At longer times, however, ligand out-diffusion dominates, and the luminescence is reduced. We have examined lower energy implantation (400 keV) and UHV-CVD in an attempt to reduce or eliminate damage and suppress the erbium complex dissociation.

## EXPERIMENT

### Ion Implantation

A standard ion implanter at an energy of 200 keV with doubly charged Er<sup>+</sup> was used to make 400 keV erbium implants in Si (100) boron-doped substrates. Oxygen was co-implanted to overlap the peak concentration of the erbium. Processing studies were done to determine the optimum annealing schedule. Spreading resistance measurements, cross-sectional TEM, and secondary ion mass spectroscopy (SIMS) were used to characterize the material.

### UHV-CVD

A hot wall UHV-CVD system was used to grow Er-doped Si (Figure 1). The reactor chamber is pumped by a turbomolecular pump which has a base pressure of  $5 \times 10^{-9}$  Torr. Partial pressures of oxidizing species such as water and oxygen are roughly  $1 \times 10^{-10}$  Torr. The process gases used are silane ( $\text{SiH}_4$ ), 1% phosphine in  $\text{H}_2$ , 1% diborane in  $\text{H}_2$ , and  $\text{H}_2$  as a carrier for the erbium metallorganic source. Two erbium sources were examined in this study;  $\text{Er}(\text{TMHD})_3$  and  $\text{Er}(\text{FOD})_3$  (Figure 2). The  $\text{Er}(\text{FOD})_3$  was loaded into a vacuum tight bubbler located in a dedicated furnace which sat in the gas delivery system. Temperature could be controlled to within  $1^\circ$ . A mass flow controller regulated the amount of hydrogen that flowed through the bubbler. For growth runs using  $\text{Er}(\text{TMHD})_3$ , however, the powder was loaded directly into the chamber after initial growth of silicon. Coarse temperature regulation was maintained by the reactor's furnace as well as heating tapes.

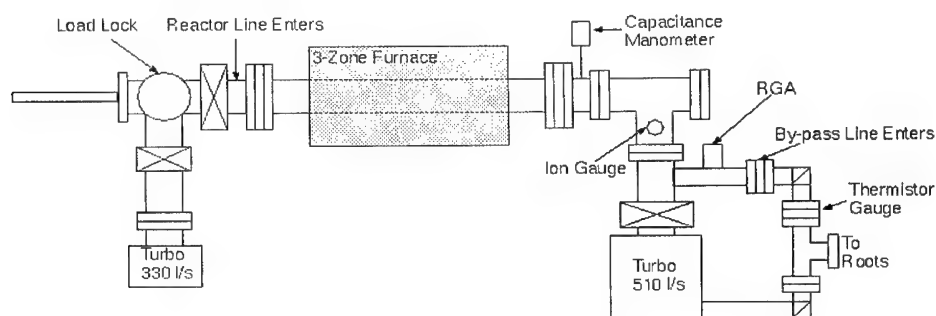


Figure 1. UHV-CVD reactor used in this experiment. The Er source either sits just inside the gate valve, or in the bubbler located in the gas manifold system.

All samples were 4 inch (100) wafers. Although the system can handle 20 wafers at a time, only 4-5 wafers were loaded per run. They were cleaned in a hot piranha solution for 10 minutes, then given an HF dip for 15 seconds before being transferred into the loadlock. Once the pressure had dropped to  $1 \times 10^{-6}$  Torr, the wafers were loaded into the reactor, where growth was initiated immediately. In all samples a doped buffer silicon film was grown prior to the Er-doped film. Some samples also had a complementary doped film was grown on the Er film to make a junction.

Growth temperatures were between 550 and 620° C, with run times varying from 30 minutes to 4 hours. SIMS and photoluminescence (PL) were used to characterize the films. The PL setup consisted of an Ar<sup>+</sup> laser, He cooled cryostat, spectrometer, and a liquid nitrogen cooled germanium detector. Standard lock-in techniques were used to improve the signal-to-noise ratio.

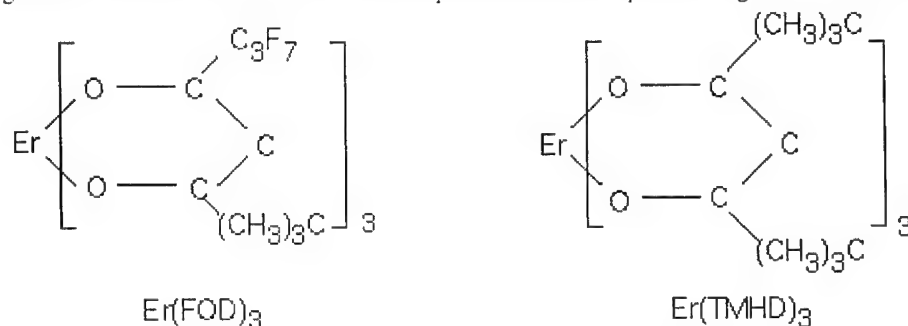


Figure 2. Structure of precursors used in this study. Each erbium is surrounded by 6 oxygen in the molecules. The Er(FOD)<sub>3</sub> can also contribute fluorine to the ligand field of erbium.

## RESULTS

Low energy implanted samples were annealed in an Ar ambient at 800, 900, and 1000° C for different times to determine the optimum PL. The best anneals were those done at 800° C for 30 minutes, which is lower in temperature than that required for the high energy implants. Cross-sectional TEM done after the anneal does not show any end-of-range secondary defect structure

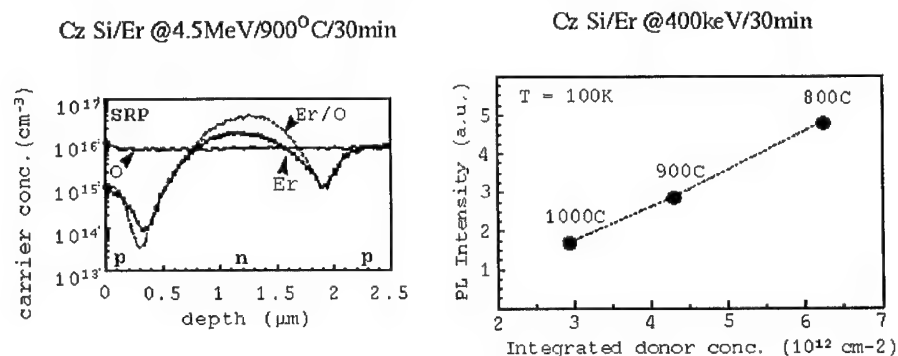


Figure 3. Spreading Resistance measurements of Er/O high energy implanted sample (left) show a maximum concentration near the projected range of the Er implant. This behavior is identical to low energy implants. By varying the annealing temperature, the donor distribution and PL intensity can be maximized.

prevalent after high energy implantation. The internal quantum efficiency was three times higher than the high energy implanted samples. Spreading resistance measurements, SIMS, and PL done on low energy implanted Er/O annealed at different temperatures strongly suggest that this could be due to the number of electrically active donors that are created and survive to the end of the process. Figure 3 shows typical results of spreading resistance of high energy implants (dose of  $3.8 \times 10^{13}/\text{cm}^2$ ) into a p-type Cz silicon wafer (low energy implantation profiles with a dose of  $3.5 \times 10^{12}/\text{cm}^2$  are identical). The carrier concentration was largest at the peak of the erbium implant in samples with both Er and O. Variations in annealing temperatures changed the spatial distribution and integrated concentration of the donors. A linear correlation between PL intensity and integrated donor dose (Figure 3) suggests that the luminescent Er centers are those which are in the electrically active Er/O donor state. This behavior is also seen in the 4.5 MeV samples as well. The maximum PL comes from the sample with the highest integrated donor density which was annealed at the lowest temperature.

Films grown by UHV-CVD were also examined by PL. Spectra of samples grown by both precursors are shown in Figure 4. The  $\text{Er(TMHD)}_3$  sample has a spectrum similar to some high dose Er/O implanted samples, with one major peak at  $1.537 \mu\text{m}$ . The  $\text{Er(FOD)}_3$  spectrum clearly looks different with a broad higher energy background and an additional sharp peak at  $1.54 \mu\text{m}$ . A broad background has also been seen in samples with high doses of fluorine in Er/F implants, suggesting the fluorine is the cause of the feature. A PL spectrum from a reference sample of  $\text{ErF}_3$  powder was compared with this PL but no match for the sharp peak at  $1.54 \mu\text{m}$  could be found. Further studies on these samples to determine the local environment are in progress.

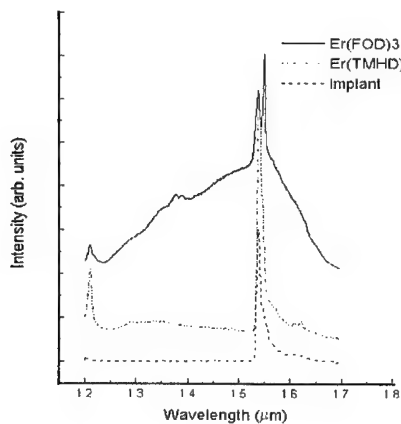


Figure 4. PL at 4 K with  $\text{Ar}^+$  laser (488nm).

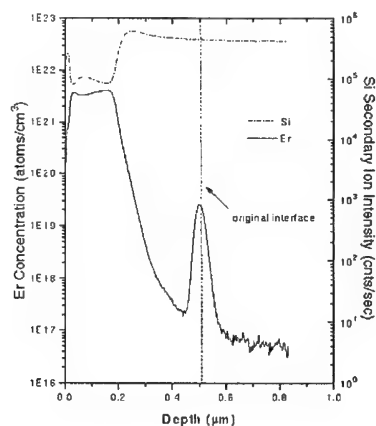


Figure 5. SIMS of Er:Si film doped with  $\text{Er(TMHD)}_3$

SIMS was done on  $\text{Er(TMHD)}_3$  samples to see how the molecule was being incorporated into the film. A representative sample is shown in Figure 5. The film has a concentration  $4 \times 10^{21} \text{ Er/cm}^3$  which is too high for good silicon film quality as the erbium adds strain to the lattice. This concentration is not unexpected as the control over Er flux in these samples was poor. Oxygen

was incorporated in such high concentrations ( $>15\%$ ) that no quantitative figure could be given. Carbon reached levels of  $10^{20}/\text{cm}^3$  as well, which has previously been a problem in a similar system [9]. This clearly shows that the precursor flux was too high. Erbium concentrations nearly 100 times lower are desired to have higher crystalline perfection and lower 'impurity' levels from other molecule fragments. The SIMS also shows that contamination from previous runs using this method of delivery is a significant problem, as the original interface has nearly monolayer coverages of precursor fragments.

Due to the high oxygen content in the films, it was possible that Er was incorporated into  $\text{SiO}_2$  instead of Si. If that was the case then the PL would only be due to optical pumping of the erbium. We varied the pump frequency of the  $\text{Ar}^+$  laser and monitored the intensity of the  $1.537\ \mu\text{m}$  line, as seen in Figure 6. For convenience, PL of  $\text{Er}_2\text{O}_3$  powder is included to show optical pumping behavior. The two vertical lines in the figure mark higher excited levels in the Er manifold which can be directly pumped. Samples grown from the two precursors do not show a response indicating optical pumping, meaning that photogenerated carriers must play a role in the excitation of the erbium.

A comparison of external quantum efficiencies was made among the high and low energy implants, as well as the CVD grown material. All samples were measured at 4 K at a power in which the material was in the linear regime. After normalizing for different pump powers and filters, and integrating the PL features due to Er, relative external quantum efficiencies were made. The UHV-CVD material doped with  $\text{Er}(\text{TMHD})_3$  was normalized to one. Under these conditions, the high energy implanted material was 35 times more efficient than the CVD material and twice as efficient as low energy implanted material. It must be re-emphasized that low energy implants had a higher quantum efficiency in electroluminescence at 100 K (not reported in this work). The low efficiency of the CVD material is not unexpected due to the quality of the initial films.

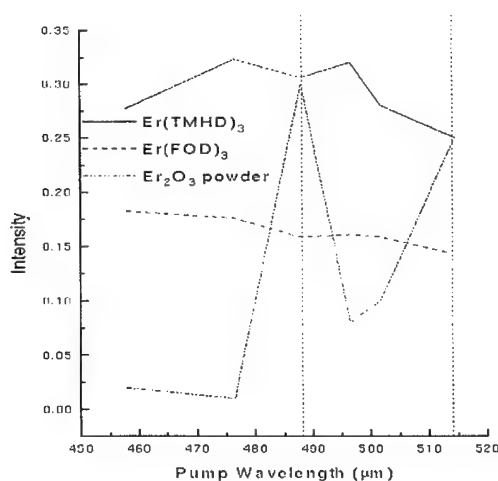


Figure 6. Intensity of  $1.537\ \mu\text{m}$  line as a function of excitation pump wavelength.

## CONCLUSIONS

Low energy ion implantation has improved the crystalline quality of Er-doped silicon. This allows for lower annealing temperatures for lattice recovery and a more stable ligand environment for the Er. A corresponding increase in the quantum efficiency has been correlated to the integrated donor concentration of Er/O states. Even lower processing temperatures have been used in UHV-CVD to further stabilize the Er/ligand complex since no damage is created which needs high temperature recovery. Initial Er-doped films have shown strong luminescence but the incorporation rate has not been controlled enough for high crystal quality. Relative external quantum efficiencies of CVD grown films are about an order of magnitude below that of implanted material, but it is expected to increase once the Er concentration is reduced.

## ACKNOWLEDGEMENTS

The authors would like to acknowledge support from the AFOSR, DARPA and collaboration with Implant Sciences Corporation.

## REFERENCES

1. H. Ennen, J. Schneider, G. Pomrenke, A. Axmann, Appl. Phys. Lett. **43**, 943 (1983).
2. B. Zheng, J. Michel, F. Ren, L.C. Kimerling, D.C. Jacobson, J.M. Poate, Appl. Phys. Lett., **64**, 2842 (1994).
3. References for these materials are throughout this proceeding.
4. Y.-H. Xie, E. Fitzgerald, Y.J. Mii, J. Appl. Phys. **70**, 3223 (1991).
5. J. Michel, J.L. Benton, R. Ferrante, D.C. Jacobson, D.J. Eaglesham, E.A. Fitzgerald, Y.-H. Xie, J.M. Poate, L.C. Kimerling, J. Appl. Phys. **70**, 2672 (1991).
6. F. Ren, Ph.D. Thesis, MIT (1994).
7. A. Polman, J.S. Custer, E. Snoeks, G.N. van den Hoven, Appl. Phys. Lett. **62**, 509 (1993).
8. P. Wetzel, L. Haderbache, C. Pirri, C.J. Peruchetti, D. Bolmont, G. Gewinner, Phys. Rev. B **43**, 6620 (1991).
9. D.B. Beach, R.T. Collins, F.K. Legoues, J.O. Chu, MRS Symposium Proceedings **282**, 397 (1992).
10. J.L. Rogers, P.S. Andry, W.J. Varhue, E. Adams, M. Lavoie, P.B. Klein, J. Appl. Phys. **78**, 6241 (1995).

## Er-DOPING OF GaN AND RELATED ALLOYS

S. J. Pearton<sup>1</sup>, C. R. Abernathy<sup>1</sup>, J. D. MacKenzie<sup>1</sup>, R. N. Schwartz<sup>2</sup>, R. G. Wilson<sup>2</sup>,  
J. M. Zavada<sup>3</sup> and R. J. Shul<sup>4</sup>

<sup>1</sup>University of Florida, Gainesville FL 3211;

<sup>2</sup>Hughes Research Laboratories, Malibu, CA 90265

<sup>3</sup>US Army Research Laboratory, RTP, NC 27709

<sup>4</sup>Sandia National Laboratories, Albuquerque NM 87185

### ABSTRACT

Er incorporation into GaN, AlN, InAlN and InGaN can be achieved using either direct ion implantation or by doping during Metal Organic Molecular Beam Epitaxy using metalorganic or elemental sources. When co-implanted with O and annealed between 600-800°C, strong luminescence at 1.54μm from optically excited Er<sup>3+</sup> is detected in both binary nitrides and there was no measurable diffusion of Er in any of the materials. The low vapor pressures of the gaseous source compounds (erbium 2, 2, 2, 6-tetramethyl-3, 5-heptanedionate for Er + O; erbium bistrimethylsilylamide for Er) makes transport difficult unless high bubbler temperatures are used. Er concentrations up to  $\sim 3 \times 10^{21} \text{ cm}^{-3}$  in AlN have been obtained using a solid Er source. Microdisk laser structures with Er-doped active layers have been fabricated using a novel KOH selective wet etch and Cl<sub>2</sub>/CH<sub>4</sub>/H<sub>2</sub>/Ar dry etching.

### INTRODUCTION

Optical communication systems depend on use of glass fibers as dielectric waveguides. A key element in these systems is the Er-doped fiber amplifier, which enables telecommunication signals at 1.54μm to be amplified in the optical domain without the need for repeater stations where the signal has to be converted to an electrical signal, amplified and then optically regenerated.[1-3] InGaAsP/InP semiconductor lasers with an emission wavelength at 1.54μm are employed as light sources, because this corresponds to a low loss transmission window in silica-based optical fibers.[4] However the lasing wavelength of these lasers is strongly temperature dependent, and there has been much interest in use of Er-doping of materials for use as light sources, because the rare earth ion Er<sup>3+</sup> has a radiative 4f electron intrashell transition  $^4I_{13/2} \rightarrow ^4I_{15/2}$  at a wavelength of 1.54μm. Incorporation of Er into Si could potentially be used for optoelectronic integrated circuits and overcome the indirect gap of this material, eliminating the need for III-V photonics.[5-11] Room temperature electroluminescence has been reported for Er-implanted pn junction Si structures.[11,12] Figure 1 shows the energy level scheme for a free Er<sup>3+</sup> ion, and the splitting of the levels in a solid.[13] The screening of the partially filled 4f subshells by the outer closed 5s<sup>2</sup> and 5p<sup>6</sup> subshells produces sharp emission spectra approximately independent of the host material. Solid state lasers such as Nd<sup>3+</sup>: YAG are based on the 4f intra-subshell transitions of the Nd<sup>3+</sup> ions, and exhibit a very stable lasing wavelength and minimal temperature dependence. Er-doped silica fiber is employed for amplification in optical communication systems operating at 1.54μm, and Pr-doped fibers are under development for 1.3μm.[14]

In Si, EXAFS analysis have shown that Er is coordinated with 12 Si atoms in low oxygen content material, and with 6 O atoms in Czochralski (high oxygen content) Si [15]. It is also



found that oxygen produces a large reduction in the temperature quenching of the 1.54 $\mu\text{m}$  emission [9,16]. The Er introduces a donor state, with maximum density of  $\sim 5 \times 10^{16} \text{cm}^{-3}$ , with the photoluminescence intensity maximized at an Er concentration of  $\sim 4 \times 10^{17} \text{cm}^{-3}$  [16].

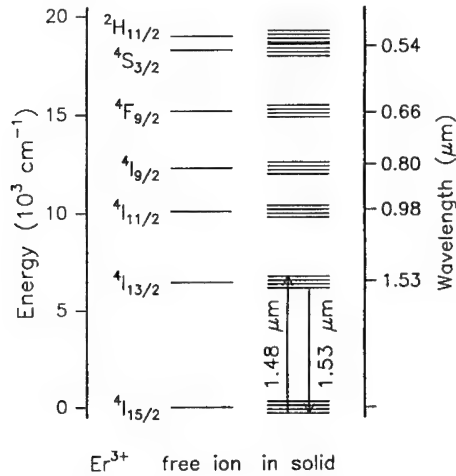


Figure 1. Energy level diagram for free  $\text{Er}^{3+}$  ion, or splitting due to Stark effect. Pump and signal wavelengths for an Er-doped amplifier are also shown [13].

In III-V semiconductors, Er has been incorporated by LPE, MBE, MOCVD, MOMBE, implantation and diffusion [4]. A few studies on lattice location have generally shown the Er to occupy a displaced tetrahedral interstitial site, with the luminescence intensity decreasing under conditions where the Er became substitutional [17,18]. The emission time decay constant is  $\sim 1 \text{ms}$ . [19] Favennec et al. [20] showed a strong dependence of the emission intensity of the  $\text{Er}^{3+}$  ions on the bandgap of the host semiconductor and on the material temperature. The emission intensity is quenched at higher temperatures for wider bandgaps, suggesting that III-V nitrides may be a good choice as a host material. Neuhalfen and Wessels [21] observed a similar temperature dependence of  $\text{Er}^{3+}$  emission for different composition  $\text{In}_x\text{Ga}_{1-x}\text{P}$  layers grown by MOCVD. Their model suggested that at elevated temperatures electrons became delocalized from the Er radiative recombination centers into the conduction band and recombine via non-radiative channels. In general optical emission in the semiconductors is not as efficient as in dielectric materials [4]. Evidence of enhancement of emission in GaP (Er) microcavity structures has recently been reported, [22] and several groups have obtained Er-emission in implanted and annealed GaN [23,24].

Epitaxial methods of Er incorporation overcome the limitation of depth associated with implantation, which typically can only produce incorporation depths of a few thousand angstroms. For gas-phase epi techniques one drawback is the low volatility of most Er sources, such as the Er cyclopentadienyl compounds [25]. Controlled Er-doping in the range  $10^{17}$ - $10^{18} \text{cm}^{-3}$  was obtained in GaAs using two new sources, (i-propylCp) $_2\text{CpEr}$  and (t-butylCp) $_3\text{Er}$  [25].

Apart from taking advantage of the wide gap of the nitrides, we would also like to consider it as a new thin film phosphor for full color self-emissive flat panel displays. For example, Maruska has reported an Er-implanted GaN film that exhibited red, green and blue

cathodoluminescence [26]. It is possible to conceive of insulating Er-doped nitride films as a replacement for ZnS in electroluminescence displays, whereas conducting films could displace ZnO in field emission displays. Figure 2 shows a typical nitride-based thin film electroluminescent display element [26]. Red emission would be achieved from Er doping and blue or green emission from InGaN or from other implanted species in GaN.

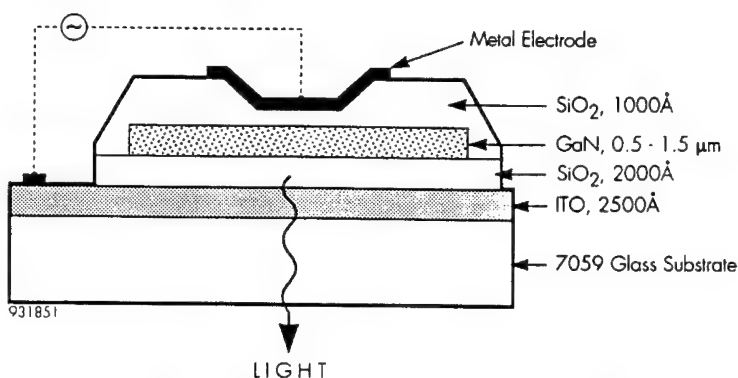


Figure 2. Schematic of GaN-based electroluminescent display element [25].

In this paper we review some of our work on growth of AlN(Er), GaN(Er) and related alloys by Metal Organic Molecular Beam Epitaxy (MOMBE). Er-concentrations up to  $3 \times 10^{21} \text{ cm}^{-3}$  have been achieved with solid Er source doping of AlN. We have concentrated on this material because of its large bandgap (6.2 eV compared to 3.4 eV for wurtzitic GaN).

## EXPERIMENTAL

The III-V nitride samples were grown by MOMBE on GaAs or  $\text{Al}_2\text{O}_3$  substrates, at typical growth temperatures of 700-900°C. The source chemicals were triethylgallium, dimethyl ethylamine alane and nitrogen from an ECR source operating at 2.45GHz [28]. Er was introduced in three different ways. In the first, metalorganic Er sources (Er 2,2,6,6-tetramethyl-3,5-heptanedionate and Er bistrimethyl silylamide) were transported by high purity  $\text{H}_2$ , but we did not achieve measurable Er incorporation. In the second method, a solid Er source was used to evaporate erbium into the growing film, as in MBE. In the third method, undoped films were implanted ex-situ with Er at typical doses of  $3 \times 10^{14} \text{ cm}^{-2}$  and an energy of 300keV, and annealed at 650-700°C. To achieve good luminescence efficiency it was found necessary to co-implant  $\text{O}^+$  ions at a similar dose to that of the Er. Emission spectra were obtained by pumping with an Ar<sup>+</sup> ion laser (458nm) and detecting with a Ge photodiode. Atomic concentrations were measured by Secondary Ion Mass Spectroscopy (SIMS), and calibrated by implant standards.

## RESULTS AND DISCUSSION

Figure 3 shows emission spectra from a GaN/ $\text{Al}_2\text{O}_3$  sample co-implanted with Er and O, as a function of measurement temperature. The spectra are centered at 1.54μm and display many of the allowed transitions between the  $^4\text{I}_{13/2}$  and the  $^4\text{I}_{15/2}$  manifolds typical of the  $\text{Er}^{3+}$  configuration. Since the laser excitation energy was below the GaN bandgap, the observed luminescence appears to be due to direct optical excitation of the  $\text{Er}^{3+}$  ions. The luminescence

intensity is nearly as strong at room temperature as at 77K, which is further evidence that widegap materials tend to suppress the temperature quenching of the  $\text{Er}^{3+}$  luminescence.

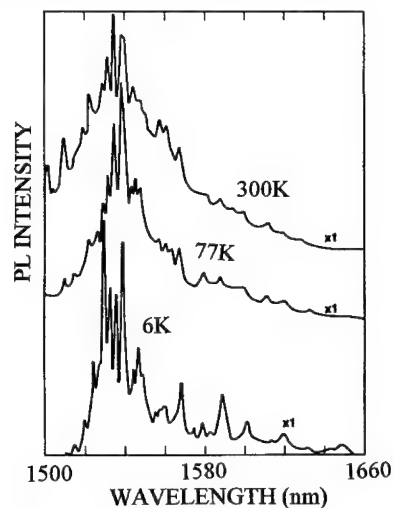


Figure 3. Emission spectra of  $\text{Er}^{3+}$  ions in Er + O implanted  $\text{GaN}/\text{Al}_2\text{O}_3$ .

Similar data are shown in Figure 4 for an Er + O implanted GaN sample grown on a GaAs substrate. The same basic features are observed in the spectrum as for the material grown on sapphire although there are some differences which need to be investigated further.

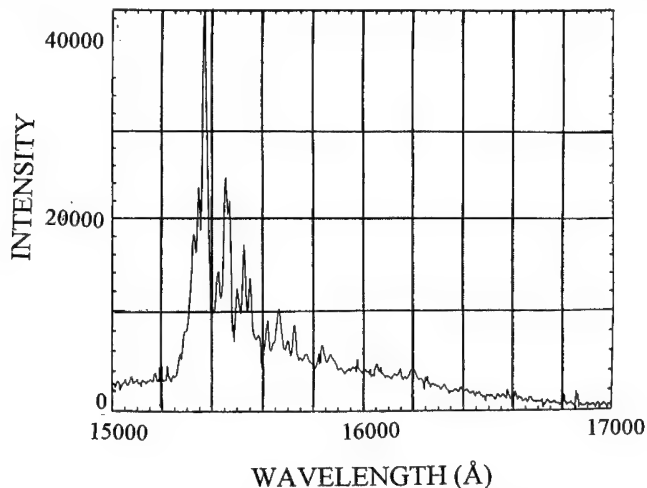


Figure 4. Emission spectra of  $\text{Er}^{3+}$  ions in Er + O implanted  $\text{GaN}/\text{GaAs}$  at 300K.

With its extremely large bandgap and affinity for incorporating large oxygen concentrations, it would appear AlN might be the most promising Er-doped nitride. Figure 5 shows an emission spectrum from an Er + O implanted AlN sample, measured at 6K. The emission intensity is very low, and suggests that the implant and anneal cycle is not optimized.

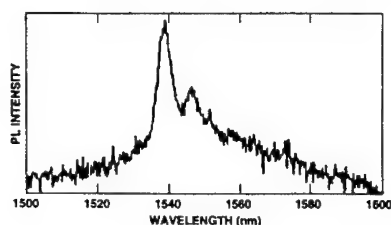


Figure 5. Emission spectra of  $\text{Er}^{3+}$  ions in Er + O implanted AlN/GaAs at 6K.

While little success has been achieved to date with use of gaseous source Er doping during growth of the III-V nitrides, solid Er doping has produced high incorporation efficiencies. Figure 6 shows SIMS profiles of Er in an AlN sample grown with two different Er flux levels. The individual layers are well separated, but there does appear to be some Er segregation during growth. At this stage we do not know how much of the Er is optically active. The luminescence efficiency is extremely strong, in the as-grown sample, with no additional oxygen incorporation.

Figure 7.

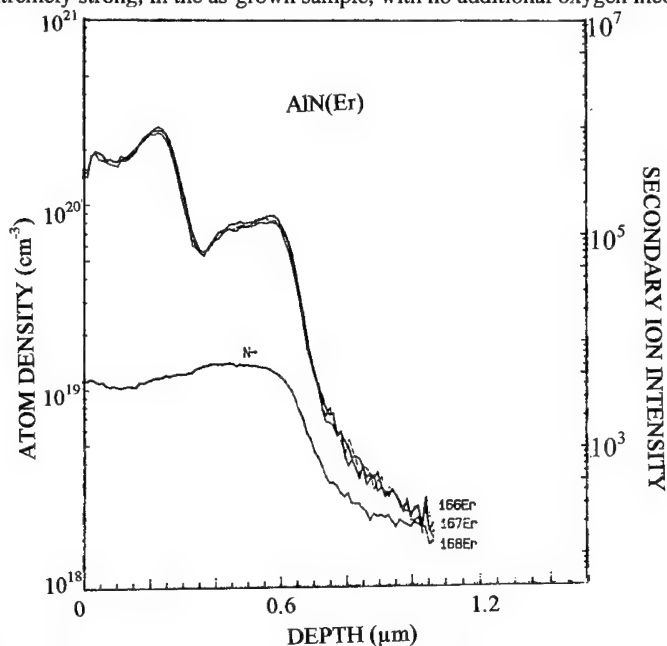


Figure 6. SIMS profiles of Er in a MOMBE grown AlN (Er) double-layer structure.

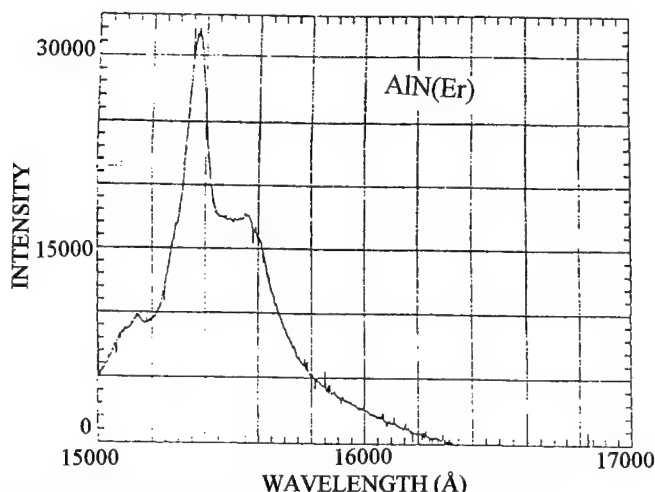


Figure 7. Emission spectra of  $\text{Er}^{3+}$  ions in the epi structure of Figure 6.

Solid source Er doping during growth has produced doping levels up to  $3 \times 10^{21} \text{ cm}^{-3}$  in AlN, as shown in Figure 8. Under these conditions the surface morphology of the AlN is quite rough as measured by scanning electron microscopy and atomic force microscopy, and the crystalline quality degrades, as measured by double crystal x-ray diffraction. For this reason we have been unable to achieve good ion channeling which would give us a clue as to the lattice site location of the Er. Note also that the oxygen concentration in these films is below the Er concentration, as shown in the SIMS profile of Figure 9. We are planning to measure the optical activity as a function of Er concentration in the AlN, and also to examine the effect of additional oxygen incorporated deliberately during growth. We also need to measure the temperature dependence of the emission signal — this is currently under investigation.

In order to examine microcavity enhancement, and possibly lasing of the emission in nitride materials, we have developed several new etching processes for GaN/AlN/InGaN structures.[29] For example, to fabricate microdisk lasers, one needs an anisotropic, non-selective dry etch. We have found that ECR plasma etching with  $\text{Cl}_2/\text{CH}_4/\text{H}_2$ ,  $\text{Cl}_2/\text{Ar}$ ,  $\text{ICl}/\text{Ar}$   $\text{BCl}_3/\text{N}_2$  or  $\text{CH}_4/\text{H}_2/\text{Ar}$  chemistries [30,31] all provide rates  $> 0.3 \mu\text{m}/\text{min}$  at moderate ion energies. KOH-based wet etch solutions have been found to selectively remove AlN while not affecting GaN, InN or  $\text{In}_x\text{Ga}_{1-x}\text{N}$ . [32] We have employed these processes to fabricate GaN (Er) microdisks on AlN buffers on  $\text{Al}_2\text{O}_3$  substrates,[29] and future work will concentrate on the optical properties of these structures.

## SUMMARY

$\text{Er}^{3+}$  emission in III-V nitrides has been achieved by ion implantation or by doping during MOMBE growth. Er concentrations up to  $3 \times 10^{21} \text{ cm}^{-3}$  have been obtained in AlN. Future work will concentrate on optimizing the oxygen concentration in these films in order to maximize the optical output, and to measure the temperature dependence of emission intensity in both unpatterned and microcavity structures.

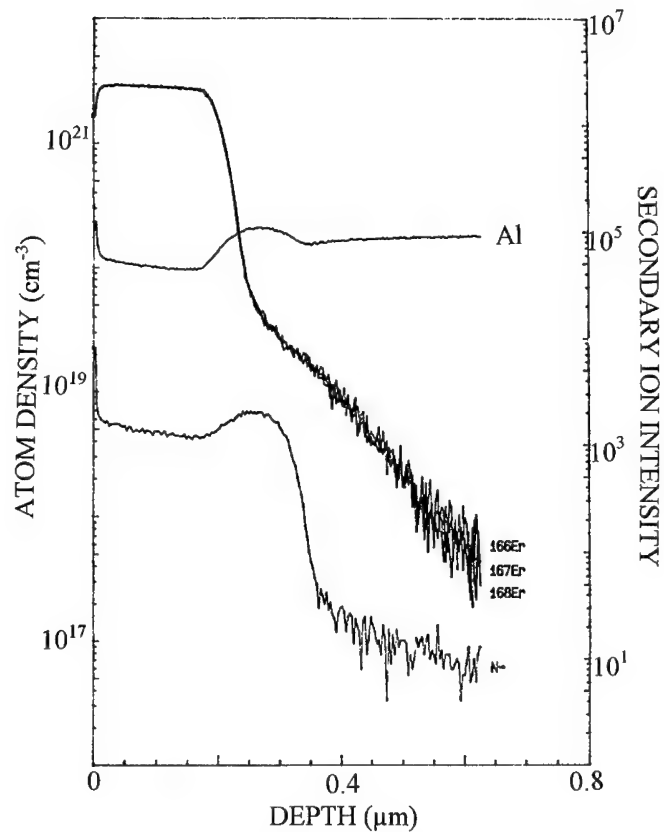


Figure 8. SIMS profiles of Er in a MOMBE grown AlN/Al<sub>2</sub>O<sub>3</sub> sample grown with high Er flux.

#### ACKNOWLEDGMENTS

The work at UF is partially supported by an ARO-AASERT grant, and is performed in the Microfabritech facility. The work at HRL is partially supported by ARO, while that at Sandia is supported by DOE contract DE-AC04-94AL85000

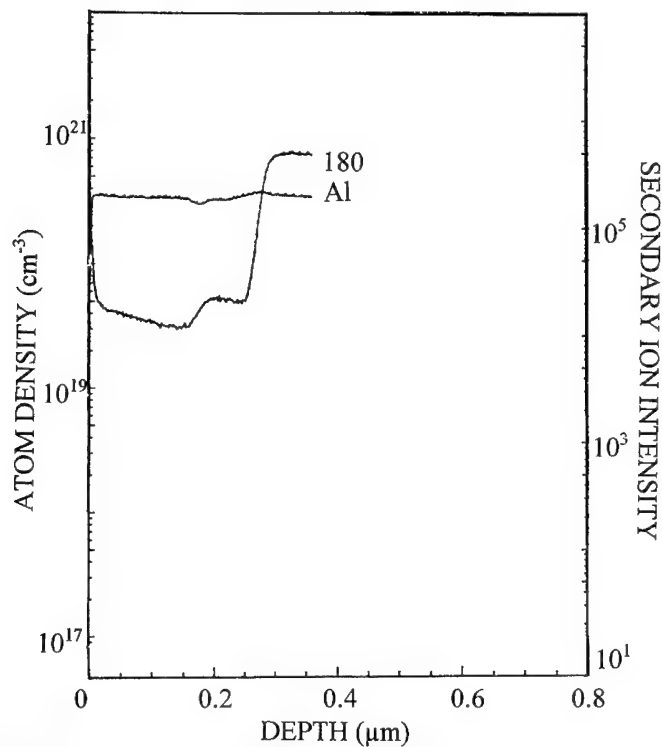


Figure 9. SIMS profile of O in the epi structure of Figure 8.

#### REFERENCES

1. S. Saito, T. Imai and T. Ito, J. Lightwave Technol. 9 161 1991
2. L. F. Mollenauer, S. G. Evangelides and H. A. Haus, J. Lightwave Technol. 9 144 (1991).
3. Integrated Optoelectronics, ed. M. Dagenais, R. F. Leheny, J. Crow (Academic Press, San Diego, 1995).
4. J. M. Zavada and D. Zhang, Solid State Electron. 38 1285 (1995).
5. S. Coffa, G. Franzo, F. Priolo, A. Polman and R. Serna, Phys. Rev. B. 49 16313 (1994).
6. H. Ennen, G. Pomrenke, A. Axmann, W. Hagyl and J. Schneider, Appl. Phys. Lett. 46 381 (1985)
7. Y. H. Xie, C. A. Fitzgerald and Y. J. Mii, J. Appl. Phys. 70 3233 (1991).

8. A. Polman, J. S. Cushter, E. Smoeks and G. N. van der Hoven, Nucl. Instr. Meth. B. 80/81 653 (1993).
9. S. Coffa, F. Priolo, G. Franzo, V. Bellani, A. Garnera and C. Spinella, Phys. Rev. B48 11782 (1993).
10. D. J. Eaglesham, J. Michel, E. A. Fitzgerald, D. C. Jacobson, J. M. Poate, J. L. Benton, A. Polman, Y. H. Xie and L. C. Kimerling, Appl. Phys. Lett. 48 2797 (1991).
11. F. Y. G. Ren, J. Michel, Z. S. Paduano, B. Zhang, H. Kitagawa, D. C. Jacobson, J. M. Poate and L. C. Kimerling, Mat. Res. Soc. Symp. Proc. 301 87 (1993).
12. G. Franzo, F. Priolo, S. Coffa, A. Polman and A. Casnera, Appl. Phys. Lett. 64 2235 (1994).
13. after G. N. van der Hovers Ph. D. Thesis (1995).
14. G. C. Jiang, L. B. Chang, G. H. Chang and L. S. Lu, J. Cryst. Growth 152 127 (1995).
15. D. L. Adler, D. C. Jacobson, D. J. Eaglesham, M. A. Marcus, J. L. Benton, J. M. Poate and P. H. Citrin, Appl. Phys. Lett. 61 2181 (1992).
16. F. Priolo, S. Coffa, G. Franzo, C. Spinella, A. Carsera and V. Bellani, J. Appl. Phys. 74 4936 (1993).
17. J. Nakata, M. Taniguchi and K. Takahei, Appl. Phys. Lett. 61 2665 (1992).
18. A. Kozanecki, M. Chan, C. Jeynes, B. J. Sealy and K. Homewood, Solid St. Comm. 78 763 (1991).
19. P. B. Klein and G. S. Pomrenke, Electron. Lett. 24 1502 (1988).
20. P. N. Favenec, H. L. Haridon, M. Salvi, D. Moutonnet and Y. L. Cuillou, Electron. Lett. 25 718 (1989).
21. A. J. Neuhaufen and B. W. Wessels, Appl. Phys. Lett. 59 2317 (1991).
22. D. Y. Chu, X. Z. Wang, W. G. Bi, R. P. Espindola, S. L. Wu, B. W. Wessels, C. W. Tu and S. T. Ho, Appl. Phys. Lett. 66 1097 (1995).
23. R. G. Wilson, R. N. Schwartz, C. R. Abernathy, S. J. Pearton, N. Newman, M. Rubin, T. Fu and J. M. Zavada, Appl. Phys. Lett. 65 992 (1994).
24. C. H. Qui, M. W. Leksono, J. I. Pankove, J. T. Toruik, R. J. Feurstein and F. Namavar, Appl. Phys. Lett. 66 562 (1995).
25. see for example J. M. Redwing, T. F. Kuech, D. C. Jordon, B. A. Vararstra and S. S. Lau, J. Appl. Phys. 76 1585 (1994).



26. H. P. Maruska (unpublished, 1994).
27. J. I. Pankove and J. A. Hutchby, Appl. Phys. Lett. 24 281 (1974).
28. C. R. Abernathy, Mat. Sci. Eng. Rep. 14 203 (1995).
29. C. R. Abernathy, S. J. Pearton, J. D. MacKenzie, J. R. Mileham, S. R. Bharatan, V. Krishnamoorthy, K. S. Jones, M. H. Crawford, R. J. Shul, S. P. Kilcoyne, J. M. Zavada, D. Zhang and R. M. Kolbas, Solid State Electron. 39 311 (1996)
30. R. J. Shul, S. P. Kilcoyne, M. H. Crawford, J. E. Parmeter, C. B. Vartuli, C. R. Abernathy and S. J. Pearton 66 1761 (1995).
31. S. J. Pearton, C. R. Abernathy and F. Ren, Appl. Phys. Lett. 64 2294 (1994).
32. J. R. Mileham, S. J. Pearton, C. R. Abernathy, J. D. MacKenzie, R. J. Shul and S. P. Kilcoyne, Appl. Phys. Lett. 67 1119 (1995).

## LOW-TEMPERATURE GROWTH OF Si:Er BY ELECTRON CYCLOTRON RESONANCE PECVD USING METAL ORGANICS

P. S. ANDRY<sup>1</sup>, W. J. VARHUE<sup>1</sup>, E. ADAMS<sup>2</sup>, M. LAVOIE<sup>2</sup>,  
P.B. KLEIN<sup>3</sup>, R. HENGHOLD<sup>4</sup> AND J. HUNTER<sup>4</sup>

<sup>1</sup>Department of Electrical Engineering, University of Vermont, Burlington, VT, 05405

<sup>2</sup>IBM Corporation, Essex Junction, VT, 05452

<sup>3</sup>Code 6874, Naval Research Laboratory, Washington, DC, 20375-5347

<sup>4</sup>AFIT / ENP, Wright-Patterson AFB, Dayton, OH, 45433-7765

### ABSTRACT

Epitaxial growth of Er-doped silicon films has been performed by plasma-enhanced chemical vapor deposition at low temperature (430°C) using an electron cyclotron resonance source. The goal was to incorporate an optically active center, erbium surrounded by nitrogen, through the use of the metal organic compound tris (bis trimethyl silyl amido) erbium. Films were analyzed by Rutherford backscatter spectrometry, secondary ion mass spectroscopy and high resolution x-ray diffraction. The characteristic 1.54  $\mu\text{m}$  emission was observed by photoluminescence spectroscopy. Previous attempts to incorporate the complex (ErO<sub>6</sub>) using tris (2,2,6,6-tetramethyl-3,5-heptanedionato) erbium (III) indicated that excessive interstitial carbon lowered epitaxial quality and reduced photoluminescent intensity. In this study, much of the carbon was introduced onto substitutional sites maintaining good epitaxial growth. A response surface method was employed to find the plasma growth parameters yielding the highest quality luminescent films. Luminescent intensity increased for anneals up to 600°C but decreased at higher temperatures.

### INTRODUCTION

In recent years, considerable interest has been focused on the use of erbium in the development of a silicon-based optoelectronic material. Since the first demonstration of Er incorporation by Ennen *et al.*<sup>1</sup>, considerable work has concentrated on increasing the photoluminescence (PL) output. The work of Priolo *et al.*<sup>2</sup>, Adler *et al.*<sup>3</sup> and Michel *et al.*<sup>4</sup> has demonstrated that the optically active center results from the symmetry and chemical nature of the ligands bound to Er, most notably B, C, N, O and F.

In the vast majority of work to date, ion implantation has been used to incorporate Er and its co-dopants into the Si host lattice. Although implantation allows the introduction of high concentrations of Er into Si, it causes a large amount of lattice damage which necessitates a high temperature anneal. During such anneals the lattice is repaired and some number of optically active centers are formed as co-implanted atoms redistribute themselves as neighbors to an Er site. Problems such as limited solubility of Er and the formation of optically inactive ErSi<sub>2</sub> precipitates<sup>5</sup> have prompted the use of alternate methods for growing Er-doped silicon. Previous approaches have included molecular beam epitaxy (MBE)<sup>6</sup>, metalorganic chemical vapor deposition (MOCVD)<sup>7</sup>, metalorganic vapor phase epitaxy (MOVPE)<sup>8</sup> and solid phase epitaxy.<sup>9</sup> All of these techniques have one aspect in common: they are all normally performed in the temperature range from 600 °C to 900 °C. These temperatures rival those used during post-implant anneals and may thus lead to some of the same deleterious effects on Er luminescence. Matsuoka *et al.* have recently demonstrated the benefits of low-temperature (500 °C) growth of Si:Er:O *in situ* by ion beam epitaxy.<sup>10</sup>

The goal of this work is to grow homoepitaxial Er-doped Si films with high PL output efficiency by employing a metal organic (MO) compound in a plasma-enhanced chemical vapor deposition (PECVD) process. The success of the technique hinges on 1) the ability to grow high quality epitaxial films at low temperatures (400 °C to 500 °C) and, 2) the ability to incorporate optically active Er complexes - contained within the MO compound - into the growing Si lattice

without creating defects. Towards the first goal, our choice of deposition technique is Electron Cyclotron Resonance (ECR) PECVD. The low ion energy (10 to 20 eV) and high ion density (up to  $10^{12} \text{ cm}^{-3}$ ) of this plasma process allows epitaxial growth to occur at substrate temperatures in the range from 360 °C to 500 °C.<sup>11</sup>

The second key factor depends on the availability of volatile metal organic precursors containing Er in promising, optically active bonding arrangements. We have shown previously<sup>12</sup> that one such MO compound, tris (2,2,6,6-tetramethyl-3-5-heptanedionato) Er (III) or "(thd)Er<sub>3</sub>" can be used to incorporate PL active ErO<sub>x</sub> complexes. This MO compound is shown in Fig. 1 a). Our hope was to incorporate intact ErO<sub>6</sub> centers, however, chemical analysis of the films revealed that the compound was dissociating in the plasma and virtually all of its constituent atoms were finding their way into the lattice. With 33 carbon atoms per Er atom, carbon "poisoning" degraded crystal quality such that no appreciable PL output could be achieved.

In this work we have used a different MO, namely tris (bis trimethyl silyl amido) Er (III) which we have dubbed the "amino" source. As can be seen in Fig. 1 b), there are several important structural differences between this molecule and the one used previously. Instead of being sixfold coordinated by oxygen, the Er atom is threefold coordinated by nitrogen. Each nitrogen is in turn bonded to two Si atoms, with each Si terminated by three methyl groups. In this case, there are 18 carbon atoms per Er atom. The optically active complex is expected to derive from the (ErN<sub>3</sub>) center and may also utilize the Si already bonded to nitrogen. It will be shown that this MO compound yields considerably improved results over the one tried previously, and that its promise appears to be linked to its special structural characteristics.

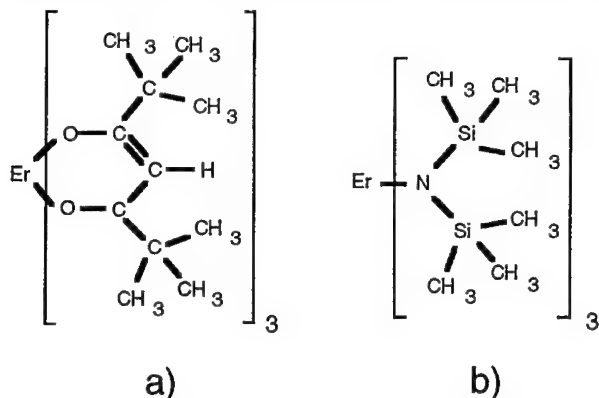


Fig. 1 Molecular structure of MO dopants: a) tris (2,2,6,6-tetramethyl-3-5-heptanedionato) Er (III) denoted "(thd)Er<sub>3</sub>", and b) tris (bis trimethyl silyl amido) Er (III) denoted "amino".

## EXPERIMENT

The ECR reactor used in these experiments has been described in detail previously.<sup>12</sup> Base pressure in the reactor is maintained at  $1 \times 10^{-8}$  Torr levels by a turbomolecular pump backed by a roots blower and a rotary mechanical pump. Samples are clamped onto a SiC-coated graphite substrate block and transferred to the reactor via a load-lock. Microwave power enters the reactor through a quartz window. The ECR region is located about 11 cm in front of the microwave window while the sample is located another ~30 cm downstream. The MO is held in a stainless steel "bottle" which is located inside a low temperature oven. A mass flow controller is used to regulate the flow of Ar carrier gas through the MO Er source. Heat tapes surrounding the gas line between the bottle and the reactor prevent condensation in the line.

All samples are 5 cm by 3 cm and are cut from (100) n-type or p-type 4 inch Si wafers. Following an *ex-situ* cleaning, samples are load-locked to  $\sim 1 \times 10^{-5}$  Torr before being transferred to the growth chamber. A plasma cleaning precedes each deposition and consists of an Ar (30 sccm) and H<sub>2</sub> (20 sccm) plasma etch for 5 min at the deposition temperature. The deposition is initiated

immediately after the cleaning without extinguishing the plasma by simultaneously cutting the  $H_2$  flow and starting the flow of 10 %  $SiH_4$  in Ar. Once film deposition is underway, the MO source and lines are heated to their pre-determined temperatures. This procedure allows a thin, intrinsic Si "buffer" layer to grow, thereby preventing the possibility of epitaxial "poisoning" at the interface by a concentration of MO species early in the growth.

Erbium concentration and crystalline quality were determined by Rutherford backscattering spectrometry (RBS). Crystalline quality is gauged by taking the ratio of the channeled backscatter intensity to the random angle backscatter intensity. This ratio, known as  $\chi_{min}$ , is commonly expressed as a percentage with 100% indicating an amorphous film and ~4% representing the limit of detection for a perfect crystal. Secondary ion mass spectroscopy (SIMS) was used to determine the impurity concentrations of carbon, oxygen and nitrogen in the silicon films.

High resolution x-ray diffraction was also used to determine the crystallographic perfection of our epitaxial thin films. A Philips Materials Research Diffractometer comprising a 3-axis Eulerian cradle, a four-crystal Ge Monochromator and a  $CuK\alpha$  x-ray source was used to record glancing angle rocking curves. Angular resolution in the  $\omega/2\theta$  scan mode was 12 arcsec ( $0.0033^\circ$ ).

Photoluminescence (PL) spectroscopy was performed at 4.2 K to verify the optical activity of the erbium in the crystalline films. Samples were illuminated at near-normal incidence using the 514.5 nm line of an Ar ion laser. For most measurements the power was fixed at 150 mW. The PL output was measured by a liquid nitrogen cooled germanium detector.

## RESULTS AND DISCUSSION

An initial series of growths were made to compare the new amino source to the (thd)Er<sub>3</sub> source used previously.<sup>12</sup> In order to compare the two MO sources on essentially equal footing, the following common growth parameters were used: 200 W microwave power, 5 mTorr reactor pressure, 30 sccm argon gas feed to the resonance chamber, 25 sccm of 10% silane in argon downstream, and a substrate temperature of 430 °C. The resulting growth rate from these conditions was approximately 30 Å/min. Only the amino MO source temperature was adjusted to give similar vapor pressures to those produced by heating the (thd)Er<sub>3</sub> source. In this case, preliminary growths were made with the amino source heated in the range from 120 °F to 140 °F. Fig. 2 shows the best PL results from this trial series (#49) plotted along with the best ever result obtained using (thd)Er<sub>3</sub> (#31). Both samples are about 3000 Å thick. The PL peak at 1.537  $\mu$ m for sample #49 is a full 8 times stronger than that of #31. Note also that two Stark lines at 1.552 and 1.577  $\mu$ m are clearly visible in the amino-doped sample. RBS yielded an Er concentration of  $2 \times 10^{19} \text{ cm}^{-3}$  and a  $\chi_{min}$  of 8% for the amino-doped sample, while the (thd)Er<sub>3</sub>-doped sample had  $5 \times 10^{18} \text{ cm}^{-3}$  of Er and a  $\chi_{min}$  of 30%.

In order to identify any important chemical differences between the films grown from different MO sources, SIMS analysis was performed samples #31 and #49, as well as an undoped Si background sample. Carbon, oxygen and nitrogen concentrations are given in Table I along with Er concentrations determined by RBS. In the case of the (thd)Er<sub>3</sub>-doped sample, we find the following ratios: C/Er ~ 16, O/Er ~ 16 and N/Er ~ 1. The C/Er ratio is not surprising considering the large supply of carbon atoms, 33 per Er atom, available from the ligands. The O/Er ratio of 16 suggests another source of O contamination present in the source or its delivery system, since there are 6 oxygens per Er in the MO, and the chamber background can account for, at most, one more. The presence of nitrogen at 8 times the level of the background also suggests a contaminant in the compound, possibly air.

For the amino-doped sample, we find the ratios: C/Er ~ 15, O/Er ~ 2.5 and N/Er ~ 3. The last of these ratios indicates that each of the three N atoms attached to Er in the MO source does in fact end up in the film, although it is impossible to confirm the final bonding arrangement by this analysis. Presence of oxygen again suggests a contaminant, most likely water or air. The C/Er ratio reveals that virtually the same proportion of C is introduced by both MO precursors. It was previously assumed that degradation of epitaxial quality was linked only with the absolute concentration of carbon in the films. These results may indicate that useful carbon incorporation is possible using the amino MO, and that a certain number of Er-C complexes may also be formed.

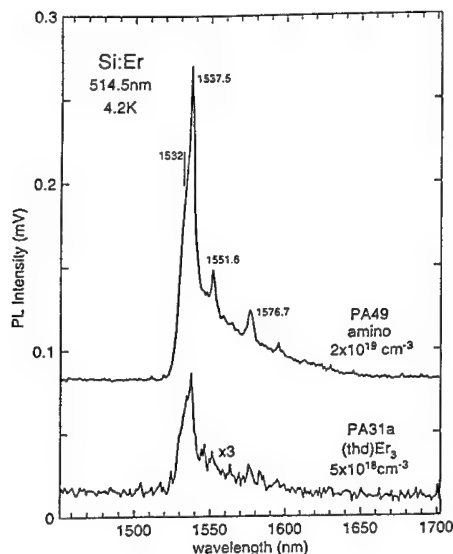


Fig. 2 Comparison of PL intensity from two Er-doped Si samples: #49 was grown using the "amino" MO; #31 shows the best result obtained using (thd)Er<sub>3</sub>.

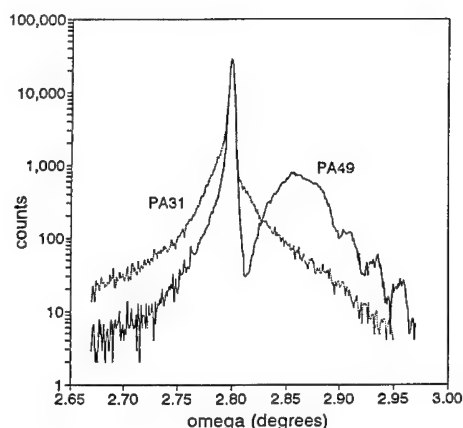


Fig. 3 Glancing incidence (113) rocking curves for the same two samples whose PL spectra are shown to the left.

**Table I.** A comparison of Er-doped samples grown using two different MO sources. Er concentration was determined by RBS; C, O and N concentrations were determined by SIMS.

Sample	MO source	Erbium (cm <sup>-3</sup> )	Carbon (cm <sup>-3</sup> )	Oxygen (cm <sup>-3</sup> )	Nitrogen (cm <sup>-3</sup> )
undoped	none	negligible	1x10 <sup>18</sup>	5x10 <sup>18</sup>	1x10 <sup>18</sup>
#31	(thd)Er <sub>3</sub>	5x10 <sup>18</sup>	8x10 <sup>19</sup>	8x10 <sup>19</sup>	4x10 <sup>18</sup>
#49	amino	2x10 <sup>19</sup>	3x10 <sup>20</sup>	5x10 <sup>19</sup>	6x10 <sup>19</sup>

Fig. 3 shows the glancing (113) rocking curves for samples #31 and #49. The difference in structure is clearly apparent. In the case of the (thd)Er<sub>3</sub>-doped sample, the flaring of the "wings" out and above the substrate reference indicates significant scattering due to defects. In contrast, the curve for the amino-doped sample shows the layer peak distinctly shifted to the right of the substrate peak. The layer peak has a well-defined single Gaussian shape (an inverted parabola on log scale), and Pendellosung fringes are clearly seen. The full-width half maximum (FWHM) of the layer peak is close to 180 arcsec while the substrate gives 16 arcsec. This film is thus of better epitaxial quality than the (thd)Er<sub>3</sub>-doped material, and furthermore its lattice parameter has shrunk significantly. Shrinkage can only result from some substitution of C for Si in the lattice. Calculation based on the layer peak shift gives between 0.17% and 0.35% carbon, ranging from the fully strained to the fully relaxed case. Since we know the actual content by

SIMS is 0.8% carbon, roughly one quarter to one half of the C atoms in this sample are substitutional. This might explain how such a large proportion of carbon may be introduced into the crystal without seriously damaging the epitaxial quality.

Having decided on exclusive use of the amino MO as our Er dopant, a factorial design experiment was run with four growth parameters under study: MO temperature, hydrogen addition, silane flow and growth time.<sup>13</sup> This study indicated that hydrogen should not be used due to an adverse reaction with the MO compound leading to poor epitaxial quality. Interestingly, PL intensity was shown to depend almost entirely on growth rate (silane flow) and total thickness (growth time), and did not show any particular dependence on Er concentration within the range from about  $1 \times 10^{18}$  to  $1 \times 10^{19} \text{ cm}^{-3}$ . Fig. 4 shows the PL response surface as a function of growth time and growth rate. Data from a total of 18 samples, grown in random order in two blocks of 9 each, were used to generate the surface. Within the parameter space defined by the figure there exists a maximum in PL intensity for films grown at a rate of about 50 Å/min for times of about 75 minutes. These results tend to confirm our notion that epitaxial film quality remains one of the most important considerations in achieving efficient luminescence.

Samples grown in the region of maximum PL intensity had an average Er content of  $4 \times 10^{18} \text{ cm}^{-3}$ . A few of these were annealed in nitrogen for one half hour at temperatures ranging from 600 °C to 900 °C. The dependence of PL intensity on anneal temperature for one such sample is shown in Fig. 5. The behavior of both the intrinsic phonon-assisted emission at 1.16 μm and the  $\text{Er}^{3+}$  peak at 1.54 μm is shown (the lines are polynomial fits). Note that the sample emits about half of its maximum luminescent power as-grown at 430 °C, and that beyond 600 °C the intensity only decreases. In contrast, ion-implanted samples must be recrystallized at temperatures which begin at 600 °C, and maximum intensity is typically found only after anneals approaching 1000 °C.<sup>14</sup> The fact that the Si indirect gap emission is a minimum where the  $\text{Er}^{3+}$  emission is a maximum may be an indication that additional optical Er centers are formed or "activated" between 430 °C and 600 °C, funneling some of the available e-h pairs away from the intrinsic Si emission path. The subsequent increase in indirect gap emission and decrease in  $\text{Er}^{3+}$  emission suggests that the band edge recombination path becomes more favorable as crystal quality improves. It may also indicate the dissociation of a portion of the optical Er centers.

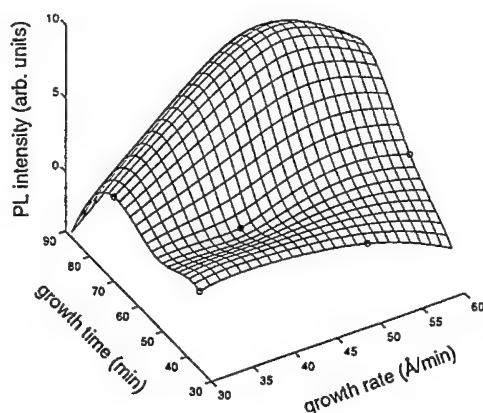


Fig. 4 Photoluminescence response surface for amino-doped samples. Fixed growth parameters: 30 sccm Ar feed, 5 mTorr pressure, 200 W microwave power, and  $T_{\text{sub}} = 430 \text{ }^{\circ}\text{C}$ .

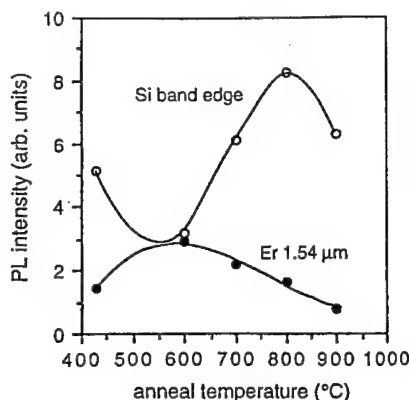


Fig. 5 Photoluminescence as a function of anneal temperature for a sample grown using optimized parameters. Anneals were 1/2 hour each in  $\text{N}_2$ .

## CONCLUSIONS

Homoepitaxial Er-doped silicon films have been grown by plasma-enhanced chemical vapor deposition at low temperature (430°C) using an electron cyclotron resonance source. The goal was to incorporate an optically active ( $\text{ErN}_3$ ) center into the growing film through the use of the MO compound tris (bis trimethyl silyl amido) erbium. The use of this "amino" compound yielded samples possessing much improved PL intensity and crystal quality compared to films grown under similar conditions using tris (2,2,6,6-tetramethyl-3,5-heptanedionato) erbium (III). SIMS analysis of an amino-doped sample yielded a N/Er ratio of 3 as expected, but also a large C/Er ratio of 15. X-ray diffraction revealed that much of the carbon found in amino-doped films is found at substitutional sites. While Er-N complexes are assumed to be the primary optical centers, the existence of Er-C complexes cannot be ruled out.

A response surface methodology was adopted in order to find the combination of growth rate (silane flow) and growth time (total thickness) leading to maximum PL intensity in our ECR-PECVD process. Epitaxial films grown at rates of close to 50 Å/min for about 75 minutes gave the best results. The average Er concentration for these samples was near  $4 \times 10^{18} \text{ cm}^{-3}$ . PL intensity was found to increase following a half hour anneal in nitrogen at 600 °C. Successively higher anneal temperatures only served to decrease the PL intensity.

## ACKNOWLEDGEMENTS

The support of the Air Force Office of Scientific Research is gratefully appreciated. The authors would also like to thank J. Lille for special graphics support.

## REFERENCES

1. H. Ennen, G. Pomrenke, A. Axmann, K. Eisele, W. Haydi and J. Schneider, *Appl. Phys. Lett.* **46** (4), 381 (1985).
2. F. Priolo, S. Coffa, G. Franzo, C. Spinella, A. Carnera and V. Ballani, *J. Appl. Phys.* **74**, 4936 (1993).
3. D. L. Adler, D. C. Jacobson, D. J. Eaglesham, M. A. Marcus, J. L. Benton, J. M. Poate and P. H. Citrin, *Appl. Phys. Lett.* **61**, 2181 (1992).
4. J. Michel, J. L. Benton, R. F. Ferrante, D. J. Eaglesham, D. C. Jacobson, E. A. Fitzgerald, Y. H. Xie, J. M. Poate and L. C. Kimerling, *J. Appl. Phys.* **70**, 2672 (1991).
5. D. J. Eaglesham, J. Michel, E. A. Fitzgerald, D. C. Jacobson, J. L. Benton, J. M. Poate, A. Polman, Y. H. Xie and L. C. Kimerling, *Appl. Phys. Lett.* **58**, 2797 (1991).
6. P. Wetzel, L. Haderbache, C. Pirri, C. J. Peruchetti, D. Bolmont and G. Gewinner, *Phys. Rev. B* **43**, 6620 (1991).
7. D. B. Beach, R. T. Collins, F. K. Legoues and J. O. Chu, *Materials Research Society Symposium Proceedings* **282**, 397 (1992).
8. J. Michel, F. Y. G. Ren, B. Zheng, D. C. Jacobson, J. M. Pote and L. C. Kimerling, *Materials Science Forum* **143-147**, 707 (1994).
9. A. Polman, J. S. Custer, E. Snoeks and G. N. van den Hoven, *Appl. Phys. Lett.* **62**, 509 (1993).
10. M. Matsuoka and S. Tohno, *J. Appl. Phys.* **78**, 2751 (1995).
11. W. J. Varhue, J. L. Rogers, P. S. Andry and E. Adams, *Appl. Phys. Lett.* **68**, 349 (1996).
12. J. L. Rogers, P. S. Andry, W. J. Varhue, E. Adams, M. Lavoie and P. B. Klein, *J. Appl. Phys.* **78**, 6241 (1995).
13. P. S. Andry, W. J. Varhue, F. Ladipo, K. Ahmed, E. Adams, M. Lavoie, P. B. Klein, R. Hengehold and J. Hunter, *J. Appl. Phys.*, in print.
14. A. Polman, G. N. van den Hoven, J. S. Custer, J. H. Shin, R. Serna and P. F. A. Alkemade *J. Appl. Phys.* **77**, 1256 (1995).

## ERBIUM DOPED GaAs BY MOCVD

\*A.C. Greenwald, \*K.J. Linden, \*\*W.S. Rees, Jr., \*\*O. Just, \*\*\*N.M. Haegel, and \*\*\*S. Donder

\*Spire Corporation, Bedford MA 01730-2396, email: spire.corp@channel1.com

\*\*Georgia Institute of Technology, Atlanta, GA 30332-0400

\*\*\*Fairfield University, Fairfield, CT 06430-7524

### ABSTRACT

The overall objective of this research is to develop temperature stable 1.54  $\mu\text{m}$  light sources based upon ionic emitters. LEDs and diode lasers were fabricated in MOCVD grown AlGaAs materials but only weak electroluminescence was observed. The III-V compound semiconductors were doped with erbium amide sources of the form:  $\text{Er}\{\text{N}[\text{Si}(\text{CH}_3)_3]\text{R}\}_3$  where R is an organic unit. These amide sources had reduced carbon and oxygen levels in a GaAs film compared to the use of a cyclopentadienyl erbium source, but did dope the semiconductor with silicon. Silicon doping levels were a function of growth temperature. Erbium photoluminescence was enhanced with oxygen co-doping, but diode electrical characteristics were degraded. PLE showed that erbium ions were excited by above bandgap light absorbed by GaAs.

### INTRODUCTION

The 1.54 micron line of erbium-doped solid state lasers is now used extensively in fiber optic communications. Temperature stabilized diode lasers can be used to initiate the signal which is further amplified. It would be advantageous to use ion-doped diode lasers with stable, temperature independent emission at 1.54  $\mu\text{m}$ . Electroluminescence from an erbium doped GaAs diode has been reported [1].

MOCVD is one potential fabrication technique that could lead to low cost 1.54  $\mu\text{m}$  sources. Experiments by ion implantation [2] have proved unsuccessful. MBE has not yet produced working devices [3]. Experiments by MOCVD using methyl- or isopropyl-substituted cyclopentadienyl derivatives of erbium lead to excess carbon in the epitaxial film. Addition of small amounts of oxygen reduced the carbon levels [4]. However, the presence of oxygen is detrimental to device performance. Previously, we reported that carbon and oxygen levels can be reduced by using erbium-amide as an MOCVD dopant source [5]. Here, we report results of epitaxial growth and device fabrication.

### MOCVD OF ERBIUM DOPED FILMS

All experimental film deposition studies were performed in a SPI-MOCVD<sup>TM</sup>450 reactor facility [6] modified to carry a high temperature precursor. Standard technology for epitaxial MOCVD of III-V compound thin films uses controlled temperature water baths and valves with KELF<sup>TM</sup> seats. Both items have a maximum temperature tolerance of 95°C, while the erbium amide source  $\text{Er}\{\text{N}[\text{Si}(\text{CH}_3)_3]\}_3$  for this work was heated to 160°C to provide adequate vapor pressure. Equipment modifications include use of an electropolished stainless-steel bubbler to hold the source, use of a temperature controlled hot oil bath to regulate source temperature, and metal sealed valves. An all-metal needle valve with graphite packing was used to control source pressure, nominally



300 torr. The source, and all valves in contact with the metalorganic material in the vapor state, were installed in a heated cabinet to improve the temperature uniformity over what can be achieved with the use of heating tapes. The pressure sensor for the source bubbler, rated at 50°C maximum, was outside the oven connected through an extension line.

Initial experiments were used to demonstrate control of the doping level of erbium in the epitaxial GaAs film. The substrate was a semi-insulating GaAs <100> wafer. All growth temperatures were 650°C, at a reactor pressure of 75 torr, carrier flow for Ga at 8 sccm (source at 0°C), and a III:V ratio of 100. An undoped GaAs buffer layer 0.5 µm thick was deposited first. This was followed by three successive layers at increasing carrier flow for erbium, of 100, 200 then 400 sccm. At the highest erbium flow rate the gallium flow was turned off for one layer to maximize erbium concentration, and then a capping layer of GaAs was added, to reduce oxidation of the highly doped erbium material.

The sample was analyzed by secondary ion mass spectroscopy (SIMS) (Figure 1) and by Rutherford backscattering spectroscopy (RBS) (Figure 2). Data clearly show that the level of erbium doping was proportional to the carrier flow, demonstrating control of this parameter. For the layer grown without any gallium flow, the maximum erbium concentration was about 30% atomic concentration.

An estimate of the diffusion coefficient for erbium in GaAs at 650°C,  $1 \times 10^{-15} \text{ cm}^2/\text{sec}$ , was derived from the erbium profile of the peak at maximum depth (Figure 1). The deepest erbium peak is the result of the erbium feed line to the reactor being pumped out before the susceptor was heated. A very thin film (few monolayers) with high erbium content was condensed on the surface of the substrate. When the substrate was heated, this layer did not completely evaporate from the surface but reacted to form an arsenide and the erbium diffused into the substrate. Note that the silicon profile associated with this same peak has a steep slope which was used to calibrate the data for the diffusion coefficient calculation.

The surface morphology, and the corresponding channeling RBS spectra, of the sample in Figures 1 and 2 was poor because of the very high erbium concentration layer. ErAs is a near lattice match to GaAs but has the NaCl cubic structure instead of the zinc blend structure of GaAs. The symmetry change created many defects, thereby affecting film growth. GaAs films with erbium concentrations below  $1 \times 10^{19} \text{ cm}^{-3}$  had a smooth surface. Channeling RBS profiles indicated that about 33% of erbium atoms (at  $10^{19} \text{ cm}^{-3}$ ) were substitutional.

In Figure 1, the minimum background level of carbon specific to this measurement was high at  $10^{19} \text{ cm}^{-3}$ . Residual oxygen levels (data not shown) were equal to the erbium concentration, which later experiments traced to a small leak in the gas system. The background silicon concentration (semi-insulating substrate) is about  $2 \times 10^{17} \text{ cm}^{-3}$ . The amount of silicon in the erbium-doped film is a function of deposition temperature, shown (Figure 3) for the erbium amide source  $\text{Er}\{\text{N}[\text{Si}(\text{CH}_3)_2]_3\}$ . This graph can be extrapolated linearly to 720°C, the growth temperature used for tests of AlGaAs films; but this point was not plotted because use of alternate chemistries (addition of trimethylaluminum) might also modify this ratio. Films deposited with an alternate amide,  $\text{Er}\{\text{N}(\text{Bu})\text{SiH}(\text{CH}_3)_2\}_3$  contained greater amounts of silicon for the same deposition temperature and growth experiments with this source were discontinued. Experiments with an ethyl substituted disilyl-amide of erbium were inconclusive.

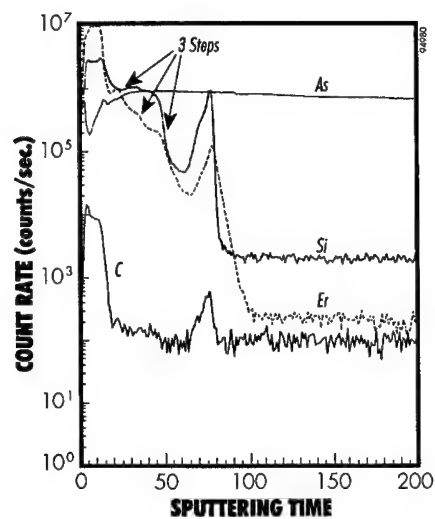


**Figure 1** SIMS depth profile using oxygen ion beam of erbium doped, GaAs epitaxial film showing control of erbium concentration with carrier flow. See depth scale in Figure 2b.

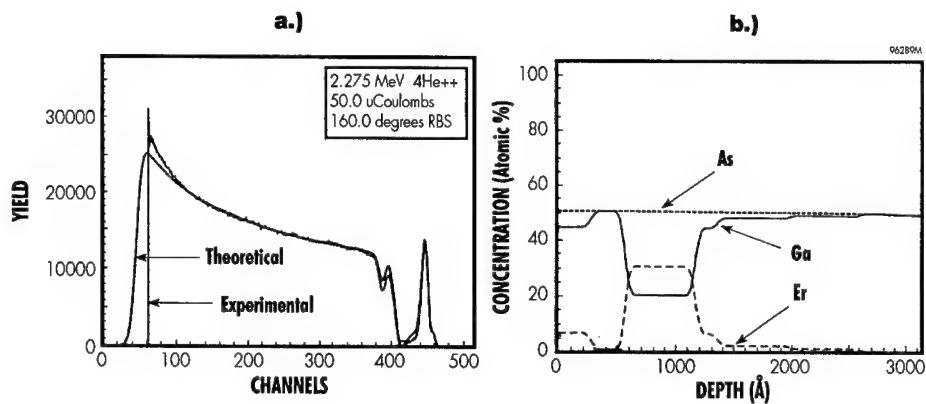


**Figure 2** RBS data and theoretical fit to the data (a) for sample in Figure 1 and (b) depth profile of erbium, gallium and arsenic used to calculate the theoretical fit in (a).

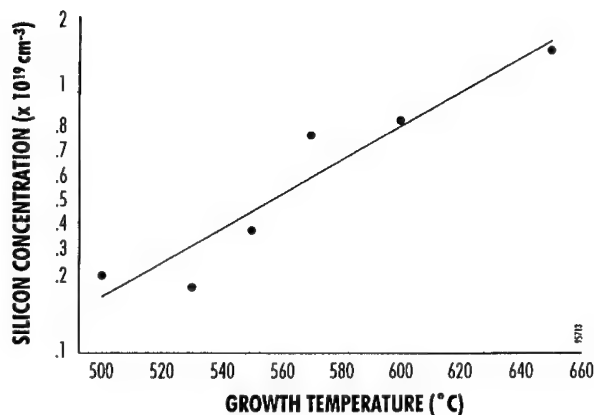


**Figure 3** *Silicon concentration in GaAs as a function of deposition temperature employing an erbium amide as the dopant source.*

#### OPTICAL PROPERTIES AND DEVICES

Photoluminescence of the erbium-doped films was easily detected, Figure 4a. The signal at room temperature (300K) was a factor of ten lower than the signal at 77K. The maximum of the PL signal from Figure 4a was used to monitor luminescent excitation as shown in Figure 4b. A tungsten lamp and a 0.25m monochromator was used as the excitation source for the PLE data. Not clearly discernable on the scale of Figure 4b is a small peak in the curve between 970 and 980 nm. The data indicate that excitation of erbium via electron-hole pairs generated by above bandgap light in GaAs is responsible for almost all of the emitted spectrum. Direct absorption of light by the erbium ions at 970 nm contributes to a very small part, if any, of the emittance.

If the erbium ions in the lattice are pumped by electron-hole pairs, as suggested by the PLE data, then an erbium doped-diode should show electroluminescence at 1538 nm. We fabricated laser diodes designed to emit at 970 nm, as shown in Figure 5a. This wavelength was chosen because it could show optical pumping of the erbium ions to increase 1540 nm emission. Without erbium doping, the diode characteristics were good, Figure 5b, and the diode showed 970 nm emission with optical or electrical excitation. With erbium doping, (Figure 5c), the diode characteristics were poor (leaky) but showed 1538 nm emission with optical pumping and 860 nm emission with electrical pumping. The change in emitted wavelength is attributed to silicon and erbium atoms shifting the junction location away from the quantum well into the GaAs confinement layers, thereby altering the effective bandgap.

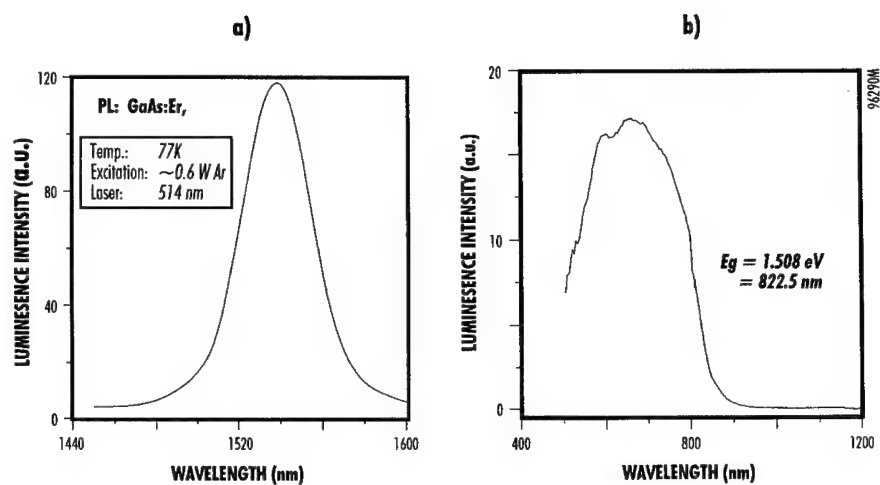


**Figure 4** Photoluminescence spectra of GaAs sample doped with erbium amide (a) and photoluminescence excitation spectra (b) showing variation of 1538 nm signal with excitation wavelength.

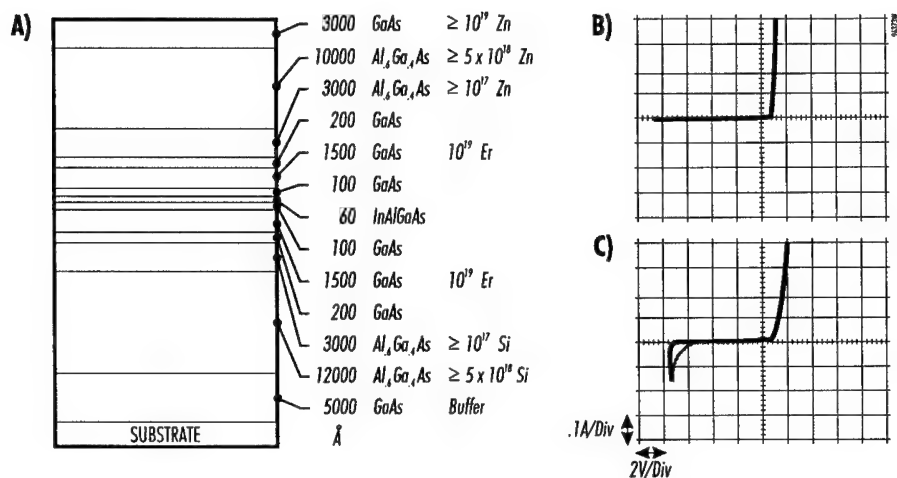


**Figure 5** Design of 970 nm laser diode used to test electroluminescence of erbium doping (a), and diode characteristics without erbium doping (b) and with erbium doping (c).

## CONCLUSIONS

We have shown that MOCVD of erbium-doped GaAs or AlGaAs, using silyl-amide sources, can result in lower carbon and oxygen content than the use of beta-diketonates or cyclopentadienyl sources. Silicon concentration in the films was temperature dependent. Low-defect, epitaxial films with substitutional dopant were obtained for erbium concentrations less than  $10^{19} \text{ cm}^{-3}$ . Photoluminescence (data not shown) was enhanced by post-CVD annealing in a hydrogen-arsine ambient at  $800^\circ\text{C}$ . Photoluminescent excitation (PLE) spectra at optical wavelengths strongly suggest that recombination of electron-hole pairs at the erbium defect site gave rise to excited levels in the erbium ion and 1538 nm emission. Oxygen co-doping to the same concentration as erbium may have contributed to enhanced photoluminescence as observed by Colon [7], but it also may have caused the high leakage current of the diodes and may have prevented electroluminescence.

## ACKNOWLEDGMENTS

This research was funded by the Ballistic Missile defense Organization and monitored by the Air Force Office of Scientific Research, Contract Number F499620-93-C-0069.

## REFERENCES

1. S.J. Cang and K. Takehei, *Appl. Phys. Lett.* **65**, 433 (1994).
2. D.W. Elsaesser, Y.K. Yeo, R.L. Hengehold, K.R. Evans, and F.L. Pedrotti, *J. Appl. Phys.*, **77**, 3919 (1995).
3. D.W. Elsaesser *et al.*, *J. Crys. Growth*, **127**, 707 (1993).
4. K. Tyakahei, A. Taguchi, Y. Horikoshi and J. Nakata, *J. Appl. Phys.*, **76**, 4332 (1994).
5. W.S. Rees, Jr., U.W. Lay, and A.C. Greenwald in Gas Phase and Surface Chemistry in Electronic Materials Processing, ed. T. J. Mountziaris *et al*, Mat. Res. Soc. Symp. Proc. **334**, (Mat. Res. Soc., Pittsburgh, PA 1994), p.207.
6. S.M. Vernon *et al.*, Proc. of 6th Int. Conf. on Indium Phosphide and Related Materials (Institute of Electrical and Electronic Engineers, cat. #94CH3369-6, New York, 1994). p137.
7. J.E. Colon, D.W. Elsaesser, Y.K. Yeo, R.L. Hengehold and G.S. Pomrenke, *Appl. Phys. Lett.* **63**, 216 (1993).

## NEODYMIUM AND ERBIUM IMPLANTED GaN

E. SILKOWSKI,\* Y. K. YEO,\* R. L. HENGHOLD,\* B. GOLDENBERG,\*\* and G. S. POMRENKE\*\*\*

\*Air Force Institute of Technology, Wright-Patterson AFB, OH 45433

\*\*Honeywell Technology Center, Bloomington, MN 55420

\*\*\*Advanced Research Projects Agency, Arlington, VA 22203

### ABSTRACT

Strong rare earth (RE) emissions from Nd and Er implanted into MOCVD grown GaN were observed through photoluminescence (PL) with below bandgap excitation from an Ar<sup>+</sup> laser. Three well resolved manifolds of 4f lines from the crystal-field split  $^4F_{3/2} \rightarrow ^4I_{9/2}$ ,  $^4F_{3/2} \rightarrow ^4I_{11/2}$ , and  $^4F_{3/2} \rightarrow ^4I_{13/2}$  transitions of Nd<sup>3+</sup> were observed at low temperature at  $\sim 0.98$ ,  $\sim 1.14$ , and  $\sim 1.46$   $\mu\text{m}$ , respectively. The Er implanted GaN showed both the  $^4I_{13/2} \rightarrow ^4I_{15/2}$  Er<sup>3+</sup> transition at  $\sim 1.54$   $\mu\text{m}$  and the  $^4I_{11/2} \rightarrow ^4I_{13/2}$  Er<sup>3+</sup> transition at  $\sim 1.00$   $\mu\text{m}$ . The Er luminescence at  $\sim 1.54$   $\mu\text{m}$  and Nd luminescence at  $\sim 1.1$   $\mu\text{m}$  persisted to room temperature. Both Er and Nd implanted samples showed increasing RE<sup>3+</sup> signal as annealing temperature increased from 700 to 1000 °C. The growth of new 4f crystal-field split-lines in the  $\sim 1.54$   $\mu\text{m}$  Er<sup>3+</sup>  $^4I_{13/2} \rightarrow ^4I_{15/2}$  manifold as annealing temperature was increased to 1000 °C suggests multiple Er<sup>3+</sup> radiative centers.

### INTRODUCTION

Several groups studying the  $\sim 1.54$   $\mu\text{m}$  Er<sup>3+</sup> emissions in semiconductor hosts have suggested that the thermal quenching of RE<sup>3+</sup> emissions decreases with increasing bandgap [1, 2]. Thus, the relatively wide 3.4 eV room temperature bandgap of GaN makes it an attractive semiconductor for producing room temperature RE luminescent devices. Recently, ion implanted GaN has attracted attention as improvements in growth processes have made high quality GaN more readily available [3, 4]. Several groups have now reported room temperature  $\sim 1.54$   $\mu\text{m}$  Er<sup>3+</sup> luminescence from Er implanted GaN co-implanted with oxygen [5, 6]. This paper reports the results of PL studies on GaN implanted with Er without oxygen co-implantation along with the PL results of Nd implanted GaN.

### EXPERIMENT

GaN was grown on sapphire by MOCVD [7]. The samples were implanted at room temperature with the energies and doses listed in Table I. Annealing was performed in a conventional tube furnace at temperatures ranging from 700 to 1000 °C for 90 min under an atmosphere of flowing NH<sub>3</sub>. Previous results with other implanted species in GaN indicated that surface damage occurred for temperatures above 1000 °C [8], thus no samples were annealed above this temperature. To further guard against sample degradation during annealing, the proximity cap method was used.

Photoluminescence was performed using an Ar<sup>+</sup> laser operating below the GaN bandgap on the 514.5 nm line. A SPEX 3/4-meter spectrometer with a liquid nitrogen cooled Ge detector was used to collect the luminescence signal. The temperature of the sample could be varied from 2 to 300 K by placing the sample in a temperature controlled optical cryostat. The spectra were not corrected for system response.

**Table I.** Er and Nd implantation energy and dose. The projected range and peak concentration were calculated using the PROFILE Code [9].

Species	Energy (keV)	Dose (cm <sup>-2</sup> )	Range (Å)	Peak Conc. (cm <sup>-3</sup> )
Er	1150	$1 \times 10^{13}$ , $5 \times 10^{13}$	1644	$9.8 \times 10^{17}$ , $4.9 \times 10^{18}$
Nd	910	$1 \times 10^{13}$ , $5 \times 10^{13}$	1623	$8.9 \times 10^{17}$ , $4.4 \times 10^{18}$

## RESULTS AND DISCUSSION

Low temperature PL performed on both Nd and Er implanted GaN annealed at 1000 °C revealed strong luminescence emissions from crystal-field split intra-4f shell transitions associated with RE<sup>3+</sup> as shown in Figure 1. Also present was an intense broad peak which was identical in

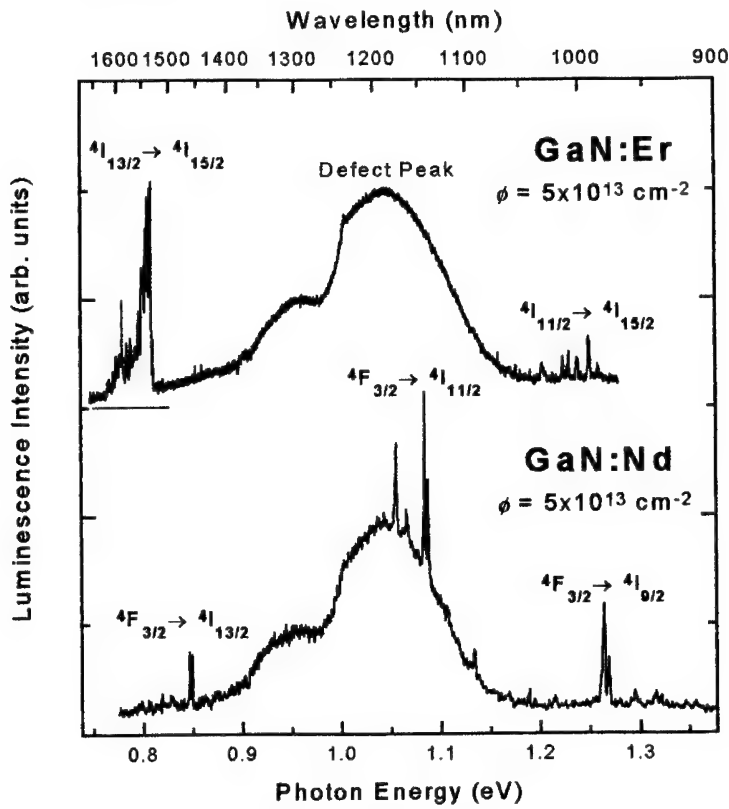


**Figure 1.** Low Temperature Photoluminescence Taken at 2 K from Er or Nd Implanted MOCVD GaN at a Dose of  $5 \times 10^{13}$  cm<sup>-2</sup> and Annealed at 1000 °C for 90 min.

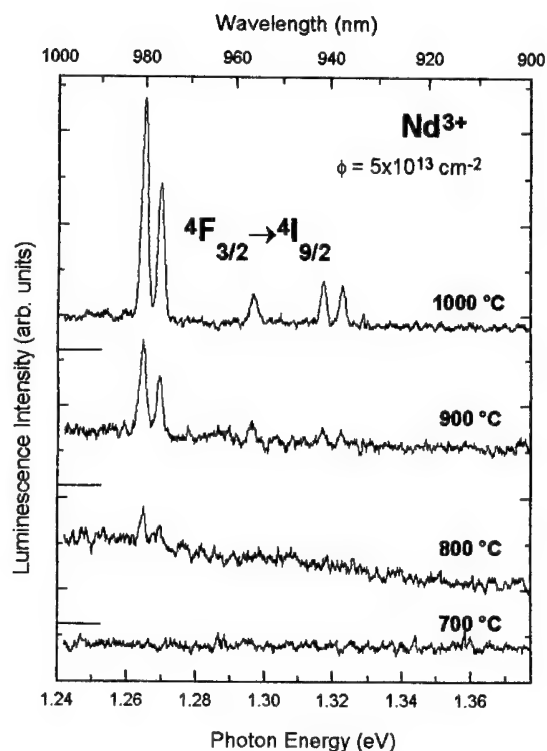


Figure 2. Annealing Temperature Dependence PL Study of Nd Implanted GaN Taken at 2 K.

observed from the 800 °C annealed sample, and the luminescence signal increased in intensity for the 900 and 1000 °C anneals. Since identical peaks were observed in all samples annealed at different annealing temperatures, only one  $\text{Nd}^{3+}$  radiative center is likely. Identical annealing temperature dependence behavior was also observed for the  ${}^4\text{F}_{3/2} \rightarrow {}^4\text{I}_{13/2}$  manifold at 1.46-1.57  $\mu\text{m}$  and the  ${}^4\text{F}_{3/2} \rightarrow {}^4\text{I}_{11/2}$  manifold at 1.09-1.20  $\mu\text{m}$ . 1000 °C was the optimal annealing temperature for all manifolds of  $\text{Nd}^{3+}$ .

Similar annealing results were observed from Er implanted GaN which is shown in Figure 3. The  $\text{Er}^{3+} {}^4\text{I}_{13/2} \rightarrow {}^4\text{I}_{15/2}$  transitions at  $\sim 1.54 \mu\text{m}$  appeared in all samples, and increased in intensity as annealing temperature was increased from 700 to 1000 °C. The luminescence associated with the  $\text{Er}^{3+} {}^4\text{I}_{11/2} \rightarrow {}^4\text{I}_{15/2}$  transition at  $\sim 1.0 \mu\text{m}$  was not observed from the 700 °C annealed sample, but appeared in the 800 °C annealed sample. The PL signal at  $\sim 1.0 \mu\text{m}$  also increased in intensity with annealing temperature through 1000 °C.

Figure 3 clearly shows the appearance and growth of several strong luminescence peaks in Er implanted GaN as annealing temperature is increased. Although there was no change in the emission peak positions as the annealing temperature increases from 700 to 1000 °C, the relative intensity among the PL peaks varied. These significant changes in relative intensity among different luminescence peaks after annealing at different temperatures indicate that these emissions

both Nd and Er implanted GaN. This peak was not present in unimplanted material, and could therefore be associated with implantation damage. Similar damage related peaks have been reported for other III-V materials implanted with RE ions [10]. The sharp drop-off in this defect peak at 1.25  $\mu\text{m}$  is believed to be an artifact of the diffraction grating which was blazed at 1.25  $\mu\text{m}$ .

Annealing studies were performed on both Nd and Er implanted GaN to determine the optimal annealing temperature for activation of the  $\text{RE}^{3+}$  intra-4f shell luminescence. Prior to annealing, no luminescence could be observed from the as-implanted samples for either species. Figure 2 shows the  $\text{Nd}^{3+}$  peaks observed at 2 K from the  ${}^4\text{F}_{3/2} \rightarrow {}^4\text{I}_{9/2}$  manifold at 0.93-0.98  $\mu\text{m}$ . The 700 °C annealed sample showed no  $\text{Nd}^{3+}$  luminescence. Weak  $\text{Nd}^{3+}$  luminescence was



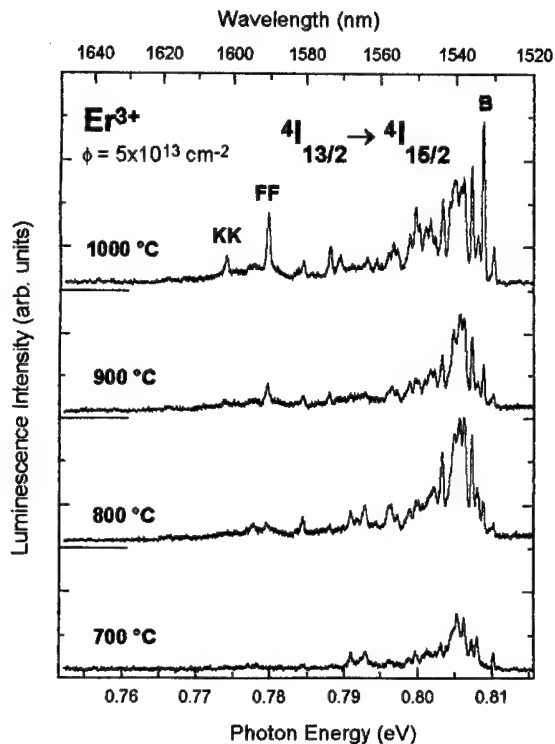


Figure 3. Annealing Temperature Dependence PL Study of Er Implanted GaN Taken at 2 K.

~1.54  $\mu\text{m}$  luminescence from GaN:Er co-implanted with oxygen decreased with annealing temperature above 700  $^{\circ}\text{C}$ . One possible explanation for these differing results is that oxygen and erbium interact to form a different RE luminescent complex center, which becomes optically active at lower annealing temperature. However, a further investigation is necessary before a definite conclusion can be drawn.

We have also investigated PL spectra taken at room temperature for both Nd and Er implanted GaN. For the Nd implanted samples, only luminescence from the  $^4\text{F}_{3/2} \rightarrow ^4\text{I}_{11/2}$  manifold was observed at room temperature. Furthermore, at 300 K, luminescence from lines at higher energy within the manifold were only observed as shown in Figure 4. However, no shift in the energetic locations of luminescence lines occurred. The other two manifolds quenched rapidly as the sample temperature was raised above 50 K.

The results of  $\text{Er}^{3+}$  PL spectra taken at room temperature are plotted in Figure 5, showing that the  $\text{Er}^{3+} ^4\text{I}_{13/2} \rightarrow ^4\text{I}_{15/2}$  luminescence persisted to room temperature. New, higher energy lines appeared as the sample temperature was increased showing the existence of 'hot' lines. Figure 5 also clearly shows that the relative intensity among PL peaks varied, implying multiple luminescence centers in GaN:Er. The integrated intensity of the entire manifold dropped by less than 50 % as temperature increased from 2 K to 300 K. 'Hot' lines were also observed in the

originated from more than one  $\text{Er}^{3+}$  luminescence center [11]. However, the peaks, labeled B, FF, and KK, were observed to grow strongly in intensity as annealing temperature was increased. Furthermore, this set of peaks grew at the same rate in PL intensity as the anneal temperature was increased. This result indicates that this set of peaks are likely of common origin.

The results of the current study indicate that a 1000  $^{\circ}\text{C}$  annealing temperature was optimal for optical activation of both Nd and Er implanted GaN. This result was similar to our observations of annealing temperature dependence for other species implanted into GaN [8], where it had been reported that 1000  $^{\circ}\text{C}$  annealing for 90 min produced the best recovery of implantation related damage, and the strongest luminescence from ion implanted GaN. In contrast to our results, Wilson *et al.* [5] reported that the

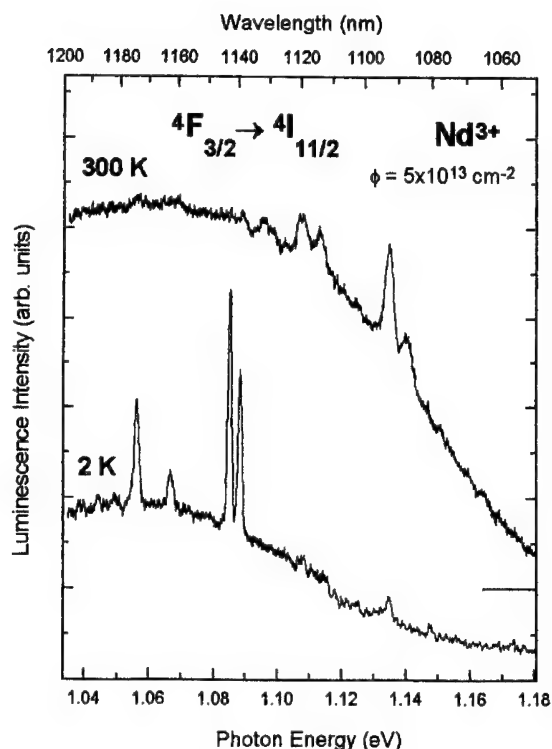


Figure 4. Photoluminescence of the  $\text{Nd}^{3+} {}^4\text{F}_{3/2} \rightarrow {}^4\text{I}_{11/2}$  Manifold Recorded at Room Temperature and Low Temperature Showing the Presence of 'Hot' Lines.

samples. However, the intensity of the main peak in each manifold was increased about three to five times for the higher dose samples. Since the difference in the two doses was a factor of five, it is believed that the doses selected have not exceeded the solubility limit of the RE in GaN.

## CONCLUSIONS

Well resolved  $\text{RE}^{3+}$  crystal-field split intra-4f shell emissions were observed by low temperature PL from both Nd and Er implanted GaN without oxygen co-doping. The strongest  $\text{Nd}^{3+}$  luminescence was observed from the  ${}^4\text{F}_{3/2} \rightarrow {}^4\text{I}_{11/2}$  manifold at  $\sim 1.14 \mu\text{m}$ , but other emissions were also observed from the  ${}^4\text{F}_{3/2} \rightarrow {}^4\text{I}_{9/2}$  manifold at  $\sim 0.98 \mu\text{m}$  and from the  ${}^4\text{F}_{3/2} \rightarrow {}^4\text{I}_{13/2}$  manifold at  $\sim 1.46 \mu\text{m}$ . The  $\text{Er}^{3+} {}^4\text{I}_{13/2} \rightarrow {}^4\text{I}_{15/2}$  transitions at  $\sim 1.54 \mu\text{m}$  were strongest, and the  ${}^4\text{I}_{11/2} \rightarrow {}^4\text{I}_{15/2}$  transitions at  $\sim 1.0 \mu\text{m}$  were also observed. In both rare earth cases, the  $\text{RE}^{3+}$  emissions showed the wavelength independence with sample temperature that is characteristic of the intra-4f shell emissions in semiconductors. 'Hot' lines were observed for all manifolds. Higher dose resulted in greater  $\text{RE}^{3+}$  intensity with identical  $\text{RE}^{3+}$  luminescence centers. The  $\text{RE}^{3+}$  emission intensity of both Nd and Er increased with annealing temperature up to  $1000^\circ\text{C}$ . Although Nd implanted

other  $\text{Er}^{3+} {}^4\text{I}_{11/2} \rightarrow {}^4\text{I}_{13/2}$  manifold as sample temperature was increased to 25 K, but the luminescence was almost completely quenched by 175 K.

The energetic positions of the  $\text{Er}^{3+}$  and  $\text{Nd}^{3+}$  transitions remained constant with sample temperature up to 300 K. This demonstrates that the 4f shells of each ion were well shielded from the GaN crystalline field environment. However, the observed number of  $\text{Er}^{3+}$  PL peaks due to crystal-field splittings was indicative of the existence of non-cubic site occupancy by  $\text{Er}^{3+}$ .

Since only two different doses were implanted for both Nd and Er, limited comparisons of dose dependence were possible. All sets of lines were observed in both doses and showed identical annealing temperature dependence. Apart from the total intensity of the  $\text{RE}^{3+}$  related luminescence, no changes in the manifolds were observed from different dose

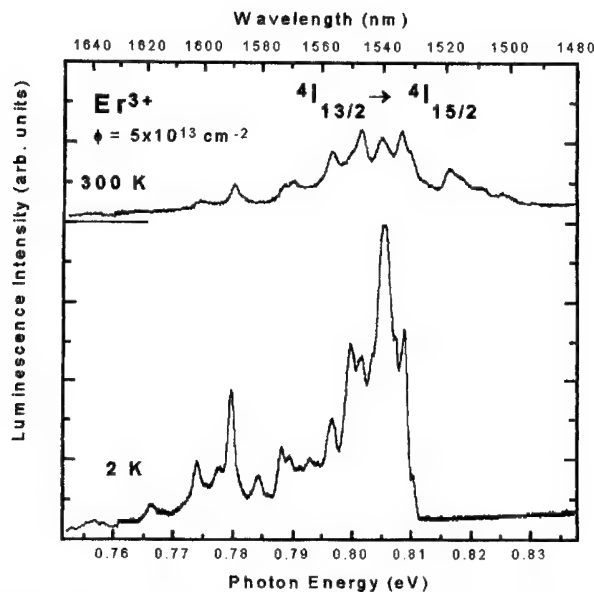


**Figure 5.** Photoluminescence Spectra of  $\text{Er}^{3+} 4I_{13/2} \rightarrow 4I_{15/2}$  Manifold Recorded at Room Temperature and Low Temperature Showing Evidence of 'Hot' Lines.

GaN showed evidence of only one type of  $\text{Nd}^{3+}$  luminescence center, the Er implanted GaN showed evidence of multiple Er luminescence centers.

## REFERENCES

1. P. N. Favennec, H. L'Haridon, M. Salvi, D. Moutonnet, and Y. Le Guillou, *Electron. Lett.* **25**, 718 (1989)
2. A. J. Neuhalfen and B. W. Wessels, *Appl. Phys. Lett.* **60**, 2657 (1992)
3. R. G. Wilson, S. J. Pearton, C. R. Abernathy, and J. M. Zavada, *Appl. Phys. Lett.* **66**, 2238 (1995)
4. S. J. Pearton, C. B. Vartuli, J. C. Zolper, C. Yuan, and R. A. Stall, *Appl. Phys. Lett.* **67**, 1435 (1995)
5. R. G. Wilson, R. N. Schwartz, C. R. Abernathy, S. J. Pearton, N. Newman, M. Rubin, T. Fu, and J. M. Zavada, *Appl. Phys. Lett.* **65**, 992 (1994)
6. C. H. Qiu, M. W. Leksono, J. I. Pankove, J. T. Torvik, R. J. Feuerstein, and F. Namavar, *Appl. Phys. Lett.* **66**, 562 (1995)
7. B. Goldenberg, J. D. Zook, and R. J. Ulmer, *Appl. Phys. Lett.* **62**, 381 (1993)
8. E. Silkowski, Y. K. Yeo, R. L. Hengehold, M. A. Khan, T. Lei, K. Evans, and C. Cerney in Gallium Nitride and Related Materials: The First International Symposium on Gallium Nitride and Related Materials, edited by R. D. Dupuis, J. A. Edmond, F. A. Ponce, and S. Nakamura (Mater. Res. Soc. **395**, Pittsburg, PA 1995)
9. PROFILE Code Version 2.1, Implant Sciences Corp., Danvars, MA (1988)
10. D. W. Elsaesser, Y. K. Yeo, R. L. Hengehold, K. R. Evans, and F. L. Pedrotti, *J. Appl. Phys.* **77**, 3919 (1995)
11. J. E. Colon, D. W. Elsaesser, Y. K. Yeo, R. L. Hengehold, and G. S. Pomrenke, *Appl. Phys. Lett.* **63**, 216 (1993)

## OPTICAL CENTERS RELATED TO LASER-DOPED ERBIUM IN SILICON

K. NAKASHIMA, O. ERYU, O. IIOKA, H. MINAMI, M. WATANABE\*

E and C Department, Nagoya Institute of Technology, Showa-ku, Nagoya 466, Japan,  
nakasima@elcom.nitech.ac.jp

\*Ion Engineering Research Institute Corporation, Tsuda, Hirakata, Osaka, Japan

### ABSTRACT

Excimer laser irradiation has been applied to dope erbium ions in silicon. Er-doping is realized with both processes of the Er-diffusion in the melted region and the subsequent solid solidification. Er atoms at the maximum concentration of  $10^{21} \text{ cm}^{-3}$  are doped in the region of 150 nm thickness without significant defect formation and amorphization. Stable Er-optical centers, emitting well known series of luminescence lines near 1.54  $\mu\text{m}$ , are formed after short term heat treatments at a relatively low temperature. Optical centers are distributed in proportional to the total Er concentration in the doped region. Oxygen atoms are found to play critical roles for stabilizing Er-optical centers and for rearranging the surroundings of Er ions. Modified bonding states of O and Er other than those in  $\text{SiO}_2$  or  $\text{Er}_2\text{O}_3$  are formed in the Er doped region during both doping and annealing processes.

### INTRODUCTION

Although stimulated efforts are devoted to enhance the luminescence intensity from Er ions doped in silicon, it is still necessary to improve several aspects until silicon-based light emitting devices come to practical use. Especially the increase in both the emission efficiency and the density of optical centers is an urgent problem to be solved. Ion implantation is a practical method to profile a desired Er ion distribution, but amorphization due to implanted ions sets the upper limit of Er concentration [1]. To improve the crystalline quality needs heat treatments at higher temperatures, but this is not desirable for device processes. It is essential to make clear the origin of the optical centers for the high emission efficiency.

In this paper we describe on the properties of Er-optical centers created by the laser-doping technique. Er-doping has been done in the liquid phase regime. The Er concentration well above the solid solubility [2] has been easily attained by both processes of the impurity-diffusion in the melted region and the subsequent solid solidification. As revealed by Rutherford backscattering spectroscopy (RBS) and channeling, and also by photoluminescence measurements, the laser doping method is a defect-free technique and needs no heat treatments to restore the crystalline quality. Here we adopted two types of doping methods which could control the oxygen concentration during the Er-doping process. It is found that the oxygen concentration determines not only the Er-related luminescence intensity, but also the emission spectrum. New bonding states of O and Er other than  $\text{SiO}_2$  and  $\text{Er}_2\text{O}_3$  are found to be formed in the Er-doped region.

### EXPERIMENTAL

Phosphorous-doped floating-zone (FZ) Si with a resistivity of 15  $\Omega\text{cm}$  was used as starting materials. We selected these materials to avoid the influence of the oxygen contained in the bulk. Two kinds of methods to dope Er into Si are investigated; firstly (a conventional method), erbium with 4 nines purity was deposited on cleaned mirror Si surfaces in a vacuum at  $5 \times 10^{-6}$  Torr, and then one shot of an excimer laser (wave length; 248 nm, pulse width; 20 ns) was incident on the

Er-deposited surface, which was set in a cryostat evacuated to  $2 \times 10^{-6}$  Torr. The laser energy density on the surface was fixed at about  $1 \text{ J/cm}^2$  which was large enough to melt the surface. Under these conditions a flat surface was kept after laser irradiation. The deposited Er-film was quickly transformed to erbium oxides when exposed to the air before laser irradiation. Therefore, oxygen atoms exceeding  $10^{21} \text{ cm}^{-3}$  were doped simultaneously in the same region as that of Er. Secondly, a single laser shot was incident on the sample surface during the Er-deposition process in a vacuum at  $1 \times 10^{-6}$  Torr ( hereafter referred to the in situ method ). This doping process could greatly reduce the oxygen concentration in the Er-doped region. All measurements such as photoluminescence (PL), RBS and x-ray photoelectron spectroscopy (XPS) were made after rinsing the samples with 1 % HF solution.

He ion backscattering and channeling ( usually along the  $\langle 111 \rangle$  direction ) were measured to reveal Er profiles using a three-axis goniometer with the 0.01 degree angle resolution. To enhance the yield of oxygen atoms we have made the He ion resonant backscattering and channeling measurements, which give rise to the O scattering cross section about 10 times larger than that for the ordinary backscattering. By this technique it is possible to detect about  $10^{20}$  oxygen atoms  $\text{cm}^{-3}$ . Unless otherwise mentioned, erbium has been doped by the conventional method. The  $\chi_{\min}$  value of the scattering yield for non-doped and Er-doped Si are 2 and 10 %, respectively. The increase in the  $\chi_{\min}$  for Er-doped Si mainly comes from He ion scattering due to the high concentration of Er in the surface region. The core-electron binding energies were measured by XPS using the  $\text{AlK}\alpha$  radiation as an excitation source. The absence of a charging effect was confirmed by neutralizing samples by an electron shower. The oxygen 1s, erbium 4f and silicon 2p spectra were monitored in both Er-doped samples, and the  $\text{SiO}_2$  and  $\text{Er}_2\text{O}_3$  films as references.

Photoluminescence was excited with the 514.5 nm line from an Ar ion laser (100 mW at the sample surface), and detected with a Ge diode cooled at liquid nitrogen temperature. The PL intensity profiles were measured after step-by-step etching of anodic oxides by the amount 20 nm thick.

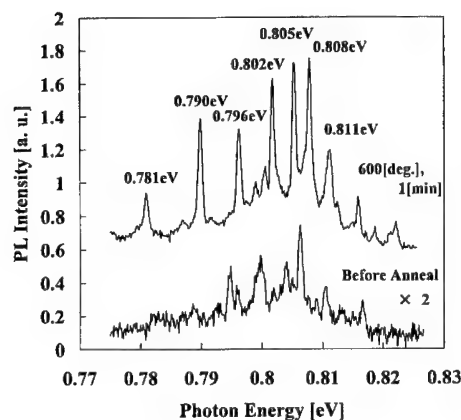


Fig.1 Photoluminescence spectra of Er ion-doped Si before and after (600°C for 1 min) annealing. Measured at 77K.

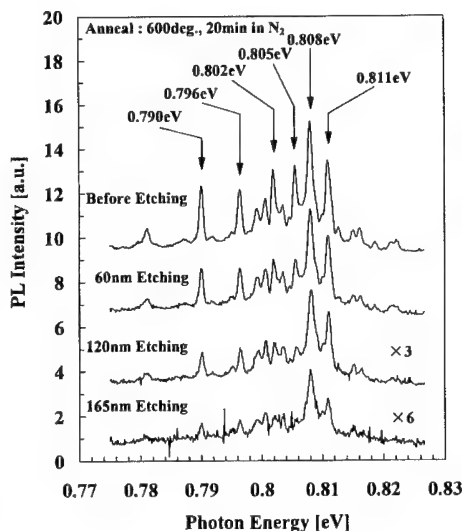


Fig.2 Photoluminescence spectra after several oxidation and etching steps. Annealed at 600°C for 20 min. Measured at 77K.

## RESULTS AND DISCUSSION

### Photoluminescence Spectra and Spatial Distribution of Er-Optical Centers

Figure 1 shows the typical photoluminescence spectra of an Er-doped sample before and after annealing. The sample was doped with the conventional method mentioned in the previous section, and was annealed in a gold image furnace purged with the nitrogen gas at 600 °C for 1 min. Detailed assignment of the spectra of the annealed sample along with the scheme given by Tang et al.[3] will be published in a separated paper; the peak at 0.808 eV corresponding to the characteristic transition between the first excited state  $^4I_{13/2}$  and the ground state  $^4I_{15/2}$ , peaks at 0.805, 0.790 and 0.781 eV representing luminescence from centers at non-cubic symmetry sites, and 0.796 and 0.787 eV from those at cubic symmetry sites. In addition, luminescence bands from unknown Er-centers are presented at 0.811, 0.802 eV and so on. Evidently, the annealing process not only increases the luminescence intensity, but also rearranges the spectra to a well-behaved one. As stated earlier, oxygen as high concentration as about  $10^{21} \text{ cm}^{-3}$  has been co-doped in the same region as that of Er. We will show in the later section that a sufficient amount of oxygen is necessary for stable optical centers to be created.

In order to investigate the spatial distribution of optical centers, a thin layer of Er-doped region was removed both with anodic oxidization in a solution of N-methylacetamide,  $\text{KNO}_3$  and  $\text{H}_2\text{O}$  and with etching in a 5 % HF solution. A uniform layer 20 nm thick was removed off at one time. Fig.2 shows the PL spectra after several etching processes. The thickness removed is attached to the respective spectra. As noted clearly, each spectral line remains at the same position, which suggests that the same kinds of optical centers are created throughout the Er-doped region. When the top layer 20 nm thick was etched off, the PL intensity increased possibly due to removal of a defective layer produced by the Er-doping process. Similar photoluminescence spectra is persistent to the depth of 165 nm, which corresponds to the tail of the doped region. The differential PL intensity emitted from the removed layer, which is the difference of the total PL intensity of all emission peaks observed after each etching step, is shown in Fig.3 against the depth from the surface. The spatial distribution of the PL intensity is roughly similar to the concentration distribution of Er, which is estimated from the RBS data. This result shows that a definite fraction

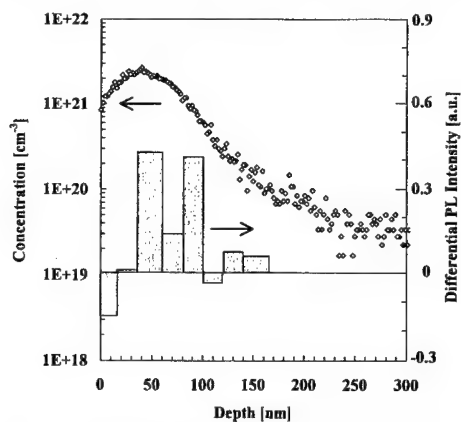


Fig.3 Spatial distribution of Er ions and the PL intensity for the sample shown in Fig.1.

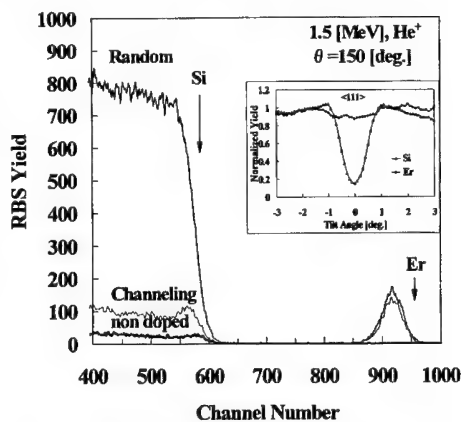


Fig.4 RBS and channeling spectra after annealing of an Er-doped sample. The inset shows the angular scan across the  $\langle 111 \rangle$  axis.

of doped Er atoms could be transformed to optically active centers through heat treatments possibly due to the combination of Er and O.

Figure 4 shows results of 1.5 MeV He ion RBS measurements ( the scattering angle:  $150^\circ$  ), in which thin and very thick lines show the channeling spectra for an annealed sample after Er-doping and a non-doped sample as a reference, respectively. Er atoms are found in the range of 130 nm with the maximum concentration  $1 \times 10^{21} \text{ cm}^{-3}$  at the depth of 60 nm. By the annealing the Er channeling yield decreases to 85 % from 95 % of as-doped samples. In the inset of the figure are shown angular scans across the  $\langle 111 \rangle$  axis for Er and for Si in the Er-doped region. A major fraction of Er atoms are located in the  $\langle 111 \rangle$  channel, while about 10 % of Er atoms are aligned along the  $\langle 111 \rangle$  atomic row by the heat treatments. The melt time of the Si substrate during the Er-doping process was estimated to be about 200 ns from measurements of the reflection of a He-Ne laser probe beam. Substituting 250 nm for the doping depth  $l$  (Fig.3) and 200 ns for  $t$  in the relation  $l = \sqrt{Dt}$ , we obtained a diffusion constant  $D = 3 \times 10^{-3} \text{ cm}^2/\text{s}$ , which is the same order as diffusion constants of impurities in the melt solution[4]. We come to the conclusion that Er atoms diffuse through the melt Si substrate, and remain there beyond the solubility limit on account of rapid solidification. A fraction of the doped Er atoms are aligned along the  $\langle 111 \rangle$  direction by the interaction of the oxygen atoms nearby during the annealing process.

#### Effect of oxygen on optical centers

In order to get insight on the effect of O on the formation of Er-optical centers, Er was doped by the in situ doping method mentioned previously, where the all doping processes were done in a vacuum at  $1 \times 10^{-6}$  Torr. As expected, the oxygen concentration was reduced below the detection limit by the conventional RBS measurements. The resonant RBS and channeling measurements of O were performed using a 2.96 MeV He ion beam at the scattering angle of  $170^\circ$ . A slight RBS yield of O could be detected in the  $\langle 111 \rangle$  aligned spectra as shown in Fig.5(a), corresponding to the oxygen concentration of  $1.8 \times 10^{21} \text{ cm}^{-3}$  at the maximum, which is about 1/4 times that for the ordinary doping method. Annealing in a vacuum at  $1 \times 10^{-6}$  Torr did not induce any change in the oxygen concentration. Figure 5(b) shows the resonant RBS and channeling spectra after annealing at  $600^\circ \text{C}$  for 1 min in a nitrogen gas ambient. It is clearly noted that the oxygen concentration

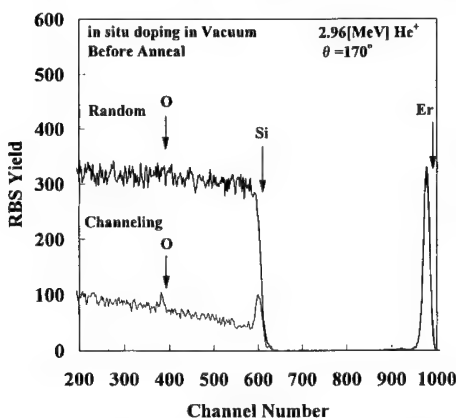


Fig.5(a) Resonant RBS and channeling spectra for a sample doped by the in situ method. All doping procedures were done in a vacuum.

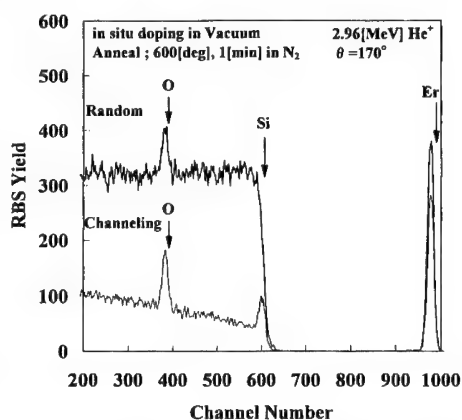


Fig.5(b) Resonant RBS and channeling spectra for an in situ doped sample annealed in the nitrogen gas ambient ( $600^\circ \text{C}$ , 1 min).

increases to  $6 \times 10^{21} \text{ cm}^{-3}$ , and the channeling yield of Er decreases by an amount of 27 %. Residual oxygen atoms in the nitrogen gas are possibly absorbed by doped Er atoms. The photoluminescence spectra measured in the similar samples to those in Fig.5(a) and (b) are presented in Fig.6. The PL spectra for an as-doped sample and after annealing in a vacuum did not show any differences in the spectral shape and the intensity. This behavior is possibly ascribed to the lack of the amount of the O concentration. The substantial amount of oxygen atoms supplied during the annealing process seems to promote the formation of optically active centers. Although the spectral resolution is lower in this case, the spectra after annealing in the nitrogen gas ambient are completely coincident with those shown in Fig.1. These results shown in Figures 5 and 6 suggest that optical centers are complexes of Er bonded with nearby O.

Figure 7(a) shows results of XPS measurements of the oxygen 1s spectra for an Er-doped sample annealed at 600°C as a function of the thickness removed by Ar ion sputtering. The number 0 nm means the top surface. In the upper part of the figure, the oxygen 1s spectra for the erbium oxide film 200 nm thick deposited on the Si substrate are shown as references ( a thin solid line ). We are able to separate the experimental curve into 3 peaks; one at 533.0 eV from the silicon dioxide and the other two at 533.3 and 530.8 eV from the erbium oxide. Solid and dotted curves are calculated fittings assuming peak energies and the Gaussian shape. The electron binding energies agree well with reported values [5] within experimental errors. The surface of the Er-doped sample is covered with a thin silicon dioxide layer. The O 1s binding energy becomes smaller inside the bulk and approaches a constant energy 531.7 eV at the depth of 4 nm, which is the intermediate value between the silicon and erbium oxide. Fig. 7(b) shows the erbium 4f spectra, which is obtained by subtracting the intensity of the Si substrate from that of an Er-doped sample. Top curves show references of the Er 4f spectra for an erbium oxide with two peaks at 10.8 and 7.2 eV [5]. At the top surface of the Er-doped sample, the spectra is possibly thought to be due to the erbium oxide. The intensity becomes higher inside the bulk, and the Er 4f binding energy becomes smaller and approaches a constant value in the region deeper than 6 nm. The increase in the Er intensity is consistent to the Er-profile estimated by RBS measurements. The 4f electron binding energies 9.3 and 5.3 eV are approximately equal to those for metal Er[5]. These results

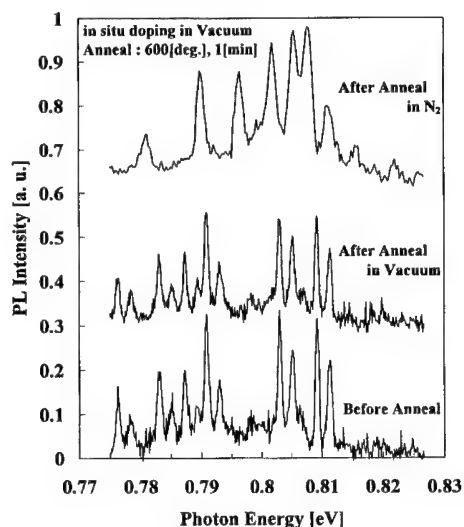


Fig.6 Photoluminescence spectra for the corresponding samples to those shown in Fig.5(a) and (b). All doping procedures were done in a vacuum. Annealing conditions: 600°C for 1 min. Measured at 77K



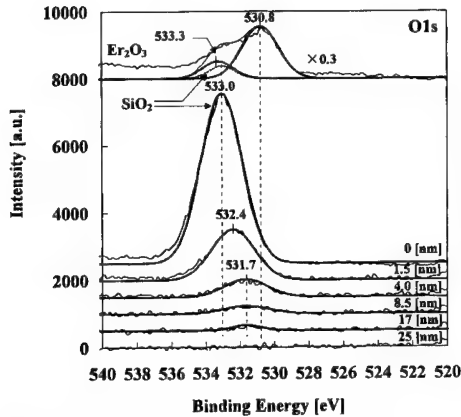


Fig.7(a) XPS spectra for O 1s electrons in an Er-doped and annealed sample. Top spectra of an erbium oxide for references.

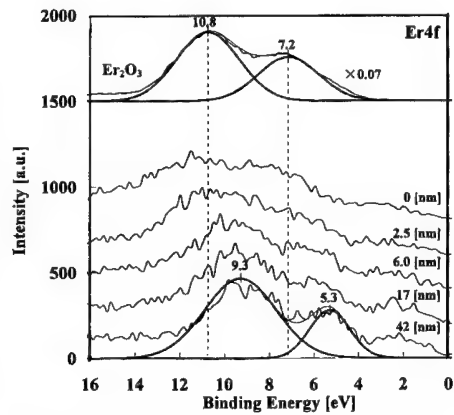


Fig.7(b) XPS spectra for Er 4f electrons of the same sample shown in Fig.7(a). Top spectra of an erbium oxide for references.

seem to suggest that a new bonding state of Er with O, which is different from that in  $\text{Er}_2\text{O}_3$ , is formed in the body of the Er-doped region.

## CONCLUSIONS

We have shown that the laser doping method using an excimer laser has advantages to dope more than  $10^{21}$  Er atoms  $\text{cm}^{-3}$  into the Si substrate without introducing significant damages in the doped region. A sufficient amount of oxygen is necessary for enhancing the Er-photoluminescence and for stabilizing Er-optical centers with the well-resolved 1.54  $\mu\text{m}$  luminescence bands. The oxygen concentration is about 5 times larger than the Er concentration in this case, which was determined quantitatively by the resonance RBS and channeling measurements. Optical centers have a similar intensity distribution profile to that of Er concentration, suggesting that the concentration of optical centers should reflect the total Er concentration. XPS measurements of the O 1s and Er 4f electron binding energies have revealed the possibility that a new bonding state of Er and O be formed in the Er-doped region.

## REFERENCES

1. A. Polman, J. S. Custer, E. Snoeks, and G. N. van den Hoven, *Appl. Phys. Lett.* **62**, p.507 (1993).
2. D. J. Eaglesham, J. Michel, E. A. Fitzgerald, D. C. Jacobson, J. M. Poate, J. L. Benton, A. Polman, Y.-H. Xie, and L. C. Kimmerling, *Appl. Phys. Lett.* **58**, p.2,797(1991).
3. Y. S. Tang, K. C. Heasman, W. P. Gillin, and B. J. Sealy, *Appl. Phys. Lett.* **55**, p.432(1989).
4. R. F. Wood, C. W. White, and R. T. Young, *Semiconductors and Semimetals*, Vol.23, Academic Press, Inc., 1984, pp.232-241.
5. B. D. Padalia, W. C. Lang, P. R. Norris, L. M. Watson, and D. J. Fabian, *Proc. R. Soc. Lond. A* **354**, p.269(1977).

## PHOTOLUMINESCENCE OF ERBIUM-DIFFUSED SILICON

H. HORIGUCHI\*, T. KINONE\*, R. SAITO\*, T. KIMURA\*, and T. IKOMA\*\*

\* University of Electro-Communications, Department of Electronic Engineering, Chofugaoka 1-5-1, Chofu, Tokyo 182, Japan

\*\*TI Tsukuba Research and Development Center Ltd., Tsukuba, Ibaragi, Japan

### ABSTRACT

Erbium films are evaporated on crystalline silicon substrates and are thermally diffused into silicon in an Ar+O<sub>2</sub> or H<sub>2</sub> flow. Very sharp Er<sup>3+</sup>-related luminescence peaks are observed around 1.54  $\mu$ m. The main peak as well as the fine structures of the luminescence spectra depend on the annealing atmosphere, suggesting different luminescence centers. The full width at half maximum (FWHM) of the main peaks is  $\leq 0.5$ nm at 20K. Thermal diffusion with Al films on top of the Er films is found to increase the intensity of the Er<sup>3+</sup>-related peaks greatly. The temperature dependence between 20 K and room temperature is relatively small, and a strong luminescence is obtained at room temperature.

### INTRODUCTION

How to incorporate rare-earth (RE) ions into semiconductors is one of the important factors for the luminescence of RE-doped semiconductors. The incorporation method affects greatly sites of RE ions in host semiconductors, ligand atoms, crystal fields and crystal defects in host semiconductors. As a result, it affects the luminescence efficiency, spectra, peak wavelength, FWHM, intensity, and thermal quenching.

Ion implantation [1], doping during crystal growth [2], electro-chemical doping into porous silicon layers with thermal treatments [3], and thermal diffusion [4-6], etc. have been used for the incorporation of RE ions into semiconductors. The above methods with the exception of thermal diffusion incorporate rare-earth ions into semiconductors under nonequilibrium conditions, and they sometimes show a number of RE-related luminescence peaks or broad bands due to the formation of different RE sites in the semiconductor lattice.

Zhao et al. have shown that thermal diffusion of Er into GaAs and InP [4] results in very sharp Er-related luminescence peaks at  $\sim 1.54$   $\mu$ m, and they ascribed the narrowness to the occupation of Er<sup>3+</sup> ions on the lattice sites, since thermal diffusion takes place under thermal equilibrium. Zhao [5] and Ren et al. [6] have diffused Er into Si and observed Er-related sharp luminescence peaks. Ren et al. have shown that the annealing atmosphere is very important for a strong luminescence of the Er-related peaks.

In thermal diffusion, the doping density cannot exceed the solubility limit of RE atoms in host semiconductors. In addition, the diffusion coefficient of Er in Si is low ( $\sim 10^{-14}$  cm<sup>2</sup>/s at 1000°C [7] and  $\sim 10^{-15}$  cm<sup>2</sup>/s at 900°C [8]) and it needs a long time and a high temperature to thermally diffuse a sufficient amount of Er ions deep into Si. M. Kechouane et al. [8] have reported that the presence of Al enhances greatly the Er thermal diffusion (2  $\mu$ m at 900°C for 2 hrs). They have grown Al:Er:O alloys in silicon by Al film evaporation, Er implantation and annealing in an O<sub>2</sub> atmosphere. They have observed a very broad luminescence around 1.54  $\mu$ m, but they have not obtained an enhancement in the luminescence intensity by Al.

In this paper we report on the Er-diffusion into crystalline silicon and on the observation of very sharp Er-related luminescence peaks with a small thermal quenching up to room temperature. We also report on the dependence of the luminescence spectrum on the annealing condition, as well as on a large enhancement in the luminescence intensity by Al.

## EXPERIMENTAL

Er films (e.g. 740 nm thick) are evaporated onto (100) Czochralski(CZ)-grown n-type Si(100) substrates with a resistivity of several  $\Omega\cdot\text{cm}$  (Er/Si samples). Samples with Al films (e.g. 610 nm thick) on top of Er/Si samples are also prepared (Al/Er/Si samples) with an intention of enhancing the Er diffusion. They are then annealed at 1100 °C for 2 to 24 hours in an Ar/O<sub>2</sub>(4 : 1) or pure H<sub>2</sub> flow. Thereafter, samples are immersed in HNO<sub>3</sub>/HCl(1:3) and in HF to remove remaining metals (Er, Al) and oxides.

Photoluminescence measurements are performed by illuminating the samples with Ar ion laser light (514.5 nm). The luminescence signal is monitored using a single-grating monochromator (Jobin-Yvon HR320) and a cooled germanium pin photodiode. The resolution is 0.48 nm.

## RESULTS

Fig.1a and b show the photoluminescence spectra of Er/Si samples at 20K annealed in an Ar+O<sub>2</sub> flow (Fig.1a) and a H<sub>2</sub> flow (Fig.1b) for 5 hours at 1100 °C, respectively. In both cases, sharp peaks are observed at around 1.54 $\mu\text{m}$  which are related to the Er 4f-4f transitions. However, the spectra are different between the two. Er/Si samples annealed in the presence of O<sub>2</sub> seem to show 7 broad luminescence bands in the 1.50 - 1.70 $\mu\text{m}$  region; at around 1.53 $\mu\text{m}$  (A), 1.55 $\mu\text{m}$  (B), 1.56 $\mu\text{m}$  (C), 1.566  $\mu\text{m}$  (D) 1.575  $\mu\text{m}$  (E), and 1.585 $\mu\text{m}$  (F), and 1.605 $\mu\text{m}$ (G). It is clearly seen that the A and B bands are composed by a number of sharp peaks, each with a relatively large base. The largest peak is at 1.5322 $\mu\text{m}$  (no.2) in the A band with an FWHM of 0.5 nm or less which is almost limited by the monochromator resolution and is among the narrowest ever observed in Er-doped Si. In the A band are also identified sharp peaks at 1.5310 $\mu\text{m}$  (no.1), 1.5338 $\mu\text{m}$  (no.3), 1.5346 $\mu\text{m}$  (no.4) etc. The 1.5346 $\mu\text{m}$  peak is strongest in samples annealed for 2 hours. The B band is characterized by a peak at 1.5509 $\mu\text{m}$  (no.7) and other peaks.

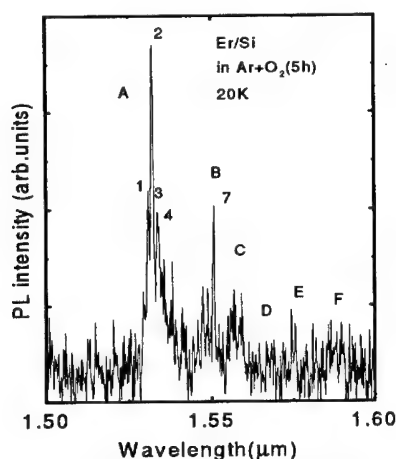


**Fig.1a** Photoluminescence spectrum of an Er/Si sample annealed at 1100 °C for 5 hours in an Ar+O<sub>2</sub> flow.

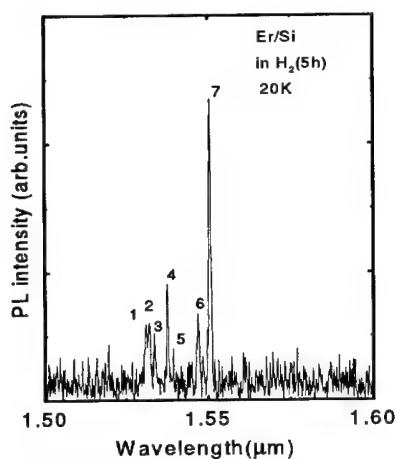


**Fig.1b** Photoluminescence spectrum of an Er/Si sample annealed at 1100 °C for 5 hours in a H<sub>2</sub> flow.

The photoluminescence of samples annealed in a  $H_2$  flow are characterized by a smaller number of sharp peaks in the A and B bands, with much smaller bases. The largest peak is the  $1.5509\mu m$  (no.7) peak in the B band with an FWHM of 0.5 nm. In the B band is also identified another peak at  $1.5469\mu m$  (no.6) at a medium intensity which cannot be clearly resolved in samples annealed in an  $Ar+O_2$  flow. In the A band are observed sharp peaks at  $1.5310\mu m$  (no.1),  $1.5322\mu m$  (no.2),  $1.5338\mu m$  (no.3),  $1.5375\mu m$  etc. Note that the intensity of the largest peak is nearly the same in both samples. Fig.1c shows the photoluminescence spectrum of samples which are annealed for 24 hours in a  $H_2$  flow. This long annealing in a  $H_2$  flow is found to make the largest  $1.5509\mu m$  peak of the B band more prominent and to suppress the peaks associated to the A band.

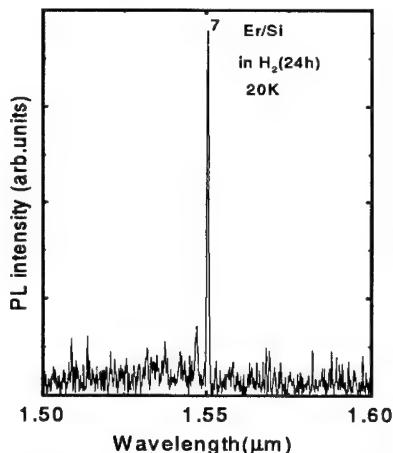


**Fig.1c** Photoluminescence spectrum of an Er/Si sample annealed at  $1100^\circ C$  for 24 hours in a  $H_2$  flow.

Fig.2 a and b show the photoluminescence spectra of Al/Er/Si samples at  $1100^\circ C$  for 5 hours in an  $Ar+O_2$  flow (Fig.2a) and a  $H_2$  flow (Fig.2b). Al films on top of the Er films are found to enhance the intensity of the luminescence peaks dramatically. In the case of annealing in an  $Ar+O_2$  flow, the largest  $1.5322\mu m$  peak as well as other peaks ( $1.5309\mu m$ ,  $1.5338\mu m$ ,  $1.5346\mu m$  etc. ) of the A band all increase in intensity by a factor of  $\sim 15$ . In contrast, the  $1.5509\mu m$  peak in the B band is increased in intensity

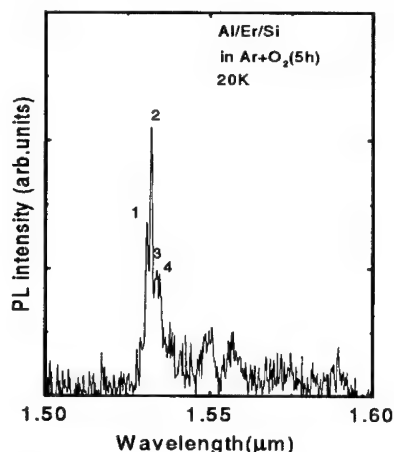


**Fig.2a** Photoluminescence spectrum of an Al/Er/Si sample annealed at  $1100^\circ C$  for 5 hours in an  $Ar+O_2$  flow.

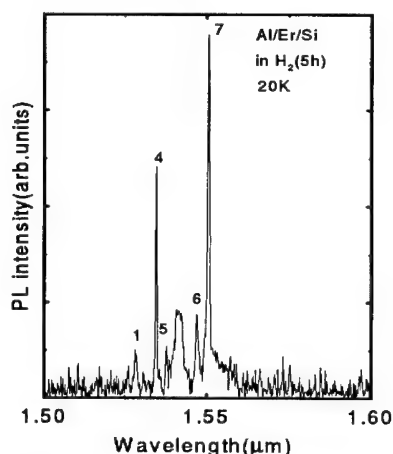


**Fig.2b** Photoluminescence spectrum of an Al/Er/Si sample annealed at  $1100^\circ C$  for 5 hours in a  $H_2$  flow.

by a factor of  $\sim 7$  and as a result the peaks of the A band are more prominent relative to the peaks of the B band.

In the case of annealing in a  $H_2$  flow, the largest peak at  $1.5509\mu m$  of the B band in Er/Si samples is increased in intensity by a factor of  $\sim 25$  by the presence of Al. Furthermore, the  $1.5346\mu m$  peak which is weak in the absence of Al becomes very strong. The  $1.5322\mu m$  peak which is the strongest in samples annealed in an Ar+ $O_2$  flow is hardly observed. These results are summarized in Table I.

Table I. Intensity enhancement of photoluminescence peaks by Al films on top of Er/Si samples

Anneal in Ar+ $O_2$ at 1100 °C for 5 hours					
band	no.	peak	without Al	with Al	intensity enhancement by Al
A	1	$1.5310\mu m$	medium	medium	$\times \sim 15$
	2	$1.5322\mu m$	very strong	very strong	$\times \sim 15$
	3	$1.5338\mu m$	medium	medium	$\times \sim 15$
	4	$1.5346\mu m$	medium	medium	$\times \sim 15$
B	7	$1.5509\mu m$	medium	weak	$\times \sim 7$
Anneal in $H_2$ at 1100 °C for 5 hours					
band	no.	peak	without Al	with Al	intensity enhancement by Al
A	1	$1.5310\mu m$	medium	weak	$\times \sim 10$
	2	$1.5322\mu m$	medium	—	small
	3	$1.5338\mu m$	medium	—	small
	4	$1.5346\mu m$	—	second strongest	extremely enhanced
	5	$1.5375\mu m$	medium	weak	$\times \sim 8$
B	6	$1.5469\mu m$	medium	medium	$\times \sim 20$
	7	$1.5509\mu m$	strongest	strongest	$\times \sim 25$

The above results suggest that the A and B bands are related with different luminescent Er centers. The difference appears also in the temperature dependence of the photoluminescence intensity. Fig.3 shows an example of the photoluminescence spectra at 20 K and 280 K of an Er/Si sample annealed in an Ar+ $O_2$  flow, and Fig.4 shows the temperature dependence of the intensity of the  $1.5322\mu m$  (A band) and  $1.5509\mu m$  (B band) photoluminescence peaks of an Er/Si sample annealed in a  $H_2$  flow for 5 hours. With increasing temperatures from 20K, the  $1.5509\mu m$  peak in the B band decreases in intensity, taking a minimum ( $\sim 1/5$  that at 20K) at about 80K and then increases slightly above 80K. The intensity of the  $1.5322\mu m$  peak in the A band shows a similar temperature dependence, but the decrease between 20K and 80K is only 40%. As a result, both peaks illuminate strongly even at room temperature, the  $1.5322\mu m$  peak becoming stronger than the  $1.5509\mu m$  peak. The FWHM of both peaks is broadened only slightly from 0.5 nm at 20K to 0.7 nm at 280 K.

## DISCUSSION

Among the five luminescence bands (A - E) detected between  $1.5\mu m$  and  $1.6\mu m$ , the first two (A and B) bands are strong and can be resolved into several sharp peaks not only at low temperatures but also at room temperature. The FWHM of 0.5 nm or less is smaller than those observed in Er-implanted silicon [1] or Er-doped MBE silicon [2] at low

temperatures. The  $1.5322\mu\text{m}$  and  $1.5346\mu\text{m}$  peaks in the A band are strong when Er/Si samples are annealed in Ar+O<sub>2</sub>, whereas they are relatively small in H<sub>2</sub>, and seem to be related with O<sub>2</sub>. The peaks  $1.5509\mu\text{m}$  and  $1.5469\mu\text{m}$  in the B band are very strong when annealed in H<sub>2</sub>, but they seem to be quenched in O<sub>2</sub>. From this annealing atmosphere dependence, it is clear that the A and B luminescence bands are originated by different Er-centers. The different temperature dependence between the peaks of the A and B bands support this speculation.

It has been shown that the Er-related luminescence in Er-doped crystalline silicon where doping is carried out under nonequilibrium conditions (ion implantation, MBE etc. ) shows a large thermal quenching above  $\sim 150\text{ K}$ , but that the thermal quenching is greatly mitigated by the presence of oxygen, and the luminescence becomes observable at room temperature. In this respect, we speculate that the peaks in the A band are related with oxygen (presumably Er-O-Si complexes), whereas the peaks in the B band with no or few oxygen.

The presence of an Al film on top of the Er film is found to increase the Er-related luminescence intensity greatly. In both Ar+O<sub>2</sub> and H<sub>2</sub> annealing atmospheres, the strongest peaks ( $1.5322\mu\text{m}$  in Ar+O<sub>2</sub> and  $1.5509\mu\text{m}$  in H<sub>2</sub> ) are enhanced by Al, suggesting that the intensity enhancement may be due to enhanced Er-diffusion into silicon.

The behavior of the  $1.5346\mu\text{m}$  peak in the A band is confusing. It is weaker than the  $1.5322\mu\text{m}$  peak in samples annealed under an Ar+O<sub>2</sub> flow for 5 hours, but is stronger when the annealing time is 2 hours. It is very weak in samples annealed in a H<sub>2</sub> flow, but is extraordinarily enhanced by the presence of Al and becomes the second strongest next to the  $1.5509\mu\text{m}$  peak in Al/Er/Si samples. We speculate at present that the  $1.5346\mu\text{m}$  peak may be related with oxygen and that oxygen impurity in Al may be responsible for the intensity enhancement of the  $1.5346\mu\text{m}$  peak. A close SIMS (secondary ion mass spectroscopy) analysis is, however, necessary to deduce a conclusive remark.

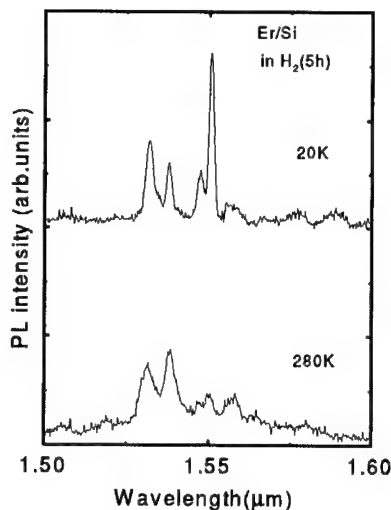


**Fig.3** Photoluminescence spectra at 20K (upper) and at 280K (lower) of an Er/Si sample annealed at 1100 °C for 5 hours in a H<sub>2</sub> flow. Note that the slit width is larger than in Fig.1b.

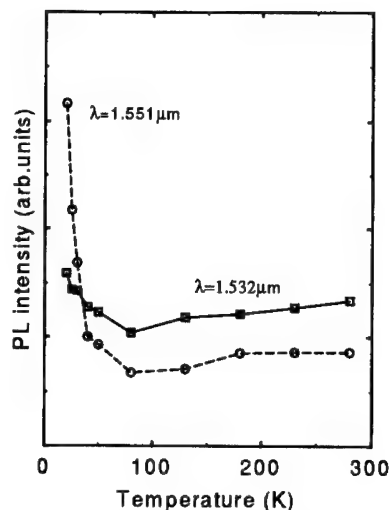


**Fig.4** Temperature dependence of the  $1.53220\mu\text{m}$  and  $1.5509\mu\text{m}$  peaks of an Er/Si sample annealed at 1100 °C for 5 hours in a H<sub>2</sub> flow.

## CONCLUSIONS

Very sharp Er-related luminescence peaks with FWHM less than 0.5 nm at 20K are observed in Er-diffused crystalline silicon. The wavelength of the strongest peak depends on the annealing atmosphere, being 1.5322 $\mu$ m in Ar+O<sub>2</sub> and 1.5509 $\mu$ m in H<sub>2</sub>. Al films on top of the Er films enhance the intensity greatly. The thermal quenching is small and the luminescence is strong at room temperature.

## ACKNOWLEDGEMENTS

We gratefully acknowledge Dr. S. Yugo, Dr. X. Zhao, Mr. A. Yokoi, Mr. T. Dejima, and Mr. Y. Nishida for their discussions. We also thank Dr. H. Ysuhara and Dr. A. Sato for their collaboration. This work is supported in part by Grant-in-Aid for Scientific Research from the Ministry of Education, Science, Sports and Culture, Japan.

## REFERENCES

1. H. Ennen, J. Schneider, G. Pomrenke, J. Schneider, J. Windscheif and A. Axmann, *J. Cryst. Growth* **64**, p.165 (1983).
2. H. Ennen, G. Pomrenke, A. Axmann, K. Eisele, W. Haydl and J. Schneider, *Appl. Phys. Lett.* **46**, p.381 (1985).
3. T. Kimura, A. Yokoi, H. Horiguchi, R. Saito, T. Ikoma and A. Sato, *Appl. Phys. Lett.* **65**, p.983 (1994).
4. X. Zhao, K. Hirakawa and T. Ikoma, *Appl. Phys. Lett.* **54**, p.712 (1989).
5. X. Zhao, private communication.
6. F. Y. G. Ren, J. Michel, Q. Sun-Paduan, B. Zheng, H. Kitagawa, D. C. Jacobson, J. M. Poate and L. C. Kimerling in *Rare Earth Doped Semiconductors*, edited by G.S. Pomrenke, P.B. Klein, and D. W. Langer (Mat. Res. Soc. Symp. Proc. 301, San Francisco, CA 1993) pp.87-95.
7. D. È. Nazarov, G. S. Kulikov and R. Sh. Malkovich, *Sov. Phys. Semicond.* **25**, p.997 (1991).
8. M. Kechouane, H. l'Haridon, M. Salvi, P.N. Favennec, D. Moutonnet, M. Gauneau, and J.P. Mercier, *Electron. Lett. (UK)*, **26**, p.1067 (1990).

## ABOUT THE ELECTRICAL AND STRUCTURAL PROPERTIES OF ERBIUM THERMALLY DIFFUSED IN SINGLE CRYSTAL SILICON

S. BINETTI, M. ACCIARRI, I. GELMI, S. PIZZINI  
INFN- Department of Physical Chemistry and Electrochemistry,  
Via Golgi, 19 I-20133 Milano (Italy)

### ABSTRACT

Having preliminarily confirmed the possibility of erbium doping by thermal diffusion, we have used this process to introduce erbium into a silicon substrate from metallic erbium or erbium oxide sources. Diffusion experiments were carried out at 1050, 1200 and 1250 °C. The Er:Si diffused samples were investigated using four probe resistivity and thermopower techniques for the measure of the concentration and type of carriers, SIMS and Auger spectroscopy for chemical analysis of the diffused layers and photoluminescence (PL) measurements at temperatures ranging from 2 to 298 K for the detection of optical activity. None of the samples prepared presented measurable PL at 2 K, except for one single sample on top of which was deposited an erbium doped silica glass. The electrical properties, instead, were deeply influenced by doping, indicating the formation of both donor and acceptors.

### INTRODUCTION

The full development of Er:Si optoelectronic devices still depends on the understanding of several problems of very basic nature. For example it would be extremely interesting to understand how the electrical and optical properties of Er:Si depend on the kind of site where Er sits in the silicon lattice, the number and type of non-silicon nearest neighbours, the dopants and, eventually, on the temperature, duration and type of preparation processes. Up to now erbium was mainly introduced in silicon by ion implantation [1] and molecular beam epitaxy. Only in the first case erbium, as  $Er^{+3}$  ion, is optically active and its photoluminescence (PL), which was originally attributed to the donor character of erbium, seems to be instead associated to the presence of oxygen, which is efficiently getterd by erbium, as donors related defects recover after suitable annealing without affecting the PL [2]. In Molecular Beam Epitaxy (MBE) samples erbium behaves instead as an acceptor and it is only very weakly photoluminescent, its PL being however enhanced by the presence of oxygen [3]. Erbium can be also introduced into the silicon lattice by thermal diffusion [5]. It has been shown by [5] using radioactive isotopes, that erbium can be diffused in silicon from an erbium chloride surface layer at temperatures between 1150 - 1250 °C. Also in this case erbium showed acceptor characteristics [4][5] and it was shown that the ionization energy of these centres is close to the ionization energy of the most common acceptor impurities like boron. It was therefore inferred from these measurements that these erbium atoms sit in substitutional position and PL measurements show that these ions are not optically active.

Aim of this work was better understanding of the correlations between the optical and electrical properties of Er:Si and to optimize the procedures of doping in presence of point defects and non metallic impurities, like oxygen, which is known to be very reactive with erbium. The materials used were single crystal silicon substrates and doping was carried out by thermal diffusion, to work with a quasi-equilibrium process. Thermal diffusion was carried out both in reducing and oxidizing conditions in order to preserve a metallic erbium source at the surface and to hinder or enhance the contemporaneous injection of self-interstitials.



## EXPERIMENTAL

**Samples preparation** The samples were cut from B and P-doped Czochralsky (CZ) and Float Zone (FZ), 4-in. diam, silicon wafers. Attempts of erbium doping by thermal diffusion processes were carried out using two kinds of erbium sources, namely metallic erbium and erbium oxide films deposited on top of the wafers. Metallic erbium films (thickness = 200 Å) were deposited on CZ n-type ( $\rho = 6.5 \pm 0.05 \Omega \text{ cm}$ ) and FZ n-type ( $\rho = 14 \pm 1 \Omega \text{ cm}$ ) samples by e-beam evaporation in Ultra High Vacuum, using high purity (> 99.99 %) erbium sources. The erbium oxide films were prepared by pyrolysis [6] of a solution of  $\text{Er}(\text{NO}_3)_3 \cdot 5\text{H}_2\text{O}$  in ethanol-ethylene glycol on top of CZ n-type  $\rho = 6.5 \pm 0.05 \Omega \text{ cm}$ , CZ p-type  $\rho = 6.14 \pm 0.32 \Omega \text{ cm}$  and FZ n-type  $\rho = 180 \pm 2 \Omega \text{ cm}$  silicon substrates. Prior to deposition, each silicon sample (usually  $1 \times 2 \text{ cm}^2$  large) was chemically cleaned using conventional wet treatments and then underwent a chemical oxidation process in distilled water for 4 hrs at 50 °C to generate a few nm thick oxide, which is required to permit the adhesion of erbium oxide. The deposition was carried out at 180 °C, with the solution which was intermittently sprayed over the silicon samples using synthetic air as carrier until the deposit is about 40  $\mu\text{m}$  thick. At the end of the deposition the samples are submitted to a final heat treatment at 700 °C for 30 min, in order to complete the decomposition of the nitrate to the oxide.

**Diffusion processes** Most of the diffusion experiments were carried out in a horizontal furnace at 1050 °C for 24 hrs using high quality quartz tubes to maintain the selected covering atmosphere. In order to study the influence of the covering atmosphere on erbium diffusion processes we used, alternatively, high purity synthetic air or a mixture of  $\text{Ar}/\text{H}_2$ , which contains about 10 ppm of oxygen. Other heat treatments at 1200 and 1250 °C for 2 hrs were carried out in a static air atmosphere, using a vertical furnace.

**Acid cleaning procedures** In order to remove the front oxides, concentrated (37% mol) HF was used, considering that it is a good solvent for silicon oxide and for rare earth oxides [7]. The surface silicon oxide removal was monitored using FTIR measurements in correspondence of the 1080  $\text{cm}^{-1}$  band which is typical of surface oxides. In order to remove thick silicon layers, instead, a CP4 mixture ( $\text{HNO}_3 : \text{HF} : \text{CH}_3\text{COOH}$ , 57:18:25) was used.

**Electrical and optical characterization** Electrical resistivity measurements were carried out using the four-probe method according to the ASTM specifications F391-87 and F84-88. The conductivity type of the samples before and after heat treatments was determined by the hot probe method (ASTM F42-88). Fourier Transform Infrared Spectroscopy (FTIR) was used to determine the oxygen concentration content and to monitor the nature of the silicon oxide formed on the sample surface after any heat treatment. Photoluminescence (PL) measurements were carried out from 70 K to 2 K using a PL spectrometer consisting of a Jasco Fourier transform IR spectrometer equipped with a InGaAs detector and with a 4W argon ion laser as the light source (excitation power 360  $\text{W}/\text{cm}^2$ ). Erbium films were monitored before and after the thermal treatment by Auger Electron Spectroscopy (AES) using a 4200 PHI Auger spectrometer.

**Erbium depth profiles measurements** Erbium depth profiles in silicon were recorded by Secondary Ion Mass Spectrometry (SIMS) using a Cameca IMS-4F Spectrometer. The depth profile of a sample implanted with erbium with a dose of  $2 \times 10^{14} \text{ at}/\text{cm}^2$  was used to calibrate the erbium concentration scale and to define the background level, which was found to be about  $10^{15} \text{ at}/\text{cm}^3$ .

## EXPERIMENTAL RESULTS

**Samples doped with metallic erbium: spectroscopical results** SEM X-ray microprobe measurements show that the metallic erbium is not uniformly distributed on the silicon surface, at least on a 10  $\mu\text{m}$  length scale. Some samples were submitted to AES and AES depth profile measurements before and after the thermal treatment to check the different surface phases. Although individual profiles are quantitatively affected by the original metallic film morpho-

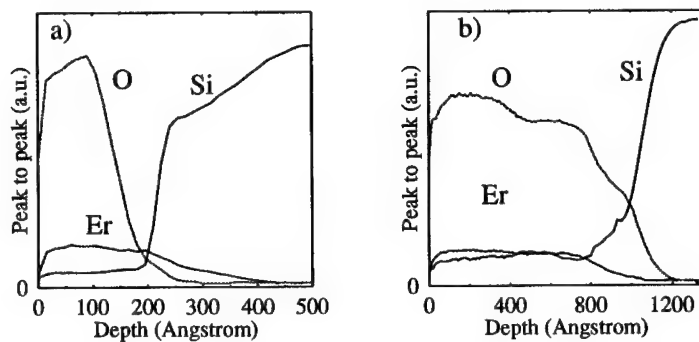


Figure 1: Auger Depth Profile of the Er-deposited CZ silicon sample a) before heat treatment, b) after heat treatment in Ar/H<sub>2</sub> at 1050 °C for 24 hrs

logy, nevertheless they show comparable features. A typical AES depth profile taken before

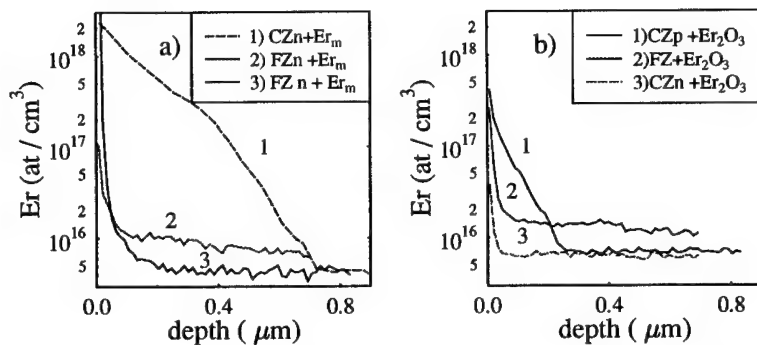


Figure 2: Erbium diffusion SIMS profiles: a) air treated metallic erbium samples at 1050 °C. b) air treated erbium oxide samples at 1050 °C after surface oxide removal with conc. HF

thermal annealing is reported in Fig. 1 a). It features a very sharp Er-Si interface at a depth corresponding to the Er-film thickness, but indicates as well the Er films are contaminated by oxygen and that a measurable amount of erbium diffused into the silicon sample. The AES depth profile measured after the heat treatment (Fig.1 b)) shows a broadening of the Si-Er interface associated to a strong decrease of the subsurface Er/Si signal and to the diffusion of oxygen into the silicon substrate. Apparently, these features indicate that both erbium and oxygen diffused into the silicon substrate during the thermal annealing process.

Being strongly affected by surface roughness, only few SIMS depth profiles could be obtained from these samples. Fig. 2 a) reports some typical SIMS depth profiles of the air treated metallic Er samples at 1050 °C after concentrated HF cleaning to remove the front thermal oxides. One recognizes a 0.7 μm thick erbium-rich subsurface region in the CZ sample. Below this region the

Sample	$\rho$ ( $\Omega\text{cm}$ ) front side	$\rho$ ( $\Omega\text{cm}$ ) back side	conductivity type front side	conductivity type back side
CZ n +Er met	$627.8 \pm 0.5$	$126.9 \pm 0.14$	p	p
CZ n +Er met	$62.5 \pm 0.4$	$205.9 \pm 0.15$	n	n
CZ n +Er met	$284.5 \pm 0.4$	$7.7 \pm 0.14$	n	n
CZ n +Er met	$581.5 \pm 1.2$	$36.3 \pm 1.3$	n	n
FZ n +Er met	$4098 \pm 10.6$	$2380 \pm 11.5$	p	p
FZ n +Er met	$726.7 \pm 7.6$	$98.3 \pm 1.6$	p	p
FZ(*)	$8961 \pm 46.3$	$2725 \pm 5.5$	n	n

Table 1: Resistivity values and conductivity type of metallic erbium-doped silicon samples after heat treatment at 1050 °C for 24hrs in air

Sample	$\rho$ ( $\Omega\text{cm}$ ) front side	$\rho$ ( $\Omega\text{cm}$ ) back side	conductivity type front side	conductivity type back side
CZ n +Er	$310.5 \pm 5.4$	$25.9 \pm 0.01$	p	p
CZ n +Er	$4592 \pm 15.5$	$26.9 \pm 0.02$	p	n
FZ n +Er	$10774 \pm 96.6$	$567.5 \pm 10.1$	p	p

Table 2: Resistivity value and conductivity type of erbium-doped silicon samples after heat treatments at 1050 °C for 24hrs in  $\text{Ar}/\text{H}_2$ .

erbium concentration is around the detection limit. On the FZ samples, instead, a homogeneous erbium doping at about  $10^{16}$  at  $\text{cm}^{-3}$  level is observed. From FTIR measurements in erbium-free samples before and after heat treatments at 1050 °C a small (about 1.5 ppm) decrease of the IR-active oxygen content is observed, almost independently of the cover gas atmosphere, indicating the occurrence of a precipitation process on preexisting nuclei.

**PL results** No evidence of PL at  $1.54 \mu\text{m}$  even at 2 K was observed in all the samples doped with either metallic erbium or erbium oxide. These results indicate that the concentration of optically active Er-O centres is extremely low in these samples. On the contrary, a typical PL peak was observed in a sample on top of it an Er-doped silica glass was deposited.

**Samples doped with metallic erbium: electrical results** The results of electrical conductivity and thermopower measurement at 1050 °C are reported in Table 1 (Air treated samples) and in Table 2 ( $\text{Ar}/\text{H}_2$  treated samples). All blank samples used as reference, for each treatment, did not show any significant change in resistivity values and conductivity type. In order to put in evidence the possible effect of traces of metallic erbium diffused on the back side during the film deposition procedures, a single FZ sample was gently etched on the back by a CP4 mixture in order to remove a  $50 \mu\text{m}$  thick silicon layer and rinsed with water before heating for 24 hrs at 1050 °C. (See FZ (\*) sample on the bottom of Table 1). Although largely influenced by some lack of uniformity of metallic films, and presumably, by the non complete reproducibility of the quenching procedures carried out manually, the results concerning both air and  $\text{Ar}/\text{H}_2$  treatments show a systematic increase of the resistivity associated to an increase of the p-type character. Furthermore, the front side is less p-type than the back. This behaviour is confirmed by the results obtained on samples treated at higher temperatures (1200 and 1250 °C in air) reported in Table 3. Apparently, the back-side conductivity could have been influenced by traces of Er diffused on the rear of the samples during the deposition, as on some back-etched samples the p-type character is less on the back than on the top (see sample FZ (\*) in Table 1). Also in this case, however, the effect of an acceptor-type impurity is well evident.

**Samples doped with erbium oxide: spectroscopical results** SEM X-ray microprobe measurements show that films of erbium oxide are homogeneously distributed on the surface.

Sample	T (°C)	$\rho$ ( $\Omega\text{cm}$ ) front side	$\rho$ ( $\Omega\text{cm}$ ) back side	conductivity type front side	conductivity type back side
CZ n Er	1200 °C	12.2 ± 0.12	342.3 ± 0.95	n	n
FZ n Er	1200 °C	4871 ± 42.2	160.3 ± 0.10	p	p
CZ n Er	1250 °C	12.7 ± 0.70	157.8 ± 0.15	n	n
FZ n Er	1250 °C	6991 ± 6.21	127.1 ± 0.13	p	p

Table 3: Resistivity values and conductivity type of metallic erbium samples after heat treatments at 1200 and 1250 °C for 2hrs in air.

Sample	atmosphere T (°C)	$\rho$ ( $\Omega\text{cm}$ ) front side	$\rho$ ( $\Omega\text{cm}$ ) back side	conductivity type front side	conductivity type back side
FZ n Er <sub>2</sub> O <sub>3</sub>	air (1050 °C)	780.8 ± 8.4	1002.9 ± 2.8	n	n
FZ n Er <sub>2</sub> O <sub>3</sub>	Ar/H <sub>2</sub> (1050 °C)	266.3 ± 0.25	264.8 ± 1.0	n	n
FZ n Er <sub>2</sub> O <sub>3</sub>	air (1200 °C)	470.3 ± 1	467.2 ± 1.3	n	n
FZ n Er <sub>2</sub> O <sub>3</sub>	air (1250 °C)	192 ± 2	193 ± 2.2	p	p

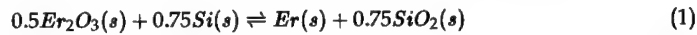
Table 4: Resistivity values and conductivity type of erbium oxide -doped FZ samples after heat treatment at 1050 °C for 24hrs and at 1200 and 1250 °C for 2hrs in air.

From SIMS depth profiles of the air-treated samples at 1050 °C, after concentrated HF cleaning to remove the front oxide, there is also in this case a subsurface accumulation of erbium in CZ samples. On the FZ samples, instead, a rather homogeneous erbium doping at about  $10^{16}$  level at  $\text{cm}^{-3}$  is observed (see Fig.2 b)

Samples doped with erbium oxide: electrical results The electrical conductivity and thermopower after heat treatment at 1050-1200-1250 °C, both in air and in Ar/H<sub>2</sub> show a significant change only in FZ samples (see Table 4).

## DISCUSSION AND CONCLUSIONS

In order to discuss the results reported in the Experimental Section, which we consider very preliminary, as most of the characterization work (spreading resistance and deep level transient spectroscopy (DLTS) experiments) are still underway, we have first to comment briefly the thermodynamics of erbium doping by Er<sub>2</sub>O<sub>3</sub> surface layers. From the known values of the free energy of formation of Er<sub>2</sub>O<sub>3</sub> and SiO<sub>2</sub> the standard free energy  $\Delta G_o$  of the reaction



(where all the solid phases are at unit activity), amounts to 271.32 kJoule/mole Er. Erbium oxide, therefore, cannot be reduced to pure erbium metal by reaction with silicon, but it could be dissolved into the silicon matrix at a concentration which can be calculated from the following equation

$$\Delta G_o = RT \ln[\text{Er}] \quad (2)$$

(where [Er] is the erbium concentration in silicon) to amount to  $1.8 \cdot 10^{12} \text{at}/\text{cm}^3$ . It appears that Er<sub>2</sub>O<sub>3</sub> is not an ideal source of metallic erbium, as it provides a solution very far from the erbium solubility conditions [2]. On the other side, a limited solubility of Er<sub>2</sub>O<sub>3</sub> can be predicted by recent literature results on erbium-oxygen co-implanted silicon[2] and in MBE grown Er-O doped layers[3], with Er, apparently sixfold coordinated with oxygen, being a strong getter for oxygen, according also to our thermodynamic predictions. Therefore, both metallic erbium and Er-O species might simultaneously diffuse into silicon. We suppose that the diffusivity data reported by Nazzyrov are a measure of the diffusivity of these erbium-oxygen species and that the erbium

doping efficiency of  $Er_2O_3$  sources depends strongly on the initial oxygen concentration of the silicon substrate. Regarding the electrical properties, Er behaves as an acceptor in Er-diffused materials, in contrast with the donor character of implanted Er ions [2]. The acceptor character of Er is also typical of MBE Er-doped silicon, where Er is mainly substitutional and the transport is shown to be hole-dominated [3] with a room temperature carrier concentration of  $10^{15} cm^{-3}$ . In most of our Er-doped CZ n and FZ n samples and only in erbium oxide-doped FZ samples, we find the presence of an acceptor species, which apparently partially compensates the preexisting donors both in the front and in the back. It apparently exhibits the character of a fast diffuser as its effect has been found to be still present at a depth of several hundred  $\mu m$ , although neither the exact value of its diffusion coefficient nor its substitutional or interstitial nature can be deduced from these present experiments. In order to explain the less p-type character observed on the front of these samples, we might suppose that a dual diffusion mechanism is operative, associated to the capability of  $Er_2O_3$ , certainly present on top of Er:Si samples (see AES profiles), to inject both metallic erbium and Er-O species, these last being the slow diffusion components, according to the Nazarov measurements. As metallic erbium in MBE samples presents acceptor properties, we might suppose that it provides the p-type character of our diffused samples, whereas the trivalent erbium of the Er-O species, which according to [2] presents a donor character, provides a partial compensation of the acceptors on the front side. The relative insensitivity of CZ -  $Er_2O_3$  : Si samples to annealing is a further evidence of the dual diffusion mechanism proposed. In fact, the solubility of  $Er_2O_3$  in oxygen-lean FZ silicon should be larger than in oxygen-rich CZ silicon, as the dissolution is limited by the solubility product  $K = [Er][O]^n$  of the Er-O species, where n is a integer.

## ACKNOWLEDGMENTS

The authors are indebted to Dr. Sandro Ferrari for the SIMS measurements and to prof. Francesco Priolo for ion implanted samples used as reference. We also thank prof. M. Guzzi and prof. E. Grilli for their assistance in PL measurements. This work has been carried out within the SiNet project of INFN, but it was partially granted by EEC under the JouleII-Multichess Project.

## REFERENCES

1. S.Coffa, F.Priolo, G.Franzò, V.Bellani, A.Carnera, C.Spinella, Phys. Rev. B **48**, 11782 (1993)
2. J.L. Benton, D.J. Eaglesham, M.Almonte, P.H. Citrin, M.A.Marcus, D.L. Adler, D.C. Jacobson, J.M.Poate, in Rare Earth doped semiconductors edited by G.S.Pomrenke, P.B.Klein, D.W.Langer (Mater.Res.Soc.Symp.Proc. **301**, Pittsburgh, PA (1993), pp. 119-124
3. F.Arnaud D'Avitaya, Y.Campidelli, J.A.Chroboczek, P.N.Favennec, H.L'Haridon, D.Moutonnet, A.Wasiela, in Rare Earth doped semiconductors edited by G.S.Pomrenke, P.B.Klein, D.W.Langer (Mat.Res.Soc.Symp.Proc. **301**, Pittsburgh, PA (1993), pp. 97-100
4. V.Aleksandrov, V.V Emtsev, D.S. Oloskin, N.A. Sobolev, E.I.Shek, Semiconduc. **28**, 1126 (1994)
5. E.Nazyrov, G.S. Kulikov, R.Sh. Malkovich, Sov. Phys. Semicond. **25**, 997 (1991)
6. D. Narducci, G.Girardi, C.Piseri, Solid State Phenomena (1996), accepted
7. Gmelins Handbuch, Teil C1 p.175, Teil C3 p.225, Springer Verlag (Berlin) 1976

## INCORPORATION OF HIGH CONCENTRATION LUMINESCENT Er CENTERS IN Si AND POROUS Si BY ELECTROPLATING

Chi Sheng, Yongming Cai, Dawei Gong, Daming Huang, Xiaohan Liu, and Xun Wang  
Surface Physics Laboratory, Fudan University, Shanghai 200433, China  
E-mail: (86)-(21)-65493232

### ABSTRACT

It is found that Er could only be deposited on a Si cathode by electrolysis of near neutral  $\text{ErCl}_3$  electrolyte with a large current density. The deposited Er hydrolytic layer reacts with Si at  $1200^\circ\text{C}$  to form the activated Er centers that emit a  $1.53\mu\text{m}$  photoluminescence peak at room temperature. By applying this process to porous Si, an apparent doping concentration of Er larger than  $10^{19}/\text{cm}^3$  in the whole porous Si layer and a strong PL intensity with little temperature quenching are achieved.

### INTRODUCTION

Erbium doped Si (Si:Er) is thought to be a promising material to fabricate Si-based optoelectronic devices. Ennen et al. first reported the infrared light emission of Er doped Si (Si:Er)<sup>1</sup> and produced the first Si:Er light emitting diode (LED) working at low temperature.<sup>2</sup> Since then, a great deal of attention has been paid to the study of Si:Er.<sup>3-16</sup> Although an Er concentration of  $10^{19}/\text{cm}^3$  has been achieved by a proper ion implantation process<sup>17</sup> and room temperature photoluminescence (PL) has been realized, it seems that increasing the Er concentration in Si and eliminating temperature quenching are still two critical factors to improve the efficiency of luminescence. The temperature quenching is due to the nonradiative recombination<sup>8</sup> and the back flow of energy from excited Er ion to the host material. It is found that the larger the bandgap of the host material, the less the temperature quenching.<sup>18</sup> Er doped  $\text{SiO}_2$ ,<sup>19</sup> SIPOS<sup>20</sup> and porous Si (PS)<sup>21,22</sup> did show a strong room temperature light emission and a weak temperature quenching.

Kimura et al.<sup>22</sup> utilized electrochemical method to incorporate a high concentration of Er in a PS layer with a thickness of  $10\mu\text{m}$  and a strong room temperature PL with weak temperature quenching was achieved. However, very critical requirements have to be met to get optically active Er in PS. We have improved the electrolysis of  $\text{ErCl}_3$  solution and easily achieved high concentration of optically active Er in Si single crystal and PS.

### EXPERIMENT AND RESULTS

#### *Doping of optically active Er in single crystal Si*

Both p-type and n-type Si(100) substrates with resistivity of  $3-5\ \Omega\ \text{cm}$  were used. The electroplating of Er was carried out in an anodic-etching cell used for preparing PS. The

substrate was negatively biased with respect to a counter graphic electrode. The electrolyte used was a specially prepared  $\text{ErCl}_3$  solution with a very low hydrogen ion concentration. Because Er is more active than hydrogen, Er atoms will not be deposited on the Si surface during the electrolysis of  $\text{ErCl}_3$  solution in ordinary condition. Hydrogen bubbles escape from the cathode instead. Decreasing the hydrogen ion concentration is in favor of the Er deposition. The  $\text{ErCl}_3$  electrolyte was prepared by first evaporating  $\text{ErCl}_3$  aqueous solution and then dissolving the precipitate again in water with limited quantity of hydrochloric acid, leaving a small quantity of residual undissolved. The pH value of the resulted solution was near 5. Even with this specially made electrolyte, Er could not deposit at the cathode unless the current density is larger than a critical value, which depends on Er concentration, pH value and temperature. In our case, the critical current density is about  $3 \text{ mA/cm}^2$  for a  $0.2 \text{ M ErCl}_3$  solution.

The electrolysis of  $\text{ErCl}_3$  was carried out with a current density larger than  $3 \text{ mA/cm}^2$ . As soon as the Er is deposited on the cathode, it immediately reacts with water. After 3-5 min, the substrate surface was covered with a thin white layer of  $\text{Er(OH)}_3$ .

The Er-deposited Si wafer was then annealed in an atmospheric ambient of 1:1 volume ratio of  $\text{O}_2$  and  $\text{N}_2$  to incorporate Er into Si. A two-step annealing process was taken. The sample was first annealed at  $200^\circ\text{C}$  to stabilize the deposited layer then followed by a rapid thermal annealing at  $1200^\circ\text{C}$  for 20 sec. During annealing the Er attacked the surface of Si resulting a rough structure as revealed by the scanning electron microscopy (SEM) observation as shown in Fig.1. The composition of this surface was detected by the x-ray photoelectron spectroscopy (XPS). Three elements of Si, Er and O were found. The spectrum of Si as shown in Fig.2 consists of two peaks representing the elemental Si and the oxide states, respectively.



Fig.1 SEM image of annealed Si:Er

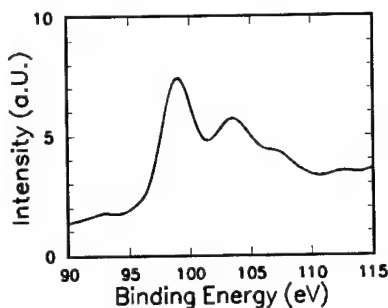


Fig.2 XPS signal of Si in annealed Si:Er

The intensity of elemental Si peak is larger than that of Si-oxide peak. This means that the reaction of Er with Si did not take place over the whole Si surface and the Er atoms were only incorporated in some areas of the Si surface. The annealed sample shows a  $1.53\mu\text{m}$  PL peak at room temperature as shown in Fig. 3 although its intensity is not very strong.

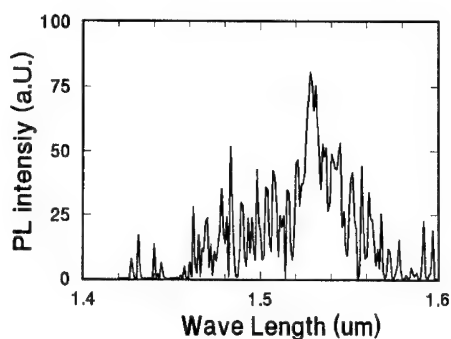


Fig.3 Room temperature PL of Si:Er

#### *Er doped into porous silicon*

The initial PS used for Er doping was made by ordinary anodic-etching method. The n-type Si wafers with a resistivity of  $1-5\ \Omega\ \text{cm}$  were anodic-etched in  $1:1\ \text{HF}:\text{C}_2\text{H}_5\text{OH}$  solution at a current density of  $3-8\ \text{mA}/\text{cm}^2$  illuminated by a 100W tungsten lamp. The as-grown PS samples emitting light with different colors were used to do the Er electroplating. The electroplating process was similar to that used for Si single crystal. To prevent non-uniform doping a pulse current was used. First a small current about  $0.05\ \text{mA}/\text{cm}^2$  was passed through the electrolysis cell for 5 min to draw  $\text{Er}^{3+}$  ions into the holes of porous Si and then a current larger than the critical value was used to electroplate Er on PS wall for 1 min. The above process was repeated several times in order to incorporate sufficient amount of Er. A similar two-step annealing was then carried out.

Secondary ion mass spectroscopy (SIMS) was used to detect the Er depth profile in PS as shown in Fig. 4. The secondary Si ion yield drops at Si surface region as shown in Fig. 4(a). This is coincident with the cone shape structure of n-PS that is anodic etched with a light illumination. The Er yield at surface is about 1.5 times of that in the depth of PS. This could be explained by the non-uniform distribution of Er concentration in the electrolyte from the



surface to the inner region of PS. The Er concentration incorporated into PS could be estimated to be  $10^{19}/\text{cm}^3$  in the bulk of PS and  $10^{20}/\text{cm}^3$  at the PS surface by using the atomic sensitivity factors of bulk Si and Er.

PL measurements were performed by illuminating samples with the 514.5 nm light of an Ar laser. The PS:Er shows a strong room temperature PL spectrum peaked at the wavelength of  $1.53\mu\text{m}$  as seen in Fig.5a. For comparison, a PL spectrum of  $\text{Er}_2\text{O}_3$  measured under the same experimental conditions is also given (curve b). The main peak of  $\text{Er}_2\text{O}_3$  is located at

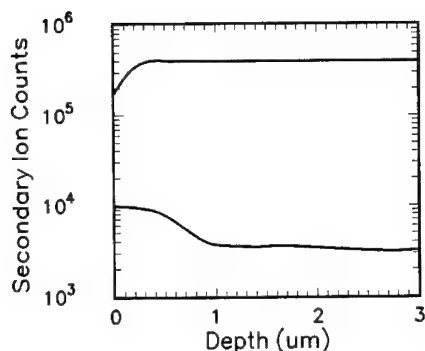


Fig.4 SIMS profile of Er in PS

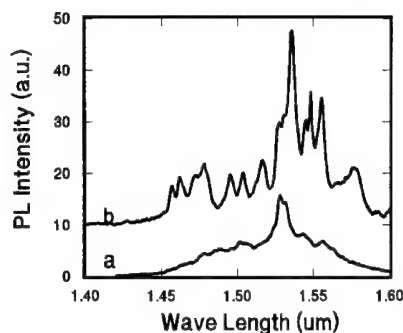


Fig.5 PL spectra at room temperature  
a. PS:Er b.  $\text{Er}_2\text{O}_3$

$1.536\mu\text{m}$  that is greatly suppressed in the PL spectrum of PS:Er. Instead, other two peaks at  $1.533$  and  $1.523\mu\text{m}$  are much pronounced. Although the transition energy of Er is kept in an atomic characteristic, the transition rate may be affected by its surrounding. In the case of PS:Er the Er atoms must also be surrounded by oxygen atoms because no light could be detected if Er were only combined with Si. The change in the fine structure of the PL spectrum for PS:Er means that the remote neighbors of Er atoms in PS are different from that of Er atoms in  $\text{Er}_2\text{O}_3$ . The possible structure of PS:Er may be composed of Er-O-Si complexes. It seems reasonable that when  $\text{Er}(\text{OH})_3$  reacts with Si the hydrogen in the (-OH) radical is easily replaced by Si resulting in the formation of Er-O-Si links. The PL intensity of PS:Er is much stronger than that of Si:Er. Due to the larger thickness of the PS layer and the high Er doping concentration, the total areal density of Er would be larger than that in the implanted Si:Er. Fig.6 shows the temperature dependence of the PL intensity of the  $1.53\mu\text{m}$  peak of a Ps:Er

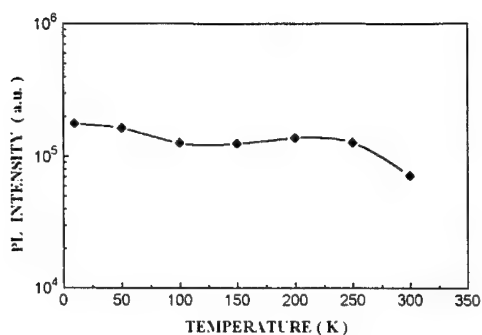


Fig.6 PL intensity at 1.53  $\mu\text{m}$  as a function of temperature for the PS:Er

sample. The PL intensity at room temperature is almost the same as that of 100K. This is benefited from the larger bandgap of PS.

## CONCLUSIONS

The room temperature PL at 1.53  $\mu\text{m}$  without remarkable temperature quenching in Er-doped PS is easily achieved by the electrochemical method combined with a post annealing at 1200°C.

## ACKNOWLEDGMENT

This work was partially supported by the National Natural Science Foundation of China.

## REFERENCES

1. H.Ennen, J.Schneider, G.Pomrenke, and A.Axmann, Appl. Phys. Lett. **43**, 943 (1983).
2. H.Ennen, G.Pomrenke, A.Axmann, K.Eisele, W.Haydl, and J.Schneider, Appl.Phys.Lett., **46**, 381 (1985).
3. J.Michel, J.L.Benton, R.I.Ferrante, D.C.Jacobson, D.J.Eaglesham, E.A.Fitzgerald, Y.H.Xie, J.M.Poate, and L.C.Kimerling, J.Appl.Phys. **70**, 2672 (1991).
4. A.Polman, J.S.Custer, E.Snoeks, and G.N.van den Hoven, Nucl.Instr.and Meth. **B80/81**, 653 (1993).
5. D.C.Adler, D.C.Jacobson, D.J.Eaglesham, M.A.Marcus, J.L.Benton, J.M.Poate, and P.H.Citrin, Appl.Phys.Lett. **61**, 2181 (1992).
6. S.Coffa, F.Priolo, G.Franzo, V.Bellani, A.Carnera, and C.Spinella, Phys.Rev. **B48**, 11782 (1993).
7. S.Coffa, G.Franzo, F.Priolo, A.Polman, and R.Serna, Phys.Rev. **B49**, 16313 (1994).

8. F.Y.G.Ren, J.Michel, Q.Sun-Paduano, B.Zheng, H.Kitagawa, D.C.Jacobson, J.M.Poate, and L.C.Kimerling, *Mat.Res.Soc.Symp.Proc.* **301**, 87 (1993).
9. G.Franzo, F.Priolo, S.Coffa, A.Polman, and A.Carnera, *Appl.Phys.Lett.* **64**, 2235 (1994).
10. K.Takahei, and A.Taguchi, *Mat.Sci.Forum* **83-87**, 641 (1992).
- 11 P.N.Favennec, H.I'Haridon, D.Moutonnet, M.Salvi, and M.Gauneau, *Jpn.J.Appl.Phys.* **29**, L524, (1990).
12. Y.S.Tang, K.C.Heasman, W.P.Gillin, and B.J.Sealy, *Appl.Phys.Lett.* **55**, 432 (1989).
13. D.Moutonnet, H.I'Haridon, P.N.Favennec, M.Salvi, M.Gauneau, F.Arnaud d'avitaya, and J.Chroboczek, *Mat.Sci.Eng.* **B4**, 75 (1989).
- 14.A.Polman, G.N.van den Hoven, J.S.Custer, J.H.Shin, R.Serna, and P.F.A.Alkemade, *J.Appl.Phys.* **77**, 1256 (1995).
15. G.Franzo, F.Priolo, S.Coffa, A.Polman, and A.Carnera, *Nucl.Instru. and Meth.* **B96**, 374 (1995).
- 16.S.Lombardo, S.U.Campisano, G.N.van den Hoven, and A.Polman, *Nucl.Instru and Meth.* **B96**, 378 (1995).
17. A.Polman, J.S.Custer, E.Snoeks, and G.N.vandenHoven, *Appl.Phys.Lett.* **62**, 507 (1993)
18. S.Coffa, G.Franzo, F.Priolo, A.Polman, and R.Serna, *Phys.Rev.* **B49**, 16313 (1994)
19. A.Polman, D.C.Jacobson, D.J.Eaglesham, R.C.Kistler, and J.M.Poate, *J.Appl.Phys.* **70**, 3778 (1991).
20. A.Lombardo, S.U.Campisano, and F.Baroetto, *Phys.Rev.* **B47**, 13561 (1993).
21. J.H.Shin, G.N.Van den Hoven, and A.Polman, *Appl.Phys. Lett.* **66**, 2379 (1995).
22. T.Kimura, A.Yokoi, H.Horiguchi, R.Saito,T.Ikoma, and A.Sato, *Appl.Phys.Lett.* **65**, 983 (1994).

**Part II**  
**Structural, Electrical, and**  
**Optical Properties**

## FACTORS GOVERNING THE PHOTOLUMINESCENCE YIELD OF ERBIUM IMPLANTED SILICON

W. JANTSCH\*, H. PRZYBYLINSKA\*\*, C. SKIERBISZEWSKI\*\*\*, S. LANZERSTORFER\*,  
L. PALMETSHOFER\*

\*Johannes Kepler Universität, A-4040 Linz, Austria, wolfgang.jantsch@jk.uni-linz.ac.at

\*\*Inst. of Physics, Polish Academy of Sciences, Al. Lotnikow 32/46, 02-668 Warsaw, Poland

\*\*\*Unipress, Polish Academy of Sciences, Sokłowska 29/37, 01-142 Warsaw, Poland

### ABSTRACT

We present a high resolution photoluminescence (PL) study of Si:Er which allows to distinguish a variety of Er centers occurring in Er-implanted Si. The lines belonging to a particular center are identified from the influence of processing parameters, temperature, excitation power, co-doping and hydrostatic pressure. The center-dependent high temperature yield is limited by the competition in efficiency of capturing excitons at Er centers or nearby defects followed by the excitation transfer to the Er-4f shell and by recombination of excitons at other, non-radiative centers. The excitation transfer probability is shown to depend on hydrostatic pressure of a few kbar. This effect indicates a new possibility to improve the efficiency of Si:Er light emitters.

### 1. INTRODUCTION

The luminescence of the trivalent erbium ion in silicon close to 1.54  $\mu\text{m}$  shows rich fine structure [1-10] and the intensity of individual lines depends strongly on the preparation conditions and on codoping with other impurities [4-10]. Particularly oxygen has attracted much attention as an abundant impurity in Czochralski (CZ)-Si since the overall photoluminescence (PL) yield due to Er in such a material can be higher by 2..3 orders of magnitude than in float zone (FZ) Si with lower oxygen content [6-11]. Additional O-doping by ion implantation or during MBE growth, the techniques commonly used also to introduce the Er at concentrations exceeding the rather low solubility limit, adds new spectral features, whereas, *e.g.*, co-implantation of N changes only the yield but does not produce new lines [11, 12].

These findings demonstrate already the complexity of the problems encountered in optimizing the PL yield. Obviously a variety of Er centers or complexes with impurities and native Si-defects are formed which differ in their efficiency of capturing the excitation from the host crystal and converting it into Er intra-4f-shell excitation followed by radiative recombination. Other defects, forming deep levels, may act as competing recombination centers but some of them might also act as co-activators providing an additional channel for the transfer of the host excitations to the 4f shell of Er. Therefore, as a first step in a systematic approach, it appears mandatory to develop tools at least to distinguish - if not to identify - different complexes in order to study their yield and its dependence on temperature and on the presence of other defects in the crystal individually.

The Er PL lines are extremely sharp owing to the exceedingly long life time of the parity forbidden  $J = 13/2 \rightarrow 15/2$  transition, the strong localization of the 4f shell, and its efficient shielding by the outer shells. The crystal field induces only a weak Stark splitting of the ground

state and excited state manifolds, perturbed by the presence of impurities in the vicinity of Er. Therefore high resolution spectroscopy is needed, and in many cases sufficient, to distinguish lines arising from different centers. The common origin of some set of PL lines can be established by the variation of several parameters like preparation conditions, excitation power, temperature and also hydrostatic pressure as presented in this paper. Other techniques, which enable identification of the microscopic structure of complexes, like electron spin resonance, have not been successfully applied so far to the optically active centers although optically inactive states were seen [10].

Owing to the strong localization of the 4f shell, hydrostatic pressure is expected to have very little influence on the intra-center transitions of Er. Pressure does affect, however, the relative positions of the bands of the host crystal as reflected also by the position of deep levels relative to the band edges [14]. Therefore an influence of pressure should bear information on the participation of deep levels in the process of the energy transfer from the host to the Er 4f shell. We observe indeed a strong influence of pressure on the PL yield in samples coimplanted with O at high doses which demonstrates another important role of O in enhancing the Er luminescence in Si.

In section 2 of this paper we review briefly the results of high resolution PL spectroscopy with respect to different centers. In section 3 we present our results for the influence of hydrostatic pressure and we discuss the implications for the energy transfer mechanism. Finally, we summarize our conclusions for the role of oxygen in the PL yield of Er in Si.

## 2. HIGH RESOLUTION LUMINESCENCE SPECTROSCOPY

Both float zone (FZ) and Czochralski (CZ) grown Si, n- and p-type wafers with resistivities of 10-20  $\Omega\text{cm}$ , were implanted with Er and some samples also with O or N. Two types of annealing procedures were applied: either annealing at temperatures up to 1100 °C for 30 min or a combination of 600 °C for 30 min and an additional short period step at 900 °C for 15 s. We use Fourier transform spectroscopy in order to achieve high resolution also for relatively weak photoluminescence (PL) spectra. Samples are mounted to the cold finger of a continuous flow He cryostat which is fitted to the self-built back chamber of a Bomem DA8.22 spectrometer. The samples are illuminated with the 514 nm line of an Ar-ion laser.

In Fig. 1 we give selected examples for the variety of spectra that can be observed in Er-implanted Si, depending on co-doping, implantation parameters (such as energy, dose, or implantation temperature) and annealing conditions. The examples chosen show a cubic center with the characteristic 5 fold splitting of the Er ground state (upper trace in Fig.1a) which has been attributed to an isolated interstitial Er ion [11-13]. Such a spectrum can be easily found in CZ-Si implanted to peak concentrations even exceeding the Er precipitation limit, especially for high energy implants performed at elevated temperatures, and annealed subsequently at 900 °C. The reported PL spectrum has been recorded for a sample implanted at 300 °C with 2 MeV energy to the peak concentration of  $3 \times 10^{18} \text{ cm}^{-3}$ , but SIMS investigations have shown that it stems from a low concentration (of the order of  $10^{17} \dots 10^{16} \text{ cm}^{-3}$ ) tail of the Er doping profile, extending to about 3  $\mu\text{m}$  into the sample. The middle trace shows the spectrum of an axial symmetry center with 7 out of 8 expected lines, which occurs exclusively in oxygen rich

material and dominates the PL for Er peak concentrations smaller than  $5 \times 10^{17} \text{ cm}^{-3}$ . The bottom trace shows a typical spectrum of lower symmetry Er complexes, usually found in samples implanted with high Er doses and annealed in two stages. The first annealing stage at 600 °C is supposed to recrystallize the layer after the amorphization caused by the implantation whereas the second, the high temperature stage, is essential to anneal the remaining point defects. Apart from the different annealing procedures applied for the samples yielding the top and bottom PL spectra, the samples themselves and their preparation are identical. The identification of the various Er centers is described in detail elsewhere [12]. The wavelength of lines belonging to different defects are given in Table 1.

In Fig. 1(b), the temperature dependent intensities of the strongest features of the three types of spectra are shown. The other lines identified as belonging to the same center behave in the same way within the experimental accuracy: their intensity is scaled only by a factor which depends neither on temperature nor on the pump power. Typically, three temperature regimes can be distinguished. At low temperatures, the intensity is constant or it increases even with increasing temperature for some centers, at intermediate temperatures (20...100 K), it decays with a center dependent activation energy of 5..15 meV and above 100 K the deactivation energy of 60..90 meV is practically the same for all Er centers within a sample. We interpret these regimes after introducing concepts for the energy transfer from the host crystal to the Er 4f shell.

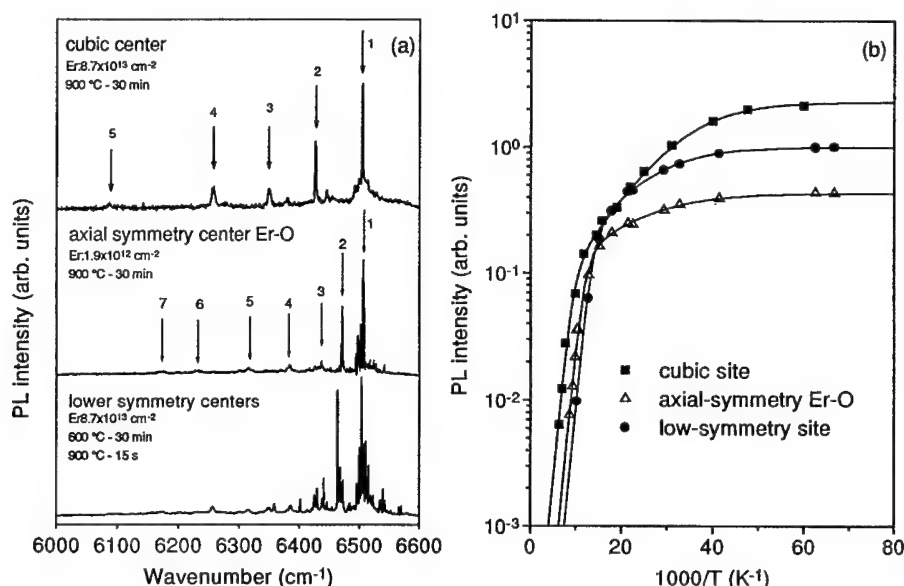


Fig.1: (a) Spectra of Er implanted into Si at 2 MeV (top and bottom) and 320 keV (middle). The Er dose and the annealing conditions are indicated in the figure. The middle trace spectrum is amplified by a factor of 50. (b) Temperature dependence of the PL intensity for the cubic center from the top spectrum in (a), as well as the Er-O complex and a lower symmetry center (denoted with O1 and ED2 in Tab. 1) measured in the same sample (bottom spectrum in (a)).

In Fig. 1b it is seen that the cubic center is the strongest luminescent center in the whole regime. There have been attempts in the literature to explain the different PL yield of different Er centers in terms of breaking of selection rules of the parity forbidden intra 4f transition. It turns out, however, in time resolved measurements that the radiative life time of these centers is practically the same [15].

### 3. ENERGY TRANSFER, QUENCHING AND THE INFLUENCE OF HYDROSTATIC PRESSURE

The originally rather weak PL yield has been substantially improved over the years by codoping with light elements and by optimizing the annealing procedures without, however, gaining much insight in the underlying physical mechanisms [4-6, 9-11]. In particular, the question, how the energy is transferred from the host crystal to the 4f shell of Er, which produces this PL, is only tentatively solved [16].

**Table 1:** Wavenumbers of some of the most characteristic PL lines observed in Er-implanted Si, depending on the implantation and annealing parameters.. Hot lines and unidentified lines were presented elsewhere [12].

Notation	Wave-number (cm <sup>-1</sup> )	Assignment	Material	Dose	Energy MeV	Annealing Temp. (°C)	Annealing time (s)	Remarks
<b>C</b>	6504.8 6426.0 6348.0 6256.0 6087.0	Interstitial Er on cubic site (Er <sub>i</sub> )	FZ, CZ	low and high	0.3, 0.6, 0.3, 0.6 2	900 600/..800 900	1800 1800/15 1800	in Er-diffused layer, close to solubility limit
<b>O1</b>	6507.5 6472.8 6437.3 6384.3 6314.5 6229.0 6173.0	Oxygen related complex	CZ only	<5x10 <sup>17</sup> cm <sup>-3</sup>	0.3, 0.6 0.3, 0.6 2	900 600/900 600/900	1800 1800/15 1800/15	Dis-sociates for T> 1000°C
<b>O2</b>	6508.6 6471.0 6438.2 6386.0 6314.5 6229.0 6173.0	Oxygen related complex	CZ only	<5x10 <sup>17</sup> cm <sup>-3</sup>	0.3, 0.6 0.3, 0.6 2	900 600/900 600/900	1800 1800/15 1800/15	Dis-sociates for T> 1000°C
<b>ED1</b>	6498.5 6498.3 6498.0 6497.5	Complex of Er and implantation defect(s)	FZ, CZ	high	0.3, 0.6 0.3, 0.6 2 2	900..1000 600/1000 900 600/900	1800 1800/15 1800 1800/15	increases with Er, O, or N dose
<b>ED2</b>	6464.4	Complex of Er and implantation defect(s)	CZ	high	2	600/900	1800/15	



It is generally accepted that localization of excitons or non-equilibrium carriers is involved in this process. In the first step, the incident photon is absorbed, generating an electron-hole pair. At low temperatures and low excitation densities the thermalized carriers form long living excitons, since due to the indirect band gap of Si exciton recombination requires the participation of a wavevector conserving phonon. Such excitons can transport near band edge excitation energy over macroscopic distances, much wider than the shallow Er-containing surface layer which is produced either by ion implantation or molecular beam epitaxy. Then these excitons are trapped at or close to an Er containing defect located near to the surface. In the next step, the excitation recombines transferring the necessary energy for the intra-4f transition from the  $J=15/2$  ground state to the excited  $J=13/2$  state. Obviously different Er configurations have different efficiencies in this transfer process which in principle should allow to optimize the PL yield by "breeding" particularly suitable Er complexes by coimplantation and short time annealing procedures (see Table 1 and Refs. 4, 6, 13).

The three temperature regimes seen in Fig. 1b can be understood in the following way. Below 20 K all excitons, either generated within or diffusing into the Er-layer, are firmly bound close to the Er centers and have sufficient time to transfer their energy. For thin, shallow implants of Er the PL intensity of some centers, the less efficient ones in exciton trapping, is even observed to increase with increasing temperature in this regime, since the excitons (which are generated within the absorption length of more than  $1\mu\text{m}$  at the applied pump wavelength) are easily trapped by other crystal imperfections, such as neutral donors or acceptors, before they reach Er ions. At slightly elevated temperatures they can be thermally released from centers with low binding energies and migrate more efficiently towards the doped layer [13, 17]. We observe a PL intensity increase activated with an energy typical for P or B exciton binding (depending on the conduction type) accompanied by a simultaneous increase of free exciton emission.

At intermediate temperatures, typically in the range of 20 to 100 K, the PL decays with an activation energy varying between 5 and 15 meV, depending only on the type of Er center but not on the sample investigated. This deactivation energy is ascribed to the thermal ionization of excitons bound at or near the Er center, which increases the probability of exciton decay at other recombination centers, distant from the optically active Er ion. This process can account for a decrease of the Er PL intensity by up to an order of magnitude at 100 K, depending on the sample preparation conditions. Moreover, it turns out that many of the nonradiative recombination defects responsible for locking the excitation away from the luminescent Er centers are introduced by implantation and annealing, as evidenced by deep level transient spectroscopy (DLTS). Even for extremely low Er implant doses ( $10^{12}\text{ cm}^{-2}$ ) a variety of deep electron trap levels has been observed after annealing [12,18]. Though the concentration profiles of those defects coincide with the as-implanted Er profile and Er evidently enters into such defects, a comparison of their annealing curves with those of the luminescent Er centers excludes the possibility that electrically and optically active Er centers are in any way related to each other. In contrast, the deep defects act as very efficient nonradiative recombination centers as the intensities of both the near band edge and Er related emissions reach a maximum for the annealing temperature of 900 °C when the total defect concentration approaches minimum. Three of the deep levels observed, with apparent enthalpies (the capture coefficient was too big for direct determination) of 0.15, 0.6 and 0.8 eV remain, however, stable up to annealing temperatures of 1000 °C and might be involved in the parasitic recombination channels.

Above 100 K, the PL intensity decays rapidly with a sample dependent deactivation energy of 60-150 meV, which seems, however, to be the same for all Er centers within one sample. This quenching regime is highly efficient owing, first of all, to the reduced efficiency of energy transfer from the host to Er because of the thermal dissociation of excitons. Moreover, the increased concentration of free carriers does not affect only the efficiency of nonradiative recombination at deep levels but it also activates new parasitic recombination paths. Since the deactivation energy does not depend on the kind of luminescent Er center obviously a common recombination channel is activated related, *e.g.*, to a level controlling the carrier concentration. As the Er luminescence decay is accompanied by a decrease of the Er lifetime, nonradiative recombination processes within Er centers are also involved. However, the frequently postulated back transfer mechanism related to nonradiative Er de-excitation with energy transfer back to the bound exciton seems to be rather improbable due to the low oscillator strengths for indirect band transitions, on the one hand, and the high thermal excitation energy needed to overcome the energy mismatch between the Er intra-shell and the exciton generation, on the other hand.

The energy transfer from the host to Er will be more efficient if the energy released is close to the intra 4f excitation energy. A small energy mismatch can be accommodated by local phonons or other low energy excitations. Now, the Er excitation energy is about 300 meV smaller than typical exciton recombination energies, which requires a large number of phonons to dissipate the energy difference. The recombination of carriers at some deep defect with a suitable energy level in the gap as intermediate step might be more efficient. Such a defect could, *e.g.*, bind one of the carriers on the level directly, which would lower the bound exciton recombination energy (as compared to energies typical of excitons bound at neutral shallow impurities in Si) and hence "tune" it to the Er transition energy. This process will also suffer from "back transfer": at elevated temperature nonradiative de-excitation of the Er ions may cause a re-excitation of the "activator" level which finally releases the bound carrier(s) by thermal excitation.

In order to test such a possibility, we have performed a study of Er in Si under hydrostatic pressure. The sample is put into a hydraulic pressure cell employing a piston and benzene as pressure transmitting medium up to a pressure of 20 kbar. The cell is attached to a cold finger cryostat and cooled to temperatures down to 10 K.

In Fig. 2a two PL spectra of Si:Er,O are shown for 0 and 12 kbar, respectively. It is clearly seen that pressure affects lines which belong to different centers in different ways: some lines increase strongly, some decrease and others seem to be unaffected. The dependence of the PL intensity for the two lines indicated in Fig. 2a by arrows on temperature is given in Fig. 2b for the two pressures of 0 and 12 kbar each. The line at  $6498\text{ cm}^{-1}$  (ED1) stems from a low symmetry Er complex with an implantation induced defect and shows the typical PL quenching with a deactivation energy of 15 meV up to 100 K and a rapid drop at higher temperatures. The PL lines occurring in the high energy spectral range (*e.g.* at  $6537.7\text{ cm}^{-1}$ ) are new features appearing only after O coimplantation to peak concentrations of about  $10^{19}\text{ cm}^{-3}$ . They originate either from small  $\text{SiO}_2$  precipitates containing Er, or from Er decorated dislocations and are not excited via energy transfer from bound excitons as the PL intensity increases with increasing concentration of free carriers (at elevated temperatures or higher pump powers), which can recombine, *e.g.*, at a dislocation related deep level transferring the excitation to the Er ions. As seen in Fig. 2b the PL yield of the Er centers with the exciton mediated excitation mechanism increases considerably under hydrostatic pressure relative to the other centers observed. (The

data in Fig. 2 have not been corrected for possible changes of the refractive index of the pressure transmitting medium but are presented "as measured".)

This type of behavior is observed only in samples with additional oxygen codoping, as shown in Fig. 3: here the temperature dependence of the normalized PL intensity of the cubic center under ambient pressure and at 11 kbar is shown for samples with and without additional oxygen. Only after oxygen coimplantation the beneficial effect of the hydrostatic pressure is observed.

We may conclude from these findings that oxygen provides an additional path for energy transfer from the Si crystal to the Er 4f shell. This additional transfer mechanism depends obviously strongly on pressure. In the case of the cubic Er center (C) and one of the centers ascribed earlier to a complex of Er and some intrinsic implantation defect (ED1 in Table 1), high hydrostatic pressure causes an increase in intensity by almost an order of magnitude in an intermediate temperature regime (140 K > T > 25 K).

In order to model the temperature and pressure dependent luminescence intensity we consider in the following simplified rate equations for the energy transfer to the 4f shell:

$$\frac{\partial N_{BE}}{\partial t} = n_{FE} c_{BE} (N - N_{BE} - N^*) - N_{BE} e_{BE} \exp\left(-\frac{E_{BE}}{kT}\right), \quad (1)$$

where  $N_{BE}$  stands for the concentration of Er centers which have a bound exciton at some center in the neighborhood (at the Er center itself or within the transfer distance). The total concentration of such Er centers is  $N$ . Out of these,  $N^*$  are in the excited state.  $c_{BE}$ ,  $e_{BE}$  and  $E_{BE}$  stand for the capture and the emission coefficients and the activation energy for the detachment (or ionization) of bound excitons, respectively.  $n_{FE}$  is the number of free excitons.

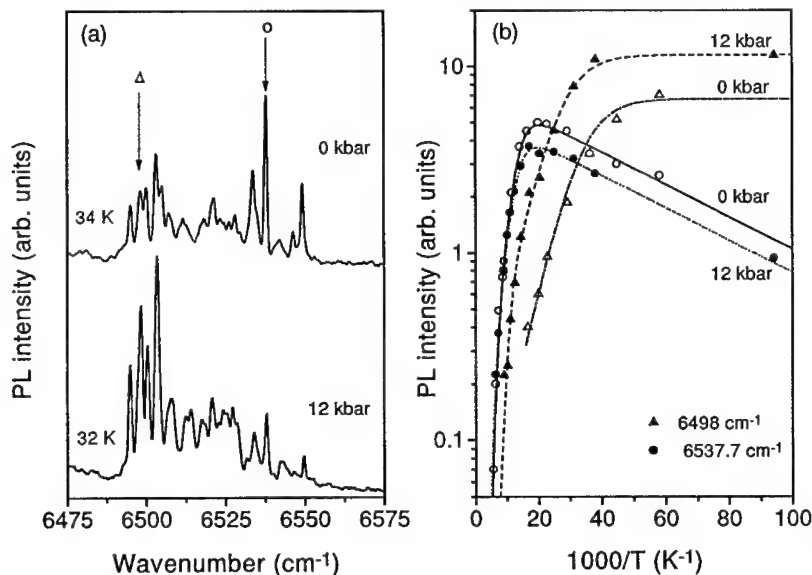


Fig. 2a) Photoluminescence of Si:Er,O without and with a hydrostatic pressure of 12kbar. b) Arrhenius plot of the luminescence intensity of two lines marked in fig. 1a (circle and triangle, respectively) with and without pressure.

The excitation and decay of the Er centers are described by the following rate equation:

$$\frac{\partial N^*}{\partial t} = \beta N_{BE} - \frac{N^*}{\tau_{Er}} \quad (2)$$

where  $\beta$  is a coupling coefficient that describes the net rate at which the energy of the bound exciton is transferred to the Er 4f shell, and  $\tau_{Er}$  is the lifetime of the  $J=13/2$  state. The third rate equation describes the generation of free excitons:

$$\frac{\partial n_{FE}}{\partial t} = G - \frac{n_{FE}}{\tau_{FE}} - n_{FE} c_{BE} (N - N_{BE} - N^*) \quad (3)$$

where  $G$  is the generation rate (proportional to the laser intensity) and  $\tau_{FE}$  is the lifetime of free excitons, which includes all the nonradiative recombination channels and trapping paths for the sake of simplicity.

In steady state, the r.h.s. of Eqs. 1-3 is zero and we obtain for the luminescence intensity, which is proportional to  $N^*$ , the expression:

$$I = I_0 \left[ 1 + \frac{c_{BE}^{\infty} \exp\left(-\frac{E_{BE}}{kT}\right)}{n_{FE} c_{BE} (1 + \beta \tau_{Er})} \right]^{-1} \quad (4)$$

Fitting such expressions (two exponentials are used in order to account for the different slopes in the two regimes of above and below 100 K) to the observed temperature dependence under pressure shows, that in the intermediate temperature regime the deactivation energy is independent of pressure, in contrast to the prefactor which is strongly affected (see Fig. 4). The prefactor, according to equ.(4) contains the transfer coupling coefficient  $\beta$  and other center independent parameters, like the lifetime of the free excitons. The latter could, in principle, depend on pressure as nonradiative recombination at deep levels might be affected by changing of the level positions relative to the band gap, but such effects should be rather negligible, at least as long as no large lattice relaxation around a defect is involved. Therefore, we attribute the observed influence to the pressure dependence of the transfer rate,  $\beta$ , i.e., to the pressure activation of an additional, oxygen mediated excitation channel contributing to the overall rate.

One of the likely candidates for such an additional Er excitation mechanism could be an exciton (or an electron-hole pair) with at least one of the carriers deeply bound at an oxygen

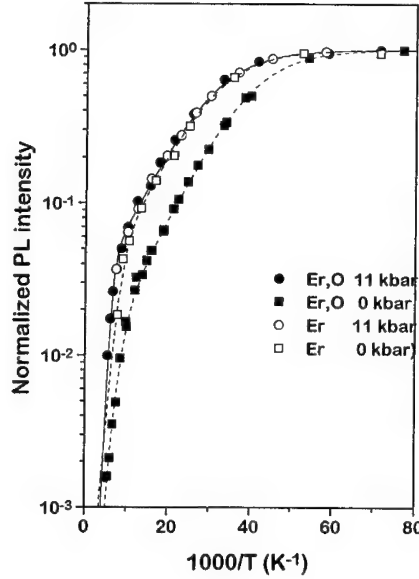


**Fig. 3:** Arrhenius plot of the luminescence intensity of Si:Er,O (full symbols) as compared to that of a sample without additional O implantation (open symbols), with and without a pressure of 11 kbar.

related deep level, which recombines nonradiatively transferring its excitation energy to the 4f shell. The recombination energy of such an exciton would depend on the level position in the Si gap and could be tuned by pressure to match better the intra-4f-shell transition energy thus increasing the transfer probability. Thermal ionization of such an exciton would occur at much higher temperatures than that of excitons bound on neutral traps. Therefore the Er PL in the intermediate temperature range would be still governed by the deactivation of the latter excitation channel, with an energy typical for loosely bound excitons. Therefore, as confirmed in the experiment, no measurable influence of pressure on the deactivation energy is expected in this temperature regime since the shallow bound excitons are extended, band-like states and like all shallow states are known to exhibit very small pressure coefficients in silicon [14].

The activation energy above 100 K, however, depends strongly on pressure: it increases from 60 meV at atmospheric pressure to more than twice this value at 17 kbar (see Fig. 4b). Apparently, within our picture, in this regime the defect state itself is activated, allowing back transfer of the excitation from the Er to the carrier system [19], or the defects ability as co-activator is impaired by a change in its equilibrium charge state. In both cases we would observe a pressure coefficient of the deep defect level relative to the bands which can be as big as the estimated values [20]. It is also possible that the observed change is due to the pressure dependence of some common level controlling, *e.g.*, the carrier concentration and thus the nonradiative recombination paths within the whole system.

The proposed mechanism requires a high concentration of these activators since their efficiency relies on the overlap of electric dipole fields which decrease strongly with distance. For lower Er and O concentrations, it might simply act as parasitic recombination center. So in this model, the activation and part of the high temperature quenching might even have a common origin. In the absence of experiments which detect the activator state and correlate it to the Er emission this explanation remains somewhat speculative. Other processes, like an Auger process, in which the back transfer consists in a heating of free carriers, may also be considered [21]. Here a pressure dependence of the free carrier concentration is also conceivable and thus an influence of pressure on the efficiency of such a process. The determination of the carrier concentration within the Er doped layer on top of a conducting crystal of 400  $\mu\text{m}$  is not trivial but an estimation both from Hall effect and C-V measurements gives a room temperature electron concentration of less than  $10^{16} \text{ cm}^{-3}$ , for which we would not expect a very strong Auger effect. However, the light induced carrier concentration might contribute here also.

#### 4. CONCLUSIONS

We have shown that the photoluminescence of Er implanted Si is governed by a rich variety of centers which show complicated line patterns. The lines belonging to one type of center are identified by their relative intensities which remain constant as experimental and preparation conditions are modified. The strongest PL lines, particularly at temperatures above 140 K, belong to a center with cubic surrounding which has been attributed to the isolated interstitial Er in Si. The temperature dependence of the PL intensities exhibit de-activation behavior. A corresponding model is developed, which considers (i) energy transfer via bound excitons and their detachment at intermediate temperatures (20..100 K) and (ii) quenching by bypass recombination via trap states at temperatures well above 100 K.

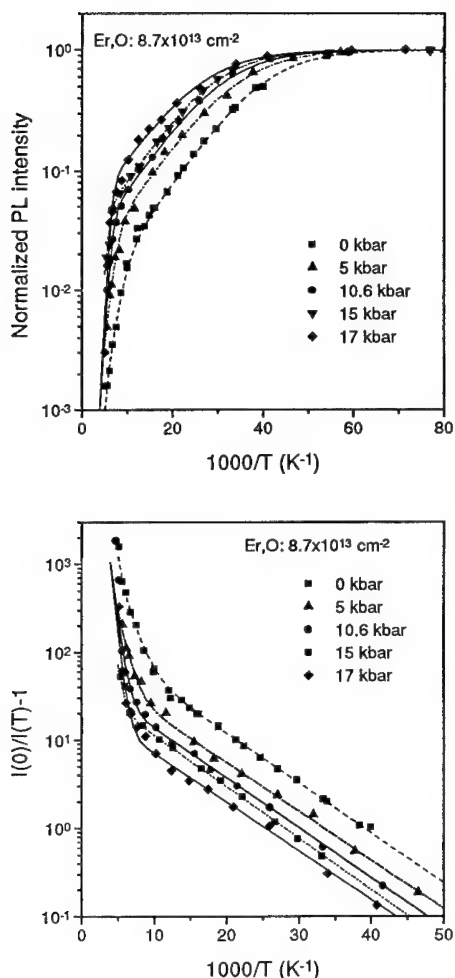


Fig. 4: Arrhenius plot of the luminescence intensity of the main cubic line in Si:Er,O for different pressures (upper diagram). In the lower part of the diagram the data are redrawn in order to linearize the slopes for the determination of the activation energies. Lines: results from fits according to equ. 4.

caused by the pressure applied in our experiments is comparable in magnitude to that occurring in short period, pseudomorphic superlattices of Si-Ge-C.

Samples with additional oxygen implantation exhibit a strong influence of pressure on the PL yield. We suggest a new mechanism for the energy transfer in such samples, namely capture and recombination of excitons at some deep, oxygen related defect state, which transmits one part of the energy released to the Er 4f state. This process is expected to work best if the energy released matches the intra-4f excitation energy and pressure allows to tune the mismatch in some range. In the intermediate temperature regime, backtransfer is not likely and quenching is governed by the competition of exciton detachment and the defect mediated transfer to the 4f shell. The latter is strongly pressure dependent. In this range, the de-activation energy is defined by the binding and/or ionization energy of the exciton which is practically independent of pressure in agreement with experiment. The pressure dependence there is caused by the coupling of the defect state and the Er 4f shell.

The pressure dependence is observed only in oxygen co-doped samples which demonstrates another beneficial role of oxygen on the luminescence yield of erbium in Si. We have seen in high resolution PL that oxygen forms low symmetry complexes with Er which contribute to the luminescence. In addition, oxygen was shown to facilitate the incorporation of Er and to prevent surface precipitation [22] and it was also shown that oxygen passivates other recombination channels [12]. The pressure mechanism indicates also new possibilities to improve the efficiency of Si:Er based light emitting devices at high temperatures: the strain

## ACKNOWLEDGMENTS

It is a pleasure to thank R.J. Wilson for some of the implantations and A. Kozanecki, A. Polman, J. Langer, and T. Gregorkiewicz for helpful discussions. Work supported by *Gesellschaft für Mikroelektronik*, Vienna, and by the *Fonds zur Förderung der Wissenschaftlichen Forschung*, Austria.

## REFERENCES

1. H. Ennen, G. Pomrenke, A. Axmann, K. Eisele, W. Haydl, and J. Schneider, *Appl. Phys. Lett.* **46**, 381 (1985)
2. Y.S. Tang, K.C. Heasman, W.P. Gillin, and B.J. Sealy, *Appl. Phys. Lett.* **55**, 432 (1989)
3. J.L. Benton, J. Michel, L.C. Kimerling, D.C. Jacobson, Y.-H. Xie, D.J. Eaglesham, E.A. Fitzgerald, and J.M. Poate, *J. Appl. Phys.* **70**, 2667 (1991)
4. S. Coffa, G. Franzo, F. Priolo, A. Polman, and R. Serna, *Phys. Rev. B* **49**, 163313 (1994)
5. F.Y.G. Ren, J. Michel, Q. Sun-Paduan, B. Zheng, H. Kitagawa, D.C. Jacobson, J.M. Poate, and L.C. Kimerling, *Mat. Res. Soc. Symp. Proc.* **301**, 87 (1993)
6. J. Michel, F.Y.G. Ren, B. Zheng, D.C. Jacobson, J.M. Poate, and L.C. Kimerling, *Materials Science Forum* **143-147**, 707 (1994)
7. D.L. Adler, D.C. Jacobson, D.J. Eaglesham, M.A. Marcus, J.L. Benton, J.M. Poate, and P.H. Citrin, *Appl. Phys. Lett.* **61** (1992) 2181
8. D.J. Eaglesham, J. Michel, E.A. Fitzgerald, D.C. Jacobson, J.M. Poate, J.L. Benton, A. Polman, Y.H. Xie, and L.C. Kimerling, *Appl. Phys. Lett.* **48**, 2797 (1991)
9. G. Franzo, F. Priolo, S. Coffa, A. Polman, and A. Carnera, *Appl. Phys. Lett.* **64**, 2235 (1994)
10. H. Przybylinska, J. Enzenhofer, G. Hendorfer, M. Schoisswohl, L. Palmetshofer and W. Jantsch, *Mat. Science Forum* **143-147**, 714 (1994)
11. H. Przybylinska, G. Hendorfer, M. Bruckner, L. Palmetshofer, and W. Jantsch, *Appl. Phys. Lett.* **66**, 490 (1995)
12. H. Przybylinska, W. Jantsch, Yu. Suprun Belevich, M. Stepikhova, L. Palmetshofer, G. Hendorfer, A. Kozanecki, R.J. Wilson, and B.J. Sealy, *PRB*, *submitted*
13. W. Jantsch, G. Hendorfer, M. Bruckner, L. Palmetshofer, and H. Przybylinska, *Proc. XXII. Int. Conference on the Physics of Semiconductors*, ed. by D. J. Lockwood, (World Scientific Publishing, Singapore 1995) p 2411
14. W. Jantsch, K. Wünnstl, O. Kumagai, and P. Vogl, *Phys. Rev. B* **25**, 5515 (1982)
15. H. Przybylinska, G. Hendorfer, M. Bruckner, W. Jantsch, and L. Palmetshofer, *Journal of Alloys and Compounds* **225**, 555 (1995)
16. Jung H. Shin, G. N. van den Hoven, A. Polman, *Appl. Phys. Lett.* **67**, 377 (1995)
17. G. Davies, *Physics Reports* **176**, 85ff (1989)
18. W. Jantsch, H. Przybylinska, Yu. Suprun Belevich, M. Stepikhova, G. Hendorfer, and L. Palmetshofer, *Materials Science Forum* **196-201**, 609 (1995)
19. K. Takarabe, T. Mizushima, S. Minomura, A. Taguchi, and K. Takahei, *Materials Science Forum* **196-201**, 645 (1995)
20. K. Wünnstl, O. Kumagai, P. Wagner, and W. Jantsch, *Appl. Phys. A* **27**, 251 (1982)
21. J.M. Langer, in *Electroluminescence*, Springer Proceedings in Physics, edited by S. Shionoya and H. Kobayashi, Vol. **38**, pp. 16-23 (Springer, Berlin Heidelberg, 1989)
22. R. Serna, M. Lohmeier, P.M. Zagwijn, E. Vlieg and A. Polman, *Appl. Phys. Lett.* **66**, 1385 (1995)

## THE EFFECTS OF IMPURITY CODOPING ON THE ELECTRICAL PROPERTIES OF ERBIUM IONS IN CRYSTALLINE SILICON

S. LIBERTINO<sup>a</sup>, S. COFFA<sup>b</sup>, R. MOSCA<sup>c</sup>, E. GOMBIA<sup>c</sup>

<sup>a</sup> *Dipartimento di Fisica, Università di Catania, Corso Italia 57, I-95129, Catania, Italy*

<sup>b</sup> *CNR-IMETEM, Stradale Primrose 50, I-95121, Catania, Italy*

<sup>c</sup> *CNR-MASPEC, Via Chiavari 18a, I-43100, Parma, Italy*

### ABSTRACT

We have investigated the effects of oxygen codoping and thermal annealing on the deep level spectrum and carrier lifetime of Er implanted crystalline Si. It is found that oxygen codoping produces a dramatic modification in the concentration and energetic position of Er-related deep levels in the Si band gap. In particular the formation of Er-O complexes is shown to produce a promotion from deep to shallow levels. This effect is the major responsible of the enhancement of Er donor behaviour in presence of oxygen and also produces a large increase in the minority carrier lifetime.

### Introduction

Rare-earth ions doping of semiconductors [1] has attracted considerable interest since it allows to combine the excellent electronic properties of semiconductors with the peculiar optical properties of rare-earth ions. These ions exhibit sharp, atomic like, emission due to transitions within their unfilled 4f shell. In particular Er has been extensively investigated because its transition at 1.54  $\mu\text{m}$  matches the maximum transmission in silica optical fibres. Er incorporation in a variety of semiconductors such as GaAs [2], InP [3] and Si [4-6] has been studied. Theoretical [7] and experimental [4,8,9] investigations of the process responsible for carrier-mediated Er excitation in semiconductors have clearly indicated that: a) Er-related deep-levels in the band gap are a pathway for the energy transfer from the electronic system of the semiconductor to the internal 4f shell of Er ions; b) the properties of these levels, such as their energy position, cross section and emissivity, determine the rate of the temperature quenching [9] of the Er photoluminescence (PL) yield which occurs above 100-150 K with an activation energy of  $\sim 0.15$  eV; c) alternative recombination routes for carriers, not ending up with Er excitation, greatly reduce the excitation efficiency: a reduction of these routes, resulting in an increase of minority carrier lifetime, produces [10, 11] a shift of the onset of the temperature quenching to higher temperature thus enhancing room temperature PL yield.

Codoping with impurities such as O and F has been shown [9, 10] to be able to both increase excitation efficiency and reduce temperature quenching. In a recent paper [8] we have demonstrated that the deep level properties of Er in crystalline Si are greatly modified by codoping with impurities such as O, F and C and we have explained these modifications in terms of the formation of Er-impurity complexes. In this work we have investigated deep and shallow levels introduced by Er and the effect of impurity codoping and thermal processes on the concentration and energetic position of these levels. The implications of these results on the comprehension of the mechanism of Er-excitation and de-excitation in Si is discussed.

### Experimental

In this work we have used  $p^+-n$  junctions realised by diffusing B in a n-type epitaxial Si wafer with a resistivity of 7  $\Omega\text{cm}$  and a thickness of 22  $\mu\text{m}$  grown on a  $n^+$  substrate. Erbium has been introduced by ion implantation at an energy of 5 MeV and to fluences in the range  $6 \times 10^{11}$ - $6 \times 10^{12}/\text{cm}^2$ . Multiple oxygen implants have also been performed on some of these wafers in order to have an almost flat oxygen concentration at  $\sim 1 \times 10^{18}/\text{cm}^3$  in the region where Er sits. For the



sake of comparison some diodes were left unimplanted and some were only implanted with O. Thermal annealing at 900°C for 30 sec or at 900°C for 30 min under nitrogen flux were performed on the different samples. On these diodes we have performed Capacitance-Voltage (C-V) measurements and Deep Level Transient Spectroscopy (DLTS) analyses in the temperature range 30-300 K. For DLTS measurements the diodes were reverse biased at -4 V in order to include all the implanted species within the depletion region. A filling pulses voltage at a +0.3 V with a duration of 1 msec were used to fill the traps. All the DLTS spectra were measured with a rate window of 1000 s<sup>-1</sup>. We also measured the lifetime of the minority carriers by monitoring the reverse recovery current transient when the diodes are switched from forward (with a current flux I<sub>F</sub> of 1 A/cm<sup>2</sup>) to reverse bias. From these measurements the hole lifetime  $\tau_p$  was calculated using the relation  $\tau_p = 2tI_R/I_F$  [12], where t is the recovery time and I<sub>R</sub> is the maximum value of the reverse current during the transient.

#### Deep and shallow Er-related levels in Si band gap

The epitaxial layer that we have used in the present study is highly pure since it contains C and O concentration below 10<sup>15</sup>/cm<sup>3</sup>. It is therefore suitable to explore the intrinsic deep-level properties of Er since the formation of Er impurity complexes is expected to be severely reduced. In Fig. 1 we compare the deep level spectra measured in the range 30-300 K on a sample implanted with Er (5 MeV, 6×10<sup>11</sup>/cm<sup>2</sup>) and on a sample which was also coimplanted with O (multiple implants resulting in a flat concentration of 10<sup>18</sup>/cm<sup>3</sup>). Both samples have been annealed at 900 °C for 30 sec. The sample only implanted with Er (solid line) exhibit at least 4 well distinct peaks with energies of 0.51 eV, 0.33 eV, 0.26 eV and 0.20 eV (all measured from the bottom of the conduction band). All these levels have been demonstrated to be Er-related [8] and associated to Er-defect complexes. A completely different picture emerges for the Er+O implanted sample (dashed line in Fig. 1). First of all a dramatic reduction (more than one order of magnitude) occurs in the concentration of very deep levels. Moreover three new distinct shallow levels at energies of 0.16 eV, 0.11 eV and ~0.08eV from the conduction band have been found. Conductance measurements as a function of the temperature (not reported) show that only the 0.11 eV level might be present in the samples only implanted with Er (solid line). Moreover, the fact that these three levels are not present in samples only implanted with O (dotted line) proves that these levels arise as a consequence of Er-O interaction.

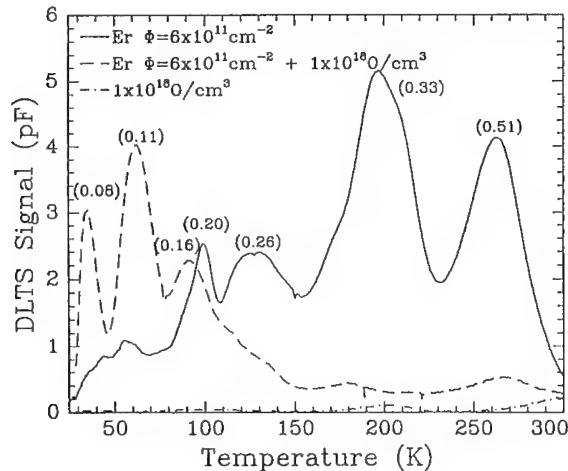


**Figure 1:** DLTS spectra of samples implanted with Er only (6×10<sup>11</sup>/cm<sup>2</sup>, 5 MeV, solid line); Er+O (dashed line), O only (multiple implants to achieve 1×10<sup>18</sup> O/cm<sup>3</sup>, dotted line). All the samples have been annealed at 900 °C for 30".

In fig. 2 we report the maximum donor concentration determined by capacitance-voltage measurements on Er and Er-O samples. Er alone (bullets in Fig. 2) introduces a maximum donor concentration of  $2 \times 10^{15}/\text{cm}^3$  ( $\sim 30\%$  of the implanted Er peak) at room temperature which rapidly decreases at temperatures below 150 K. This donor activity is due to the observed deep levels: the carriers associated to these donors can be promoted to the conduction band at high temperatures but are frozen at lower temperatures. The deep levels of the Er-O implanted sample also exhibit a donor behaviour and give an almost constant donor concentration in the temperature range 30-300 K (triangles in Fig. 2). This proves that indeed very shallow levels dominate the donor activity. The observed promotion from deep to shallow Er-related levels caused by O codoping is responsible of the previously reported [13] enhancement produced by O of the donor behaviour of Er in silicon since a much higher density of free carriers can be provided by the shallowest levels present in the Er+O implanted sample. The modifications of the deep level spectrum produced by O-codoping are likely to be responsible for the enhancement in the Er luminescence yield and for the reduction of the temperature quenching of this yield which are known [10] to occur in presence of O. In fact, Er excitation is thought to occur [7] by e-h recombination at an Er-related level in the gap with a transfer of the recombination energy to the internal 4f shell of Er. The levels that can provide efficient Er excitation at high temperature must meet at least three requirements: a) they cannot be too shallow: in fact, while very shallow levels can produce Er excitation at low temperatures ( $< 100$  K), at higher temperatures electron thermalization to the conduction band will occur before hole capture and will inhibit Er excitation; b) they cannot be too deep otherwise the recombination energy of carrier trapped at these levels is lower than 0.8 eV and hence unable to excite Er (but still these defects will provide recombination routes for carriers); c) they must be Er-related: any level due to e.g. defects will only affect the minority carrier lifetime providing alternative recombination routes for the carriers not ending up with Er excitation. Taking into account these constraints the ideal level should be located in the range 0.1-0.3 eV from the conduction band. As clearly shown in Fig. 1, O codoping simultaneously reduces the concentration of those levels which are too deep for efficient Er excitation and enhances the concentration of the levels that sit in the optimum energy window.

#### Role of thermal annealing and oxygen precipitation around Er

A fundamental question to be answered is that of the thermal stability of these levels. For only Er implanted samples, we have found that the concentration of the deep levels monotonically decreases by increasing the temperature or the time of the thermal process as result of the dissociation of Er-defect complexes. A different behaviour is found for the levels which dominate in the Er+O sample. For example, upon increasing the annealing temperature the level at 0.16eV first increases, reaches a maximum at 900 °C and then decreases. This behaviour has been

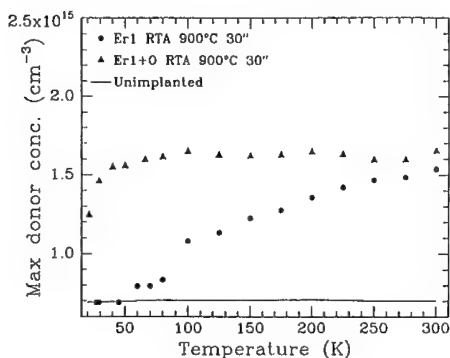


**Figure 2:** Maximum donor concentration as a function of the temperature for samples implanted with Er (5 MeV,  $6 \times 10^{11}$  Er/cm<sup>2</sup>, bullets); Er+O (multiple O implants to achieve  $1 \times 10^{18}$  O/cm<sup>3</sup>, filled triangles), unimplanted samples (solid line). All the samples have been annealed at 900 °C for 30'.

interpreted in terms of the formation of Er-O complexes and their successive dissociation or growth into more complex structures above 900 °C. Indeed, in spite of the fact that these levels are more stable, i.e. capable to stand higher thermal budgets, severe modifications occur in the relative intensity of the different levels when the thermal budget is changed. For example in Fig. 3 we compare the DLTS spectra measured on Er+O samples after 900 °C 30 sec (solid line) and 900 °C 30 min (dashed line). It should be noted that the longer thermal process causes a reduction in the concentration of the levels at  $E_C-0.16$  eV and  $E_C-0.11$  eV and a large increase in the concentration of the shallowest level. This effect also produces an increase in the maximum donor concentration of this sample from  $2 \times 10^{15}$  to  $3 \times 10^{15}/\text{cm}^3$  (which means that 50% of the Er atoms introduce a donor). On the other hand we have estimated that only 1 to 3% of the total Er concentration introduces the level at  $E_C-0.16$  eV, which is the one which gives the highest probability of Er pumping at high temperature being the deepest among the levels suitable for pumping. We have also verified that this particular level is a donor. As shown in Fig. 4, sampling regions of stronger electric field, by increasing the amplitude of the filling pulse, moves the peak to lower temperature suggesting that a Poole-Frenkel effect (i.e. emission enhanced by electric field) is operative. Hence this level is a donor as also confirmed by the large cross section for electron capture that we have measured for this centre ( $2 \times 10^{-14} \text{ cm}^2$ ). Finally it should be noted in Fig. 3 that the thermal process at 30 min also results in the introduction of a very deep centre at  $E_C-0.78$  eV. This centre might be of noticeable interest since its energy is almost resonant with that of Er excitation and it could be therefore an efficient pathway for excitation and deexcitation processes. The results so far presented show large modifications in the electronic properties of Er in Si arising from the strong interaction between Er and O. It is known from EXAFS [14] that in an oxygen-rich material Er is surrounded by a cage containing 4 to 6 O atoms, and EPR analyses identify O atoms as first neighbours of the Er ions. It is interesting to observe that oxygen precipitates in Si exhibit a donor behaviour introducing shallow levels at  $E_C-0.16$  and  $E_C-0.08$  eV, i.e. very similar to those which results from Er-O interaction. Normally the formation of the oxygen related donor [15] requires annealing at very low temperatures ( $\sim 400$  °C) and long annealing times in order to have a large rate of homogeneous O precipitation. However, in our case the strong Er-O interaction can provide a very high driving force for heterogeneous O precipitation around Er, producing the well known cage of oxygen. The modifications in the relative concentration of the shallow donor levels for larger thermal budgets, might be associated, as in the case of oxygen related thermal donors [15], to the formation of larger precipitates,

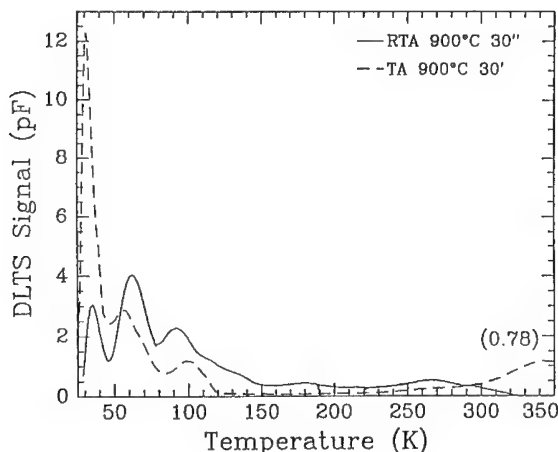


**Figure 3:** DLTS spectra of samples coimplanted with Er and O (5 MeV,  $6 \times 10^{11} \text{ Er}/\text{cm}^2$ , multiple oxygen implants to achieve a concentration of  $10^{18} \text{ O}/\text{cm}^3$ ), annealed at 900 °C 30'' (solid line), or 900 °C 30' (dashed line).

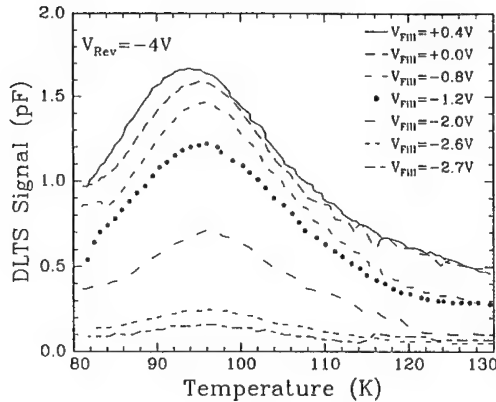


**Figure 4:** DLTS spectra as a function of the filling pulse voltage, showing the donor character of the Er-O related level at  $E_C - 0.16$  eV.

possibly containing a different number of O atoms. On the other hand if the thermal budget is too low, O is unable to reach Er and precipitate around it. Therefore an optimum thermal process exists that is expected to be strongly dependent on the absolute concentration of O and on the ratio between the concentration of Er and O atoms.

#### Measurements of minority carrier lifetime

The large reduction in the concentration of the deep levels produced by O coimplantation also produces a large increase in carrier lifetime. We checked this by performing measurements of the reverse recovery characteristics of Er and Er+O implanted diodes. When the diode is switched from forward to reverse bias the current first inverts and then reaches its equilibrium value when the full recombination of the minority carriers injected during forward bias operation is completed. From a measurement of the transient information on the carrier lifetime can therefore be achieved. In fig. 5 the recovery curves of unimplanted (solid line), only Er implanted (dashed line) and Er+O implanted sample (dotted line) are reported. All the samples were processed in a rapid thermal furnace at 900 °C for 30 sec. It should be noted that the transient duration is significantly reduced for Er implanted sample compared to the unimplanted diode; this suggests that a large reduction in the lifetime arises as a consequence of carrier recombination at the Er-related deep levels. On the other hand for Er+O implanted samples the duration of the transient returns very close to that of the unimplanted diode. In this sample in fact the concentration of deep levels is strongly

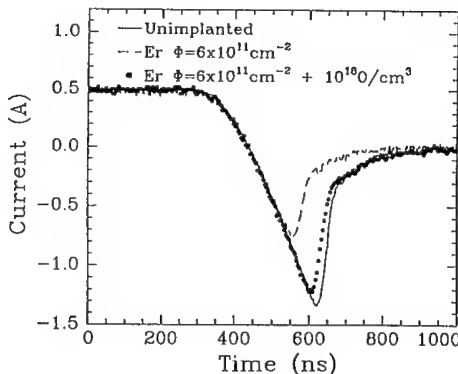


**Figure 5:** Reverse recovery curves of  $p^+-n$  diodes: unimplanted (solid line); only implanted with Er ( $6 \times 10^{11} / \text{cm}^2$ , dashed line); Er coimplanted with O ( $1 \times 10^{18} \text{ O/cm}^3$ , dotted line). The diode is switched from forward to reverse bias at  $t = 300$  nsec.

reduced (see Fig. 1) and the minority carriers lifetime returns very close to that observed in the unimplanted diode. From these measurements and from Eq. 1 we obtain  $\tau_p \sim 2\mu\text{sec}$ ,  $0.69\mu\text{sec}$  and  $1.7\mu\text{sec}$  for unimplanted, Er implanted and Er+O implanted diodes respectively. An identical behaviour (not shown) has been observed for samples implanted with higher Er fluence (up to  $6 \times 10^{12}/\text{cm}^2$ ): in the samples only implanted with Er, lifetime is reduced upon increasing the Er concentration while in Er+O implanted samples the carrier lifetime always returns towards the value characteristic of unimplanted diodes.

### Conclusion

We have shown that oxygen codoping of Er-implanted crystalline Si produces severe modifications of the electronic properties of Er with at least three noteworthy effects: 1) a reduction in the concentration of very deep levels with a consequent increase of the minority carrier lifetime; 2) an increase in the concentration of the Er-related levels which fall within the optimum window (0.1 to 0.3 eV from the conduction band) for efficient Er excitation at high temperature; 3) a large enhancement in the donor behaviour of Er in crystalline Si: as a result of this the incorporation of a high Er concentration is concomitant with the achievement of a high density of free electrons which can provide alternative recombination routes for the carriers or alternative paths of non radiative deexcitation for the excited Er ions.

### Acknowledgements

We wish to thank Antonio Marino, Nico Parasole and Aldo Spada for the expert technical assistance. Romeo Letor is also gratefully acknowledged for his help in performing the lifetime measurements. This work has been performed in the framework of the project SCOOP (Silicon Compatible Optoelectronics) supported by the European Community.

### References

- [1] Rare Earth Doped Semiconductors, vol. 301, Materials Research Society Symp. Proc. edited by G. S. Pomrenke, P. B. Klein, D. W. Langer (1993)
- [2] S. J. Chang and K. Takahei, *Appl. Phys. Lett.* **65**, 433 (1994)
- [3] H. Issiki, K. Kobayashi, S. Yugo, T. Kimura and T. Ikoma, *Appl. Phys. Lett.* **58**, 484 (1991)
- [4] J. Michel, J. L. Benton, R. I. Ferrante, D. C. Jacobson, D. J. Eaglesham, E. A. Fitzgerald, Y. H. Xie, J. M. Poate and L. C. Kimerling, *J. Appl. Phys.* **70**, 2672 (1991)
- [5] S. Coffa, F. Priolo, G. Franzò, V. Bellani, A. Carnera, C. Spinella, *Phys. Rev. B* **48**, 11782 (1993)
- [6] A. Polman, J. S. Custer, E. Snoeks, G. N. Van den Hoven, *Nucl. Instr. Meth. B* **80**, 653 (1993)
- [7] I. N. Yassievich and L. C. Kimerling, *Semiconductor Sci. Technol.* **8**, 718 (1993)
- [8] S. Libertino, S. Coffa, G. Franzò, F. Priolo, *J. Appl. Phys.* **78**, 3867 (1995)
- [9] F. Priolo, G. Franzò, S. Coffa, A. Polman, S. Libertino, R. Barklie and D. Carey, *J. Appl. Phys.* **78**, 3874 (1995)
- [10] S. Coffa, G. Franzò, F. Priolo, A. Polman and R. Serna, *Phys. Rev B* **49**, 16313 (1994)
- [11] J. Michel, F. Y. G. Ren, B. Zhang, D. C. Jacobson, J. M. Poate and L. C. Kimerling, *Proceedings of ICDS 17 Grumden (Austria)*
- [12] S. M. Sze, *Physics of Semiconductor Devices*, John Wiley & Sons, New York, 108 (1981)
- [13] J. L. Benton, J. Michel, L. C. Kimerling, D. C. Jacobson, Y. H. Xie, D. J. Eaglesham, E. A. Fitzgerald and J. M. Poate, *J. Appl. Phys.* **70**, 2667 (1991)
- [14] D. L. Adler, D. C. Jacobson, D. J. Eaglesham, M. A. Marcus, J. L. Benton, J. M. Poate, and P. H. Citrin, *Appl. Phys. Lett.* **61**, 2181 (1992)
- [15] A. Borghesi, B. Pivac, A. Sassella and A. Stella, *J. Appl. Phys.* **77**, 4169 (1995) and reference therein.

## LUMINESCENCE DECAY OF THE 1.54 $\mu\text{m}$ EMISSION FROM ERBIUM IN SILICON

J. HARTUNG\*, J.H. EVANS\*, P. DAWSON \*\*, A.P. SCHOLLES\*, T. TASKIN\*, M.Q. HUDA\*, C. JEYNES\*\*\* and A.R. PEAKER\*

\*Centre for Electronic Materials and Department of Electrical Engineering and Electronics, University of Manchester Institute of Science and Technology, PO Box 88, Manchester M60 1QD, UK, CEM@UMIST.AC.UK

\*\*Centre for Electronic Materials and Department of Physics, University of Manchester Institute of Science and Technology, PO Box 88, Manchester M60 1QD, UK

\*\*\* Department of Electronic and Electrical Engineering, University of Surrey, Guildford, Surrey GU2 5XH, UK

### ABSTRACT

Photoluminescence of silicon implanted with erbium and oxygen was measured in the time domain focussing on the temperature and excitation density dependence of the intra-4f-shell emission from  $\text{Er}^{3+}$ . The decay of this luminescence is similar for the different optically active crystal field split Er-centres. At low temperatures the luminescence transients consist of a fast initial non-exponential component followed by slower exponential behaviour. An increase in excitation density results in a higher proportion of the luminescence decaying with the faster decay time. Our results indicate a relation of the fast component to nonradiative processes. Auger recombination is proposed as a possible mechanism.

### INTRODUCTION

There is currently intense interest in rare-earth doped silicon, because of its possible application in silicon based opto-electronic devices and systems. Erbium in silicon is especially attractive because the intra-4f-shell transition between the  $^4\text{I}_{13/2}$  excited and the  $^4\text{I}_{15/2}$  ground state emits at 1.54  $\mu\text{m}$  [1], a wavelength coincident with minimum loss in silica optical fibres. Although the radiative recombination from the  $\text{Er}^{3+}$ -ion is quite strong at low temperatures only very weak room temperature electroluminescence has been reported [2, 3]. The detailed mechanisms of excitation and the nonradiative aspects of de-excitation of erbium in silicon are still under debate. The energy transfer process into the erbium atom and the reduction of the competing nonradiative recombination [4] are key issues which need to be addressed to achieve useable emission power densities at room temperature.

The energy level scheme of the 4f states of a rare earth embedded in a semiconductor is modified by the host lattice resulting in crystal field split spin-orbit states and allowing an intra-4f-shell optical transition with a long spontaneous lifetime. The crystal field split energy level schemes of three types of Er-centres with different local symmetries have been very accurately determined in a high resolution photoluminescence study [5].

A knowledge of the efficiency and lifetime of the Er-transition is a prerequisite for the development of Si:Er optoelectronic devices. In the present paper we report preliminary results from a detailed time-resolved photoluminescence analysis of the internal transition from  $\text{Er}^{3+}$  in silicon. These are discussed in terms of the various contributions of the radiative and the nonradiative decay rates.

## EXPERIMENTAL DETAILS

The samples used in this study were n-type float zone silicon with a resistivity of 20–30  $\Omega$ -cm, into which oxygen and erbium were implanted. Er was implanted with energies between 1–2 MeV and doses between  $7.5\text{--}15 \times 10^{13} \text{ cm}^{-2}$  into the (100) silicon. For an overlapping oxygen profile, oxygen was implanted with energies between 140–300 keV; the doses varied between  $1.2\text{--}5 \times 10^{14} \text{ cm}^{-2}$ . For a complete amorphization of the sample from the surface to the maximum penetration depth of the Er ions additional Si-implants were performed with energies between 80–480 keV. The Er-profile peaks at 0.55  $\mu\text{m}$  below the surface with a concentration of  $3 \times 10^{18} \text{ cm}^{-3}$ . The oxygen peak concentration was  $1 \times 10^{19} \text{ cm}^{-3}$ . The O- and Er-concentration profiles were calculated - checked using secondary ion mass spectroscopy. After the implantation the samples were annealed either at 550°C for 3 h followed by a rapid thermal anneal at 1025°C for 90 s (NS3-3) or at 900°C for 90 s only (NS3-1).

The luminescence was excited using the 514.5 nm line of an argon ion laser, which was modulated by an acousto-optic modulator. The luminescence was detected by a fast North Coast Ge-detector with a response time of 200/400 ns, cooled to 77 K. Spectral discrimination could be achieved either by a 1 m Jobin-Yvon grating monochromator or a specially produced interference filter, with a pass band centred at 1.54  $\mu\text{m}$  encompassing the transitions into the crystal field split  $^4I_{15/2}$  ground state. The photoluminescence decay measurements described in the following examine the luminescence decay after a pulse of sufficient length to achieve equilibrium (typically 5–10 ms for the excitation densities used). The luminescence decay was measured using a boxcar-detector and after digitizing was read into a computer. During the photoluminescence measurements the sample temperature could be varied between 6–300 K in a closed-cycle He cryostat and controlled with an accuracy of 0.5 K. The decay time was found by either curve fitting or determining the point at which the intensity fell to 1/e of its original value.

## EXCITATION AND RECOMBINATION

A rare earth doped semiconductor undergoing an excitation necessary to create photoluminescence can be considered as two coupled systems. The first system is the semiconductor host in which minority carriers and/or excitons are generated. Some of these transfer energy to the rare earth while the remainder are lost via other recombination channels [4]. In silicon, these “other” recombination channels are predominantly nonradiative and will exhibit some temperature dependence according to the mechanisms involved. A measurement of the minority carrier or exciton lifetime monitors the summation of these first system processes. The rare earth ion and its immediate atomic environment constitutes the second system. The two systems are coupled by the excitation processes and in some circumstances by a de-excitation process.

In an uncoupled system exhibiting exponential decay of the radiative emission, the measured decay time  $\tau_{\text{eff}}$ , contains both the radiative lifetime  $\tau_{\text{rad}}$  and the nonradiative lifetime  $\tau_{\text{nonrad}}$ . For a simple impurity or band to band system this can be written as

$$1/\tau_{\text{eff}} = 1/\tau_{\text{rad}} + 1/\tau_{\text{nonrad}}. \quad (1)$$

The value of  $\tau_{\text{nonrad}}$  results from several nonradiative components. If we consider the erbium ion these fall into two main categories. The first and most obvious are processes which

remove excitation from the f-shell of the erbium. Conceptually, Auger processes must figure high on the list of possibilities, indeed such behaviour has been postulated for several rare earth/host combinations [6, 7]. The second category is a rather more subtle effect, in which the nonradiative processes in the bulk have an indirect effect on the erbium excitation. These processes have been referred to generically as "back transfer" [8, 9]. The mechanism is rather ill-defined (at least at a fundamental level) but in essence is a leakage of excitation from the erbium f-shell back to the lattice. Taking a kinetic view, two parameters are of significance firstly the strength of the back transfer path and secondly the carrier/exciton lifetime in the rare earth doped region of the semiconductor. If the only recombination route for excited carriers is via the rare earth, then the "back transferred" excitation may be recycled (a common phenomena in highly efficient band to band systems) and re-excite the rare earth.

## RESULTS AND DISCUSSION

The dependence of the decay of the integrated intensity of the  $^4I_{13/2} \rightarrow ^4I_{15/2}$  transition from the  $\text{Er}^{3+}$ -ion on the excitation density at low temperature is shown in figure 1. All the temporal decays of the Er-luminescence in sample NS3-3 exhibit an exponential component at long times. This exponential component is characterised by a decay time of  $\sim 870 \mu\text{s}$ . A faster non-exponential behaviour within the first  $\sim 400 \mu\text{s}$  after the laser pulse is observed. However the initial fast decay gets more dominant with increasing excitation density. This initial fast decay, which is faster than the lifetimes observed for rare earths in semiconductors suggests the existence of a competing process present even at low temperatures. A comparison of the increase in luminescence intensity with excitation density over the range used for figure 1 reveals a sublinear dependence. This indicates a reduction in luminescence efficiency with an increased excitation density. This is unlikely to be due primarily to saturation of the  $^4I_{13/2} \rightarrow ^4I_{15/2}$  optical transition as the intensity of the  $1.54 \mu\text{m}$  emission does continue to increase and the sample structure is such that quasi-saturation phenomena are unlikely (increase of saturated active volume with excitation). Consequently, we attribute the initial fast part of the transient to nonradiative processes, which obviously become more significant at high excitation densities. This is quite evident when we compare plots of the

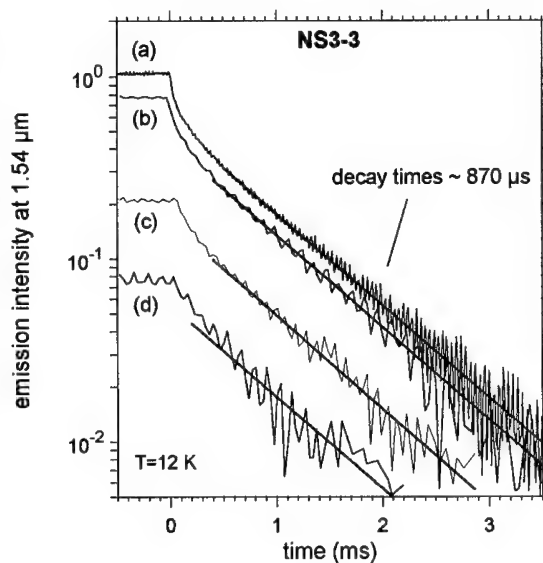


**Figure 1:** Decay of the integrated luminescence at  $1.54 \mu\text{m}$  after a laser pulse at different excitation densities: (a) 1400, (b) 700, (c) 40 and (d) 5  $\text{mW}/\text{cm}^2$ .



decay time as a function of excitation density using alternative methods of analyzing the decay transient, as shown in figure 2.

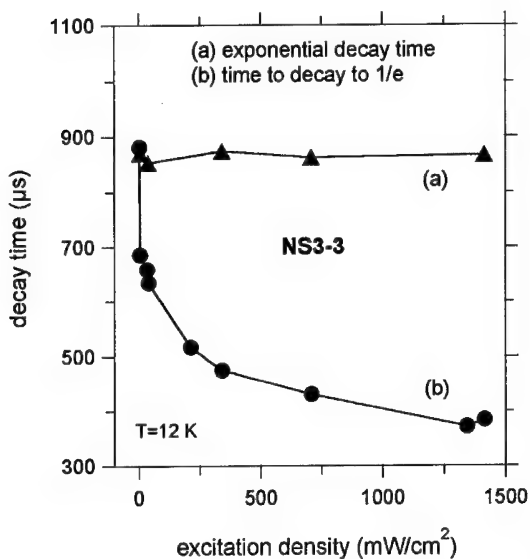


Figure 2: Dependence of the decay time on the excitation density.

ms [10]. Because of the highly efficient luminescence in these dilute systems, it is often assumed that this value approximates to the radiative lifetime with little or no nonradiative processes present.

In a semiconductor host the effective lifetime could be reduced by nonradiative processes or by a change in the local environment of the  $\text{Er}^{3+}$ -ion affecting the probability of the  $^4\text{I}_{13/2} \rightarrow ^4\text{I}_{15/2}$  transition. Although it is very difficult to predict the exact magnitude of either of these effects, an experimental distinction can be made. If the reduction in the decay time is a result of the existence of additional active nonradiative channels the photoluminescence efficiency should also be reduced. However, if the reduction of the luminescence decay time is caused by a change in the local environment of the Er-atom e.g. a change in the crystal field, the efficiency should increase. Over a wide range of samples exhibiting a different amount of the various Er-centres, we observe a reduced decay time to be accompanied by a reduced photoluminescence efficiency. This may imply that the effects related to a change in the local surrounding of the Er-atom are less significant than nonradiative processes.

To separate the contribution of nonradiative  $\tau_{\text{nonrad}}$  and radiative lifetimes  $\tau_{\text{rad}}$  to the measured decay time  $\tau_{\text{eff}}$  for constant symmetry we investigated the temperature dependence of the luminescence intensity and decay. With increasing temperatures between 6–200 K the photoluminescence intensity decreased and the transients became faster. The decay times of the transients measured at temperatures higher than 170 K could not reliably be evaluated by either the numerical or the 1/e method, described above. It can be seen

There we have plotted the luminescence decay time derived from the exponential part of the transient by curve fitting and also the time for the emission to decay to 1/e of its initial value. This latter decay time provides a semi-quantitative measure which takes into account the fast initial decay as well as the exponential component. Over the range of excitation densities used for this sample the exponential part of the decay is essentially independent of the excitation density e.g. the initial luminescence intensity, as depicted in figure 1. However, the magnitude of the fast component of the decay is excitation dependent. The exponentially decaying part of the transient can be described by equation (1) namely a contribution of both a radiative component and a nonradiative component.

In glasses the luminescence decay time has been measured to be up to several

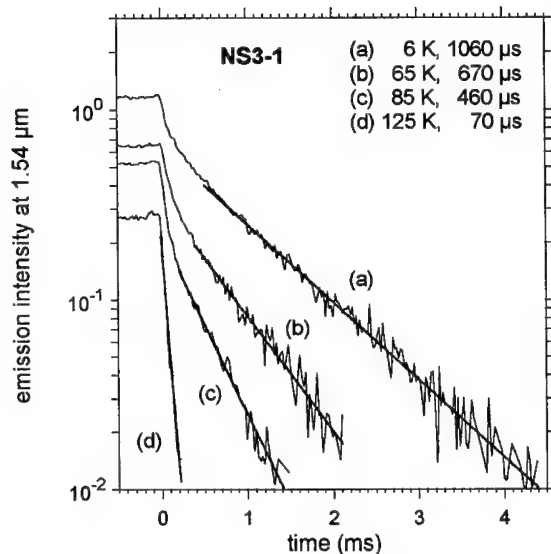


Figure 3: Decay of the integrated  $\text{Er}^{3+}$ -emission measured at different sample temperatures excited with a 7 ms laser pulse.

Here we show the decay times from the purely exponential part of the transients as triangles and the times for the emission intensity to decay to  $1/e$  of its initial value as crosses. In spite of the scatter of the various data points both the  $1/e$ -decay times and the fitted exponential decay times have a trend. The line in figure 4 is a fit to the exponential decay times assuming that the temperature dependence of  $\tau_{\text{eff}}$  relates only to a temperature dependence of the non-radiative lifetime  $\tau_{\text{nonrad}}$ , equation (1). The proportion of the initial fast ("non-radiative") part of the transient also increases with increasing temperature - compare figure 3 - as well as with increasing excitation density (figure 1). The form of this temperature dependence and that of the excitation dependence are consistent with an Auger process according to [11]. It appears that all the data points and the fit from fig-

from figure 3, that the exponential decay rate increases with increasing temperature. There is also a less pronounced increase in the rate of the initial decay - at a fixed excitation density - with increasing temperature. The dependence of the shape of the luminescence transients in our study were found to be different from the one reported earlier [9]. It is quite clear that at higher temperatures the nonradiative component is much stronger resulting in a decrease in decay time as well as luminescence intensity. The term "nonradiative component" is used in the broad sense previously defined to include "back transfer" as well as more conventional processes. The relationship is evident from a plot of the luminescence intensity against luminescence decay time, as indicated in figure 4.

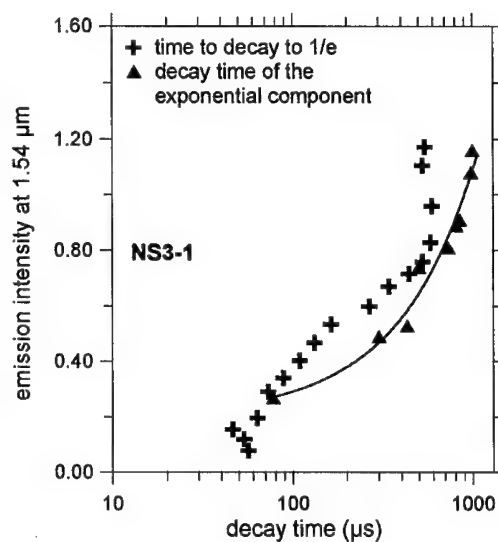


Figure 4: Intensity of the  $1.54 \mu\text{m}$  emission versus decay time, derived from the temperature dependence over the range of 6–165 K.

ure 4 show a trend, which is consistent with a basic assumption, that the radiative lifetime is essentially constant over the measured temperature range while the net nonradiative processes are temperature dependent. This is also supported by the fact that with increasing temperature, decreasing intensity respectively, the “1/e-decay time” such as in figure 4 represents mainly the fast initial component of the decay.

## CONCLUSIONS

The present study of the time dependence of the intra-4f-shell transition of Er in silicon reveals that the luminescence decay generally consists out of an initial non-exponential component and a slower exponential behaviour. However, the form of the decay curve depends in detail on the excitation density, because of the strong dependence of the initial part of the decay on the excitation density. We assign the initial fast part of the luminescence transient to predominantly nonradiative processes, which become more significant as the excitation density is increased and may be due to an Auger process. The observed temperature quenching of the luminescence at lower excitation densities is attributed to an increased strength of the nonradiative path acting to de-excite the erbium-atom.

## ACKNOWLEDGEMENTS

This work was done under a contract funded by the UK EPSRC. We thank Ian D. Hawkins and Eric Whittaker for their prompt help and their continuous support. The technical assistance of Mr. A. Mulryan and Mr. A. Lee is gratefully acknowledged.

## REFERENCES

- [1] H. Ennen, J. Schneider, G. Pomrenke and A. Axmann, Appl. Phys. Lett. **43**, 943 (1983)
- [2] B. Zheng, J. Michel, F. Y. G. Ren, L. C. Kimerling, D. C. Jacobson and J. M. Poate, Appl. Phys. Lett. **64**, 2842 (1994)
- [3] G. Franzò, F. Priolo, S. Coffa, A. Polman and A. Carnera, Appl. Phys. Lett. **64**, 2235 (1994)
- [4] T. Taskin, M. Q. Huda, A. Scholes, J. H. Evans, A. R. Peaker, P. Hemment, C. Jeynes and Z. Jafri in *Thin Films for Integrated Optics Applications*, edited by B.W. Wessels, S.R. Marder and D.M. Walba (Mat. Res. Soc. Symp. Proc. Vol. 392, Pittsburgh, PA 1995), p. 223
- [5] H. Przybylinska, G. Hendorfer, M. Bruckner, L. Palmetshofer and W. Jantsch, Appl. Phys. Lett. **66**, 490 (1995)
- [6] J. M. Langer and L. V. Hong, J. Phys. C:Solid State Physics **17**, L923 (1984)
- [7] W. Körber and A. Hangleiter, Appl. Phys. Lett. **52**, 114 (1988)
- [8] K. Thonke, K. Pressel, G. Bohnert, A. Stapor, J. Weber, M. Moser, A. Molassioti, A. Hangleiter and F. Scholz, Semicond. Sci. Technol. **5**, 1124 (1990)
- [9] S. Coffa, G. Franzò, F. Priolo, A. Polman and R. Serna, Phys. Rev. B **49**, 16 313 (1994)
- [10] S.Q. Gu, S. Ramachandran, E.E. Reuter, D.A. Turnbull, J. T. Verdeyen and S. G. Bishop, Appl. Phys. Lett. **66**, 670 (1995)
- [11] R. Haug, Phys. Status Solidi B **108**, 443 (1981)

## DEFECT ENGINEERING IN Si:ER TECHNOLOGY

N.A. SOBOLEV, O.V. ALEXANDROV, M.S. BRESLER, V.V. EMTSEV,  
O.B. GUSEV, D.S. POLOSKIN, E.I. SHEK

Ioffe Physico-Technical Institute, St. Petersburg 194021, Russia, NSobolev@optl.pti.spb.su

### ABSTRACT

Recent results contributing to our understanding of mechanisms of defect formation and excitation of Er luminescence in Si:Er system are presented. An essential role of non-equilibrium intrinsic point defects in Er-related defects formation for both implanted and in-diffused Si:Er structures is demonstrated.

The data of electroluminescence (EL) measurements evidence that the  $\text{Er}^{3+}$  excitation occurs via capture of free excitons on neutral Er-related donor centers with subsequent Auger-recombination of bound excitons.

### INTRODUCTION

Room temperature EL from Er:Si was recently observed. Nevertheless, the EL intensity has to be increased by several orders of magnitude for practical use in optoelectronics devices. To solve this problem, more comprehensive understanding of Er-related luminescence mechanisms as well as development of defect engineering techniques for preparing Si:Er with optimal properties must be achieved. Whereas many possibilities of introduction of ligand impurities (firstly, oxygen and fluorine) for formation of electrically and optically active centers have been studied in detail [1,2], little attention has been given to the impact of process-induced intrinsic point defects on defect formation.

As concerns the excitation of Er-related luminescence, it has been shown in [1] that excitation occurs via recombination of free carriers generated optically or electrically. However, there were no experimental data showing a more detailed picture of the excitation.

In this paper we report some results which point to the possible ways of defect engineering to control the electrical and optical properties of Si:Er structures and give additional information clarifying the mechanism of Er-related luminescence.

### EXPERIMENT

To reveal the role of non-equilibrium intrinsic point defects in defect formation during high temperature (1200-1250°C) annealing, erbium was introduced by ion implantation and diffusion techniques into n-Cz-Si with resistivity of 1-10  $\Omega$  cm. Er ions at energies 1.0-1.2 MeV were implanted at a dose of  $1 \cdot 10^{13} \text{ cm}^{-2}$ . In-diffusion introduction of Er was carried out at 1250°C for 0.25 hr in flowing argon-oxygen gaseous mixture from tetraethoxysilane-based films containing erbium chloride. Protection against the impact of annealing atmosphere on the defect formation was provided by means of silicon nitride films with a depth of 0.1  $\mu\text{m}$ . The use of various ambients allows to control the type of dominant excess intrinsic point defects: annealing in flowing argon results in the generation of excess vacancies and annealing in flowing oxygen leads to the Si supersaturation with self-interstitials [3].

For studies of the mechanism of excitation of Er-related luminescence, Er ions at energies of 0.8-2.0 MeV and a dose of  $1 \cdot 10^{13} \text{ cm}^{-2}$  and O ions at energies of 0.1-0.25 MeV and a dose of  $1 \cdot 10^{14} \text{ cm}^{-2}$  were co-implanted in p-type Cz-Si with a resistivity of  $7.5 \Omega \text{ cm}$ . Postimplantation annealing was carried out at  $900^\circ\text{C}$  for 0.5 hr in a chlorine-containing atmosphere. In some of the samples P ions at an energy of 75 keV were implanted a dose of  $1 \cdot 10^{16} \text{ cm}^{-2}$ . In this case postimplantation annealing was carried out at  $900^\circ\text{C}$  for 0.25 hr in nitrogen.

Contacts to light-emitting structures were prepared by evaporation of Ti-Ni-Au. A mesa-like edge contour of diodes was formed by chemical etching. The working area was about  $7 \text{ mm}^2$ .

For studying the properties of Si:Er we used the following methods: SIMS, capacitance-voltage and differential conductivity measurements, bevelling and staining techniques and EL. EL measurements were performed by passing current pulses through the diode in the forward direction. The emitted radiation was collected by a lens, dispersed using a 822 mm monochromator and detected by a liquid-nitrogen-cooled Ge detector. Spectra were recorded using the lock-in detection method.

## RESULTS

### Defect formation during high temperature annealing of Si:Er

To reveal some important features of formation of Er-related electrically active centers in implanted and in-diffused samples, we made annealing studies of the test structures supersaturated with intrinsic point defects at high temperatures ( $\geq 1200^\circ\text{C}$ ). Fig. 1 shows schematically the cross section of test structures after annealing in oxygen and argon. Annealing of the in-diffused

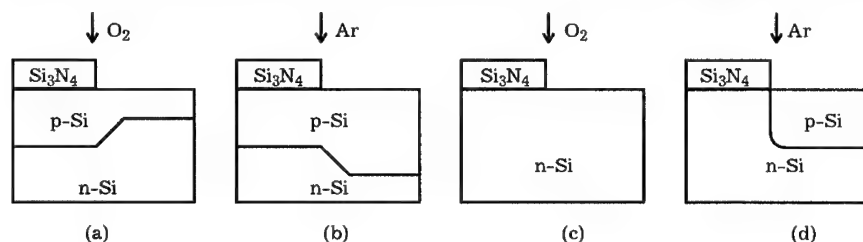


Fig. 1. Schematic cross section of the in-diffused (a and b) and implanted (c and d) structures after annealing in oxygen (a and c) and argon (b and d).

structures leads to formation of p-type layers, independent of annealing conditions. The concentration profile of acceptor centers under the surface protected by films of silicon nitride does not depend on annealing ambients. The concentration of acceptor centers and p-layer depth increase in sequence: annealing of Si wafers without silicon nitride protective films in flowing oxygen - annealing of samples under protective films - annealing of wafers without protective films in flowing argon (Fig. 1a and b). For example, the samples annealed at  $1200^\circ\text{C}$  for 4 hrs are characterized by the surface concentrations ( $N_s$ ) and p-layer depths ( $x_j$ ) as follows:  $N_{SA} = 2 \cdot 10^{18} \text{ cm}^{-3}$ ,  $N_{SNA} = N_{SNO} = 2 \cdot 10^{17} \text{ cm}^{-3}$ ,  $N_{SO} = 6 \cdot 10^{16} \text{ cm}^{-3}$  and  $x_{JA} = 5.3 \mu\text{m}$ ,  $x_{JNA} = x_{JNO} = 4.8 \mu\text{m}$ ,  $x_{JO} = 4.0 \mu\text{m}$  (the subscripts denote that annealing was made in an argon (A) or oxygen (O) ambient under silicon nitride protective films (N)).

In the case of implanted test structures, the formation of layers of p-type conductivity is observed only provided Si wafers are not protected by silicon nitride films in flowing argon (see

Fig. 1c and d). These results show that the introduction of erbium by ion implantation techniques leads to formation of very stable Er-related defects with high binding energies. For removal of Er atoms from these defects, high concentrations of excess vacancies are needed, along with high temperatures.

Note that a thin surface Si layer (its depth equals only some percent of the depth of p-type layers) is removed during annealing of samples with unprotected surface in an argon ambient (not shown in Fig. 1b and d). This evaporation of surface Si layers is responsible for generation of excess vacancies.

The study of annealing of in-diffused samples in argon shows that the concentration profile of Er-related acceptor centers is described by a Gauss function modified in the case of two-stage diffusion of impurity. The estimated diffusivity is equal to  $1 \cdot 10^{-12} \text{ cm}^2/\text{s}$  at  $1200^\circ\text{C}$  and  $4.5 \cdot 10^{-12} \text{ cm}^2/\text{s}$  at  $1250^\circ\text{C}$ .

Fig. 2 shows some experimental concentration profiles of Er-related acceptor centers after

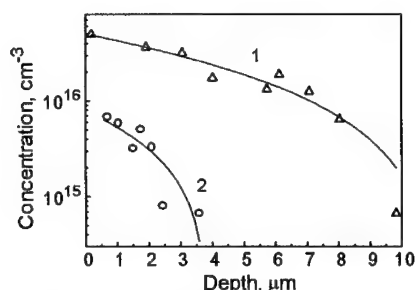


Fig. 2: Concentration profiles of acceptor Er-related centers after annealing of implanted samples at  $1250^\circ\text{C}$  (1) and  $1200^\circ\text{C}$  (2) for 4 hrs in argon.

annealing of Er-implanted samples with unprotected surface at different temperatures for 4 hrs in argon. These profiles are well described by a Gauss function with a displaced maximum. The diffusivities of Er at  $1250^\circ\text{C}$  in the cases of in-diffused and implanted samples are practically equal. The diffusivity at  $1200^\circ\text{C}$  for the implanted sample is by a factor of 2.4 lower than that for in-diffused sample. It seems reasonable to related this difference between the diffusivities to a decrease in the erbium activation degree for the implanted sample with decreasing temperature of annealing.

Hall effect measurements showed that erbium diffusion at high temperatures results in formation of acceptor centers with shallow levels at  $E_v + 45 \text{ meV}$  [4]. Analysis of the

experimental results led to the conclusion that these centers belong to substitutional erbium atoms [4]. The similarities in the formation of acceptor centers during annealing of in-diffused and implanted samples suggest that Er-related acceptor centers introduced during annealing of Er-implanted Si belong to the Er atoms in substitutional lattice positions. It is very important to emphasize that oxidation enhanced diffusion of Er impurity has been not observed, in contrast to other dopant elements of the group III of the Periodical Table.

#### Mechanism of excitation of EL in Er-implanted Si structures

Fig. 3a represents the dependence of the intensity of EL line at  $1.537 \mu\text{m}$  (Er-related line) on pumping current for Si:Er:O (1) and Si:Er:O:P (2) samples (at 77 K). A threshold in dependence of EL signal on pumping current is observed for the structure doped additionally with phosphorus (curve 2). Fig. 3b shows that the threshold current decreases with an increasing temperature of measurements.

EL spectra for these samples at pumping currents at which saturation of the Er-related EL line takes place are shown in Fig. 4 (curves a and b for 36 mA and 200 mA, respectively). The  $1.537 \mu\text{m}$  line corresponds to electron transition from the lowest level of the first excited state,  $^4I_{13/2}$ , to the lowest level of the ground state,  $^4I_{15/2}$ . The shoulder of this line at  $1.550 \mu\text{m}$  appears

due to the transition to the next levels of the ground state. A group of lines near  $1.4\ \mu\text{m}$  is related to EL of implantation defects. The line of free exciton at  $1.124\ \mu\text{m}$  is also observed in the spectrum of the Si:Er:O sample (curve a). There is no luminescence of free excitons in the Si:Er:O:P sample (curve b).

Peculiarities observed in dependences of intensity of  $1.537\ \mu\text{m}$  luminescence line on the pumping current and EL spectra can be explained in the framework of the following model of

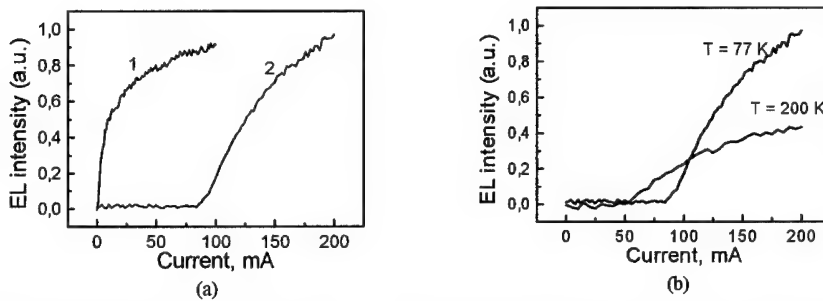


Fig. 3: Dependences of intensity of EL of Er-related line on the pumping current (a) for Si:Er:O (1) and Si:Er:O:P (2) samples at 77 K and (b) for Si:Er:O:P sample at 77 K (1) and 130 K (2).

f-shell excitation of optically active Er ions. The excitation of Er ions occurs via two stages: (i) capture of free excitons by neutral donor Er-related level and (ii) recombination of a bound exciton with a simultaneous Auger-excitation of the f-shell of Er ion. Let us consider the diagrams of energy levels for Si:Er:O and Si:Er:O:P samples at 77 K at different pumping currents (Fig. 5).

These samples differ by concentrations of phosphorus atoms:  $N_{P1} \ll N_{P2}$ . All the P-related levels in the Si:Er:O sample at 77 K are ionized (Fig. 5a). Therefore, there are Er-related and free-exciton-related lines in the sample spectrum (Fig. 4a). When the pumping current in the Si:Er:O:P sample is less than the threshold current ( $j_2 < j_{thr}$ ), only part of the P-related levels is ionized (Fig. 5b). In this case the most part of excitons will be captured by shallow centers. Therefore, Er-related and free-exciton-

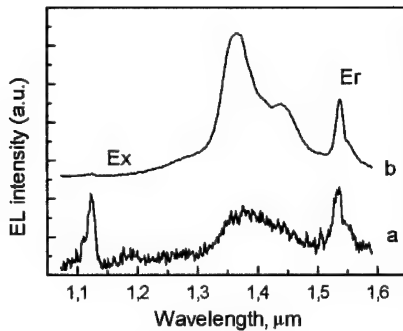


Fig. 4: EL spectra for Si:Er:O (a) and Si:Er:O:P (b) samples at 77 K.

related lines are not observed in the EL spectrum. An increase of the pumping current above the threshold current ( $j_3 > j_{thr}$ ) results in ionization of all the P-related levels (or their larger part) (see Fig. 5c) and capture of free excitons by deeper levels. This leads to appearance of  $1.537\ \mu\text{m}$  line luminescence. As was shown in [5], an increase of free exciton line intensity begins when Er-related line intensity is saturated.

A decrease of the threshold of the pumping current with an increase of the measurement temperature in the Si:Er:O:P sample (see Fig. 3b) is associated with thermal ionization of P-related levels.

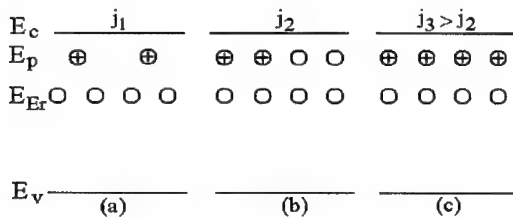


Fig. 5: Diagrams of energy levels for Si:Er:O (a) and Si:Er:O:P (b and c) samples at different pumping current ( $j_1 < j_2 < j_3$ ).

Participation of the free excitons in excitation of Er ions was firstly proposed in [6]. A first direct observation of correlation between luminescence of Er ions and free excitons was reported by us in [5,7,8]. This mechanism is supported also by the data of other authors presented in [9,10]. A detailed theory of excitonic excitation of Er ions is given in [11].

## CONCLUSIONS

An important role of intrinsic point defects during formation of electrically active Er-related centers is demonstrated. In particular, it is shown that annealing of implanted Si:Er leads to the formation of acceptor Er-related centers only at high temperatures ( $\geq 1200^\circ\text{C}$ ) under Si supersaturation with excess vacancies. A threshold in dependence of EL on the pumping current was observed in Si:Er:O structures co-implanted with phosphorus. This provides additional experimental evidence that the excitation of luminescence is associated with recombination of excitons bound to Er-related levels in the energy gap of Si.

## ACKNOWLEDGMENTS

The authors are grateful to E.O. Parshin and L.F. Tarasova for their assistance in preparing of samples and I.N. Yassievich for useful discussions. This work was partly supported by International Science and Technology Center (grant 168) and the Russian Foundation for Basic Research (grants 96-02-17901a and 95-02-04163a).

## REFERENCES

1. J. Michel, J.L. Benton, R.F. Ferrante, D.C. Jacobson, D.J. Eaglesham, E.A. Fitzgerald, Y.H. Xie, J.M. Poate and L.C. Kimerling, *J. Appl. Phys.* **70**, p. 2,672 (1991).
2. F. Priola, S. Coffa, G. Franzo, C. Spinella, A. Carnera and B. Bellany, *J. Appl. Phys.* **74**, p. 4936 (1993).
3. Yu. V. Vyzhigin, N.A. Sobolev, B.N. Gresserov and E.I. Shek, *Semicond.* **26**, p. 1,087 (1992).
4. O.V. Alexandrov, V.V. Emtsev, D.S. Poloskin, N.A. Sobolev and E.I. Shek, *Semicond.* **28**, p. 2,045 (1994).
5. M.S. Bresler, O.B. Gusev, B.P. Zakharchenya, P.E. Pak, N.A. Sobolev, E.I. Shek, I.N. Yassievich, M.I. Makoviichuk and E.O. Parshin, *Semicond.* **30**, p. 898 (1996).



6. S.Coffa, F.Priolo, G.Franzo, V.Bellani, A.Carnera and S.Spinella, Phys. Rev. **B48**, p. 11,782 (1993).
7. N.A.Sobolev, O.V.Alexandrov, M.S.Bresler, O.B.Gusev, E.I.Shek, M.I.Makovijchuk and E.O.Parshin, Mater. Sci. Forum **196-201**, p. 597 (1995).
8. M.S.Bresler, O.B.Gusev, M.I.Makoviichuk, P.E.Pak, E.O.Parshin, E.I.Shek, N.A.Sobolev, I.N.Yassievich, B.P.Zakharchenya, Proc. SPAI **2,706**, p. 272 (1995).
9. J.H.Shin, G.N. van den Hoven and A.Polman, Appl. Phys. Lett. **67**, p. 377 (1995).
10. I.Tsimperidis, T.Gregorkiewicz and C.A.J.Ammerlaan, Mater. Sci. Forum **196-201**, p. 591 (1995).
11. M.S.Bresler, O.B.Gusev, B.P.Zakharchenya and I.N.Yassievich, Solid State Physics **38**, p. 165 (1996).

## Photoluminescence of Erbium Implanted in SiGe

S. J. Chang, D. K. Nayak<sup>1</sup> and Y. Shiraki<sup>1</sup>

Department of Electrical Engineering, National Cheng Kung University, Taiwan, ROC

<sup>1</sup>Research Center for Advanced Science and Technology, University of Tokyo,  
Tokyo, Japan

*The optical properties of an Er-implanted SiGe sample have been studied. Sharp and temperature-stable Er-related PL peaks were observed at around 1.5  $\mu\text{m}$ , which correspond to the Er  $^4I_{13/2}$  to  $^4I_{15/2}$  transition. It was found that the Er ions form more than three noncubic luminescence centers in the SiGe host. Although the PL intensity quenches at high temperatures, the Er-related PL signal can still be observed at room temperature. For a  $\text{Si}_{0.87}\text{Ge}_{0.13}\text{:Er}$  sample annealed at 850  $^{\circ}\text{C}$  for 20 min, the activation energy is 130 meV which is slightly smaller than that of the Er-doped Si.*

Rare-earth (RE) -doped semiconductor is an interesting system that has attracted much attention. <sup>1-4)</sup>Unlike the semiconductor band-gap-related emission, the luminescence of RE ions is extremely sharp and temperature stable since the transition energies of the RE 4f levels are insensitive to the external host environment and the surrounding temperature. <sup>1-4)</sup>If we can pump the RE ions through the host semiconductor efficiently, we can use the RE-doped semiconductor as a good optical source that can be used in optoelectronic integrated circuits. Among the various RE ions, Er seems to be the most useful element since it emits luminescence at 1.54  $\mu\text{m}$  which corresponds to the minimum absorption region of the silica-based optical fiber. <sup>5)</sup>

In the 80's, numerous studies concentrated on the optical properties of Er-doped Si were carried out. <sup>2-4)</sup> Recently, the microstructure and defect properties of Er-implanted Si have also been reported. <sup>6,7)</sup> An Er-doped Si-based light-emitting diode (LED) has also been demonstrated. <sup>4)</sup> To excite Er ions in the Si host, we must create electron-hole pairs. The Er ions are excited when the electrons and holes recombine, and a portion of the recombination energy is transferred to the Er ions. It has been reported that, for the RE ions in III-V semiconductor hosts, the energy mismatch between the RE 4f-shell transition energy and the band-gap energy of the host semiconductor is an important parameter. <sup>8)</sup> By changing this energy mismatch, we might be able to achieve a higher energy transfer efficiency. In SiGe-based host, we can change the Ge fraction so as to

change the host band-gap energy and thus change the energy mismatch. Also, if we want to realize an Er-doped semiconductor laser on Si substrates, it is very likely that we will have to dope Er in a quantum well structure such as Si/SiGe:Er/Si. Therefore, doping Er ions into SiGe hosts becomes an important issue. Previously, Efeoglu *et al.*<sup>9)</sup> reported a study on Er-doped SiGe prepared by molecular beam epitaxy. They found that, compared with Si:Er, the photoluminescence ( PL ) peaks of  $\text{Si}_{0.9}\text{Ge}_{0.1}\text{:Er}$  is slightly broadened due to the variation in atom size of the host matrix. They also observed that the presence of 10% germanium changes the siting of erbium for growth at 500 °C. In this study, we report the optical properties of SiGe: Er samples prepared by implanting Er ions into SiGe epitaxial layers.

In the experiment,  $\text{Si}_{0.87}\text{Ge}_{0.13}$  layers were grown on an n-type silicon ( 100 ) substrate by gas source molecular beam epitaxy ( GSMBE ) .<sup>10)</sup> prior to the growth of the  $\text{Si}_{0.87}\text{Ge}_{0.13}$  layer, a 180 nm Si buffer layer was grown at 800 °C . The growth temperature of the subsequent  $\text{Si}_{0.87}\text{Ge}_{0.13}$  layer was 700 °C . The thickness of the undoped  $\text{Si}_{0.87}\text{Ge}_{0.13}$  epilayer is 2  $\mu\text{m}$ . Since this thickness is greater than its critical thickness,  $h_c$ , the epilayer is relaxed.<sup>11)</sup> Er-doped SiGe samples were obtained by implanting Er into the  $\text{Si}_{0.87}\text{Ge}_{0.13}$  samples at room temperature. The implantation energy was 250 keV with a dose of  $10^{14} \text{ cm}^{-2}$ . In order to obtain the maximum PL efficiency, the samples were annealed at various temperatures for various times in vacuum after Er implantation. PL spectra of the annealed SiGe:Er samples were measured at different temperatures. In the PL experiment, an argon 514.5 nm ion laser was used as the excitation source. The emission spectra were monitored through a Spex monochromator and a liquid-nitrogen-cooled germanium *p-i-n* photodiode. Standard lock-in technology was used for signal analysis.

Figure 1 ( a ) shows the PL spectrum of a  $\text{Si}_{0.87}\text{Ge}_{0.13}\text{:Er}$  sample, annealed at 850 °C for 20 min, measured at 4.2K. These extremely sharp PL peaks, with full width at half maximum ( FWHM ) less than 1 nm, originated from the Er intra-4f-shell transitions. It is known that the  $\text{Er}^4\text{I}_{13/2}$  state will split into five levels (  $3 \times \Gamma_8, \Gamma_7$  and  $\Gamma_6$  ) and the  $^4\text{I}_{15/2}$  state will also split into five levels (  $2 \times \Gamma_8, \Gamma_7$  and  $\Gamma_6$  ) if the Er center is surrounded by a crystal field of cubic symmetry. In a crystal field of noncubic symmetry, the  $\text{Er}^4\text{I}_{13/2}$  and  $^4\text{I}_{15/2}$  states will further split into seven and eight levels, respectively.<sup>4)</sup> Thus, at low temperatures in the  $\text{Er}^4\text{I}_{13/2} \rightarrow ^4\text{I}_{15/2}$  1.5  $\mu\text{m}$  transition region, five PL peaks are expected if the Er luminescence center is surrounded by a crystal field of cubic symmetry and eight PL peaks are expected if the Er luminescence center is surrounded by a crystal field of noncubic symmetry. From Fig.1 ( a ) , we can clearly identify more than twenty PL peaks. This result not only suggests that the Er ions in the SiGe host are surrounded by a crystal field of noncubic symmetry, but also that there

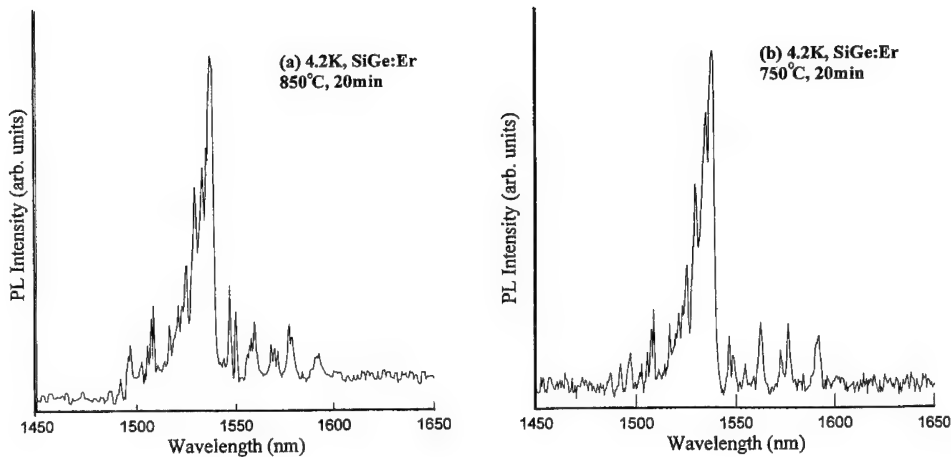


Fig. 1. PL spectrum of the  $\text{Si}_{0.87}\text{Ge}_{0.13}:\text{Er}$  sample, (a) annealed at  $850^\circ\text{C}$  for 20 min, measured at 4.2 K and (b) annealed at  $750^\circ\text{C}$  for 20 min, measured at 4.2 K.

are more than three Er Luminescence centers which coexist in this  $\text{SiGe:Er}$  sample. Figure 1 (b) shows the PL spectrum of a  $\text{Si}_{0.87}\text{Ge}_{0.13}:\text{Er}$  sample, annealed at  $750^\circ\text{C}$  for 20 min, also measured at 4.2 K. Comparing Figs. 1 (a) and 1 (b), we found that although these two PL spectra look similar, the exact PL peak positions and the relative PL peak intensities are different. This indicates that the optically active Er centers were different in these two samples.

Figure 2 (a) shows the integrated PL intensity as a function of annealing temperature for  $\text{Si}_{0.87}\text{Ge}_{0.13}:\text{Er}$  samples measured at 4.2 K. The annealing time is 20 min. It can be seen that samples annealed at  $850^\circ\text{C}$  emit the strongest luminescence signal. The dependence of the integrated PL intensity measured at 4.2 K, for the  $\text{Si}_{0.87}\text{Ge}_{0.13}:\text{Er}$  samples annealed at  $850^\circ\text{C}$ , is shown in Fig. 2 (b). From Fig. 2(b), we found that the integrated PL intensity increases initially as the annealing time increases and reaches saturation when the annealing time is around 5 min. However, for annealing time longer than 20 min, the integrated intensity starts to decrease. Figure 3 (a), 3 (b) and 3 (c) show the PL spectra of the  $\text{Si}_{0.82}\text{Ge}_{0.18}:\text{Er}$  sample, annealed at  $850^\circ\text{C}$  for 20 min, measured at higher temperatures (i.e., 60K, 150K and 300K). Comparing Figs. 1 (a) and 3 (a), we can see that as the sample temperature increased from 4.2 K to 60 K, additional peaks appeared in the high-energy region. These "hot-lines" are transitions from the higher energy states of the  $\text{Er } ^4\text{I}_{13/2}$  level. Although the number of PL peaks increases and the intensity decreases

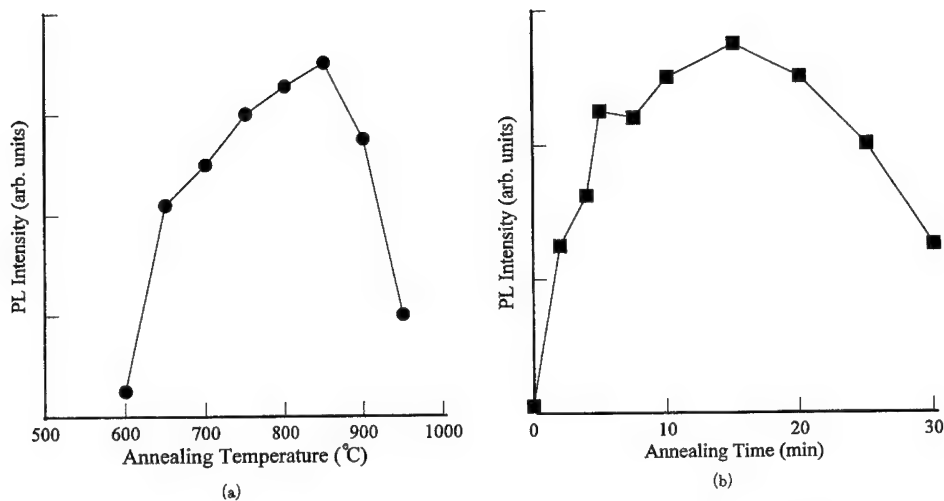


Fig. 2. (a) The integrated PL intensity as a function of annealing temperature for  $\text{Si}_{0.87}\text{Ge}_{0.13}:\text{Er}$  samples measured at 4.2 K. The annealing time is 20 min. (b) The integrated PL intensity as a function of annealing time for  $\text{Si}_{0.87}\text{Ge}_{0.13}:\text{Er}$  samples measured at 4.2 K. The annealing temperature is 850°C.

at higher temperatures, the peak positions of the PL lines remain practically unchanged. This is characteristic of RE 4f-shell transition. As shown in Fig. 3 (c), reasonably strong Er-related luminescence signals can still be observed at room temperature. Similar room-temperature Er signals have also been observed in Si:Er and GaAs:Er.<sup>12)</sup> The integrated PL intensity as a function of sample temperature for the  $\text{Si}_{0.87}\text{Ge}_{0.13}:\text{Er}$  sample, annealed at 850°C for 20 min, is shown in Fig. 4. From Fig. 4, we found that the activation energy of this  $\text{Si}_{0.87}\text{Ge}_{0.13}:\text{Er}$  sample is about 130 meV, which is slightly smaller than that of the Si:Er sample reported earlier.<sup>12)</sup> It is likely that this value is related to the energy mismatch between the energy band-gap of the host  $\text{Si}_{0.87}\text{Ge}_{0.13}$  and the Er 4f-shell transition energy. By changing the Ge fraction, we might obtain a different value of the activation energy.

In summary, we have implanted Er ions into the GSMBE-grown  $\text{Si}_{0.87}\text{Ge}_{0.13}$  epitaxial layers. The optical properties of the implanted SiGe:Er samples were evaluated and we found that more three Er luminescence centers coexist in the SiGe host. Reasonably strong Er-related PL signals can be observed at room temperature. At higher temperatures, the integrated PL intensity decreases with an activation energy of 130 meV for the  $\text{Si}_{0.87}\text{Ge}_{0.13}:\text{Er}$  sample annealed at 850°C for 20 min.

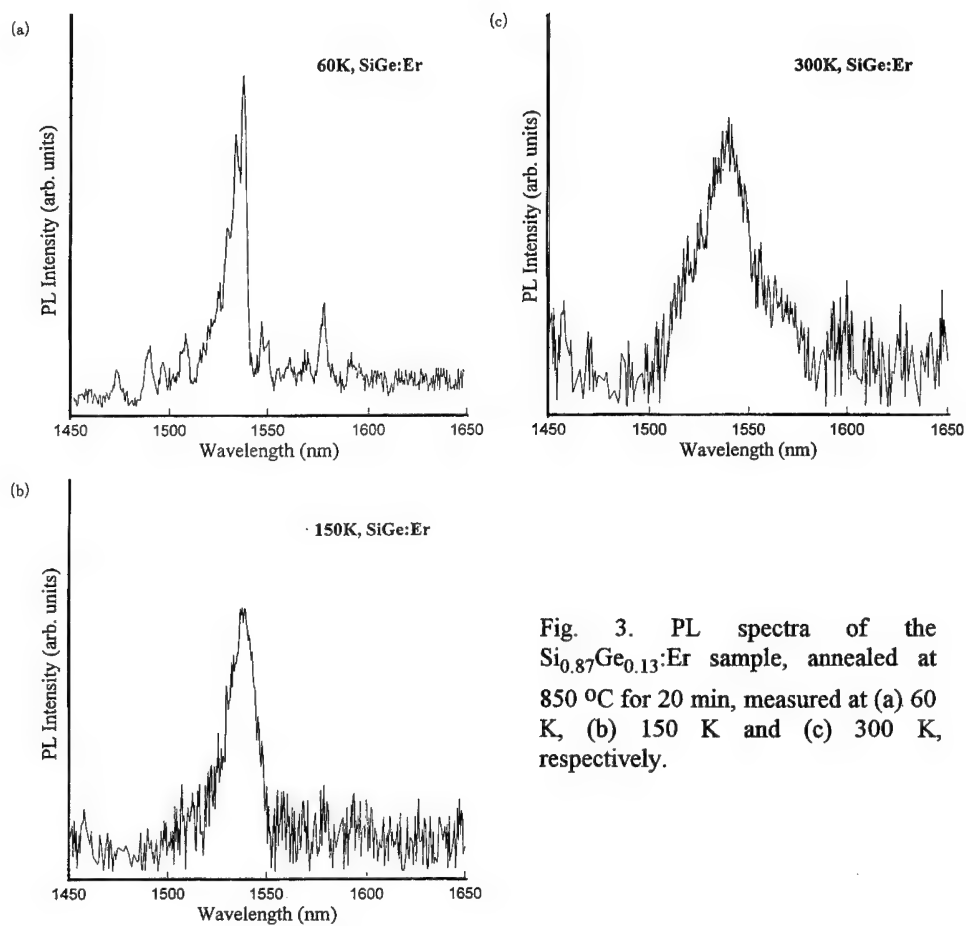


Fig. 3. PL spectra of the  $\text{Si}_{0.87}\text{Ge}_{0.13}\text{:Er}$  sample, annealed at  $850^\circ\text{C}$  for 20 min, measured at (a) 60 K, (b) 150 K and (c) 300 K, respectively.

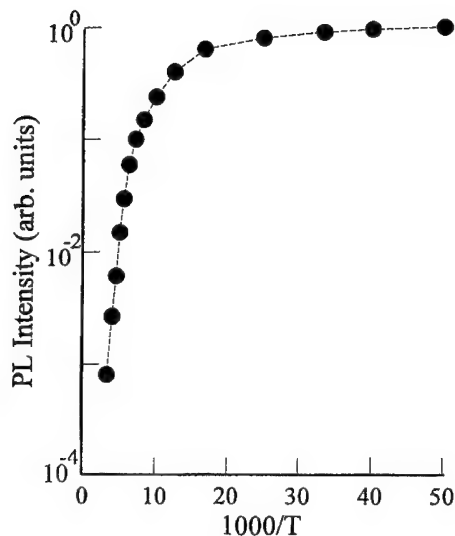


Fig. 4. The integrated PL intensity of the  $\text{Si}_{0.87}\text{Ge}_{0.13}\text{:Er}$  sample, annealed at 850°C for 20 min, as a function of sample temperature.

#### Acknowledgments

The authors would like to thank Dr. K. Takahei and Dr. A. Taguchi of NTT Basic Research Laboratories for their helpful discussions. This work is supported by National Science Council under contract number NSC 82-0404-E-006-306-T.

- 1) A. Taguchi, K. Takahei and J. Nakata: *Mater. Res. Symp. Proc.* **301** (1993) 139.
- 2) H. B. Dietrich, P. B. Klein and B. J. Mrstik: *Proc. SPIE* **530** (1985) 195.
- 3) Y. S. Tang, K. C. Heasman, W. P. Gillin and B. J. Sealy: *Appl. Phys. Lett.* **55** (1989) 432.
- 4) H. Ennen, G. Pomrenke, A. Axmann, K. Kisele, W. Haydl and J. Schneider: *Appl. Phys. Lett.* **45** (1989) 381.
- 5) F. Y. G. Ren, J. Michel, Q. Sun-Paduan, B. Zheng, H. Kitagawa, D. C. Jacobson, J. M. Poate and L. C. Kimerling: *Mater. Res. Symp. Proc.* **301** (1993) 87.
- 6) D. J. Eaglesham, J. Michel, E. A. Fitzgerald, D. C. Jacobson, J. M. Poate, J. L. Benton, A. Polman, Y. H. Xie and L. C. Kimerling: *Appl. Phys. Lett.* **58** (1991) 2797.
- 7) J. L. Benton, J. Michel, L. C. Kimerling, D. C. Jacobson, Y. H. Xie, D. J. Eaglesham, E. A. Fitzgerald and J. M. Poate: *J. appl. Phys.* **70** (1991) 2667.
- 8) A. Taguchi, M. Taniguchi and K. Takahei: *Appl. Phys. Lett.* **60** (1992) 965.
- 9) H. Efeoglu, J. H. Evans, T. E. Jackson, B. Hamilton, D. C. Houghton, J. M. Langer, A. R. Peaker, D. Perovic, I. Poole, N. Ravel, P. Hemment and C. W. Chan: *Semicond. Sci. Technol.* **8** (1993) 236.
- 10) S. Fukatsu, H. Yoshida, N. Usami, A. Fujiwara, Y. Takahashi, Y. Shiraki and R. Ito: *Jpn. J. Appl. Phys.* **31** (1992) 1319.
- 11) R. People: *IEEE J. Quantum Electron.* **22** (1986) 1696.
- 12) J. Michel, J. L. Benton, R. F. Ferrante, D. C. Jacobson, D. J. Eaglesham, E. A. Fitzgerald, Y. H. Xie, J. M. Poate and L. C. Kimerling: *J. Appl. Phys.* **70** (1991) 2672.

## Characterization of visible and infrared (1.54 $\mu\text{m}$ ) luminescence from Er-doped porous Si

R. White\*, X. Wu\*, U. Hömmerich\*<sup>†</sup>, F. Namavar\*\*, and A. M. Cremins-Costa\*\*

\*Hampton University, Research Center for Optical Physics, Department of Physics  
Hampton, VA 23668

\*\* Spire Corporation, One Patriots Park, Bedford, MA 01876

<sup>†</sup> e-mail: hommeric@gprc.hamptonu.edu

### ABSTRACT

Results of a photoluminescence excitation (PLE) study of Er-implanted porous Si (Er: PSi) are presented. Erbium was implanted at a dose of  $1 \times 10^{15}$  Er/cm<sup>2</sup> at 380 keV and annealed for 30 minutes at 650°C. We observed a nearly identical PLE intensity behavior from 1.54  $\mu\text{m}$  and visible-emitting Er: PSi. This observation indicates that both visible and infrared photoluminescence (PL) arise from carrier mediated processes, and that the 1.54  $\mu\text{m}$  Er<sup>3+</sup> PL is related to the porous Si nanostructures. Measurements of the temperature dependence (15-375K) of Er<sup>3+</sup> PL intensity and lifetime are also reported.

### INTRODUCTION

Er-doped porous silicon has recently attracted significant attention because of its possible applications in Si-based opto-electronics. Porous silicon emits brightly in the visible wavelength range due to the quantum confinement of carriers in silicon nanograins [1,2]. Erbium can be introduced into porous silicon either through ion implantation, electrolysis, or spin-on. In each case, an intensive 1.54  $\mu\text{m}$  Er<sup>3+</sup> photoluminescence (PL) is observed at room temperature [3-6]. These results suggest a high concentration of optically active Er<sup>3+</sup> ions and a weak Er<sup>3+</sup> PL quenching in Er-doped porous Si (Er: PSi). The weak temperature quenching of the Er<sup>3+</sup> PL has been explained by the large bandgap of porous Si ( $\sim 1.8$ -2.0 eV) [3-7].

The exact excitation mechanism of Er<sup>3+</sup> in porous silicon and its relation to porous silicon nanostructures remain unclear. It was proposed that efficient Er<sup>3+</sup> excitation resulted from the recombination of spatially-confined photocarriers in silicon nanograins near the incorporated Er [3-5]. We previously reported that the temperature quenching of Er<sup>3+</sup> PL depends on the porosity of porous silicon, which implies a correlation between Er<sup>3+</sup> PL and porous Si nanostructures [8]. In this paper, we present a comparison of the photoluminescence excitation (PLE) behavior of visible and infrared PL in Er: PSi. Our results strongly support that Er<sup>3+</sup> photoluminescence (PL) arises from Er<sup>3+</sup> ions located in the nanostructures of porous Si. Additional results of the temperature dependence of Er<sup>3+</sup> PL intensity and lifetime are also discussed.

### SAMPLE AND MEASUREMENT

The erbium implanted porous silicon sample was prepared at Spire Corporation. The porous silicon was obtained by anodically etching three-inch p-type Si <100> wafers (0.1-1.2  $\Omega$  cm) in a HF:ethanol (1:1) solution under constant current conditions (10-100 mA/cm<sup>2</sup>) for one hour. Erbium was implanted at a dose of  $1 \times 10^{15}$  Er/cm<sup>2</sup> at 380 keV and annealed in N<sub>2</sub> at 650°C for 30 minutes.



For PL excitation measurements, an Optical Parametric Oscillator (Surelite OPO, Continuum) pumped with a Q-switched Nd:YAG laser (Surelite II, Continuum) was used as excitation source. PL was dispersed with a 1-m monochromator and detected with either a photomultiplier or liquid-nitrogen cooled Ge detector. The PLE signal was recorded as the ratio between PL intensity and excitation power.

For PL spectra and lifetime measurement, the 488 nm line of an argon ion laser (Coherent Innova 400) was used as excitation source. The laser beam was focused onto a chopper wheel and mechanically chopped at 55 Hz. The luminescence spectra were recorded using a 1-m monochromator equipped with a liquid-nitrogen cooled Ge detector. The signal was processed by a boxcar averager (SR250 Stanford Research Systems). PL lifetime measurements were performed by directly monitoring the signal of a fast-response Ge detector (403HS, Applied Detector Corp.) on an averaging digitizing oscilloscope (Tektronix TDS 420A). The overall time resolution of the system was 20  $\mu$ s. The sample was cooled on the cold finger of a two stage closed cycle refrigerator capable of reaching temperatures as low as 12 K.

#### EXPERIMENTAL RESULTS AND DISCUSSION

Figure 1 shows the low temperature (15 K) visible and infrared PL spectrum of Er-implanted porous Si following pulsed excitation at 450 nm. The visible PL features a broad band spanning from 500 to 850 nm, peaking at 750 nm. This bandgap luminescence has been attributed to quantum confinement effects within crystalline Si [1].

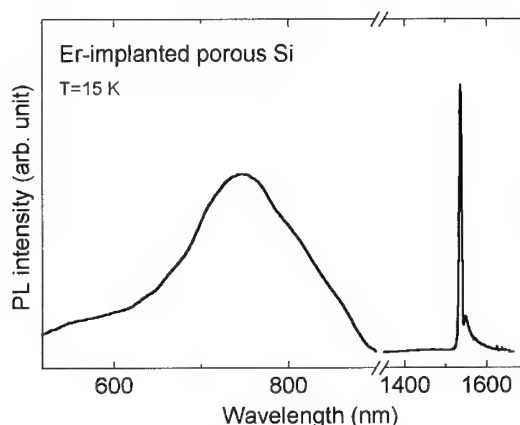


Figure 1. Visible and infrared luminescence spectra of Er-implanted porous silicon at 15 K, following the pulsed excitation at 450 nm.

The infrared spectrum exhibits a characteristic luminescence at 1.54  $\mu$ m arising from the  $^4I_{13/2} \rightarrow ^4I_{15/2}$  transition of  $\text{Er}^{3+}$  ions. The relatively large bandwidth (35  $\text{cm}^{-1}$  FWHM) of the infrared PL spectrum indicates that  $\text{Er}^{3+}$  ions occupy a range of sites in porous Si and that the luminescence spectrum is mainly inhomogeneously broadened.

Figure 2 shows the low temperature (15 K) PLE spectra of both the visible and infrared PL on a logarithmic scale. The visible PL was monitored at 750 nm and the infrared PL at 1.54  $\mu$ m. A significant increase of the PLE signal monitored at the two wavelengths occurred at around 600

nm ( $\sim 2.0$  eV), indicating that  $\text{Er}^{3+}$  ions are excited through a carrier mediated process. Since the PLE spectrum monitored at 750 nm represents a characteristic band edge of porous silicon [2], the nearly identical behavior between the visible and infrared PLE spectrum strongly suggests that  $\text{Er}^{3+}$  ions are located in the nanograins of porous silicon.

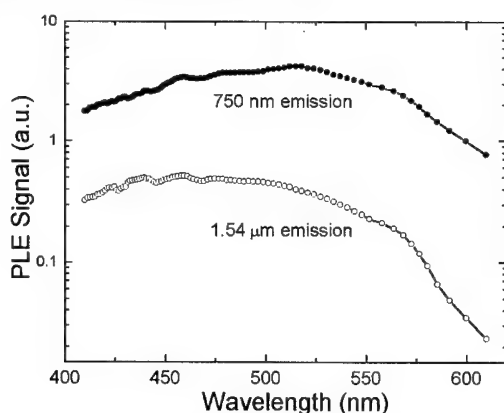


Figure 2. PLE spectra of Er-implanted porous silicon at a temperature of 15 K. The PL was monitored at 750 nm and 1540 nm, respectively.

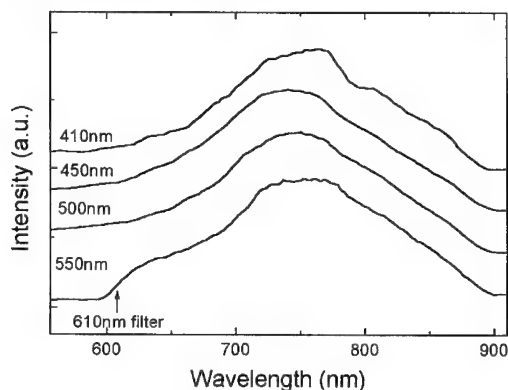


Figure 3. Visible luminescence spectra of Er-implanted porous silicon at 15 K following pulsed excitation at 410, 450, 500, and 550 nm.

The PLE signal monitored at a specific wavelength may alter for different excitation wavelength because of changes in the luminescence line shape and/or peak position. To eliminate these possible variations in our PLE measurement, we recorded the visible PL spectra of porous Si after pulsed excitation at 400, 450, 500, and 550 nm. As shown in figure 3, PL from the porous Si substrate exhibited essentially the same line shape and peak position, independent of excitation wavelength. Therefore, the error in the visible PLE measurement, resulting from changes in luminescence spectrum, is negligibly small.

In Figure 4 the PL lifetime of  $\text{Er}^{3+}$  in porous Si is depicted. As can be seen in Figure 4 A, the luminescence decay is non-exponential. It is noted that following a fast initial decay ( $\sim 140 \mu\text{s}$ ), the PL decays with a long lifetime of  $\sim 1.3$  ms. Similar features have been reported for other Er-doped Si-based materials [9-11]. The transient at each temperature can be fitted to a double exponential decay. The fast and slow component were determined to be  $145 \mu\text{s}$  ( $122 \mu\text{s}$ ) and  $1.37$  ms ( $1.02$  ms) at  $15$  K ( $300$  K), respectively. The intensity ratio of the fast to slow component was found to be constant ( $\sim 0.9$ ) in the temperature range from  $15$  to  $375$  K, suggesting the existence of two types of  $\text{Er}^{3+}$  sites in porous Si.

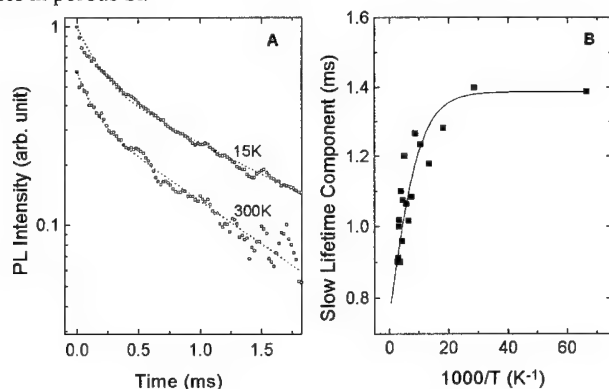


Figure 4.  $\text{Er}^{3+}$  Lifetime in Er-implanted porous silicon. (A) This Figure shows the  $\text{Er}^{3+}$  decay curves at  $15$  and  $300$  K. The dotted lines are the fits to a double exponential decay, with the parameters given in text. (B) This Figure depicts the lifetime of slow decaying component as a function of reciprocal temperature. The solid line is the fit generated by Eq. (1).

Since the slow decaying component accounts for more than 80% (ratio of slow to fast lifetime) of the total  $\text{Er}^{3+}$  PL intensity, it can be considered as the characteristic PL lifetime. Figure 4 B shows the slow lifetime component as a function of reciprocal temperature. At  $375$  K the lifetime is reduced to 65% of its value at  $15$  K. The weak  $\text{Er}^{3+}$  lifetime reduction is most likely due to the onset of energy back transfer [4]. The temperature dependence of the  $\text{Er}^{3+}$  lifetime was fitted to the relationship:

$$\tau(T) = \tau(0) \left[ 1 + A e^{-\frac{E}{kT}} \right]^{-1} \quad (1)$$

where  $\tau(0)$  is the low temperature lifetime,  $E$  is the thermal activation energy, and  $A$  is the ratio between radiative and non-radiative decay rate. The theoretical fit with  $E=15.5$  meV ( $125 \text{ cm}^{-1}$ ),  $\tau(0)=1.37$  ms, and  $A=0.84$  is shown as the solid line in Figure 4 B. The activation energy ( $E$ ) for the weak thermal quenching between  $15$  and  $150$  K in  $\text{Er}^{3+}$ : porous Si is comparable to the value obtained for  $\text{Er}^{3+}$ : Si ( $20$  meV) [9,10]. In both cases energy back transfer has only a small contribution to the  $\text{Er}^{3+}$ -PL quenching.

Figure 5 shows the infrared PL intensity at various temperatures ( $15$ - $375$  K) excited with the  $488$  nm line of an argon laser. For temperatures below  $150$  K, the PL intensity quenching follows closely the lifetime quenching. However, for temperatures above  $150$  K the PL intensity decreases faster than the lifetime. At  $375$  K the PL intensity is reduced to 45 % of that at  $15$  K, whereas the lifetime at  $375$  K is 65 % of that at  $15$  K.

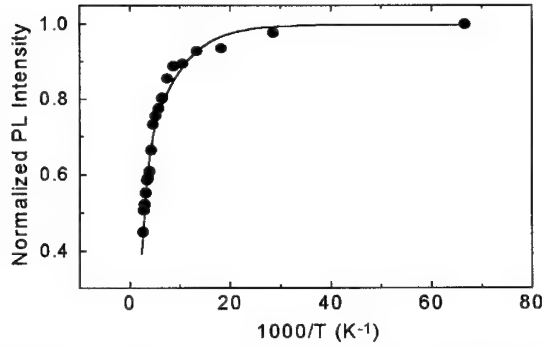


Figure 5. Temperature dependence of the infrared 1.54  $\mu\text{m}$   $\text{Er}^{3+}$  PL. The solid line is the fit generated by the Eq.(4) with the parameters given in text.

Based on our experimental data, the enhanced thermal quenching observed above 150 K is interpreted using the following  $\text{Er}^{3+}$  excitation scheme. Assuming the observed  $\text{Er}^{3+}$  luminescence arises from  $\text{Er}^{3+}$  ions incorporated in the nanograins of porous silicon, the excitation of Er ions occurs through recombination of an exciton bound to an Er-related trap site. Assuming that most of the  $\text{Er}^{3+}$  ions are in the ground state, the concentration ( $n^*$ ) of excited Er is given by the rate equation [10]:

$$\frac{dn^*}{dt} = \frac{n_c}{\tau_{tr}} - \frac{n^*}{\tau} \quad (2)$$

where  $n_c$  is the concentration of e-h complexes,  $\tau_{tr}$  is the time required for energy transfer, and  $\tau$  is the  $\text{Er}^{3+}$  PL decay time. At steady state the PL intensity as a function of temperature can be written as

$$I(T) = \frac{n_c(T)}{\tau_{tr}} \frac{\tau(T)}{\tau(T=0)} \quad (3)$$

As a first order approximation, we assume that the concentration of e-h complexes  $n_c$  is determined by the equilibrium between the formation and dissociation rate of the complexes [10]. The dissociation of e-h pairs provides a temperature dependent quenching mechanism for the  $\text{Er}^{3+}$  PL, which, in contrast to energy backtransfer, does not reflect in the Er PL lifetime. Considering thermalization of bound electrons from the Er-related level to the conduction band, the concentration  $n_c$  is proportional to  $[1+B\exp(-\Delta/kT)]^{-1}$  [10].  $\Delta$  is the energy gap between the Er-related level and the conduction band. B is assumed to be constant and includes the density of trap states, the carrier lifetime, optical generation rate of e-h pairs, and the capture cross-section for electrons and holes [10]. The overall temperature dependence of the  $\text{Er}^{3+}$  PL intensity is given by

$$I(T) = I(0) \frac{\tau(T)}{\tau(0)} \frac{1}{1 + B \exp(-\frac{\Delta}{kT})} \quad (4)$$

A fit of Eq. (4) to the observed  $\text{Er}^{3+}$  PL temperature quenching is shown as a solid line in Figure 5, with  $\Delta=0.104$  eV, and  $B=10.6$ . The energy gap  $\Delta$  is comparable to those measured in Er: Si (0.15-0.51 eV) [10]. Whereas the value of  $B$  is two orders of magnitude smaller in Er: Porous Si than in  $\text{Er}^{3+}$ : Si, which is consistent with the weak  $\text{Er}^{3+}$  PL quenching in Er: PSi [10].

## SUMMARY

We have performed PLE measurements on Er-implanted porous silicon. Although our result is not exclusive, it strongly supports that the 1.54  $\mu\text{m}$  infrared PL in Er-doped porous Si originates from  $\text{Er}^{3+}$  ions located in the nanograins of porous silicon. In addition, the PLE spectrum demonstrates that  $\text{Er}^{3+}$  excitation occurs via a carrier mediated process, which most likely includes the recombination of e-h complexes bound to a Er-related trap site. The temperature dependencies of both  $\text{Er}^{3+}$  PL intensity and lifetime shows that the thermal quenching of  $\text{Er}^{3+}$  PL above 150 K is dominated by the thermalization of electrons bound to Er-related levels.

## ACKNOWLEDGMENTS

The authors from Hampton University would like to acknowledge financial support by NASA through Grant NAGW-2929. The work at Spire Corporation was supported in part by an SBIR program funded by the Air Force of Scientific Research and monitored by Lt. Col. G. S. Pomrenke.

## REFERENCES

1. L. T. Canham, Appl. Phys. Lett. **57**, 1046 (1990).
2. Lei Wang, M. T. Wilson, and N. M. Haegel, Appl. Phys. Lett. **62**, 1113 (1993).
3. F. Namavar, F. Lu, C. H. Perry, A. Cremins, N. M. Kalkhoran, R. A. Soref, J. Appl. Phys. **77**, 4813 (1995).
4. T. Kimura, A. Yokoi, H. Horiguchi, R. Saito, T. Ikoma, and A. Sato, Appl. Phys. Lett. **65**, 983 (1994).
5. A. M. Dorofeev, N. V. Gaponenko, V. P. Bondarenko, E. E. Bachilo, N. M. Kazuchits, A. A. Leshok, G. N. Troyanova, N. N. Voroso, V. E. Borisenko, H. Gnaser, W. Bock, P. Becker, and H. Oechsner, J. Appl. Phys. **77**, 2679 (1995).
6. J. H. Shin, G. N. van den Hoven, and A. Polman, Appl. Phys. Lett. **66**, 2379 (1995).
7. P. N. Favenec, H. L'Haridon, D. Moutonnet, M. Salvi, and M. Gauneau, Mat. Res. Soc. Symp. Proc. **301**, 181 (1993).
8. U. Hömmerich, F. Namavar, A. M. Cremins-Costa, and K. L. Bray, Appl. Phys. Lett. **68**, 1951 (1996).  
U. Hömmerich, X. Wu, F. Namavar, A. M. Cremins-Costa, and K. L. Bray, Mat. Res. Soc. Symp. Proc. Vol. **405**, 1996, in press.
9. S. Coffa, F. Priolo, G. Franzò, V. Bellani, A. Carnera, and C. Spinella, Phys. Rev. **B 48**, 16313 (1994).
10. F. Priolo, G. Franzò, S. Coffa, A. Polman, S. Libertino, R. Barklie and D. Carey, J. Appl. Phys. **78**, 3874 (1995).
11. G. N. van den Hoven, J. H. Shin, A. Polman, S. Lombardo and S. U. Campisano, J. Appl. Phys. **78**, 2642 (1995).

## TO PROBE THE ABSORPTION EDGE OF POROUS SILICON BY ERBIUM

Xinwei Zhao\*, Shuji Komuro\*\*, Shinya Maruyama\*\*, Hideo Isshiki\*, Yoshinobu Aoyagi\* and Takuo Sugano\*

\*Frontier Research Program, The Institute of Physical and Chemical Research (RIKEN), Wako, Saitama 351-01, Japan

\*\*Faculty of Engineering, Toyo University, Kawagoe, Saitama 350, Japan

Intra-4f-transitions from erbium atoms are proposed as a probe to determine absorption edges of the hosts. This idea was firstly applied on erbium-doped porous silicon materials. Intense and sharp 1.54  $\mu\text{m}$  luminescence from erbium triply ionized ions as well as visible emissions from porous silicon were observed up to room temperature. Photoluminescence excitation spectroscopy investigations of the samples indicate identical absorption edges for both the 1.54  $\mu\text{m}$  and the visible emissions. No 1.54  $\mu\text{m}$  luminescence can be observed by directly exciting the erbium triply ionized ions. This fact suggests that the erbium ions are excited by energy transfer process from the excited carriers in the hosts. From this result, we can propose that erbium could behave as a good probe to determine the absorption edge or the bandgap of the host material even it is not luminescent.

## INTRODUCTION

To dope erbium (Er) into silicon (Si) is a subject of great interest in view of its potential applications to optoelectronic devices. Er ion in its trivalent state ( $\text{Er}^{3+}$ ,  $4f^{11}$ ) shows sharp photoluminescence (PL) at 1.54  $\mu\text{m}$ , one of the standard wavelengths in silica fiber-based optical communication technology. Although a lot of papers on the doping and PL of  $\text{Er}^{3+}$  ions have been published, [1] there is a lack of sufficient understanding of the luminescence mechanism at present. In the case of Er-doped Si, an acceptable suggestion is that the Er luminescence may be enhanced by energy transfer from excitons or electron-hole pairs to the  $\text{Er}^{3+}$  ions. [2] Because of the 1.54  $\mu\text{m}$  PL is caused by the transition of the spin-orbit split  $4I_{13/2}$  to  $4I_{15/2}$  of 4f electrons which are shielded by outer  $5s^25p^6$  shells, the influence of the host lattice is weak. Indeed, the wavelength of the PL from  $\text{Er}^{3+}$  ions is almost the same in various hosts. The intensity of the PL, however, is very different. Key points of obtaining efficient Er emission are to increase the doping level and to increase the energy transfer probability from the excited carriers in the host. It is reported in literature that Er shows more intense PL in wider bandgap hosts. [3] Porous Si fabricated by anodization of Si in dilute HF solution exhibits bright visible PL at room temperature. [4] Although the origin of the visible PL from porous Si is not clear at present, optical absorption measurements indicated that porous Si is a semiconductor or a semi-insulating material with a bandgap near 2 eV. [5] The micro- and nano-pores in porous Si layer formed by the anodization allow a higher doping density of Er than in single crystalline Si (c-Si), too. It is interest to investigate the optical transition process between the Er emission and the visible emission from porous Si. The first work of doping Er into porous Si was reported by Kimura et al using an electrochemical process. [6] The paper claimed that the  $\text{Er}^{3+}$  ions were optically activated only by annealing the sample at very high temperature (1300  $^{\circ}\text{C}$ ) in an oxygen ( $\text{O}_2$ ) atmosphere. The porous Si, which contains a large quantity of oxygen (Si:O~1:1), is easily oxidized in such high temperature resulted in an Er-doped Si dioxide ( $\text{SiO}_2$ ) system. Indeed, the PL spectra obtained in the paper were very similar to that of Er-implanted

SiO<sub>2</sub> or Er-doped optical fiber. [6] Then, it is hard to understand the optical transition mechanism between the Er<sup>3+</sup> ions and the host porous Si by the above mentioned doping process.

In this paper, we demonstrated a process of doping Er into porous Si by immersing the sample in ErCl<sub>3</sub>:C<sub>2</sub>H<sub>5</sub>OH saturated solution and post-annealing at relatively low temperature (800 °C). A sharp Er<sup>3+</sup>-related 1.54 μm emission peak was observed up to room temperature. The visible PL was also observed from the same sample. It was demonstrated that the Er<sup>3+</sup> ions were excited by energy transfer process from optically excited electron-hole pairs in the host porous Si. No Er<sup>3+</sup>-related PL can be observed by direct excitations. These results suggest that the Er<sup>3+</sup>-emission could be used as a probe to measure the absorption edge of the host even it is not luminescent. We applied the idea to Er-doped porous Si, for the first time, and demonstrated that the Er<sup>3+</sup>-related emission had identical absorption edges with the host porous Si layers. Because of the PL intensity and peak energy of porous Si strongly depend on the preparing process, Er should be a valid probe in such materials.

## EXPERIMENTAL PROCEDURE

The porous Si samples were fabricated by anodization of p-type Si (100) wafers (boron doped, 10-12 Ωcm) in a dilute HF (HF:C<sub>2</sub>H<sub>5</sub>OH:H<sub>2</sub>O=1:2:1) solution using a platinum grid electrode. The anodization was performed with current densities of 10-100 mA/cm<sup>2</sup> for 5 min under the light illumination of a 500 W tungsten lamp. The illumination power density was about 1 W/cm<sup>2</sup> at the surface of the samples. Porous Si layers with thicknesses of 2 μm having different microstructures and different PL spectra were fabricated. After the anodization, the samples were rinsed by C<sub>2</sub>H<sub>5</sub>OH and immersed in saturated ErCl<sub>3</sub>:C<sub>2</sub>H<sub>5</sub>OH solution for 1-10 min and then rinsed in deionized water and dried by nitrogen (N<sub>2</sub>) blowing. The solutions for both the anodization and the immersion were maintained at room temperature during the process.

Afterwards, the samples were annealed in N<sub>2</sub> atmosphere. A two-step annealing process was used. The samples were first baked at 200 °C for 10 min to turn out the remained C<sub>2</sub>H<sub>5</sub>OH and then, were annealed at 800 °C for 5 min to resolve ErCl<sub>3</sub> and to activate Er atom to Er<sup>3+</sup> state. The density of Er atoms in the sample after 3 min immersing and annealing was determined to be 3~5×10<sup>19</sup> cm<sup>-3</sup> by secondary ion mass spectroscopy measurements. The depth profile of Er atoms was almost flat in the porous Si layer.

Temperature-dependent and time-resolved PL measurements of the samples were carried out from 18 K to 300 K. In PL excitation (PLE) measurements carried out at 18 K two excitation sources, a pulsed N<sub>2</sub> laser with a wavelength of 337 nm and a pulse width of 0.3 ns and a dye laser pumped by the N<sub>2</sub> laser were used for over-bandgap tunable excitations. The dye laser was tuned over a wavelength range from 400 nm to 650 nm to excite electron-hole pairs selectively to a certain excitation level. In order to maintain the photoexcited-carrier density to be constant in the host, a constant excitation density of 1.0×10<sup>13</sup> photons/pulse was used by carefully controlling the laser power at each wavelength. To directly excite the Er<sup>3+</sup> ions, a titanium (Ti)-doped sapphire laser was used. The wavelength range of the Ti-doped sapphire laser was from 700 nm to 820 nm. The PL signal was detected by a photomultiplier tube for the visible wavelength region and a germanium p-i-n detector for the infrared region and processed by a boxcar averager with a gate width of 100 μs.

## RESULTS AND DISCUSSIONS

Figure 1 shows the 18 K PL spectra of porous Si layers doped with and without Er after annealing at 800 °C for 5 min in the visible wavelength region (a) and in the infrared region (b) under 337 nm

excitation of the pulsed N<sub>2</sub> laser. The annealed porous Si doped without Er (as-annealed) shows a luminescence band at the blue-green wavelength region (350 nm-600 nm) and a broad background PL at around 1.54  $\mu$ m. In contrast, the porous Si layer doped with Er shows an additional sharp peak at 1.538  $\mu$ m (0.806 eV) on the background of the porous Si. The full width at half maximum (FWHM) of the sharp peak was determined to be 5.2 meV at 18 K. No change on the peak position and on the FWHM was observed by changing the excitation density and the measuring temperature, indicating that the peak at 1.538  $\mu$ m is originated from the intra-4f shell transitions in the Er<sup>3+</sup> ions. Furthermore, the sample which exhibited

weaker visible emission gave rise to more intense Er<sup>3+</sup>-emission and vice versa. Both the visible emission from porous Si and the Er<sup>3+</sup>-emission were observed up to the room temperature. The intensity of the Er<sup>3+</sup>-emission at room temperature was about 30% of that at 18 K. This fact suggests that porous Si is a good host to obtain efficient Er-related emission at room temperature and that Er-doped porous Si might be a suitable material for Si-based optoelectronic device applications. All of the samples investigated in this work for immersing time from 1 to 10 min and annealed at 800 °C for 5 min showed Er<sup>3+</sup>-emission. The most intense 1.54  $\mu$ m PL was obtained from the sample immersing for 3 min. Long immersing time and higher annealing temperature induced an intensity reduction of the Er<sup>3+</sup>-emission. For the samples annealed in O<sub>2</sub> atmosphere only very poor 1.54  $\mu$ m PL was detected.

The PL intensity decay curve of Er<sup>3+</sup>-related 1.54  $\mu$ m emission is shown in Fig. 2. The curve can be fitted by a single-exponential equation and the lifetime of the 1.54  $\mu$ m emission is deduced to be 1.2 ms. This value is very similar to that reported in literature. [6] However, the lifetime of the visible and infrared emissions from porous Si were much shorter. [7] The lifetimes of the emissions at around 1.5  $\mu$ m were in the microsecond order. So that it is easily to remove the background and only detect the Er<sup>3+</sup>-emission by delay the detection time for 100  $\mu$ s for the spectra shown in Fig. 1(b). After removing the background a linear relationship between the excitation power density and the intensity of the 1.54  $\mu$ m PL was demonstrated.

In order to investigate the energy transfer mechanism of the excited electron-hole pairs to the 4f shell in Er<sup>3+</sup> ions, PLE measurements were carried out at 18 K. For the excitation energy higher and around the bandgap of the host

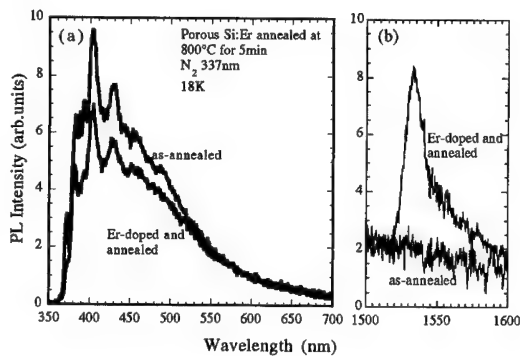


Figure 1. Photoluminescence spectra of porous Si doped with and without Er in the visible wavelength region (a) and in the infrared region (b) measured at 18 K. The Er-related emission at 1.54  $\mu$ m was observed up to room temperature.

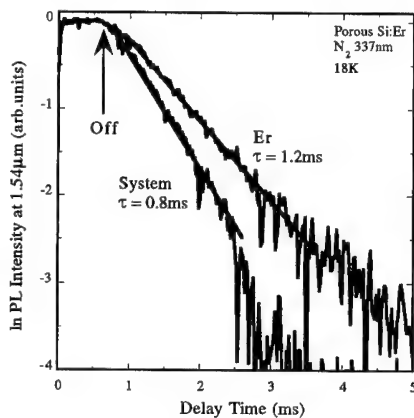


Figure 2. Intensity decay curve of the Er-related 1.54  $\mu$ m photoluminescence of Er-doped porous Si measured at 18 K. The response of the system is also shown in the figure.



porous Si, the N<sub>2</sub> laser and the N<sub>2</sub> laser pumped dye laser were used. The wavelength of the dye laser was tuned from 400 nm to 650 nm (3.10 eV to 1.91 eV). The excitation level was kept to be constant by maintaining the photon flux to be  $1 \times 10^{13}$  photons/pulse at each excitation wavelength. Shown in Fig. 3 are the PL spectra of the visible emission (a) and Er<sup>3+</sup>-emission (b) for several excitation wavelengths. For each excitation wavelength, the PL spectra were recorded from the wavelength which was 60 nm longer than that of the excitation in the visible region and from 1500 nm to 1600 nm in the infrared region.

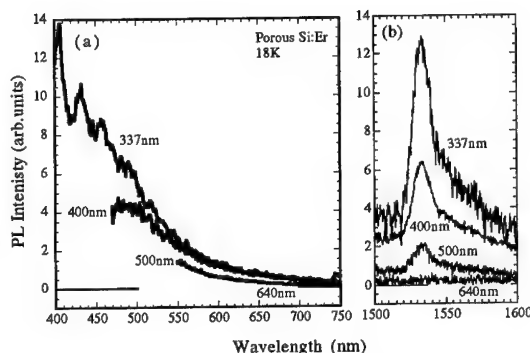


Figure 3. Photoluminescence spectra of Er-doped porous Si in the visible wavelength region (a) and in the infrared region (b) under various excitation wavelengths at 18 K.

Then, the PL intensities were obtained by integrating the spectra in the same wavelength range. The background was removed in calculating the integrated PL intensity of Er<sup>3+</sup>-emission. The PL of porous Si decreased their intensities by increasing excitation wavelength and vanished for excitation wavelength longer than 640 nm (1.94 eV). The background PL from porous Si in the infrared region showed the same behavior as the visible emission. It is considered that the optical absorption edge or the bandgap of the sample is 1.94 eV or larger, and the background PL band in the infrared region should be due to some deep levels inside the bandgap which are excited by a carrier capturing process. The intensity reduction of the PL from porous Si by decreasing the excitation energy should be caused by the reduction of the density of states in the conduction band for the same energy value. It should be pointed out that the intensity of the Er<sup>3+</sup>-emission at 1.54  $\mu$ m decreases by decreasing excitation energy, too.

The Er<sup>3+</sup>-emission disappears at the same energy there the emission from porous Si vanishes. This result suggests that the Er<sup>3+</sup> ions are excited by energy transfer process from the optically excited electron-hole pairs in the host porous Si. A similar model was firstly proposed by Taguchi et al to understand the excitation mechanism of ytterbium-doped InP. [8]

Next, a below bandgap excitation of the sample was performed using the Ti-doped sapphire laser at 18 K. The laser wavelength was continuously changed from 700 nm to 820 nm (1.77 eV to 1.51 eV) in which the third excited state  $^4I_{9/2}$  of Er<sup>3+</sup> ion exists (790-800 nm, 1.57-1.55 eV). In contrast to the over bandgap excitation, no detectable Er<sup>3+</sup>-related luminescence could be observed. The lu-

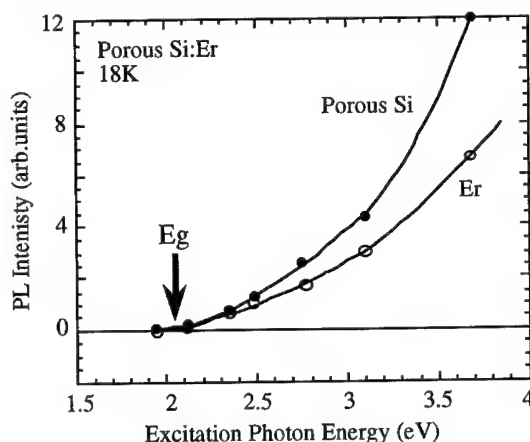


Figure 4. Excitation photon energy dependence of integrated photoluminescence intensities of Er-related emission and porous Si emission. Eg is the deduced absorption edge of the host porous Si.

minescence from porous Si at the infrared region could not be observed, too. The fact indicates that the  $\text{Er}^{3+}$  ions in porous Si can only be excited by interactions with the excited electron-hole pairs but not by direct excitation.

Although the energy transfer mechanism from the excited carriers to the 4f shells of  $\text{Er}^{3+}$  ions is not completely understood at present, it is considered that the  $\text{Er}^{3+}$  ions should have the same absorption edge in the excitation process as the host porous Si material at very low temperature and that the  $\text{Er}^{3+}$  ions are excited by the existence of the excited electron-hole pairs in the host even their radiative recombination rate is very poor. Thus, it is possible to measure the absorption edge or the bandgap of the host only by measuring the absorption edge of the doped Er in it. If there is an efficient absorption of excitons in the host material, however, the measured absorption

edge should be lower than the bandgap energy by the exciton energy. Figure 4 shows the PLE spectra of Er-doped porous Si at 18 K. The open circles show the integrated intensities of  $\text{Er}^{3+}$ -emissions at 1.54  $\mu\text{m}$  and the solid circles show that of the visible emissions from porous Si, respectively. The integration was carried out by the above-mentioned method. The fitting curves of both  $\text{Er}^{3+}$ - and porous Si- emissions indicate an identical absorption edge noted as Eg. Four samples of Er-doped porous Si with different PL spectra were investigated in this work and extremely same absorption edges were demonstrated for every sample, as shown in Fig. 5.

Porous Si is formed by anodization of Si in HF dilute solution. The PL behavior of porous Si strongly depends on the starting material and the fabricating condition. The PL peak position can change from the blue-green wavelength region to the infrared. The PL intensity can vary violently, too. Some of them even show no detectable luminescence. It is also difficult to carry out an optical absorption or reflection measurement because of the porous Si is a fragile and thin layer formed on Si substrate with a rough surface. The  $\text{Er}^{3+}$ -emission, however, is a good probe to measure the absorption edges of such porous Si materials. One only need to dope Er into the host porous Si and measure the PLE of the 1.54  $\mu\text{m}$  emission. The 1.54  $\mu\text{m}$  emission is stable and sharp at a wide temperature range which enables us to investigate it by using a simple experiment set up. The here reported probe effect should be valid in other Er-doped semiconductors, such as in Er-diffused GaAs and InP. [9] The lattice position and crystal symmetry of  $\text{Er}^{3+}$  ions doped into porous Si, on the other hand, are not clarified at present. A detailed study of it is needed which would be helpful in understanding the origin of the visible luminescence from porous Si.

## CONCLUSIONS

Er has been successfully doped into porous Si host by immersing the porous Si sample in a saturated  $\text{ErCl}_3:\text{C}_2\text{H}_5\text{OH}$  solution and post annealing at 800  $^\circ\text{C}$ . A sharp and intense  $\text{Er}^{3+}$ -related luminescence peak at 1.538  $\mu\text{m}$  was observed up to room temperature. It is demonstrated that the  $\text{Er}^{3+}$  ions doped in porous Si are excited only by an energy transfer process from excited electron-hole pairs of the host to the intra-4f-electrons in the ions. From this fact we proposed that the  $\text{Er}^{3+}$  luminescence

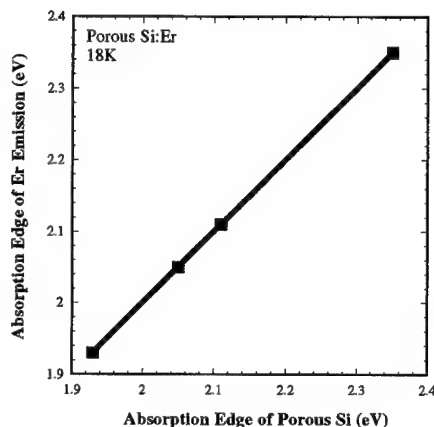


Figure 5. Relationship between the absorption edge of the Er-related emission and that of the host porous Si.

could behave as a good probe to measure the absorption edges of the host materials. The idea was firstly applied on Er-doped porous Si and the validity of the idea was demonstrated by this work. It is considered that the probe effect of Er should be able to apply on other host materials.

## REFERENCES

1. For example, see *Rare Earth Doped Semiconductors*, edited by G. S. Pomrenke, P. B. Klein, and D. W. Langer (Mater. Res. Soc. Proc. **301**, Pittsburgh, PA 1993).
2. S. Coffa, F. Priolo, G. Franzo, V. Bellani, A. Carnera and C. Spinelle, Phys. Rev. B **48**, 11782 (1994).
3. P. N. Favenec, H. L'Haridon, M. Salvi, D. Moutonnet and Y. Le Guillou, Electron Lett. **25**, 718 (1989).
4. L. T. Canham, Appl. Phys. Lett. **57**, 1046 (1990).
5. V. Lehmann and U. Gosele: Appl. Phys. Lett. **58**, 856 (1991).
6. T. Kimura, A. Yokoi, H. Horiguchi, R. Saito, T. Ikoma and A. Saito, Appl. Phys. Lett. **65**, 983 (1994).
7. S. Komuro, T. Kato, T. Morioka, P. O'Keeffe and Y. Aoyagi, Appl. Phys. Lett. **68**, 949 (1996).
8. A. Taguchi, H. Nakagome and K. Takahei, J. Appl. Phys. **70**, 5604 (1991).
9. X. Zhao, K. Hirakawa and T. Ikoma, Proc. of 2nd ICMPC for VLSI, 549 (Shanghai 1991).

## LUMINESCENCE OF RARE EARTH DOPED POROUS SILICON

T. Kimura\*, I. Hosokawa\*, Y. Nishida\*, T. Dejima\*, R. Saito\* and T. Ikoma\*\*

\*Univ. Electro-Communications, Chofu-shi, Tokyo 182, Japan,

\*\*TI Tsukuba Research Development Center, Tsukuba-shi, Ibaragi 305, Japan

### ABSTRACT

Photoluminescence characteristics of porous silicon layers (PSLs) doped with Er or Yb ions are studied. 10 $\mu$ m thick PSLs with a luminescence centered at  $\sim 0.8\mu$ m are formed by anodic etching of p-type silicon wafers of several  $\Omega$ -cm resistivity. Rare-earth ions are electrochemically incorporated into PSLs. The Er<sup>3+</sup>-related luminescence at 1.54 $\mu$ m as well as the Yb<sup>3+</sup>-related luminescence at 1.0 $\mu$ m is observed at room temperature after annealing at high temperatures ( $> 900^\circ\text{C}$ ). The Er-related luminescence is enhanced after annealing in O<sub>2</sub>, whereas the Yb<sup>3+</sup>-related luminescence needs oxygen-free atmosphere (H<sub>2</sub>) for the optical activation. The luminescence decay time of the rare earth ions as well as the host PSLs is measured and the energy transfer mechanism is discussed.

### INTRODUCTION

An efficient room-temperature luminescence of rare earth (RE) doped silicon is expected for the realization of silicon-based optoelectronic devices. To obtain a sufficient luminescence intensity, a RE density higher than 10<sup>19</sup>/cm<sup>3</sup> may be necessary, and the incorporation method should be as simple as possible from a technical as well as an economical point of view. In addition, the luminescence energy of RE ions is limited below the bandgap energy of host semiconductors, i.e.  $\sim 1.1$  eV in the case of crystalline silicon. RE ions are incorporated into crystalline silicon by ion implantation [1], molecular beam epitaxy [2], etc. The authors group has shown for the first time that Er ions are very easily incorporated into porous silicon layers (PSLs) and a strong room-temperature luminescence of Er-related 1.54  $\mu$ m peaks is obtained [3]. Recently, the same group has also reported the Yb-related 0.98  $\mu$ m luminescence from Yb-doped PSLs [4]. Because of the simple two-level energy scheme of the 4f-electrons of Yb<sup>3+</sup> (<sup>2</sup>F<sub>5/2</sub> and <sup>2</sup>F<sub>7/2</sub>), it is obvious that Yb<sup>3+</sup> 4f-electrons are excited by photocarriers generated in PSLs, which becomes possible due to the enlarged energy bandgap of crystalline silicon by anodic etching.

In this paper, we report on the close luminescence characteristics of Er- or Yb-doped PSLs in relation with the PSLs and annealing conditions. The luminescence decay time of the rare earth ions as well as the host PSLs is measured and the energy transfer mechanism is discussed.

### EXPERIMENTAL

PSLs of 10 $\mu$ m thickness are formed by anodic etching of (100) p-Si substrates of several  $\Omega$ -cm resistivity. Thereafter, PSLs are dipped into an ethanol solution with ErCl<sub>3</sub> or YbCl<sub>3</sub>, and the RE<sup>3+</sup> ions are electrochemically incorporated into the PSLs by applying a negative

bias to the PSLs. Measurements by secondary ion mass spectroscopy reveal that  $\text{RE}^{3+}$  ions can be incorporated into the  $10\text{ }\mu\text{m}$  thick PSLs almost uniformly, and a typical  $\text{RE}^{3+}$  ion density used in this study is  $3 - 4 \times 10^{19}/\text{cm}^3$ . After the incorporation, the samples are annealed in a pure Ar,  $\text{Ar}/\text{O}_2(4 : 1)$  or pure  $\text{H}_2$  flow. Photoluminescence measurements are performed by illuminating samples with an Ar laser line ( $514.5\text{ nm}$ ). The luminescence signal is monitored using a single-grating monochromator (Jobin-Yvon HR320) and a cooled germanium p-i-n photodiode.

## RESULTS

### Er-related luminescence

Fig.1 shows typical photoluminescence spectra of an Er-doped PSL at 12K, with the annealing temperature as a parameter (the annealing is in  $\text{Ar}+\text{O}_2$  for 30 sec). Just after the Er incorporation, an Er-doped PSL shows only a luminescence band centered at  $\sim 0.8\mu\text{m}$  which is almost the same as that of a nondoped PSL. The Er-related  $1.54\mu\text{m}$  luminescence begins to appear after annealing at  $\sim 900^\circ\text{C}$ , and it grows rapidly with increasing annealing temperatures.

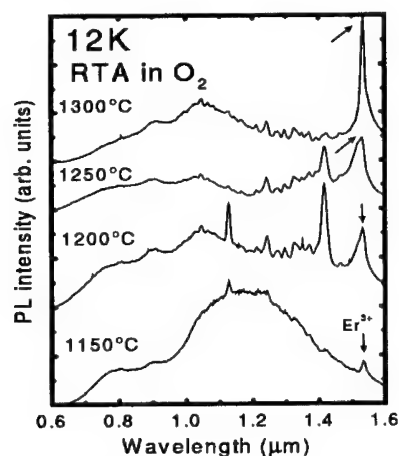


Fig.1 Typical photoluminescence spectra of an Er-doped PSL at 12K for different annealing temperatures (annealing: in  $\text{Ar}+\text{O}_2$  for 30 sec).

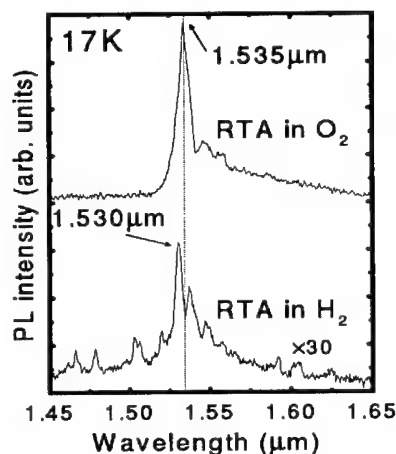


Fig.2 Photoluminescence spectra of an Er-doped PSL annealed in  $\text{Ar}+\text{O}_2$  (upper) and in  $\text{H}_2$  (lower) (annealing: at  $1300^\circ\text{C}$  for 30 sec).

The Er-related luminescence is also observed when samples are annealed in  $\text{H}_2$ . Fig.2 compares the luminescence spectrum of an Er-doped PSL annealed in  $\text{Ar}+\text{O}_2$  with that annealed in  $\text{H}_2$  (annealed at  $1300^\circ\text{C}$  for 30 sec). The intensity of the latter is smaller than that of the former (a factor of  $\sim 30$  in Fig.2). The spectra are also different from each other. The main peak is at  $1.535\text{ }\mu\text{m}$  for the former, whereas at  $1.532\text{ }\mu\text{m}$  for the latter. The full width at half maximum (FWHM) is  $\sim 10\text{ nm}$  for both. The thermal quenching of the luminescence intensity is small for both peaks as shown in Fig.3. The intensity at

low temperatures decreases gradually with increasing temperatures to about a half at room temperature.

#### Yb-related luminescence

Fig.4 shows photoluminescence spectra of an Yb-doped PSL sample at 20K and room temperature, annealed at 1100 °C for 30sec in H<sub>2</sub>. The peak at 0.98 μm which is located at the same wavelength for both temperatures is identified as the luminescence due to the intrashell 4*f*-4*f* transitions  $^2F_{5/2} \rightarrow ^2F_{7/2}$  of Yb<sup>3+</sup>. This Yb-related luminescence cannot be obtained when Yb-doped PSLs are annealed under Ar+O<sub>2</sub>.

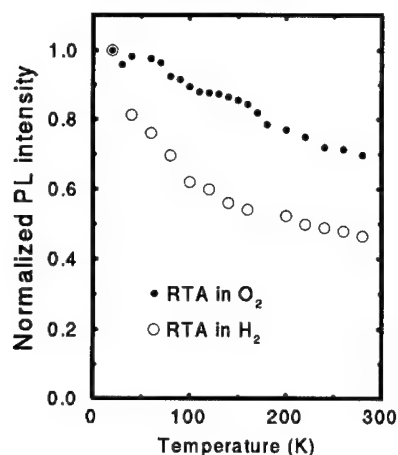


Fig.3 Comparison of the temperature dependence of the luminescence intensity of the main peak between Er-doped PSLs annealed in Ar+O<sub>2</sub> and in H<sub>2</sub> (annealing: at 1300 °C for 30 sec. ).

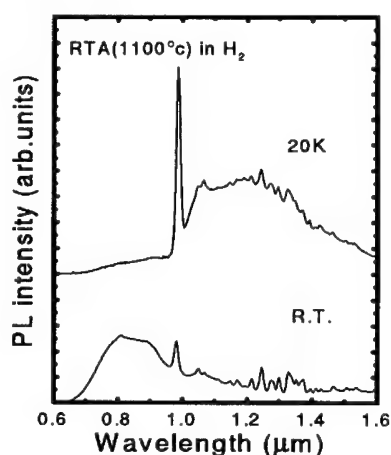


Fig.4 Photoluminescence spectra of an Yb-doped PSL at 20K and at room temperature (annealing: at 1100 °C for 30sec in H<sub>2</sub>).

#### Host PSL dependence

Because the Yb 4*f* electronic state consists of only two energy levels, the Yb 4*f* electrons are excited without doubt by the recombination energy of electrons and holes which are generated in the host PSLs, and therefore the energy transfer from the host PSLs to Yb<sup>3+</sup> ions may be related with the properties of the host PSLs. First, the effective bandgap of the PSLs should be larger than the Yb<sup>3+</sup> luminescence energy. The host PSLs used in this study show a luminescence energy at 1.5-1.4 eV (0.8-0.9 μm) just after anodic etching and is larger than the luminescence energy of Yb<sup>3+</sup> (1.26 eV). Second, the radiative as well as the nonradiative recombination lifetime of electrons and holes generated in PSLs affects the energy transfer efficiency. The lifetime is greatly reduced by the increase of dangling bonds at the surface of microcrystals. These dangling bonds may be passivated with O or H atoms just after anodization and therefore PSLs illuminate strongly. However, when PSLs

are annealed at several hundreds °C, these passivating atoms are considered to be desorbed and the dangling bonds become active, leading to the quenching of the luminescence of PSLs [5,6].

Fig.5 compares the photoluminescence spectra of Er or Yb-doped PSLs, unannealed, annealed in Ar+O<sub>2</sub>(4:1) and in pure H<sub>2</sub>. The as-anodized PSL shows an intense luminescence centered at 0.8 μm. When the PSLs are annealed isochronally (30sec) in Ar+O<sub>2</sub>, the luminescence first disappears at low annealing temperatures (500 - 900 °C), then grows again above ~900 °C. However, its spectrum changes into a broad band with a peak red-shifted. In the case of annealing in H<sub>2</sub>, the luminescence of the PSLs is very weak but does not disappear totally, and both Er- and Yb-related peaks are obtained. As for Yb-doped PSLs, when PSLs are first oxidized at 900 °C for 3 min. in Ar+O<sub>2</sub>, thereafter Yb<sup>3+</sup> ions are incorporated and then the samples are annealed at high temperatures in H<sub>2</sub>, the luminescence of the PSLs at 0.8 μm does not disappear. At the same time, the Yb-related luminescence becomes very strong (×10) (the second spectrum from the top in Fig.5).

In the case of annealing in Ar+O<sub>2</sub>, the dangling bonds may be passivated with O atoms. In the case of H<sub>2</sub>, a part of the dangling bonds may be passivated with H atoms. When the PSLs are annealed at 900 °C for a little bit longer time to passivate the dangling bonds with O atoms and thereafter annealed at higher temperatures for the optical activation of Yb<sup>3+</sup> ions in H<sub>2</sub>, the PSLs are stable and Yb<sup>3+</sup> ions are excited more effectively from the host PSL.

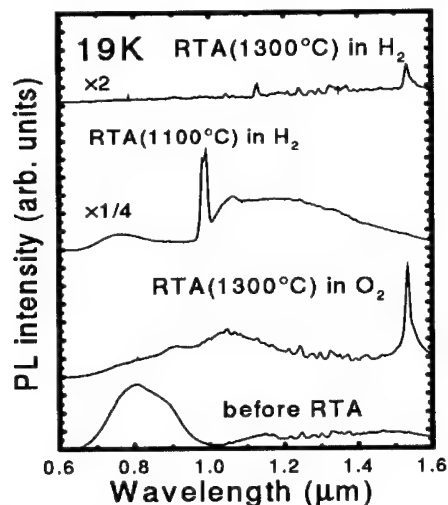


Fig.5. Photoluminescence spectra of RE<sup>3+</sup>-doped PSLs at 19K. Top: Er<sup>3+</sup>-doped, annealed at 1100 °C in H<sub>2</sub>. Second from the top: Yb<sup>3+</sup>-doped, pretreated at 900 °C for 3 min, in Ar+O<sub>2</sub> before the Yb-incorporation. Third from the top: Er-doped, annealed in Ar+O<sub>2</sub> at 1300 °C. Bottom: Er-doped, unannealed.

#### Time decay

The decay of the luminescence of PSLs is known to be dependent on the anodization conditions as well as on the wavelength. Since the as-anodized PSLs used in this study illuminate at ~0.8 μm, the decay at this wavelength is compared with that of Yb-related 0.98 μm peak. Fig.6 shows the decay at 15K of a sample annealed at 1100°C for 30 sec in H<sub>2</sub>. The decay of the PSL luminescence at 0.8 μm is nearly exponential (linear in the semilogarithmic plots). On the other hand, the decay of the Yb-related peak is nonexponential and is fitted with two decay times (a fast decay time  $\tau_f$  and a slow decay time  $\tau_s$ ). The faster decay time is almost comparable to that of Yb-doped InP [7], but this fast decay is not dominant

in the whole decay curve especially at higher temperatures and is followed with a slower decay which is several hundreds microseconds.

Fig.7 shows the decay time as a function of temperature. As for the Yb-related peak, the time for the 90% decay ( $\tau_{90}$ ) is plotted in the figure. With increasing temperatures,  $\tau_{90}$  which is closer to  $\tau_f$  at low temperatures approaches  $\tau_s$  at high temperatures and rather increases slightly. When  $\tau_{90}$  is compared with the decay time of the PSL at 0.8  $\mu\text{m}$  ( $\tau_{PSL}$ ), the latter is longer at low temperatures, but becomes shorter at high temperatures, presumably due to the increase in the nonradiative recombination at dangling bonds. The cross point is around 100K. This point agrees roughly with the onset of the thermal quench of the Yb-related peak (see insert).

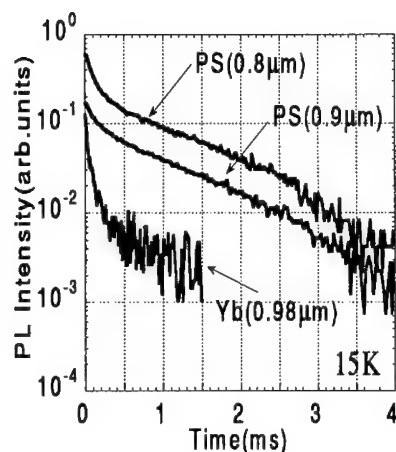


Fig.6 Luminescence decay of Yb (at 0.98  $\mu\text{m}$ ) and PSL (at 0.8  $\mu\text{m}$  and 0.9  $\mu\text{m}$ ) at 15K (annealing: at 1100°C for 30 sec in  $\text{H}_2$ ).

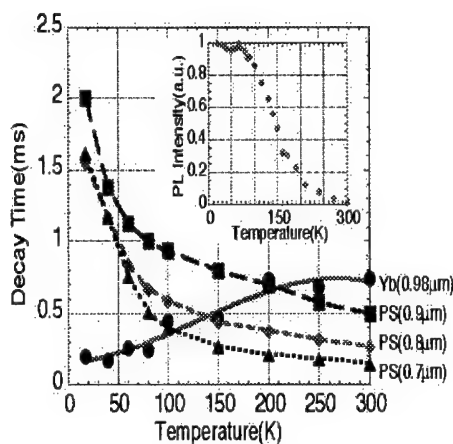


Fig.7 Temperature dependence of the luminescence decay times of Yb  $\tau_{90}$  (90% decay at 0.98  $\mu\text{m}$ ) and PSL ( $\tau_{90}$  at 0.8  $\mu\text{m}$  and 0.9  $\mu\text{m}$ ). The insert shows the temperature dependence of the Yb (0.98  $\mu\text{m}$ ) intensity (annealing: at 1100°C for 30 sec in  $\text{H}_2$ ).

#### Usefulness of PSLs as hosts for the RE-related luminescence

From the above results, we can deduce the following conclusive remarks and point out useful features of PSLs as host semiconductors.

1. RE-ions are easily incorporated into nanometer-size pores of PSLs at high density ( $\sim 10^{20}/\text{cm}^3$ ) by electrochemical incorporation or simply dipping in an alcohol/ $\text{RECl}_3$  solution.
2. The bandgap of PSLs becomes larger than the crystalline silicon and is controlled by the anodization condition. The enlargement in the bandgap makes possible the RE-related luminescence at energies higher than the bandgap of crystalline silicon. It also



may possibly suppress the energy backflow from RE ions to host PSLs as is observed in wide bandgap semiconductors such as GaN.

3. The recombination lifetime of electrons and holes generated in PSLs are relatively long (several microseconds to milliseconds). This may lead to an effective energy transfer of the recombination energy to RE-ions.
4. A high temperature anneal is necessary for the optical activation of RE-ions after incorporation into PSLs. However, the optical properties of PSLs as well as RE ions are greatly influenced by the annealing after anodization. The passivation of dangling bonds is the most important factor for the effective excitation of RE ions.
5. It may be possible to form a RE-doped PS waveguide on the crystalline silicon substrate. This may open the way to the silicon-based opto-electronic devices.

## CONCLUSION

Strong room-temperature luminescence of Er-doped porous silicon at  $\sim 1.54 \mu\text{m}$  and of Yb-doped porous silicon at  $\sim 0.98 \mu\text{m}$  is obtained. The emission intensity as well as the spectrum depends on the atmosphere of the annealing after RE-ion incorporation. The enlargement of the bandgap due to the formation of nanometer size microcrystals by anodization makes possible the luminescence of Yb at  $0.98\mu\text{m}$ , increases the energy transfer efficiency, and may possibly suppress the energy backflow.

## ACKNOWLEDGEMENTS

The authors would like to thank Mr. A. Yokoi and Mr. H. Horiguchi for the cooperation. They also express their thank to Dr. H. Morisaki, Dr. H. Isshiki and Dr. K. Takahei for their helpful discussions. This work is supported in part by Grant-in-Aid for Scientific Research from the Ministry of Education, Science, Sports and Culture, Japan.

## REFERENCES

1. H. Ennen, J. Schneider, G. Pomrenke, J. Schneider, J. Windscheif, and A. Axmann, *J. Cryst. Growth* **64**, p.165 (1983).
2. H. Ennen, G. Pomrenke, A. Axmann, K. Eisele, W. Haydl and J. Schneider, *Appl. Phys. Lett.* **46**, p.381 (1985).
3. T. Kimura, A. Yokoi, H. Horiguchi, R. Saito, T. Ikoma and A. Sato, *Appl. Phys. Lett.* **65**, p.983 (1994).
4. T. Kimura, A. Yokoi, Y. Nishida, R. Saito, S. Yugo and T. Ikoma, *Appl. Phys. Lett.* **67**, p.2687 (1995).
5. C. Tsai, K.-H. Li, J. Sarathy, S. Shin, J.C. Cambell, B.K. Hance and J. M. White, *Appl. Phys. Lett.*, **59**, 2814-2816 (1991).
6. N. Ookubo, H. Ono, Y. Ochiai, Y. Mochizuki, and S. Matsui, *Appl. Phys. Lett.*, **61**, 940-942 (1992).
7. K. Takahei, A. Taguchi, H. Nakagome, K. Uwai and P. S. Whitney, *J. Appl. Phys.* **66**, 4941 (1989).

## EXAFS AND X-RAY CTR SCATTERING CHARACTERIZATION OF Er DOPED IN InP BY OMVPE

M. TABUCHI, D. KAWAMURA, K. FUJITA, N. MATSUBARA, N. YAMADA,  
H. OFUCHI, S. ICHIKI, Y. FUJIWARA, Y. TAKEDA

Department of Materials Science and Engineering, Nagoya University, Nagoya 464-01,  
Japan, tabuchi@numse.nagoya-u.ac.jp

### ABSTRACT

Er-doped semiconductors are considered to be important for optical communication systems since one of the prominent luminescent peaks of Er is in the minimum absorption region of silica based fiber and wavelength of the luminescence is insensitive to the ambient temperature. In this work, OMVPE grown InP samples uniformly and  $\delta$ -doped with Er were investigated by EXAFS and X-ray CTR measurements. The EXAFS measurement revealed that the uniformly doped Er atoms in InP grown at 580°C formed NaCl-structure ErP, and at 530°C occupied the In-sites. The X-ray CTR measurement revealed that the  $\delta$ -doped Er atoms in InP at 530°C formed NaCl-structure ErP. In the sample, the total number of Er was analyzed to be about 0.171ML(monolayer), and the FWHM of Er distribution was about 5ML. By comparing the results of PL measurement with those of the EXAFS and the X-ray CTR measurements, it was suggested that the Er atoms on In-sites show high efficiency of luminescence and the Er atoms in the NaCl-structure ErP low efficiency.

### INTRODUCTION

The rare earth elements are known to show stable luminescence spectra even when environments such as temperature and chemical bonding are changed[1]. One of the luminescent peaks of Er is observed at 1.54 $\mu$ m. Since the wavelength(1.54 $\mu$ m) is just in the minimum absorption region of silica based optical fibers, Er-doped materials are considered to be important for optical communication systems. Er-doped optical fiber amplifier is an example which shows the ability of Er in optics. However, the fiber amplifier is a relatively complicated system composed of optical excitation system and Er-doped fiber. Therefore, if the Er can be excited directly by electricity, it is much more useful for optical communication systems.

For this purpose, Er-doped semiconductors have been studied. In our laboratory, Er-doped InP samples were grown by OMVPE (organometallic vapor phase epitaxy), and investigated by SIMS (secondary ion mass spectroscopy), Hall effect, PL (photoluminescence), PR (photorefectance), EXAFS (extended X-ray absorption fine structure), and X-ray CTR (crystal truncation rod) measurements. The PL measurement showed that spectra and intensity of the Er luminescence depend strongly on growth temperatures[1]. It suggests that Er atoms form more than one type of luminescent centers of high and low luminescent efficiency, and that the ratio of concentrations of the luminescent centers varies with the growth temperature. In order to apply the Er-doped semiconductors to optical communication systems, it is necessary to control the generation of the luminescent centers of high and low efficiency. Therefore, the structures of luminescent centers must be studied to understand how these centers are formed. In this paper, results of the EXAFS and the X-ray CTR measurements are discussed with results of the PL measurement. The EXAFS measurement is a powerful

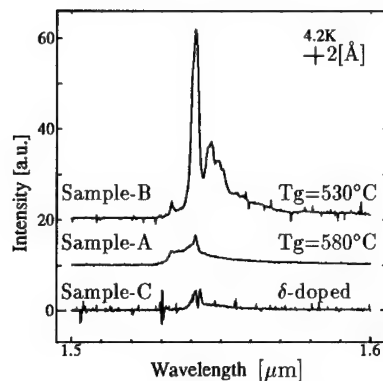


Fig. 1: Measured PL spectra at the same excitation power.

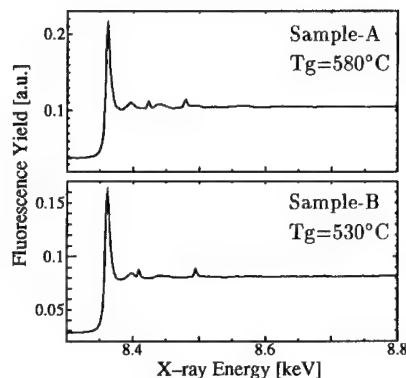


Fig. 2: Measured EXAFS spectra for samples-A and -B.

technique to investigate a local structure around an element[2, 3, 4]. The X-ray CTR is sensitive to the structure of crystals as thin as 1ML [5, 6, 7, 8].

## EXPERIMENTS

All samples were prepared by OMVPE using TMI(trimethylindium), TBP(tertiarybutylphosphine), and Er(MeCp)(tris(methylcyclopentadienyl)erbium) as source materials[1].

Three samples were investigated in this work. Two samples were uniformly doped InP with Er, and the third sample was  $\delta$ -doped InP with Er. One of the uniformly Er-doped InP was grown at 580°C(sample-A), and another was grown at 530°C(sample-B). The concentration of Er in both samples were  $8 \times 10^{18} \text{cm}^{-3}$  measured by SIMS. The  $\delta$ -doped sample (sample-C) was grown at 530°C. The  $\delta$ -doped layer was prepared by exposing the InP surface to Er(MeCp) for 5min with TBP. Then the Er-exposed surface was capped by 100Å InP. Total number of the Er contained in the sample was about  $2 \times 10^{14} \text{cm}^{-2}$  measured by SIMS.

Figure 1 shows the result of PL measurement for the three samples. The luminescence from the sample-B was stronger than those from the samples-A and -C. The spectra of the samples-A and -C were very similar with each other. Thus, it was considered that in the samples-A and -C the Er atoms formed the same type of luminescent center which was different from that formed in the sample-B.

In this work, the uniformly doped samples(A and B) were investigated by Er  $L_{III}$ -edge fluorescence EXAFS measurement, and the  $\delta$ -doped sample(C) was investigated by the X-ray CTR measurement. Both of the measurements were conducted using synchrotron radiation at the Photon Factory in the National Laboratory for High Energy Physics at Tsukuba. For the EXAFS and the X-ray CTR measurement, Beam Line 12C and Beam Line 6A<sub>2</sub> were used, respectively.

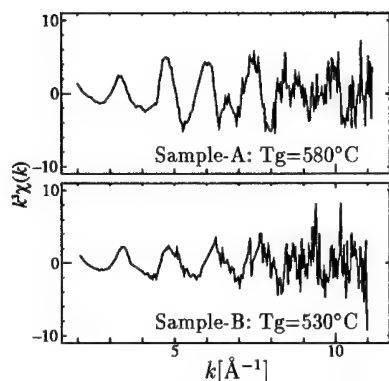


Fig. 3: EXAFS  $k^3\chi(k)$  spectra.

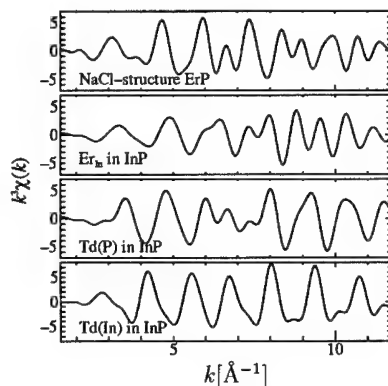


Fig. 4: Theoretically calculated EXAFS  $k^3\chi(k)$  spectra.

## RESULTS OF EXAFS

Figures 2 and 3 show measured fluorescence yield spectra and  $k^3\chi(k)$  spectra, respectively. The  $k^3\chi(k)$  spectra of the samples-A and -B are different from each other. For example, a peak appeared about at  $k = 6.5[\text{\AA}]$  in the spectrum of the sample-A was not observed in the spectrum of the sample-B. For comparison, theoretically calculated EXAFS  $k^3\chi(k)$  spectra were shown in Fig. 4. These spectra were calculated with several assumed crystal structures and occupation sites for Er, such as NaCl-structure ErP, Er on In-site of InP, Er on Td(tetrahedral)-site (P nearest) of InP, and on Td-site (In nearest). For the sample-A, the calculated spectrum of NaCl-structure ErP fit best to the experimental EXAFS. In table-I, best fit parameters are listed. Er-P bond length was obtained to be  $2.77 \pm 0.005\text{\AA}$  for the sample-A. Since the lattice constant of NaCl-structure ErP is  $5.606\text{\AA}$ , the Er-P bond length in the NaCl-structure ErP is calculated to be  $2.803\text{\AA}$  which was close to the measured bond length. Number of neighboring atoms obtained from the analysis was about 7, which was only 20% different from that of the assumed NaCl-structure ErP, i.e., 6.

It was difficult to choose which calculated spectrum fits best to measured one only by their shapes for the sample-B. Therefore, after fitting every calculated spectrum to the measured spectrum, the spectrum calculated with the assumption that Er atoms were on In-sites in the zincblende-structure InP matrix was chosen as the best fit. Number of neighboring atoms obtained from the analysis was about 4. The number is consisted with the nearest neighbor atoms number in the assumed zincblende-structure, i.e., 4.

Table-I: Parameters obtained from EXAFS data analysis at the best fit.

sample	$r_{\text{Er-P}}[\text{\AA}]$	N	$\sigma[\text{\AA}^{-1}]$	R-factor
A: 580°C	2.77	7.3	0.11	0.163
B: 530°C	2.67	3.9	0.11	0.035

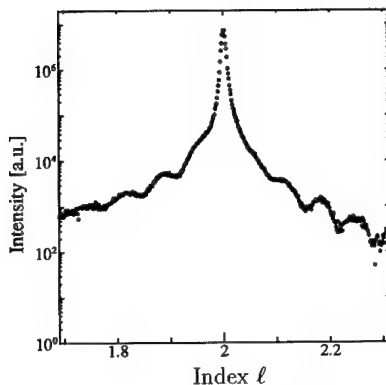


Fig. 5: Measured X-ray CTR scattering spectra for sample-C.

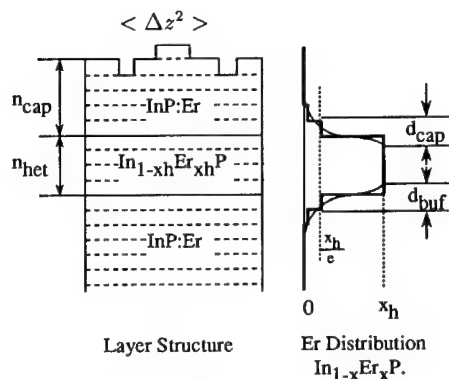


Fig. 6: Model of Er distribution for theoretical calculation.

## RESULTS OF CTR

Figure 5 shows a measured X-ray CTR spectrum for the sample-C. The measured data was analyzed by comparing the spectrum with calculated ones with several assumed crystal structures and occupation sites for Er. Distribution of Er atoms, as shown in Fig. 6, was also treated as a parameter to calculate each spectrum. The calculated spectra and the measured one were compared as shown in as shown in Fig. 7. It was obvious that the calculated spectrum of NaCl-structure ErP fit best to the measured X-ray CTR spectrum. The distribution of Er atoms which gave the spectrum Fig. 7-(a) is shown in Fig. 8. The total number of Er atoms contained in the sample-C was calculated to be 0.171ML, which was well consisted with the result of RBS measurement. The FWHM(full width at half maximum) of the Er distribution was successfully analyzed as 5ML. Such high resolution

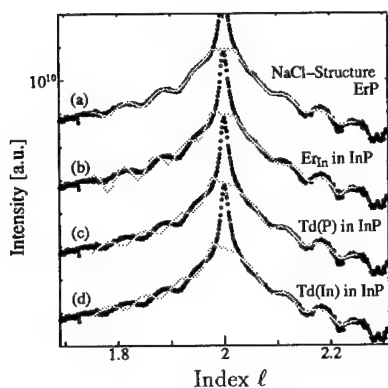


Fig. 7: Theoretically calculated spectra fit to measured data.

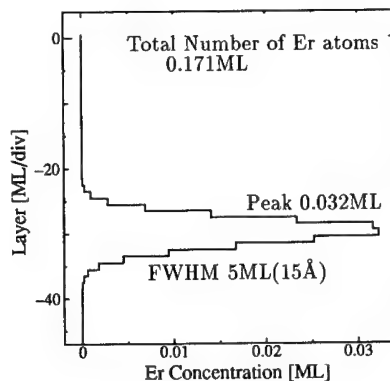


Fig. 8: Measured distribution of Er.

had never obtained before the present X-ray CTR measurement.

## DISCUSSIONS

As shown in the previous sections, in the samples-A and -C Er atoms formed the NaCl-structure ErP, and in the sample-B Er atoms were on In-sites in InP matrix. These results were considered to correspond to the results of the PL measurement. As shown in Fig. 1, only the luminescence of the sample-B showed a high efficiency. The samples-A and -C showed a low efficiency of luminescence, and the spectra of them were very similar. The EXAFS and X-ray CTR measurements investigated only major (in number) structures formed with Er. Therefore, it was not still clear that those structures were directly related to luminescence or not. However, these results were considered to suggest that the Er atoms which showed a high efficiency of luminescence occupied the In-sites in InP, and that the Er atoms which showed a low efficiency of luminescence formed NaCl-structure ErP.

## CONCLUSIONS

OMVPE grown InP samples uniformly and  $\delta$ -doped with Er were investigated by the EXAFS and the X-ray CTR measurements. The EXAFS measurement revealed that the uniformly doped Er atoms in InP at 580°C formed NaCl-structure ErP, and at 530°C occupied the In-sites. The X-ray CTR measurement revealed that the  $\delta$ -doped Er atoms in InP at 530°C formed NaCl-structure ErP. The total number of Er was about 0.171ML, and the FWHM of Er distribution was about 5ML. By comparing the results of the PL measurement with those of the EXAFS and the X-ray CTR measurements, it was suggested that the Er atoms on In-sites showed a high efficiency of luminescence, and the NaCl-structure ErP showed a low efficiency of luminescence.

## ACKNOWLEDGMENTS

This work was performed as a part of the project (Project No. 94G330 and No. 94G240) accepted by the Photon Factory Program Advisory Committee. This work was supported in part by the Grant-in-Aid for Scientific Research (B) No. 0745507, and for Developmental Scientific Research (B) No. 07555100 from the Ministry of Education, Science and Culture.

## References

1. Y. Fujiwara, N. Matsubara, J. Yuhara, M. Tabuchi, K. Fujita, N. Yamada, Y. Nonogaki, Y. Takeda, and K. Morita, *Inst. Phys. Conf. Ser.*, (in press).
2. J.B. Boyce and J.C. Mikkelsen, Jr., *J. Cryst. Growth*, **98**, p.37 (1989).
3. H. Oyanagi, T. Matsushita, H. Tanoue, T. Ishiguro, and K. Kohara, *Jpn. J. Appl. Phys.*, **24**, p.610 (1985).
4. Y. Takeda, H. Oyanagi, and A. Sasaki, *J. Appl. Phys.*, **68**, p.4513 (1990).
5. Y. Takeda, Y. Sakuraba, K. Fujibayashi, M. Tabuchi, and T. Kumamoto, *Appl. Phys. Lett.*, **66** pp.332-334 (1995).

6. M. Tabuchi, Y. Takeda, Y. Sakuraba, T. Kumamoto, K. Fujibayashi, I. Takahashi, J. Harada, and H. Kamei, *J. Cryst. Growth*, **146** pp.148-152 (1995).
7. M. Tabuchi, N. Yamada, K. Fujibayashi, T. Kumamoto, Y. Takeda, I. Takahashi, J. Harada, *J. Electron. Mat.*, in April 1996 issue.
8. M. Tabuchi, K. Hagiwara, A. Kobashi, N. Yamada, K. Fujibayashi, and Y. Takeda, *Inst. Phys. Conf. Ser.*, (in press).

## THE 4f INTRASHELL TRANSITIONS OF YTTERBIUM IN INDIUM PHOSPHIDE

INGRID DE MAAT-GERSDORF\*, T. GREGORKIEWICZ\*, C.A.J. AMMERLAAN\*,  
P.C.M. CHRISTIANEN\*\* and J.C. MAAN\*\*

\*Van der Waals-Zeeman Instituut, Universiteit van Amsterdam, Valckenierstraat 65-67,  
NL-1018 XE Amsterdam, The Netherlands

\*\*Laboratorium voor Hoge Magneet Velden, Katholieke Universiteit Nijmegen, Toernooiveld 1,  
NL-6525 ED Nijmegen, The Netherlands

### ABSTRACT

Zeeman measurements in magnetic fields up to 16 T have been performed on the no-phonon lines labelled #3, #4, and #8 of the spectrum of ytterbium impurities in indium phosphide. A strong polarization effect and changes in intensities were observed. An energy level diagram is presented that satisfactorily explains the magnetic field effect and the relative intensities of the photoluminescence lines and is consistent with experiments described in the literature.

### INTRODUCTION

Rare-earth doped semiconductors are lately intensively investigated in the prospective of their possible application in optoelectronic devices. The presence of an incompletely filled 4f shell offers an attractive possibility of inducing intrashell excitations, with a sharp atomic-like spectrum, practically independent of the host crystal.

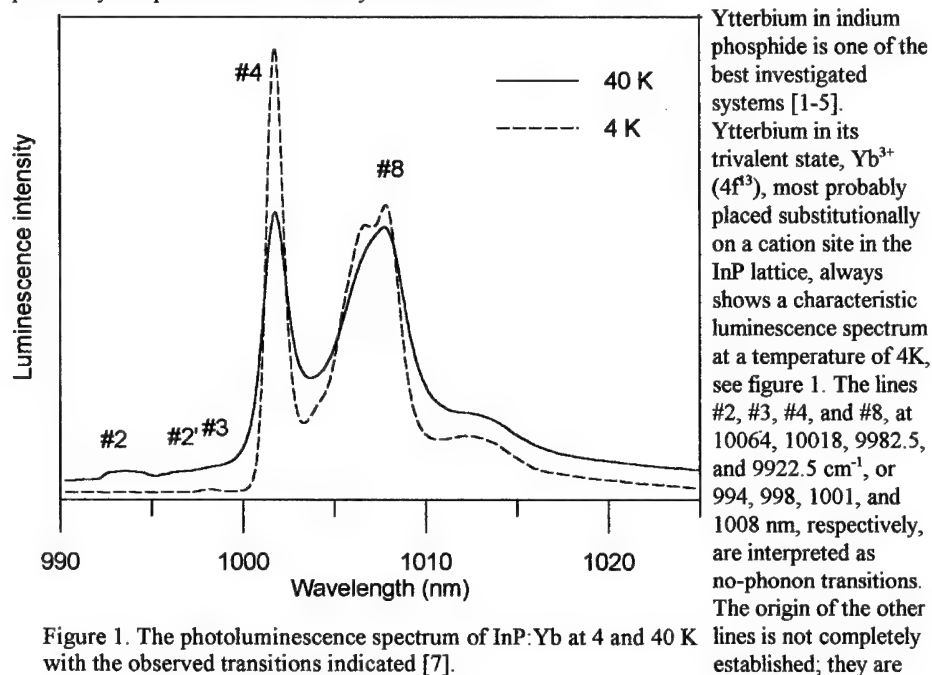


Figure 1. The photoluminescence spectrum of InP:Yb at 4 and 40 K with the observed transitions indicated [7].



described as phonon replica's [3] or assigned to a non-cubic centre [4]. The zero-phonon lines are shown to result from a cubic defect centre and arise from transitions between the spin-orbit levels  $^2F_{5/2}$  and  $^2F_{7/2}$ . Due to the cubic crystal field the lower  $^2F_{7/2}$  level is split in three,  $\Gamma_6$ ,  $\Gamma_7$ , and  $\Gamma_8$  sublevels, and the  $^2F_{5/2}$  in two, a  $\Gamma_7$  and a  $\Gamma_8$  sublevel.

Zeeman measurements [3] show an eightfold splitting of line #3 in high magnetic fields. Following this study an energy level diagram for the 4f sublevels, as shown in figure 2, has been established. This scheme has an unusual reversal of the  $\Gamma_7$  and  $\Gamma_8$  sublevels at the excited state that cannot be explained by the crystal field calculations [6], and is in contrast to the predictions of a point charge model for an ytterbium atom on a substitutional cation site [8]. Further, in this scheme one is unable to explain the relative intensities of the lines #3, #4 and #8 in photoluminescence and the surprising increase of the luminescence intensity of line #3 when applying a magnetic field, see later.

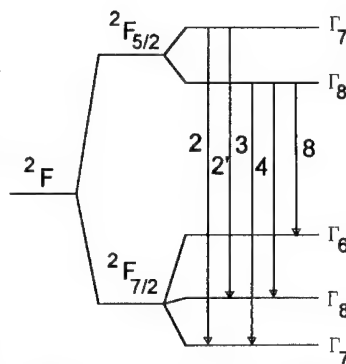


Figure 2. The energy level diagram of InP:Yb according to Ref. [3].

Optically detected magnetic resonance (ODMR) has been observed in the lowest state of the  $^2F_{5/2}$  level [4]. The ODMR signal is not isotropic but depends on the crystal orientation relative to the magnetic field; this can be interpreted as a confirmation of the reversed order of the crystal field states in the  $^2F_{5/2}$  level.

## EXPERIMENTAL RESULTS AND DISCUSSION

Lines #3, #4 and #8 in the luminescence spectrum of Yb in InP have been studied by investigating their Zeeman effect at a temperature of 4 K in magnetic fields up to 16 tesla. The luminescence was excited with a cw argon-ion laser operating at a wavelength of 514.5 nm. A 0.64 m monochromator, with an unblazed 1200 grooves  $\text{mm}^{-1}$  grating, was used in a backscattering geometry with  $\lambda/4$  and polarization filters. The light emerging parallel to the field direction was observed. The magnetic field was changed 180 degrees to measure the different polarizations; in this paper an arbitrarily chosen direction will be referred to as positive.

Two samples were used in this study:

- One crystal was grown by metal-organic chemical vapour deposition (MOCVD). The total Yb concentration was approx.  $10^{18}$  atoms/ $\text{cm}^3$ . The surface was the [100] plain.
- The other crystal was grown by the high pressure gradient freeze synthesis method. By this method, Yb was diluted in indium phosphide with a concentration of about  $10^{17}$  atoms/ $\text{cm}^3$ . The surface of this sample was off-axis oriented.

When investigating the transitions that are possible in this system selection rules should be taken into account. For the magnetic field split levels these are  $\Delta\mu = 0$  or  $\pm 1$ , with  $\mu$  the lowest (absolute) value of the magnetic quantum number  $m$ . For electrical dipole-transitions  $\Delta\mu = 0$ , linear polarized light will be emitted perpendicular to the magnetic field. In the case of  $\Delta\mu = \pm 1$  transitions circular polarized light will be emitted parallel or antiparallel to the magnetic field. Since the experiment was done in the latter configuration the selection rules are  $\Delta\mu = \pm 1$ .

We will first investigate what to expect for the different transitions of Yb in a  $\langle 100 \rangle$  direction. The forbidden  $\Gamma_7 \rightarrow \Gamma_7$  transition has four possible components: one with  $\Delta\mu = +1$ , one with  $\Delta\mu = -1$  and two with  $\Delta\mu = 0$ ; the allowed transitions are the inner ones. According to this scheme the  $\Gamma_7 \rightarrow \Gamma_7$  transition is permitted; probably in  $T_d$  symmetry the different contributions of this line will sum up to zero because of destructive interference. Without field there is no line but as soon as the Zeeman splitting is bigger than the natural line width two strong lines will be seen. The  $\Gamma_7 \rightarrow \Gamma_6$  transition has also two allowed components  $\Delta\mu = \pm 1$  but they are the outer ones and the other two have  $\Delta\mu = 2$ . The  $\Gamma_7 \rightarrow \Gamma_8$  transition and the  $\Gamma_8 \rightarrow \Gamma_7$  transition will both have in total eight components two  $\Delta\mu = 0$ , two  $\Delta\mu = 2$  and four allowed transitions; the allowed ones are the inner ones. The  $\Gamma_8 \rightarrow \Gamma_6$  transition is similar, with the allowed lines being the outer ones. Finally, for  $\Gamma_8 \rightarrow \Gamma_8$  there are four  $\Delta\mu = 2$ , four  $\Delta\mu = 0$  and eight allowed transitions, the inner ones.

When the field is in an arbitrary direction, no transitions will be forbidden. In this case a doubling of the number of lines is expected when compared to the situation for the  $\langle 100 \rangle$  direction. In what follows the results obtained for the individual spectral components will be discussed.

#### Line #8

In the Zeeman splitting of line #8 at 1007.7 nm, two lines were resolved for the  $\langle 100 \rangle$  direction, and four for the off-axis direction, see figures 3 and 4. The total splitting width is about 4 nm in a field of 16 T. More components observed in this region are most probably due to the lines #5 - #7. The intensity of the four lines changed with increasing field. The intensity of the lines seen in the positive polarization got somewhat higher and the intensity of the lines seen in negative direction decreased, see figure 5.

In theory the Zeeman components are expected to repel each other, see figure 6. In the

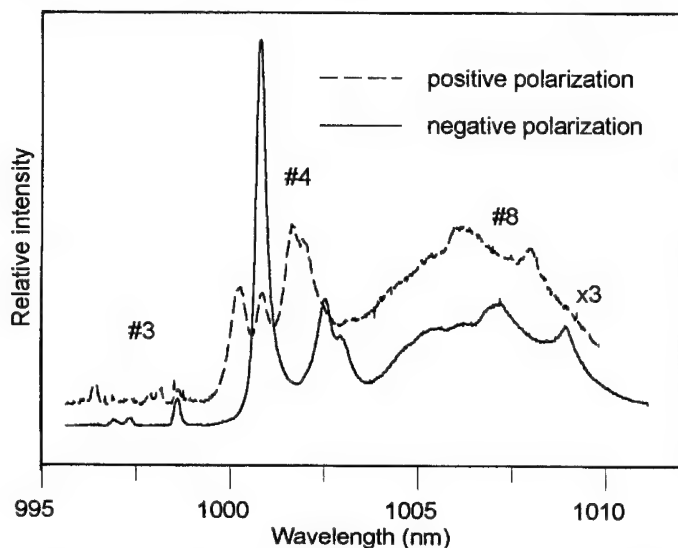


Figure 3. The Zeeman spectra observed in the positive and negative polarization at 14 T, in the off-axis oriented sample.

experiment a deviation from the expected behaviour is seen indicating that a rather strong second-order effect is present. One can assume that also lines #3 and #4 are influenced by this effect and this will disturb correct qualitative analysis of the Zeeman effect.

The very clear splitting of line #8 into two components for the  $\langle 100 \rangle$  oriented sample and four in the low-symmetry direction indicates that this line must correspond to a  $\Gamma_7 \rightarrow \Gamma_7$  or a  $\Gamma_7 \rightarrow \Gamma_6$  transition. Also the fact

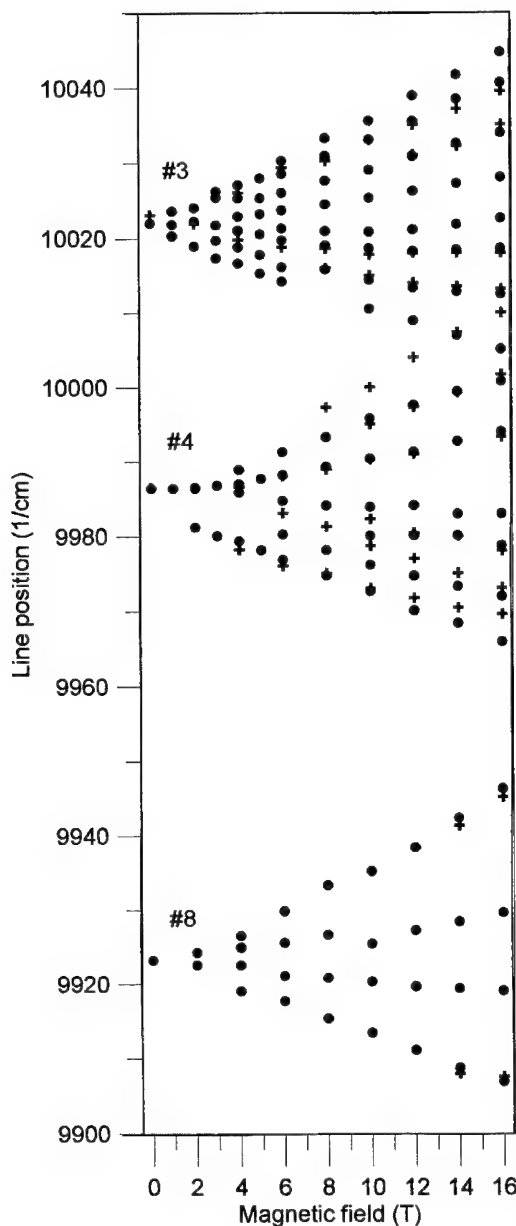


Figure 4. The Zeeman splitting of PL lines #3, #4, and #8 in the  $\langle 100 \rangle$  (crosses) and the off-axis (circles) oriented sample.

that the two lines, that can be seen for both measurements, are more or less in the same position indicates that no anisotropic  $g$  tensor, characteristic for  $\Gamma_8$ , is involved. The observation that the two outer lines are seen in the  $\langle 100 \rangle$  direction, fixes line #8 unequivocally as the  $\Gamma_7 \Rightarrow \Gamma_6$  transition. Also the magnitude of the experimentally found Zeeman splitting agrees with the theoretical expectations for this transition, see figure 6, and thus supports such an assignment.

#### Line #4

Line #4, at about 1001.3 nm was shifted, in the  $\langle 100 \rangle$  oriented specimen, to higher energies by about  $1 \text{ cm}^{-1}/\text{T}$ , and several lines with low intensity appeared at both sides of it, see figures 3 and 4.

One strong line was seen in the positive polarization and the other ones were of equal intensity up to 8 T. Also in this case the lines with the negative polarization decreased in higher fields, see figure 5. Both samples show slightly different spectra, but at a sufficiently high field always six lines appear, with the total splitting of approx. 5 nm in 16 T. Since line #4 splits in more than four components it is likely to arise from the  $\Gamma_7 \Rightarrow \Gamma_8$  transition. Only six of the expected eight lines were observed, but the relative splitting and the trend of the lines are in agreement with the theoretical expectations. For the two samples the lines are found in somewhat different positions indicating some anisotropy and, therefore the possible involvement of a  $\Gamma_8$  level.

The decrease of the intensity of the lines seen in the negative polarization can be explained by the fact that these arise from the higher sublevel of the lowest excited state. The life times for all these forbidden transitions is sufficiently long to obtain an equilibrium Boltzmann distribution. When

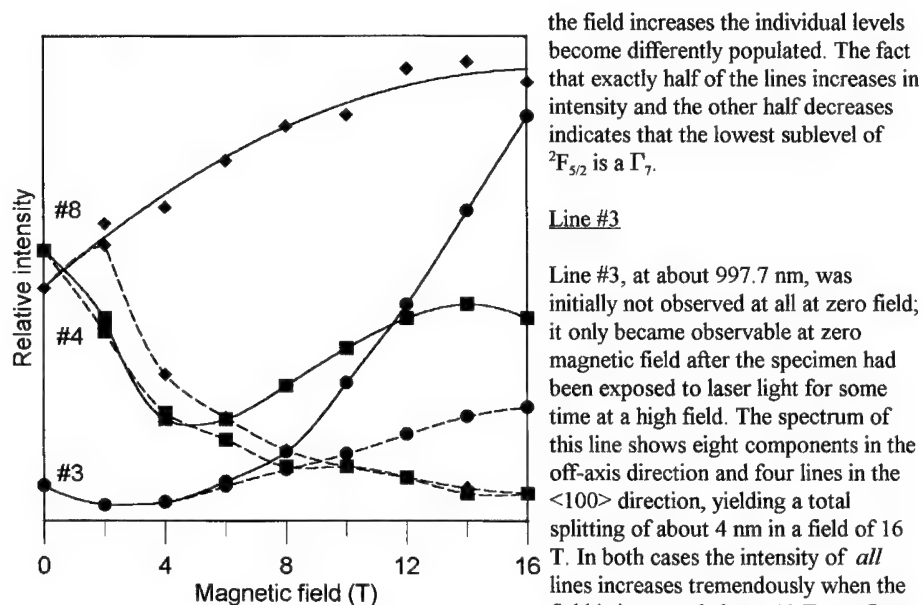


Figure 5. The relative intensities of the PL lines under positive and negative (dashed line) polarizations. The lines are a guide for the eyes.

the field increases the individual levels become differently populated. The fact that exactly half of the lines increases in intensity and the other half decreases indicates that the lowest sublevel of  $^2F_{5/2}$  is a  $\Gamma_7$ .

#### Line #3

Line #3, at about 997.7 nm, was initially not observed at all at zero field; it only became observable at zero magnetic field after the specimen had been exposed to laser light for some time at a high field. The spectrum of this line shows eight components in the off-axis direction and four lines in the  $\langle 100 \rangle$  direction, yielding a total splitting of about 4 nm in a field of 16 T. In both cases the intensity of *all* lines increases tremendously when the field is increased above 10 T, see figure 4. One line, seen in positive polarization at the lowest energy became four times stronger than the other ones which had approximately

equal intensity. Strong circular polarization of the light was detected, see figure 3.

The origin of the lines seen in the "line #3 region" is still unclear.

As discussed before a  $\Gamma_7 \rightarrow \Gamma_7$  transition is expected to have two inner lines in the  $\langle 100 \rangle$  direction and four lines in the off-axis direction, while the intensity of the lines could increase until their splitting is twice the natural line width. This is clearly not the case.

A  $\Gamma_8 \rightarrow \Gamma_7$  or  $\Gamma_7 \rightarrow \Gamma_8$  transition is expected to have four lines for the  $\langle 100 \rangle$  direction and eight for the random orientation with the lines in the first case being the inner ones. In contrast, the experiment shows clearly a different pattern of intensities. For an identification with a  $\Gamma_8 \rightarrow \Gamma_7$  or a  $\Gamma_7 \rightarrow \Gamma_8$  transition there is no reason that all the lines increase in intensity.

Finally, a  $\Gamma_8 \rightarrow \Gamma_8$  transition should have 8 and 16 lines when measured for a  $\langle 100 \rangle$  and a random orientation, respectively. It is possible that not all the lines are observed because of transition probabilities or low occupation of the higher levels. In this case it could also be possible that the lines can only be seen in the higher magnetic field, where the lowest sub-levels of the highest excited state have sufficiently shifted in order to gain population. A  $\Gamma_8 \rightarrow \Gamma_8$  transition can, however, not explain the positions of the lines. The fact that identical positions of the lines were found for both samples seems to indicate that the anisotropic  $\Gamma_8$  is not involved. The fact that both the positively and the negatively polarized lines increase in intensity in higher magnetic field indicates that not the same  $\Gamma_7$  level is involved as for lines #4 and #8.

In view of the above it is possible that the origin of these lines cannot be found in this energy level diagram and that a different defect is involved. Since in the magnetic field line #3 splits into many

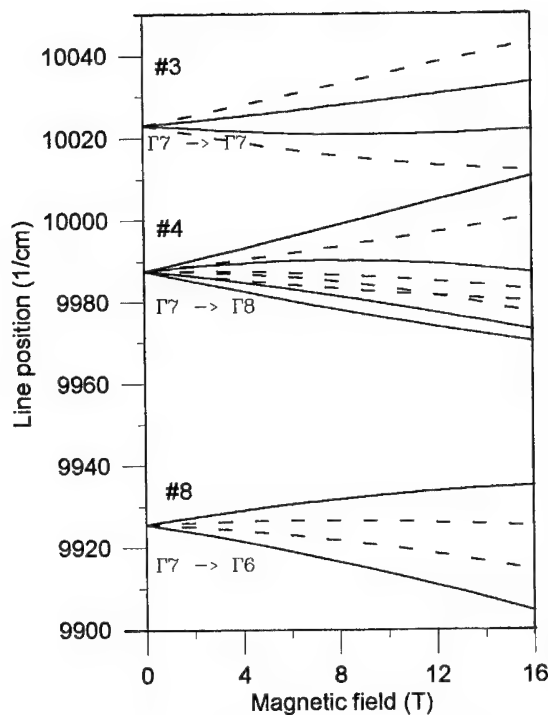


Figure 6. The theoretically expected Zeeman lines, the dashed lines are forbidden in the  $\langle 100 \rangle$  direction.

since it correspond in this case to the forbidden  $\Gamma_7 \rightarrow \Gamma_7$  transition.

#### REFERENCES

1. V.F. Masterov, V.V. Romanov, and K.F. Shtel'makh, Sov. Phys. Solid State **25**, 824 (1983).
2. J. Wagner, J. Windscheif, and H. Ennen, Phys. Rev. B **30**, 6230 (1984).
3. G. Aszodi, J. Weber, Ch. Uihlein, L. Pu-lin, H. Ennen, U. Kaufmann, J. Schneider, and J. Windscheif, Phys. Rev. B **31**, 7767 (1985).
4. R. Kallenbach, H.J. Reyher, J. Unruh, A. Winnacker, and H. Ennen, Mat. Sci. Forum **10-12**, 681 (1986).
5. T. Gregorkiewicz, B.J. Heijmink Liesert, I. Tsimperidis, I. de Maat-Gersdorf, C.A.J. Ammerlaan, M. Godlewski, and F. Scholz, Mat. Res. Soc. Symp. Proc. **301**, 239 (1993).
6. K.R. Lea, M.J.M. Leask and W.P. Wolf, J. Phys. Chem. Solids. **23**, 1381 (1962).
7. I. de Maat-Gersdorf, T. Gregorkiewicz, C.A.J. Ammerlaan, P.C.M. Christianen and J.C. Maan, to be published.
8. R.K. Watts and W.C. Holton, Phys. Rev. **173**, 417 (1968).

components, the symmetry of such a defect should be high, and so it cannot be related to line #1, identified with a trigonal  $\text{Yb}^{3+}_{\text{In}} - \text{X}_p$  centre [3].

The fact that for both samples identical intensity of the components, relative to line #4 has been found indicates that line #3 could be connected to the not yet explained lines #5 - #7 and #9 which are always present in the photoluminescence spectrum of  $\text{InP}:\text{Yb}$  with the same relative intensities.

#### CONCLUSIONS

Based on the Zeeman measurements for lines #4 and #8 it seems reasonable to propose an ordering of levels where  $\Gamma_7$ , and not  $\Gamma_8$ , is the lowest level of the  $F_{5/2}$  state. Such a scheme is also in agreement with the crystal field analysis and the expectations that the Yb atom takes a substitutional position on an In site. It can also explain the low intensity of line #3 in the photoluminescence spectrum,

## OPTICAL ANISOTROPY OF Er CENTERS IN GaAs:Er,O

R.A. HOGG, K. TAKAHEI, A. TAGUCHI, and Y. HORIKOSHI

*NTT Basic Research Laboratories,*

*3-1 Morinosato-Wakamiya, Atsugi-shi, Kanagawa, 243-01, Japan. e-mail: hogg@will.brl.ntt.jp*

### ABSTRACT

For GaAs:Er,O the anisotropic photoluminescence (PL) properties of the Er-2O center and its preferential alignment within the GaAs matrix have been revealed by the polarization dependence of host-excited PL when detecting emission polarized along certain crystallographic directions. In the present paper, a polarized intra-4f-shell photoluminescence excitation (PLE) spectroscopic study of Er centers incorporated in GaAs is reported. This technique is not only sensitive to those centers which luminesce under host-excitation, but also to other Er centers incorporated in the host, thus allowing the polarized PL properties of most Er centers to be studied. A comparison of the polarization characteristics of host-excited PL and direct intra-4f-shell PLE, due to the difference in the excitation mechanisms, is made and the information which may be gained from such measurements is discussed. For the Er-2O center, we confirm the optical anisotropy and preferential alignment of the center previously observed in host-excited PL. Incorporation mechanisms for the Er-2O center which could result in the observed polarization dependence are discussed.

### INTRODUCTION

There has been considerable recent interest in rare-earth (RE) doped semiconductor materials due to the intra-4f-shell transitions of the incorporated RE atoms. Er doped III-V materials and silicon have been shown to exhibit luminescence at 1.54  $\mu\text{m}$  due to  $^4I_{13/2} \rightarrow ^4I_{15/2}$  intra-4f-shell transitions [1], which lie in the minimum loss region of silica fibers. Although much attention has been paid to this class of materials, the microscopic nature of these luminescent centers has so far remained rather unclear.

The introduction of molecular  $\text{O}_2$  into the growth atmosphere of metalorganic chemical vapor deposition (MOCVD) grown GaAs:Er has been shown to have a drastic effect [2,3]. A sharp, simple intra-4f-shell photoluminescence (PL) spectrum of  $\text{Er}^{3+}$  atoms is produced. The host-excited PL of GaAs:Er,O samples obtained at low temperature is dominated by seven transitions (from the lowest lying crystal-field-split  $^4I_{13/2}$  level to the crystal-field-split  $^4I_{15/2}$  levels) attributed to one center [4]. This center has been identified as an Er atom substituting for Ga associated with two O atoms (hereafter referred to as Er-2O) [5], and has been determined to exhibit  $C_{2v}$  symmetry (with either substitutional or interstitial O) [5,6]. Under host-excitation the energy transfer process of the Er atom in the case of Er-2O is considered to be via the non-radiative recombination of an exciton bound to the Er-2O related trap level [7]. In addition to host-excitation and subsequent energy transfer, a photon of energy equal to the intra-4f-shell transitions may be absorbed and excite the 4f-shell of an Er center directly. This method of excitation may be used to study the nature of Er centers, such as their optical anisotropy.

The "latent" optical anisotropy of crystals containing anisotropic luminescence centers has been studied in detail [8]. Such crystals are termed "latently" anisotropic as each center possesses anisotropic optical properties on the microscopic level, while the ensemble of centers as a whole exhibits isotropic optical properties. Techniques utilized to study such centers rely upon the perturbation of the crystal in order to render certain crystallographic directions inequivalent, such as the application of uniaxial stress, magnetic, or electric field. In another technique, polarized PLE

spectroscopy, luminescence centers oriented along certain crystallographic directions may be preferentially excited using linearly polarized light. An anisotropic distribution of excited centers is thus produced, the excitation being either atomic (e.g. intra-4f-shell) or excitonic (creation of an exciton localized at the center). If the absorbed energy is emitted as luminescence, and the center originally excited luminesces before energy migration, then the luminescence should be partially or wholly polarized. A previous study of  $\text{Er}^{3+}$  related centers in  $\text{InP}$  and  $\text{In}_{0.92}\text{Ga}_{0.08}\text{P}$  allowed the symmetry of the centers to be determined to be no higher than  $C_{3v}$  [9].

Recently we reported the preferential alignment of the Er-2O center within the GaAs host which was revealed by host-excited polarized PL [10]. A polarization dependence of the ensemble of Er-2O centers indicated that the Er-2O center itself exhibited anisotropic PL properties, and that there must be a preferential alignment of the center within the GaAs host. The Er-2O center may take up several different crystallographic orientations within the host. In the present paper, a polarized PLE spectroscopic study of various Er-related centers in  $\text{GaAs:Er,O}$  is presented. For the Er-2O center, we discuss how the difference in excitation mechanisms in host-excited PL and intra-4f-shell PLE are reflected in the observed optical anisotropy. In addition, anisotropy of those centers silent by host-excitation will be discussed.

## EXPERIMENTAL

The sample described in this study was grown by low pressure MOCVD at  $500^\circ\text{C}$  on a (001)-oriented undoped GaAs substrate, with  $\text{O}_2$  codoping as detailed previously [3,4]. The Er concentration of this sample (as measured by SIMS) was  $1.4 \times 10^{18} \text{ cm}^{-3}$ .

PLE spectra were obtained under normal incident excitation to the (001) plane of the sample at 5 K using a continuous mode color center laser ( $\text{NaCl:OH}$ ). The electric field vector was polarized parallel to the  $[110]$  and  $[\bar{1}10]$  crystallographic directions, which were differentiated by the observation of etch pits following etching in molten KOH. Luminescence was collected normal to the (001) plane and was detected by a liquid nitrogen cooled Ge-detector, using standard lock-in techniques. For each excitation polarization, the subsequent luminescence polarized parallel to the  $[110]$  and  $[\bar{1}10]$  directions was detected. A spectral range centered at 0.78 eV (1590 nm) with a band pass of 22 meV (45 nm) was detected by using suitable color and interference filters, and by varying the slit width of the double monochromator used to disperse the light. This spectral region has been shown to include PL from many different Er centers which are silent by host excitation, but which may be excited directly [4], in addition to the Er-2O center. The PLE spectra were corrected for the spectral dependence of the laser output power.

All spectra were corrected for the response of the measurement system to light of different polarization. This was done using a sample with InGaAs layers lattice matched to InP, grown by liquid phase epitaxy. This sample exhibited isotropic luminescence in the spectral region discussed for emission perpendicular to the plane of growth.

## RESULTS

The preferential alignment of the Er-2O center within the GaAs host was revealed by host-excited polarized PL [10]. Figure 1 shows host-excited PL (three highest energy  $^4I_{13/2} \rightarrow ^4I_{15/2}$  transitions) with detection polarization along  $[110]$  and  $[\bar{1}10]$ . A clear polarization dependence of the PL intensity is observed, with a  $19 \pm 2\%$  reduction in intensity when detecting luminescence polarized parallel to  $[110]$  as opposed to  $[\bar{1}10]$  for all the  $^4I_{13/2} \rightarrow ^4I_{15/2}$  Er-2O transitions. For the four lower energy Er-2O transitions, within experimental error ( $\pm 5\%$ ), equal polarization dependences were observed. This polarization dependence was observed to be independent of the polarization of the HeNe excitation light. PL spectra with identical intensities were obtained when the detection polarization was  $[100]$  and  $[010]$ . This polarization dependence of the host-excited

PL was attributed to both an anisotropy in the PL behavior of the Er-2O center, and a preferential alignment of the center within the host. The preferred orientation of the center was deduced to be such that both O atoms lie in a plane "above" or "below" the Er atom with respect to the growth direction. These two different configurations of the Er-2O center, one of which was deduced to be incorporated preferentially, are shown schematically in Fig. 2. Four other configurations of the Er-2O center are possible, all of which consist of one oxygen atom above and one below the Er atom with respect to the growth direction. The concentrations of these centers (if they are non-zero) were deduced to be equal. When carrying out measurements with polarization along the  $[110]$  and  $[\bar{1}10]$  directions, the components from these centers are equal, so any polarization dependence of the PL is due entirely to a change in the contribution from the two centers with both O atoms "above" or "below" the Er atom.

Figure 3 shows intra-4f-shell PLE spectra for the same sample in the region of the strongest peak in Fig. 1. Polarized PLE spectra were obtained with excitation parallel to  $[110]$  and  $[\bar{1}10]$ . For each excitation polarization luminescence polarized parallel to  $[110]$  and  $[\bar{1}10]$  was detected.

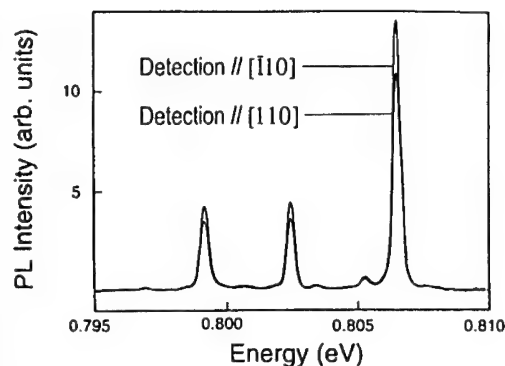


**Figure 1.** PL spectra at 5K for collection perpendicular to the (001) plane. The detection polarization is indicated for each spectrum.

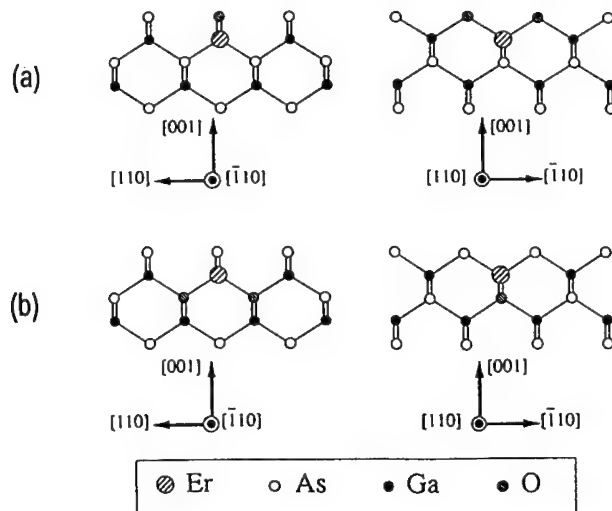


**Figure 2.** Schematic diagrams of the Er-2O center in GaAs for two possible incorporation mechanisms where Er precedes (a) or is preceded by (b) O in the incorporation of Er-2O. The growth direction is  $[001]$ .



For a detection polarization along  $[\bar{1}10]$ , spectra with excitation polarization along  $[\bar{1}10]$  and  $[110]$  are labeled h and i, respectively. For a detection polarization along  $[110]$ , spectra with excitation polarization along  $[\bar{1}10]$  and  $[110]$  are labeled j and k, respectively. Three separate peaks are observed in the energy range studied. A site-selective PL measurement has shown that the highest energy peak, centered at 0.80562 eV, is due to the Er-2O center, and corresponds to a transition from the lowest lying level of the  $^4I_{15/2}$  manifold to the lowest lying level of the  $^4I_{13/2}$  manifold [11], and subsequent radiative transition from this level to the higher lying levels of the  $^4I_{15/2}$  manifold. The two peaks at lower energies are due to other Er centers and shall be discussed later. The observed width of the peaks in these measurements is limited by the width of the excitation laser, due to its multi-mode operation. For the Er-2O related transition a clear increase in the peak height, and hence oscillator strength, when excitation is by light polarized along  $[\bar{1}10]$  can be seen in Fig. 3 (compare h with i, and j with k). For the same excitation polarization, the peak heights increase when the detection polarization is along  $[\bar{1}10]$  (compare h with j, and i with k). The experimentally obtained peak intensities from these PLE measurements, relative to the intensity of the strongest peak are shown in Table 1, with their corresponding errors. The magnitude of the polarization dependence of this transition is determined by subtracting the background luminescence (see Fig. 3). This background is attributed to deep luminescence from the GaAs, and from Er aggregates which emit a broad luminescence.

In order to discuss the polarized PL and PLE results for the Er-2O center, the difference in host-excitation and direct intra-4f-shell excitation must be considered. Under host-excitation the ratio of the concentrations of excited centers in different orientational configurations (for example the ratio of excited Er-2O centers with both oxygen atoms above the Er atom to those with both oxygen atoms below) is given by the ratio of the concentrations of these centers within the host. The anisotropic optical cross-section of the center is unimportant in its excitation (the formation of an exciton at the Er center being the excitation method). The polarization dependence of the luminescence emitted by the excited centers, however, does depend on the anisotropic optical cross-section of the Er-2O center. The observed polarization dependence in host-excited PL is therefore due to the anisotropic optical cross-section and preferential alignment of the center. In general the contribution to the host-excited PL from centers in a specific orientation may be described by: [concentration of the center]  $\times$  [relevant emission optical cross-section].

In the case of direct intra-4f-shell excitation, however, polarized excitation light will result in the probability of excitation for the Er-2O centers in different configurations being given by the product of both the concentration of the centers in that configuration, and the relevant optical cross-section, corresponding to the orientation of the polarized light. For emission, the optical

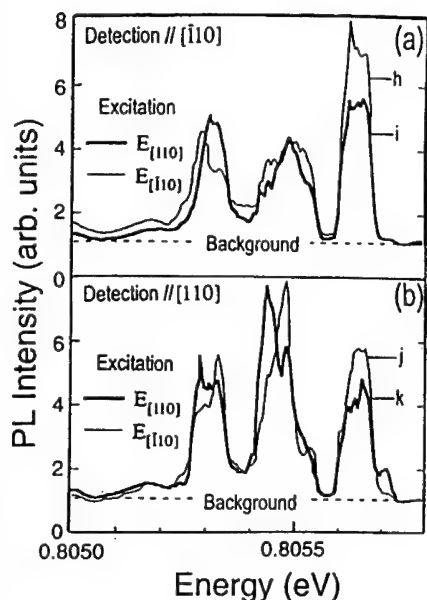


**Figure 3.** Intra-4f-shell PLE spectra at 5K for collection perpendicular to the (001) plane with detection polarized parallel to (a)  $[\bar{1}10]$  and (b)  $[110]$ . Excitation polarization is along  $[\bar{1}10]$  (thin line) and  $[110]$  (thick line).

anisotropic cross-section of the center will once more be included, depending this time on the detection polarization. The contribution from centers in one orientation to the PLE signal obtained for polarized excitation and emission may be described by: [relevant excitation optical cross-section]  $\times$  [concentration of center]  $\times$  [relevant emission optical cross-section]. In PLE measurements the optical cross-section for emission (lower energy transitions) may be different to that of the excitation (highest energy transition). For the Er-2O center, the optical cross-sections (excitation and emission cross-section should be the same for the same transition) for the different transitions was observed to be the same from host-excited PL.

**Table1.** Dependence of relative PLE peak intensities upon excitation and detection polarization.

Excitation	Detection	Normalised ratio of PLE peak intensities
$[\bar{1}10]$	$[\bar{1}10]$	1
$[110]$	$[\bar{1}10]$	$0.73 \pm 0.05$
$[\bar{1}10]$	$[110]$	$0.77 \pm 0.05$
$[110]$	$[110]$	$0.56 \pm 0.08$

For both host-excitation and intra-4f-shell excitation, the contribution to the measured signal from each of the six configurations of the Er-2O center must be resolved along the  $[110]$  and  $[\bar{1}10]$  directions. This analysis becomes somewhat complicated and will not be discussed in any great quantitative detail here. However, it is possible to make the following qualitative points. It is clear that the polarization dependence observed in host-excited PL and intra-4f-shell PLE contain different information. In host-excited PL, the intensity of luminescence detected along  $[110]$  is 0.81 times that observed along  $[\bar{1}10]$ . For intra-4f-shell PLE for excitation polarization along  $[\bar{1}10]$  luminescence detected along  $[110]$  is  $\sim 0.75$  times that observed along  $[\bar{1}10]$ . An equivalent factor is observed for excitation along  $[110]$ . This difference is attributed to the difference in the excitation mechanism in host-excitation and intra-4f-shell excitation (i.e. in intra-4f-shell PLE the optical cross-section is included twice). Polarized intra-4f-shell PLE measurements have confirmed the polarization dependence observed in host-excited PL, thus confirming the preferential alignment of the Er-2O center within the GaAs host. Polarized intra-4f-shell PLE measurements, in addition to polarized host-excited PL measurements, therefore provide a powerful tool in determining the polarization dependence of the center and the sample as a whole, and also provide information regarding the concentration of centers in different orientations.

The present results suggest that the nucleation core is preferentially formed when Er and O couple with either both O "above" or "below" the Er atom. This nucleation core is subsequently overgrown, resulting in the observed preferential alignment of the center. Figure 2 shows a schematic diagram of two possible configurations of the Er-2O center, taking a side view of the GaAs crystal (with respect to the growth direction). These configurations result when either Er precedes the O atoms (Fig. 2(a)), or being preceded by both O atoms (Fig. 2(b)). The inequivalence of the  $[110]$  and  $[\bar{1}10]$  direction at the surface during growth must be responsible for the observed polarization dependence of the sample. The inequivalence of the  $[110]$  and  $[\bar{1}10]$  directions at the surface during growth [12] has been attributed to a number of phenomena involving a polarization dependence of excitonic emission [13] and far infra-red absorption [14] of impurity complexes in GaAs.

The two peaks to lower energies in Fig. 3 are attributed to the direct intra-4f-shell excitation for centers which are silent in PL by host excitation [4]. The local structure of these centers is unknown. For the two non Er-2O related peaks the following points can be made. Firstly, some additional structure is observed for both peaks. This indicates that each peak is due to several different centers. We attribute the peak centered at 0.8053 eV to at least two transitions, the peak centered at 0.80545 to at least three transitions. Secondly, these transitions exhibit a different polarization dependence, indicating that some of these centers are optically anisotropic and preferentially oriented in some crystallographic directions.

## CONCLUSIONS

A polarized spectroscopic study of GaAs:Er,O has been presented. We have confirmed by polarized intra-4f-shell PLE the optical anisotropy and hence preferential alignment of the Er-2O center. The use of this technique in gaining information on the relative concentration of centers in different orientational configurations, and the optical anisotropy of luminescent centers has been discussed. In the light of these measurements, possible incorporation mechanisms for the Er-2O center have been discussed. The anisotropic optical properties of a number of other Er centers incorporated in the sample have also been shown.

## ACKNOWLEDGMENTS

The authors thank Toshimasa Amano and Hideo Sugiura for the provision of InGaAs/InP samples, Kazuhiko Nozawa for technical assistance, and Selvakumar Nair for fruitful discussions.

## REFERENCES

- [1] *Rare Earth Doped Semiconductors, Materials Research Society Symposium Proceedings 1993*, edited by G.S. Pomrenke, P.B. Klein, and D.W. Langer (Materials Research Society, Pittsburgh, PA, 1993), Vol. 301.
- [2] K. Takahei, A. Taguchi, J. Appl. Phys. **74**, 1979, (1993).
- [3] K. Takahei, A. Taguchi, Jpn. J Appl. Phys. **33**, 709, (1994).
- [4] K. Takahei, A. Taguchi, J. Appl. Phys. **77**, 1735, (1995).
- [5] K. Takahei, A. Taguchi, Y. Horikoshi, J. Nakata. J. Appl. Phys. **76**, 4332, (1994).
- [6] D. Haase, A. Dörnen, K. Takahei, A. Taguchi. Presented at this conference.
- [7] A. Taguchi, K. Takahei. *Proceedings to the 18th International Conference on Defects in Semiconductors*. Materials Science Forum, **197**, 633, (1995).
- [8] P.P. Feofilov, A.A. Kaplyanskii. Sov. Phys. Uspekhi. **5**, 79, (1962).
- [9] I.A. Buyanova, A.J. Neuhalfen, BW Wessels. Appl. Phys. Lett. **61**, 2461, (1992).
- [10] R.A. Hogg, K. Takahei, A. Taguchi, Y. Horikoshi. Appl. Phys. Lett. In Press.
- [11] K. Takahei. Unpublished results.
- [12] J.H. Neave, B.A. Joyce, P.J. Dobson, N. Norton. Appl. Phys. **A31**, 1, (1983).
- [13] M.S. Skolnick, T.D. Harris, C.W. Tu, T.M. Brennan, M.D. Sturge. Appl. Phys. Lett. **46**, 427, (1985). M.S. Skolnick, C.W. Tu, T.D. Harris. Phys. Rev. **B33**, 8468, (1986).
- [14] B.R. Davidson, R.C. Newman, T. Kaneko, O. Naji. Phys Rev. **B50**, 12250, (1994). B.R. Davidson, R.C. Newman, K.H. Bachem. Phys. Rev. **B52**, 5179, (1995).

## Rutherford Backscattering and Photoluminescence Studies of Erbium Implanted GaAs

S.E. Daly<sup>\*\*</sup>, M.O. Henry<sup>\*</sup>, E. Alves<sup>§</sup>, J.C. Soares<sup>§§</sup>, R. Gwilliam<sup>&</sup>, B.J. Sealy<sup>&</sup>, K. Freitag<sup>%</sup>, R. Vianden<sup>#</sup> and D. Stievenard<sup>#</sup>.

<sup>\*</sup> School of Physical Sciences, Dublin City University, Dublin 9, Ireland.

<sup>§</sup> Departamento de Fisica, Instituto Tecnológico e Nuclear, Estrada Nacional 10, Sacavém, Portugal.

<sup>§§</sup> Centro de Fisica Nuclear da Universidade de Lisboa, Av. Prof. Gama Pinto, 2, 1699 Lisboa, Portugal.

<sup>&</sup> Department of Electrical and Electronic Engineering, University of Surrey, Guildford, GU2 5XH, U.K.

<sup>%</sup> Institut für Strahlen und Kernphysik der Universität Bonn, D-53115 Bonn, Germany.

<sup>#</sup> Institut Supérieur d'Electronique du Nord, 41 Boulevard Vauban, 59046 Lille, France.

The results of parallel RBS and photoluminescence studies of erbium implanted GaAs are presented. Low dose implantations do not produce any significant PL signals, and the dose must be in the range  $1 \times 10^{14}$  to  $1 \times 10^{15}$  /cm<sup>2</sup> in order that Er related emission dominates in the PL spectrum. A comprehensive analysis of the effects of coimplantation with oxygen on the Er luminescence is reported and the data are compared to those of GaAs:Er and AlGaAs:Er samples grown by MBE. The evidence indicates that, at high doses, ErAs precipitates are formed unless oxygen is co-implanted, and that the Er atoms which produce the luminescence occupy substitutional Ga sites.

### Introduction

The luminescence behavior of rare earth (RE) ions in semiconductors has been studied extensively during recent years. The doping of III-V compounds like GaAs or AlGaAs with Er receives much attention due to the intra 4f shell transition with a wavelength of 1.54  $\mu$ m at which the minimum absorption for silica-based optical fibers occurs. This characteristic makes Er doped semiconductors potential candidates for optoelectronic device applications. However, to produce efficient devices it is important to achieve high luminescence efficiencies. For that it is necessary to introduce large concentrations of Er into optically active sites and to excite Er efficiently.

The incorporation of high concentrations of Er into GaAs is possible both during the growth process by molecular beam epitaxy[1,2] (MBE) and metalorganic chemical vapour deposition[3,4] (MOCVD) or by ion implantation[5-7]. However our previous work [8] on Er doped MBE GaAs has shown that Er atoms occupy non optically active sites when the concentration reaches a value of the order of  $10^{20}$  cm<sup>-3</sup> (well above the solid solubility limit of  $7 \times 10^{17}$  cm<sup>-3</sup>) [9]. In that case we observed that the Er was located in an interstitial position which is compatible with the formation of ErAs precipitates. Furthermore, in the same study we observed luminescence in two AlGaAs samples doped with lower Er concentrations, having the optically active Er localized in substitutional sites. Recently, Takahei et al [10] have shown that

<sup>\*\*</sup> Present address: Physics Department, Dublin Institute of Technology, Kevin St., Dublin 8.  
email: sedaly@dit.ie

codoping MOCVD Er-doped GaAs with O increases the photoluminescence (PL) intensity. They consider that Er is incorporated into Ga sites forming complexes with O and creating an efficient luminescent center. This study reports the luminescence behavior of GaAs doped with Er and O by ion implantation. For the Er implanted samples we measure an increase in the PL intensity with the Er dose. When we co-implant Er and O we observe a significant change in the PL spectrum and intensity indicating the formation of a well defined optical center. Combining the PL and RBS/channeling techniques we show that O increases the fraction of Er in substitutional sites which we believe to be the lattice sites occupied by the optically active ions.

### **Experimental**

Samples were produced from LEC - grown n-type (100) GaAs wafers. The Er ions were implanted in the range of  $7.5 \times 10^{11} \text{ cm}^{-2}$  to  $7.5 \times 10^{14} \text{ cm}^{-2}$  with 100 keV and 250 keV in order to produce a reasonably flat profile over a depth of 70nm. Some of the samples were further implanted with O ions with fluences in the range of  $10^{13} \text{ cm}^{-2}$  to  $10^{15} \text{ cm}^{-2}$ . The energy of the O ions was 25 keV in order to overlap the Er and O depth profiles. All the implantations were carried out at room temperature. After implantation the samples were capped with a protective  $\text{Si}_3\text{N}_4$  layer and annealed at  $850^\circ\text{C}$  for 15 min.

The RBS/channeling analysis were done using a collimated beam of 1.6 MeV of  $\text{He}^+$  and the backscattered particles were detected with two surface barrier detectors placed at  $140^\circ$  and  $180^\circ$  with respect to the beam direction. The angular scans were performed using a two-axis goniometer and in order to avoid radiation effects due to the ion beam a fresh spot on the sample was used for each measurement. Computer simulations [11] were performed to model the angular scans and determine the Er lattice site accurately.

For the PL measurements the samples were mounted in a helium flow cryostat. Argon ion laser excitation of wavelength 514.5nm was used. A Bomem DA8 FT spectrometer fitted with a liquid nitrogen cooled germanium detector (North Coast) was used to record the luminescence spectra.

### **Results**

Figure 1 shows representative PL spectra recorded at 4.2K. The spectra associated with the Er implanted samples were obtained for Er doses of  $7.5 \times 10^{12}$ ,  $7.5 \times 10^{13}$  and  $7.5 \times 10^{14} \text{ ions/cm}^2$ . In all cases, the luminescence is rather broad and featureless indicating that the Er - implanted regions of the samples are quite inhomogeneous. The luminescence is barely detectable for the sample with the lowest dose but there is a systematic increase in the intensity of the luminescence in the  $1.54\mu\text{m}$  region of the Er dose is increased.

The effects of co-doping with oxygen are evident in the spectra, Er and O doses are as indicated in the figure. The co-implantation of oxygen has significant effects in this case, as is found by other authors in similar cases [10,12]. Firstly, sharp lines due to the series of intra - 4f - shell transitions are observed, as expected, although the line widths are greater than those obtained using epitaxially grown samples [10]. The abundance of spectral lines observed at highest dose indicates that more than one type of defect is present in the samples, when compared to the spectra recorded by other authors [10]. Comparing samples of equivalent Er doses we see that in the lower dose regime the presence of oxygen produces a significant increase in the PL

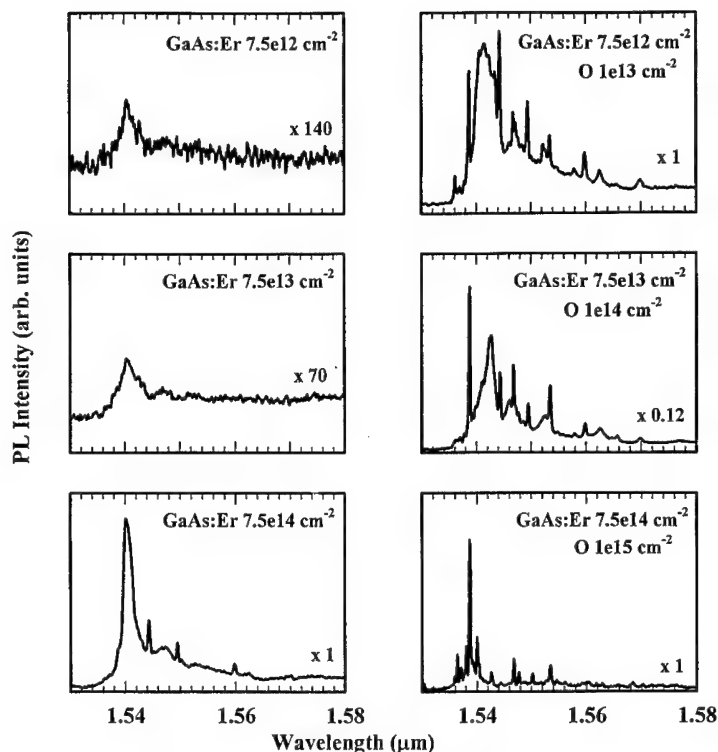


**Figure1:** Photoluminescence spectra recorded at 4.2 K of Er implanted GaAs and GaAs coimplanted with Er and O.

intensity, in the case of the highest dose sample there is no corresponding increase in the PL intensity with the addition of oxygen.

The RBS/channeling results obtained with the sample implanted with the highest Er dose is shown in figure 2. The data show the complete recrystallization of the amorphous layer produced by the implantation after the annealing at 850°C. The measured value of minimum yield (5%) is greater than that expected for a virgin sample (2.3%), which suggests the existence of some residual defects. The Er concentration profile, shown in the

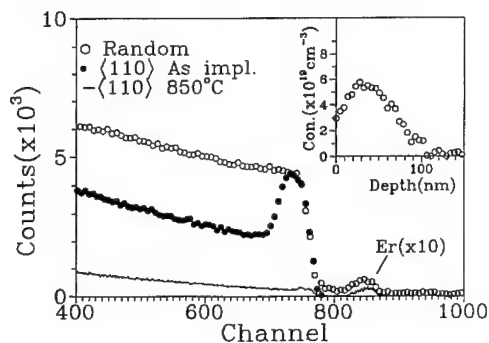


**Figure 2:** Random and aligned RBS spectra before and after annealing obtained with a 2 MeV He<sup>+</sup> for GaAs:Er to a dose of 7.5e14 cm<sup>-2</sup>. The inset shows the concentration profile of Er after background subtraction.

inset, does not change during the annealing process and is in good agreement with that predicted by the TRIM code for the implantation conditions used.

Figures 3a and 3b show detailed angular scans of the  $\langle 110 \rangle$  axis along the (110) plane (the vertical plane normal to the paper in the projections of figure 4) for the samples implanted with  $7.5 \times 10^{13} \text{ cm}^{-2}$  and  $7.5 \times 10^{14} \text{ cm}^{-2}$  Er doses respectively. As can be seen, the results obtained for Er are completely different in both cases. A dip in the flux peak is observed for the sample with lowest Er dose, and a peak for the higher Er dose. The solid lines in the figure represent the best fit to the experimental data, obtained with the simulation program previously described [13]. The fit in figure 3a was obtained assuming that 80% of the Er is occupying a substitutinal site, 5% is in the form of ErAs precipitates and 15% are randomly distributed in the GaAs lattice. We contend that the large non-substitutinal Er fraction observed in the sample with the highest Er dose is due to ErAs micro - precipitates in the sample. Evidence for this is shown in figure 3. The data are compared to theoretical curves for two situations (i) ErAs precipitates produced with the Er atoms on Ga sites (shown by the solid curve) and (ii) Er atoms on the ideal tetrahedral site (shown by the dotted curve). Agreement is far superior for case (i). The higher shoulder in the left part of the scan was due to a small misalignment between the scan direction and the (110) plane. The fit in 3b was obtained assuming 55% of the Er to be ErAs precipitates, 35% to be distributed in randomly in the lattice and 10% to be occupying substitutinal sites. The asymmetry in the flux peak with respect to the GaAs curve is attributed to the existence of ErAs precipitates.

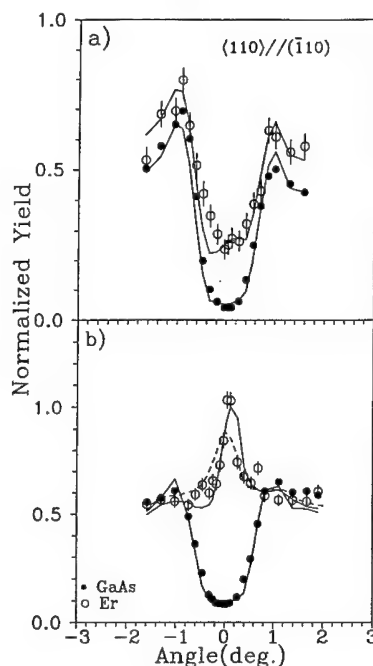


**Figure 3:** Detailed angular scans for the  $\langle 110 \rangle$  axis along the (110) plane. (a) Sample implanted with Er to a dose of  $7.5 \times 10^{13} \text{ cm}^{-2}$ . (b) Sample implanted with Er to a dose of  $7.5 \times 10^{14} \text{ cm}^{-2}$ . The solid and dashed curves were obtained using a Monte Carlo simulation.

Figure 4 shows the relevant crystal structures associated with both cases discussed. In figure 4a the NaCl type lattice of ErAs can be lattice matched to the ZnS structure of GaAs through the sharing of the As atoms in the (001) plane. Therefore, by increasing the Er concentration the formation of these precipitates is favoured not only by the structural compatibility (lattice mismatch  $\sim 1.5\%$ ) but also due to the high value of the heat of formation (the heat of formation of ErAs is  $-316 \text{ kJ/mol}$  while for GaAs it is only  $-91 \text{ kJ/mol}$ ). The asymmetry of the Er position with respect to the lattice in the  $\langle 110 \rangle$  direction is visible in the projection shown in figure 4a. The flux peak can also be observed if Er is occupying the regular interstitial tetrahedral site shown in figure 4b. However in this case we have two GaAs curves.

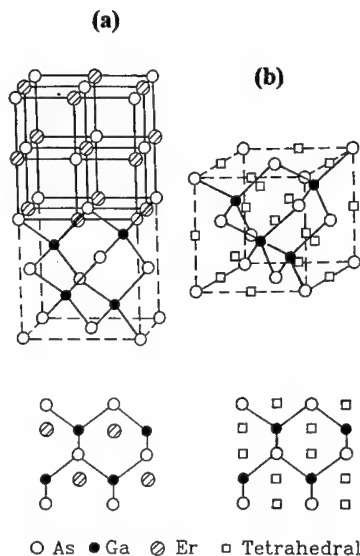


**Figure 4:** (a) interface structure of ErAs (NaCl type lattice) and GaAs (ZnS type lattice). The projection in the plane perpendicular to the  $\langle 110 \rangle$  axis shows the asymmetry of the Er ions with respect to the GaAs lattice.

(b) The zinc-blende lattice of GaAs showing all of the possible interstitial tetrahedral sites and their projections in the plane normal to the  $\langle 110 \rangle$  axis.

This situation is reproduced by the dashed line in figure 3b using the same Er fractions of the best fit (continuous line) and as is evident the agreement with the experimental data is very poor. The conclusion that Er on Ga sites is the source of the luminescence is in agreement with results reported for MBE - grown GaAs:Er&O samples [10].

The introduction of O produces some changes in the fraction of Er incorporated into the substitutional lattice sites. Figure 5 shows the angular scan for the sample implanted with the same dose of Er as the one shown in Figure 4a but codoped with O. As we see now the minimum yield is much lower which indicates a substantial increase of Er in substitutional sites. The continuous line represents the best fit and was obtained considering 95% of Er in substitutional positions and 5% in random sites.

### Conclusions:

Detailed RBS and PL measurements on the same samples of GaAs implanted with Er alone and with Er and O point towards two key effects.

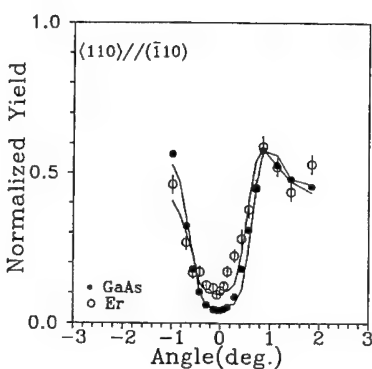


**Figure 5:** Detailed angular scan of the  $\langle 110 \rangle$  axis along the  $(110)$  plane for GaAs co-implanted with Er and O to doses of  $7.5 \times 10^{14} \text{ cm}^{-2}$  and  $1 \times 10^{15} \text{ cm}^{-2}$  respectively.



Firstly, the addition of oxygen to Er - implanted GaAs both simplifies and intensifies the 1.54 $\mu$ m luminescence. Secondly, the RBS data show that a consequence of oxygen codoping is to increase substantially the fraction of Er on substitutional sites. We propose that these results can be readily reconciled if the luminescence is attributed to Er atoms which are substitutional, rather than interstitial. We attribute the 1.54  $\mu$ m Er luminescence to Er<sup>3+</sup> ions on Ga sites. High Er concentrations - well above the solubility limit - result in the absence of oxygen in the formation of ErAs precipitates. The addition of oxygen to such samples has the effect of increasing the solubility limit thereby preventing the formation of precipitates during thermal annealing.

#### **Acknowledgments:**

This research has been supported by the EU under contract ERBCHRXCT930363 and by the Irish Science and Technology Agency (Forbairt) under grant SC/93/189 and under the Optronics Ireland Program in Advanced Technology.

#### **References:**

1. H.Ennen, J.Wagner, H.D.Muller and R.S.Smith. J.Appl. Phys. 61 (1994) 4171.
2. D.Seghier, T.Benyattou, A.Kalboussi, S.Moneger, G.Marrakchi, S.Guillot, B.Lambert and A.Guivarch. J. Appl. Phys. 75 (1987) 4877.
3. K.Takahei, Peter S.Whitney, Horoshi Nakagonne, Kunihiko Uwai. J. Appl. Phys. 65 (1989) 1257.
4. Joyoji Nakata, Moriyuki Taniguchi, K. Takahei. Appl. Phys. Lett. 61(1992) 2665.
5. Gernot S. Pomrenke, H. Ennen and W. Haydl. J. Appl. Phys. 59(1986) 601.
6. P.N. Favennec, H.L. Haridon, D. Moutonnet, M.Salvi, M. Gauneau and A.C. Papadopoulos. Inst Phys. Conf. Ser. 106 (1989) 333.
7. A. Kozanecki, M. Chang, C. Jeynes, B. Sealy and K. Homewood. Solid State Commun. 78 (1991) 763.
8. E. Alves, M.F. daSilva, A.A. Melo, J.C. Soares, G.N. van den Hoven, A. Polman K.R. Evans and C.R. Jones. Mat. Res. Soc. Symp. Proc. 301 (1993) 175.
9. I. Poole, K.E. Singer and A.R. Peaker. J. Cryst. Growth 121 (1992) 121.
10. K. Takahei, A. Taguchi, Y. Horikoshi and J. Nakata. J. Appl. Phys. 76 (1994) 4332.
11. D.W. Elsaesser, Y.K. Yeo, R.L. Hengehold, K.R. Evans and F.L. Pedrotti. J. Appl. Phys. 77 (1995) 3919.
12. J. Michel, J.L. Benton, R.F. Ferrante, D.C. Jacobson, D.J. Eaglesham, E.A. Fitzgerald, Y.-H. Xie, J.M. Poate, and L.C. Kimmerling, J. Appl. Phys. 70 (1991) 2672.
13. P.J.M. Smulders and D.O.Boerma. Nucl. Instr. and Meth. B29 (1987) 471.

## STUDY OF THE ZEEMAN EFFECT OF $\text{Er}^{3+}$ IN $\text{GaAs:Er}_2\text{O}_3$

DIETER HAASE, ACHIM DÖRNEN, KENICHIRO TAKAHEI\*, and  
AKIHITO TAGUCHI\*

4. Physikalisches Institut, Universität Stuttgart, D-70550 Stuttgart, Box 80 11 40,  
Federal Republic of Germany; A.Doernen@physik.uni-stuttgart.de

\*NTT Basic Research Laboratories, 3-1 Morinosato-Wakamiya, Atsugishi-shi, Kanagawa,  
243-01, Japan; takahei@will.brl.ntt.jp

### ABSTRACT

We analyze the Zeeman effect of the  $^4I_{13/2} \rightarrow ^4I_{15/2}$  transition of  $\text{Er}^{3+}$  in  $\text{GaAs:Er}_2\text{O}_3$  grown by metal-organic vapor-phase epitaxy. The photoluminescence spectrum has been assigned previously to one specific Er-O complex. The dominant optical transition at 1538 nm ( $6499.5 \text{ cm}^{-1}$ ), which shows a full width at half maximum of only  $0.05 \text{ cm}^{-1}$ , has been investigated by high-resolution Zeeman spectroscopy. A highly anisotropic Zeeman pattern is found which indicates the low symmetry of the underlying complex. A detailed analysis shows that the defect has a predominant rhombic symmetry  $C_{2v}$ . Additionally, smaller contributions of a crystal field with a monoclinic symmetry  $C_{1h}$  are found. The results provide further arguments that an  $\text{ErO}_2$  complex is the responsible center observed.

### INTRODUCTION

Erbium in various host crystals gives rise to the characteristic transition  $^4I_{13/2} \rightarrow ^4I_{15/2}$  at  $1.55 \mu\text{m}$  due to the  $4f^{11}$  electron configuration. Gallium arsenide doped with erbium either during growth by molecular beam epitaxy (MBE) or by implantation gives rise to a broad emission band centered at  $1.5 \mu\text{m}$  indicating a huge variety of Er-related centers rather a specific center [1, 2]. Only under specific conditions of the MBE growth process a sharp line spectrum of a single Er-related center was observed and identified as a center with a low symmetry by photoluminescence (PL), photoluminescence excitation (PLE) [3] and Zeeman spectroscopy [4].

When erbium is introduced by metal-organic vapor-phase epitaxy (MOVPE), also several centers can be identified in PL by a series of sharp lines. Recently, it was shown that only one center appears in PL when erbium is codoped with oxygen in the ambient during the MOVPE growth [5, 6]. The luminescence is much stronger than without the oxygen codoping. By site-selective (intra-center) excitation of the PL and by PLE it was shown that at least two other Er-related centers are present but are not excited by above band-gap excitation in the PL [7, 8]. It was concluded that the latter centers are not strongly coupled to the host states and thus are not efficiently excited by capturing free carriers or excitons. The center found in the MOVPE-grown sample is different from the above mentioned MBE-specific center by the clearly different spectroscopic position of the optical lines [5].

In a following paper the microscopic structure of the optical center in  $\text{GaAs:Er}_2\text{O}_3$  has been investigated [9]. By adding a small fraction of aluminum during the MOVPE growth a drastic change in the fine structure of the PL is observed. Instead the strong single

line in GaAs:Er,O at 1538 nm up to at least eight lines in  $\text{Al}_{0.01}\text{Ga}_{0.99}\text{As}$  were observed, which indicates that the energy level structure of the center is changed by the presence of aluminum atoms. To account for the large number of lines found, a coordination of the erbium ion in rhombic symmetry ( $C_{2v}$ ) has been favored in form of an  $\text{ErO}_2$  complex.

In a tetrahedral environment the  $^4I_{13/2}$  level of the  $4f^{11}$  shell splits into the series of states  $2\Gamma_6 + \Gamma_7 + 2\Gamma_8$  and the ground state  $^4I_{15/2}$  splits into the sequence  $\Gamma_6 + \Gamma_7 + 3\Gamma_8$  [10]. Depending on the crystal-field parameters five PL lines are expected when the lowest excited state of  $^4I_{13/2}$  transforms like  $\Gamma_8$ , whereas only four lines are expected when the lowest state transforms like  $\Gamma_6$  or  $\Gamma_7$ . Similarly in PLE only up to five lines should be observable. Experimentally, in PL and PLE 7 and 6 lines are found, respectively, indicating a symmetry of the Er-2O complex less than tetrahedral [5, 7]. From the number of lines alone the defect symmetry cannot be concluded further since for any symmetry lower than  $T_d$  the degeneracy is lift and only Kramers doublets remain which can be split further only by a magnetic field. Therefore, an analysis of the Zeeman effect on the dominant PL line of the Er-2O center at 1538 nm ( $6499.5 \text{ cm}^{-1}$ ) was carried out to further understand the microscopic structure of the center.

## RESULTS

Zeeman measurements at 4.2 K were carried out in a cryostat equipped with a split-coil magnet, which allows to collect light in the Faraday and Voigt configuration. The PL was excited by the 647 nm line of an  $\text{Kr}^+$  laser and analyzed by a Fourier spectrometer equipped with a *Northcoast* germanium *p-i-n*-detector.

A series of Zeeman spectra of the line at  $6499.5 \text{ cm}^{-1}$  (1538 nm) is depicted in Fig. 1 for the field oriented along the three principal directions [001], [111], and [110]. Obviously, the splitting is strongly anisotropic with different numbers of lines showing up in each direction. With increasing field  $B$  the line intensities of the two most intense lines change. For low fields always a distribution of intensities is found which is symmetric to the center of gravity. As the field is increased the distribution becomes asymmetric, for example for  $B$  along [001] the high-energetic component gains intensity whereas the low-energetic line gets weaker. A similar thermalization has been found for the Er-related center in the MBE-grown sample [4].

For the field along the direction [111], the linear Zeeman splitting of several lines is superposed by a non-linear shift due to the coupling to the other crystal-field states of the  $^4I_{15/2}$  ground-state manifold. The coupling is weaker for the field along [001], mainly the center of gravity shifts to higher energies. To avoid the non-linear effects, we first consider the Zeeman splitting for low fields up to 1 Tesla and then return to the high-field splitting.

From the number of Zeeman components observed, the low symmetry of the center is evident. As discussed above, for symmetries lower than  $T_d$  only two-fold degenerate Kramers doublets (effective spin  $S = 1/2$ ) originate from the crystal-field splitting. In the magnetic field the degeneracy is fully removed. Therefore, the PL transition of each center results in four Zeeman lines according to  $\Delta m_S = 0, \pm 1$ . The magnetic field also removes the geometrical degeneracy of the various orientations of the center in the host crystal. For a completely arbitrary direction of the field generally each orientation results in a different Zeeman splitting. Removal of electronic and geometrical degeneracy leads to the complexity of the Zeeman spectra in the present case. From the Zeeman splitting at

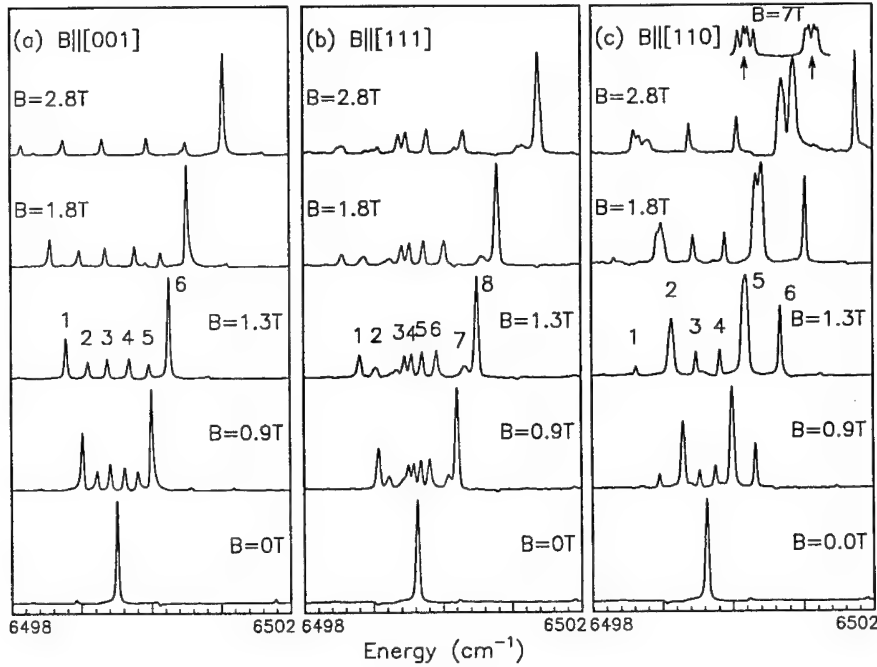


Figure 1: Zeeman splitting of the dominant PL line of the center Er-2O. Marks in (c) represent the monoclinic contribution for  $\delta = 7^\circ$ .

low fields a rhombic symmetry follows for the center as will be discussed below. Figure 2 illustrates how the magnetic field removes the geometrical degeneracy for rhombic centers. The cuboids labeled *a* through *f* represent the six equivalent orientations of the center as well as the anisotropic *g* tensors which are diagonal in the primed coordinate system.

The orbital degeneracy for the field along various directions can be seen from Fig. 2. The Zeeman measurement were carried out in the standard geometry, where the sample is rotated around a  $[1\bar{1}0]$  direction with the field perpendicular to this axis. By a sweep over  $90^\circ$  all three principal directions are hit, see Fig. 2. In this geometry for an arbitrary angle the centers labeled *c* and *e* are equivalent with respect to the magnetic field as are the centers *d* and *f*. Thus the field distinguishes between four different classes: (a), (b), (c,e), and (d,f), where the centers in each class have the same Zeeman splitting. Since each class contributes four Zeeman lines, in total the four classes result in 16 lines. If the field is along the high symmetric directions the degree of orbital degeneracy is higher [11]: (i) for  $B \parallel [001]$  ( $\theta = 0$ ) with 2 classes of equivalent orientations (a,b) and (c,d,e,f) resulting in 8 lines, (ii) for  $B \parallel [111]$  ( $\theta = 54.74^\circ$ ) with 2 classes (a,d,f) and (b,c,e) giving 8 lines, and (iii) for  $B \parallel [110]$  ( $\theta = 90^\circ$ ) with 3 classes (a), (b), and (c,d,e,f) resulting in 12 lines.

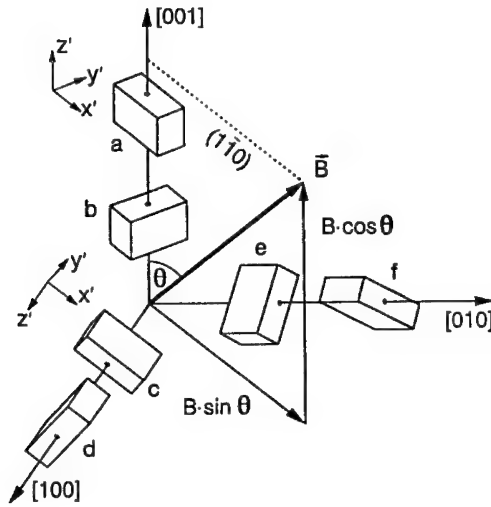


Figure 2: Cuboids represent the six possible orientations of a rhombic center in a tetrahedral host crystal. Zeeman spectra were taken with the field  $\vec{B}$  in the  $(1\bar{1}0)$  plane.

To describe the linear Zeeman splitting we use a Hamiltonian which includes an anisotropic  $g$  tensor for the ground state and the excited state

$$\mathcal{H} = \mu_B \{ \mathbf{B}' \cdot \mathbf{g}_i \cdot \mathbf{S}' \} \quad i = \text{I, II} \quad (1)$$

where  $\mathbf{S}'$  denotes the Pauli-spin matrices for a state of  $S = 1/2$  with the primed coordinate system aligned along the rhombic axes as shown in Fig. 2. The index  $i$  labels the initial and final state of the optical transition and the other symbols have their usual meaning. Therefore the six components of the both diagonal  $g$  tensors determine the Zeeman splitting completely.

To identify the various Zeeman lines with the corresponding orientations, angular-dependent Zeeman spectra were taken at 1.0 Tesla, see Fig. 3. These data and the spectra in Fig. 1 can be understood consistently on the background discussed above. From the angular dependence the branches, which are due to the classes (a), (b), (c, e), and (d, f), are identified as shown in Fig. 3. The energetic position of the transitions  $\Delta m_s = \pm 1$  is given by the sum of the  $g$  factors of the ground state and the excited state. For example, the position of branch a and b at  $\theta = 0$  is given by  $g_{x, \text{I}} + g_{x, \text{II}}$ . At  $\theta = 90^\circ$  branch a is given by  $g_{x, \text{I}} + g_{x, \text{II}}$ , whereas branch b provides  $g_{y, \text{I}} + g_{y, \text{II}}$ , compare Fig. 2.

As discussed above, generally, for a rhombic center at  $B$  along  $[001]$  ( $\theta = 0$ ) eight lines are expected because of the two classes (a, b) and (c, d, e, f). But even for the maximum field only 6 Zeeman components show up. On the other hand angular dependence reveals that for  $\theta = 0$  the lines 2 and 5 of Fig. 1(a) split into at least three lines for  $\theta > 0$ . Therefore, when the field is moved away from the direction  $[001]$  not only the geometrical degeneracy between the orientations a and b is removed but also electronic levels are separated. Thus the  $g$  factor of the corresponding state,  $g_{x, \text{II}}$ , has to be zero. Similar arguments for branch b yield  $g_y$  of state I has to be zero, too. Therefore, five relations are obtained from the

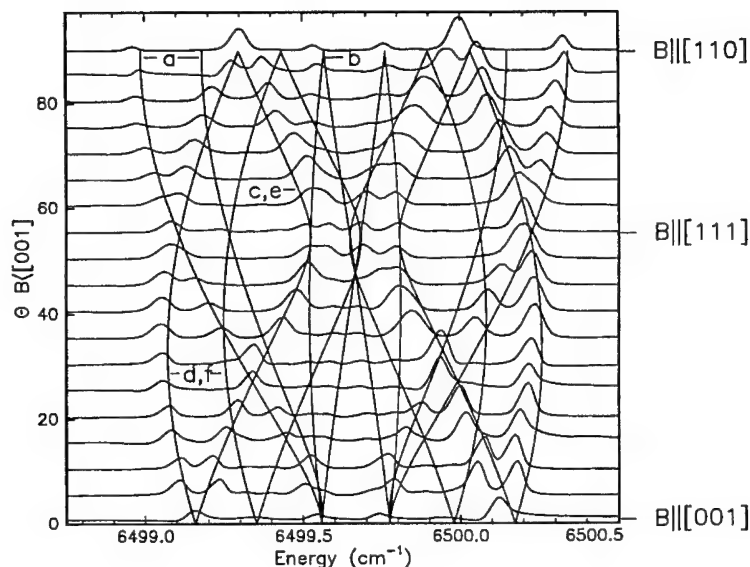


Figure 3: Angular dependent Zeeman splitting of line 1 at a field of 1.0 Tesla. The angle  $\theta$  is defined as given in Fig. 2. The lines result from Hamiltonian Eq. 1 and from the  $g$  tensor as given in the text.

angular dependence. An additional relation is obtained to fit the position of the lines 2 and 5 in Fig. 1(a). With this procedure all six elements of the both  $g$  tensors are given:

	$g_x$	$g_y$	$g_z$
I	2.7	0.0	0.5
II	0.45	0.45	0.0

With these data the lines drawn in the Fig. 3 were calculated. We find an overall agreement with the spectroscopic positions though some lines match better than others. The deviations are most probably due to the coupling with the crystal-field states of  $^4I_{13/2}$ . As obtained from Fig. 1(b) the coupling is found to be strongest for the line 3 with the magnetic field along [111]. The non-linear behavior is also responsible that the evolution of the Zeeman pattern is not symmetrical to the zero-field position of the line (Fig. 3). This additional effect is beyond the description used here.

As depicted in Fig. 1(c) if the magnetic field is along the direction [110] the both lines 2 and 5, which are assigned to the centers  $c$  through  $f$ , are split if the field is considerably higher than 1 Tesla. The high-energetic component first splits into two equally strong components. Finally, the latter ones are split further into four components, each having a FWHM identical to the zero-field line. Thus a further splitting at even higher fields is most unlikely. The two-fold splitting at medium fields indicates that the center has a symmetry

which is monoclinic  $C_{1h}$ . In the present case the monoclinic contribution is rather small, since the low-field case has been described successfully by the higher symmetric point group  $C_{2v}$ . For a monoclinic center there are 12 equivalent orientations, twice as much as for a rhombic center. The 12 eigensystems of such a center are derived from the 6 rhombic orientations by rotating the axis  $z'$  and  $x'$  around the axis  $y'$  by an angle of  $+\delta$  and  $-\delta$ , respectively [11,4]. The value of  $\delta$ , which is specific for the monoclinic part of the crystal field, is derived by matching the two components of line 5 as indicated in Fig. 1(c). The small value of  $\delta = 7^\circ$  shows that the deviation from the rhombic symmetry is rather small.

The further splitting of line 2 and 5 into eight components at high fields is due to a small misalignment of the sample during the Zeeman measurements, which results in a small departure of  $\vec{B}$  from the [110] direction at  $\theta = 90^\circ$ . As a consequence the monoclinic centers derived from the rhombic centers  $c$  through  $f$  are all inequivalent and show a slightly different Zeeman splitting. The number of in total eight components agrees with the eight monoclinic positions corresponding to positions  $c$  through  $f$ . If the center would be purely rhombic a slight misalignment will result in only four lines corresponding to the positions  $c$  through  $f$ . Therefore, the eightfold splitting of line 2 and 5 also shows, that the center is slightly distorted to monoclinic symmetry.

## DISCUSSION

The  $g$  factors found for the center Er-2O are different from those reported by Thonke *et al.* [4] found for the MBE-specific center. Also the Zeeman spectra shown here are different from those in [4], too. Although, in both cases a monoclinic symmetry of the center has been found. As a characteristic difference in the present case for each state two values of the  $g$  tensor are non-zero, whereas for the center of Ref. [4] only the  $g_y$  values are non-zero.

The slightly monoclinic contribution found is also in accordance with an complex  $\text{ErO}_2$  proposed in Ref. [9] if we assume that the two Er-O bonds are not completely symmetrical. A similar situation is found for the well known radiation-induced center in silicon, which is observed by optical spectroscopy as the so called 0.97-eV( $G$ ) center and as the center  $G11$  by electron paramagnetic resonance. The center is made of two substitutional carbon atoms  $C_s$  on next-neighbor sites embracing a silicon interstitial ( $\text{Si}_i$ ) in the configuration  $C_s\text{-Si}_i\text{-C}_s$  [12]. In this complex the both carbon atoms are not completely equivalent. As has been shown in the isotope effects of the local mode replica  $E'$  of the optical transitions [13] as well as in the hyper-fine structure in the optically detected magnetic resonance [12] the two bonds  $C_s\text{-Si}_i$  are slightly different. A similar case could be present for two oxygen atoms bound to the erbium atom. By favoring one Er-O bond the system relaxes from the higher symmetric rhombic symmetry to the lower monoclinic symmetry  $C_{1h}$ .

Though we cannot conclude the position of the constituents of the defect from the experiment these results provide the present view of the Er-2O center: An erbium ion is residing on a gallium site and two oxygen atoms are placed on arsenic sites adjacent to erbium in an almost  $C_{2v}$ -like configuration. An inequivalence between the two Er-O bonds may be responsible for the slightly distorted monoclinic complex.

## ACKNOWLEDGEMENTS

We thank M. H. Pilkuhn for his steady interest in our work.

## REFERENCES

1. G. S. Pomrenke, H. Ennen, and W. Haydl, *J. Appl. Phys.* **59**, 601 (1986).
2. R. S. Smith, H. D. Müller, H. Ennen, P. Wennekers, and M. Maier, *Appl. Phys. Lett.* **50**, 49 (1987).
3. H. Ennen, J. Wagner, H. D. Müller, and R. S. Smith, *J. Appl. Phys.* **61**, 4877 (1987).
4. K. Thonke, H. U. Hermann, and J. Schneider, *J. Phys. C* **21**, 5881 (1988).
5. K. Takahei and A. Taguchi, *J. Appl. Phys.* **74**, 1979 (1993).
6. K. Takahei and A. Taguchi, *Jpn. J. Appl. Phys.* **33**, 709 (1994).
7. K. Takahei and A. Taguchi, *Appl. Phys. Lett.* **77**, 1735 (1995).
8. K. Takahei and A. Taguchi, *J. Appl. Phys.* **78**, 5614 (1995).
9. K. Takahei, A. Taguchi, Y. Horikoshi, and J. Nakata, *J. Appl. Phys.* **76**, 4332 (1994).
10. K. R. Lea, M. J. M. Leask, and W. P. Wolf, *J. Phys. Chem. Solids* **23**, 1381 (1962).
11. A. A. Kaplyanskii, *Opt. Spectrosc.* **16**, 329 (1964).
12. K. P. O'Donnell, K. M. Lee, and G. D. Watkins, *Physica* **116B**, 258 (1982).
13. K. Thonke, H. Klemisch, J. Weber, and R. Sauer, *Phys. Rev. B* **24**, 5874 (1981).



## ACTIVATION OF Yb LUMINESCENCE IN GaAs BY GROUP VI ELEMENTS CODOPING

V.M.Konnov, T.V.Larikova, N.N.Loyko, V.A.Dravin, V.V.Ushakov, A.A.Gippius

P.N.Lebedev Physical Institute of the Academy of Sciences of Russia,  
Leninsky prospect 53, Moscow 117924, Russia, gippius@sci.fian.msk.su

### ABSTRACT

Yb in GaAs is generally believed to be optically inactive due to very low fraction of Yb in substitutional position. In the present work it is demonstrated that Yb can be rendered optically active in GaAs if it is incorporated in three-component complexes (Yb+O+S/Se/Te).

### INTRODUCTION

Rare-earth (RE) doped Si and III-V semiconductors have received increased attention for their possible use in optoelectronic devices which are expected to combine sharp, temperature stable, atomic-like emission due to internal electronic transitions within 4f-shell of RE impurities with the efficient electrical pumping of this emission by the energy transfer from the excited system of electrons and holes.<sup>1</sup>

Intensity of f-f luminescence in RE doped semiconductors is determined, among other factors by the efficiency of energy transfer from electrons and holes to RE luminescence centres and probability of optical transitions within 4f shell of RE centres. These two characteristics depend upon the structure of luminescence centres, that is on the lattice position of RE impurity and on its possible association with other impurities and/or defects. Due to high chemical activity of RE elements, their associations with other chemical dopants are quite common. It is known that co-doping of RE in II-VI compounds is a prerequisite for their optical activity<sup>2</sup> and photoluminescence efficiency of RE in ionic hosts is usually highest for RE complexes. So it was quite natural to look for some co-dopants in the case of RE doped Si and III-V compounds. For Er-doped silicon it has been reported that the addition of oxygen and fluorine enhanced the Er<sup>3+</sup> emissions<sup>3</sup>. In III-V compounds the intensity of luminescence of Er<sup>3+</sup> in Al<sub>x</sub>Ga<sub>1-x</sub>As was found to be dramatically increased by oxygen co-doping. On the other hand, oxygen co-implantation into GaAs:Er generally resulted in weaker Er<sup>3+</sup> emission than those for the samples implanted with Er alone<sup>4</sup>. An explanation was that (Er+Al+O) complexes, formed in the ternary compounds, might be more efficient emitters than other Er-related centres.

As far as ytterbium is concerned much attention was given to the excitation mechanism of Yb 4f-shell, particularly to the Auger type transfer of energy from the recombining electron-hole pair at the acceptor-like electron trap level introduced by Yb at 30 meV below the bottom of the conduction band of InP<sup>5</sup>. It was found that in InP the luminescent properties of Yb are independent of the growth and doping techniques and that Yb atoms occupy only one type of lattice site (the most probable — substitutional location Yb<sub>in</sub>) which is made possible by size matching of the Yb<sup>3+</sup> and In<sup>3+</sup> ions and favoured also by the admixture of ligand (<111> directional) wave function (covalency effects)<sup>6</sup>. It was suggested that optical activity of Yb in III-V compounds must be related to its substitutional location largely due to covalency effects which relax the parity selection rule and make parity forbidden dipole transition in the 4f-shell possible<sup>7</sup>. It was found that optical activity of Yb implanted in III-V binary and ternary compounds

correlated with the substitutional fraction of Yb as determined by Rutherford back scattering (RBS)/channeling technique. In GaAs the substitutional fraction of Yb was below the sensitivity of the method<sup>6</sup>, it was thought to be the reason for very weak (if any) Yb luminescence generally reported for GaAs doped with Yb either by ion implantation or during epitaxial growth.

In the present work we demonstrate that Yb can be rendered optically active in GaAs if it is associated with other impurities (in our case oxygen and chalcogenes S, Se, Te) which enhances the optical transitions probabilities and/or the efficiency of energy transfer from electrons and holes to Yb luminescence centres.

## EXPERIMENT

GaAs samples of various origin were implanted at "High Voltage Engineering Europa" implanter at room temperature by ions of Yb and co-activators (O, S, Se, Te) using a set of energies and doses to produce a flat profile of dopants with concentrations in the range  $(10^{17} \div 10^{19}) \text{ cm}^{-3}$  up to a depth 150 nm. After the implantation the samples were covered with a  $\text{Si}_3\text{N}_4$  protective layer and then annealed up to 800°C. The photoluminescence (mostly at 77K) was recorded by the standard lock-in technique using liquid-nitrogen-cooled photomultiplier.

## RESULTS

We have performed systematic studies of oxygen co-doping of Yb-implanted GaAs basing upon our previous results on Yb-implanted InP and GaAs where it was found that of the three co-dopant used (O, F, Li) oxygen produced the largest enhancement of Yb luminescence<sup>8,9</sup>. Implantation of Yb or Yb in combination with oxygen was performed into GaAs samples with various concentration of background impurities controlled by secondary ions mass spectroscopy (SIMS) technique.

Implantation of Yb alone (up to concentrations of  $10^{19} \text{ cm}^{-3}$ ) into GaAs samples with background impurities concentration of about  $10^{17} \text{ cm}^{-3}$  produced no luminescence characteristic of f-f  $\text{Yb}^{3+}$  transitions, in agreement with the data reported in the literature. Combined implantation (Yb+O) into the same samples produced a number of luminescence lines (to be discussed further) in the spectral range of  $\text{Yb}^{3+}$  ( $^2\text{F}_{5/2} - ^2\text{F}_{7/2}$ ) transitions. For the series of samples with background impurities (Se, O, Si, C etc) concentration of about  $10^{18} \text{ cm}^{-3}$  the implantation of Yb alone produced appreciable  $\text{Yb}^{3+}$  luminescence. Its intensity varied by more than an order of magnitude within this series of identically implanted samples. Combined implantation (Yb+O) produced much more intense  $\text{Yb}^{3+}$  luminescence with much lower dispersion of the intensity within the series. In all cases the  $\text{Yb}^{3+}$  luminescence was observed within the range of annealing temperatures (550÷700)°C. It can be concluded from these results that oxygen (implanted or background) plays a crucial role in the optical activation of Yb atoms implanted in GaAs.

Let us consider the spectra of  $\text{Yb}^{3+}$  related luminescence. The characteristic  $\text{Yb}^{3+}$  lines are observed in the range (9800÷10200) Å, i.e. (1.264÷1.215) eV, where in some samples more than one hundred lines can be found, and in the range (10300÷11000) Å, i.e. (1.203÷1.126) eV, with much less intensity. Basing upon the analysis of the spectra for various samples and for various annealing conditions it was possible to separate and nominate for convenience several most important groups of lines referring to various centres (Fig. 1):

- $X_1$  and  $X_2$  systems with emission lines at 10060 Å (1.2321 eV) and 10054 Å (1.2329 eV) respectively;
- $Y_1$  and  $Y_2$  systems differing by the ratio of intensities of lines at 9886 Å (1.2533 eV), 9898 Å (1.2518 eV), 9905 Å (1.2509 eV) and 9908 Å (1.2505 eV).

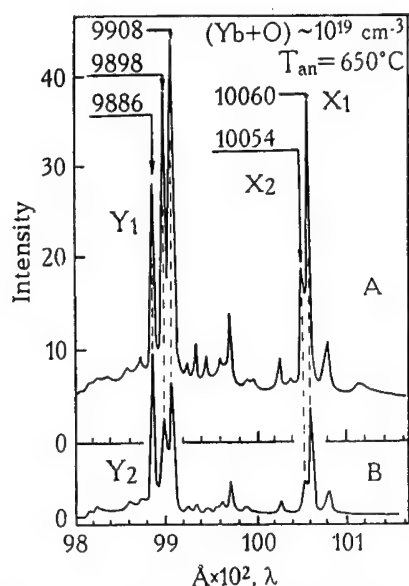


Fig. 1. Luminescence spectra of Yb-related X and Y centres for various (A and B) samples.

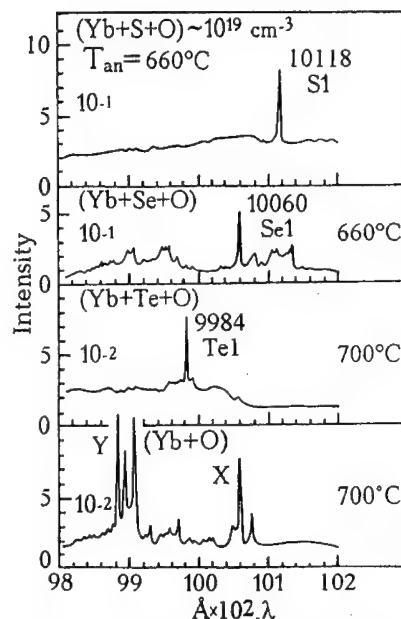


Fig. 2. Spectra of Yb-related centres for various combinations of co-dopants.

The lines of  $X_1/X_2$  and  $Y_1/Y_2$  systems were found to correlate with much weaker groups of lines from the range (10200–11000) Å. The energy shifts between the correlated lines are 70.6 meV and 69.5 meV for  $X_1$  and  $X_2$  systems respectively and ~67 meV for  $Y_1/Y_2$  systems. These weaker lines can be attributed to phonon assisted transitions. Occurrence of various combinations of (Yb+O)-related lines in various samples subjected to identical implantation and annealing procedures suggested that the Yb luminescence centres might be complexes incorporating (besides oxygen) some other components. The role of radiation defects in the formation of Yb-related centres is not clear. Certainly we can not exclude the participation of radiation defects under the conditions of strong radiation damage produced by ion implantation, but as far as luminescence centres mentioned are concerned, there is no direct evidence that these centres incorporate radiation defects.

It was natural to look for unidentified components of Yb-related complexes among the background impurities detected in part of our samples by SIMS technique (Se, O, Si, C etc). To establish the role of at least some of these impurities we performed the co-doping of Yb-implanted GaAs samples (containing relatively low concentration of background impurities) with chalcogene impurities S, Se and Te. In the first experiment we implanted Yb in combination with either S or Se or Te. No Yb-related luminescence was found. In the second experiment three species were implanted in the same samples: Yb, O and either S or Se or Te. In this case the Yb-related luminescence was observed (which confirmed the important role played by oxygen in the optical activation of Yb in GaAs) with lines specific for each of the chalcogenide impurities. These lines could be seen starting from the concentration of co-dopants  $10^{18} \text{ cm}^{-3}$  (which is

comparable to or higher than the concentration of background impurities). At the concentration of about  $10^{19} \text{ cm}^{-3}$  they dominated in the spectra. The following are the data on these luminescence structures referring to (three-components) Yb-related centres (Fig. 2).

**Sulfur ( $S_1$  centre):** implantation of (Yb+O+S) produced a line at  $10115 \text{ \AA}$  (1.2254 eV) which at sulfur concentration  $10^{19} \text{ cm}^{-3}$  dominated in the spectrum and was an order of magnitude more intense than X and Y systems at the reference (implanted by Yb+O) parts of the samples. Similar to X and Y systems we found a weak line at  $10924 \text{ \AA}$  (1.1347 eV), supposedly phonon-assisted transition, shifted by 90.7 meV from the zero-phonon line.

**Tellurium ( $Te_1$  centre):** in (Yb+O+Te) implanted samples we found a line at  $9984 \text{ \AA}$  (1.2415 eV), accompanied by a weak line at  $10462 \text{ \AA}$  (1.1848 eV), shifted by 56.7 meV. The  $Te_1$  line, similar to the case of sulfur, dominated in the spectrum at tellurium concentration  $10^{19} \text{ cm}^{-3}$  being about an order of magnitude lower in intensity than the  $S_1$  line.

**Selenium ( $Se_1$  centre):** in the case of (Yb+O+Se) implantation it was difficult to separate the Se-related line at implants concentration  $(10^{17}+10^{18}) \text{ cm}^{-3}$ . It was only at Se concentration  $10^{19} \text{ cm}^{-3}$  that the line at  $10060 \text{ \AA}$  (1.2321 eV), previously referred to as  $X_1$ , became dominant in the spectrum, so it was evident that  $X_1$  centre was in fact (Yb+O+Se) complex.

Basing upon these results it can be suggested that considerable fraction (if not all) of luminescence lines observed in (Yb+O) implanted samples might be due to other background impurities, still to be identified. Formation and destruction of Yb related complexes implies complicated reactions between their components, at least some of them being mobile at the corresponding annealing temperatures. It is worth noting that our preliminary studies have demonstrated that even more complicated aggregates can be formed comprising, for instance, implanted Yb, O, S and background Se atoms.

Basing upon our data we can draw some preliminary conclusions concerning the correlation of the atomic structure of Yb-related complexes and their energy characteristics. In the Table the energies of (zero-phonon) optical transitions ( $E_0$ ) for all the centres mentioned in the present work are given along with the photon energy for the weak lines attributed to phonon-assisted transition ( $E_{ph}$ ) and the energies of corresponding phonons ( $\hbar\omega_{ph}$ ). Also given are the reference energy ( $E_f$ ) of free  $Yb^{3+}$  ion transition and the differences between this energy and transition energies of various centres ("nepheloxetic shift")  $\delta=E_f-E_0$ .

**Table.** Energy characteristics of Yb-related luminescence centres.

Luminescence centre	$E_0$ (eV)	$\delta=E_f-E_0$ (meV)	$E_{ph}$ (eV)	$\hbar\omega_{ph}$ (meV)
$X_1$	1.2321	38.4	1.1615	70.6
$X_2$	1.2329	37.6	1.1634	69.5
$Y_1/Y_2$	1.2518	18.7	1.1849	66.7
$Z_1$	1.2440	26.5	1.1791	64.9
$Z_2$	1.2430	27.5	1.1765	66.5
$S_1$	1.2254	45.1	1.1347	90.7
$Se_1$	1.2321	38.4	1.1615	70.6
$Te_1$	1.2415	29.0	1.1848	56.7

$E_f=1.2705 \text{ eV}$  — energy of free  $Yb^{3+}$  ion transition ( $^2F_{5/2}-^2F_{7/2}$ ),

$E_0$  — zero-phonon transition energy,

$E_{ph}$  — phonon-assisted transition energy,

$\hbar\omega_{ph}=E_0-E_{ph}$  — phonon energy.

Let us note first of all that the Table stresses the identity of one of the X-centres ( $X_1$ ) with (Yb+O+Se) complex. As far as trends are concerned, one can see systematic change of the optical transition energy within a group of similar centres: Yb+O+S/Se/Te, that is the transition energy increases and the nepheloxetic shift decreases with the increase of the coactivator size. If we accept the assignment of weak lines in the region (10200÷11000) Å to phonon-assisted transitions then another trend is seen: the phonon energy decreases with the increase of the S/Se/Te coactivator mass.

Basing upon the present data it is not possible to separate the roles of the two coactivators as far as the energy structure of the luminescence centres is concerned: the definite correlation between the transition energies and properties of one of the coactivators (S/Se/Te) does not exclude the contribution of another (oxygen). Oxygen seems to be an ever-present component of Yb-related luminescence centres in GaAs (though no centres with oxygen co-activator alone have so far been found), so it is possible that its main role is in the energy transfer process.

## CONCLUSIONS

In the present work we have shown that, contrary to the general belief, ytterbium in GaAs can be optically active. Among optically active Yb-related centres we have identified complexes comprising Yb, O and chalcogene impurities S, Se, Te. These complex luminescence centres are rather efficient, the intensity of luminescence of, say, (Yb+O+S) complex is comparable to the intensity of Yb related luminescence in GaP and even in InP, where high optical activity of Yb was attributed to isolated substitutional  $\text{Yb}^{3+}$  ions.

It should be born in mind that the correlation between optical activity of Yb and Er and their lattice position is not definitely established. First of all, it is not evident that the substitutional RE atoms detected by RBS/channeling measurements are the same RE atoms that are seen in luminescence experiments. Moreover there are some data which show that Er atoms loose their optical activity when located substitutionally<sup>10</sup>. It is not excluded that Yb atoms can move from interstitial sites to substitutional sites when they form optically active complexes with O and S (or Se, Te), as it was observed for (Er+O) doping of GaAs<sup>11</sup>. It can be suggested that lattice position of RE atoms might not be the only (and even not the most important) factor of their optical activity if they are incorporated in some complex aggregated centres.

## ACKNOWLEDGEMENTS

This work was supported by the Russian Foundation for Basic Research (project № 96-02-18206a) and by the National Program "Physics of Solid State Nanostructures" (project № 1-008).

## REFERENCES

1. Rare Earth Doped Semiconductors, ed. by G.S.Pomrenke, P.B.Klein, D.W.Langer (Material Research Society Symposium Proceedings 301, Material Research Society, Pittsburgh, Pennsylvania 1993).
2. R.Boyn, Phys. Stat. Sol. (b), **48**, pp.11-47 (1988).
3. J.Michel, J.L.Benton, R.F.Ferrante, D.C.Jacobson, D.J.Eaglesham, E.A.Fitzgerald, Y.-H.Xie, J.M.Poate and L.C.Kimerling, J. Appl. Phys. **70**, No.5, pp.2672-2677 (1991).
4. J.E.Colon, D.W.Elsaesser, Y.K.Yeo, R.L.Hengehold and G.S.Pomrenke in [1], pp.169-174.

- 
5. T.Gregorkiewicz, B.J.Heijmink Liesert, I.Tsimperidis, I. de Maat-Gersdorf, C.A.J.Ammerlaan and M.Godlewski in [1], pp.239-250.
  6. A.Kozanecki and R.Graetzel, J. Appl. Phys. **68**, No.2, pp.517-522 (1990).
  7. A.Kozanecki in [1], pp.219-224.
  8. V.M.Konnov and N.N.Loiko, Bulletin of the Lebedev Physics Institute, No.12, pp.20-23 (Allerton Press, Inc./New York, 1993).
  9. V.M.Konnov, N.N.Loiko and V.A.Dravin, Bulletin of the Lebedev Physics Institute, No.3, pp.20-23 (Allerton Press, Inc./New York 1994).
  10. A.Kozanecki, M.Chan, C.Jeynes, B.Sealy and K.Homewood, Sol. St. Comm. **78**, No.8, pp.763-766 (1991).
  11. K.Takahei, A.Taguchi and Y.Horikoshi, J. Appl. Phys. **76**, No.7, pp.4332-4339 (1994).

## CHARACTERIZATION OF Er-DOPED III-V NITRIDE EPILAYERS PREPARED BY MOMBE

J. M. Zavada\*, R. G. Wilson\*\*, R. N. Schwartz\*\*, J. D. MacKenzie\*\*\*, C. R. Abernathy\*\*\*,  
S. J. Pearton\*\*\*, X. Wu\*\*\*\* and U. Hömmerich\*\*\*\*

\*U.S. Army Research Office, Research Triangle Park, NC 27709

\*\*Hughes Research Laboratories, Malibu, CA 90265

\*\*\*MSE Department, University of Florida, Gainesville, FL 32611

\*\*\*\*Hampton University, Research Center for Optics, Department of Physics, Hampton, VA 23668

### ABSTRACT

Er-doped AlN epilayers have been grown using metal-organic molecular beam epitaxy (MOMBE) with controlled Er densities. Cell temperatures greater than 1000°C were required for the Er solid source in order to achieve significant Er concentrations in the epilayers. Er densities in the  $10^{19}$  to  $10^{20}$  cm<sup>-3</sup> range were confirmed using secondary ion mass spectrometry (SIMS), quantified using implanted standards. The epilayers were optically excited using an argon-ion laser and infrared luminescence spectra were measured over the temperature range 13 to 300 K. The spectra are centered at 1.54  $\mu$ m and display features typical of the Er<sup>3+</sup> configuration. These data demonstrate that high densities of Er atoms can be incorporated in AlN films during epitaxial growth and that the Er atoms give rise to the intra-4f transitions of the trivalent Er<sup>3+</sup> ion.

### INTRODUCTION

The III-V nitride semiconductors are of significant interest for optoelectronics, largely due to the commercial development of high-brightness, blue and green, light emitting diodes (LEDs) [1,2]. The recent demonstration of a room temperature, pulsed quantum well laser [3] has added to the activity in this material system and indicates that efficient ultraviolet/blue lasers are a definite possibility in III-V nitride materials.

Optoelectronic materials doped with Er atoms are also receiving widespread attention due to their impact on optical communication systems. The intra-shell 4f transitions of the Er<sup>3+</sup> ions produce optical emissions at about 1.54  $\mu$ m. Optical amplifiers based on Er-doped fibers have demonstrated major improvements in link distance, data rates, and reduced needs for signal regeneration. Semiconductors doped with Er offer the prospect of very stable, temperature-insensitive, low-noise laser diodes and efficient optical amplifiers. Previous studies have indicated that the room temperature luminescence of Er-doped semiconductors is strongly dependent upon the energy bandgap of the material host [4]. Consequently, because of their wide bandgaps, the III-V nitrides may be excellent materials to be used for rare earth doped electroluminescent devices.

Here we give the first report, to our knowledge, of Er incorporation in III-V nitride semiconductors during epitaxial growth. In particular, AlN epilayers were grown on sapphire substrates using metal-organic molecular beam epitaxy (MOMBE) and Er densities in the  $10^{19}$  cm<sup>-3</sup> to  $10^{20}$  cm<sup>-3</sup> range were attained. These densities were confirmed using secondary ion mass spectrometry (SIMS) using implanted standards. Furthermore, the Er atoms were optically active as Er<sup>3+</sup> ion centers. Photoluminescence (PL) characterization of the Er-doped AlN layers resulted in bright, room temperature, emission spectra centered at 1.54  $\mu$ m.

### INCORPORATION OF Er ATOMS

Several different methods can be used to incorporate Er atoms into III-V semiconductor materials, including diffusion, ion implantation, and epitaxial growth. To date, there does not seem to be any report of Er incorporation into these III-V nitride semiconductors using diffusion. Wilson *et al.* [5] introduced Er into GaN and AlN materials using ion implantation and observed infrared luminescence centered at 1.54  $\mu$ m. However, co-implantation with O and subsequent furnace annealing was needed to achieve this luminescence.

In the present experiments, the AlN epilayers were grown on sapphire substrates at ~700°C

using a gas source Gen II MOMBE system. Dimethylethylamine alone was used as the Al source. Atomic nitrogen was generated by a 200 W, 2.45 GHz electron cyclotron resonance (ECR) source (Wavemat MPDR) system [6]. The films were single crystalline hexagonal and layer thicknesses were 0.5 - 1.0  $\mu\text{m}$ .

With MOMBE various Er sources may be used for synthesizing Er-doped epilayers. In our initial experiments, gaseous Er precursors, ErTMHD and ErBTSiN, were selected. The gaseous precursors provide a greater surface mobility which was expected to be effective in producing a higher concentration of optically active Er in the epilayers. These sources also allow for the incorporation of other impurities such as oxygen, which may improve the luminescence. However, the resulting epilayers did not exhibit observable light emission at 1.54  $\mu\text{m}$  and SIMS measurements indicated that the Er concentration was below  $10^{17} \text{ cm}^{-3}$ . However, it was found that with a solid elemental Er source and high cell temperatures, significant densities of Er could be achieved.

### SIMS PROFILES OF Er

Atomic depth profiles of Er in the AlN epilayers were obtained with SIMS using a PHI 6600 quadrupole instrument. The SIMS measurements were made using  $\text{O}_2$  ion bombardment and positive secondary ion detection for the Er atoms. An Er-implanted specimen of another AlN film provided the calibration standard necessary for quantification. The density scales were calibrated by setting the integrals of the depth profiles equal to the implant fluences. The background subtracted SIMS detection sensitivity for Er in the AlN material is approximately  $10^{17} \text{ cm}^{-3}$ . However, due to atomic mass interferences, the background subtracted SIMS detection sensitivity was difficult to achieve. The depth scales of the profiles were calibrated by measuring the SIMS crater depths using surface profilometry.

An example of a SIMS depth profile of Er in one of the AlN samples is given in Fig. 1.

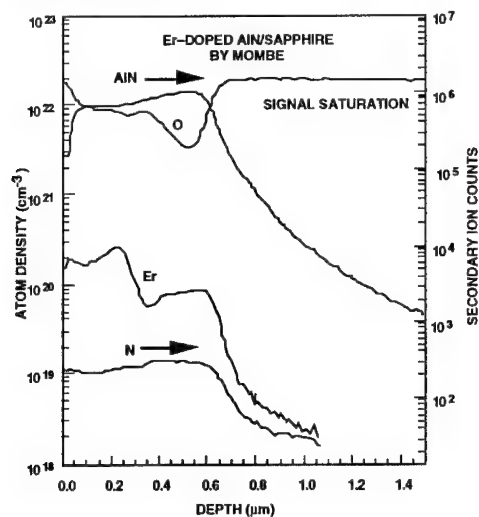


Fig. 1. Atomic depth distribution of Er incorporated in an AlN film during epitaxial growth.

Two different Er cell temperatures were used in this sample. The lower cell temperature, 955°C, resulted in an Er density of  $\sim 1.2 \times 10^{20} \text{ cm}^{-3}$ . The higher cell temperature, 1043°C, yielded a density of  $\sim 2.4 \times 10^{20} \text{ cm}^{-3}$ . The total thickness of the epilayer was approximately 0.6  $\mu\text{m}$ . While the SIMS measurements confirm the high levels of Er in the AlN films, no information is



provided concerning whether the Er atoms occupy interstitial or substitutional sites.

Note also in Fig. 1 that the as-grown AlN contains a high concentration of oxygen that presumably assists in the efficient luminescence from the Er centers. It will be interesting to compare the efficiency of Er in other III-V nitrides, especially GaN, with that in AlN because the oxygen content will be lower in Al-free materials.

### Er<sup>3+</sup> LUMINESCENCE

In general, optical emission of Er in semiconductors is not as efficient as in the dielectric materials. It may be that the more ionic bonds found in dielectrics are more effective in forming the Er<sup>3+</sup> energy levels than the covalent bonds present in most III-V semiconductors. The III-V nitride semiconductor crystals are somewhat like the dielectrics in that the bonds are highly ionic and there is a large energy bandgap.

The Er-doped AlN films were optically excited at 488 nm and infrared photoluminescence (PL) spectra were recorded in the temperature range 13 to 300 K. For the PL measurements, an optical parametric oscillator (Surelite OPO, Continuum) pumped by a Q-switched Nd:YAG laser, was used for the excitation source. The PL was dispersed with a 1-m monochromator and detected with a cooled Ge detector. As shown in Fig. 2, the emission spectra measured at various temperatures are centered at ~1.54  $\mu\text{m}$  and correspond to transitions between the weakly crystal-field split levels of the Er<sup>3+</sup> <sup>4</sup>I<sub>13/2</sub> and <sup>4</sup>I<sub>15/2</sub> multiplets.

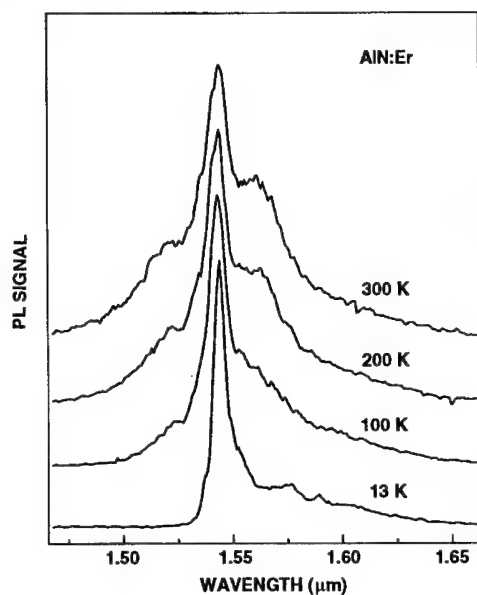


Fig. 2. PL spectra of Er<sup>3+</sup> incorporated in an AlN film during epitaxial growth.

It should also be noted that the room temperature spectrum shown in Fig. 2 resembles the one taken by Wilson *et al.* at 6 K from an Er-implanted AlN film [5]. The main difference between these two spectra is that the one from the Er-doped film is nearly 500 times brighter than the one from the Er-implanted film reported in [5]. In fact, no room temperature emission spectrum could be measured from the Er-implanted AlN film. It should also be noted that for AlN:Er, the 1.54  $\mu\text{m}$

$\text{Er}^{3+}$  luminescence is quenched only by a factor of approximately two between 6 K and room temperature. Favennec *et al.* reported a strong dependence of the  $\text{Er}^{3+}$  ions on the bandgap of the host semiconductor and on the material temperature [7]. The present results provide further evidence that wide bandgap materials, such as AlN ( $E_g \sim 6.2$  eV), tend to suppress the temperature dependence of the  $\text{Er}^{3+}$  luminescence.

Photoluminescence excitation (PLE) spectra were also measured and shown in Fig. 3 is the spectrum recorded at 15 K.

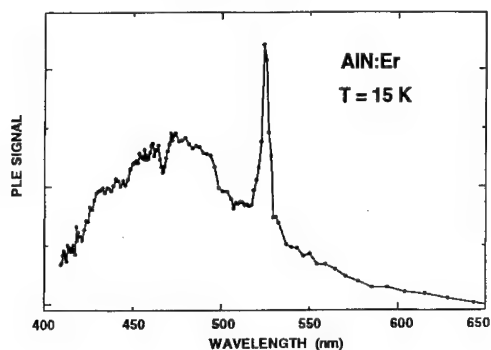


Fig. 3. PLE spectrum of  $\text{Er}^{3+}$  incorporated in an AlN film during epitaxial growth.

For these measurements, the same OPO system as described above was used for the excitation source. The PLE signal was recorded as the ratio between the PL intensity detected at  $1.54 \mu\text{m}$  and the excitation power. The sharp feature at  $\sim 524$  nm suggests that a direct optical excitation mechanism via an intra- $4f$  transition (e.g.,  $^4I_{15/2} \rightarrow ^4S_{3/2}$ ) may be operative. The broad feature peaking at  $\sim 475$  nm may be indicative of a photocarrier mediated mechanism. Work is in progress in order to understand the details of the optical excitation mechanism of  $\text{Er}^{3+}$  in AlN:Er.

## CONCLUSIONS

The present experiments represent a significant breakthrough in the incorporation of Er atoms in the III-V nitride semiconductor materials. The data demonstrate that high densities of Er atoms can be incorporated in AlN during epitaxial growth in a controlled manner. Furthermore, the Er atoms give rise to infrared emission spectra typical of the trivalent  $\text{Er}^{3+}$  configuration. These results indicate that multilayer structures needed in electroluminescent devices can be fabricated using wide bandgap materials, such as AlN. However, difficulties remain concerning the incorporation of Er atoms in GaN materials. The proper growth and processing conditions necessary for incorporation and optical activation need to be established. Further studies are in progress to determine the optimum conditions.

## REFERENCES

1. S. Nakamura, T. Mukai, and M. Senoh, Appl. Phys. Lett. **64**, 1687 (1994).
2. S. Nakamura, M. Senoh, N. Iwasa, and S. Nagahama, Jpn. J. Appl. Phys. **34**, L 797 (1995).
3. S. Nakamura, M. Senoh, S. Nagahama, N. Iwasa, T. Yamada, T. Matsushita, H. Kiyoku, and Y. Sugimoto, Jpn. J. Appl. Phys. **35**, L 74 (1996).

- 
4. J. M. Zavada and D. Zhang, *Solid-St. Electron.* **38**, 1285 (1995) and references therein.
  5. R. G. Wilson, R. N. Schwartz, C. R. Abernathy, S. J. Pearton, N. Newman, M. Rubin, T. Fu, and J. M. Zavada, *Appl. Phys. Lett.* **65**, 992 (1994).
  6. C. R. Abernathy, *J. Vac. Sci. Technol. A* **11**, 869 (1993).
  7. P. N. Favenec, H. L'Haridon, M. Salvi, D. Moutonnet, and Y. L. Guillou, *Electron. Lett.* **25**, 718 (1989).

## ANNEALING STUDY OF ERBIUM AND OXYGEN IMPLANTED GALLIUM NITRIDE

JOHN T. TORVIK<sup>(a)</sup>, ROBERT J. FEUERSTEIN<sup>(a)</sup>, CHANG H. QIU<sup>(b)</sup>, MOELJANTO W. LEKSONO<sup>(b)</sup>, JACQUES I. PANKOVE<sup>(a,b)</sup>, FERREYDOON NAMAVAR<sup>(c)</sup>.

<sup>(a)</sup>Department of E&CE, University of Colorado, Boulder, CO 80309-0425.

<sup>(b)</sup>Astralux, Inc., Boulder, CO 80303.

<sup>(c)</sup>Spire Corporation, Bedford, MA 01730-2396.

### ABSTRACT

A systematic study of photoluminescence (PL) of Er and O ion implanted and annealed n-type GaN grown on R-plane sapphire ( $\text{Al}_2\text{O}_3$ ) was performed. The Er implants ranged from  $2 \times 10^{13}$  to  $1 \times 10^{15} \text{ Er}^{++}/\text{cm}^2$ , and the O co-implants ranged from  $10^{14}$  to  $10^{16} \text{ O}^+/\text{cm}^2$ . The resulting nine different combinations of GaN:Er,O were annealed at 600 °C (4 hrs. in  $\text{N}_2$ ), 700 °C (1.5 hrs. in  $\text{N}_2$ ), 800 °C (0.75 hr. in  $\text{NH}_3$ ), and 900 °C (0.5 hr. in  $\text{NH}_3$ ). Following each annealing step, the  $\text{Er}^{3+}$ -related PL at 1.54  $\mu\text{m}$  was measured from each sample at 77K, when pumped directly with  $\sim 135 \text{ mW}$  of power at 980 nm. The three samples with the highest dose of Er ( $1 \times 10^{15} \text{ Er}^{++}/\text{cm}^2$ ), regardless of O co-dopant dose, yielded the strongest PL peak intensity at 1.54  $\mu\text{m}$  after all the anneals. The integrated PL from 1.52 to 1.58  $\mu\text{m}$  was reduced by 62 % when going from 77 K to room temperature (RT).

### INTRODUCTION

Rare-earth doped semiconductors have been extensively studied as a potential material system for use in optical communications. Possible applications include a low power, temperature insensitive, broad band CW source of IR (1.54  $\mu\text{m}$  or 1.3  $\mu\text{m}$ ) radiation, or lossless Y-junction splitters for curbside signal processing.

The rare-earth element erbium (Er) has been shown to luminesce at a particularly important wavelength, approximately  $\lambda = 1.54 \mu\text{m}$  (0.806 eV) corresponding to an intra 4f-shell transition between levels  $^4\text{I}_{13/2}$  and  $^4\text{I}_{15/2}$  in triply charged Er ( $\text{Er}^{3+}$ ) under the influence of a crystal field from various host semiconductors [1, 2]. At this wavelength there is low loss [3], and no dispersion [4] in some silica based optical fibers. Er has almost exclusively been used as the active element in optically pumped fiber (glass) amplifiers and lasers [5]. However, it was found that the impact excitation cross section for Er in Si is  $\sim 9 \times 10^{-16} \text{ cm}^2$  [6, 7]. This is about 4 - 5 orders of magnitude larger than the optical absorption cross section  $\sim (4.1 - 7.9) \times 10^{-21} \text{ cm}^2$  [8]. Several groups have fabricated RT Er-doped electroluminescent LEDs in Si, GaAs, InP and GaP operating at 1.54  $\mu\text{m}$  [9, 10, 11]. Even so, the quantum efficiencies achieved to date have been too low for any practical application, in part due to the low solubility of Er, which has been found to be  $< 1 \times 10^{18} \text{ Er ions/cm}^3$  in Si [12].

Another practical problem with Si:Er which must be overcome is the observed thermal quenching of the  $\text{Er}^{3+}$ -related PL and electroluminescence (EL) at 1.54  $\mu\text{m}$  [13]. The PL and EL, from Si and GaAs have been observed to be quenched between 100 - 1000 times, when going from 77 K to RT. This figure has been improved upon by co-doping with lighter elements, such as O and F along with the Er [14,15]. Recently, the EL from a reverse biased (impact excitation) Si:Er:O p<sup>+</sup>n<sup>+</sup> LED operating at 1.54  $\mu\text{m}$ , was shown to be reduced by only a factor of 4 when going from 77 K to RT [11].

On the other hand, Favennec et al. suggested the temperature dependent  $\text{Er}^{3+}$ -related PL intensity at 1.54  $\mu\text{m}$  from semiconductors is correlated to the band gap of the host [13]. In hosts

with small band gaps such as Si with  $E_g = 1.11$  eV (RT) and GaAs with  $E_g = 1.43$  eV (RT), the PL was quenched by a factor of more than 100 at RT with respect to 77 K, while in CdS:Er with  $E_g \sim 2.42$  eV (RT) the PL was temperature independent up to RT. Temperature dependent PL and cathodoluminescence (CL) studies of Er doped GaN, a large bandgap host ( $E_g = 3.4$  eV at RT), have since shown a decrease in power at  $1.54 \mu\text{m}$  of 50% (PL) and 5 % (CL), from 6 K to RT [16, 17]. The inconsistency in these results with respect to Favennec et al.'s findings [13], is perhaps due to the fact that the GaN:Er samples were co-implanted with O, whereas the materials in [13] were not. An alternative explanation may be related to defect levels in GaN, which provide non-radiative relaxation paths. We also note that the integrated PL intensity from Er-implanted in two polytypes of SiC (4H with  $E_g = 3.26$  eV at RT and 6H with  $E_g = 3.0$  eV at RT) at  $1.54 \mu\text{m}$ , was constant from 2K to 400 K, when excited by a 46-mW HeCd laser [18].

Wide bandgap hosts, such as GaN, have been demonstrated to be suitable room temperature hosts for Er. The first step in reaching the ultimate goal of an electrically-pumped Er-doped-GaN active device is the characterization of implantation and annealing conditions of Er and O in GaN.

## EXPERIMENT

To determine the optimum sample preparation conditions for Er- and O-implanted GaN, a systematic implantation and annealing study was performed. The "best sample" was defined to be the sample which exhibited the strongest relative PL intensity at the  $\text{Er}^{3+}$ -related emission wavelength,  $\lambda = 1.54 \mu\text{m}$ , at 77 K.

The implantation parameters investigated were the Er and O implantation doses. The first set (set I) of samples investigated consisted of a large piece of GaN film grown on R-plane sapphire, with mobility  $\mu \sim 100 \text{ cm}^2/\text{V-s}$ , and carrier concentration  $n \sim 2 \times 10^{18} \text{ cm}^{-3}$ , which was cut into 10 smaller samples. In preparation for implantation, the GaN samples were cleaned in hot acetone and methanol, before mounting on a Si wafer as shown in Fig. 1. The samples were subsequently ion-implanted with Er and O at doses ranging from  $2 \times 10^{13}$  to  $1 \times 10^{15} \text{ Er}^{++}/\text{cm}^2$ , and  $1 \times 10^{14}$  to  $1 \times 10^{16} \text{ O}^+/\text{cm}^2$ , yielding 9 different combinations of Er and O. The Er was implanted at 350 keV, and the O was implanted at 80 keV. Using RBS, the Er was found to be located within  $0.2 \mu\text{m}$  of the surface. One control sample was implanted with  $1 \times 10^{15} \text{ Er}^{++}/\text{cm}^2$  only.

After implantation the samples were removed from the Si wafer, and cleaned once again in

hot acetone and methanol. A second set (set II) of samples consisting of four GaN films, with similar mobility and carrier concentration, was prepared identically to set I. This set was implanted with  $1 \times 10^{15} \text{ Er}^{++}/\text{cm}^2$ , at 350 keV, and co-implanted with  $1 \times 10^{16} \text{ O}^+/\text{cm}^2$ , at 80 keV. These doses correspond to sample #9 from set I.

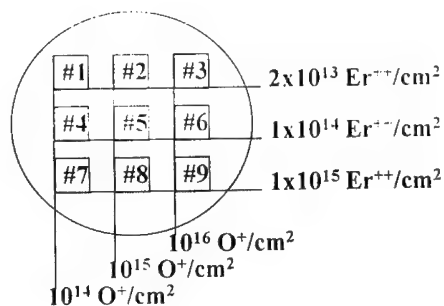


**Fig. 1.** Implantation chart. A single piece of n-type GaN on sapphire was sliced into 9 smaller pieces and ion-implanted with erbium and co-implanted with oxygen at the doses shown in the figure.

For the annealing study, the GaN:Er,O samples were characterized using PL after each annealing step. The samples were mounted on a LN<sub>2</sub>-cooled cold finger, and excited with ~ 135 mW at 980 nm from a laser diode through a fused silica window. The PL was collected by a lens (effective NA = 0.13), and focused into a single-pass Instruments SA, Inc. grating monochromator and detected by a LN<sub>2</sub>-cooled North Coast Ge detector. The grating was blazed at 1.5  $\mu$ m. A bandpass filter with a fairly flat spectral response in the 1510 nm to 1600 nm region was placed in front of the detector. The light was chopped at 11 Hz, and a lock-in amplifier was employed. No correction was made for the filter or detector response.

The pumping was performed at 980 nm, which directly pumps the second excited state of Er<sup>3+</sup> ( $^4I_{15/2} \rightarrow ^4I_{11/2}$ ). The bandgap of GaN is  $E_g = 3.4$  eV at RT, so that the energy of the pump laser ( $E_{\text{pump}} = 1.27$  eV) was not high enough to excite the Er indirectly through the recombination of electron-hole pairs, as is commonly done with Si:Er [15]. For an Er dose of  $1 \times 10^{15}$  Er/cm<sup>2</sup>, and with an optical absorption cross section of  $\sim 5 \times 10^{-21}$  cm<sup>2</sup>, only an estimated 560 nW was actually absorbed by the Er.

The implanted GaN:Er,O samples from set I were annealed in a tantalum sample holder inside a quartz tube which was heated in a furnace. The samples were successively annealed under atmospheric pressure at: 600 °C (4 hrs. in N<sub>2</sub>), 700 °C (1.5 hrs. in N<sub>2</sub>), 800 °C (0.75 hr. in NH<sub>3</sub>), and 900 °C (0.5 hr. in NH<sub>3</sub>). After each annealing step each sample was characterized using PL as described above, and compared to a reference sample. After the characterization of set I, a similar study for the samples from set II was performed at annealing temperatures of 800 °C and 900 °C.

## RESULTS

It is important to incorporate, and to optically activate as many Er ions as possible. The luminescence intensity of an LED, and the gain in a laser are directly proportional to the density of optically active elements. The total implanted densities were approximately  $1 \times 10^{18}$  Er ions/cm<sup>3</sup>,  $5 \times 10^{18}$  Er ions/cm<sup>3</sup>, and  $5 \times 10^{19}$  Er ions/cm<sup>3</sup> in set I, and  $5 \times 10^{19}$  Er ions/cm<sup>3</sup> in set II. The highest implant density,  $5 \times 10^{19}$  Er ions/cm<sup>3</sup>, was 50 times larger than the reported solubility limit of  $\sim 1 \times 10^{18}$  Er ions/cm<sup>3</sup> for Er in Si [11].

No Er<sup>3+</sup>-related PL at 1.54  $\mu$ m was detected in any sample before the anneals. A typical PL spectra taken at 77 K from one of the Er and O implanted GaN samples

( $10^{15}$  Er<sup>3+</sup>/cm<sup>2</sup> and  $10^{16}$  O<sup>2+</sup>/cm<sup>2</sup>) after the annealing sequence of 600 °C (N<sub>2</sub>), 700 °C (N<sub>2</sub>), 800 °C (NH<sub>3</sub>), and 900 °C (NH<sub>3</sub>) is shown in Fig. 2.

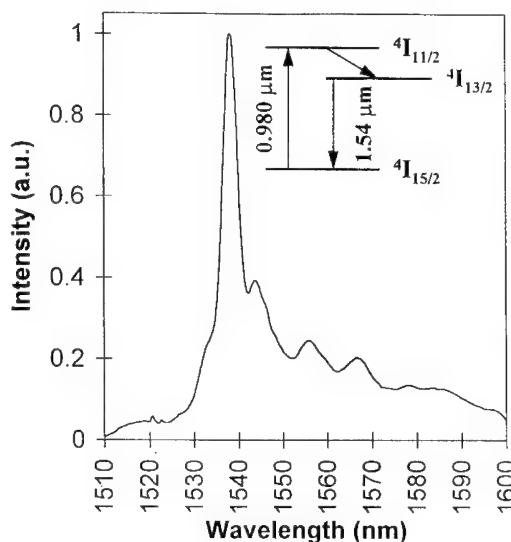


**Fig. 2.** A typical PL spectrum taken at 77 K of a Er ( $10^{15}$  Er<sup>3+</sup>/cm<sup>2</sup>) and O ( $10^{16}$  O<sup>2+</sup>/cm<sup>2</sup>) implanted GaN film, after anneals at 600 °C, 700 °C, 800 °C, and 900 °C.

All the GaN:Er,O samples in set I were annealed at 600 °C (N<sub>2</sub>), 700 °C (N<sub>2</sub>), 800 °C (NH<sub>3</sub>), and 900 °C (NH<sub>3</sub>). The peak PL power of the Er<sup>3+</sup>-related emission at 1.54 μm was measured after each annealing step, and plotted against the annealing temperature. All the intensities were normalized to the largest value found from sample #9 at 800 °C. The results are shown in Fig. 3.

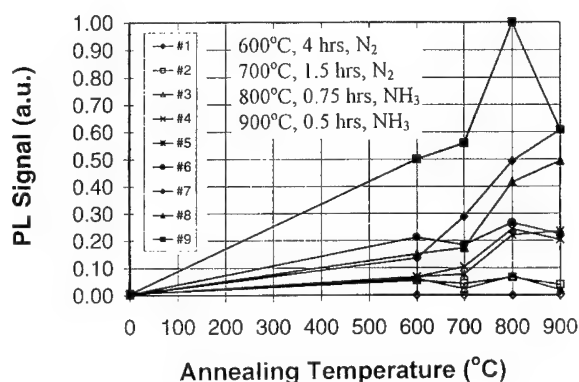


**Fig. 3.** Peak intensity of the Er<sup>3+</sup>-related PL line at 1.54 μm measured at 77 K versus annealing temperature, while pumped with 150 mW at 980 nm.

Although the Er concentration in samples 1,2, and 3 was substantial at  $1 \times 10^{18}$  Er/cm<sup>3</sup>, they did not yield a distinct Er signature at 1.54 μm after any of the annealing steps. Instead, a rather broad PL signal around 1.54 μm was detected. Excluding samples 1-3, it was found that the samples with the most oxygen present ( $1 \times 10^{16}$  O<sup>+</sup>/cm<sup>2</sup>), samples 6 and 9, became optically active at the lowest annealing temperature (600 °C). We can speculate that at 600 °C the large number of O atoms can move only slightly to form complexes with the Er ions.

The anneal at 700 °C did not effect the Er<sup>3+</sup>-related PL intensity significantly, but the anneals at 800 °C and 900 °C did. We speculate that the high temperature anneals helped to recrystallize the implantation-damaged lattice, and reduce non-radiative decay. The recrystallization of the GaN during the anneals at 800 °C and 900 °C was visually apparent because the samples which had turned "milky" after the Er and O implants, regained their transparent appearance following the anneals.

It is clear from Fig. 3 that the luminescence efficiency was strongly dependent upon the Er dose and much less so the O dose. Samples 7-9, all with an Er dose of  $1 \times 10^{15}$  Er/cm<sup>2</sup>, exhibited the largest PL signal. Samples 4-6, all with Er dose of  $1 \times 10^{14}$  Er/cm<sup>2</sup>, exhibited PL approximately a factor 2-3 weaker than samples 7-9. However, the PL from samples 4-6 was about a factor of 5 larger than the PL from samples 1-3, which had 5 times less Er ions. This suggests for the lower Er doses that the PL is directly proportional to the number of Er ions. We can therefore speculate that the Er solubility limit in GaN was not reached. However, the PL intensity difference between samples 4-6, and 7-9 was only about a factor of 2-3, while their dose ratio was 10. Since this increase in the Er dose by a factor of 10 only led to an increase in the PL by a factor of 2-3, one can speculate that the percent of optically active Er atoms dropped when the Er concentration increased from  $0.5 - 5 \times 10^{19}$  Er/cm<sup>3</sup>.

The control sample which was implanted with  $1 \times 10^{15}$  Er/cm<sup>2</sup>, and no O, was annealed along with samples 1-9. The control sample had no detectable Er-related luminescence. This demonstrates the need for co-dopants to optically activate the Er. This is consistent with the report that O enhances the luminescence output from Er in Si up to three orders of magnitude [15]. However, increasing the O dose from  $1 \times 10^{14}$  O/cm<sup>2</sup> to  $1 \times 10^{16}$  O/cm<sup>2</sup> did not affect the PL noticeably after the anneals at 800 °C and 900 °C.

The annealing study of set I showed that the anneals at 800 °C and 900 °C enhanced the PL intensity the most. The anomalous peak in the PL intensity at 800 °C for sample #9, needed verification. Set II was therefore annealed at 800 °C and 900 °C, to investigate the difference between the two temperatures. One piece of each sample (1a, 2a, 3a, 4a) was annealed at 800 °C in NH<sub>3</sub> for 30 min, and subsequently characterized using PL as described above. These samples were annealed again along with the other half of the samples (1b, 2b, 3b, 4b) at 900 °C in NH<sub>3</sub> for 30 min. The PL spectra for two of the samples (1a and 1b) are shown in Fig. 4 a and b.

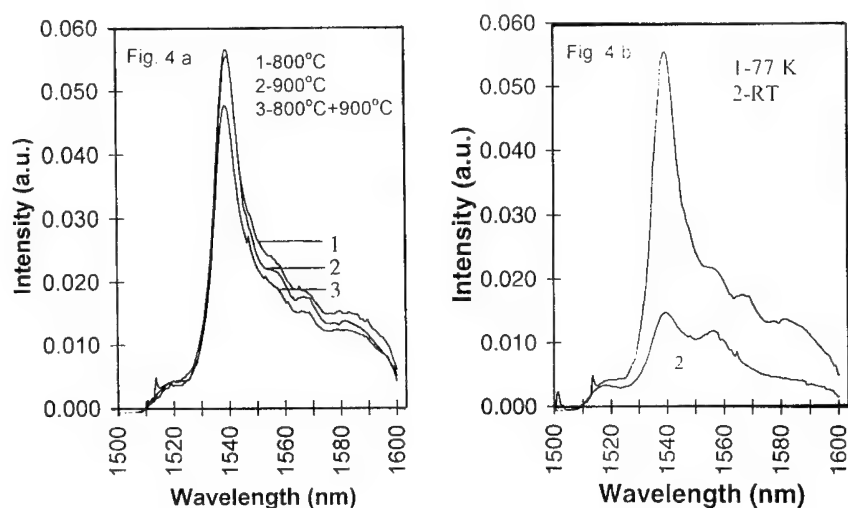


**Fig. 4.** a) PL of sample 1 in sample set II at 77 K after anneals at (1) 800 °C, (2) 900 °C, and (3) 800 °C and 900 °C. b) PL of sample 1a at 77 K and RT after anneal at 800 °C.

These spectra were typical for samples 1, 2, and 3, while sample 4 showed the same relative PL output after anneals at 800 °C or 900 °C or 800 °C and 900 °C. From Fig. 4a, the anneals at 800 °C for 30 min, and the anneal at 900 °C for 30 min proved to be roughly equivalent, but the sample which was annealed at *both* 800 °C (0.75 hr) and 900 °C (0.5 hr) showed a slight decrease in PL intensity.

In Fig. 4b one can compare the PL at 77 K and RT. The room temperature integrated signal is reduced to 38 % of its value at 77 K, which is comparable to 50 % PL power reduction reported by Wilson et al. [16]. In both these PL studies, the laser photon energy is below the bandgap energy of GaN. Compared to the temperature quenching in PL, the smaller quenching in CL signal (5%) [17] may be due to the electron excitation, as is the case of smaller EL temperature quenching in Si [11].



The anneals did not shift the peak wavelength of the  $\text{Er}^{3+}$ -related emission, which remained constant at 1.539  $\mu\text{m}$ . The anneals may have broadened the linewidth. However, these measurements were broadened by the large slit width used on the monochromator to collect as much light as possible from the weakest samples. The slit widths were kept constant throughout the experiments.

## CONCLUSIONS

A systematic PL study of Er and O ion implanted and annealed n-type GaN was performed. The optimum implantation and annealing conditions to optically activate GaN:Er,O films were found to be  $1 \times 10^{15} \text{ Er}^{++}/\text{cm}^2$  at 350 keV, and  $1 \times 10^{16} \text{ O}^-/\text{cm}^2$  at 80 keV, followed by a single post-implant anneal at 800 °C in flowing  $\text{NH}_3$  for 30 min. The integrated  $\text{Er}^{3+}$ -related PL in the 1.54  $\mu\text{m}$  spectral region was reduced to approximately 38 % when going from 77 K to room temperature.

## ACKNOWLEDGMENTS

This work was supported by AFOSR Grant No. F49620-95-I-0301, and AFOSR AASERT Grant No. F49920-93-I-0384.

## REFERENCES

1. H. Ennen, J. Schneider, G. Pomrenke, and A. Axmann, *Appl. Phys. Lett.* **43**, 943 (1983).
2. H. Nakagome, K. Uwai, and K. Takahei, *Appl. Phys. Lett.* **53**, 1726 (1988).
3. T. Miya, Y. Terunuma, T. Hosaka, and T. Miyashita, *El. Lett.* **15**, 106 (1979).
4. C. T. Chang, *El. Lett.*, **15**, 765 (1979); *Appl. Opt.*, **18**, 2516 (1979).
5. M. J. F. Digonnet, *Rare Earth Doped Fiber Lasers and Amplifiers*, Dekker, New York, 1993.
6. T. Kimura, H. Isshiki, H. Ishida, S. Yugo, R. Saito, T. Ikoma, *J. Appl. Phys.* **76**, 3714 (1994).
7. S. Lomardo, S. U. Campisano, G. N. van den Hoven, and A. Polman, *J. Appl. Phys.* **77**, 6504 (1995).
8. W. J. Miniscalco, *IEEE/OSA J. Lightwave Technol.*, **LT-9**, 234-250 (1991).
9. X. Z. Wang and B. W. Wessels, *Appl. Phys. Lett.*, **65**, 584 (1994).
10. B. Zheng, J. Michel, F. Y. G. Ren, L. C. Kimerling, D. C. Jacobson, and J. M. Poate, *Appl. Phys. Lett.* **64**, 2842 (1994).
11. G. Franzo, F. Priolo, S. Coffa, A. Polman, A. Carnera, *Appl. Phys. Lett.* **64**, 2235 (1994).
12. D. J. Eaglesham, J. Michel, E. A. Fitzgerald, D. C. Jacobson, J. M. Poate, J. L. Benton, A. Polman, Y.-X. Xie, and L. C. Kimerling, *Appl. Phys. Lett.* **58**, 2797 (1991).
13. P. N. Favennec, H. L'Haridon, M. Salvi, D. Moutonnet, and Y. Le Guillou, *El. Lett.* **25**, 718 (1989).
14. P. N. Favennec, H. L'Haridon, D. Moutonnet, M. Salvi, and Y. Le Guillou, *Jpn. J. Appl. Phys.* **29**, L524 (1986).
15. J. Michel, J. L. Benton, R. F. Ferrante, D. C. Jacobson, D. J. Eaglesham, E. A. Fitzgerald, Y.-H. Xie, J. M. Poate, and L. C. Kimerling, *J. Appl. Phys.* **70**, 2672 (1991).
16. R. G. Wilson, R. N. Schwartz, C. R. Abernathy, S. J. Pearton, N. Newman, M. Rubin, T. Fu, and J. M. Zavada, *Appl. Phys. Lett.* **65**, 992 (1994).
17. C. H. Qiu, M. W. Leksono, J. I. Pankove, J. T. Torvik, R. J. Feuerstein, and F. Namavar, *Appl. Phys. Lett.* **66**, 562 (1995).
18. W. J. Choyke, R. P. Devaty, L. L. Clemen, M. Yoganathan, G. Pensl, and Ch. Hassler, *Appl. Phys. Lett.* **65**, 1668 (1994).

**Part III**  
**Excitation Mechanisms**

## EXCITATION AND DE-EXCITATION OF $\text{Yb}^{3+}$ IN $\text{InP}$ AND $\text{Er}^{3+}$ IN $\text{Si}$ : PHOTOLUMINESCENCE AND IMPACT IONIZATION STUDIES

T. GREGORKIEWICZ\*, I. TSIMPERIDIS\*, C.A.J. AMMERLAAN\*, F.P. WIDDERSHOVEN\*\*,  
AND N.A. SOBOLEV\*\*\*

\*Van der Waals - Zeeman Institute, University of Amsterdam, Valckenierstraat 65-67, NL-1018  
XE Amsterdam, The Netherlands, tom@phys.uva.nl

\*\* Nederlandse Philips Bedrijven B.V., Prof. Holstlaan 4, NL-5656 AA Eindhoven, The Netherlands

\*\*\* Ioffe Physical-Technical Institute, Politechnicheskaya ul. 26, St Petersburg, Russia

### ABSTRACT

In the paper the existing information on the optical excitation of the erbium ion in crystalline silicon is critically reviewed. The proposed excitation mechanism is compared to the one which is believed to be responsible for the luminescence of ytterbium in indium phosphide. To this end the influence of constant and microwave electric field on the photoluminescence of both systems is inspected. It is shown that, although both systems show some similarities, their analogy is limited.

The particular role of excitons and electrons in both the excitation as well as the de-excitation mechanism is investigated for the  $\text{Si:Er}$  system. The results of photoluminescence decay studies ( $T=4.2$  K) are presented. It is argued that a nonradiative energy transfer to conduction electrons is responsible for the limitation of the energy transfer to the Er core and for its nonradiative recombination. Also, a prominent role of excitons in the energy transfer mechanism is confirmed. Finally, the origin of the 873 meV photoluminescence band recently reported in Er-implanted Si is discussed in relation to a possible defect-mediated activation of Er.

### INTRODUCTION

#### Rare Earth Ions in Semiconductors

Rare earth (RE) atoms are characterized by an incompletely filled 4f electron shell. Excited states of this shell give rise to characteristic photoluminescence (PL). Since the 4f shell is well screened from external influence the photoluminescence spectrum shows very little dependence on the host crystal and is very similar to that of a free atom. Because it is due to internal atomic transitions the energy of the PL spectrum is independent of temperature. These characteristic features of their PL make RE's very attractive for practical applications and they stimulated intensive investigations. Most research effort so far has been focused on ytterbium in indium phosphide and erbium in silicon.

The photoluminescence of Yb in InP is relatively best understood. This follows from the fact that the PL spectrum has in this case rather strong intensity and energies which are identical regardless of the sample preparation method or parameters of the matrix; identical spectra have been observed in InP crystals doped during different growth techniques (MOCVD, LPE, high-pressure gradient freeze synthesis), and also in implanted material. The spectrum has been identified with a substitutional  $\text{Yb}^{3+}$  ion on an In site. However, the precise assignment of individual spectral components to particular transitions between the two lowest manifolds is still not fully resolved [1,2]. It is nevertheless established that the structure of the spectrum is due to the crystal field splitting of the ground and excited states.

In comparison to Yb in InP the understanding of the  $\text{Si:Er}$  system is still at a lower level. This is somewhat disappointing since the photoluminescence of Er ions implanted in crystalline silicon and related materials ( $\text{SiO}_2$ , SIPOS, amorphous and porous silicon) is intensively investigated in the prospect of possible applications. This is stimulated by the fact that the sharp, atomic-like emission of Er coincides with the absorption minimum of glass fibers commonly used in telecommunications. The studies on Er-doped silicon form part of a much broader effort aimed at the development of optical devices compatible with the highly successful silicon technology.

However, in spite of a continued effort, the intense emission at room temperature has not yet been demonstrated. This is mainly due to the complicated character of energy transfer between the rare-earth ion core and silicon crystal as well as to the forbidden character of the intrashell transition responsible for radiative recombination. In comparison to Yb in InP, the case of Er in Si appears to be more complicated. Although the PL emission always takes place around the  $1.6\ \mu\text{m}$  wavelength value the particular spectrum and overall PL efficiency exhibit a clear dependence on the preparation conditions and other defects/dopants simultaneously present in the material. In that situation it has been suggested that Er in Si forms complexes of varying symmetry and atomic composition; each particular complex being characterized by an individual PL spectrum. It has been established that oxygen is especially effective in promoting the Er PL and the formation of Er-O clusters has been postulated.

#### Excitation and De-excitation Mechanism

As already mentioned before the sharp spectra emitted by RE ions are due to the internal atomic character of involved transitions. This implies that the interaction between the RE core and the host crystal is very weak. As a consequence, the energy transfer between the crystal and RE ion is inefficient. In the case of InP:Yb it is rather generally assumed that the excitation of the core is mediated by a formation of an exciton bound to the RE ion via a local potential. Indeed, various DLTS studies reported on the existence of an Yb-related electron trap, relatively shallow with respect to the conduction band. The core excitation is then accomplished in an Auger process involving the nonradiative recombination of the bound exciton (BE) with a simultaneous energy transfer to an electron localized in the 4f shell, with the energy mismatch of about 100 meV being compensated by phonon emission. In the case of Er in silicon the situation is again more complicated as no states, which could unambiguously be related to Er, have been found in the band gap. Nevertheless, also here evidence for an electron trap has been reported. In contrast to InP:Yb the reported level has a deep character; for the binding energy values as high as 150 meV [3] or 260 meV [4] have been given. Also in this case the postulated energy transfer mechanism involves recombination of an exciton captured at this trap with a simultaneous Auger excitation of a core electron and a phonon-compensated energy difference.

Apart from an indirect, and therefore not very efficient, excitation, the RE PL suffers also from low efficiency. This follows from the fact that the internal 4f transitions are parity-forbidden and become only partially allowed due to crystal-field-induced mixing of the states. Consequently the radiative recombination times should be long. In contrast to that, the experimentally measured low-temperature decay time of Yb PL in InP is only about  $10^{-2}$  ms [5]. For Er PL in Si the decay time at  $T=4.2\ \text{K}$  is approx. 1 ms [6], but decreases quickly for higher temperatures. This effective shortening of the life time is ascribed to an efficient nonradiative de-excitation channel competing with the radiative recombination. As a possible mechanism responsible for this quenching a nonradiative Auger process, involving conduction electrons, has frequently been postulated.

In the studies of RE luminescence in semiconductors various experimental techniques have been used. In this paper we concentrate on the influence of an electric field on the PL spectra of both above discussed systems, and on the decay characteristics of photoluminescence of Er-implanted float zoned silicon (Fz-Si).

#### PHOTOLUMINESCENCE UNDER APPLICATION OF AN ELECTRIC FIELD

Application of an electric field of moderate amplitude alters the carrier capture rate at impurity centers [7]. The effect is predominantly due to the heating of the electron gas which diminishes the number of low energy electrons at the bottom of the band, which are preferentially being localized by local potentials at impurity/defect sites. The actual magnitude of the lowering of the capture rate is proportional to the effective electron temperature  $T_e$ . The heating of the (free) electron gas will take place in a constant (DC) as well as in a microwave electric field. (In the latter case cyclotron resonance might be observed if a magnetic field is simultaneously applied). For stronger electric fields the carrier capture rate will additionally be influenced by another mechanism - the effective lowering of a (Coulombic) potential of a trap due to the so-called *Poole-Frenkel* effect. As a result of both mechanisms, the capture of carriers at shallow traps can

be significantly reduced. Such an effect blocks the recombination which proceeds via such traps, effectively enhancing alternative de-excitation paths. For moderate electric fields ( $\mathcal{E} \leq 10^2$  V/cm) the increase of the electron temperature usually does not exceed values of approximately 25 K.

#### Ytterbium in Indium Phosphide

Figure 1 presents a comparison of the behavior of the PL spectrum of Yb-doped InP under the influence of the microwave and DC electric fields.

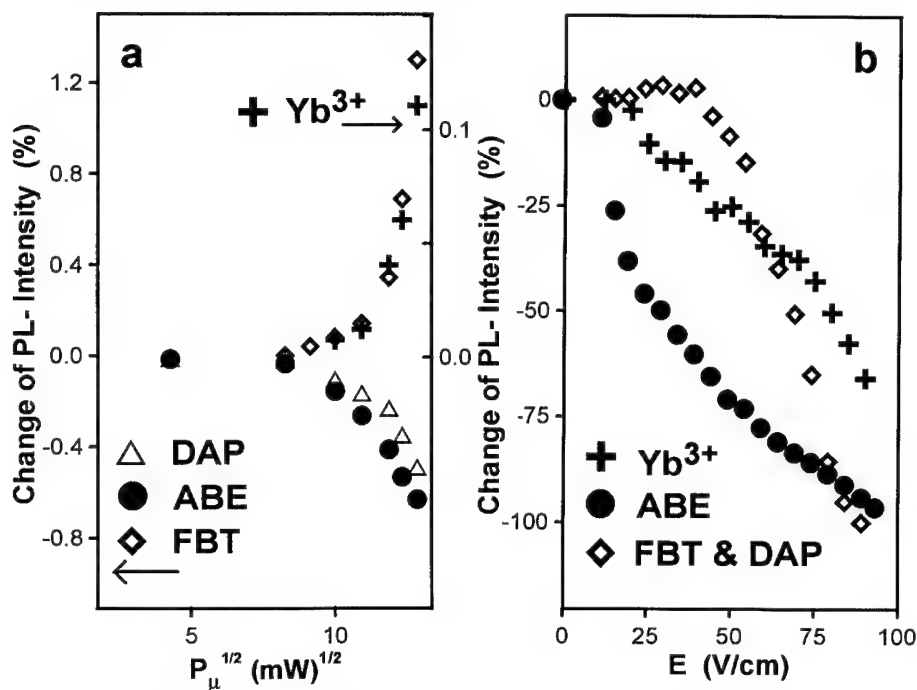


Figure 1. Relative intensity of PL bands observed in InP:Yb (at LHe temperature) as a function of the microwave (a) and the DC (b) electric fields. (For the microwave field the square root of the power  $P_\mu$  is given). The individual behavior for the Yb-related, bound-exciton (ABE), donor-acceptor pair (DAP), and free-to-bound (FBT) recombinations is shown.

In the experiment the sample was either placed in the microwave cavity (Q band, 35 GHz) with optical access, or metal contacts were made to which the DC voltage could be applied. The measurements were performed at liquid helium (LHe) temperature under an argon laser excitation. Details of the experiment and sample preparation can be found elsewhere [8]. Without the electric field the spectrum was characterized by three PL bands corresponding to bound excitons (ABE), a donor-acceptor pair (DAP) band superimposed with a free-to-bound (FBT) transition to acceptor states, and a characteristic Yb luminescence. As can be concluded from Fig. 1a, upon increase of the microwave electric field, (given in the plot as a square root of the microwave power  $P_\mu$ ), the photoluminescence corresponding to band-edge excitons and DAP recombination is quenched. Based on the earlier presented reasoning one can explain it by an increase of the electron temperature which lowers the capture cross section of shallow centers involved in these recombination channels. At the same time the Yb photoluminescence and the FB transition

involving acceptor states are enhanced. Such an effect could be an indication that these two recombination channels involve deeper states which are less affected by the microwave heating of the free carriers and are being enhanced at the expense of the shallower ones. In this case there should be a linear correlation between the quenching and the enhancing effects. Careful analysis of the data shows that although the changes are indeed co-linear for small electric field values, they become decoupled as the microwave power increases. Therefore, another mechanism has to be called upon in order to account for the experiment. Such a conclusion is further supported by a similar set of measurements performed on another InP:Yb sample whose PL spectrum consisted of the Yb-related band only. Also in that case the Yb luminescence increased upon application of the microwave field [8]. Since such an increase of Yb-related PL is not accompanied by a simultaneous decrease of any other radiative recombination, the effect must be explained either by a microwave-induced quenching of a nonradiative recombination channel, or by an influence on the Yb PL itself; this could proceed via an increase of the efficiency of the radiative recombination at Yb, or by enhancement of the excitation of Yb core. Although an existence of nonradiative recombination channels, related to shallow levels in the gap of semiconducting host, cannot be excluded, and indeed has been reported for MBE-grown silicon and Si-Ge superlattices [9], it does not appear very likely since i) the effective nonradiative recombination centers usually have midgap levels and, therefore, should be rather insensitive to small variations of the effective electron temperature, and ii) if the microwave-induced quenching of nonradiative recombination was indeed important it should also demonstrate itself in the data depicted in Fig.1, as an increase of all the radiative recombination channels - an effect which is not observed. We conclude therefore that the enhancement of Yb luminescence in the microwave field is independent of other recombination channels available in a particular material and is rather connected to the mechanism of Yb PL itself. In view of the above, a microwave-induced quenching of the nonradiative de-excitation of Yb has been postulated [10].

Fig.1b shows the influence of a DC electric field on the PL spectrum of the same sample for which the effect of the microwave field has been studied. As can be concluded, in this case the behavior of the PL bands is somewhat different. Already a relatively small electric field of approximately 10 V/cm effectively quenches the band-edge exciton PL. This can be explained by an earlier mentioned Poole-Frenkel effect which diminishes the capture cross section for shallow exciton traps. For a somewhat higher value of the electric field, also the Yb band lowers its intensity. At the same time the intensity of the acceptor-related FB transition slightly increases - it can be quenched only for substantial electric fields, most probably as an effect of the free carrier sweeping. The similar behavior of the Yb-related and the band-edge exciton PL bands, as evidenced by the presented DC field dependence of the PL spectrum, is consistent with the excitonic mechanism of Yb photoluminescence. As mentioned in the introduction, the existence of a BE state in the excitation scheme of Yb in InP has been postulated but its actual fingerprint could not be given until now. The current results also show that the local potential, that binds an exciton to an ytterbium ion, is not very deep; it can be influenced by an electric field of approximately 20 V/cm. It remains, however, unaffected by microwave-induced carrier heating.

#### Er in Silicon

The influence of a microwave field on the photoluminescence of erbium in silicon has been reported in the past [11]. The effect is illustrated in Fig.2, where the spectral dependence of the Er-doped (Czochralski-grown) silicon PL under application of a microwave field is depicted. (For details on sample preparation see Ref.[11]). As can be seen, the microwave field quenches the intensity of the band-edge-exciton-related PL and simultaneously enhances the Er band. While the first effect can again be explained by a reduction of the capture coefficient of shallow exciton traps upon increase of the free carrier temperature, the origin of the enhancement of the Er PL is more difficult to account for. Possible explanations include the decrease of a nonradiative quenching of the excited erbium ions [11] and an increased efficiency of the Er core excitation upon carrier heating [12].

Fig.3 shows the influence of the DC electric field application on the photoluminescence of Er. The effect is in this case remarkably different from that discussed in the preceding paragraph for

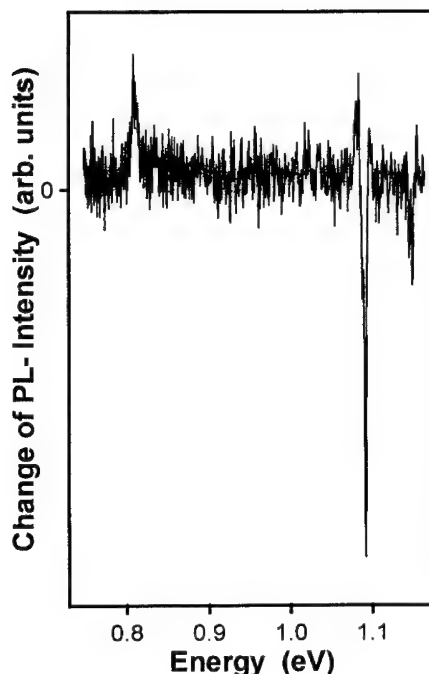


Figure 2. Spectral dependence of the microwave induced changes of the PL spectrum of Er implanted Cz-Si. The microwave power is 200 mW,  $T=1.8$  K.

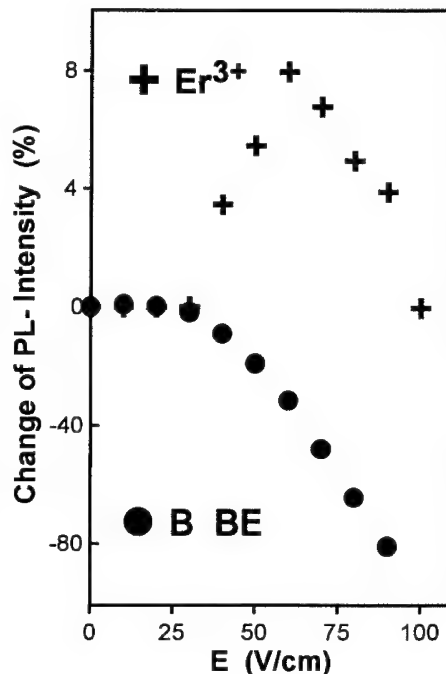


Figure 3. Relative intensity of PL spectrum in Si:Er as a function of DC electric field. The experimental data for the Er-related and boron BE PL bands are given. (Note change of scale)

InP:Yb. While the excitonic PL band is quenched for electric fields  $\mathcal{E} > 30$  V/cm, the erbium PL does not follow this behavior; in contrast to the results for Yb in InP the intensity of Er PL band starts to increase its intensity for the same field value. This strongly suggests that both processes are correlated. The observed effect illustrates the importance of deep electron trap in the Er excitation scheme [3]. We can rationalize the observed field dependence of Er PL by assuming that the Poole-Frenkel effect diminishes capture at shallow traps which, in turn, leads to a lower BE recombination rate. Consequently, this effect will increase the free electron concentration and promote their capture by deep traps, and among them also at an Er-related level. The existence of this trap has been postulated from the DLTS measurements [4] and from the temperature dependence of erbium PL intensity. The observed increase of the intensity of Er PL could alternatively be explained by an increase of its radiative efficiency. However, this possibility has been ruled out experimentally by showing that the decay time of Er PL does not change upon the application of the DC electric fields up to 50 V/cm. As will be discussed in the next section, such a result means that the nonradiative recombination of excited Er atoms, (which strongly competes with the radiative de-excitation), cannot be affected by an application of electric fields.

Finally, it should be mentioned that special care must be taken when comparing results obtained for constant electric fields with those for microwave fields. Similarly to the case of the resistivity measurements, one should keep in mind that for highly nonhomogeneous samples both methods can yield very different results: the microwave field will heat carriers available in the more conductive parts of the sample where the DC potential will be negligible. In contrast to

that, the DC potential will be effectively applied only to the resistive parts of the material and will be short-circuited for the regions of low resistivity. It can therefore happen that, for a very inhomogeneous material, different parts of the sample will contribute to the PL spectrum measured under application of the DC and microwave electric fields.

## MEASUREMENTS OF PHOTOLUMINESCENCE DECAY TIME FOR Er IN Si

### Role of Electrons in the Photoluminescence Mechanism

As can be concluded from the electric field measurements presented in the preceding section, electron capture at a relatively deep level plays an important role in the luminescence of Er in Si. In a recent contribution [3] it is argued that the temperature dependence of the electron capture rate at Er-related trap at approximately 150 meV below the bottom of the conduction band (CB) determines thermal quenching of Er photoluminescence for the higher temperature range  $T > 70$  K. For lower temperatures, the thermal dependence of Er PL is reported to be governed by a process with an activation energy of 10-15 meV [13-15], i.e. similar to the dissociation energy of excitons. Also the power dependence of Er PL confirms the prominent role of excitons in the activation of erbium atoms [16].

On the other hand more evidence is being gathered that CB electrons have also a prominent role in limiting the efficiency of Er PL. In a model likely to account for the kinetics of Er photoluminescence the interaction with free electrons in CB limits the energy transfer to the erbium core, and also provides a nonradiative way of de-excitation of Er, alternative to the radiative recombination. The second process shortens the effective life time of the excited state of Er atoms and thus influences a parameter which can be directly measured in an experiment.

In a probable description of the kinetics of Er PL in silicon [17] it is assumed that the 4f-shell is excited by recombination of a bound exciton system which is formed via free excitons generated upon laser illumination. However, the nonradiative energy transfer between an exciton bound at the Er-related trap and the 4f-shell is hampered by an alternative de-excitation route involving an energy transfer to electrons in CB. Also for an excited Er atom (at least) two recombination paths exist; a radiative one giving rise to the characteristic PL band at  $1.6 \mu\text{m}$ , and a nonradiative one based on an Auger mechanism involving again the energy transfer to CB electrons. A relevant set of rate equations comprises then:

$$\frac{d}{dt}n = I\sigma - \alpha n^2, \quad (1)$$

$$\frac{d}{dt}N^{ex} = \alpha n^2 - \frac{N^{ex}}{\tau_{eff}^{ex}}, \quad (2)$$

$$\frac{d}{dt}N^* = \frac{N^{ex}}{\tau_{TR}} - \frac{N^*}{\tau_{eff}^{Er}}, \quad (3)$$

where  $I\sigma$  corresponds to the generation rate and is proportional to the laser power density,  $\alpha$  is a coefficient describing exciton formation at the expense of free electrons and holes, and  $N^{ex}$  and  $N^*$  are concentrations of excitons mediating Er excitation and excited Er atoms, respectively. Further,  $\tau_{eff}^{ex}$  and  $\tau_{eff}^{Er}$  are effective life times of Er-trapped excitons and excited Er atoms, respectively. In such a scheme equations 1, 2, and 3 describe the time dependence of the concentrations of free carriers, excitons capable of transferring their energy to Er atoms, and excited Er atoms capable of luminescence, respectively. In the process description given by the above equations several simplifications, in respect to the real situation, have been included. The most important here are the assumptions that i) the laser energy absorbed by the crystal is mainly converted into exciton generation, that ii) the energy transfer to erbium is not saturated (i.e. the concentration of excited Er atoms is much smaller than that of the "excitable" ones and therefore does not limit the energy transfer process), and that iii) all the generated (free) excitons can transfer their energy to Er core. The last assumption means that an important step in the excitation scheme - a transformation from free excitons (FE) to Er BE system - is not explicitly included. To a certain



extent the fact that not all the generated free excitons will be bound at Er-related traps can be incorporated in the exciton generation constant  $\alpha$ , but in this way the influence of the Er atom itself on the capture of an exciton cannot be accounted for. Both effective life times can be seen as superpositions of 2 independent components corresponding to alternative decay mechanisms:

$$\frac{1}{\tau_{eff}^{ex}} = \frac{1}{\tau_{TR}} + \frac{1}{\tau_{A1}} = \frac{1}{\tau_{TR}} + c_{A1}n, \quad (4)$$

$$\frac{1}{\tau_{eff}^{Er}} = \frac{1}{\tau_R} + \frac{1}{\tau_{NR}} = \frac{1}{\tau_R} + c_{A2}n, \quad (5)$$

where  $\tau_{TR}$  is the time constant characteristic for the energy transfer between the BE and Er core,  $\tau_R$  is the radiative recombination time of excited Er atoms, and  $\tau_{A1} = (c_{A1}n)^{-1}$  and  $\tau_{NR} = (c_{A2}n)^{-1}$  are the nonradiative recombination time constants describing the Auger energy transfer to CB electrons from Er BE and excited Er core, respectively. The observed Er-related PL intensity will then be proportional to the concentration of the excited erbium atoms  $N^*$  and their radiative life time:

$$I_{PL} \propto \frac{N^*}{\tau_R}. \quad (6)$$

#### PL Decay Measurements

Upon a steady excitation level equilibrium concentrations of electrons  $n_0$ , excitons  $(N^{ex})^0$ , and excited erbium atoms  $(N^*)^0$  will be reached. These will lead to particular values of both effective life times  $\tau_{eff}^{ex}$  and  $\tau_{eff}^{Er}$  and of PL intensity. When the excitation is terminated, the equilibrium concentrations will decay with their kinetics determined by the rate equations (1-3). The fastest decay will be that of excess electrons in the conduction band. When  $n$  has been annulled then, following Eq.(2), we can write:

$$\frac{d}{dt}N^{ex} = \alpha n^2 - \frac{N^{ex}}{\tau_{eff}^{ex}} = -\frac{N^{ex}}{\tau_{TR}}. \quad (7)$$

As a solution we get an exponential decay of the exciton concentration, with the decay time being now the transfer time  $\tau_{TR}$ :

$$N^{ex} = (N^{ex})^0 \exp\left(-\frac{t}{\tau_{TR}}\right). \quad (8)$$

(In view of a very short life time of excess electrons  $n$  we have assumed here the equilibrium exciton concentration  $(N^{ex})^0$  as the initial value of the decay). The onset of the exponential decay of Er-bound excitons will coincide with the beginning of the decay of boron-bound excitons which could be observed experimentally in the same sample. The exponential decay of the excitons will lead also to the decay of the concentration of excited erbium atoms. Following Eq.(3) this process, which determines the decay of the Er-related PL, can be described by:

$$\frac{d}{dt}N^* = \frac{(N^{ex})^0}{\tau_{TR}} \exp\left(-\frac{t}{\tau_{TR}}\right) - \frac{N^*}{\tau_R}. \quad (9)$$

The first term gives here an increase of the concentration of the excited Er atoms due to the energy transfer from bound excitons, and the second one corresponds to their radiative decay. (Since the excess electron concentration  $n = 0$  the nonradiative decay of Er is no longer possible and  $\tau_{eff}^{Er} = \tau_R$ ). Solving the above equation we get:

$$N^*(t) = \frac{(N^*)^0}{\tau_R - \tau_{TR}} \left\{ \tau_R \exp\left(-\frac{t}{\tau_R}\right) - \tau_{TR} \exp\left(-\frac{t}{\tau_{TR}}\right) \right\}. \quad (10)$$

(Here again we have neglected the decrease of  $N^*$  during the decay of excess electrons). The photoluminescence decay will then be given as:

$$I_{PL}(t) \propto \frac{1}{\tau_R} N^*(t) = \frac{(N^*)^0}{\tau_R(\tau_R - \tau_{TR})} \left\{ \tau_R \exp\left(-\frac{t}{\tau_R}\right) - \tau_{TR} \exp\left(-\frac{t}{\tau_{TR}}\right) \right\} . \quad (11)$$

The above formula describes the decay of the erbium-related photoluminescence when the excitation source is turned off and when the excess electrons are no longer present in the sample. In terms of an experiment it should describe the decay curve starting from the moment determined by the onset of boron BE luminescence decay. Since the Er radiative recombination time  $\tau_R$  is of an order of milliseconds and therefore longer than the excitation transfer time  $\tau_{TR}$ , it will govern the PL decay in its later phase. However, in the initial part also the second exponential term will be important and will lead to a relatively slow change of the Er photoluminescence intensity. This follows from the fact that, although no new Er-bound excitons are being generated, the ones already existing in the crystal continue to excite Er, while their effective life time is considerably increased, since the excess carriers concentration diminished and the energy transfer to CB is no longer possible. Therefore the exponential decay of Er PL will start with some time delay whose magnitude is related to the ratio between the radiative recombination time  $\tau_R$  and excitation time  $\tau_{TR}$ . Such an effect has been observed experimentally before [18] and is consistent with the intensity behavior described by Eq.(11).

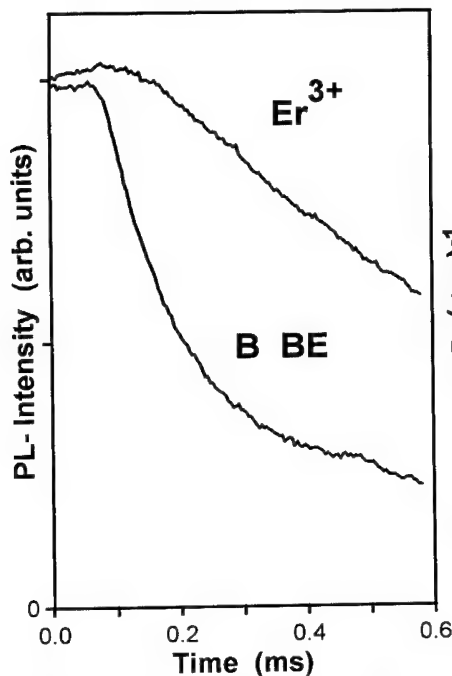


Figure 4. Comparison of the decay curves for Er-related and boron BE PL bands measured in the same sample; for Er  $\tau \approx 900\mu s$ ,  $T=4.2$  K.

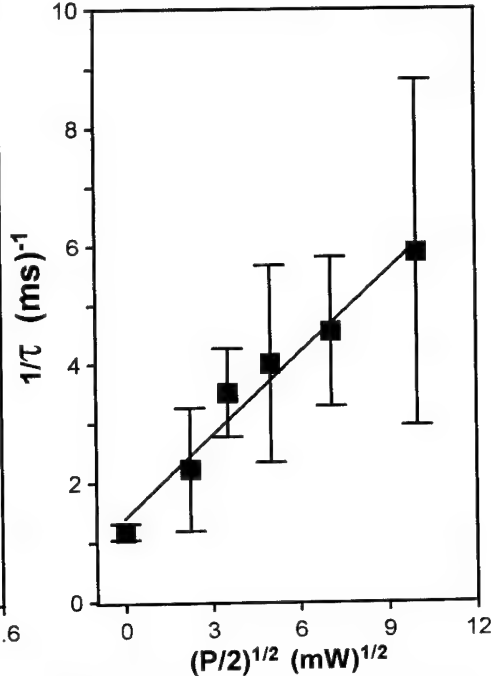


Figure 5. Dependence of the inverse decay time on the square root of the background excitation power for Si:Er. For details see text.

Fig.4 shows the decay of Er and boron BE luminescence as measured under on/off modulated laser power of 100 mW at LHe temperature. The material used for the decay measurements was

Fz-Si, implanted (1100 keV) at a temperature of 500°C to a dose of  $10^{14}$  Er/cm<sup>2</sup> - for details see Ref.[4]. The decay time, as determined from the depicted measurement, is approximately  $\tau \approx 900\mu s$ . Also a considerable delay in an onset of the Er decay curve, when compared to that of boron BE, can be seen. (In view of an extremely short life time of BE in Si, the depicted decay curve for B BE is illustrative for the response time of the experimental setup; all the measurements performed in this study concern decay constants which are clearly longer than the response time). As discussed before, the magnitude of the delay is related to the excitation transfer time  $\tau_{TR}$ . Based on the presented measurement its value can be estimated as  $\tau_{TR} \approx 50\mu s$ . This is an order of magnitude more than the estimation given in Ref.[17]. We should, however, bear in mind that in Ref.[17] an oxygen-rich material was investigated, while the PL decay results presented here have been obtained for float-zone (FZ), oxygen-lean samples, where the energy transfer to Er is known to be more difficult.

In order to investigate the influence of conduction electrons on the mechanism of Er photoluminescence we followed changes of PL decay characteristics in an experiment where the excitation laser beam was modulated to approximately 50% of its intensity, instead of the normally applied on/off chopping. This was accomplished by the use of a chopper blade made of a partially transparent material. In its concept such a measurement is similar to the two-beam experiment described in Ref.[15]. Under conditions of the partially, low-frequency modulated excitation the intensity of the photoluminescence spectrum will alternate between equilibrium values determined by laser power levels corresponding to 100% and 50% of the set value. Fig.5 shows the effective time constant of the intensity decay from the higher to the lower equilibrium levels as a function of the laser power applied during the decay, i.e. 50% of the nominal laser power  $P$ . The time constants given in the plot were always determined for the "later" part of the decay curve. According to the earlier presented description, for the partially modulated excitation, the effective decay time  $\tau_{eff}^{Er}$  will be given by Eq.(5), where the excess carrier concentration  $n$  is now a steady, time-independent value corresponding to the equilibrium value for the laser excitation at half power  $P/2$ :

$$\frac{1}{\tau_{eff}^{Er}} = \frac{1}{\tau_R} + f\left(\frac{P}{2}\right). \quad (12)$$

It should be noted that all the measurements depicted in Fig.5 were taken outside the saturation range, i.e. for the region where PL intensity is linearly proportional to excitation power, and which is well described by the rate equations set (1-3). As can be seen from the figure, the experimental data are linear in respect to the square root rather than to the full background excitation power level and could be fitted with the formula:

$$\frac{1}{\tau_{eff}} = A + B\sqrt{\frac{P}{2}}. \quad (13)$$

We conclude therefore that the equilibrium concentration  $n$  of the excess carriers is governed by the relaxation mechanism proportional to  $n^2$ . Such a result confirms the prominent role of exciton generation in the mechanism of Er luminescence in silicon. At the same time the observed data directly indicate a strong influence of the free carriers concentration  $n$  on the effective life time of the excited Er atom. This conclusion is evident when one compares the photoluminescence decay measured under on/off and partially modulated excitation.

In Fig.6 the decay of Er PL upon laser excitation of 25 mW is compared for the standard on/off and the partial modulation. In this case the zero on the time scale corresponds to the onset of the boron BE decay. The upper curve, taken without the background excitation, is characterized by a long delay of approximately  $\tau_d \approx 80\mu s$ , followed by a slow decay corresponding to the life time  $\tau \approx 800\mu s$ . The lower curve, which shows the decay under the background illumination corresponding to 12.5 mW, shows practically no delay ( $\tau_d < 20\mu s$ ), and is characterized by an almost 3 times faster decay  $\tau \approx 300\mu s$ . This dramatic shortening of the effective life time of the excited Er under background illumination confirms the important role of carriers in the de-excitation process and is consistent with the assumed nonradiative quenching of Er PL. As discussed before, a delay in the photoluminescence decay curve is due to the excitons, bound at Er-related trap,

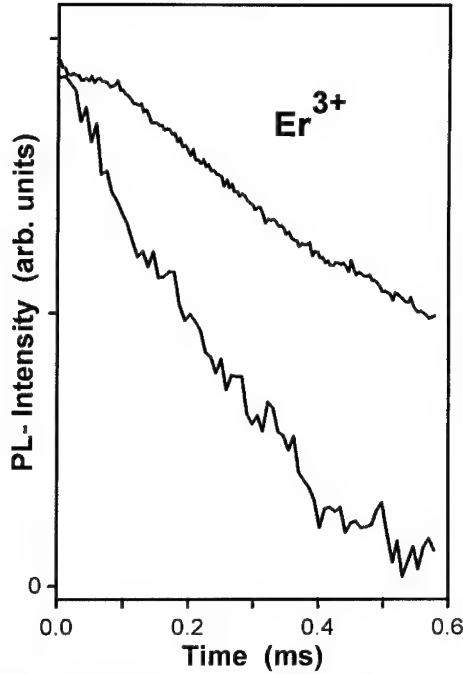


Figure 6. Decay of Er-related PL without - upper curve,  $\tau \approx 800\mu s$ , and with background excitation - lower curve,  $\tau \approx 300\mu s$ ,  $T=4.2$  K.

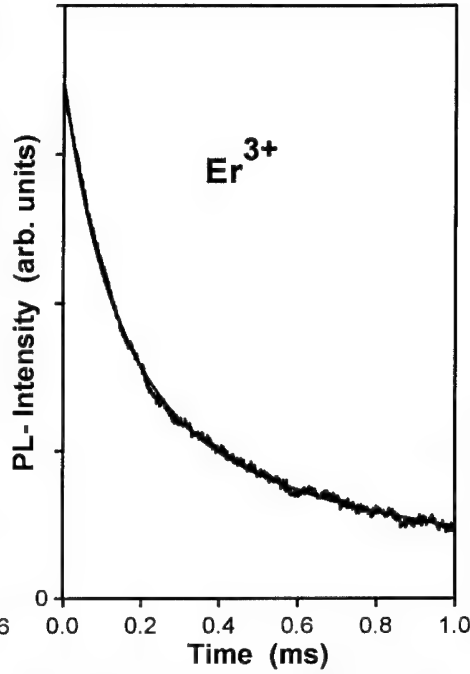


Figure 7. PL decay of Si:Er under 50 mW argon laser excitation,  $T=4.2$  K. For details of the fit - see text.

which continue to excite the Er core when the laser power is reduced, and is therefore linked to the effective life time of these states. The evident reduction of the delay time  $\tau_d$  shows the involvement of CB electrons in the quenching of the Er-related BE state. In this way the results presented here give an experimental confirmation of the free carrier quenching of the excitonic state intermediating Er luminescence. We can therefore conclude from our experiment that free carriers indeed limit both: the energy transfer to the Er core as well as its subsequent radiative recombination. This conclusion supports therefore the important role of these two processes as assumed in the rate equations Eqs.(1-3).

Fig.7 presents the Er PL decay as measured for an on/off modulated argon laser excitation (nominal power 50 mW). The experimental data can be fitted as a superposition of two exponential curves: a faster one with  $\tau_1 \approx 500 \mu s$  and a slower one with  $\tau_2 \approx 2ms$ . The coexistence of a fast and a slow components in the Er decay curve was observed before in oxygen-rich material [19] and attributed to two different Er-related centers. Here we report a similar effect also for Er-implanted FZ silicon. The data presented in Fig.7 could be alternatively fitted when we assumed that excited Er atoms could also transfer their energy to another center whose concentration diminished exponentially with time. In this case the PL decay would be described with the pseudo-exponential decay characterized by an effective life time  $\tau_{eff}^{Er}$  given as:

$$\frac{1}{\tau_{eff}^{Er}} = \frac{1}{\tau_R} + cN_x \exp\left(-\frac{t}{\tau_x}\right), \quad (14)$$

where  $c$  is the coupling constant, and  $N_x$  and  $\tau_x$  initial concentration and life time of the deacti-

vator, respectively. Using Eq.(14) a good fit to the experiment could be obtained yielding in that case both time constants of approx. 2 ms. Further studies are necessary to explore which of the alternative descriptions is more adequate.

#### POSSIBLE DEFECT-RELATED EXCITATION OF Er PL IN Si

We finally turn our attention to the 873 meV band reported recently in Er-implanted Cz-Si annealed briefly at 1100°C temperature [20,11]. We note that, in a sample where the intensity of this band is big - see Fig.8, the width of the PL line appearing in the region of Er luminescence is increased and its maximum is shifted toward higher energies. The positions of both, very strong in this case, PL bands coincide nearly precisely with the D1 and D2 lines reported earlier in silicon annealed under stress and identified with dislocations [21]. The same lines were later detected also in laser-annealed ion-implanted silicon [22]. In this situation an interesting question arises whether the PL bands depicted in Fig.8 are related to Er, as expected from the sample preparation conditions and supported by an appearance of a band, which certainly overlaps with the PL spectrum usually assigned to Er, or to defects, as suggested by a close coincidence of their energies. In an attempt to solve that dilemma we studied the temperature dependence of the intensity of the spectrum and this turned out to be different from the one reported for D-lines [23]. Also the saturation behavior of both lines is puzzling - upon increased excitation power a strong asymmetric broadening on the high energy side develops for both lines. Such a behavior is characteristic for free-to-bound transitions and is difficult to reconcile with the intrashell character of Er luminescence, but also with the reported bound-to-bound character of the D1 line [22]. One cannot, however, exclude that a rapid annealing of heavily (Er) implanted material could result in formation of dislocations in the subsurface Er-rich layer. In such a case the close coincidence of the energy of D1 line with that of the 4f-shell transitions of  $\text{Er}^{3+}$  could offer a defect-related channel of a near-resonant transfer of energy to and from the Er core. This interesting situation clearly requires further studies. Even more so, since the 873 meV energy of the D2 line again coincides rather perfectly with one of the transitions for the  $4f^{12}$  configuration of the  $\text{Er}^{2+}$  ion.

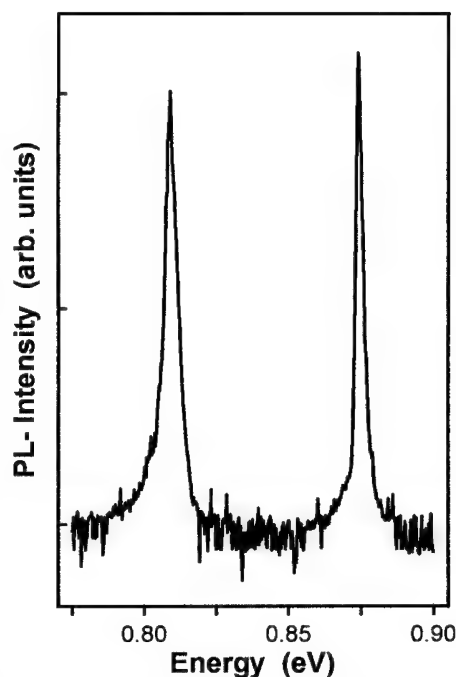


Figure 8. PL spectrum observed in Er implanted Cz-Si, annealed briefly at 1100°C,  $T=4.2$  K.

#### CONCLUSIONS

By investigating the influence of an electric field on the PL spectrum of Yb in InP we confirmed the excitonic character of its generation and found evidence for dissociation of the Yb BE system. Similar measurements for Si:Er show importance of a deep trap in the excitation scheme. By studying the photoluminescence decay of this system we could give experimental fingerprint of excess carrier-related processes limiting the energy transfer to the Er core and its subsequent radiative recombination.

# ACKNOWLEDGMENTS

The authors would like to thank E.O. Parshin and E.I. Shek for their help in preparing the samples. This project was partially sponsored by the Netherlands Foundation for Fundamental Research on Matter [Stichting voor Fundamenteel Onderzoek der Materie (FOM)] and Russian Fund for Fundamental Research (grant 96-02-17901a).

# REFERENCES

1. G. Aszodi, J. Weber, Ch. Uihlein, L. Pu-lin, H. Ennen, U. Kaufmann, J. Schneider, and J. Windscheif, *Phys. Rev.* **B31**, 7767 (1985).
2. I. de Maat-Gersdorf, T. Gregorkiewicz, C.A.J. Ammerlaan, P.C.M. Christianen, and J.C. Maan, proceedings of this symposium.
3. F. Priolo, G. Franzò, S. Coffa, A. Polman, S. Libertino, R. Barklie, and D. Carey, *J. Appl. Phys.* **78**, 3874 (1995).
- 4 F.P. Widdershoven and J.P.M. Naus, *Mat. Sci. Eng.* **B4**, 71 (1989).
5. P.B. Klein, *Solid State Commun.* **65**, 1097 (1988).
6. G.N. van den Hoven, J.H. Shin, A. Polman, S. Lombardo, and S.V. Campisano, *J. Appl. Phys.* **78**, 2642 (1995).
7. V.N. Abakumov, V.I. Perel, and I.N. Yassievich in Nonradiative Recombination in Semiconductors, Modern Problems in Condensed Matter Science **33**, edited by V.M. Agranovich and A.A. Maradudin, Elsevier Science Publishers B.V., Amsterdam 1991, pp. 172-188.
8. I. Tsimperidis, T. Gregorkiewicz, C.A.J. Ammerlaan, M. Godlewski, F. Scholz, and B. Lambert, *J. Appl. Phys.* **77**, 1523 (1995); I. Tsimperidis, T. Gregorkiewicz, and C.A.J. Ammerlaan, to be published.
9. W. M. Chen, I.A. Buyanova, A. Henry, W.-X. Ni, G.V. Hansson, and B. Monemar, *Mat. Sci. Forum* **196-201**, 473 (1995).
10. T. Gregorkiewicz, B.J. Heijmink Liesert, I. Tsimperidis, I. de Maat-Gersdorf, C.A.J. Ammerlaan, M. Godlewski, and F. Scholz in Rare Earth Doped Semiconductors, edited by G.S. Pomrenke, P.B. Klein, and D.W. Langer (*Mater. Res. Soc. Proc.* 301, Pittsburgh, PA 1993), pp. 239-250.
11. I. Tsimperidis, T. Gregorkiewicz, and C.A.J. Ammerlaan, *Mat. Sci. Forum* **196-201**, 591 (1995).
12. M.S. Bresler, O.B. Gusev, I.N. Yassievich, and B.P. Zakharchenya, to be appear in *Solid State (Fizika Tverdogo Tela* **38**, 5 (1996).
13. D.T. Xuan Thao, T. Gregorkiewicz, and C.A.J. Ammerlaan, to be published.
14. E. Efeoglu, J.H. Evans, T.E. Jackman, B. Hamilton, D.C. Houghton, J.M. Langer, A.R. Peaker, D. Perovic, J. Poole, N. Ravel, P. Hemment, and C.W. Chan, *Semicond. Sci. Technol.* **8**, 236 (1993).
15. J. Michel, J. Palm, F. Gan, F.Y.G. Ren, B. Zheng, S.T. Dunham, and L.C. Kimerling, *Mat. Sci. Forum* **196-201**, 585 (1995).
16. M.S. Bresler, O.B. Gusev, M.I. Macoviichuk, P.E. Pak, E.O. Parshin, E.I. Shek, N.A. Sobolev, I.N. Yassievich, and B.P. Zakharchenya in Tenth Feofilov Symposium on Spectroscopy of Crystals Activated by Rare-Earth and Transitional-Metals Ions, edited by A. Ryskin and V.F. Masterov, *Proc. SPIE* 2706, pp. 31-37 (1996).
17. J. Palm, F. Gan, and L.C. Kimerling in - see Ref.[16].
18. Jung H. Shin, G.N. van den Hoven, and A. Polman, *Appl. Phys. Lett.* **67**, 377 (1995).
19. S. Coffa, G. Franzò, F. Priolo, A. Polman, and R. Serna, *Phys. Rev. B* **49**, 16313 (1994).
20. N.A. Sobolev, O.V. Alexandrov, M.S. Bresler, O.B. Gusev, E.I. Shek, M.I. Makoviichuk, and E.O. Parshin, *Mat. Sci. Forum* **196-201**, 597 (1995).
21. N.A. Drozdov, A.A. Patrin, V.D. Tkachev, *Pis'ma Zh. Eksp. Teor. Fiz.* **23**, 651 (1976); *Sov. Phys. JETP Lett.* **23**, 597 (1976).
22. R.H. Vebbing, P. Wagner, H. Baumgart, and H.J. Queisser, *Appl. Phys. Lett.* **37**, 1078 (1980).
23. R. Sauer, J. Weber, J. Stolz, E.R. Weber, K.-H. Küsters, and H. Alexander, *Appl. Phys.* **A36**, 1 (1985).

# INCORPORATION, EXCITATION AND DE-EXCITATION OF ERBIUM IN CRYSTAL SILICON

M. J. A. DE DOOD, P. G. KIK, J. H. SHIN and A. POLMAN  
FOM Institute for Atomic and Molecular Physics  
Kruislaan 407, 1098 SJ Amsterdam, The Netherlands, e-mail : kik@amolf.nl

## ABSTRACT

Temperature quenching of the 1.54  $\mu\text{m}$  photoluminescence intensity and lifetime of Er in crystal Si was investigated between 12 K and 150 K. A p-type Czochralski-grown Si (100) wafer was doped with Er to a peak concentration of  $5 \times 10^{18} \text{ cm}^{-3}$  using 1.5 MeV ion implantation. The Er doped layer was co-implanted with N to a peak concentration of  $6 \times 10^{19} \text{ N cm}^{-3}$ . The sample was annealed at 490 °C for 2 hours and at 600 °C for 1 hour. The 1.54  $\mu\text{m}$  photoluminescence intensity shows a weak temperature quenching between 12 and 75 K, characterised by an activation energy of 1-10 meV. For temperatures above 75 K, a strong intensity quenching with an activation energy of  $210 \pm 10 \text{ meV}$  is observed. The luminescence lifetime decreases from 420  $\mu\text{s}$  at 12 K to 1  $\mu\text{s}$  at 170 K, and shows strong quenching behaviour above 75 K, characterised by an activation energy of  $135 \pm 5 \text{ meV}$ . The results are interpreted in terms of an impurity Auger energy transfer model. The lifetime quenching is attributed to a phonon assisted backtransfer process which becomes dominant at high temperatures. Intensity quenching is attributed to both the backtransfer process and a carrier de-trapping process which reduces the Er excitation rate. Spectral response measurements on Er implanted solar cells confirm the presence of a backtransfer process at room temperature.

## INTRODUCTION

In recent years much research has been done on trivalent rare earth ions as possible optical dopants in optoelectronic materials. When incorporated in Si these ions could provide a solution for the problem of the indirect bandgap, which precludes efficient light emission from Si. Erbium is an interesting dopant, because the transition within the  $\text{Er}^{3+}$  4f-shell from the first excited state ( $^4\text{I}_{13/2}$ ) to the ground state ( $^4\text{I}_{15/2}$ ) occurs at 1.54  $\mu\text{m}$  (0.8 eV), a standard telecommunication wavelength.

Several reports on the luminescence of Er in crystal Si have been made, and strong temperature quenching of the luminescence is observed in many cases [1 - 5]. To describe this quenching behaviour a model [3] has been proposed that includes trapping (T in Fig. 1) of an electron hole pair at an Er-related defect level in the Si bandgap, followed by excitation (E) of the Er through an Auger process, as well as two quenching

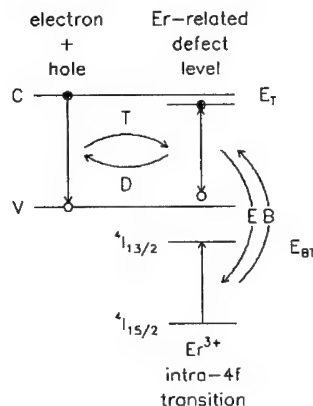


**Figure 1** Schematic picture of the excitation of  $\text{Er}^{3+}$  in Si. C and V denote the Si conduction and valence band, respectively. Trapping (T), Excitation (E), De-trapping (D) and Backtransfer (B) processes are indicated.

mechanisms: 1) de-trapping (D) of a bound e-h pair before it can transfer its recombination energy to the Er, and 2) a non-radiative backtransfer process (B) from an excited  $\text{Er}^{3+}$  ion to an excited state in the Si electronic system. Both quenching processes are phonon-assisted and are therefore more effective at high temperature. De-trapping and backtransfer will cause a reduction in the photoluminescence (PL) intensity. Backtransfer will also cause quenching in the PL lifetime. The aim of this paper is to investigate the effectiveness of both quenching processes.

## EXPERIMENTAL

A single crystal Czochralski-grown (CZ) Si wafer (p-type [100], B doped,  $1.0 - 10 \Omega\text{cm}$ ), was implanted with Si, Er and N at room temperature at a base pressure below  $10^{-6}$  mbar. To avoid channelling effects all implantations were performed at an angle of  $7^\circ$  off the surface normal. The sample was first implanted with  $3.5 \times 10^{15} \text{ cm}^{-2}$  450 keV Si to form a 700 nm thick buried amorphous layer, starting 160 nm below the surface. 225 keV N was implanted to a dose of  $1 \times 10^{15} \text{ cm}^{-2}$ . 1.46 MeV Er ions were implanted into the buried amorphous layer to a dose of  $1.6 \times 10^{14} \text{ cm}^{-2}$ . After implantation the sample was annealed at  $490^\circ\text{C}$  for 2 hours to sharpen up the amorphous-crystal interfaces, followed by a  $600^\circ\text{C}$  anneal for 1 hour to recrystallize the amorphous region from both sides. The anneals were done in a vacuum furnace at a background pressure of  $10^{-7}$  mbar. Er depth profiles were measured with Rutherford backscattering spectrometry (RBS) using a 2 MeV  $\text{He}^+$  beam at a scattering angle of  $165^\circ$  with a detector resolution of 14 keV. N depth profiles were measured using secondary ion mass spectrometry (SIMS) using a 6 keV  $\text{O}_2^+$  beam.

PL measurements were done using the 515 nm line of an Ar ion laser as a pump beam. The laser beam was modulated using an acousto-optic modulator. The peak pump power ranged from 1 mW to 100 mW in a 1 mm diameter spot. The sample was mounted in a closed-cycle helium cryostat, using silver paint to ensure good thermal contact. The temperature was varied between 12 and 150 K. The luminescence signal was collected by a 48 cm monochromator in combination with a liquid nitrogen cooled Ge detector using standard lock-in techniques. The spectral resolution was 3 nm. Luminescence lifetimes were measured using 1 ms pump pulses with a power of 1 W and a repetition frequency of 20 Hz, by monitoring the detector signal on an averaging digital oscilloscope. The overall system response time was 0.5  $\mu\text{s}$ .

In this paper we also analyse spectral response measurements on passivated emitter, rear locally-diffused (PERL) Si solar cells, which were implanted with 3.5 MeV Er ions to doses of  $1 \times 10^{13} \text{ cm}^{-2}$  and  $3 \times 10^{13} \text{ cm}^{-2}$  and were annealed at  $1060^\circ\text{C}$  for 60 min. and  $1000^\circ\text{C}$  for 75 min. The solar cells were made at the University of New South Wales, and their detailed electrical characteristics are reported in ref. [6]. From these measurements the absolute external quantum efficiency was determined, defined as the number of electron-hole pairs collected per incoming photon.

## RESULTS

Figure 2 shows the Er depth profile after annealing (solid line). The Er distribution is described by a Gaussian profile peaking at a depth of 490 nm, showing a full width at half maximum (FWHM) of 310 nm and a peak concentration of  $5 \times 10^{18} \text{ cm}^{-3}$ . No difference was observed between random or channelling RBS spectra in the Er part of the spectrum, indicating that the Er is distributed randomly in the Si.

The N concentration profile is also shown in Fig. 2, as indicated by the dashed line. It shows a peak concentration of  $6 \times 10^{19} \text{ cm}^{-3}$  at a depth of 580 nm and a FWHM of 200 nm. No redistribution of the Er [7] was observed after recrystallizing the a-Si. This is



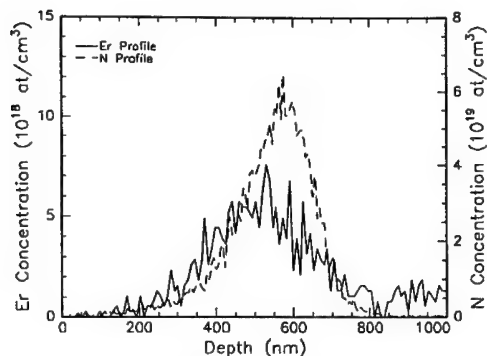


**Figure 2** Er concentration profile as measured by RBS (solid line), and N concentration profile as measured by SIMS (dashed line).

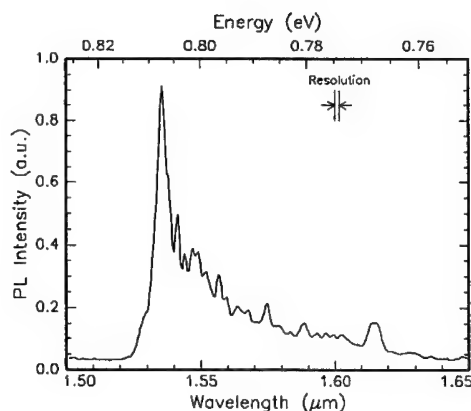


**Figure 3** PL spectrum of Er doped Si measured at 12 K, at a pump power of 20 mW and a spectral resolution of 3 nm.

attributed to the fact that N, like other impurities as O and C, prevents Er segregation [4, 8].

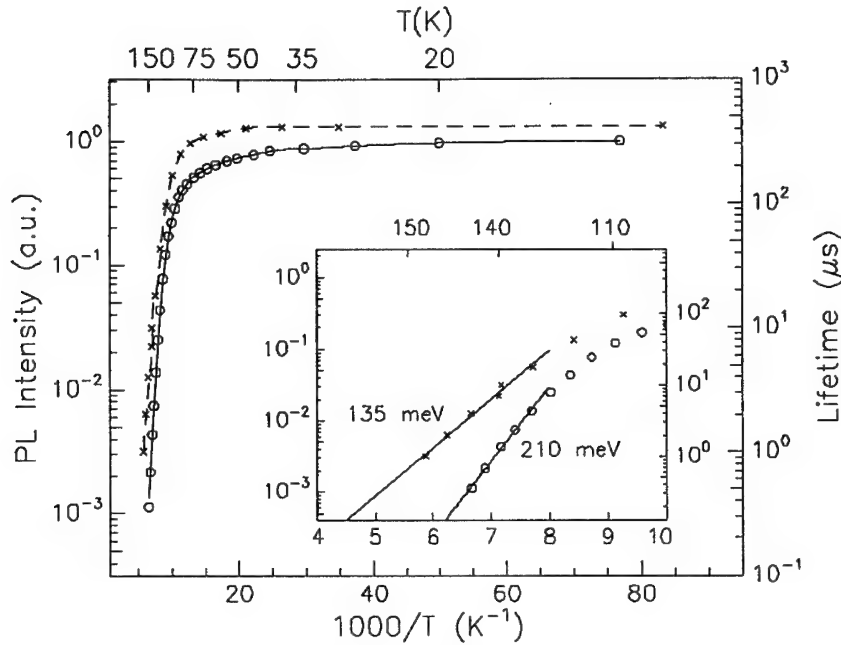
Figure 3 shows the PL spectrum of the sample at 12 K, pumped with a laser power of 20 mW. The main peak around 1.536  $\mu\text{m}$  is due to radiative decay from the first excited state ( $^4I_{13/2}$ ) to the ground state ( $^4I_{15/2}$ ) of  $\text{Er}^{3+}$ . The luminescence lifetime at 1.54  $\mu\text{m}$  is 420  $\mu\text{s}$ . The small peak around 1.615  $\mu\text{m}$  has a lifetime shorter than 30  $\mu\text{s}$  and is known from heavy-ion irradiated CZ Si [9] and is probably not related to Er. The remaining structure in the spectrum is due to transitions between the different Stark-split levels in the manifolds. Measurements of PL spectra at various temperatures between 12 and 150 K show that no significant shift in the peak wavelength occurs as function of temperature.

Figure 4 shows the 1.54  $\mu\text{m}$  integrated  $\text{Er}^{3+}$  luminescence intensity as a function of temperature. All intensity measurements were made in a pump power range which showed a linear dependence of the PL intensity on pump power, i.e. no saturation effects occurred. Measurements at different temperatures were made at different pump powers, but all intensity measurements were normalised to

the value for a fixed pump power for the whole temperature range. As can be seen in Fig. 4 the PL intensity quenches by 3 orders of magnitude between 12 and 150 K.

Figure 4 also shows the PL lifetime as a function of temperature. The measured Er decay traces were not single exponential, therefore the lifetimes in Fig. 4 are defined as  $1/e$  decay times. As can be seen from the figure, the lifetime decreases from 420  $\mu\text{s}$  at 12 K to 1  $\mu\text{s}$  at 170 K. The quenching behaviour for lifetime and intensity show a similar trend. This shows that lifetime quenching, i.e. a backtransfer process (see Fig. 1), plays a significant role in the intensity quenching.

Figure 5 shows spectral response measurements at 300 K of PERL solar cells implanted with either  $1 \times 10^{13} \text{ Er cm}^{-2}$  or  $3 \times 10^{13} \text{ Er cm}^{-2}$  taken from ref. [6]. A spectral shape typical for Er absorption is observed for wavelengths around 1.54  $\mu\text{m}$ . The dashed



**Figure 4** Arrhenius plot of the integrated  $\text{Er}^{3+}$  luminescence intensity (open circles) and lifetime (crosses). The lines through the data are guides to the eye. The inset shows the high temperature data in detail. The lines are linear fits to the data, to determine the quenching activation energies.

lines indicate a background which is also seen in Si implanted solar cells and is attributed to implantation defects [6]. Implantation of a 3 times higher Er fluence results in a 3 times higher absorption. These data indicate that optically excited Er generates free carriers that are collected in the solar cell. This is direct experimental evidence for the existence of a non-radiative quenching process in which excited Er decays by the generation of a free electron-hole pair.

## DISCUSSION

To quantitatively analyse the observed temperature quenching of the  $\text{Er}^{3+}$  luminescence in Si in Fig. 4, the model of Fig. 1 is used. In this model a small fraction of the e-h pairs generated by the laser are trapped (T in Fig. 1) at an Er related defect level. With this trapping process an energy difference  $E_T$  is associated. The bound e-h pair can either recombine and excite the Er (E) or it can dissociate again (D). An excited  $\text{Er}^{3+}$  ion can decay by emission of a 1.54  $\mu\text{m}$  photon or by backtransfer (B) of the energy to a state in the Si electronic system. With this backtransfer process an activation energy  $E_{BT}$  is associated. The decay rate  $W$  of an excited  $\text{Er}^{3+}$  ion is given by :

$$W = W_{\text{rad}} + W_{\text{BT}} \cdot e^{-E_{BT}/kT} \quad (1)$$

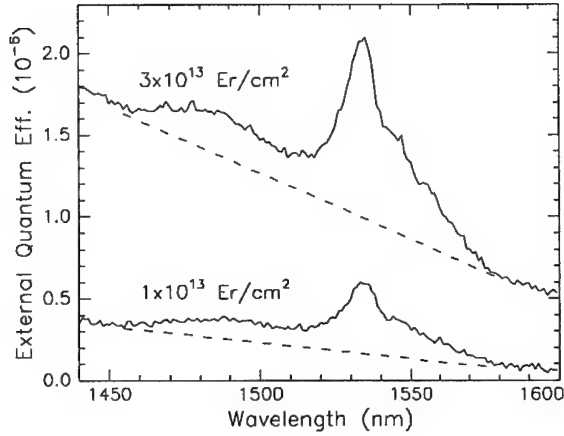


**Figure 5** Spectral response of PERL solar cells implanted with  $1 \times 10^{13} \text{ Er cm}^{-2}$  and  $3 \times 10^{13} \text{ Er cm}^{-2}$ . From ref. [6].

where  $W_{rad}$  is the radiative decay rate,  $W_{BT}$  is a pre-factor for the backtransfer process,  $k$  is Boltzmann's constant and  $E_{BT}$  is the activation energy for backtransfer. Priolo et al. [3], have developed a rate equation model which takes into account the de-trapping, but assume a constant  $W$ . Substituting Eqn. (1) in their model we find in the low pump power regime :

$$I \propto \frac{1}{W} \cdot \frac{1}{1 + C \cdot e^{-E_T/kT}} \quad (2)$$

in which  $E_T$  is the activation energy for de-trapping an e-h pair and  $C$  is given by :

$$C = \frac{\sigma_n \cdot N_C}{\sigma_p \cdot G_L \cdot \tau_C} \quad (3)$$

with  $\sigma_n$  and  $\sigma_p$  the capture cross-sections for an electron and a hole at the Er-related defect level,  $N_C$  the effective density of states at the bottom of the conduction band,  $G_L$  the optical generation rate and  $\tau_C$  the minority carrier lifetime. In general  $C$  is a function of temperature, as both  $N_C$  and  $\tau_C$  are temperature dependent. If we take  $N_C \propto T^{3/2}$  [10] and  $\tau_C \propto T^{1/2}$  by assuming that the carrier lifetime is determined by uni-molecular recombination, then  $C \propto T$ .

The inset of Fig. 4 shows the quenching behaviour for high temperatures in more detail. According to Eqns. (1) and (2), the slope for the high temperature lifetime data should yield  $E_{BT}$  and the slope for the intensity data should yield  $E_{BT} + E_T$ . Linear fits to the 5 highest temperature data points result in  $E_{BT} = 135 \pm 5 \text{ meV}$  and  $E_T = 75 \pm 10 \text{ meV}$ . Fitting the data to Eqns. (1) and (2) for high temperatures, and varying the temperature dependence of  $C$  from constant to  $\propto T$  yields the same result for the activation energies within the error bars. Fitting the lifetime data to Eqn. (1) yields an estimate of  $W_{BT} = 10^8 - 10^{10} \text{ s}^{-1}$ .

Below 75 K the intensity shows a very small quenching characterised by an activation energy of 1-10 meV, which is not seen in the lifetime quenching and is attributed to a second de-trapping process, possibly the dissociation of the weakly bound hole.

The energy difference between the Si bandgap (1.12 eV) and the Er excitation energy (0.81 eV) is around 300 meV. However, in this experiment the observed activation energies add up to only  $215 \pm 10$  meV. This suggests that the excitation and de-excitation processes involve different defect levels. Also, it is possible that the levels are broader than indicated in Fig. 1.

The spectral response measurement in Fig. 5 can be used to estimate the quantum efficiency (QE) for the backtransfer process. Assuming a smoothly decreasing background for the sample implanted with  $3 \times 10^{13}$  Er cm<sup>-2</sup>. The external QE at 1.54  $\mu$ m is found to be  $10^{-6}$ . This external QE is the product of the probability for absorption of a photon by an Er<sup>3+</sup> ion and the probability for an excited Er<sup>3+</sup> ion to de-excite and generate a free e-h pair. The probability for absorbing a photon is given by:  $N_{Er} \cdot \sigma_{abs}$ , with  $N_{Er}$  the optically active Er fluence and  $\sigma_{abs}$  the absorption cross-section. Assuming that all implanted Er is optically active and taking a typical value for the cross section ( $6 \times 10^{-20}$  cm<sup>2</sup> [11]), the absorption probability is estimated to be  $2 \times 10^{-6}$ . The QE for de-excitation can then be estimated to be on the order of 50 %, showing that the de-excitation process for Er can be quite efficient. The above estimate can be taken as an upper limit for the QE for de-excitation, as internal reflections in the solar cell were neglected. In reality, multiple reflections will take place in these PERL solar cells [12], which can significantly reduce the 50 % estimate.

## CONCLUSIONS

The 1.54  $\mu$ m Er<sup>3+</sup> luminescence intensity in crystal Si, co-doped with  $6 \times 10^{19}$  N cm<sup>-3</sup>, quenches by three orders of magnitude as the temperature is increased from 12 K to 150 K. The luminescence lifetime decreases from 420  $\mu$ s at 12 K to 1  $\mu$ s at 170 K. An impurity Auger model, which involves trapping of carriers at an Er related defect level, followed by energy transfer to the Er<sup>3+</sup> ion, is used to describe the data. Carrier de-trapping, characterised by an activation energy of  $75 \pm 10$  meV, results in a reduction in the Er excitation rate at high temperature. In addition, a non-radiative de-excitation process, with an activation energy of  $135 \pm 5$  meV reduces the Er luminescence efficiency at high temperature. Spectral response measurements on Er-implanted Si solar cells provide direct evidence for such a non-radiative quenching process, in which excited Er<sup>3+</sup> decays by the generation of a free electron-hole pair.

## Acknowledgements

F. W. Saris is acknowledged for stimulating discussions and work on Er-implanted Si solar cells. P. F. A. Alkemade is acknowledged for the SIMS measurement. This work is part of the research program of the Foundation for Fundamental Research on Matter (FOM) and was made possible by financial support from the Dutch Organisation for the Advancement of Research (NWO), the Foundation for Technical Research (STW), the IC Technology Program (IOP Electro-Optics) of the Ministry of Economic Affairs and the ESPRIT program (SCOOP) of the European Community.

## References

1. P. N. Favennec, H. l'Haridon, D. Moutonnet, M. Salvi, and M. Gauneau, *Jpn. J. Appl. Phys.* **29**, L524 (1990).
2. J. Michel, J. L. Benton, R. F. Ferrante, D. C. Jacobson, D. G. Eaglesham, E. A. Fitzgerald, Y. -H. Xie, J. M. Poate and L. C. Kimerling, *J. Appl. Phys.* **70**, 2672 (1991)

3. F. Priolo, G. Franzò, S. Coffa, A. Polman, S. Libertino, R. Barklie and D. Carey, J. Appl. Phys. **78** 3874 (1995)
4. A. Polman, G. N. van den Hoven, J. S. Custer, J. H. Shin, R. Serna and P. F. A. Alkemade, J. Appl. Phys. **77** 1256 (1995)
5. S. Coffa, G. Franzò, F. Priolo, A. Polman and R. Serna, Phys. Rev. B, **49**, 16313 (1994)
6. M. J. Keevers, F. W. Saris, G. C. Zhang, J. Zhao, M. A. Green and R. Elliman, Proceedings 13th European Photovoltaic Solar Energy Conference, Nice, Oct. 1995, p. 1215
7. J. S. Custer, A. Polman, and H. M. van Pinxteren, J. Appl. Phys. **75** 2806 (1994)
8. F. Priolo, S. Coffa, G. Franzo, C. Spinella, A. Camera, V. Bellani, J. Appl. Phys., **74**, 4936 (1993)
9. G. Davies, Physics Reports **176**, 83 (1989)
10. S. M. Sze, *Physics of Semiconductor Devices*, 2nd Ed., (Wiley, New York, 1981) p. 17
11. W. L. Barnes, R. I. Laming, E. J. Tarbox and P. R. Morkel, IEEE J. Quantum Electron. **27**, 1004, (1991)
12. M. A. Green, *Silicon Solar Cells*, (University of New South Wales, Sydney, 1995) Ch. 6

## THE POSSIBLE MECHANISM OF EXCITATION OF THE f - f EMISSION FROM Er-O CLUSTERS IN SILICON

V.F.MASTEROV, L.G.GERCHIKOV

Department of Experimental Physics, St.Petersburg State Technical University,  
St.Petersburg 195251, Russia, masterov@tuexph.spb.su

### ABSTRACT

The  $\text{Er}_2\text{O}_3$  quantum dot (cluster) with dimensions about  $1.2\text{nm}$  in silicon is discussed as the possible source of the Er related emission in  $\text{Si:Er}_2\text{O}_3$ , excited by photogenerated carriers or in a light-emitting diodes (LED) at forward bias. This quantum dot is represented as a spherical quantum well  $0.9\text{eV}$  in depth. The electron level with energy about  $0.15\text{eV}$  below the bottom of the silicon conduction band plays role of an electron trap. The trapped electron interacts with a hole in valence band of silicon forming "indirect" exciton bonded to quantum well. The energy is transferred to f - shell of erbium by the Auger electron - hole recombination.

### INTRODUCTION

The problem of an energy transfer from photogenerated carriers to f - electron of the rare-earth center in semiconductor is a primary consideration in physics of the rare-earth doped semiconductors. It is a complicated problem, especially in the case of complex centers involving the rare-earth ion and the other impurity atoms. The  $\text{Er}^{3+} - \text{O}(6)$  complex is known to be an optically active center in  $\text{Si:Er}_2\text{O}_3$  [1]. It was suggested [2] that the annealed f - f emission spectra originate in (111) c- $\text{Er}_2\text{O}_3$  nanoplatelets with dimensions  $1\text{nm} \times 2.5\text{nm}^2$ . The two strong peaks originate from recombination at the two inequivalent Er sites of the 16 formula unit cell of  $\text{Er}_2\text{O}_3$ . However, the process of energy transfer from silicon bulk to erbium in nanoplatelets was not discussed in [2].

In this paper we proposed the simple model of the mechanism of an excitation of the Er related emission in cluster  $\text{Er}_2\text{O}_3$  in silicon by Auger recombination of an electron localized within quantum well (QW) with a hole in the silicon valence band. In this model the  $\text{Er}_2\text{O}_3$  cluster forms a spherical quantum well in the silicon band structure. The photogenerated electron is trapped on a level within the well and interacts with a hole in valence band of silicon forming "indirect" exciton bonded to the well. The energy is transferred to erbium ion by the electron-hole Auger recombination.

### MODEL

The basis for our model is the quantum dot of  $\text{Er}_2\text{O}_3$  (nanoplatelet in [2]) with dimensions in the order of the lattice parameter  $a(\text{Er}_2\text{O}_3) \approx 1.05\text{nm}$  in silicon. It is necessary to add to this size the correction  $d$  which represents an adaptation or transition length needed to change the cation coordination number  $N_c$  from  $N_c = 6$  in  $\text{Er}_2\text{O}_3$  to  $N_c = 4$  in silicon. According to [2] this length is equal to about  $0.12\text{nm}$ . Hence, the characteristic dimension of  $\text{Er}_2\text{O}_3$  dot is about  $1.2\text{nm}$ . As a first approximation, we assume that this dot represents a spherical quantum well with radius  $R \approx 0.6\text{nm}$  in an energy scheme of  $\text{Si:Er}_2\text{O}_3$ . The depth of the well may be obtained from band gaps of erbium oxide and silicon  $E_g(\text{Er}_2\text{O}_3) = 5.4\text{eV}$ ,  $E_g(\text{Si}) = 1.17\text{eV}$  (at  $T = 0\text{K}$ ), and the energy parameters of oxygen and silicon atoms. The top of valence band in  $\text{Er}_2\text{O}_3$  is formed by  $2p$  states of oxygen [3] and by  $3p$  states - in silicon. That's why we should estimate the energies of  $p$  states in free atoms

O and Si. Using the method of determination of an atomic parameters, proposed previously [4], we obtained  $E_p(O) = -13.6eV$  and  $E_p(Si) = -8.15eV$ . Thus the valence band edge in the Er-O complex  $E_V(Er_2O_3)$  lies about  $5eV$  below the position of the valence band edge in the bulk  $E_V(Si)$ . So the complex represents a weakly transparent barrier of  $5eV$  high for holes while for electrons it acts as quantum well with the depth of  $U=0.9eV$  which has the discrete electron level with binding energy  $0.15eV$ . The f - levels lie close to the bottom of well according to band structure of rare-earth metal oxides [3]. The described energy scheme is presented in Fig. 1.

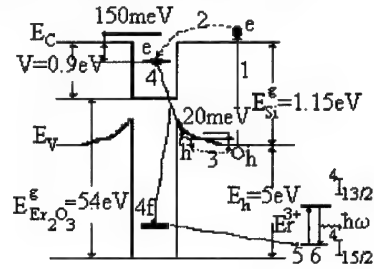


Fig. 1 The schematic illustration of the quantum well  $Er_2O_3$  in silicon; 1-photogeneration of electron-hole pair; 2-capture of an electron on the level within well; 3-capture of a hole, forming of exciton; 4-Auger process; 5- $Er^{3+}$  ion excitation; 6-f-f emission.

Certainly, it's needed a quantum-chemical calculation of the energy structure of the Si- $Er_2O_3$  system to receive further support of this scheme. Nevertheless the proposed model offers a clearer view of the process of excitation of the Er related emission in silicon codoped with erbium and oxygen. The electron level within the well plays role of an electron trap. The trapped electron attracts by Coulomb interaction a hole in valence band of silicon forming "indirect" (in space) exciton. Then the Auger recombination of an electron and a hole takes place, as a result of which some energy is transferred to one of  $Er^{3+}$  ions in  $Er_2O_3$  dot. It should be noted that twenty-four of the rare-earths are on sites with twofold rotational symmetry ( $C_2$ ) and eight are on sites with threefold rotary inversion symmetry ( $C_{3i}$ ) in the unit cell of erbium oxide [5].

The electron and hole energies as well as their wave functions should be calculated in order to determine time of the Auger process. This time plays the important role in an efficiency of Er related emission because it dictates the number of the erbium ions which can be excited in a given quantum dot.

## THE ENERGIES AND WAVE FUNCTIONS

Now we estimate the energy  $E_e$  of electron bound to the Er-O complex using the above proposed model. The electron effective mass should be different inside and outside the QW. Inside the QW we put the effective mass equal to the free electron mass  $m_0$  and in the bulk semiconductor we take the average mass  $m_c$  of the silicon conduction band. There is a single spherical symmetric electronic state with the energy determined by the transcendental equation

$$\tan(kR) = -\frac{km_c}{\kappa}, \quad (1)$$

where  $k = \sqrt{2m_0(U + E_e)} / \hbar$  is the electron wave vector in the QW region,  $\kappa = \sqrt{2m_c(-E_e)} / \hbar$  is the wave function decrement in the bulk, the electron energy  $E_e$  is measured from the conduction

band edge in silicon  $E_c$ . The result of solution Eq.(1) is shown in the Fig. 2. Certainly the proposed model is very rough. The aim of this simulation is to demonstrate that the electron localized within the Er-O complex with the characteristic radius  $R \approx 0.6nm$  has energy which corresponds to the position of the real electron level  $E_e = -0.15eV$ . Indeed, the electron wave function presented in the Fig. 3 shows that the main part of the electron density is concentrated in the QW. We have also provided the similar calculation for the infinity deep QW and have obtained the results close by the order of magnitude.

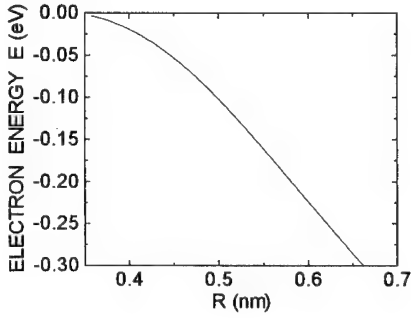


Fig. 2. Electron energy level as a function of Er-O complex radius.

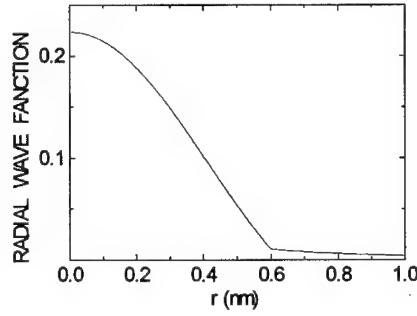


Fig 3. Radial wave function  $R_0$  of electron state bound to Er-O complex with  $R = 0.6nm$

Electron bound to the Er-O complex can trap the hole. Below the hole binding energies and wave functions are calculated within the spherical Luttinger model[6]. In this model hole states are characterized by the angular momentum  $J$  and the parity. The hole wave functions in the spherical symmetrical potential is of the form [7]:

$$\Psi_h(\mathbf{r}) = R_l(r)\Omega_{JM} + R_{l+2}(r)\Omega_{JM,l+2}, \quad (2)$$

where  $\Omega_{JM} = \sum_{\mu=\pm\frac{3}{2}, \pm\frac{1}{2}} C_{l,M-\mu,3/2,\mu}^{JM} Y_{l,M-\mu}(\vartheta, \varphi) u_{M-\mu}$ ,  $u_\mu$  is the valence band Bloch function,  $C_{lm,3/2,\mu}^{JM}$

are the Clebsh-Gordon coefficients,  $l = J - 3/2$  or  $l = J - 1/2$  depending on the parity. We will be interested in the lowest hole states of the both parity which have  $J = 3/2$ ,  $l = 0$  for even and  $l = 1$  for odd state. As it will be shown the character size of the hole orbit proves to be a few times larger than the Er-O complex radius. So we can take the electron potential as  $-e^2/\epsilon r$ ,  $\epsilon$  is the dielectric permeability. The radial wave functions obey the following equations [7]:

$$\gamma_1 \left( \frac{\partial}{\partial r} - \frac{1}{r} \right) \left( \frac{\partial}{\partial r} + \frac{3}{r} \right) R_2 + 2\gamma_2 \left( \frac{\partial}{\partial r} - \frac{1}{r} \right) \frac{\partial}{\partial r} R_0 = \frac{2m_0}{\hbar^2} \left( E - E_v - \frac{e^2}{\epsilon r} \right) R_2 \quad (3a)$$

$$\gamma_1 \left( \frac{\partial}{\partial r} + \frac{2}{r} \right) \frac{\partial}{\partial r} R_0 + 2\gamma_2 \left( \frac{\partial}{\partial r} + \frac{2}{r} \right) \left( \frac{\partial}{\partial r} + \frac{3}{r} \right) R_2 = \frac{2m_0}{\hbar^2} \left( E - E_v - \frac{e^2}{\epsilon r} \right) R_0 \quad (3b)$$

for even state and



$$\begin{aligned}
\left(\gamma_1 + \frac{8}{5}\gamma_2\right)\left(\frac{\partial}{\partial r} - \frac{2}{r}\right)\left(\frac{\partial}{\partial r} + \frac{4}{r}\right)R_3 + \frac{6}{5}\gamma_2\left(\frac{\partial}{\partial r} - \frac{2}{r}\right)\left(\frac{\partial}{\partial r} - \frac{1}{r}\right)R_1 &= \frac{2m_0}{\hbar^2}\left(E - E_v - \frac{e^2}{\epsilon r}\right)R_3 \\
\left(\gamma_1 - \frac{8}{5}\gamma_2\right)\left(\frac{\partial}{\partial r} + \frac{3}{r}\right)\left(\frac{\partial}{\partial r} - \frac{1}{r}\right)R_1 + \frac{6}{5}\gamma_2\left(\frac{\partial}{\partial r} + \frac{3}{r}\right)\left(\frac{\partial}{\partial r} + \frac{4}{r}\right)R_3 &= \frac{2m_0}{\hbar^2}\left(E - E_v - \frac{e^2}{\epsilon r}\right)R_1
\end{aligned} \quad (4)$$

for odd state.

Here  $E_v$  denotes the valence band position,  $\gamma_1$  and  $\gamma_2$  are the Luttinger constants which are expressed through the hole masses  $\gamma_1 = m_0(m_{lh}^{-1} + m_{hh}^{-1})/2$  and  $\gamma_2 = m_0(m_{lh}^{-1} - m_{hh}^{-1})/4$ . We assume that the Eqs.(3,4) describe the hole motion in the bulk semiconductor and in the Er-O complex as well. Since the Er-O complex represents a weakly permeable barrier for holes the parameters of Eqs.(3,4) in the QW region are not very essential for the hole binding energy. So we take the same value for heavy hole mass  $m_{hh}$  in the QW and in the bulk. For light holes we take into account in the Kane model [9] the nonparabolisity of the energy spectrum caused by the mixing of the valence states and the states of the QW bottom which lies quite close to the hole energies. The numerical solution of Eq.(3,4) gives the following results for the hole binding energies:  $E_h - E_v = 0.021\text{eV}$  for even state and  $E_h - E_v = 0.011\text{eV}$  for odd state. Note that using the zero boundary conditions for the hole wave functions on the QW surface gives the similar results. The radial parts of the hole wave functions are shown in the Fig. 4.

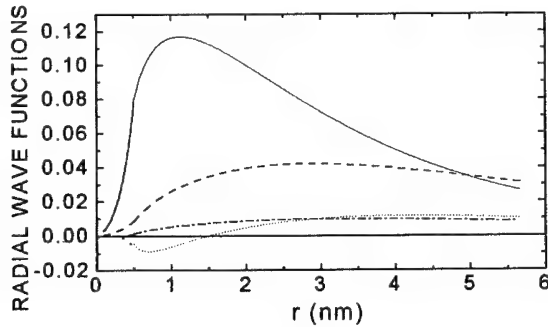


Fig.4. Radial wave functions of the hole bound to the Er-O complex. For even state  $R_0$  (solid line) and  $R_2$  (dot line). For odd state  $R_1$  (dashed line) and  $R_3$  (dash and dot line).

#### THE AUGER PROCESS

With the help of the obtained electron and hole wave functions we can calculate the matrix element of the Auger recombination of electron and hole bound to the Er-O complex and excitation of an Er f-electron from the ground level  $f$  to the excited level  $f'$  [8]:

$$\begin{aligned}
M_{Ex} &= \int V(\mathbf{r}) \Psi_h^*(\mathbf{r}) \Psi_e(\mathbf{r}) d\mathbf{r}, \\
V(\mathbf{r}) &= \int \frac{e^2}{|\mathbf{r} - \mathbf{r}'|} \Psi_{f'}^*(\mathbf{r}') \Psi_f(\mathbf{r}') d\mathbf{r}'
\end{aligned} \quad (5)$$

where  $\Psi_h, \Psi_e$  are the wave functions of the hole and the electron bound to the Er-O complex,  $\Psi_{f'}, \Psi_f$  and are the wave functions of Er f-electrons. Since the characteristic value of the f-shell radius  $r' \approx r_f \approx 0.08nm$  is much smaller than the radius of the electron and the hole motion the multipolar expansion for  $V(\mathbf{r})$  can be used

$$V(\mathbf{r}) = \frac{ed_{ff'}}{r^2} P_1(\cos(\theta)) + \frac{eQ_{ff'}}{r^3} P_2(\cos(\theta)) \quad (6)$$

where  $P_l$  are Legendre polynomials,  $d_{ff'}$  and  $Q_{ff'}$  are the dipole and quadrupole Er matrix elements. The zero term of the expansion  $\propto 1/r$  does not contribute to the Eq.(6) due to orthogonality of Er wave functions  $\Psi_{f'}, \Psi_f$ .

As it will be shown the main contribution to the Auger matrix element gives the area of the bulk semiconductor near the Er-O complex where we can write the electron and the hole wave functions, according to the effective mass approximation, as a composition of distinct components corresponding to the different energy bands of silicon

$$\Psi_{e,h} = \sum_i \Psi_i^{(e,h)} u_i, \quad (7)$$

where  $u_i$  are the Bloch functions of the  $i$ -th band and  $\Psi_i^{(e,h)}$  are the envelope wave functions. The conduction band is the nearest to the electron level and might have the largest wave function component of the electron state, but as it was shown [8] the overlapping integral of valence and conduction band Bloch functions gives zero contribution to the  $M_{ex}$ . So we shall consider the valence component of the electron wave function  $\Psi_v^{(e)}$ . The latter may be easily written down if we again use here the assumption concerning the mixing of the conduction and valence band states in the Er-O complex according to the Kane model [9] and also that the valence band envelope wave functions are continuous on the Er-O complex surface. The  $\Psi_v^{(e)}$  is of the form of the free light hole wave function with  $J = 1/2$  and  $l = 1$ . Its magnitude is determined by the condition of valence band wave function continuity on the QW surface

$$\Psi_v^{(e)} = \frac{\frac{\partial}{\partial r} R_0 \Big|_{r=R}}{\sqrt{2m_0 E_{s_{Er_2O_3}}}} \frac{k_1(\kappa_{lh} r)}{k_1(\kappa_{lh} R)} \Omega_{1/2, M, 1}. \quad (8)$$

Here

$$R_0(r) = \sqrt{\frac{2}{R + \frac{m_c(\kappa^2 m_o^2 + k^2 m_c^2)}{\kappa(\kappa^2 m_o^2 + k^2 m_c^2)}}} \frac{\sin(kr)}{r} \quad (9)$$

is the radial electron wave function in the QW region,  $E_{s_{Er_2O_3}}$  is  $Er_2O_3$  energy gap,  $\kappa_{lh} = \sqrt{2m_{lh}(E_{s_{Si}} + E_e)}$  is the modulus of light hole wave vector in silicon at  $E = E_e$ ,  $k_1(x)$  is the spherical McDonald function. Thus, the silicon part of Auger matrix element is of the form:

$$M_1 = \int_{r>R} V(\mathbf{r}) \Psi_v^{(h)*}(\mathbf{r}) \Psi_v^{(e)}(\mathbf{r}) d\mathbf{r}, \quad (10)$$

where the hole wave function  $\Psi_v^{(h)}$  (2) is determined by solution Eqs.(3,4). Within the spherical model only the even hole state with  $l=0$  takes part in the dipole transition, while the odd state with  $l=1$  takes part in the quadrupole transition. The numerical calculations give the following results for this kind of transitions:  $M_{d_1} = 5.2 \cdot d_{ff} / er_f meV$  and  $M_{Q_1} = 4.8 \cdot 10^{-2} Q_{ff} / er_f^2 meV$ .

We have also estimated the contribution of the internal QW region into the Auger matrix element  $M_2$  using the same consideration as for  $M_1$ . The largest overlapping might have here the wave function components corresponding to the Er-O conduction states. The electron wave function we write as

$$\Psi_c^{(e)} = \frac{R_0}{\sqrt{4\pi}} u_\mu, \quad (11)$$

where  $R_0$  is determined by Eq.(9),  $u_\mu$  is the Bloch function with spin  $\mu$ . For the hole state we assume the continuity of the wave function component corresponding to the energy band with symmetry similar to  $Er_2O_3$  conduction states. We supply that the  $\Gamma_2$  band states of the silicon Brillouin zone center have such symmetry and can easily mix with conduction states of  $Er_2O_3$ . Mixing between the  $\Gamma_2$  and valence band hole states can be described in the Kane model. Thus using the continuity boundary condition at the QW surface we get

$$\Psi_c^{(h)} = \frac{\left( \frac{\partial}{\partial r} R_0 + \left( \frac{\partial}{\partial r} + \frac{3}{r} \right) R_2 \right) \Big|_{r=R}}{\sqrt{4m_{hh} \Delta E}} \frac{i_1(\kappa r)}{i_1(\kappa R)} \Omega_{3/2, M, 1} \quad (12)$$

for even hole state and

$$\Psi_c^{(h)} = \frac{\left( \left( \frac{\partial}{\partial r} - \frac{1}{r} \right) R_1 + 3 \left( \frac{\partial}{\partial r} + \frac{3}{r} \right) R_3 \right) \Big|_{r=R}}{\sqrt{20m_{hh} \Delta E}} \frac{i_2(\kappa r)}{i_2(\kappa R)} \Omega_{3/2, M, 2} \quad (13)$$

for odd hole state.  $R_l(r)$  are the hole radial wave functions which obtained from the solution the differential equations (3,4),  $\Delta E \approx 4eV$  is the energy distance between the top of the valence band and the  $\Gamma_2$  band edge. Here we neglect the Coulomb potential in comparison with kinetic energy so the radial wave functions dependence is described by the modified spherical Bessel functions  $i_l(x)$  with decay decrement  $\kappa = \sqrt{2m_0(E_c - U - E_h)} / \hbar$ . After numerical integration

$$M_2 = \int_{r<R} V(\mathbf{r}) \Psi_c^{(h)*}(\mathbf{r}) \Psi_c^{(e)}(\mathbf{r}) d\mathbf{r}, \quad (14)$$

we obtained  $M_d = -1.3 \cdot d_{ff'} / er_f \text{ meV}$  and  $M_{Q_2} = 1.5 \cdot 10^{-2} Q_{ff'} / er_f^2 \text{ meV}$ . Comparing these results with  $M_1$  we see that the main contribution to Auger matrix element gives the area of the bulk semiconductor close to the Er-O complex. Combining  $M_1$  and  $M_2$  we finally obtain

$$\begin{aligned} M_d &= 4 \cdot d_{ff'} / er_f \text{ meV}, \\ M_Q &= 6 \cdot 10^{-2} Q_{ff'} / er_f^2 \text{ meV}. \end{aligned} \quad (15)$$

Since the  $ff'$  optical transition is forbidden by the parity the dipole matrix element is small  $d_{ff'} / er_f \approx 10^{-3}$  [8] while  $Q_{ff'} / er_f^2 \approx 1$ . So the quadrupole transitions turns out to be more effective in the Auger recombination processes. In the used spherical model only the even hole state takes part in this transition. But actually the shape of Er-O complex is no longer spherical [2] so the even hole state can also contribute to  $M_Q$ . Note that the ratio of the numerical factors in the Eq.(15) is much smaller than the parameter of the multipolar expansion  $r_f / R$ . It is caused by the additional smallness of the hole wave function near the Er-O complex surface for odd state (see Fig. 4) and connected with the action of centrifugal barrier. The minimum orbital angular momentum value of the even state  $l = 0$  and its wave function  $R_0$  is larger than the  $R_1$  ( $l=1$ ) near the Er-O complex surface. Therefore the real value of Auger matrix element can be larger then  $M_{Ex} \approx 6 \cdot 10^{-2} \text{ meV}$  according to the Eq.(15) if we take into account participation of the even hole state in the quadrupole transition.

## DISCUSSION

As indicated above the energy of exciton bound to the Er-O complex  $E_{ex} = E_e - E_h = 0.96 \text{ eV}$  is larger than the energy of transition between the first excited state  $^4I_{13/2}$  and the ground state  $^4I_{15/2}$  of  $\text{Er}^{3+}$  ion  $\hbar\Delta_{ff'} = 0.8 \text{ eV}$ . Thus, from the conservation of energy it follows that the energy excess  $\Delta E \approx 0.2 \text{ eV}$  should be transferred to a "third body". Usually (see, for example, [8]) this difference is ascribed to electron-phonon interaction. So following [8] we shall take into account possibility of the multiphonon transitions accompanying the Auger pumping. In that work the following expression for probability of such process was obtained in the one mode model and Condon approximation:

$$W = \frac{2\pi}{\hbar} \frac{|M_{Ex}|^2}{\hbar\omega_p} \frac{S^N}{N!} e^{-S}, \quad (16)$$

where  $S = (\Delta_{ff'} - \hbar\omega_p) / 2\hbar\omega_p$  is the Huang-Rhys factor,  $\hbar\omega_p$  is the Er luminescence energy,  $\hbar\omega_p$  is the local phonon energy and  $N = (E_{ex} - \Delta_{ff'}) / \hbar\omega_p$  is the number of local phonons emitted during the Auger pumping. The local phonon energy  $\hbar\omega_p$  may be estimated [10] for rare-earth center in semiconductors as equal  $\sim 40 \text{ meV}$ . However, from the photoluminescence excitation spectrum in  $\text{GaAs:Er}$  [11] and from the comparison between emission and absorption spectra of the ion in phosphate glass [12] it follows that difference  $(\Delta_{ff'} - \hbar\nu_{ff'})$  is much smaller than  $\hbar\omega_p$ . Consequently, the Huang - Rhys factor approaches zero and the Auger process time  $\tau_A = 1/W \approx 1.5 \cdot 10^{-6} / S^5$  according to Eq.(16) tends to infinity. Besides, the optical phonons taken into account in this case have a finite energy. That is why it is impossible to satisfy exactly the conservation of energy law.

So we shall discuss the another Auger excitation processes where the energy excess  $\Delta E$  is transferred to the free carriers (electron or hole) in the host semiconductor. These processes are shown in Fig.5(a,b). In the first place, we consider the case of n-type semiconductor (Fig.5a) when free electron in the silicon conduction band receives the energy excess  $\Delta E$

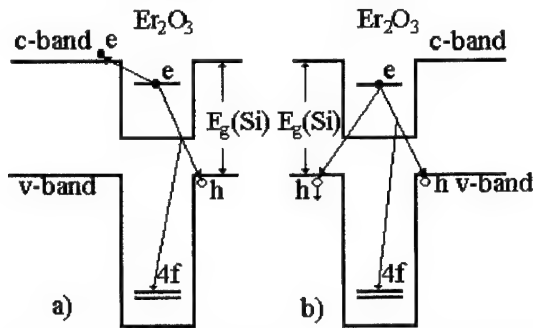


Fig.5 The diagrams of the f-f emission excitation by Auger process;  $\Delta E$  is transferred to electron (a), to hole (b).

The Feynman diagram of this process is presented in Fig.6a. Notice that the electron energy in intermediate state is quite close to the energy of the discrete level  $E_e$ . It only differs by the energy  $\Delta E$  from  $E_e$ . Since  $\Delta E \approx 0.2eV$  is much smaller than the electron quantum size energy  $\hbar^2 / m_0 R^2 \approx 1eV$  the main contribution to the Auger recombination amplitude is given by the term where the intermediate state is the electron level bound to the Er-O complex.

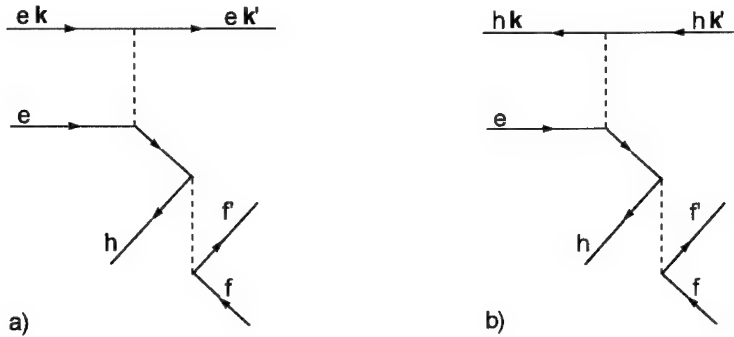


Fig.6 The Feynman diagrams of the processes presented in Fig.5.  $\Delta E$  is transferred (a) to electron, (b) to hole. Indexes  $f$  and  $f'$  denote  $f$ -shell states of Er,  $e$  and  $h$  denote electron and hole states bound to the Er-O complex,  $e\mathbf{k}$  and  $h\mathbf{k}$  denote the free electron and hole states.

So the given Auger recombination has a resonance character. It proceeds mostly via the discrete electron level  $E_e$ . In the resonance approximation we can write the Auger recombination amplitude as

$$M = \frac{M_A M_{Ex}}{\Delta E}, \quad (17)$$

where

$$M_A = \int \Psi_e^*(\mathbf{r}) \Psi_e(\mathbf{r}) \frac{e^2}{|\mathbf{r} - \mathbf{r}'|} \Psi_{\mathbf{k}'}^*(\mathbf{r}') \Psi_{\mathbf{k}}(\mathbf{r}') d\mathbf{r} d\mathbf{r}' \quad (18)$$

is the Auger amplitude which corresponds to the upper part of the Feynman diagram Fig. 6a,  $\Psi_e$  is the wave functions of the discrete electron level and  $\Psi_{\mathbf{k}}, \Psi_{\mathbf{k}'}$  are free electron wave functions of the initial and final states with wave vectors  $\mathbf{k}$  and  $\mathbf{k}'$  respectively. Taking into account that characteristic value of the bound electron coordinates  $r \approx R$  while free electron radius vector  $r' \approx \lambda = 1/k' > R$  and also that  $\Psi_e \approx R^{-3/2}$ ,  $\Psi_{\mathbf{k}} \approx 1$  we obtain the following estimation for  $M_A \approx \frac{e^2}{\lambda} \lambda^3$ .  $M_{Ex}$  is amplitude of Auger pumping (5) which corresponds to the lower part of the Feynman diagram Fig. 6a. It was evaluated earlier (see the Ex.(15)).

According to the Fermi golden rule the probability of the Auger processes is given by

$$W = \frac{2\pi}{\hbar} \int |M|^2 f_e(k) \delta\left(\frac{\hbar^2 \mathbf{k}'^2}{2m_e} - \frac{\hbar^2 \mathbf{k}^2}{2m_e} - \Delta E\right) \frac{d\mathbf{k}}{(2\pi)^3} \frac{d\mathbf{k}'}{(2\pi)^3}, \quad (19)$$

where  $f_e(k)$  is electron distribution function. After integration over the  $\mathbf{k}'$  and  $\mathbf{k}$  and substituting the Eq.(17) and estimation for  $M_A$  we obtain

$$W \approx \frac{|M_{Ex}|^2 e^4 m_e}{\pi \hbar^3 \Delta E^2} (n_e \lambda^3). \quad (20)$$

Here  $\lambda = \hbar / \sqrt{2m_e \Delta E}$  is the wave length of outgoing electron,  $n_e$  is the electron concentration. Thus the rate of this Auger process is concentration dependent. Expression (20) is proportional to the number of electrons in the reaction area ( $n_e \lambda^3$ ). According to Eq.(20) the Auger pumping time equals  $\tau_A \approx 10^{12} n_e^{-1}$ .

In the p-type semiconductor the energy excess is transferred to the free hole. The diagrams corresponding to this process are shown in the Fig.5b and the Fig.6b. In this case we obtained the results described by Eq. (20) with changing  $n_e$  by  $n_h$  and  $m_e$  by  $m_h$ . The heavy hole wave length is  $\sqrt{m_h / m_{hh}}$  times smaller than for the light hole. So the energy excess is transferred mostly to the light holes. Thus in the both cases the efficiency of the Auger pumping is determined by the concentration of the major carriers  $n$ . If  $n \geq 10^{18}$  time of the Auger recombination turns out to be small enough  $\tau_A \leq 10^{-6} s$  to excite the major part of the Er ions in the Er-O complex. However at high electron concentration the probability of trapping of two electrons by the QW becomes significant and the energy level of two electron state may raise into the conduction band of silicon, if the Hubbard energy has positive value. It will decrease efficiency of Er related emission. That is why the p - silicon seems to be preferable for the emitting devices.

The electron concentration on the Er-O complex can be essentially larger if two electrons occupy the energy level within the QW. It may take place in semiconductors having larger band gap where the QW should be deeper. It is necessary to take into account that the energy of two electron level is larger then the one electron sate energy due to the Hubbard energy  $U_H$ . So the

condition  $|E_e| < U_H$  takes place. We estimate the Hubbard energy as  $U_H \approx 0.3 \text{ eV}$ . Note that in this case the exciton energy  $E_{\text{Ex}} = E_e - E_h$  can be larger than  $1.2 \text{ eV}$  and the  $\text{Er}^{3+}$  ion may be excited also into the  $^4I_{1/2}$  state. The excess energy  $\Delta E = E_{\text{Ex}} - \hbar\Delta_{ff}$  is transferred to second electron which is excited into conduction band of silicon. The Feynman diagram is same one as presented in Fig. 6a but all initial electron states are localized. For the Auger amplitude of this process we have changed the free electron wave function  $\Psi_{\mathbf{k}}(\mathbf{r})$  by the wave function of localized electron  $\Psi_e(\mathbf{r})$  in Eq.(18). It leads to the following estimation for  $M_A \approx \frac{e^2}{R} R^{3/2}$ . The probability of the considered process is

$$W = \frac{2\pi}{\hbar} \int |M|^2 \delta\left(\frac{\hbar^2 \mathbf{k}^2}{2m_c} - E_e - \Delta E\right) \frac{d\mathbf{k}}{(2\pi)^3}, \quad (21)$$

where  $\mathbf{k}$  is a momentum of the ionized electron. After integrating over the electron wave vector and substitution the expression for  $M$  we obtain

$$W \approx \frac{e^4 |M_{\text{Ex}}|^2 m_c R}{\pi \hbar^4 \Delta E^2} \sqrt{2m_c E_k}. \quad (22)$$

where  $E_k$  is the kinetic energy of ionized electron in silicon conduction band. Notice that the considered Auger pumping is a threshold process, therefore its probability is proportional to  $\sqrt{E_k}$ . It is necessary to transfer to second electron a sufficient amount of energy to excite it into the conduction band, i.e.  $E_k = \Delta E + E_e > 0$ . For characteristic value  $E_k \approx 100 \text{ meV}$  Eq.(22) gives the following estimation for Auger pumping time  $\tau_A \approx 3 \times 10^{-8} \text{ s}$ . Such short time is the result of high effective concentration of localized electron on Er-O complex  $n_e \approx 10^{21} \text{ cm}^{-3}$ .

The temperature dependence of the f - f emission intensity in Si:Er at excitation by the Auger recombination of a bonded exciton was discussed in [13]. The following expression for  $I(T)$  have been obtained in that work:

$$I \propto \frac{A}{1 + B e^{-0.15 \text{ eV} / kT}}, \quad (23)$$

where

$$A = \frac{\tau}{\tau_{\text{rad}} \tau_A} N_{\text{Er}}. \quad (24)$$

Here  $\tau$  is the decay lifetime of erbium related emission;  $\tau_{\text{rad}}$  is the radiative lifetime;  $\tau_A$  is the Auger process time;  $N_{\text{Er}}$  is the concentration of erbium, and  $B$  is value which is determined by a carriers parameters. As a first approximation, the authors [13] assumed that the dominating contribution to the temperature quenching arose from the exponential term in the dominator of the Eq(23). In our model the two exponents with energies  $E_h \approx 20 \text{ meV}$  and  $E_e \approx 150 \text{ meV}$  should appear in the Eq(23). Really it has been found experimentally [14] that from 100 to 200K, the electroluminescence intensity (at forward bias on  $p$ - $n$  junction) decays with an activation energy of approximately  $17 \text{ meV}$ . Above 200K a much steeper decay with an activation energy of about  $200 \text{ meV}$  occurs. A similar dependence was also observed in photoluminescence studies of Si:Er.

. From the preceding text it follows that the Auger process time falls far short of the measured decay time which is equal to  $\tau \approx 10^{-4} \text{ s}$  for the fast component of the Er related emission spectrum

of silicon. We take into account that the decay time is determined by the lifetime of the excited state of  $\text{Er}^{3+}$  ion. Such a large time is caused by the forbidding of the f - f dipole optical transition by parity. The carriers times are of about  $10^{-12}$  s, that's why for the time  $10^{-4}$  s almost all erbium ions in  $\text{Er}_2\text{O}_3$  dot should be excited by Auger process. On the other hand,  $\tau \approx \tau_{\text{rad}}$  and  $A \approx N_{\text{Er}}/\tau_A$ , consequently, the Auger process determines the f - f emission intensity.

Turning back to the model of a quantum dot, it should be noted that the severe dependence of the efficiency of the Er related emission from parameters of the postimplantation annealing should take place. At prolonged or high-temperature annealing, the  $\text{Er}_2\text{O}_3$  clusters with large size are produced. For large crystallite the misfit between the nanocrystallites and the host semiconductor will generate a high density of interfacial defects which increase the rate of nonradiative recombination. Besides an electron level in within wide quantum wells will lie close to its bottom, and the difference in energy  $E_e - E_h$  will be less than  $\Delta_{\text{ff}}$ . The experimental data suggest that intensity of Er related emission in silicon depends on temperature and time of annealing (see for example [15,16]).

It should be noted that there are 32 rare-earth ions and 48 oxygens in a cubic unit cell of c- $\text{Er}_2\text{O}_3$  [5]. Twenty-four of the rare-earths are on sites with twofold rotational symmetry ( $C_2$ ) and eight are on sites with threefold rotary symmetry ( $C_{3i}$ ). That is why in the PL and EL spectra there are two types of an optical activity centers having the different decay times because the  $C_2$  centers have a low symmetry in comparison with the  $C_{3i}$  centers. Certainly, the Er-O complexes in semiconductors do not all have dimensions which is equal to the lattice parameter of  $\text{Er}_2\text{O}_3$ . That is why according to literature data only from 10% to 50% of erbium ions are optically active centers. Besides at low electron (hole) concentration the Auger process time will be something like the radiative time. In this case efficiency of the f-f emission will be 30 times lower its maximum because one exciton will be excite only one of 32 Er ions in Er-O complex.

## CONCLUSIONS

The model of excitation of the Er related emission in silicon codoped with erbium and oxygen is proposed. This model offers a clearer view of how the energy is transferred from photogenerated carriers in host semiconductor to  $\text{Er}^{3+}$  ions in Er - O clusters. The proposed mechanism allows to explain the basic experimental facts: i) two types of the optically active centers with a different decay times; ii) two activation energies in temperature dependence of the Er related emission; iii) the strong dependence of the EL and PL intensity on annealing temperature and time.

This mechanism of the f - f emission excitation allows also to direct the ways for increasing the efficiency of the Er related emission in semiconductors codoped erbium and oxygen. In the first place, it is an increasing of a band gap of semiconductor or, more precisely, a rising of the bottom of conduction band. In this case the quantum well barrier is increased and the temperature range of effective emission should be expanded if two localized electrons take part in the Auger process. May be, this conception takes place in the case of the Er related photoluminescence of SIPOS [17], which have band gap of about  $2\text{eV}$ . Secondly, the increasing of the Auger recombination rate by way of a resonance transfer of energy from electron - hole pair to rare-earth ion may be possible. Thirdly, the oxygen concentration must be higher than the erbium concentration because ratio between oxygens and Er atoms in the unit cell of c- $\text{Er}_2\text{O}_3$  is 3:2.

## ACKNOWLEDGMENTS

We are grateful to Dr.G.Pomrenke and Dr.M.Markow for support, and to Dr.G.Zegrya and



Dr.N.II'in for helpful discussion. The work is supported by AFOSR in frame of Contract SPC-95-4037, Grant F-49620-94-1-0390 and by Science Counsel on Fundamental Spectroscopy (Russia).

#### REFERENCES

1. D.L.Adler, D.C.Jacobson, M.A.Marcus, J.L.Benton, J.M.Poate, P.H.Citrin, *Appl.Phys.Lett.* **61**, p.2181 (1992).
2. J.C.Phillips, *J.Appl.Phys.*, **76**, p.5896 (1994).
3. A.A.Samokhvalov in Rare-Earth Semiconductors, edited by V.P.Zhuze and I.A.Smirnov, (Leningrad, Russia 1977), p.5-47 (in Russian).
4. A.E.Vasil'ev, N.P.II'in, V.F.Masterov, *Sov.Phys.-Semicond.* **22**, p.1253 (1988).
5. R.M.Moon, W.C.Koehler, H.R.Child, and I.J.Raubenheimer, *Phys.Rev.*, **176**, p.722 (1968)
6. J.M.Luttinger, *Phys.Rev.* **102**, p.1030 (1956).
7. B.L.Gel'mont, M.I.D'yakov, *ZhTEF* **62**, p.713 (1972) (in Russian).
8. I.N.Yassievich, L.C.Kimerling, *Semicond.Sci.Technol.* **8**, p.718 (1993).
9. E.O.Kane, Semiconductors and Semimetals, Acad.Press Inc., **1**, p.75 (1966).
10. K.Uwai, H.Nakagome, K.Takahei, *Appl.Phys.Lett.* **50**, p.977 (1987).
11. H.Ennen, J.Wagner, H.D.Muller, and R.S.Smith, *J.Appl.Phys.* **61**, p.9877 (1987).
12. T.Ohtsuki, N.Peyghambarian, S.Honkanen, S.I.Najafi, *J.Appl.Phys.* **78**, p.3617 (1995).
13. F.Priolo, G.Franzo, S.Coffa, A.Polman, S.Libertino, R.Barklie, D.Carey, *J.Appl.Phys.* **78**, p.3874 (1995).
14. B.Zheng, J.Michel, F.Y.G.Ren, L.C.Kimerling, D.C.Jacobson, J.M.Poate, *Appl.Phys.Lett.* **64**, p.2842 (1994).
15. J.S.Custer, A.Polman, H.M.van Pinxteren, *J.Appl.Phys.* **75**, p.2809 (1994).
16. R.Serna, E.Shoeks, G.N.van den Hoven, A.Polman, *J.Appl.Phys.* **75**, p.2644 (1994).
17. G.N.van den Hoven, Jung H.Shin, A.Polman, S.Lombardo, S.U.Camprisano, *J.Appl.Phys.* **78**, p.2642 (1995).

## LUMINESCENCE QUENCHING IN ERBIUM-DOPED HYDROGENATED AMORPHOUS SILICON

A. POLMAN, JUNG H. SHIN, R. SERNA,<sup>a</sup> and G.N. VAN DEN HOVEN<sup>b</sup>  
FOM Institute for Atomic and Molecular Physics  
Kruislaan 407, 1098 SJ Amsterdam, The Netherlands, e-mail: polman@amolf.nl

W.G.J.H.M. VAN SARK and A.M. VREDENBERG  
Department of Atomic and Interface Physics, Debye Institute, University of Utrecht  
P.O. Box 80000, 3508 TA Utrecht, The Netherlands

S. LOMBARDO and S.U. CAMPISANO  
Dipartimento di Fisica, Università di Catania,  
Corso Italia 57, I-95129 Italy

### ABSTRACT

Hydrogenated amorphous silicon thin films, co-doped with oxygen, are made using low-pressure chemical vapor deposition (LPCVD) or plasma-enhanced chemical vapor deposition (PECVD). The films are implanted with Er to a peak concentration of 0.2 at.%. Room-temperature photoluminescence at 1.54  $\mu\text{m}$  is observed in both amorphous materials, after thermal annealing at 300-400 °C. The PECVD films with low O content (0.3, 1.3 at.%) show a luminescence intensity quenching by a factor 7-15 as the temperature is raised from 10 K to room temperature. The quenching is well correlated with a decrease in luminescence lifetime, indicating that non-radiative decay of excited  $\text{Er}^{3+}$  is the dominant quenching mechanism as the temperature is increased. In the LPCVD films, with 31 at.% O, the quenching is only a factor 3, and no lifetime quenching is observed. The results are interpreted in the context of an impurity Auger excitation model, taking into account the fact that oxygen modifies the Si bandgap and the Er-related defect levels in the gap.

### INTRODUCTION

Pure silicon is an impractical opto-electronic material. Due to its indirect band gap, the probability for direct band-to-band transitions is small, and charge carriers, generated either optically or electrically, will recombine non-radiatively. An interesting way to turn Si into a possibly practical opto-electronic material is by the doping with rare earth ions.<sup>1</sup> These ions have an incompletely filled internal 4f shell, shielded from the host by closed outer 5s and 5p shells. As a result, relatively sharp interatomic transitions can be obtained. Erbium has a transition from the first excited state to the ground state at 1.54  $\mu\text{m}$  (0.8 eV), an important telecommunication wavelength. The achievement of efficient photo- and electroluminescence from erbium in silicon depends on three critical factors:

- high concentrations of Er must be incorporated,
- the Er must be incorporated in an optically active configuration with high quantum efficiency (i.e. high luminescence lifetime), and
- the Er must be efficiently excited.

Until today, most of the work on these issues has focused on the incorporation of Er in crystal Si (c-Si) by ion implantation or molecular beam epitaxy.<sup>1</sup> High Er concentrations ( $10^{20}$  Er/cm<sup>3</sup> and higher) can be trapped in the Si crystal. However, it has been difficult to

fully activate such high concentrations. In fact, the maximum Er concentration<sup>2</sup> that can be optically activated in Czochralski-grown c-Si (CZ-Si) is only  $3 \times 10^{17}$  Er/cm<sup>3</sup>. In addition, strong temperature quenching of the 1.54  $\mu$ m Er<sup>3+</sup> luminescence intensity, a factor 300 between 77 and 300 K, is observed in Er-doped CZ-Si.<sup>3</sup>

The addition of impurities such as oxygen to Er-doped c-Si increases the Er active concentration, and causes a reduction in the temperature quenching<sup>3</sup> to a factor 30. As a result, room-temperature photoluminescence<sup>4,5,6</sup> and electroluminescence<sup>7,8</sup> at 1.54  $\mu$ m have been observed from Er-doped c-Si. Yet, the absolute internal luminescence quantum efficiencies for optimized O-co-doped c-Si:Er layers are below  $10^{-4}$ , too low for practical application. It seems therefore interesting to study other Si-based hosts for Er.

Amorphous silicon (a-Si) is a promising host material for Er. Being amorphous, it allows to side-step the problem of limited solubility of Er in crystalline semiconductors,<sup>9</sup> and to incorporate more of the impurities such as oxygen and carbon that are known to enhance the luminescence.<sup>4,6</sup> Our earlier work on Er doping of pure amorphous Si has shown luminescence only at low temperature (77 K).<sup>10</sup> The disadvantage of this material is that its electrical quality is rather poor, and it is therefore interesting to investigate amorphous materials with better electrical quality.

The advantage of hydrogenated amorphous Si (a-Si:H) is that it is a well characterized, mature semiconductor, with the possibility of direct deposition on optical materials, and it shows excellent electrical properties. In this paper, we present a photoluminescence characterization of lightly (0.3, 1.3 at.%)<sup>11</sup> and heavily (31 at.%)<sup>12</sup> oxygen doped hydrogenated amorphous silicon films, doped with Er by ion implantation. These films show room-temperature 1.54  $\mu$ m photoluminescence from Er<sup>3+</sup>, with an intensity higher than has been achieved in c-Si so far. Measurements of the temperature dependence of the luminescence of Er in a-Si:H show relatively small quenching (a factor 3-15), depending on the O content. The data are interpreted in terms of a model that assumes that the presence of O modifies the Si bandgap as well as the Er-related defect levels in the gap.

## EXPERIMENTAL

a-Si:H films were fabricated in two ways. 340 nm thick a-Si:H layers were deposited on Si(100) by low-pressure chemical vapor deposition (LPCVD) from SiH<sub>4</sub> and N<sub>2</sub>O at 620 °C. The H and O content in these films was 10 at.% and 31 at.%, respectively. Erbium was implanted at 500 keV to a dose of  $1 \times 10^{15}$  Er/cm<sup>2</sup>. The peak Er concentration, at a depth of 150 nm, was 0.2 at.%. These samples were annealed at 400 °C to obtain optimum luminescence. In addition, 250 nm thick films were deposited on glass (Corning 7059) by plasma enhanced chemical vapor deposition (PECVD) of SiH<sub>4</sub> at 230 °C. The H content in the films was 10 at.%, and a background concentration of 0.3 at.% O was also present, as measured using elastic recoil spectrometry. Erbium was implanted at 125 keV to a dose of  $4 \times 10^{14}$  Er/cm<sup>2</sup>, corresponding to a peak concentration (at a depth of roughly 35 nm) of 0.2 at.%. In some samples, additional O was implanted at 25 keV to a dose of  $7 \times 10^{15}$  O/cm<sup>2</sup>, resulting in a total peak O concentration of 1.3 at.%, which overlaps with the Er profile. After implantation, samples were annealed in vacuum (base pressure  $< 1 \times 10^{-6}$  mbar) for 2 hr. at various temperatures.

Photoluminescence (PL) spectra were measured using the 515 nm line of an Ar laser as the excitation source at a nominal power of 50 mW, and employing a mechanical chopper and standard lock-in techniques. All spectra were corrected for detection sensitivities.

A closed-cycle helium cryostat was used for low temperature measurements, and an averaging, digitizing oscilloscope was used for photoluminescence lifetime measurements.

## RESULTS

### LPCVD a-Si:H

Figure 1 shows a PL spectrum for the Er-implanted LPCVD (31 at.% O) film, annealed at 400 °C, measured at room temperature. The spectrum shows the characteristic  $\text{Er}^{3+}$  luminescence, peaked at 1.54  $\mu\text{m}$ . Figure 2(a) shows the temperature dependence of the 1.54

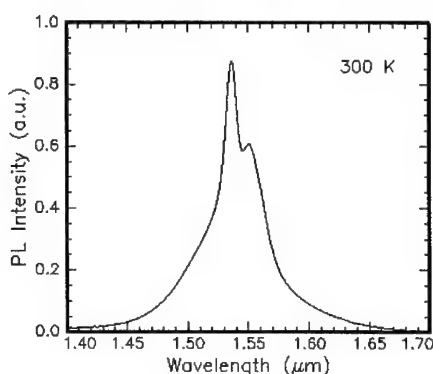


Fig. 1 Room temperature PL spectrum of Er-implanted LPCVD a-Si:H, annealed at 400 °C.  $\lambda_{\text{pump}} = 515 \text{ nm}$ .

$\mu\text{m}$  PL intensity of this sample (pump power 50 mW). A very weak temperature quenching of only a factor three is observed. For comparison, the quenching in typical Er-implanted CZ-Si samples (with and without co-doping with 0.2 at.% O, pump power 200 mW) is also shown. Clearly, the amorphous film shows higher PL intensities over the whole temperature range with much less quenching.

Luminescence lifetime measurements at 1.54  $\mu\text{m}$  have also been made. The decay curves showed a double exponential behavior with lifetimes of around 160 and 800  $\mu\text{s}$ ,<sup>12</sup> independent of temperature in the range 77-300 K, as can be seen in Fig. 2(b). The contribution of each decay component was independent of temperature. This lifetime behavior is quite different than for O or N co-doped crystal-Si which showed a lifetime quenching by a factor 10-500 between 10 and 200 K.<sup>3,13</sup>

Photoluminescence excitation spectroscopy experiments<sup>12</sup> (not shown) have indicated that the total areal density of optically active  $\text{Er}^{3+}$  in the LPCVD film amounted to  $(2 \pm 1) \times 10^{13} \text{ Er/cm}^2$ , i.e.  $2 \pm 1$  % of the implanted fluence.

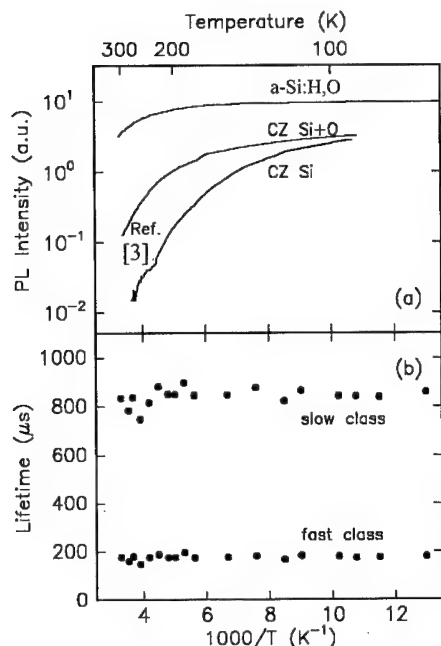


Fig. 2 (a) Temperature dependence of the 1.54  $\mu\text{m}$  PL intensity of Er-implanted LPCVD a-Si:H (pump power 50 mW) compared to that for Er-implanted CZ-Si from ref. 3 (pump power 200 mW) (b) Temperature dependence of the two lifetime components in the luminescence decay measurement for LPCVD a-Si:H.

#### PECVD a-Si:H

Figure 3 shows the room temperature PL spectra of Er-implanted PECVD a-Si:H films (0.3 at.% and 1.3 at.% O), annealed at 400 °C, displaying characteristic Er<sup>3+</sup> luminescence at 1.54  $\mu\text{m}$ . The inset shows the Er<sup>3+</sup> luminescence intensity at 1.54  $\mu\text{m}$  as a function of the annealing temperature. As can be seen, samples annealed at 300-400 °C display the optimum Er<sup>3+</sup> luminescence. No erbium related luminescence can be observed from either the as-implanted samples nor from the samples annealed at 500 °C.

The increasing and decreasing trends in the inset are attributed to the competing effects of removal of irradiation-induced defects and out diffusion of hydrogen as the annealing temperature is increased. Hydrogen is essential for passivating the defects inherent in a-Si:H and it has been

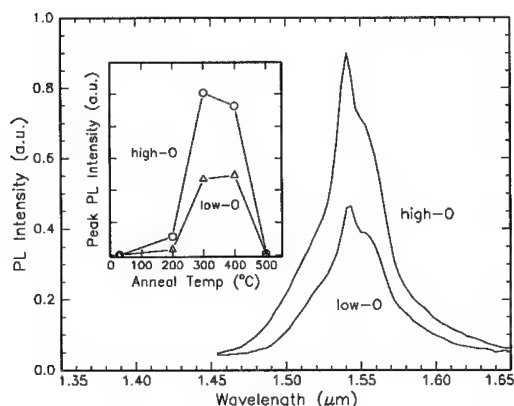


Fig. 3 Room temperature PL spectra of Er-implanted PECVD a-Si:H, O (0.3 and 1.3 at.% O), annealed at 400 °C. The inset shows the 1.54  $\mu\text{m}$  PL intensity as a function of annealing temperature.

shown before that Er in pure a-Si without hydrogen does not luminesce at room temperature.<sup>10</sup> The room-temperature PL peak intensity for the high-O sample is more than a factor 10 larger than that for Er-doped crystal Si co-doped with oxygen and annealed for optimum luminescence, and measured under identical conditions.

Figure 4 shows the temperature dependence of both the integrated  $\text{Er}^{3+}$  PL intensity and lifetime for the Er-implanted low-O a-Si:H film (0.3 at.% O), annealed at 400 °C. The inset shows the data above 160 K in detail, as well as data for the high-O sample (1.3 at.% O). All intensity data are normalized to the value at 10 K. Between 10 K and 110 K, the integrated  $\text{Er}^{3+}$  PL intensity shows a slight increase as the temperature increases. At the same time, the lifetime decreases. Above 110 K, a 15-fold reduction in the  $\text{Er}^{3+}$  luminescence intensity is observed as the temperature is increased to 300 K. Up to 250 K, the temperature quenching of the  $\text{Er}^{3+}$  luminescence intensity correlates well with that of the lifetime (see inset in Fig. 4). No lifetime measurements could be made at temperatures above 250 K as it became shorter than the system response time (30  $\mu\text{s}$ ). However, extrapolating the lifetime data to higher temperatures, it becomes clear that most of the intensity quenching above 160 K can be attributed to lifetime quenching. The high-O sample shows less quenching (only a factor 7 between 10 and 300 K), and again the trend in the intensity is correlated with the change in lifetime.

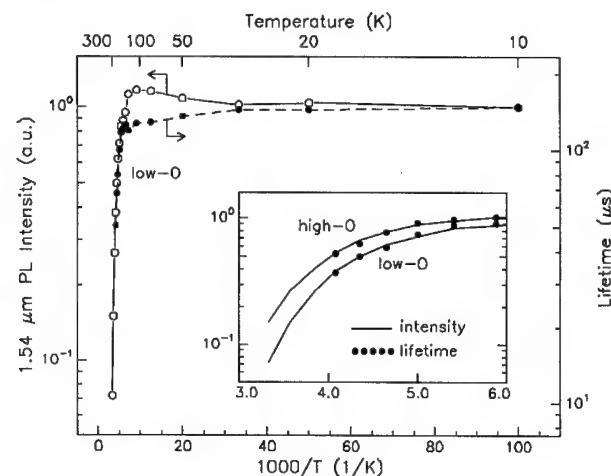


Fig. 4 Arrhenius plot of the normalized, integrated PL intensity (open circles and solid line) and lifetime (filled circles and dashed line) of Er-implanted PECVD a-Si:H:O (0.3 at.% O), annealed at 400 °C. The inset shows the curves in a smaller temperature range. Data for the high-O sample (1.3 at.% O) are also shown in the inset.

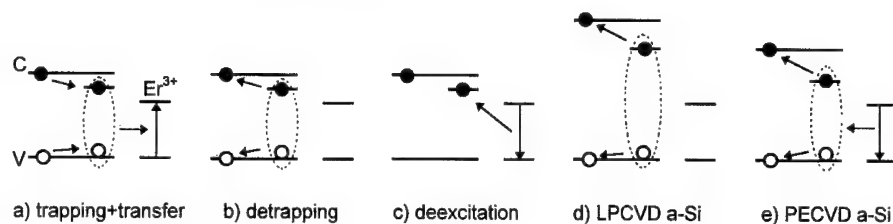


Fig. 5 Schematic of the excitation (a) and quenching (b,c) processes of Er in crystal Si, and of the quenching mechanisms in (d) LPCVD a-Si:H (30 at.% O), and (e) PECVD a-Si:H (0.3, 1.3 at.% O).

## DISCUSSION

The excitation of Er in Si most likely takes place through an Er-related level in the Si bandgap. An electron-hole pair may be bound to this level, recombine, and then transfer its recombination energy to the  $\text{Er}^{3+}$  ion through an Auger process. Subsequently, the excited  $\text{Er}^{3+}$  ion can decay by the emission of a photon. This model is indicated schematically for the case of crystalline Si in Fig. 5(a), which shows the Si conduction (C) and valence band (V), the  $\text{Er}^{3+}$  ground and first excited state (plotted relative to the valence band to facilitate comparison) and the Er-related defect level in the Si bandgap. Note that the mismatch between the Er transition energy (0.8 eV) and the Si bandgap (1.1 eV) is around 0.3 eV. Consequently, the Er-related defect level is located within 0.3 eV from the conduction band. In this model, the temperature quenching of the luminescence intensity in Er-doped Si can be a result of two distinct processes:

- a reduction in the excitation rate of  $\text{Er}^{3+}$  due to de-trapping of electrical carriers trapped at the Er-related level in the Si bandgap (Fig. 5(b)).<sup>6</sup> These processes decrease the luminescence intensity but do not affect the  $\text{Er}^{3+}$  luminescence lifetime.
- an increase in the non-radiative de-excitation rate of excited  $\text{Er}^{3+}$  due to coupling to defect levels in the Si bandgap, e.g. to the Er-related level itself or to other defect levels in the gap. In this case the Er ion decays to the ground state and an electron is excited from the valence band to a trap level. These non-radiative processes decrease the luminescence lifetime as well as the  $\text{Er}^{3+}$  PL intensity.

Both of these processes require the annihilation of phonons to account for the energy mismatch between initial and final state, and as a result their probability will increase with temperature. In crystal Si both these quenching processes take place.<sup>13</sup>

The data for LPCVD a-Si:H (31 at.% O) show no lifetime quenching (see Fig. 2). Hence there is no non-radiative de-excitation of excited  $\text{Er}^{3+}$  at higher temperatures. This may be associated to the fact that this material, due to the high O content, has a large bandgap (2.0 eV)<sup>14</sup>, and as a result a large energy mismatch gap has to be bridged for a de-excitation process to defect levels near the conduction band (see Fig. 5(d)). The small (factor 3) quenching in the intensity measured in Fig. 2 is then attributed to a small decrease in the excitation rate due to carrier de-trapping as the temperature is increased. The fact that this effect is small implies that the Er-related level is positioned relatively deep in the forbidden band (as indicated in Fig. 5(d)).

The PECVD a-Si:H films (0.3, 1.3 at.% O) do show lifetime quenching (see Fig. 4), indicating that in this material non-radiative de-excitation of Er can take place at elevated temperature. Indeed, this material has a smaller bandgap (1.6 eV) than the LPCVD material and as a result the non-radiative de-excitation of an excited  $\text{Er}^{3+}$  ion may involve a smaller energy mismatch (see Fig. 5(e)). The magnitude of the lifetime quenching accounts for most of the intensity quenching and therefore the de-trapping rate of carriers is only slightly temperature dependent. This implies that also in the PECVD material the Er-related level is positioned relatively deep in the forbidden band (see Fig. 5(e)).

The fact that in both types of a-Si:H the excitation rate is only slightly temperature dependent (i.e. small carrier de-trapping) contrasts the behavior of Er in crystalline Si, where it has been argued that the carrier de-trapping effect is important.<sup>6,13</sup> Consequently, in both a-Si:H<sub>2</sub>O materials the Er-related level is positioned deeper in the forbidden gap than in c-Si. Our data also correlate with previous work on III-V and II-VI semiconductors doped with Er,<sup>16</sup> that has shown the trend that the luminescence quenching is reduced as the bandgap is increased.

## CONCLUSION

In conclusion, we have observed room temperature 1.54  $\mu\text{m}$  photoluminescence from Er implanted PECVD and LPCVD grown a-Si:H thin films, co-doped with O at different concentrations (0.3, 1.3 and 31 at.%). The temperature quenching of the luminescence intensity between 10 and 300 K ranges from a factor 15 at low O content to only a factor 3 at the highest O content. In the low-O films, the quenching is primarily due to an increase in the non-radiative de-excitation rate of excited  $\text{Er}^{3+}$  at high temperature. For the material with 31 at.% O this de-excitation does not take place, and the temperature quenching is attributed to a slight reduction in the Er excitation efficiency with increased temperature.

## Acknowledgments

C.H.M. van der Werf is acknowledged for depositing a-Si:H films. Salvo Coffa is gratefully acknowledged for stimulating discussions on the topic of this paper. This work is part of the research program of FOM and made possible by financial support from NWO, STW, IOP-Electro Optics, and the ESPRIT program (SCOOP) of the European Community.

## References

- a) present address: Instituto de Optica, CSIC, Serrano 121, 28006 Madrid, Spain.
- b) present address: Philips Research Laboratories, Prof. Holstlaan 4, 5656 AA Eindhoven, The Netherlands.
- 1 See, for example, *Rare Earth Doped Semiconductors*, edited by G.S. Pomrenke, P. B. Klein, D. W. Langer, *Mat. Res. Soc. Symp. Proc.* **301** (1993), and this proceedings: *Rare Earth Doped Semiconductors II*, edited by S. Coffa, A. Polman, and R.N. Schwartz, *Mat. Res. Soc. Symp. Proc.* **422** (1996).
- 2 A. Polman, G.N. van den Hoven, J.S. Custer, J.H. Shin, R. Serna, and P.F.A. Alkemade, *J. Appl. Phys.* **77**, 1256 (1995).
- 3 S. Coffa, G. Franzò, F. Priolo S, A. Polman, and R. Serna, *Phys. Rev. B* **49**, 16313 (1994).
- 4 J. Michel, J.L. Benton, R.F. Ferrante, D.C. Jacobson, D.J. Eaglesham, E. A. Fitzgerald, Y.H. Xie, J.M. Poate, and L.C. Kimerling, *J. Appl. Phys.* **70**, 2672 (1991).
- 5 R. Serna, E. Snoeks, G.N. van den Hoven, and A. Polman, *J. Appl. Phys.* **75**, 2644 (1994).
- 6 F. Priolo, G. Franzò, S. Coffa, A. Polman, S. Libertino, R. Barklie, and D. Carey, *J. Appl. Phys.* **78**, 3874 (1995).
- 7 G. Franzò, F. Priolo, S. Coffa, A. Polman, and A. Carnera, *Appl. Phys. Lett.* **64**, 2235 (1994).
- 8 B. Zhen, J. Michel, F. Y. G. Ren, L. C. Kimerling, D. C. Jacobson, and J. M. Poate, *Appl. Phys. Lett.* **64**, 2842 (1994).
- 9 D.J. Eaglesham, J. Michel, E.A. Fitzgerald, D.C. Jacobson, J.M. Poate, J.L. Benton, A. Polman, Y.-H. Xie, and L.C. Kimerling, *Appl. Phys. Lett.* **58**, 2797 (1991).
- 10 J. S. Custer, E. Snoeks, and A. Polman, *Mat. Res. Soc. Symp. Proc.* **235**, 51 (1992).
- 11 Jung H. Shin, R. Serna, G.N. van den Hoven, A. Polman, W.G.J.H.M. van Sark, and A.M. Vredenberg, *Appl. Phys. Lett.* **68**, 997 (1996).
- 12 G.N. van den Hoven, Jung H. Shin, A. Polman, S. Lombardo, and S.U. Campisano, *J. Appl. Phys.* **78**, 2642 (1995).
- 13 M.J.A. de Dood, P.G. Kik, Jung H. Shin, and A. Polman, this proceedings: *Mat. Res. Soc. Symp. Proc.* **422** (1996).
- 14 S. Libertino, S. Coffa, G. Franzò, and F. Priolo, *J. Appl. Phys.* **78**, 3867 (1995).
- 15 G. Compagnini, S. Lombardo, R. Reitano, and S.U. Campisano, *J. Mater. Res.* **10**, 885 (1995).
- 16 P. N. Favenec, H. L'Haridon, D. Moutonnet, M. Salvi, M. Ganneau, *Mat. Res. Soc. Symp. Proc.* **301**, 181 (1993).



## RARE-EARTH DOPED EPITAXIAL InGaP AND ITS OPTICAL PROPERTIES

B. W. WESSELS

Dept. of Materials Science and Engineering and the Materials Research Center, Northwestern University, Evanston, Ill. USA

### ABSTRACT

The optical properties of rare-earth impurities in InGaP and the factors which influence their luminescence efficiency are presented. Basic energy transfer processes are described. Practical devices that utilize characteristic rare-earth luminescence are reported.

### INTRODUCTION

Rare -earth (RE) doped semiconductors are of interest because of their potential for use in light-emitting devices as a result of the sharp and temperature stable emission originating from the RE ions. The utilization of p-n junctions enables excitation of the rare earth ions by electrical injection as proposed by Bell in 1963.(1) Indeed the characteristic 4f emission by RE ions has been observed in a number of semiconductor hosts including Si and III-V compounds.(2) While strong characteristic emission has been observed at low temperatures for a number of RE ions, the observation of relatively efficient emission at room temperature has only been recently realized.(3) The observed thermal quenching of luminescence depends on both the ion and the host. To date practical RE based semiconductor lasers have not been fabricated. In order to attain these devices a number of key questions need to be answered including the mechanisms of excitation and thermal quenching of the luminescence. Suitable device structures need to be developed. In this report the rare-earth luminescence of InGaP semiconductor alloys is discussed. Of special interest are the excitation and de-excitation mechanisms for the characteristic RE luminescence in the InGaP system. Recent results on room temperature electroluminescence for forward biased Er-doped GaP junctions are presented. The potential of these junctions for laser emission is discussed.

### EXCITATION PROCESSES

The origin of the optical emission from RE doped semiconductors is well understood and is attributed to intra-4f shell transitions; however the nature of the energy transfer processes leading to excitation and the thermal quenching of the emission is a subject of controversy. Recently several models for the luminescence excitation and quenching have been proposed. These models involve the transfer of energy from the free carriers in the band to the 4f electrons. The currently accepted model for excitation of the 4-f emission is that the free carriers are trapped at the RE center and form a bound exciton. The exciton subsequently recombines transferring energy to the 4f shell electron as shown in Fig. (1). The excited 4f shell electron upon undergoing a transition to the ground state emits the characteristic emission. Inherent in this description is that the RE centers can bind carriers. The centers are considered to be isoelectronic in III-V semiconductors since addition of rare-earths does not change the net carrier

concentration.(4) However at low temperature the carriers can be trapped and effectively lower the carrier concentration. An important parameter necessary to understand the energy transfer processes is the position of the trapping level of the isoelectronic center with respect to the conduction and valence band edge. This will determine the energy available for excitation

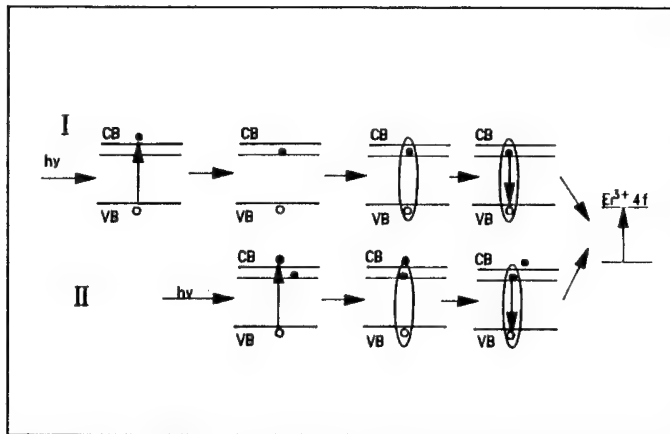


Figure 1 Model for 4f shell electron excitation

of the 4f electron upon the recombination of the bound exciton. Clearly if there is a mismatch between the two energies, other processes must be involved in the excitation process to accommodate the energy mismatch. It has been proposed that the position of this level also determines the thermal quenching of the characteristic luminescence. (4) If the RE trap is shallow then the bound carriers will thermalize at low temperatures and consequently not be available for excitation of the characteristic luminescence. Thus the larger the binding energy, the higher the temperature for which the thermal quenching that will be observed.

Therefore an important parameter necessary to understand the kinetics of energy transfer is the position of the isovalent RE level relative to the bandedge. The position of the levels remains a subject of controversy both theoretically and experimentally. Initial experiments on the thermal quenching of the rare-earth luminescence in InAsP alloys have yielded information pertaining to the position of these levels.(4) It was observed that the thermal quenching was an activated process and the measured activation energy was associated with the thermalization energy of a bound carrier. It was noted that the activation energy depended upon the alloy composition, decreasing with increasing arsenic concentration. Concurrently, the degree of luminescent quenching at high temperatures increased significantly. Thus the measured luminescence intensity was strongly host dependent.

Likewise for rare-earths in InGaP alloys including Er, Yb and Tm, the magnitude of the activation energy depends upon the alloy composition, increasing with increasing gallium content as shown in Fig. (2). While it was observed earlier that thermal quenching depended on the host bandgap, it was later observed that different ions had different quenching properties. The temperature at which the RE emission quenched depended on the specific ion type for a given alloy composition and could not be explained in terms of band gap size alone.

The observed dependence of the binding energy could be explained in terms of a vacuum referred binding energy model in which the RE related isoelectronic level are referenced to the

vacuum level instead of the host bandedge.(5) This can be seen in Fig.(3) which plots the position of the Er isoelectronic trap level with respect to the vacuum level as a function of InGaP alloy composition. Here the trap level is determined from the activation energy for thermal quenching. The bandedge position is determined by measuring the work function by photoemission. Note that the valence bandedge for these alloys is only weakly composition dependent. Thus if the activation energy is associated with the thermalization of an electron from the Er isoelectronic center to the conduction band, the trap energy gets larger with increasing Ga composition. Concurrently the bandgap also gets larger. It should be noted that once a particular RE level has been placed with respect to the vacuum level, it is possible to predict its binding energy in any III-V alloy, provided the position of the valence band edge is known. The thermal quenching data indicates that the Er level is 4.43 eV below the vacuum level. Recent photoconductivity and photocapacitance data supports this assignment.(6)

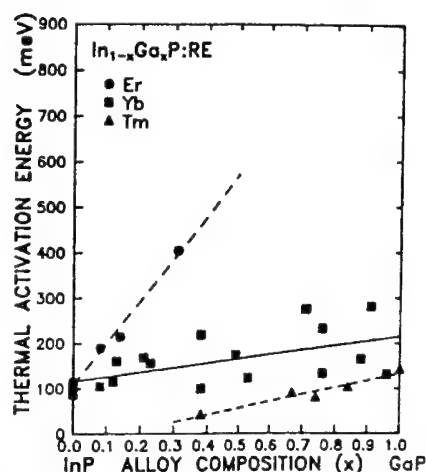


Figure 2 Activation energies for RE PL intensity vs. alloy composition after Ref.5

The vacuum referred binding energy model indicates that in order to get efficient room temperature RE emission the semiconductor host should have a bandgap energy greater than the 4f electron transition energy. The bandgap should also be of sufficient size so that the trapping level associated with the rare-earth center is deep to minimize thermal emission. Thus large bandgap semiconductors are preferred as hosts. Nevertheless if the bandgap is too large then there will also be a mismatch between the exciton energy and the 4f transition energy leading to a lower overall efficiency. Conversely if the isoelectronic level is resonant with the conduction or valence band, then no RE luminescence would be observed since the exciton state would be unstable.

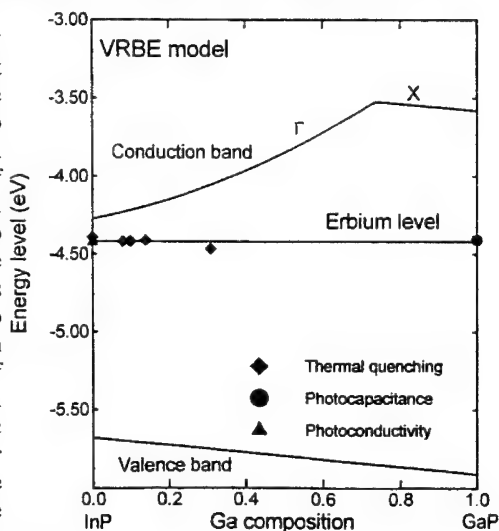


Figure 3 Energy level position with respect to vacuum level.

For the aforementioned model nothing is assumed about the nature of the center other than that it contains a rare-earth impurity and it is isovalent. The center could be substitutional, or interstitial. Moreover it could be just a single RE atom or a RE complex. By changing the composition of the center, it would be expected that its trapping energy would also change. Thus different complexes should have different quenching temperatures. Presumably by forming the appropriate complex, efficient characteristic emission at room temperature could be obtained even though the emission of the simple substitutional atom was weak. Oxygen has been indicated to form stable complexes with rare-earths in III-V semiconductors. Indeed intense emission has been observed from Er:GaAs co-doped with oxygen.(7)

#### EFFICIENCY ISSUES

The intensity for photoluminescence emission is given by the equation:

$$I = fN\sigma (I_p/h\nu) \tau / \tau_{rad}$$

where  $f$  is the fraction of active ions,  $N$  is the areal density of RE ions,  $\sigma$  the pump absorption cross section,  $I_p$  is the pump intensity,  $h\nu$  is the pump photon energy,  $\tau$  is the measured radiative decay lifetime and  $\tau_{rad}$  is the radiative decay time.

It can be seen that the intensity depends linearly on the ion concentration and is inversely proportional to the radiative lifetime. Thus increasing the solubility of the rare-earths in the III-V semiconductors is essential for increasing the luminescent efficiency of the material. This has been somewhat problematic in that concentrations are usually limited to  $10^{18}$  to  $10^{19}$  cm<sup>-3</sup>. While the use of low temperature deposition techniques such as molecular beam epitaxy and metalorganic vapor phase epitaxy have enabled non-equilibrium incorporation, the concentrations are still at the utmost  $10^{19}$  cm<sup>-3</sup>. It is also noted that the radiative lifetimes for RE ions are long, of the order of one millisecond for Er in compound semiconductors.

The measured decay lifetime will be determined by competing radiative and non-radiative processes. A competitive non-radiative process that has been proposed is quenching by Auger processes involving free electrons.(8) The lifetime when Auger processes predominate is given by:

$$\tau = 1/C_A n$$

where  $C_A$  is the Auger constant and  $n$  is the electron concentration. Fig. (4) shows the Er emission intensity as a function of carrier concentration for InP. Note that the dependence of intensity on  $n$  is not monotonic but appears to have a logarithmic dependence. The intensity is only weakly dependent on carrier concentration, decreasing only by a factor of four for more than a two order increase in carrier concentration. Auger processes appear to be unimportant for carrier concentrations of the order of  $10^{17}$  cm<sup>-3</sup> in contrast to earlier theoretical predictions. (8) It is interesting to note that for  $10^{19}$  cm<sup>-3</sup> carriers, strong characteristic RE emission is still observed.

To explain the relative weakness of the free carrier Auger effect in these materials, a model was recently proposed whereby the interaction of 4f electrons with free electrons was

effectively screened by valence electrons of the Er center.(9) For the analysis a simple screened Coulombic model potential was used so as to include the effect of the outer valence electrons. It was found that the luminescence quenching at high carrier concentrations could be explained for the most part by a model whereby screening by free carriers was important. In this case the overall intensity dependence was given by:

$$I = 1/(A + Bn/(n + n_0))$$

where A and B are constants, n is the free carrier concentration and  $n_0$  is a critical carrier concentration above which luminescence quenching occurs. The solid curve in Fig. (4). is a best fit to the above equation.

Based upon the above discussions, a high RE luminescence efficiency at room temperature should be attainable using a semiconductor with a bandgap of the order of 1.6 to 2.3 eV to minimize thermal quenching and moderate electronic dopant concentrations to minimize non-radiative processes.

#### LIGHT-EMITTING DIODES AND LASER STRUCTURES

The question then arises whether or not rare-earth doped III-V light -emitting diodes and lasers can be realized. Recently diffused diodes were prepared from epitaxial GaP doped with Er. Strong electro-luminescence at 0.80 eV was observed under both forward and reverse bias.(10,11) For the reverse bias case, the maximum internal power emitted was estimated to be 30 microwatts which was comparable to the calculated theoretical limit of 50 microwatts assuming a radiative efficiency of 100% for the excited Er centers. For the calculations an active volume of  $2 \times 10^{-7} \text{ cm}^3$  was used. The radiative lifetime was taken as 1 msec. and the Er concentration was taken as  $2 \times 10^{18} \text{ cm}^{-3}$ .

Fig. (5) shows the electroluminescence spectrum for p-n Er doped GaP diode under forward bias at several temperatures including room temperature. Note strong characteristic emission was also observed. The emitted power was of the same order as the reverse bias case with the emitted power equal to 12 microwatts.

As to the possibility of laser emission from these materials the optical gain needs to be considered. The optical gain  $\beta$  is given by:

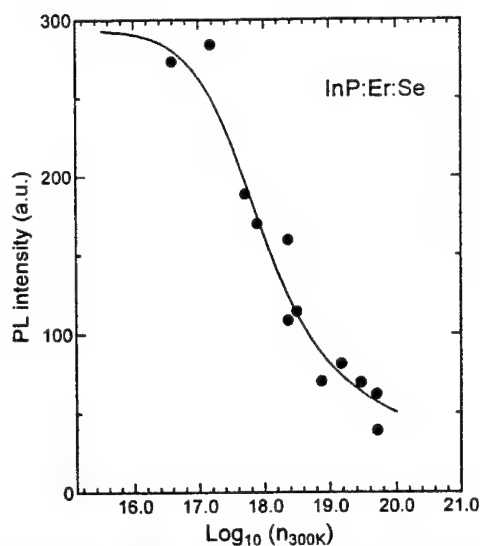


Figure 4 PL intensity vs. free carrier concentration for Er:InP

$$\beta = \lambda^4 N / 8\pi n^2 \tau \Delta\lambda$$

where  $N$  is the rare earth concentration,  $n$  is the refractive index,  $\tau$  the spontaneous radiative lifetime, and  $\Delta\lambda$  the emission linewidth. The calculated threshold current density is given by:

$$J_{th} = \alpha / \beta$$

where  $\alpha$  is the loss due to absorption and scattering in the laser cavity as well as end losses.

In Fig (6) the threshold is plotted as a function of loss for different emission linewidths. Currently the Er emission linewidth is of the order of 100 angstroms and concentrations are of the order of mid  $10^{18} \text{ cm}^{-3}$ . Thus laser structures with thresholds of  $10^2$  to  $10 \text{ A/cm}^2$  should be realizable. This is not the lower limit by any means since Er emission with a linewidth of the order of 1 angstrom has been observed in Er doped GaAs at low temperatures. (7)

Recently an Er PL emission linewidth of 2.6 angstroms was observed in our GaP which was selectively excited at low temperatures.

To realize stimulated emission in the present materials, high gain structures have been fabricated. Enhanced Er intra-4f shell emission was observed from a microdisk resonator due to the microcavity effect.(12) At low pumping power densities, the photoluminescence from the microdisks was an order of magnitude stronger than that from a thin film sample. As to whether or not stimulated emission was observed this is still under study.

In our studies on the dependence of EL intensity on current for p-n junction electroluminescent diodes we have noted that the sublinear dependence normally observed was not observed in some cases. In fact the EL intensity was found to be linearly dependent on current and subsequently became superlinear indicating that gain may be present.(13) The clear presence of a threshold was observed. At higher current densities saturation was observed and attributed to saturation of the optical centers. As to whether stimulated emission processes are occurring it is again too early to judge. However preliminary calculations suggest that this may indeed be the case. As shown in Figure 6, for a loss of  $1 \text{ cm}^{-1}$  and a line width of 100

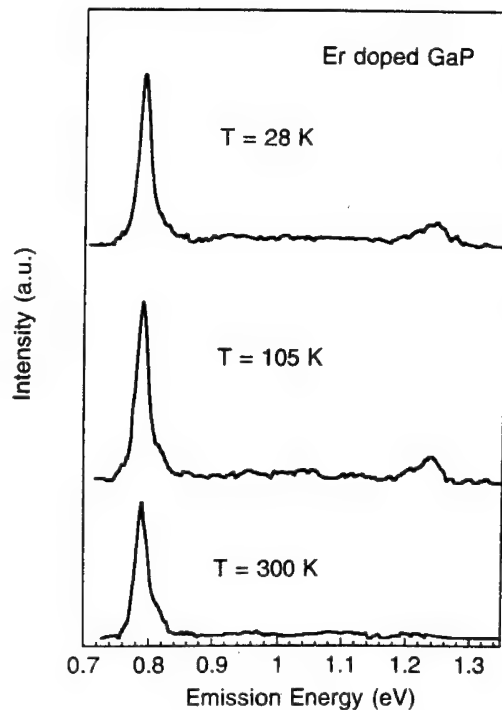


Figure 5 Electroluminescence spectrum for Er:GaP.

angstroms, the threshold for laser emission is calculated to be 50 A/cm<sup>2</sup>, which is comparable to the threshold observed. Experiments are underway to verify calculations.

#### FUTURE DIRECTIONS

In order to attain efficient laser emission from RE-doped III-V semiconductors further material improvements are required.

Presumably the concentration of rare earth ions is limited to 10<sup>19</sup> cm<sup>-3</sup>. Therefore in order to improve the gain, narrower linewidths are necessary. The cause of the inhomogeneous linewidth broadening in these materials is not well understood, but could be associated with rare-earth ions occupying multiple sites or forming complexes. The observed emission band could also be strain broadened. Future progress will depend upon understanding the nature and the identity of the rare-earth centers in the semiconductors. Further improvements may also be obtained by using rare-earths other than Er that have shorter spontaneous lifetimes for example Nd. While GaP as a host material has produced excellent electroluminescence, there may be other hosts that have even better properties.

#### ACKNOWLEDGEMENTS

This work was a collaborative effort with A. J. Neuhalfen and X. Z. Wang. Recent experiments on p-n junction electroluminescence were carried out by G. Ford. This work was sponsored by the National Science Foundation of the U. S. under grant No. DMR 930357.

#### REFERENCES

1. R. Bell, J. Appl. Phys. **12** 1563 (1963)
2. V. F. Masterov, Semiconductors **27** 791 (1993) and references therein.
3. A. J. Neuhalfen and B. W. Wessels, Appl. Phys. Lett. **59** 2317 (1991).
4. A. J. Neuhalfen and B. W. Wessels, Materials Science Forum **83-87** 689 (1992).
5. A. J. Neuhalfen and B. W. Wessels, MRS Proc. **240** 195 (1992).
6. X. Z. Wang and B. W. Wessels, Materials Science Forum **196-201** 663 (1995).

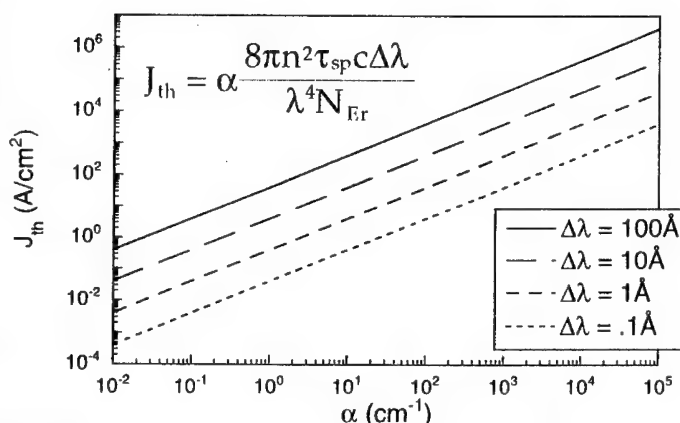


Figure 6 Calculated threshold for lasing as a function of loss in Er-doped GaP.

- 
7. K. Takahei and A. Taguchi J. Appl. Phys. 74 1979 (1993).
  8. J. Langer and Le Van Hong, J. Phys. C. 17 L923 (1984).
  9. X. Z. Wang and B. W. Wessels, Materials Science Forum 196-201 657 (1995).
  10. X. Z. Wang and B. W. Wessels, Appl. Phys. Lett. 65 584 (1994).
  11. G. Ford and B. W. Wessels, Appl. Phys. Lett. 68 1126 (1996)
  12. D. Chu et al. Appl. Phys. Lett. 66 2843 (1995).
  13. G. Ford and B. W. Wessels, (MRS Proc. 1996) Symposium D.



# On the Excitation Mechanism of Erbium and Ytterbium in the Quaternary Compounds InGaAsP

Peter Wellmann\* and Albrecht Winnacker

Institute of Materials Science 6 , University of Erlangen, Germany.

Gerhard Pensl

Institute of Applied Physics, University of Erlangen, Germany.

## Abstract

An efficient transfer of excitonic energy to rare earth (RE) ions is crucial for possible optoelectronic applications of RE doped semiconductors. In order to investigate the energy transfer mechanism to RE ions after optical above bandgap excitation we studied the intensity of the  $^4I_{13/2} \rightarrow ^4I_{15/2}$ -transition of  $Er^{3+}$  ( $1.54\mu m$ ) and the one of the  $^2F_{5/2} \rightarrow ^2F_{7/2}$ -transition of  $Yb^{3+}$  ( $1\mu m$ ) doped into InGaAsP-layers lattice matched to InP. By varying the composition of the quaternary compounds, the bandgap energy together with the RE bound exciton energy were tuned relative to the RE excitation energy, and the effect on the RE luminescence intensity was observed. The results can be interpreted by stating a) that the energy transfer to the RE proceeds via the RE bound exciton, and b) that the intensity of the RE luminescence is essentially determined by the rate of back transfer of the RE excitation energy  $E_{RE}$  to the bound exciton (with excitation energy  $E_{be}$ ). In this back transfer the energy of the excited RE ion plus the energy of 0, 1, 2 ... LO-phonons (energy  $E_{lo}$ ) is used to reexcite the bound exciton, instead of being emitted as an RE luminescence photon. For compositions where  $E_{be} = E_{RE} + n \cdot E_{lo}$  ( $n = 0, 1, 2 \dots$ ) we have a maximum of back transfer and correspondingly a minimum in RE luminescence. In between the intensity has a maximum.

## 1 Introduction

Since the early work of Ennen et al. [1], almost every semiconductor has been incorporated with rare earth ions. The sharp and temperature stable luminescence of the 4f-shell luminescence in the near infrared make rare earth ions interesting for applications in optoelectronic devices. The most investigated rare earths are erbium and ytterbium. The latter one has attracted much interest as a studying object and has been successfully doped in InP. It occupies an Indium site and has a simple two-level excitation scheme in its trivalent state  $Yb^{3+}$ . Erbium in its trivalent state is of particular interest due to its luminescence at  $1.54\mu m$ , because this wavelength coincidences with the absorption minimum of glass fibers.

\*current address: Dep. Mat. & Elec. Engr. , Univ. of California, Santa Barbara, CA 93106

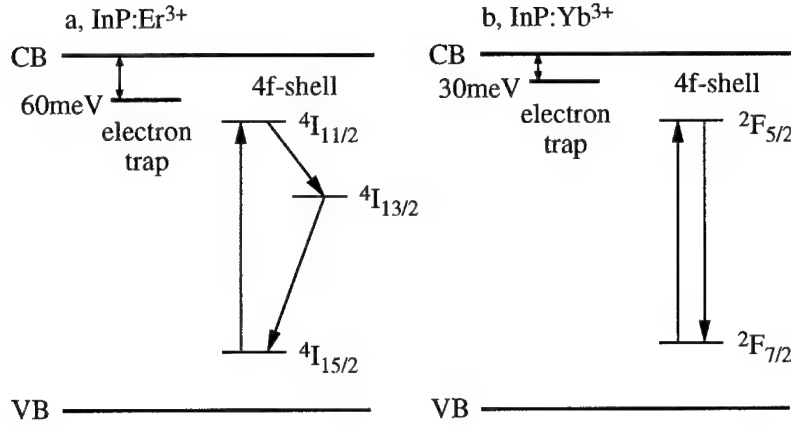


Figure 1: Band diagram of In(GaAs)P doped with erbium (a) and doped with ytterbium (b). The relative energetic position of the 4f shell is arbitrary.

Up to now no electroluminescence devices on the basis of RE doped semiconductors are available commercially. The main hindrance is the low efficiency of the rare earth luminescence. Connected with this, the excitation and deexcitation mechanisms have not been clarified in a sufficient manner, and there is only little knowledge about the physical limits of the rare earth luminescence efficiency.

But there has also been considerable progress in the knowledge of the physical properties of the rare earths erbium and ytterbium in semiconductors, especially in InP. For example it is well known from temperature dependent hall measurements (TDH)[2][3] and from deep level transient spectroscopy (DLTS) [2] that the rare earths erbium and ytterbium form an acceptorlike electron trap at 60 meV and 30 meV, respectively, below the conduction band (figure 1). The model is that the rare earth ion (RE<sup>3+</sup>) introduces a short range deformation potential which attracts electrons. EPR-measurements (electron-paramagnetic-resonance) [3] have shown that the capture of an electron does not change the charge state of the RE ion itself. The electron trapped means the RE ion causes a long range Coulomb interaction which is attractive to holes and leads to the creation of a bound exciton. Recently Godlewski et al. [4] and Kozanecki et al. [5] presented results, which give a direct evidence for the existence of such a bound exciton in ytterbium-doped InPAs. Temperature dependent luminescence measurements under cw and pulsed excitation have often been used to study the excitation mechanism of the RE ions [6][7][8] in semiconductors. The thermal quenching of the rare earth luminescence intensity and lifetime has indicated that the bound exciton plays an important role in the excitation and deexcitation of the RE 4f shell.

Our experimental results give a direct experimental proof that the bound exciton is crucial for the energy transfer processes to and from the RE 4f shell.

To investigate the excitation mechanism we have studied the influence of the size of the semiconductor band gap  $E_g$  on the 4f-shell luminescence efficiency. Our experimental approach differs from the work of Neuhaufen and Wessels [7], who investigated the quenching temperature of the erbium luminescence as a function of the band gap  $E_g$  in  $In_{1-x}Ga_xP$ . The underlying idea of our experiment is that the energy transfer from the semiconductor

to the 4f shell might critically depend on the relative size of  $E_g$  and the 4f-shell excitation energy, for instance through a resonant transfer etc. . We have investigated the erbium and ytterbium luminescence efficiency at  $T = 10K$ , where the thermal quenching of the 4f-shell luminescence is negligible. Erbium and ytterbium-doped  $In_{1-x}Ga_xAs_yP_{1-y}$ -layers were grown lattice matched on  $InP$ -substrates. The band gap  $E_g$  was tailored in a wide range from  $1.416eV$  to  $1.210eV$  in small steps of about  $13meV$  by varying the composition parameters  $x$  and  $y$ .

The paper is organized in the following way. In section 2 we describe the sample preparation and the experimental procedure. In section 3 the measurements on erbium and ytterbium-doped  $InGaAsP$ -layers are presented. We have investigated the evolution of the luminescence efficiency with a varying band gap  $E_g$  and as a function of lattice temperature and laser excitation. The interpretation of our results will be given in section 4. We will point at the role of the bound exciton on the excitation mechanism of erbium in  $InGaAsP$ . On the basis of the results of the ytterbium-doped samples an energy back transfer from the excited 4f shell is taken into consideration. The relevance of this process for erbium-doped samples will be discussed as well. Section 5 gives a summary of our paper.

## 2 Sample preparation and experimental setup

### 2.1 Sample preparation

The  $In_{1-x}Ga_xAs_yP_{1-y}$ -layers were grown by liquid phase epitaxy at  $600^\circ C$  (erbium-doped sample set 1) and  $700^\circ C$  (erbium-doped sample set 2 and ytterbium-doped samples) lattice matched on semi-insulating  $InP:Fe$  and  $n-InP:S$  substrates. The composition of the quaternary layers was varied between  $y = 0 \dots 0.30$  ( $E_g = 1.414 \dots 1.210eV$ ) for the erbium-doped layers (thickness:  $2.5\mu m$  (set 1) and  $0.2\mu m$  (set 2)) and between  $y = 0 \dots 0.11$  ( $E_g = 1.416 \dots 1.322eV$ ) for the ytterbium-doped layers (thickness:  $0.5\mu m$ ). Erbium doping was done by ion implantation at an energy of  $350keV$  and a dose of  $5 \cdot 10^{13}cm^{-2}$ . The depth of the implanted region is about  $0.2\mu m$ , the doping concentration is estimated to be about  $10^{18}cm^{-3}$ . After implantation the samples of each set (1 and 2) were annealed simultaneously<sup>1</sup> for  $t = 15min$  at  $T = 625^\circ C$ . Ytterbium doping was done during the epitaxy of the  $InGaAsP$ -layers by adding  $0.01at\%$  metallic ytterbium powder to the melt.

### 2.2 Experimental setup

The measurement of the photoluminescence (PL) spectra was done in a helium closed cycle cryostat at  $T = 10 \dots 200K$  using the  $514nm$  line of an argon laser, a  $0.6m$  spectrometer and a cooled germanium detector. The laser spot was spread to a spot diameter of  $d = 3mm$ ; the excitation density was about  $I_{exc} = 0.5W/cm^2$ . The change of the spectral efficiency of the germanium detector has been taken into account.

<sup>1</sup>The annealing procedure affects the erbium luminescence efficiency due to the percentage of the activated  $Er^{3+}$ -centers. To avoid such a variation between samples, all layers of each sample set have been annealed simultaneously. To exclude other possible preparation errors, we have investigated two independent sample sets (1 and 2).

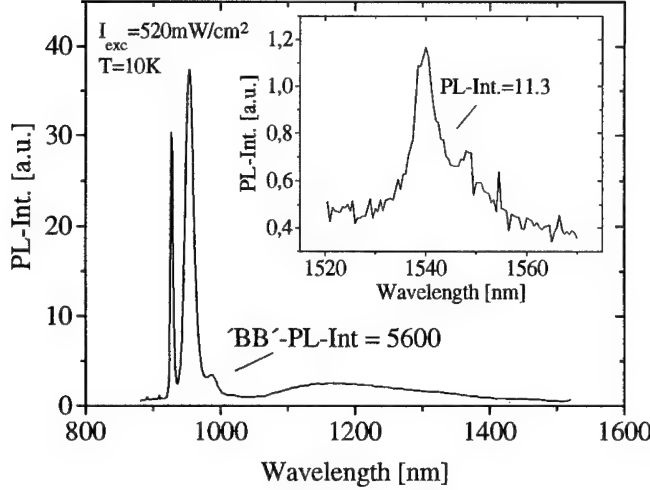


Figure 2: PL spectra of an erbium-doped InGaAsP-sample at  $T = 10K$ .

### 3 Results

#### 3.1 Erbium-doped InGaAsP-samples

A typical PL spectrum of an erbium-doped InGaAsP-sample at  $T = 10K$  is shown in figure 2. The band gap  $E_g$  can be extracted approximately from the peak position of the conduction band/donor-valence band transitions. The integral PL-intensity of the InGaAsP host luminescence ( $I_{BB}$ ) is about 500 times larger than that of the erbium 4f shell around 1540nm ( $I_{Er}$ ). In the following, we define the ratio  $I_{Er}/I_{BB}$  as the erbium photoluminescence efficiency.

Figure 3 shows the dependence of the erbium PL efficiency on the band gap  $E_g$  of the erbium-doped sample set 1 and set 2. For a better understanding we have chosen  $E_g - E_{4I11/2}$  as the horizontal axis;  $E_{4I11/2}$  represents the energy of the 4f-shell transition of  $Er^{3+}$  from the ground state  $^4I_{15/2}$  to the second excited state  $^4I_{11/2}$ . Zero in this graph means that the band gap  $E_g$  and the 4f-shell transition energy  $E_{4I11/2}$  are equal. A negative/positive value indicates a band gap that is smaller/larger than the erbium transition energy from the ground state to the second excited state. Due to a systematic deviation in the determination of the band gaps of sample set 1<sup>2</sup>, the data of sample set 1 have been shifted on the horizontal axis of the plot for +12meV relative to the ones of sample set 2.

A low erbium PL efficiency is found in the region  $-50meV \dots +60meV$ . At about +60meV the erbium PL starts to rise and reaches a high value (about three times enhanced)

<sup>2</sup>Due to a higher diffusion coefficient of phosphorus (P) than arsenic (As) in the liquid phase epitaxy melt, the band gap  $E_g$  of thick layers ( $d \geq 1\mu m$ ) rises during the growth. This means for sample set 1 ( $d = 2.5\mu m$ ) that the band gap of the implanted surface region ( $\approx 0.2\mu m$ ) is larger than the band gap estimated from the peak position of the conduction band/donor-valence band transition, because in the PL-experiment one measures the average band gap over the whole layer thickness. Therefore, the estimated values of  $E_g$  of sample set 1 have to be corrected by +12meV.

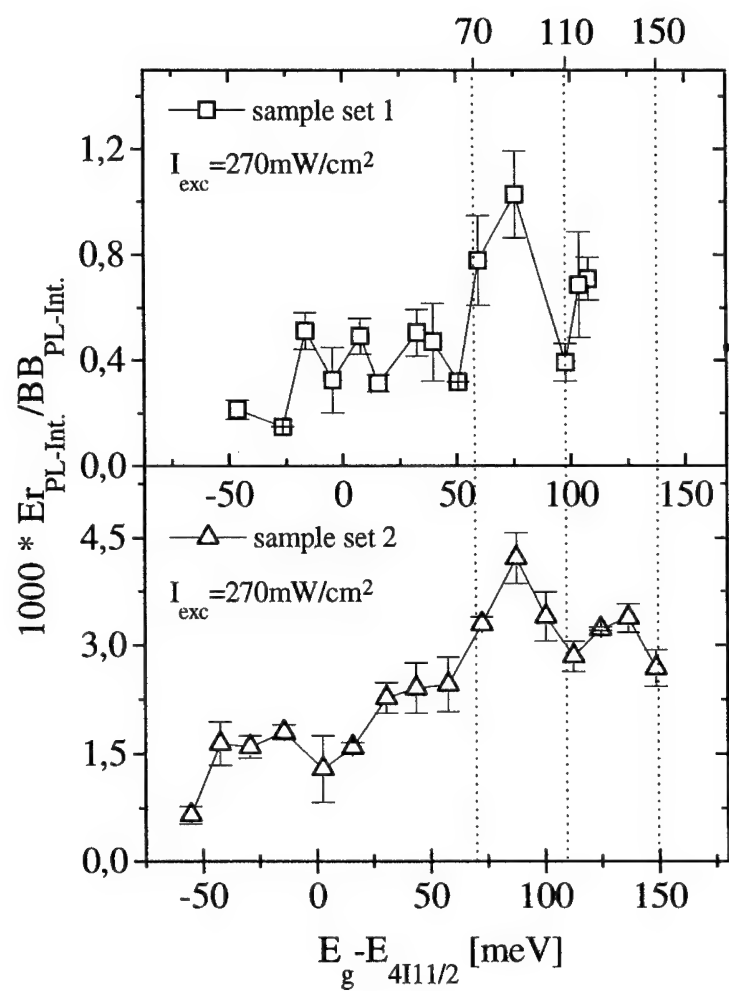


Figure 3: Erbium PL efficiency as a function of  $E_g - E_{4I11/2}$  for sample set 1 and set 2 at  $T = 10K$ .

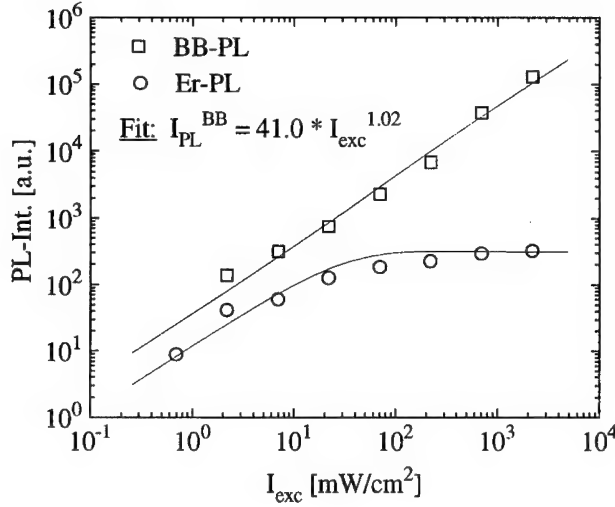


Figure 4: Erbium (*Er*) and band edge (*BB*) photoluminescence versus excitation intensity  $I_{exc}$  at  $T = 10K$ .

in the region  $+70meV \dots 150meV$ . At  $+110meV$  a local minimum appears in the erbium PL efficiency. This behavior will be discussed later in section 4.1 and 4.2. The measurements in figure 3 were done at an laser excitation intensity  $I_{exc} = 270mW/cm^2$ . At this value the erbium PL efficiency is saturated (see figure 4).

Figure 4 shows the dependence of the erbium ( $I_{Er}$ ) and the InGaAsP near band edge ( $I_{BB}$ ) luminescence on the laser excitation intensity  $I_{exc}$  at  $T = 10K$ . The semiconductor host related luminescence rises over the whole excitation range linearly with  $I_{exc}$ . The erbium related luminescence rises at a low excitation linearly with  $I_{exc}$  but saturates at an excitation intensity of about  $100mW/cm^2$ . The lines indicate a model calculation, which will be published elsewhere [9].

Figure 5 shows the dependence of the erbium PL intensity on the lattice temperature. The experimental data have been fitted by a double exponential equation [3].

$$I_{Er} = \frac{I_0}{1 + A_{hole} \exp\left(\frac{-E_{hole}}{k_B T}\right) + A_{trap} \exp\left(\frac{-E_{trap}}{k_B T}\right)} \quad (1)$$

In our case equation 1 can be understood as the thermal quenching of a bound exciton at the rare earth ion.  $I_0$  is the erbium PL-intensity at  $T = 10K$ , where the exponentials are negligible.  $E_{trap}$  is the energy of the acceptor like electron trap of the rare earth ion below the conduction band.  $E_{hole}$  is the binding energy of a hole, which forms a bound exciton with the electron at the rare earth trap.  $A_{hole}$  and  $A_{trap}$  are free fitting parameters and contain the corresponding capture cross sections. An energy back transfer as discussed in section 4.2 has been neglected in equation 1, because the investigated sample (figure 5) did not show a (relative) minimum of the erbium luminescence efficiency at  $T = 10K$ .

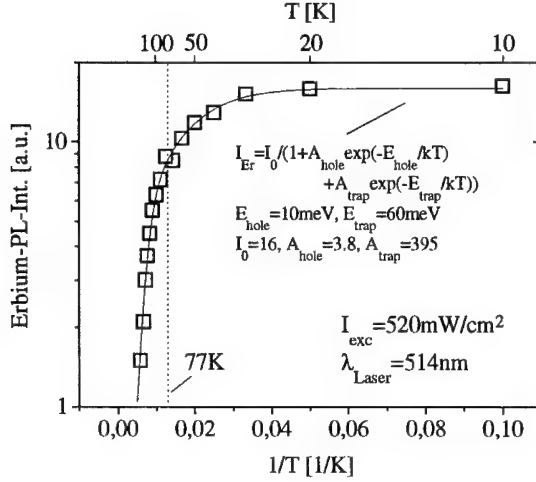


Figure 5: Erbium PL intensity  $I_{Er}$  versus lattice temperature  $T$  ( $E_g - E_{4I11/2} \approx 100meV$ , sample set 2).

### 3.2 Ytterbium-doped InGaAsP-samples

Figure 6 shows the evolution of the rare earth PL efficiency with the band gap  $E_g$  of the ytterbium-doped samples. The energy of the ytterbium 4f-shell transition  $^2F_{7/2} \rightarrow ^2F_{5/2}$  ( $E_{2F_{5/2}} = 1.24eV$ ) is always smaller than  $E_g$  of the InGaAsP-layers. In the case of ytterbium it is not possible to tune the band gap of the semiconductor host over the energy of the excitation level of the 4f shell. The problem is that the ytterbium PL transition, which is equal to the excitation transition, will be covered by near band edge luminescence like donor acceptor transitions and related phonon replicas. In the case of the erbium-doped samples this circumstance did not appear; here  $E_g$  was varied over the transition from the ground state to the second excited state, whereas PL was observed from the transition from the first excited state to the ground state.

The most remarkable feature of figure 6 is that the ytterbium luminescence almost vanishes at  $E_g = 1.349eV$  ( $y = 0.08$ ), showing a pronounced minimum there as a function of  $E_g$ . For a further illustration of this striking fact figure 7 shows the spectrum for this composition, as well as the ones of the two neighboring band gaps. A preparation error of the sample at  $E_g = 1.349eV$  can be excluded, because a second sample with a nominally equal composition of  $y = 0.08$  ( $E_g = 1.345eV$ ) shows as well a nearly zero ytterbium luminescence intensity. We attribute the vanishing of the ytterbium luminescence intensity to an efficient energy back transfer from the excited 4f shell to the semiconductor host (section 4.2). At  $E_g = 1.392eV$  ( $y = 0.03$ ) the ytterbium luminescence intensity shows a further minimum. Please note that the difference of the PL minima ( $1.349eV$  versus  $1.392eV$ ) is about  $40meV$ .

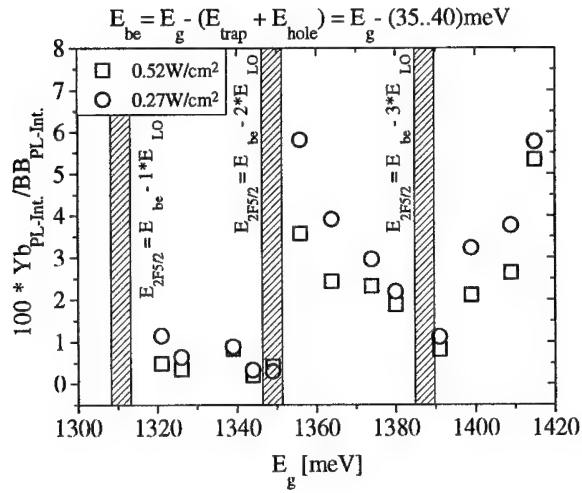


Figure 6: Ytterbium PL efficiency as a function of band gap energy  $E_g$  at  $T = 10K$ . The energy of the  $^2F_{7/2} \rightarrow ^2F_{5/2}$  transition is  $1.24eV$ .

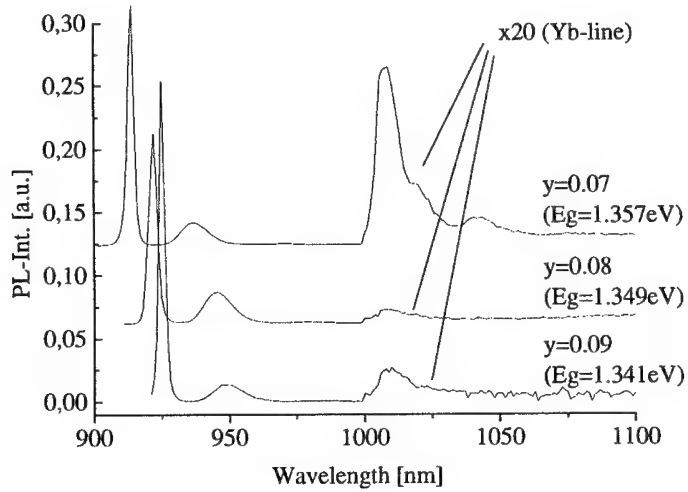


Figure 7: PL spectra of three ytterbium-doped InGaAsP samples with a different band gap at  $T = 10K$ . The ytterbium PL efficiency shows a minimum for a quaternary composition of  $y = 0.08$ .



## 4 Discussion

### 4.1 Excitation mechanism via bound exciton

The dependence of the erbium luminescence efficiency on the band gap energy  $E_g$  (figure 3) helps us to understand the energy transfer from the semiconductor host to the RE ion.

If the recombination of free electrons and holes played a crucial role for the excitation mechanism of the 4f shell one would obviously expect an enhancement of the energy transfer and hence an increase of the erbium luminescence at  $E_g - E_{4I_{11/2}} = 0\text{meV}$ . At this value of  $E_g$  the energy of free electron hole pairs would suffice to excite the 4f shell from the ground state into the first excited state ( $^4I_{13/2}$ ) as well as into the second excited state ( $^4I_{11/2}$ ). The experimental data in figure 3 show no significant rise of the erbium PL in the region  $E_g - E_{4I_{11/2}} = -50 \dots +60\text{meV}$ . This indicates that the recombination of free charge carriers is not relevant for the excitation of the 4f shell.

At  $E_g - E_{4I_{11/2}} = +70\text{meV}$  the erbium luminescence has started to rise about a factor two to three. Please note that the energy of a bound exciton ( $E_{\text{trap}} + E_{\text{hole}}$ ) at the RE ion amounts to approximately  $70\text{meV}$ .  $E_{\text{trap}}$  is known to be  $60\text{meV}$  [3] in InP, whereas the Coulomb binding energy of the hole ( $E_{\text{hole}}$ ) can be estimated to be  $10\text{meV}$ . For band gaps with  $E_g - E_{4I_{11/2}} < +70\text{meV}$  the energy of the bound exciton suffices only to excite the rare earth ion from the ground state ( $^4I_{15/2}$ ) into the first excited state ( $^4I_{13/2}$ ). At  $E_g - E_{4I_{11/2}} > +70\text{meV}$  it is possible to excite the erbium 4f shell not only into the first excited state ( $^4I_{13/2}$ ) but also into the second excited state ( $^4I_{11/2}$ ). Due to this enhanced energy transfer probability the erbium luminescence rises.

The participation of the bound exciton is also confirmed by an independent experiment: the temperature dependent PL measurements (figure 5) of the erbium line. As stated in section 3.1 it is possible to fit the experimental data with an equation, which describes the thermal emission of a bound exciton from the rare earth trap (equation 1). The fitting parameters  $E_{\text{trap}} = 60\text{meV}$  and  $E_{\text{hole}} = 10\text{meV}$  in figure 5 coincidence with the above estimation that the energy of a bound exciton amounts to  $70\text{meV}$ .

The absence of an enhanced erbium luminescence at  $E_g - E_{4I_{11/2}} = 0\text{meV}$  and its increase at  $E_g - E_{4I_{11/2}} > +70\text{meV}$  leads us to the conclusion that the main energy transfer to the 4f shell occurs from the recombination of an exciton, bound to the RE trap.

Another excitation mechanism discussed in the literature, the impact excitation [10][11], has been disregarded. The impact excitation process requires hot electrons, which are, e.g., generated in electroluminescence devices for instance.

### 4.2 Energy back transfer

Two types of energy back transfer processes from the excited 4f shell to the semiconductor host have been discussed in the literature in detail [12][8]. Godlewski et al. [12] suggested an Auger like energy transfer from the excited 4f shell to a bound exciton that has been captured at the RE trap. The excited 4f shell transfers its energy nonradiatively to the bound exciton and emits the electron and the hole into the conduction and valence band, respectively. One would expect that this process should depend only slightly on the energy gap of the semiconductor. We cannot exclude the Auger like energy back transfer at all. But it is not possible to explain the strong ytterbium luminescence quenching in figure 6 at certain semiconductor band gaps ( $E_g = 1.349\text{eV}$  and  $E_g = 1.392\text{eV}$ ).

A more suitable energy back transfer model for our measurements has been proposed by Taguchi et.al.[8]. The idea is that the excited 4f shell creates a bound exciton at the ytterbium trap. The missing of energy will be provided by the absorption of phonons. If we assume that the absorption of LO-phonons dominates in our experiment, it is possible to understand our results. The energy back transfer occurs most efficiently in the case that the energy difference between the excited 4f shell and the bound exciton is a multiple of LO-phonons ( $E_{lo} \approx 38meV$  for InP).

To mark this, broad lines indicate in figure 6 the situation where the energy difference between the excited 4f shell and the bound exciton corresponds 1, 2 or 3 LO-phonons. The ytterbium trap has been set to the value  $E_{trap} = 30meV$  [2], whereas the binding energy of the hole has been assumed to be  $E_{hole} = 5 \dots 10meV$ . At  $E_g = 1.349eV$ , the ytterbium luminescence nearly vanishes. This is in coincidence with an energy difference of the bound exciton and the excited 4f shell of 2 LO-phonons. At  $E_g = 1.392eV$ , the ytterbium luminescence has another minimum, the energy difference amounts 3 LO-phonons. The energy back transfer is less effective at  $E_g = 1.392eV$  than at  $E_g = 1.349eV$ , because the probability to absorb 3 LO-phonons is lower than in the case of 2 LO-phonons at  $E_g = 1.349eV$ .

The question arises how it could be possible for the excited 4f shell to absorb LO-phonons at  $T = 10K$ . Due to Bose-statistic it is not expected that a high number of LO-phonons is present in the semiconductor at this temperature. But we have to keep in mind, however, that the lattice is not in a thermodynamical equilibrium. Due to the laser excitation with the 514nm argon line, each electron hole pair is generated with an excess energy of about 0.9eV in InP and emits more than twenty LO-phonons while relaxing to the band edge. The phenomenon that a small energy band of phonons is not in equilibrium with the lattice due to optical excitation (phonon bottleneck) is also known from other parts in spectroscopic research. For example Geschwind et al. [13] found an anomalous occupation of electronic levels in optical detected EPR-measurements in  $Al_2O_3 : Cr^{3+}$ -crystals due to such a phonon bottleneck.

Due to high resolution PL measurements of the ytterbium lines and its phonon replicas (figure 8) we find that there is a strong interaction of the 4f shell with LO-phonons of the semiconductor host. From the intensity ratios of the phonon replicas it is possible to estimate the Huang-Rhys factor  $S$  (equation 2) [14];  $n$  is the number of the emitted LO-phonons. We find a value of  $S = 0.14 \pm 0.02$ .

$$I_n = \frac{S^n \exp(-S)}{n} \quad (2)$$

For comparison, the Huang-Rhys factor of the donor acceptor transition is only  $S = 0.08 \pm 0.02$ .

We conclude from our results that there will be a resonant like energy back transfer from the excited 4f shell to the semiconductor host, if the energy difference of the excited 4f shell and the bound exciton is equal to a multiple of  $n$  LO-phonons ( $n = 0, 1, 2, 3 \dots$ ). The energy will be used to recreate a bound exciton at the RE trap.

The question arises, whether this energy back transfer is of more general nature and does also occur in the erbium-doped samples. The energy difference of the 4f shell in its first excited state ( $^4I_{13/2}$ ) and the bound exciton is about 14 LO-phonons in InP. The probability to absorb 14 LO-phonons is supposed to be too weak to give rise to a visible effect by an energy back transfer. But if the 4f shell is in its second excited level ( $^4I_{11/2}$ ), the energy difference to the bound exciton is only about 2 LO-phonons in InP. The dotted lines at

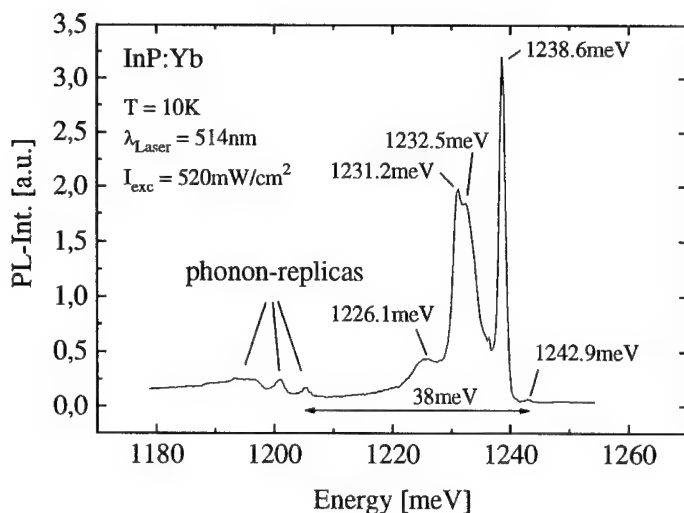


Figure 8: High resolution PL measurement of the ytterbium line in InGaAsP:Yb.

70 meV, 110 meV and 150 meV in figure 3 points at those band gaps, for which the energy difference of the excited 4f shell ( $^4I_{11/2}$ -level) and the bound exciton is 0, 1 and 2 LO-phonons. The experimental data show that the erbium luminescence is decreased in these samples. For 110 meV clearly a minimum is observed. 150 meV is the last data point of set 2. So no minimum can be seen, but certainly the erbium PL intensity decreases. Both facts would be in agreement with an energy back transfer via LO-phonon absorption. Even the data at 70 meV could be interpreted in this way: At  $E_g - E_{4I_{11/2}} = 70$  meV the energy of the bound exciton would suffice to excite the RE into the second excited state, see 4.1. However, the maximum is only reached at 90 meV due the back transfer at 70 meV. Between the 70 meV, 110 meV and 150 meV points, at 90 meV and 130 meV, the erbium luminescence has a correspondingly maximum.

As in the case of ytterbium-doped InGaAsP, we conclude that an energy back transfer from the excited 4f shell to the bound exciton occurs in erbium-doped InGaAsP. The effect is smaller than in the case of ytterbium, because only an energy back transfer from the second excited erbium level should be relevant. An interesting aspect of this result is that the energy back transfer should also appear if the 4f shell has been excited by impact excitation. The impact excitation for example has been favored for electroluminescence devices on the basis of InP which work at room temperature. Especially at room temperature there will be a high amount of LO-phonons in the lattice which should lead to a quenching of the rare earth luminescence.

## 5 Conclusions

In conclusion, we have studied the erbium and ytterbium luminescence efficiency as a function of the InGaAsP composition and band gap. We have tuned the energy of the rare earth bound

exciton relative to the 4f-shell excitation energy. The experimental data indicate that the bound exciton is crucial for the excitation and deexcitation of the rare earth ion.

In the case of erbium-doped InGaAsP we found an enhanced rare earth luminescence efficiency if the energy of the bound exciton suffices to excite the 4f shell not only into the first excited state  $^4I_{13/2}$  but also into the second excited state  $^4I_{11/2}$ . However, from this we have concluded that the excitation due to recombination of free electrons plays a minor role, the excitation rather occurs via the bound exciton.

Furthermore we found experimental evidence for a strong energy back transfer from the excited 4f shell of ytterbium to the bound exciton. If the energy difference of the excited 4f shell and the bound exciton is a multiple of the LO-phonon energy, the 4f shell reexcites the bound exciton instead of emitting a photon. The energy mismatch will be provided by the absorption of LO-phonons. This energy back transfer was found to occur in the erbium-doped samples too.

## References

- [1] H. Ennen, U. Kaufmann, G. Pomrenke, J. Schneider, J. Windscheif, and A. Axmann. *J.Cryst.Growth* **64**,165 (1983).
- [2] P.S. Whitney, K. Uwai, H. Nakagome, and K.Takahei. *Appl.Phys.Lett.* **53**(21),2074 (1988).
- [3] B. Lambert, A. LeCorre, Y. Toudic, C. Lhomer, G. Grandpierre, and M. Gauneau. *J.Phys.Condens.Matter.* **2**,479 (1990).
- [4] M. Godlewski, A. Kozanecki, J.P. Bergman, and B. Monemar. *Appl.Phys.Lett.* **66**(4),493 (1995).
- [5] A. Kozanecki and A. Szczerbakow. *Appl.Phys.Lett.* **66**(26),3630 (1995).
- [6] C. Lhomer, B. Lambert, Y. Toudic, A. LeCorre, M. Gauneau, F. Clerot, and B. Sermage. *Semic.Sci.Tec.* **6**,916 (1991).
- [7] A.J. Neuhaufen and B.W. Wessels. *Appl.Phys.Lett.* **60**(21),2657 (1992);
- [8] A. Taguchi, K. Takahei, and Y. Horikoshi. *J.Appl.Phys.* **76**(11),7288 (1994).
- [9] P. Wellmann and A. Winnacker. *submitted to J.Appl.Phys.*.
- [10] H. Isshiki, H. Kobayashi, S. Yugo, T. Kimura, and T. Ikoma. *Appl.Phys.Lett.* **58**(5),484 (1991).
- [11] S.J. Chang and K. Takahei. *Appl.Phys.Lett.* **65**(4),433 (1994).
- [12] M. Godlewski, K. Swiatek, and B. Monemar. *J.Luminescence* **58**,303 (1994).
- [13] S. Geschwind, G.E. Devlin, R.L. Cohen, and S.R. Chinn. *Phys.Rev.* **137**(4A),A1087 (1965).
- [14] Ingrid de Maat-Gersdorf, T. Gregorkiewicz, C.A. Ammerlaan, and N.A. Sobolev. *Semi-cond.Sci.Technol.* **10**,666 (1995).

## ENERGY-TRANSFER PROCESSES IN OXYGEN-CODOPED GaAs:Er

K. TAKAHEI, R.A. HOGG and A. TAGUCHI

*NTT Basic Research Laboratories*

*3-1 Morinosato-Wakamiya, Atsugi-shi, Kanagawa 243-01, Japan. takahei@will.brl.ntt.jp*

### ABSTRACT

GaAs grown by metalorganic chemical vapor deposition and codoped with Er and oxygen shows a simple spectrum with sharp luminescence lines due predominantly to one type of Er center. This center is identified as an Er atom substituting a Ga site, coupled with two oxygen atoms. Photoluminescence measurements under host excitation and photoluminescence excitation measurements that directly excite the 4f-shell of the  $\text{Er}^{3+}$  ion indicate that this center is excited much more efficiently than other Er centers simultaneously present in the same sample. A possible energy-transfer mechanism and its implications are discussed.

### I. INTRODUCTION

Rare-earth (RE) atoms in solid-state laser materials are activated by intra-4f-shell optical excitation, and those in electroluminescence panels using II-VI compound semiconductor hosts are activated by accelerated carriers. A recent interest in RE atoms in III-V compound semiconductors and group IV semiconductors is motivated by the possibility of efficiently activating RE atoms in these semiconductors by minority carrier injection in a p-n junction, a technique that has been proved to be a very efficient way of exciting the host semiconductor hosts. To excite the RE atoms in this way, there must be a transfer of energy from electron-hole (e-h) pairs in the semiconductor hosts to the 4f-shell electrons of RE atoms in the host. Luminescence from RE atoms has been observed when various RE atoms are incorporated into various semiconductors, thus indicating that there is a universal mechanism that transfers the energy of e-h pairs in the semiconductor hosts to the 4f-shell electrons of RE atoms. Identification of the energy transfer mechanisms in most cases, however, has been difficult because of the simultaneous presence of various RE centers and of other defects in the semiconductors. Theoretical treatment of the energy transfer mechanism is also difficult because the energy is transferred from a spatially extended state of an e-h pair to a very localized 4f-shell electrons which are screened by outer electronic shells.

The energy transfer process has been best studied for Yb in InP because Yb in InP forms only one type of luminescence center regardless of the way the sample is synthesized. Although Er is a technologically more important RE atom because it shows luminescence at the 1.5  $\mu\text{m}$  region which is suitable for optical-fiber communication systems, the Er-related luminescence spectrum of Er-doped semiconductors depends on the way the samples are synthesized and on how they are heat-treated. Reported luminescence spectra of Er generally consist of many lines or of broad bands, suggesting the simultaneous presence of many types of Er centers and indicating that the Er atom does not have a stable site in the lattice of a semiconductor host. Er atoms must be incorporated into semiconductors in the form of complexes with native defects or impurities, or in the form of Er-rich aggregates. Many papers concerning the improvement of luminescence efficiency have been published [1], and we recently found that the codoping of oxygen (O) in Er-doped GaAs (GaAs:Er) by metalorganic chemical vapor deposition (MOCVD) has a marked effect on the formation of Er centers and on luminescence characteristics. This paper reviews experimental results on Er-doped GaAs with O codoping (GaAs:Er,O) and discusses the process by which energy is transferred between e-h pairs in the GaAs host and the 4f-shell electrons of  $\text{Er}^{3+}$  ions.

## II. EFFECTS OF O-CODOPING ON GaAs:Er

Photoluminescence (PL) spectra observed at 2 K under host photo-excitation for Er-doped GaAs with and without O codoping are shown in Fig. 1 [2]. The samples were grown at 2  $\mu\text{m/h}$  on (100)-oriented GaAs substrates at 500°C. A sample with O codoping always shows seven lines indicated by arrows, and the width of the strongest luminescence line is below the resolution of our spectrometer (0.01 nm). A sample without O codoping, on the other hand, shows many lines and broad features. The O-codoped sample shows sharp spectral lines even at room temperature but the width of the strongest line is about 2 nm [3].

To investigate the role of deliberately doped O, an experiment was carried out using an  $^{18}\text{O}$  isotope gas source [4], so that the deliberately doped  $^{18}\text{O}$  and the unintentionally incorporated naturally abundant  $^{16}\text{O}$  isotope could be distinguished. The concentrations of  $^{18}\text{O}$  and  $^{16}\text{O}$  measured by secondary ion mass spectroscopy (SIMS), normalized against the Er concentration (about  $10^{19}\text{cm}^{-3}$ ), are shown in Fig. 2 as a function of the  $^{18}\text{O}_2$  gas concentration in the growth atmosphere. Ratios rather than absolute values of concentrations are plotted here because the concentrations of both isotopes changed in proportion to Er concentration. When an epitaxial layer without Er doping was grown in an atmosphere containing a similar O concentration, we observed that the concentration of O in the layer was below the limit of detection for SIMS measurements (i.e., below  $10^{17}\text{cm}^{-3}$ ) [2]. This indicates that O present in concentrations exceeding this amount is incorporated into epitaxial layers only in the form of Er-O complexes. As can be seen from Fig. 2, when  $^{18}\text{O}_2$  is not injected into the furnace during growth, the ratio of concentrations of  $^{18}\text{O}$  to  $^{16}\text{O}$  in the layer due to the unintentionally incorporated O impurities is close to the ratio of their natural abundances, which is about  $2 \times 10^{-3}$ .

Although such a sample contains a high concentration of  $^{16}\text{O}$ , it shows a spectrum similar to the one shown in Fig. 1(a). When  $^{18}\text{O}_2$  gas is injected into the furnace, the PL spectrum becomes simple with sharp lines even when the sample is grown with an  $^{18}\text{O}_2$  concentration of 0.1 ppm in the growth

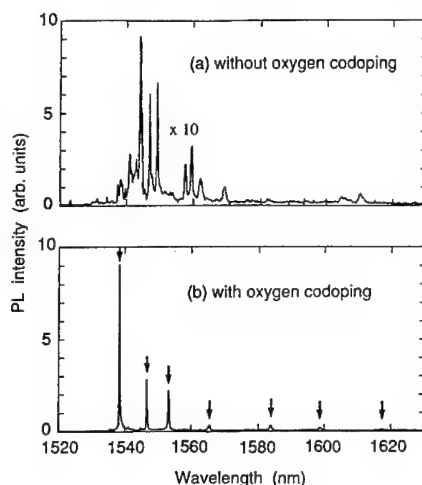


Fig. 1. PL spectra of Er-doped GaAs grown by MOCVD (a) without and (b) with deliberate O codoping. The spectra were measured at 2 K with a resolution of 0.26 nm. The features indicated by arrows in (a) are due to the  $\text{Er}_{\text{Ga}}\text{-2O}$  center discussed in Sec. III.

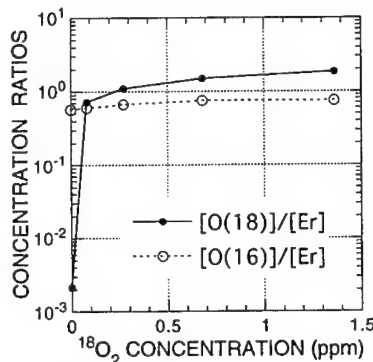


Fig. 2. Ratios of  $^{18}\text{O}$  and  $^{16}\text{O}$  concentrations (normalized against Er concentration) in MOCVD-grown GaAs:Er,O versus  $^{18}\text{O}_2$  concentration in the growth atmosphere. The Er concentration was about  $1 \times 10^{19}\text{cm}^{-3}$ .

atmosphere. The changes in the spectra are, of course, not due to the different isotopes. An identical change in the PL spectra is observed even when  $^{16}\text{O}_2$  is used instead of  $^{18}\text{O}_2$ .  $^{18}\text{O}$  is introduced into the furnace as oxygen molecules. The difference in the spectra indicates that unintentionally doped  $^{16}\text{O}$  was introduced into the furnace in the form of oxygen compounds such as alkoxides. The probable origin of  $^{16}\text{O}$  is residual Er-oxygen complexes in the Er source itself. Er-O complex centers formed in GaAs from such compounds do not contribute to the formation of the Er center responsible for the spectrum shown in Fig. 1(b).

The processes forming the Er centers at different growth temperatures with and without O codoping were studied by *in situ* monitoring of the surface roughness during the growth (Fig. 3). The intensity of light scattered from the growth surface was monitored by irradiating the surface with an Ar laser. The horizontal axis in Fig. 3 shows the distance from the interface between the substrate and the epitaxial layer. The vertical axes show (a) scattered light intensity, (b) growth temperature, and (c) flow rate of argon (Ar) gas containing 100 ppm  $\text{O}_2$ . As seen in regions A and B, when the growth temperature is  $500^\circ\text{C}$  the surface morphology is smooth regardless of  $\text{O}_2$  concentration in the growth atmosphere. At the growth temperatures of  $550$  and  $600^\circ\text{C}$ , however, the surface retains a smooth morphology only when  $\text{O}_2$  is injected into the reactor (regions C and E). When there is no  $\text{O}_2$  in the atmosphere the surface becomes rough as the growth proceeds, and the rate of roughening with the growth is higher at a higher temperature (region D and F).

We think this behavior is related to the formation of Er-rich aggregates on the growth surface. The rate of roughening is higher at a higher temperature because the segregation of Er atoms out of the grown epilayer becomes larger and the mobility of Er atoms on the growth surface is higher. Both these phenomena facilitate the formation of Er aggregates on the surface. Since Er has a strong tendency to form complexes with O, we speculate that the changes in the light scattering intensity are caused by the coupling of Er atoms with O atoms. This coupling would suppresses the formation of large Er-rich aggregates that become the origin of the morphology that scatters light. When Er atoms couple with O atoms on the GaAs surface, the complexes are probably more easily incorporated into the GaAs host before large aggregates can form.

This speculation is consistent with the temperature dependence of the PL spectrum of Er-doped GaAs, which reflect the different types of Er centers formed. At a high growth temperature — such as  $600^\circ\text{C}$  or more, which is normally used in the growth of high quality GaAs — an Er-related luminescence spectrum shows several broad bands. As the growth temperature becomes lower, the broad bands splits into a number of lines as shown in Fig. 1(a). The number of luminescence lines in the spectrum becomes smaller and their intensity higher in O-codoped sample as shown in Fig. 1(b).

Not only the growth temperature and the O source but also the orientation of the substrate has a large effect on the formation of the Er centers [5]. When the substrate is misoriented from the (100) plane, the intensity

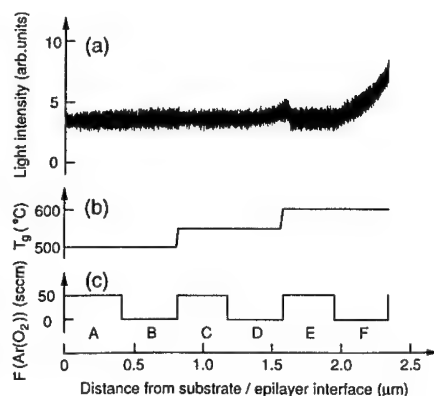


Fig. 3. Intensity of light scattered from the surface of Er-doped GaAs growth with and without added  $\text{O}_2$ . The horizontal axis is the distance between the surface and the substrate/epilayer interface. The vertical axes are (a) scattered light intensity, (b) growth temperature, and (c) flow rate of Ar gas containing 100 ppm  $\text{O}_2$  gas.

of the sharp lines observed in Fig. 1(b) decreases. This behavior can be accounted for by considering the role of atomic steps on the vicinal planes. Therefore, the microscopic structure of the growth surface is related to the atomic configurations of Er centers formed in GaAs. This result, as well as the effects of growth temperature and the O source show that Er centers may be formed in a controlled manner by choosing appropriate growth conditions.

### III. ATOMIC CONFIGURATIONS OF Er CENTERS IN GaAs:Er,O

What is the atomic configuration of the Er center showing the sharp line spectrum shown in Fig. 1(b)? It must be a complex of Er and O. The formation of large aggregates is suppressed in the O-containing growth atmosphere. The extremely small linewidths suggests that this Er center is not in Er-rich aggregates incorporated in various ways in the lattice of the GaAs host, since the luminescence spectrum of a sample with such Er atoms should show inhomogeneous broadening. The number of lines observed in the spectrum indicates that it is a non-cubic center [6].

Additional evidence related to the atomic configuration of the Er center was obtained from PL spectra of  $\text{Al}_x\text{Ga}_{1-x}\text{As:Er,O}$  with low Al concentrations [7]. We added a small amount of Al in the GaAs:Er,O and measured high-resolution PL spectra in the region of the highest luminescence line in Fig. 1(b). This region is most suitable for a detailed analyses since the line in this region has the smallest width of the seven lines by this Er center. A small change in the spectra due to the formation of different Er centers may be observed. Figure 4 compares the PL spectra of four samples with different Al concentrations. The peak intensities of the spectra are normalized to the same values. Comparing the spectrum for the pure GaAs host and that for the  $\text{Al}_{0.01}\text{Ga}_{0.99}\text{As}$  host, it is surprising to see that adding just 1% Al results in the appearance of so many lines. At the wavelength of the strongest line indicated by an arrow in Fig. 4(a) for the sample with a pure GaAs host, there still is a luminescence line in Fig. 4(b) for the sample with the  $\text{Al}_{0.01}\text{Ga}_{0.99}\text{As}$  host. Comparing Fig. 4(b) and 4(c), we can see that the spectra change according to the Al composition, but relatively strong lines are observed at the same wavelengths in the  $\text{Al}_{0.01}\text{Ga}_{0.99}\text{As}$  host and in the  $\text{Al}_{0.04}\text{Ga}_{0.96}\text{As}$  host. These observations indicate that various types of new Er centers with well defined atomic configurations are formed when a small amount of Al is added to the GaAs doped with Er and O. Moreover, these Er centers have the same

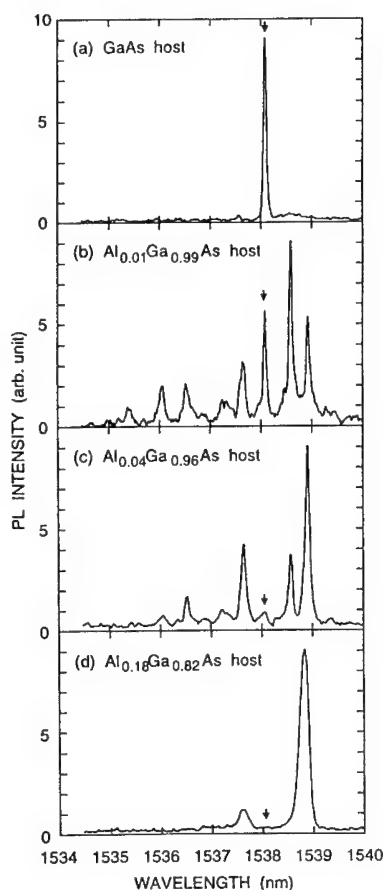


Fig. 4. High resolution PL spectra of  $\text{Al}_x\text{Ga}_{1-x}\text{As:Er,O}$  for various Al concentrations: (a) 0%, (b) 1%, (c) 4%, and (d) 18%. The spectra, measured at 2 K with a resolution of 0.04 nm, are normalized by the peak intensity of the strongest luminescence line in each spectrum. The wavelength of the main peak in GaAs:Er,O is indicated by an arrow in each spectrum.



atomic configurations in the alloy hosts with different Al concentrations up to 4%. These results thus differ from frequently observed experimental results obtained in alloy systems where the spectrum changes continuously with change in alloy composition.

Rutherford back-scattering channeling experiments indicate that Er atoms tend to occupy a location close to substitutional sites in GaAs when O is codoped [7]. The most probable site would be the Ga site. The fact that the luminescence lines in Fig. 1(b) are seen only when O is codoped indicates that the Er center responsible for the luminescence is an Er-O complex. The simplest atomic configuration of the center consistent with such experimental evidence would be an Er atom occupying the Ga site and an O atom located either at the nearest neighbor As site or tetrahedral interstitial site. The former case is shown in Fig. 5(a). The drastic change in the PL spectra with only 1% Al may be understood as due to preferential occupation of Al atoms at the three next nearest neighbor sites of the O atom, substituting for Ga atoms. This configuration is shown schematically in Fig. 5(a), indicated with three sites that can be occupied either by Ga or Al atoms. If we assume that different numbers of Al atoms occupying these sites correspond to different lines observed in Fig. 4, we would expect only four lines. This atomic configuration therefore does not explain the observed changes in the PL spectra. On the other hand, if we assume that two O atoms are coupled with an Er atom as shown in Fig. 5(b), ten different atomic configurations can be formed as discussed in more detail in Ref. 7. This is consistent with the number of luminescence lines observed in the spectra of alloy hosts in Fig. 4(b) and 4(c).

There are several experimental results that further support the proposed atomic configuration. The atomic configurations shown in Fig. 5(a) and 5(b), respectively, have  $C_{3v}$  and  $C_{2v}$  symmetry. A Zeeman measurement of the luminescence indicates that the symmetry of the Er center is close to  $C_{2v}$  [8]. In PL measurements, an anisotropy of polarization was observed for GaAs:Er,O, showing that a specific axis of this Er center is preferentially aligned toward the growth direction [9,10]. This anisotropy can be understood assuming that the Er atom at the Ga site is coupled with two O atoms, either at the nearest neighbor As sites or tetrahedral interstitial sites. We therefore think that the Er center responsible for the sharp luminescence lines in Fig. 1(b) is an Er atom at the Ga site with two adjacent O atoms, an  $\text{Er}_{\text{Ga}}\text{-2O}$  center. The site of the atoms is probably displaced somewhat from the regular lattice sites. Additional defects such as vacancies, hydrogen or carbon might also be involved in the atomic configuration, but no experimental evidence of such has yet been found.

#### IV. EXCITATION PROCESSES OF RARE-EARTH CENTERS IN SEMICONDUCTORS

A RE ion in a semiconductor host may be excited in several ways (Fig. 6). The simplest way is the direct optical excitation of the 4f-shell electrons from the ground state to the excited state. Radiative relaxation from the excited state to a lower-energy state results in luminescence. The efficiency of such excitation depends on the optical cross section (or oscillator strength) of the

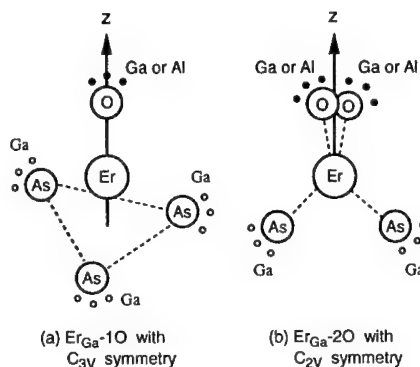


Fig. 5. Possible atomic configurations of (a) an  $\text{Er}_{\text{Ga}}\text{-1O}$  center with  $C_{3v}$  symmetry and (b) and  $\text{Er}_{\text{Ga}}\text{-2O}$  center with  $C_{2v}$  symmetry. The sites of the Ga sublattice adjacent to the As atoms are shown by open circles, and the sites of the Ga sublattice adjacent to the O atoms are shown by closed circles.

transition and on the concentration of the center. The intensity of luminescence depends also on the efficiency of radiative relaxation, decreasing if there are other energy dissipation mechanisms such as non-radiative relaxation and energy transfer to other centers.

A RE ion in a semiconductor host can also be excited by energy transfer from e-h pairs in the host. An e-h pair can be created by current injection into a p-n junction or by photo-excitation of the host by a photon whose energy exceeds the bandgap of the host. Alternatively, when the RE ion in some atomic configuration forms a trap level within the bandgap of the host, photo-excitation of a carrier from either the valence band or the conduction band to the trap level creates a bound e-h pair or a bound exciton. Successive energy transfer to the 4f-shell electrons may also activate the electrons in the 4f-shell.

The energy transfer from an e-h pair bound at the RE center to the 4f-shell electrons of the RE center seems to be the most plausible mechanism of the Er-related luminescence under host photo-excitation. This mechanism was found to be consistent with experimental results on Yb-doped InP [11]. This model, schematically shown in Fig. 7, assumes that the energy mismatch between the recombination energy of an e-h pair bound at the RE center and the energy required to excite the 4f-shell electrons from the ground state to the excited state is compensated by multi-phonon emission [12]. The excitation rate  $W_e$  and de-excitation rate  $W_a$  (the rate of energy back-transfer by non-radiative relaxation in the 4f-shell and creation of an e-h pair bound at the RE center with phonon absorption) are expressed as

$$W_e = W_0(n_q + 1)^p \exp(-2n_q s) \quad (1)$$

and

$$W_a = W_0(n_q)^p \exp(-2n_q s), \quad (2)$$

where

$$p = E_0 / \hbar \nu.$$

Here,  $W_0$  is the transition matrix element for the energy transfer between the bound e-h pair and the 4f-shell electrons,  $n_q$  is the phonon density (which is the only temperature-dependent factor in the equation),  $s$  is the Huang-Rhys factor,  $\hbar \nu$  is the optical phonon energy, and  $E_0$  is the difference between the recombination energy of the e-h pair bound at the RE center and the excitation energy

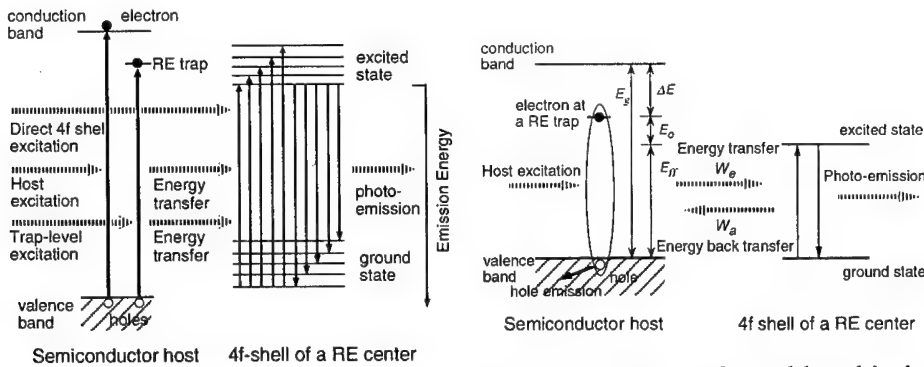


Fig. 6. A schematic diagram of the energy bands of a semiconductor host, and the ground and the first excited states of 4f-shell electrons of a RE atom in the semiconductor. Three methods of excitation are shown.

Fig. 7. The energy transfer model used in the calculations [12].  $E_s$  is the bandgap of the host semiconductor and  $\Delta E$  is the depth of RE-related carrier trap, which is assumed to be an electron trap.  $W_e$  and  $W_a$  are the transition probabilities given by Eqs. (1) and (2).

of the 4f-shell electrons,  $E_{ff}$

Luminescence at  $1.5\mu\text{m}$  due to the  $^4I_{13/2}$  (excited state)  $\rightarrow$   $^4I_{15/2}$  (ground state) transition of the  $\text{Er}^{3+}$  ion has been observed by host photo-excitation for various Er-doped semiconductors. The total luminescence efficiency of the Er centers is on the same order in AlGaAs alloy hosts of various Al concentrations shown in Fig. 4. Er also shows luminescence in InGaAsP alloy hosts with bandgap energies ranging from 0.8 to 1.4 eV [13]. The exact resonance of some energy donor in the host and the 4f-shell electronic system, the energy acceptor, does not seem to be required for the energy transfer. The energy transfer model in Fig. 7 is consistent with this observation, the energy mismatch being compensated by a multi-phonon process.

If we assume this mechanism, thermal quenching of RE-related luminescence may be explained by the energy back-transfer process expressed by Eq. (2). A comparison of this equation and the experimentally observed thermal quenching behavior of luminescence decay time allows an estimation to be made of the important parameters  $W_0$  and  $\Delta E$ , where  $\Delta E = E_g - E_{ff} - E_o$ . The application of such an analysis to GaAs:Er,O will be discussed in Sec. VI.

In this paper we will not discuss another conceivable excitation mechanism where the  $\text{Er}^{3+}$  ions are resonantly excited by distant energy donors, such as donor-acceptor pairs. This kind of process is observed in insulating materials [14], but we have not found any evidence of such an energy donor present in GaAs:Er,O. Neither will we discuss the mechanism in which the energy mismatch is compensated by carriers in the host (Auger process), because, for samples with similar Er concentrations, luminescence of the  $\text{Er}_{\text{Ga}}\text{-2O}$  center is dominant and not so different in p- and n-type hosts (with carrier concentrations on the order of  $10^{16}\text{cm}^{-3}$ ) as well as in semi-insulating hosts. We think that the Auger process is not the essential process in the excitation of the  $\text{Er}_{\text{Ga}}\text{-2O}$  center, although it probably is important in the quenching of the luminescence especially at higher carrier concentrations, as was shown for InP:Yb [15].

## V. DIRECT 4f-SHELL PLE SPECTROSCOPY OF GaAs:Er,O

Figure 1(b) is the spectrum of GaAs:Er,O under above-bandgap photo-excitation. It shows luminescence due predominantly to the  $\text{Er}_{\text{Ga}}\text{-2O}$  center. There may, however, be other Er centers that do not show luminescence in this spectrum because of a low efficiency of energy transfer from the host. As discussed in the previous section,

one way to evaluate such Er centers in a sample is by measuring a direct 4f-shell photoluminescence excitation (PLE) spectrum. Figure 8 shows such PLE spectra of a GaAs:Er,O sample, monitoring the luminescence at 1600 or 1545 nm with a bandwidth of 26 nm [16,17]. The selection of such wide wavelength regions allows simultaneous detection of PLE signals from various Er centers in the sample. On the other hand, a PLE measurement monitoring a narrow wavelength region predominantly from one Er center (which is called a site-selective PLE measurement) allows identification of excited-state energy levels for a specific type of Er center corresponding to the monitored luminescence line. Such a measurement was carried out for  $\text{Er}_{\text{Ga}}\text{-2O}$  samples, and the features indicated by arrows in Fig. 8 have been found to be due to the  $\text{Er}_{\text{Ga}}\text{-2O}$  center. Figure

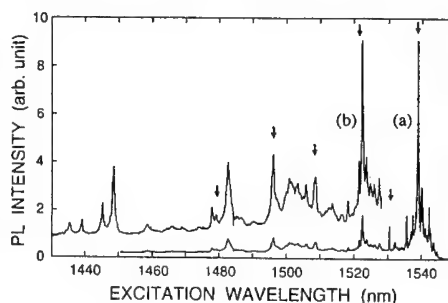


Fig. 8. Non-site-selective PLE spectra of GaAs:Er,O measured by monitoring the PL centered at (a) 1600 nm and (b) 1545 nm. The monitored bandwidth is 26 nm. The arrows indicate the wavelengths of the features observed in the site-selective PLE spectrum for the PL peak at 1617 nm in Fig. 1(b), which is due to the  $\text{Er}_{\text{Ga}}\text{-2O}$  center.

9(a) shows a PL spectrum obtained by exciting the peak at 1530.5 nm in Fig. 8. Seven distinct features were consistently observed for samples grown under similar conditions. Their wavelengths and relative intensities coincide with those in Fig. 1(b) when measured with the same spectral resolution, confirming that the seven PL lines in Fig. 1(b) are due to the  $\text{Er}_{\text{Ga}}\text{-2O}$  center.

Other features in the PLE spectrum shown in Fig. 8 must therefore be due to other Er centers. The PL spectrum shown in Fig. 9(b) was obtained by exciting the peak at 1448.6 nm, which is one of the sharp lines observed in Fig. 8. We compared spectra for several samples and confirmed that the six lines indicated by arrows in Fig. 9(b) and two additional weak lines at 1667 and 1672 nm (not shown) are due to one type of Er center. Corresponding to the sharpness of the PLE line, this type of Er center shows a sharp PL spectrum comparable to that of the  $\text{Er}_{\text{Ga}}\text{-2O}$  center. The wavelengths of their highest peaks, near 1538 nm, almost coincide under the present spectral resolution but actually differ by about 0.3 nm. No lines observed in Fig. 9(b) are observed in the host-excited PL spectrum shown in Fig. 1(b). Thus the Er center with the spectrum shown in Fig. 9(b) must have a negligible efficiency of excitation through the host compared to the Er-2O center. The peak intensity of the line at 1448.6 nm in Fig. 8 is comparable to that of lines due to the  $\text{Er}_{\text{Ga}}\text{-2O}$  centers, suggesting that their Er concentrations are comparable. This is true, however, only if the oscillator strengths of the transitions for the two centers are nearly equal and non-radiative relaxation of the excited states is negligible in the both centers.

Figure 9(c) shows a PL spectrum excited at 1500.0 nm, which is a region of a broad feature in the PLE spectrum shown in Fig. 8. In addition to the two Raman lines, a large number of lines and broad features are observed, indicating that Er centers with various atomic configurations are simultaneously excited. PL spectra excited at slightly different wavelengths show similar spectra with somewhat different intensities of the fine structures. These features suggest

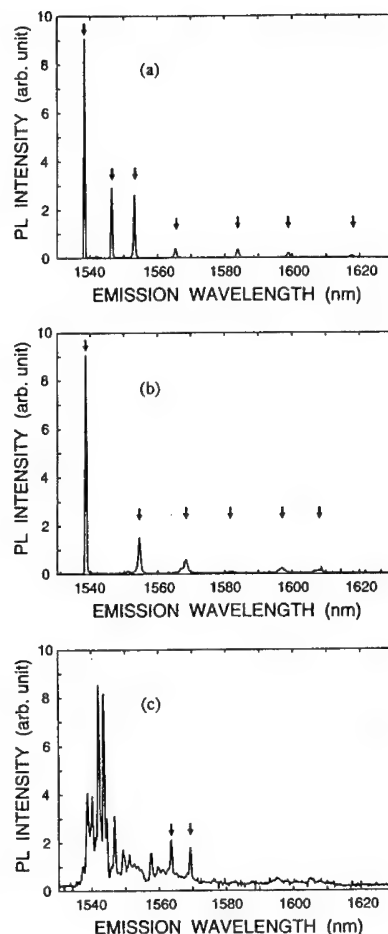


Fig. 9. Site-selective PL spectra of GaAs:Er,O excited at (a) 1530.5 nm, (b) 1448.8 nm, and (c) 1500.0 nm. They were measured at 2 K with a spectral resolution of 0.7 nm. The arrows in (a) indicate the wavelengths of the features due to the  $\text{Er}_{\text{Ga}}\text{-2O}$  center, and the arrows in (b) indicate the wavelengths of features due to another type of Er center. The lines indicated by arrows in (c) are Raman signals, while other features are Er-related luminescence.

that the photon energy absorbed by a specific Er center is migrating to other Er centers with slightly different atomic configurations having quasi-resonant 4f-shell energy-levels. This kind of spectrum is probably due to Er-rich aggregates with a high density of  $\text{Er}^{3+}$  ions rather than to Er centers uniformly dispersed in the host. Within an aggregate, the energy absorbed by a specific Er center can easily migrate to other Er centers with slightly different atomic configurations. Luminescence from Er centers in various atomic configurations may then be observed even under photo-excitation at a specific wavelength. The broadness of the feature is also consistent with such a speculation, since such aggregates might be incorporated in the zincblende structure of the GaAs host in various ways and there could be various distortion around  $\text{Er}^{3+}$  ions. As discussed in Sec. II, codoping of O in the growth of Er-doped GaAs suppresses the segregation of Er atoms, but some Er atoms may still segregate in GaAs:Er,O. In Fig. 1(b), a weak and broad PL feature in the wavelength region between 1535 and 1570 nm is observed under host excitation. This wavelength region and its feature are similar to those of the luminescence shown in Fig. 9(c). The Er-rich aggregates thus seem to show some luminescence under host excitation.

So three types of Er centers coexist in one sample. The type I center shows a spectrum with sharp lines and high peak luminescence intensity under host photo-excitation. This type of center has a very high efficiency of energy transfer from an e-h pair in the host. An Er center of this type has also been observed in MBE-grown GaAs:Er [6]. This center must have an atomic configuration different from that of the  $\text{Er}_{\text{Ga}}\text{-2O}$  center because its PL spectrum is different from that of the Er-2O center. This Er center was observed also in MOCVD-grown samples, but only at a low Er concentration [2].

The type II center shows little or no luminescence under host photo-excitation, but it shows a luminescence spectrum with sharp lines under direct 4f-shell excitation. This type of center must have a very small energy transfer efficiency from an e-h pair in the host. The type III center shows a luminescence spectrum with many lines whose widths are generally greater than those of lines due to type I and II centers. Because of the greater linewidths, the peak intensities of these lines are generally lower than those of type I and II centers for similar concentrations. There may also be some other Er centers, a type IV center, which do not show luminescence even by direct 4f-shell excitation because of some PL quenching process occurring in the samples. We have, however, no way to directly observe such centers at present.

The  $\text{Er}_{\text{Ga}}\text{-2O}$  center is a center of type I which is the most important type for device application of this kind of materials. Some noteworthy characteristics of the  $\text{Er}_{\text{Ga}}\text{-2O}$  centers are the following:

- (1) It shows a very sharp line spectrum under host photo-excitation, suggesting that it is dispersed in the host and has a very high efficiency of energy transfer from the host.
- (2) The temperature dependence of the wavelengths of the lines are very small as expected for the intra-4f-shell transitions [3].
- (3) It shows relatively sharp luminescence even at room temperature. The linewidth increases to a few nanometers and the integrated intensity decreases about one order compared to that observed at temperatures below 200 K [3].
- (4) It is efficiently formed only at a low growth temperature below 500°C but is thermally stable once formed. A post-growth anneal at 750°C for 30 min. does not change any PL characteristics.

## VI. ENERGY-TRANSFER PROCESSES IN GaAs:Er,O

Device applications of Er-doped semiconductors require that a high luminescence intensity be obtained by minority carrier injection. For an efficient energy transfer from an e-h pair injected in the host to the 4f-shell electrons of  $\text{Er}^{3+}$  ions, the following five requirements have to be met.

- (1) A large concentration of optically active Er centers must be formed in a high-quality host. Formation of aggregates distorts the host crystal forming non-radiative recombination

- centers and also reduces the effective concentration of Er centers accessible by e-h pairs.
- (2) There must be a mechanism that brings e-h pairs within an interaction distance of Er centers. Formation of carrier traps with large capture cross sections by Er centers themselves seems to be a very effective mechanism.
  - (3) After an e-h pair is trapped at an Er center, there must be a high probability that it recombines and transfers its energy to the 4f-shell of the  $\text{Er}^{3+}$  ion. The probability will be high if the recombination energy of the e-h pair is in resonance with the excitation energy of the 4f-shell electrons. This, however, does not seem to be always the case, since the 4f-shell luminescence at  $1.5\mu\text{m}$  is observed in various hosts and for various types of Er centers. Clear evidence of resonance has not been reported, so it seems that there must be some universal energy compensation mechanism for the energy transfer. In the case  $\text{GaAs:Er,O}$ , an Auger process by carriers can be excluded as discussed in Sec. IV, and an alternative energy compensation mechanism by a multi-phonon process was proposed. This mechanism explains various experimental results obtained in  $\text{InP:Yb}$  and may also explain the observed properties of  $\text{GaAs:Er,O}$ .
  - (4) The efficiency of energy transfer depends not only on the energy compensation mechanism but also on the nature of the e-h pair and the micro-structure of Er center which determines  $W_0$  in Eqs. (1) and (2) in Sec. IV.  $W_0$  must be large compared with other rates of competing energy relaxation processes. A rigorous theoretical estimation of  $W_0$  requires detailed knowledge of the Er centers and has not yet been reported for any Er center. An empirical estimation of  $W_0$  will be discussed later in this section.
  - (5) After the 4f-shell is excited, a radiative probability has to be greater than any non-radiative probability. The observed luminescence intensity indicates that a carrier-related non-radiative relaxation rate is not very high if majority carrier concentrations are on the order of  $10^{16}\text{ cm}^{-3}$  for n- and p-type samples. Thermal quenching of the luminescence intensity is observed even for samples with semi-insulating hosts. Since it is accompanied by the reduction of the lifetime of the  $^4\text{I}_{13/2}$  excited state, it must be due to some non-radiative relaxation of the excited center rather than the decrease in the excitation efficiency of the center. This quenching is probably caused by a back-transfer process such as that observed in the case of  $\text{InP:Yb}$ , where the excited 4f-shell electrons relax to the ground state and the relaxation energy along with thermally activated phonon energy create an e-h pair bound at the Er center (see Fig. 7). This is the reverse process of the activation of 4f-shell electrons and is a process that can occur regardless of other defects in the host.

As discussed in Sec. V, at least three types of Er centers coexist in the  $\text{GaAs:Er,O}$  sample studied. The type III centers which show weak luminescence under host photo-excitation in  $\text{GaAs:Er,O}$  do not satisfy the requirement (1) mentioned above for high luminescence efficiency. The formation of large aggregates not only reduces excitation efficiency but also increases the linewidths and reduces the peak intensity of the luminescence lines. In laser applications, a high peak intensity is essential for a low-threshold operation.

That the type II centers satisfy the requirement (1) can be inferred from the sharp absorption and luminescence lines observed, respectively, in PLE and site-selective PL measurements. These centers also satisfy the requirement (5), since luminescence is observed under direct 4f-shell excitation. Then the fact that no luminescence is observed under host excitation indicates that at least one requirement among (2), (3) or (4) is not satisfied, but we do not, at present, know which requirement actually are not met.

The high luminescence efficiency of the  $\text{Er}_{\text{Ga}}\text{-2O}$  center, a type I center, indicates that this center meets all five requirements fairly well. If we assume the energy transfer mechanism discussed in Sec. IV, some physical parameters for this center can be estimated from the temperature dependence of the life time of the  $^4\text{I}_{13/2}$  excited state, which can be obtained by measuring the decay time as a function of temperature. A result of such a measurement for the

highest luminescence line in Fig. 1(b) is shown in Fig. 10. In the present model, the temperature dependence is mainly determined by the back-transfer process (Fig. 7). An e-h pair recombination at the Er center emitting a photon is neglected because such luminescence is not observed experimentally. Equations for the energy transfer according to Eqs. (1) and (2), and additional equations for energy dissipation processes such as e-h pair dissociation and radiative relaxation of the 4f-shell electrons were solved. Best-fit parameters were obtained by comparing the temperature dependencies of the PL decay time experimentally obtained and that analytically calculated based on the proposed model [18]. They are shown in Fig. 10. The important parameters obtained in this way are the position of the trap level from the bandedge,  $\Delta E$ , and the matrix element that determines the rate of energy transfer from the e-h pair to the 4f-shell electrons,  $W_0$ . Estimated values for  $\Delta E$  and  $W_0$  are 0.42 eV and  $4 \times 10^9 \text{ sec}^{-1}$ , respectively.

This calculation cannot distinguish whether  $\Delta E$  is the value measured from the bottom of the conduction band or the top of the valence band. A study to experimentally identify the trap level of the  $\text{Er}_{\text{Ga}}\text{-2O}$  center and possibly the type II Er centers found by PLE measurements is under way. Such a study should clarify the role of trap levels in determining the optical characteristics of type I and type II Er centers, but the simultaneous presence of various centers has so far made it difficult to identify the trap level corresponding to the Er centers responsible for a specific luminescence spectrum.

The estimated  $W_0$  value for the  $\text{Er}_{\text{Ga}}\text{-2O}$  center is comparable to the band-to-band radiative transition rate of an e-h pair often observed. Such a high rate of transition from the extended state of the e-h pair to the screened and very localized 4f-shell electrons is surprising. It is, however, consistent with the fact that the luminescence of an e-h pair bound at the Er trap is not experimentally observed but the intra-4f-shell luminescence of Er is observed. A theoretical consideration taking into account the microscopic structure of the  $\text{Er}_{\text{Ga}}\text{-2O}$  center will be required in order to verify such a high transition rate. The estimation of  $W_0$  is important in the application of this material to lasers, since this process may become a bottleneck of the lasing scheme if it is too slow compared to other energy-transfer processes.

## VII. SUMMARY

The luminescence spectrum of MOCVD-grown Er-doped GaAs shows a marked change when oxygen is codoped. The roles of oxygen in the formation of Er-O complex centers were clarified by using oxygen isotope gases ( $^{16}\text{O}_2$  and  $^{18}\text{O}_2$ ) and by monitoring the growth surface *in situ*. PLE measurements in which the 4f-shells of Er centers are directly excited and PL measurements in which the GaAs host is excited showed that although there are many types of Er centers simultaneously present in the sample, only one type of Er center shows predominant luminescence due to the transfer of energy from electron-hole pairs in the host. This Er center was identified as an Er atom substituting for a Ga site and coupled with two oxygen atoms. The reasons why only this center has a high energy-transfer efficiency by photo-excitation of the host were discussed and an energy-transfer model was proposed. The temperature dependence of the

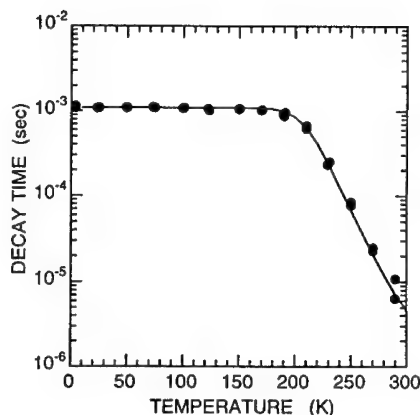


Fig. 10. Temperature dependence of decay time of the  $\text{Er}_{\text{Ga}}\text{-2O}$  center. Circles denote experimental results and solid lines are calculated results using best-fit parameters.

decay time of the  $\text{Er}_{\text{Ga}}\text{-2O}$  center was explained by the proposed model, and two physical parameters of the center were obtained: the depth of the trap level formed by this center, and the rate of energy transfer from the electron-hole pair at the trap to the 4f-shell electrons. Implications of these experimentally determined values were discussed.

#### ACKNOWLEDGMENTS

We would like to express our gratitude to Dr. Yoshiji Horikoshi for discussions on the mechanisms of the  $\text{Er}_{\text{Ga}}\text{-2O}$  formation and the energy transfer processes.

#### REFERENCES

- [1] For example, *Rare Earth Doped Semiconductors*, edited by G. S. Pomrenke, P. B. Klein, and D. W. Langer (Mater. Res. Soc. Symp. Proc. **301**, San Francisco, CA, 1993).
- [2] K. Takahei and A. Taguchi, *J. Appl. Phys.* **74**, p. 1979 (1993).
- [3] K. Takahei, P. S. Whitney, H. Nakagome, and K. Uwai, *J. Appl. Phys.* **65**, p. 1257 (1989).
- [4] K. Takahei and A. Taguchi, *Jpn. J. Appl. Phys.* **33**, p. 709 (1994).
- [5] K. Takahei, Y. Horikoshi and A. Taguchi, in *Defects in Semiconductors 18*, edited by M. Suezawa and H. Katayama-Yoshida, (Mater. Science Forum **196-201**, Sendai, Japan, 1995), pp. 639-643.
- [6] H. Ennen, J. Wagner, H. Müller, and R. Smith, *J. Appl. Phys.* **61**, p. 4877 (1987).
- [7] K. Takahei, A. Taguchi, Y. Horikoshi, and J. Nakata, *J. Appl. Phys.* **76**, p. 4332 (1994).
- [8] D. Haase, A. Dörnen, K. Takahei, and A. Taguchi, submitted to the Mater. Res. Soc. Symp. Proc. **422**, San Francisco, CA, 1996.
- [9] R. A. Hogg, K. Takahei, A. Taguchi, and Y. Horikoshi, *Appl. Phys. Lett.* in press.
- [10] R. A. Hogg, K. Takahei, A. Taguchi, and Y. Horikoshi, submitted to the Mater. Res. Soc. Symp. Proc. **422**, San Francisco, CA, 1996.
- [11] A. Taguchi, K. Takahei, and J. Nakata, in *Rare Earth Doped Semiconductors*, edited by G. S. Pomrenke, P. B. Klein, and D. W. Langer (Mater. Res. Soc. Symp. Proc. **301**, San Francisco, CA, 1993), pp. 139-150.
- [12] A. Taguchi, K. Takahei, and Y. Horikoshi, *J. Appl. Phys.* **76**, p. 7288 (1994).
- [13] C. Rochaix, A. Rolland, P. N. Favennec, B. Lambert, A. Le Corre, H. L'Haridon, and M. Lalvi, *Jpn. J. Appl. Phys.* **27**, p. L2348 (1988).
- [14] S. Hüfner, *Optical Spectra of Transparent Rare Earth Compounds*, Academic Press Inc., New York, 1978, Chp. 5.
- [15] K. Takahei, A. Taguchi, H. Nakagome, K. Uwai, and P. S. Whitney, *J. Appl. Phys.* **66**, p. 4941 (1989).
- [16] K. Takahei and A. Taguchi, *J. Appl. Phys.* **77**, p. 1735 (1995).
- [17] K. Takahei and A. Taguchi, *J. Appl. Phys.* **78**, p. 5614 (1995).
- [18] A. Taguchi and K. Takahei, in *Defects in Semiconductors 18*, edited by M. Suezawa and H. Katayama-Yoshida, (Mater. Science Forum **196-201**, Sendai, Japan, 1995), pp. 633-637.



## EXCITATION PROPERTIES OF Er-DOPED GaP FROM PHOTOLUMINESCENCE AND HIGH PRESSURE STUDIES

T.D. Culp\*, X.Z. Wang\*\*, T.F. Kuech\*, B.W. Wessels\*\*, and K.L. Bray\*

\*Department of Chemical Engineering, University of Wisconsin, Madison WI 53706  
e-mail: bray@engr.wisc.edu

\*\*Department of Materials Science and Engineering, Northwestern University, Evanston IL 60208

### ABSTRACT

The photoluminescence properties of MOCVD GaP:Er were investigated as a function of temperature, applied hydrostatic pressure, and excitation wavelength. Four sharp peaks are observed on the high energy side of the 1.54  $\mu\text{m}$   $\text{Er}^{3+}$  emission. These peaks are selectively excited by below-gap energies and have a significantly shorter lifetime than the main  $\text{Er}^{3+}$  emission, suggesting that at least two distinct  $\text{Er}^{3+}$  centers contribute to the luminescence. The low temperature photoluminescence excitation (PLE) spectrum of the 1.54  $\mu\text{m}$  emission was also measured. Strong broad excitation of the  $\text{Er}^{3+}$  centers occurs with energies well below the indirect bandgap energy. In fact, the  $\text{Er}^{3+}$  emission intensity is significantly stronger when excited with below-gap wavelengths than with above-gap wavelengths. This result has been explained in terms of competition between  $\text{Er}^{3+}$  excitation and nonradiative deep level recombination for free carriers under above-gap excitation. With below-gap excitation, carriers are promoted directly into the  $\text{Er}^{3+}$  excitation pathway via absorption at an erbium-related trap. At 42 kbar, below-gap excitation is no longer more efficient than above-gap excitation, suggesting that competitive capture of free carriers by deep levels has been reduced.

### INTRODUCTION

Rare-earth doped semiconductors have been the subject of much research over the past several years because of their potential to combine sharp, temperature stable rare earth luminescence with the convenience of electrical excitation via the semiconductor host.  $\text{Er}^{3+}$  doped materials are of particular interest because the  $^4\text{I}_{13/2} \rightarrow ^4\text{I}_{15/2}$  emission of  $\text{Er}^{3+}$  at 1.54  $\mu\text{m}$  matches the minimum loss region of silica fibers used in optical communications. An important objective of research on rare-earth doped semiconductors is the development of efficient optical devices based upon the electronic transitions of rare earth ions.

Progress toward practical devices based on rare-earth doped semiconductors has been hindered by low room temperature efficiencies. In order to improve the efficiency, a better understanding of the nature of rare-earth centers in the semiconductor lattice and the basic mechanism of rare-earth excitation needs to be further developed. Er-doped GaP has been shown to be a promising system, because the 1.54  $\mu\text{m}$   $\text{Er}^{3+}$  emission intensity only decreases by a factor of 2 as the temperature is increased from 12 to 300 K.<sup>1</sup>

In this work, we examined the luminescence properties of GaP:Er as a function of temperature, applied hydrostatic pressure, and excitation wavelength. We found that several different  $\text{Er}^{3+}$  centers contribute to the luminescence. We also observed that the  $\text{Er}^{3+}$  emission intensity is significantly stronger when excited at energies below the indirect bandgap energy than when excited with above-gap energies. This result is discussed in terms of competition between  $\text{Er}^{3+}$  excitation and nonradiative deep level recombination.

## EXPERIMENT

Epitaxial GaP films were prepared by atmospheric pressure metal-organic chemical vapor deposition (MOCVD) using  $\text{Ga}(\text{CH}_3)_3$  and  $\text{PH}_3$  as reactants.<sup>1</sup> Palladium diffused  $\text{H}_2$  was used as the carrier gas. Erbium doping was accomplished by sublimating tris-tetramethylheptanedionate erbium  $[\text{Er}(\text{thd})_3]$  and transporting the vapor to the reaction zone with  $\text{H}_2$  gas. The layers were deposited on S-doped (100) oriented GaP substrates at  $700^\circ\text{C}$ . Layers were typically  $2\ \mu\text{m}$  thick with an erbium concentration of  $\sim 10^{18}\ \text{cm}^{-3}$ .

For photoluminescence (PL) measurements, samples were cooled in a closed-cycle helium refrigeration system. Samples were excited with either an argon ion laser or a tunable dye laser. Luminescence was dispersed with a one-meter monochromator and detected with either a photomultiplier tube or a liquid-nitrogen cooled Ge detector. Pressure experiments were performed by loading thinned samples into a diamond anvil cell, using a 4:1 ethanol:methanol mixture as the pressure-transmitting fluid and ruby as the pressure calibrant.

## RESULTS AND DISCUSSION

### Spectral Characteristics: Pressure and Temperature Dependence

The low temperature PL spectrum of GaP:Er is shown in Figure 1. A weak, sharp peak at 537 nm (2.309 eV) can be attributed to the recombination of donor-bound excitons ( $\text{D}^0\text{X}$ ) involving unintentionally doped sulfur.<sup>2</sup> Next, the broad peak observed at 559 nm (2.22 eV) is due to donor-acceptor pair recombination. This peak was accompanied by two LO phonon replicas, spaced by  $\sim 49\ \text{meV}$ . The identity of the donor and acceptor is arguable, but the position of the  $\text{D}^0\text{A}^0$  peak suggests a sulfur donor and a silicon or magnesium acceptor.<sup>2,3</sup> These are common unintentional impurities in MOCVD precursors.<sup>4</sup>

Two broad overlapping peaks at  $\sim 700\ \text{nm}$  (1.77 eV) and  $\sim 760\ \text{nm}$  (1.63 eV) originated from the S-doped GaP substrate. It has been proposed that this emission is due to recombination

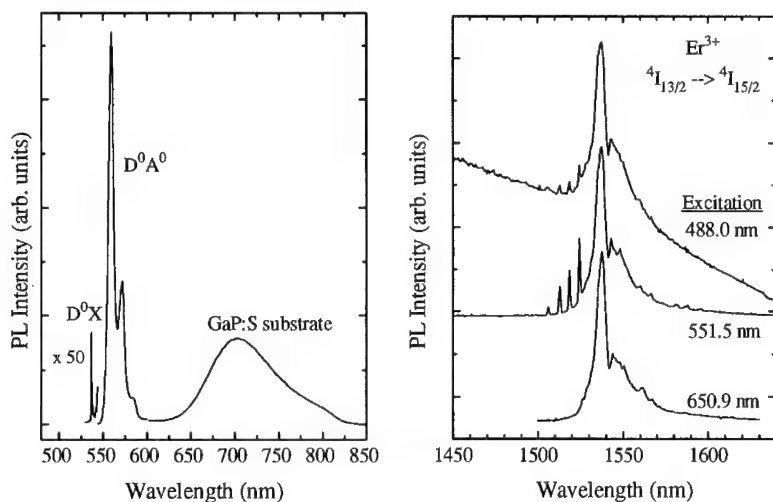


Figure 1: Visible and near-infrared PL spectra of GaP:Er at 12 K.

of excitons bound on sulfur-vacancy complexes.<sup>5</sup> This emission from the substrate was extremely strong, glowing visibly red. A tail of the emission extended into the near-infrared, creating background luminescence underneath the  $^4I_{13/2} \rightarrow ^4I_{15/2}$   $\text{Er}^{3+}$  emission at 1.54  $\mu\text{m}$ .

The 1.54  $\mu\text{m}$   $\text{Er}^{3+}$  emission contained many features in itself. The main peak is at 1537.6 nm with a width of  $\sim 28 \text{ cm}^{-1}$ . A second peak occurs at 1544 nm with a shoulder at 1549 nm. Additionally, four sharp peaks appear on the high energy side, spaced by 3.0 to 3.7 meV. We have confirmed that these sharp peaks are erbium related and not due to any sort of optical interference, including Fabry-Perot resonance. Upon close examination, there are at least 9 identifiable peaks or shoulders altogether. Because the  $^4I_{15/2}$  ground state will be split into at most 8 levels at lowest site symmetry, and emission will only occur from the lowest  $^4I_{13/2}$  level at 12 K, at least two  $\text{Er}^{3+}$  centers must contribute to these peaks. Furthermore, the main peak is much broader than emission lines known to come from a single, well-defined center, such as the  $\text{Er}_{\text{Ga}}-(\text{O}_{\text{As}})_2$  center in  $\text{GaAs:Er,O}$  which has a main peak width of only  $0.1 \text{ cm}^{-1}$ .<sup>6,7</sup> This suggests that there are in fact numerous slightly different centers contributing to the luminescence.

The pressure dependence of the  $\text{Er}^{3+}$  spectrum is shown in Figure 2. As the pressure was increased, the emission peaks shifted away from each other, with rates ranging from -0.034 to +0.042 meV/kbar. The crystal field strength is expected to increase as pressure decreases the distance between the  $\text{Er}^{3+}$  ion and its nearest neighbors. The increasing crystal field strength would then increase the splittings between levels, consistent with the observed diverging nature of the peaks. However, the  $\text{Er}^{3+}$  shift rates are extremely small when compared to the shift rates of the X and  $\Gamma$  conduction band edges, which are -1.6 and +10.5 meV/kbar, respectively.<sup>8</sup> The small  $\text{Er}^{3+}$  shift rates result because transitions within the 4f electron shell are shielded from changes in the crystal host by the filled outer 5s and 5p electron shells.

The effect of temperature upon the  $\text{Er}^{3+}$  spectrum is shown in Figure 3. As reported previously, the  $\text{Er}^{3+}$  emission intensity was not strongly quenched in this material, decreasing only by a factor of  $\sim 2$  as the temperature was increased from 12 to 295 K.<sup>1</sup> Furthermore, the peak

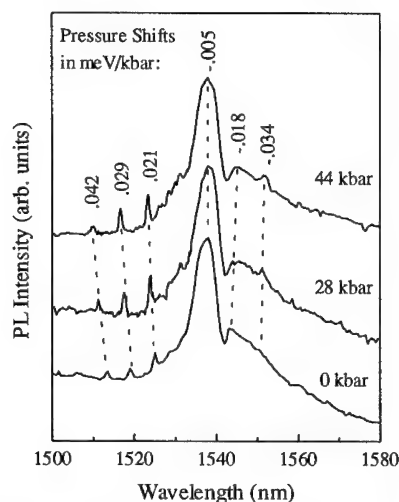


Figure 2: Pressure dependence of the 1.54  $\mu\text{m}$   $\text{Er}^{3+}$  emission in  $\text{GaP:Er}$  at 45 K. Excitation at 488.0 nm.

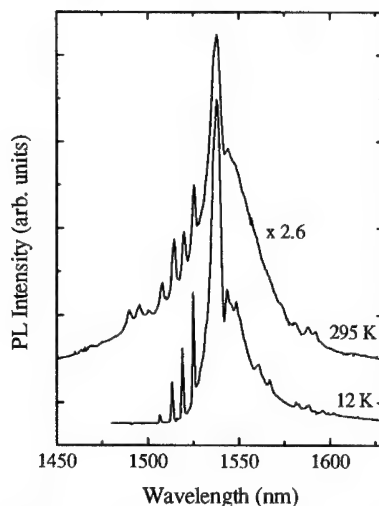


Figure 3: Temperature dependence of the 1.54  $\mu\text{m}$   $\text{Er}^{3+}$  emission in  $\text{GaP:Er}$  at ambient pressure. Excitation at 571.8 nm.

positions were largely independent of temperature. Over this temperature range, the main peak did not shift significantly, and the other peaks shifted only 5-10 Å to longer wavelength at room temperature. Again, this is because the inner 4f electrons are screened from interaction with the crystal host. As the temperature was increased, the only changes in the spectrum included slight broadening of the emission features, and the appearance of three new peaks at higher energy in the range of 1490-1500 nm. These peaks are presumably due to transitions from higher levels within the  $^4I_{13/2}$  manifold, which are more likely to be populated at higher temperatures.

#### Excitation Characteristics

Three representative spectra of the 1.54  $\mu\text{m}$   $\text{Er}^{3+}$  emission under excitation with different wavelengths are shown in Figure 1. The most surprising observation is that there was strong  $\text{Er}^{3+}$  luminescence even with excitation by wavelengths well below the bandgap energy ( $\lambda > 534$  nm). This fact will be discussed in greater detail below. It should be noted that the broad background apparent under the  $\text{Er}^{3+}$  emission with 488.0 nm excitation is due to a near-infrared tail of the strong substrate-related emission. This emission was only observed with above-gap excitation.

Under below-gap excitation, the four sharp peaks on the high-energy side gained in intensity relative to the main peak. These peaks were greatly enhanced by excitation with wavelengths between 534 nm and 608 nm. Beyond 608 nm, these high-energy peaks disappeared altogether, although the rest of the  $\text{Er}^{3+}$  emission remained strong. This behavior suggests that one  $\text{Er}^{3+}$  center is responsible for the four high-energy peaks, whereas other centers are responsible for the relatively broad main peak and low-energy peaks.

The exact nature of this center is undetermined. The linewidth of the four high-energy peaks was only  $1.1 \text{ cm}^{-1}$ , which is approaching the value expected for a single, well-defined  $\text{Er}^{3+}$  site. Furthermore, the PL decay lifetime of these peaks was less than 180  $\mu\text{sec}$ , the limit of our Ge detector. On the other hand, the luminescence decay of the main 1538 nm peak was much longer with two components of 1.2 and 0.3 msec. These observations suggest that a fraction of the  $\text{Er}^{3+}$  may be in some sort of aggregated crystalline phase in which the  $\text{Er}^{3+}$  ions occupy a well-defined site. Cross-relaxation between relatively close  $\text{Er}^{3+}$  ions may be responsible for the short lifetime of the sharp peaks. More work is needed to verify this possibility.

To further characterize the strong excitation by below-gap energies, low temperature photoluminescence excitation (PLE) spectra were measured using a dye laser. The excitation intensity was kept constant at 50 mW for all excitation wavelengths. The PLE spectra for the 1.54  $\mu\text{m}$  emission at ambient pressure and 42 kbar are shown in Figure 4. The PLE spectrum at ambient pressure shows that there was strong broad excitation of the  $\text{Er}^{3+}$  centers at energies well below the indirect bandgap energy. In fact, the  $\text{Er}^{3+}$  emission intensity was three times as strong when excited with below-gap wavelengths than with above-gap wavelengths. One possible explanation is that the  $\text{Er}^{3+}$  emission is weaker with above-gap excitation because highly competitive capture of free carriers by deep levels or other nonradiative processes reduces the number of carriers available for  $\text{Er}^{3+}$  excitation. On the other hand,  $\text{Er}^{3+}$  luminescence with below-gap excitation is much stronger as carriers are promoted directly into the  $\text{Er}^{3+}$  excitation pathway via some mid-gap state.

There are several possible origins of this mid-gap state. The PLE peak lies roughly 80-90 meV below the bandedge. The donor-acceptor pair transition is also at this energy, so it is possible that absorption occurs at the pairs, followed by energy transfer to the  $\text{Er}^{3+}$  centers. However, the PLE peak is an order of magnitude broader than the  $\text{D}^0\text{A}^0$  emission and shows no similar structure. Alternately, direct  $\text{Er}^{3+}$  absorption from the  $^4I_{15/2}$  ground state to the upper  $^4F_{9/2}$ ,  $^4S_{3/2}$ , or  $^2H_{11/2}$  manifolds could be occurring in this range, but much sharper features would be

observed. Finally, the below-gap transition could be absorption directly at the erbium-related trap which is expected to lie beneath the conduction band.<sup>9</sup> After an electron is promoted from the valence band to the Er-related trap, a hole is captured to form a bound exciton which recombines and excites the  $\text{Er}^{3+}$  ion.<sup>9,10</sup>

A PLE spectrum at 42 kbar is also shown in Figure 4. At this pressure, the bandgap energy decreased by  $\sim 70$  meV.<sup>8</sup> This figure shows that although below-gap excitation was still strong, it was no longer more efficient than above-gap excitation. If competing deep level recombination upon above-gap excitation is quenched at higher pressures, the  $\text{Er}^{3+}$  excitation pathway can more effectively contend for free carriers. As a result, above-gap excitation would increase relative to below-gap excitation at high pressures, as was observed. The efficiency of nonradiative recombination at a deep level is highest when the level is at the center of the gap, and decreases monotonically as the level moves away from midgap.<sup>11,12</sup> Thus, if pressure causes the deep level to shift away from the center of the gap, this pressure-induced reduction of deep level recombination would be expected.

Unfortunately, the characteristics of the competing deep level recombination are unknown, and direct evidence that it is inhibited at high pressures is lacking at this time.

However, the excitation power dependence of the  $\text{Er}^{3+}$  emission may provide some indirect evidence of this pressure quenching. At excitation powers below 50 mW, the  $\text{Er}^{3+}$  emission intensity increased roughly as  $P^{1/2}$ . This square-root dependence is commonly observed in  $\text{GaAs:Er}$  and  $\text{Al}_x\text{Ga}_{1-x}\text{As:Er}$ , and has been previously attributed to Auger transfer of the bound exciton energy to a free carrier rather than the  $\text{Er}^{3+}$  ion,<sup>13,14</sup> although there is recent evidence that free carrier Auger processes are not important.<sup>15</sup> However, at 1 atm, the  $\text{Er}^{3+}$  emission intensity saturated at higher excitation powers. At 44 kbar, the square-root dependence was maintained at high excitation powers, and no such saturation was observed even at 200 mW. The  $\text{Er}^{3+}$  emission at ambient pressure could have saturated due to competition with deep level recombination. Deep level recombination (rate typically  $\propto P$ ) will increase faster with excitation power than the  $\text{Er}^{3+}$  emission ( $I \propto P^{1/2}$ ), ultimately dominating free carrier capture. Because no saturation of the  $\text{Er}^{3+}$  emission was observed at 44 kbar, it is possible that competition by deep level recombination has been reduced. This observation is tentative and requires further study.

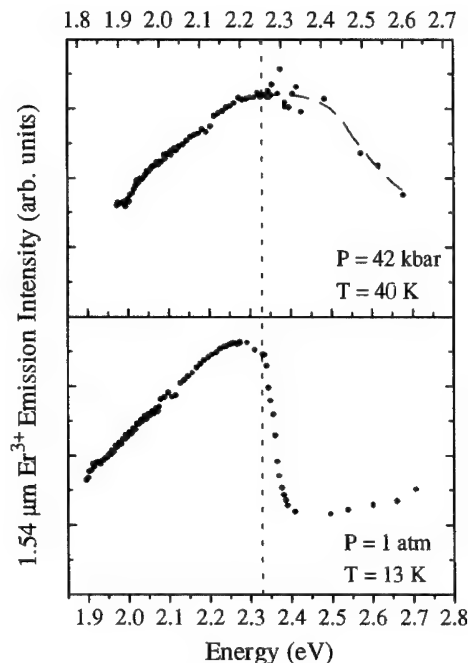


Figure 4: PLE spectra for the  $1.54 \mu\text{m}$   $\text{Er}^{3+}$  emission in  $\text{GaP:Er}$  at 1 atm and 42 kbar. Both spectra are aligned relative to the bandgap energy at the corresponding pressure, as marked by the vertical line. Although the spectra above are at slightly different temperatures, we have confirmed that the PLE spectrum does not change significantly over this small temperature range.

## CONCLUSIONS

In conclusion, the photoluminescence properties of MOCVD GaP:Er were investigated as a function of temperature, applied hydrostatic pressure, and excitation wavelength. The 1.54  $\mu\text{m}$   $\text{Er}^{3+}$  emission peaks exhibited extremely small temperature and pressure shifts, consistent with the shielded nature of the intra-4f transitions. Multiple  $\text{Er}^{3+}$  centers contribute to the luminescence, as evidenced by four sharp higher-energy peaks which are selectively excited by below-gap wavelengths and have a significantly shorter lifetime than the main  $\text{Er}^{3+}$  emission.

The low temperature photoluminescence excitation (PLE) spectrum of the 1.54  $\mu\text{m}$  emission showed that there was strong broad excitation of the  $\text{Er}^{3+}$  centers at energies well below the indirect bandgap energy. In fact, the  $\text{Er}^{3+}$  emission intensity was significantly stronger when excited with below-gap wavelengths than with above-gap wavelengths. This result has been attributed to highly competitive capture of free carriers by deep levels or other nonradiative processes under above-gap excitation. With below-gap excitation, carriers are promoted directly into the  $\text{Er}^{3+}$  excitation pathway via absorption at an erbium-related trap. At higher pressure, below-gap excitation was no longer more efficient than above-gap excitation, suggesting that competition by deep level recombination was reduced.

## ACKNOWLEDGMENTS

We gratefully acknowledge financial support under grants from the National Science Foundation and Army Research Office, as well as a National Science Foundation Graduate Research Fellowship.

## REFERENCES

1. X.Z. Wang and B.W. Wessels, *Appl. Phys. Lett.* **64**, 1537 (1994).
2. H. Alawadhi, R. Vogelgesang, T.P. Chin, J.M. Woodall, and A.K. Ramdas, *Bull. of the Amer. Phys. Soc.* **41**, 476 (1996).
3. D.G. Thomas, M. Gershenson, and F.A. Trumbore, *Phys. Rev.* **133**, A269 (1964).
4. T.F. Kuech, *Mat. Sci. Reports* **2**, 1 (1987).
5. T. Monteiro, E. Pereira, F. Domingue-Adame, and J. Piqueras, *Mat. Sci. Forum* **117-118**, 375 (1993).
6. H. Nakagome, K. Uwai, and K. Takahei, *Appl. Phys. Lett.* **53**, 1726 (1988).
7. K. Takahei, A. Taguchi, Y. Horikoshi, and J. Nakata, *J. Appl. Phys.* **76**, 4332 (1994).
8. H. Abid, N. Badi, B. Soudini, N. Amrane, M. Driz, M. Hammadi, H. Aourag, and B. Khelifa, *Mat. Chem. and Phys.* **38**, 162 (1994).
9. K. Takahei and A. Taguchi, *Mat. Sci. Forum* **83-87**, 641 (1992).
10. X.Z. Wang and B.W. Wessels, *Mat. Sci. Forum* **196-201**, 663 (1995).
11. J. Bourgoin and M. Lannoo, *Point Defects in Semiconductors II* (Springer-Verlag, New York, 1983), ch. 6.
12. S.T. Pantelides, *Rev. Modern Phys.* **50**, 797 (1978), p. 804.
13. T. Benyattou, D. Seghier, G. Guillot, R. Moncorge, P. Galtier, and M.N. Charasse, *Mat. Res. Soc. Symp. Proc.* **163**, 69 (1990).
14. T. Benyattou, D. Seghier, G. Guillot, R. Moncorge, P. Galtier, and M.N. Charasse, *Appl. Phys. Lett.* **58**, 2132 (1991).
15. X.Z. Wang and B.W. Wessels, *Mat. Sci. Forum* **196-201**, 657 (1995).

## PHOTOLUMINESCENCE KINETICS MODEL OF P-TYPE GaAs:Nd

U. K. Saha, and H. J. Lozykowski, , School of Electrical Engineering and Computer Science, Ohio University, Athens, Ohio 45701

### ABSTRACT

In this work we have developed a model for the kinetics of the energy transfer from the host lattice to the core states of rare earth (RE) centers. We have derived a set of kinetics differential equations of RE luminescence in p-type semiconductor. Numerically computed rise and decay time of RE luminescence as a function of excitation power shows good agreement with the experimental data obtained for p-type GaAs:Nd.

### INTRODUCTION

Rare earth (RE) doped III-V semiconductors are very attractive for new light emitting device applications such as lasers and LEDs. In this case emission is no more Band to Band recombination but on the internal emission of the  $RE^{3+}$  ions. Among the rare earth doped in III-V semiconductors InP:Yb has been the most extensively studied. It was found that Ytterbium in InP replaces indium on a substitutional site and creates an isoelectronic electron trap at 30 meV below the conduction band (CB). For the case of Nd in GaAs, Takahei [1] proposed similar trap level ranging 80 - 120 meV exists below the CB. Nd in III-V semiconductor is of particular interest due to its four-level laser scheme. In this article, we have developed photoluminescence (PL) kinetics model for p-type III-V semiconductors doped with  $RE^{3+}$  ions, where  $RE^{3+}$  replaces the element from column III. A numerical approach was encountered to solve the rise and decay of the luminescence of the developed kinetic model for p-type GaAs:Nd. Study of the rise time at different excitation intensities and pulse duration, and temperatures can provide important information about the energy transfer and recombination (radiative and non-radiative) processes.

### EXPERIMENTAL SETUP

The experimental data used in this paper were obtained at NTT Basic Research Laboratory in Tokyo [2]. Nd-doped GaAs epitaxial layers were grown by low-pressure metal organic chemical vapor deposition (MOCVD). The p-type GaAs:Nd with the hole concentration  $1.4 \times 10^{14} \text{ cm}^{-3}$  at room temperature was investigated in this study. The PL measurements were carried out using an argon-ion laser ( $Ar^+$ ) operating at 514.5 nm. The pulse excitation for kinetic measurements was obtained by acousto-optic light modulator (model A140 CS). The detecting electronics consisted of Hamamatsu R632-1S photo multiplier. The signals from the photo multiplier was fitted through to the photon counters SR 430 to measure the PL rise and decay kinetics. Different excitation intensities were used to see the variation of rise and decay time. The complete PL spectrum of Nd-doped GaAs is shown in figure 1a. These emission lines correspond to the  $Nd^{3+}$  ion intra-4f-shell transitions  $^4F_{3/2} \rightarrow ^4I_{13/2}$  at 0.9 eV,  $^4F_{3/2} \rightarrow ^4I_{11/2}$  at 1.1 eV, and  $^4F_{3/2} \rightarrow ^4I_{9/2}$  at 1.346 eV respectively. Figure 1b shows PL emission lines peaking at 921.0 nm (1.346 eV) which are attributed to the transition  $^4F_{3/2} \rightarrow ^4I_{9/2}$  of the  $Nd^{3+}$  ion. The PL rise and decay kinetics of  $Nd^{3+}$  transition  $^4F_{3/2} \rightarrow ^4I_{9/2}$  at 921 nm as a function of excitation intensity was investigated for p-type GaAs doped with neodymium.

This wavelength was chosen since the photocounting system with photomultiplier had the long wavelength limit at about 1100 nm.

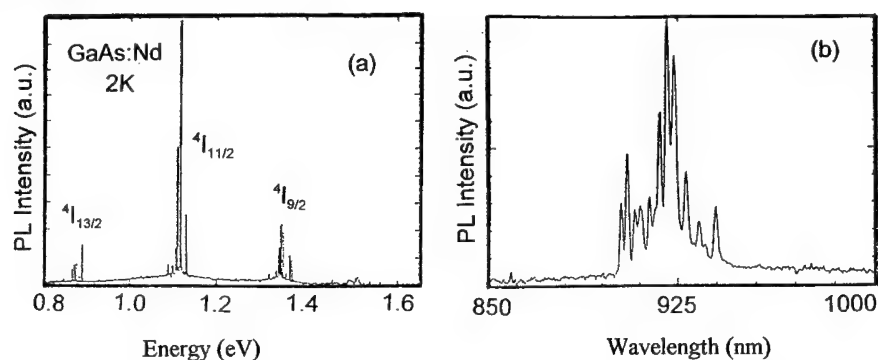


Fig. 1: PL spectra of p-type GaAs:Nd. (a) complete emission spectrum of  $Nd^{3+}$  in GaAs [3], and (b) emission spectra attributed to transition  $4F_{3/2} \rightarrow 4I_{9/2}$  peaked at 921.0 nm.

## KINETIC MODEL AND COMPUTATION RESULTS

The RE structured isoelectronic centers can exist in six possible states. These are (1) neutral unoccupied trap (concentration  $N_0$ ), (2) neutral excited trap (concentration  $N_o^*$ ), (3) exciton occupied trap (concentration  $N_x$ ), (4) negatively charged trap (concentration  $N_-$ ), (5) excited negatively charged trap (concentration  $N_-^*$ ), and (6) excited exciton occupied trap (concentration  $N_x^*$ ). The RE luminescence is due to the radiative transitions between  $4f^n$  core states of the RE element. Total intensity of the RE emission is the sum of the radiative transition of  $N_o^*$ ,  $N_-^*$ , and  $N_x^*$  to  $N_0$ ,  $N_-$ , and  $N_x$  respectively. The radiative recombination of excited  $RE^{3+}$  ions in crystals occurs predominantly by magnetic and electric dipole transitions [4]. Electric-dipole transitions between  $4f^n$  levels are strictly parity forbidden (Laporte's selection rule). The parity prohibition can be lifted by the influence of the crystal lattice. If the RE ion is located at a site that is a center of symmetry in the crystal lattice the parity prohibition cannot be lifted and only magnetic-dipole transitions are allowed. For RE ions residing in a lattice site lacking inversion symmetry like semiconductors with  $T_d$  symmetry, the parity prohibition can be canceled by mixing the  $4f^n$  configuration with a state possessing a different parity. Typically the lifetime of the magnetic-dipole transition is  $10^4 - 10^5$  times longer than the lifetime of a level that recombines via an allowed electric-dipole transitions. In InP:Yb and GaAs:Nd semiconductors the radiative lifetime at low temperature is in the range of 12  $\mu$ s and is probably dominated by electric-dipole transition.

In our model we will assume that isoelectronic trap is an electron trap such as  $Yb^{3+}$  in InP. With the intrinsic excitation the electron from the valence band will go to CB and may fall into the isoelectronic trap and create  $N_-$  (Fig. 2a). From this stage two important energy transfer processes may occur to core state of REI impurities. First, the  $N_-$  center can be transformed to the  $N_o^*$  center through an Auger process where the recombination energy of the bound electron with free hole is transferred non-radiatively to the core states with a rate,  $r_T = B_T N_- p$ , where  $B_T$  is the energy transfer coefficient, and  $p$  is the free hole concentration.



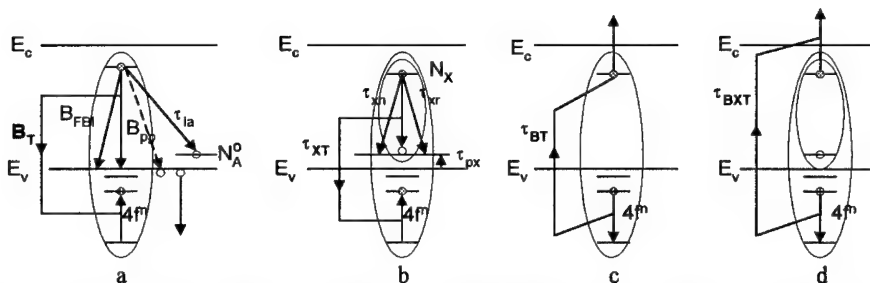


Fig. 2. Auger energy transfer processes to core states (a) from the annihilation energy of the bound electron to free hole, (b) from the bound exciton on a REI trap. Energy back transfer processes: (c) from the excited core states to bound electron on the trap, and (d) from the excited REI-trap to bound exciton.

Second, electron on the trap can attract a hole from valance band with time  $\tau_{px}$  and create a bound exciton ( $N_X$ ) (Fig. 2b). The striking feature of this bound exciton is a long luminescence decay time, ranging from few hundred to few thousand nanoseconds [5]. For example, the lifetime of an exciton bound to a Bi isoelectronic trap in InP is about 200 ns [5]. Energy of that bound exciton on a REI trap may transfer non-radiatively via Auger process to core states with the rate  $r_{XT} = B_{XT} N_X$ , where  $B_{XT}$  is the transfer coefficient, and  $\tau_{XT}$  is the characteristics time. The radiative recombination of the bound exciton on REI trap has long lifetime compare to the energy transfer time  $\tau_{XT}$ . That's why we do not observe the luminescence of excitons bound to REI trap. The bound exciton to isoelectronic trap  $N_X$  can thermally dissociate by either of two processes: (1) it can dissociate into a free exciton ( $X$ ) and neutral  $N_0$  and (2) it can dissociate with the liberation of a hole or an electron with time  $\tau_{xp}$  or  $\tau_{et}$  respectively. If the initial and final states are not resonant, the energy mismatch must be accommodated in some way such as phonon emission or absorption.

The  $N_0$  may also recombine radiatively or non-radiatively (via the Auger process) with a hole in the valence band with transition rate  $r_{FBI} = B_{FBI} (N_0 \text{ or } N_0^*) p$  and  $r_{pp} = B_{pp} (N_0 \text{ or } N_0^*) p^2$ , respectively (Fig. 2a), or recombine radiatively with a hole trapped on a distant acceptor. These three processes transform the  $N_0$  center into the  $N_0^*$  neutral trap. The exciton bound to  $N_X$  can thermally dissociate by several processes. It can dissociate a free exciton and neutral trap ( $N_0$ ) or it can dissociate with liberation of hole or electron with time  $\tau_{xd}$ . The result of the two energy transfer processes to core states defined by  $B_T$  and  $r_{XT}$  leads neutral excited trap ( $N_0^*$ ). If the lifetime of the  $N_0^*$  is long, an electron can be captured into that trap and transformed into an  $N_0^-$  center. The  $N_0^-$  may lose the electron through processes described above (Fig. 2a), or by an auto-deionization Auger process ( $N_0^- \rightarrow N_0 + e_{kinetic}$ ) with characteristic time  $\tau_{BT}$  described in figure 2c. This process is called Auger back transfer process. Electron trapped on  $N_0^-$  can also create an excited bound exciton,  $N_X^*$  and it may be dissociated with the liberation of hole or electron with characteristic time  $\tau_{BXT}$  by the de-excitation energy transition between  $4f^n$  core states (Fig. 2d) and become  $N_0$ . Exciton bound to excited REI trap,  $N_X^*$ , can thermally dissociate into free exciton and becomes  $N_0^*$ .

Figure 3a shows an example of non-radiative recombination involving the interaction of a  $N_0^*$  with an electron trapped on  $N_0$  and an electron trapped on a  $N_0^-$ . The de-excitation

energy of  $N_o^*$  may be transferred non-radiatively via Auger process creating "hot" hole in the valence band by ejecting electron from the valence band to acceptor level (Fig. 3b) or to a hole by ejecting it into the deep valence band (Fig. 3c). Wang and Wessels [6] reported that free carrier Auger processes play a limited role in determining the  $Er^{+3}$  luminescence efficiency in InP crystal. This is because probability of formation of bound excitons at the rare earth centers increases with the increase of free carrier concentration from  $10^{13}$  to  $10^{17}$ . Considering this situation in our model we have ignored the free carrier Auger processes.

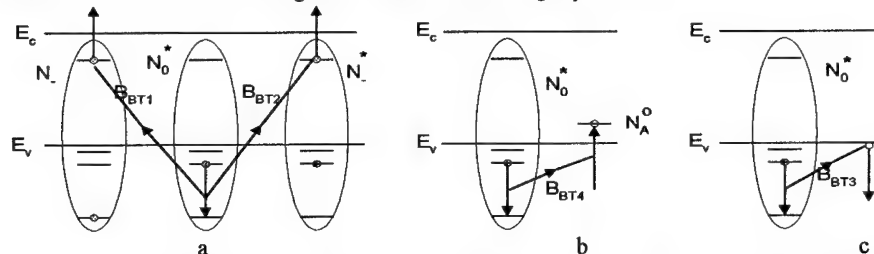


Fig. 3: Auger nonradiative recombination involving the interaction of the core excited REI-trap ( $N_o^*$ ) with (a) an electron trapped on separate centers  $N$  and  $N^*$ , (b) an electron in the valence band, and (c) a hole in the valence band.

The excited RE ion may decay by radiating, by a cross relaxation process (which is not important at low RE concentration used), or by the multiple emission of phonons. Investigations in different host materials [5] show that nonradiative recombination involving the generation of more than five phonons is weaker than the radiative process. Nonradiative recombination for Er and Nd in GaAs and Yb in InP would require the generation of 21, 36 and 27 LO phonons, respectively. In GaAs oxygen related centers produced the IR absorption bands centered at  $845\text{ cm}^{-1}$  (104.7 meV) and  $715\text{ cm}^{-1}$  (88.6 meV) due to localized vibrational modes (LVM) [7]. Oxygen atoms due to ability of forming strong bonds create impurities complexes and show IR absorption spectra. Oxygen can also create complexes with rare earth ions [8]. The very high energy optical phonons derive from internal vibrational modes of the oxygen complexes, may interact with the RE ions differently from the low-energy lattice LO phonons [9]. The quenching process involving vibration modes required additional study planned for the near future. Energy migration due to the quenching center can also play an important role in the quenching of RE luminescence at high temperature.

According to above discussion we have developed the kinetic equations (3) to (13). To solve this system we have assumed the band gap excitations take place at low temperature (in our experiment 2 K) so that thermal activation of the trapped carriers is negligible. That is, terms explicitly dependent on temperature were ignored, and only trapping, transferring, and recombination transitions were considered. The numerical solution was obtained using the fitting parameters stated in table 1. The experimental and numerically simulated luminescence rise and decay are shown in figure 4 at different excitation intensities. All profiles are normalized to unity at maximum. The rise and decay time of the dominant component of the double exponential fitting are shown in table 2. From table 1 we see that Auger energy transfer coefficient of bound electron to free hole ( $B_T$ ) is  $3 \times 10^{-5}\text{ cm}^3$  per sec. But for semi-insulating (SI) InP:Yb,  $B_T$  was equal to  $4 \times 10^{-10}\text{ cm}^3$  per second [5], which indicates that

$$\frac{dN_-}{dt} = \frac{n}{\tau_{et}} \left( \frac{N_0}{N} \right) + \frac{N_-^*}{\tau_3} + \frac{1}{\tau_{px}} \left( \frac{N_x}{N} \right) \frac{N_v}{\beta_h} \exp\left(-\frac{E_h}{kT}\right) - \frac{1}{\tau_{et}} \left( \frac{N_-}{N} \right) \beta_l N_c \exp\left(-\frac{E_l}{kT}\right) - \frac{p}{\tau_{px}} \left( \frac{N_-}{N} \right) \quad (3)$$

$$- B_{FBI} (N_-) p - B_{BT1} N_0^* (N_-) - B_T (N_-) p \quad (4)$$

$$\frac{dN_x}{dt} = \frac{N_x^*}{\tau_3} + \frac{p}{\tau_{px}} \left( \frac{N_-}{N} \right) - N_x \left( \frac{1}{\tau_2} + \frac{1}{\tau_{xT}} + \frac{1}{\tau_{xd}} \right) - \frac{1}{\tau_{px}} \left( \frac{N_x}{N} \right) \frac{N_v}{\beta_h} \exp\left(-\frac{E_h}{kT}\right) \quad (5)$$

$$\frac{dN_0^*}{dt} = \frac{N_x}{\tau_{xT}} + B_T (N_-) p + \frac{1}{\tau_{et}} \left( \frac{N_-}{N} \right) \beta_l N_c \exp\left(-\frac{E_l}{kT}\right) - \frac{n}{\tau_{et}} \left( \frac{N_0^*}{N} \right) - \frac{N_0^*}{\tau_3} - B_{BT1} (N_-) (N_0^*) \quad (6)$$

$$- B_{BT4} (N_A^0) (N_0^*)$$

$$\frac{dN_-^*}{dt} = \frac{n}{\tau_{et}} \left( \frac{N_0^*}{N} \right) + \frac{1}{\tau_{px}} \left( \frac{N_x}{N} \right) \frac{N_v}{\beta_h} \exp\left(-\frac{E_h}{kT}\right) - N_-^* \left( \frac{1}{\tau_3} + \frac{1}{\tau_{BT}} \right) - B_{FBI} (N_-^*) p - \frac{p}{\tau_{px}} \left( \frac{N_-^*}{N} \right) \quad (7)$$

$$- \frac{1}{\tau_{et}} \left( \frac{N_-^*}{N} \right) \beta_l N_c \exp\left(-\frac{E_l}{kT}\right) - B_{BT2} N_0^* (N_-^*)$$

$$\frac{dN_x^*}{dt} = \frac{p}{\tau_{px}} \left( \frac{N_x}{N} \right) - N_x^* \left( \frac{1}{\tau_2} + \frac{1}{\tau_3} + \frac{1}{\tau_{xd}} + \frac{1}{\tau_{BXT}} \right) - \frac{1}{\tau_{px}} \left( \frac{N_x^*}{N} \right) \frac{N_v}{\beta_h} \exp\left(-\frac{E_h}{kT}\right) \quad (8)$$

$$\frac{dn}{dt} = G + N_x^* \left( \frac{1}{\tau_{xd}} + \frac{1}{\tau_{BXT}} \right) + \left( \frac{N_- + N_-^*}{N} \right) \frac{1}{\tau_{et}} \beta_l N_c \exp\left(-\frac{E_l}{kT}\right) + \frac{N_x}{\tau_{xd}} + \frac{N_-^*}{\tau_{BT}} - \frac{n}{\tau_{et}} \left( \frac{N_0 + N_0^*}{N} \right) \quad (9)$$

$$+ B_{BT1} N_0^* (N_-) + B_{BT2} (N_0^*) N_-^*$$

$$\frac{dp}{dt} = G + \frac{\beta_A}{\tau_{px}} \left( \frac{N_x}{N} + \frac{N_x^*}{N} \right) - \frac{p}{\tau_{px}} \left( \frac{N_-}{N} + \frac{N_-^*}{N} \right) - B_{FBI} (N_- + N_-^*) p + B_{BT4} N_0^* N_A^0 \quad (10)$$

$$- \left( 1 - \frac{N_A^0}{N_A} \right) \frac{p}{\tau_{pA}} + \left( \frac{N_A^0}{N_A} \right) \left( \frac{1}{\beta_A} \right) \frac{N_v}{\tau_{pA}} \exp\left(-\frac{E_A}{kT}\right)$$

$$\frac{dN_A^0}{dt} = \left( 1 - \frac{N_A^0}{N_A} \right) \frac{p}{\tau_{pA}} - \left( \frac{N_A^0}{N_A} \right) \left( \frac{1}{\beta_A} \right) \frac{N_v}{\tau_{pA}} \exp\left(-\frac{E_A}{kT}\right) - B_{BT4} N_0^* N_A^0 \quad (11)$$

$$N = N_0 + N_- + N_x + N_0^* + N_-^* + N_x^* \quad (12)$$

$$N_A = N_A^0 + N_A^- \quad (13)$$

$$p = n + N_- + N_-^* - \left( 1 - \frac{N_A^0}{N_A} \right) N_A$$

Table 1: Parameters describing Rise and Decay kinetics of GaAs:Nd

Symbol	Unit	Parameter value
$\tau_3$	second	$11.7 \times 10^{-6}$
$\tau_{BT}$	second	$500 \times 10^{-9}$
$\tau_{XT}$	second	$1 \times 10^{-9}$
$\tau_{BXT}$	second	$9 \times 10^{-6}$
$\tau_{et}$	second	$1 \times 10^{-8}$
$\tau_{px}$	second	$4.91 \times 10^{-12}$
$\tau_{xd}$	second	$1 \times 10^{-12}$
$\tau_{pA}$	second	$500 \times 10^{-9}$
$B_T$	cm <sup>3</sup> /second	$3 \times 10^{-5}$
$B_{FBI}$	cm <sup>3</sup> /second	$1 \times 10^{-15}$
$B_{BT1}$	cm <sup>3</sup> /second	$1 \times 10^{-14}$
$B_{BT2}$	cm <sup>3</sup> /second	$1 \times 10^{-14}$
$B_{BT4}$	cm <sup>3</sup> /second	$4 \times 10^{-18}$

transfer rate of the annihilation energy of bound electron to free hole to the core states is faster in p-type GaAs:Nd than in SI InP:Yb. All other parameters used for fitting are in the same range which are used in SI InP:Yb. From table 2 it is easily found that computed rise time is always higher than the experimental rise time. However decay times almost matches with the experimental data. In conclusion the developed PL kinetic model for p-type semiconductor doped with RE gives estimation of the energy transfer process to core states when fitted with the experimental data.

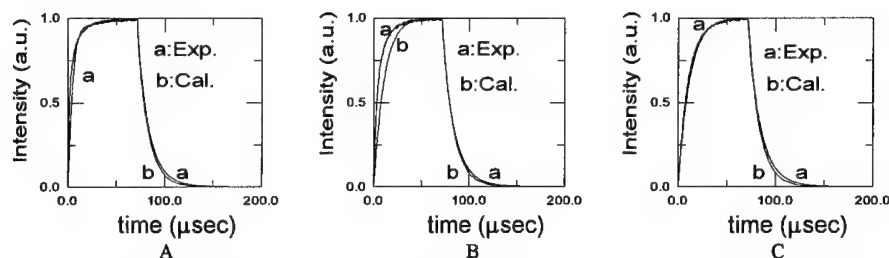


Fig. 4: Experimental (a) and calculated (b) luminescence rise and decay as a function of time, for three excitation intensities, A) 18 mW, B) 2.24 mW, and C) 0.24 mW. Pulse width is 71.4  $\mu$  sec.

Table 2: Theoretical and experimental rise and decay times as a function of power.

Excitation power	Rise time ( $\mu$ sec.)		Decay time ( $\mu$ sec.)	
	Experimental	Theoretical	Experimental	Theoretical
18 mW	1.91	3.1	9.421	9.421
2.243 mW	5.4	9	10.5	11.2
0.24 mW	9	10	13.1	12.52

This work was supported by AFOSR grant No. F49620-1-0024, Ohio University CMSS Program, and Ohio University SEECS Stocker Fund.

## REFERENCES

1. M. Taniguchi, H. Nakagome and K. Takahei, Appl. Phys. Lett. **58**, 2930 (1991).
2. H. J. Lozykowski, and K. Takahei, unpublished.
3. H. Nakagome and K. Takahei, Jap. J. Appl. Phys. **28**, 2098 (1989).
4. M. J. Weber, Phys. Rev. Vol. 171, 283 (1968).
5. H. J. Lozykowski, Phys. Rev. **B48**, 17758 (1993), and references cited therein.
6. X. Z. Wang and B. W. Wessels, Appl. Phys. Lett. **65**, 845 (1994).
7. M. Skowronski in, *Deep Centers in Semiconductors* Edited by S.T. Pantelides (Gordon and Breach Science Publishers, Philadelphia, 1992), p.379.
8. H.J. Lozykowski, A. K. Alshawa, and I. Brown, Mat. Res. Soc. Symp. Proc. **417** (1995), in print.
9. E.D. Reed, Jr. And H.W. Moos, Phys. Rev. **B8**, 980 (1973), and references cited therein.

---

## EXCITATION AND RECOMBINATION PROCESSES IN RARE EARTH DOPED II-VI SEMICONDUCTORS

M. GODLEWSKI

Institute of Physics, Polish Academy of Sciences, 02-668 Warsaw, Al. Lotników 32/46, Poland  
e-mail: godlew@delta2.ifpan.edu.pl

### ABSTRACT

Rare Earth (RE) doped II-VI semiconductors are currently used for production of thin film light emitting electroluminescence devices. The excitation and recombination processes in RE activated wide band gap II-VI semiconductors (ZnS, ZnSe, SrS and CaS) are reviewed. Mechanisms relevant for obtaining bright photoluminescence (energy transfer processes, RE ionisation and exciton binding), electroluminescence (impact excitation and impact ionisation) and cathodoluminescence are described based on the recent experimental results. Efficiency of the light emission from RE doped II-VI materials is limited by several processes of nonradiative recombination. The Auger-type energy transfer processes and electric field- or thermally-activated processes responsible for 4f-4f nonradiative recombination of RE ions are discussed.

### INTRODUCTION

The first powder electroluminescence (EL) phosphor based on ZnS was prepared by Destriau [1] in 1936, whereas the first thin film EL display was reported by Inoguchi et al. [2] for Mn doped ZnS. At present efficient multi-color displays are commercially available. Rare earth (RE) activated ZnS and SrS are currently used for green (ZnS:Tb) and blue (SrS:Ce) color EL. In this paper we review excitation and deexcitation mechanisms of RE activated semiconducting phosphors and analyse recent experimental results for Ce doped SrS. A detail discussion of these processes can be found in the recent review of the present author [3].

### PROPERTIES OF RARE EARTH IONS

RE ions substitute cations in wide band gap II-VI compounds. Most of RE ions appears in the trivalent charge state, in which three valence  $5d^1 6s^2$  electrons are ionised. The unfilled 4f electron shell of RE ions is screened from the environment by the outer filled 5s5p shells. In the result the optical properties of RE ions are free ion like, with the influence of the crystalline environment regarded as a small perturbation. This is why a sharp atomic like emission can be obtained in RE activated phosphors. This emission weakly depends on ambient temperature, which is a very attractive property of RE activated phosphors.

The electric dipole transitions within 4f shell are forbidden due to the parity selection rules. Low symmetry electric field at the RE site may admix higher (5d) states of the opposite parity to the ground and excited 4f states relaxing the parity selection rules of the 4f-4f transition. Unfortunately, due to screening of the 4f shell by the external 5s, 5p shells, the crystal field effects are small for RE ions. In consequence, parity selection rules are not relaxed and 4f - 4f transitions of REs are not efficient. This limits wider application of RE ions in optoelectronics devices.

Trivalent RE ions in II-VI compounds require charge compensation. For close associates of RE ions with compensating ions crystal field effects can be relatively strong. For such complex centers of RE ions mixing of 4f and 5d wave functions can relax the parity selection rules for 4f-4f

intra-shell transitions. This is why complex RE sites often dominate in optical transitions. Even though isolated RE sites are often quite common, they play only a minor role in photoluminescence (PL) or cathodoluminescence (CL), which is dominated by light emission from low symmetry RE centers.

#### DAP-RE ENERGY TRANSFER

Early studies of photoluminescence and cathodoluminescence of RE doped II-VI materials indicated a high efficiency of indirect excitation processes of RE ions. PL and CL emissions of undoped II-VI compounds are dominated by recombination transitions of electrons on donors with holes on acceptors (donor - acceptor pair (DAP) emission). The DAP emissions are often observed also in RE doped samples, which is due to a relatively high concentration of DAP centers and their large excitation and emission rates. In such case the 4f-4f emission of the RE ion can be excited by an indirect process of an energy transfer from excited DAP center to RE ion. The theoretical description of the process was given by Schaffer and Williams [4], who have modified the Dexter [5] model of energy transfer process. In the model of Schaffer and Williams the DAP-RE transfer rate is proportional to an energy overlap between the DAP emission and the RE absorption. Since DAP bands in ZnS, and in other wide band gap II-VI compounds, are relatively broad we expect that the energy overlap between the DAP emission and the RE absorption should be identical for different RE sites and different RE ions. In consequence, the PL excitation (PLE) spectra should be identical for various RE ions or various RE complexes. Already early works of Anderson et al. [6] showed that this is not the case. Different PLE spectra were observed for Tb, Nd, Tm and Dy ions in ZnS lattice. This result was confirmed later on by several other authors, and the relevant experimental results were summarised in the reviews of Brown et al. [7] and Boyn [8].

The explanation of different PLE spectra for different RE ions or the same RE ion at different lattice sites or in different complexes was discussed by several authors. The accumulated experimental results (see e.g. Ref. [9]) indicate that the transfer proceeds between closely associated RE ions and compensating centers. It was convincingly shown that the adjacent DAP - RE centers dominate in the PL process. It may mean that one of the components of the DAP acts simultaneously as RE compensator and as sensitizer, i.e., donor or acceptor center of the pair acts as a charge compensator for the RE ion.

#### IMPACT EXCITATION PROCESSES

Excitation mechanisms of RE ions in EL structures are different from those active in PL and CL phosphors. The energy transfer mechanism between DAP and RE, important for PL and CL phosphors, is not efficient in the limit of high electric fields often present in EL devices [10]. The relevant excitation process, impact excitation mechanism, was proposed by Krupka [11] for ZnS:Tb. In this process, shown in Fig. 1, the intra-shell emission of the RE ion is excited by impact with a hot carrier accelerated by the strong electric field present in the EL device. The process of impact excitation can, thus, be treated as inelastic scattering of hot carrier on RE site.

The cross-section of the impact excitation process depends on the electric dipole transition rate [12,13]. Since for most of the RE ions the excitation proceeds within the 4f shell, this is a parity forbidden process with a small electric dipole transition rate. Much larger cross sections of the impact excitation are achieved for extended complexes and clusters of RE ions. Such molecular centers of RE ions are called lumocens and may have impact cross sections larger than  $10^{-16} \text{ cm}^2$  [14-15]. For example, Okamoto et al. [16] increased the EL efficiency of ZnS:Tb by optimising

codoping with either fluorine and/or oxygen. The luminance of ZnS:Tb is the highest for F/Tb ratio close to 1 [17]. The best luminance was obtained for Tb present in large molecules of TbSF and TbOF [16]. It was also shown that a good luminance of ZnS grown by atomic layer epitaxy and doped with metallic Tb relates to formation of  $(\text{TbO})_n^+$  molecules in the layer [18].

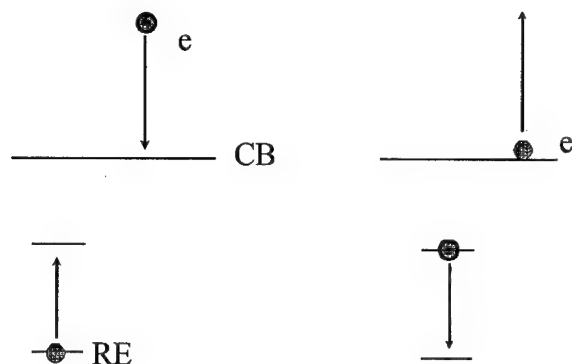


Fig. 1 Impact excitation (left) and one center Auger recombination (right) processes of RE activated EL structures.

There are two reasons for an increased efficiency of EL excitation for complex RE centers. If impact with hot electron excites first a compensating ion, then the energy transfer to RE center is more effective for close pairs. Moreover, for a close compensation a lowering of symmetry of the local electric field results in relaxing of the selection rules for 4f-4f excitation and for subsequent RE emission.

The large efficiency of the impact excitation is also expected for RE ions with a low lying 5d excited state. 4f - 5d transition is a parity allowed process characterised by relatively large excitation and recombination rates. Such a favourable energy structure of RE ion excited state, occurring e.g. for  $\text{Eu}^{2+}$  ion in CaS and SrS, is however rather rare for RE ions in II-VI compounds.

Efficiency of the impact excitation process is limited by Auger-type nonradiative recombination transitions of RE ions (see Fig. 1). RE excitation energy can be transferred to a nearby free carrier, which is excited high into continuum of the conduction (electron) or valence (hole) bands. This process is called one center Auger recombination and can severely limit the luminance efficiency. The matrix element describing the impact process is identical to the one for the Auger process, in which RE ion is deexcited by the interaction of the excited RE site with a free carrier. Thus, the quantum efficiency of the impact excitation process should be reduced by 50 %. In high field EL structures electron is immediately swept from the excited RE center and the reduction of the emission efficiency can be lower. Still the efficiency of the one center Auger transition can be large, as was confirmed experimentally [19-23].

In addition to the one center Auger recombination, two center processes can be important. In the two center Auger process RE excitation energy is transferred to the carrier bound at electron or hole trap.

### IMPACT IONISATION PROCESSES

The cross - section of impact excitation process is small due to the parity selection rules. Even though the impact cross - sections are larger for complex centers still they are often too small for practical application. The larger impact cross - sections (two to four orders of magnitude larger than those for the impact excitation mechanism [12]) are expected for ionisation transitions of RE ions in wide band gap sulphides [12]. The ionisation of RE ion will result in its intra-shell emission if an ionised carrier is retrapped via an excited state of the RE. The concept of such three - step RE excitation (shown in Fig. 2) was introduced by Allen [12]. The RE ion is first ionised by impact with a hot carrier. This process is characterised by a large impact cross - section. The ionised carrier should be recaptured onto the excited state of the RE center, which is followed by 4f-4f or 5d-4f recombination to the ground state of RE ion.

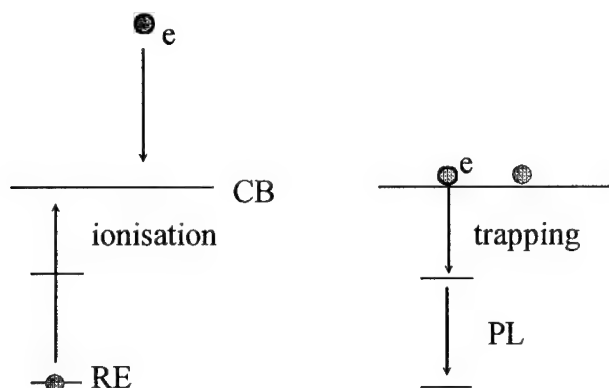


Fig. 2 Impact ionisation mechanism of the RE excitation. RE ion is ionised by collision with hot electron (left). The ionised electron is retrapped via an excited state of the RE ion, which is followed by the intra-shell RE emission.

The experimental results for Pr doped ZnS and SrS [24,25] and the electron spin resonance (ESR) investigations of Eu doped SrS [26] indicated that at least some of the RE ions in ZnS and other wide band gap sulphides can change their charge state. Similar excitation mechanism was proposed for Eu in ZnS [27,28], Yb in ZnS [29], Sm in ZnS [30], Tm in ZnS [31], Eu in ZnSe [32] and Eu in CaS and SrS [33,34]. In the case of the Eu and Yb ions in ZnS RE ionisation could be observed directly in the ESR study and the ionisation energy was determined from the photo-sensitivity of the ESR signals [27,28,29,32]. In other cases RE ionisation was concluded from indirect observation of e.g. appearance of strong PLE bands in RE doped samples [30,31].



Experimentally determined energies of  $3+ \rightarrow 2+$  ionisation allow to predict the  $3+$  to  $2+$  ionisation energies for other RE ions in wide band gap sulphides and selenides. The theoretical two - zigzag curve shown in Fig. 3 was calculated [35,36] with a refined spin pairing theory (RESPET) developed by Jörgensen [37]. A given RE ion can change its charge state from  $3+$  to  $2+$  if the ionisation energy is smaller than the band gap energy of the host material. We can thus predict which RE ions can be ionised comparing the ionisation energy (solid line in Fig. 3) with the band gap energies of the II-VI compounds (broken lines in Fig. 6).

For most of the RE ions the initial  $3+$  charge state of the ion is changed to the  $2+$  state. However,  $4+$  charge state may be stable for some of the RE ions as is suggested for e.g. cerium in SrS. At present we do not know if  $4+$  charge state is possible in the wide band gap II-VI compounds.

Fig. 3 indicates that for some of the RE ions excitation by the impact ionisation mechanism can occur in CaS and SrS but not in ZnS. In fact such situation was confirmed experimentally for Pr ion [38,39]. Comparing PL and EL efficiencies it was possible to verify experimentally the expected large gain in efficiency of the RE emission, which should follow the replacement of the impact excitation process of the EL excitation with the impact ionisation process.

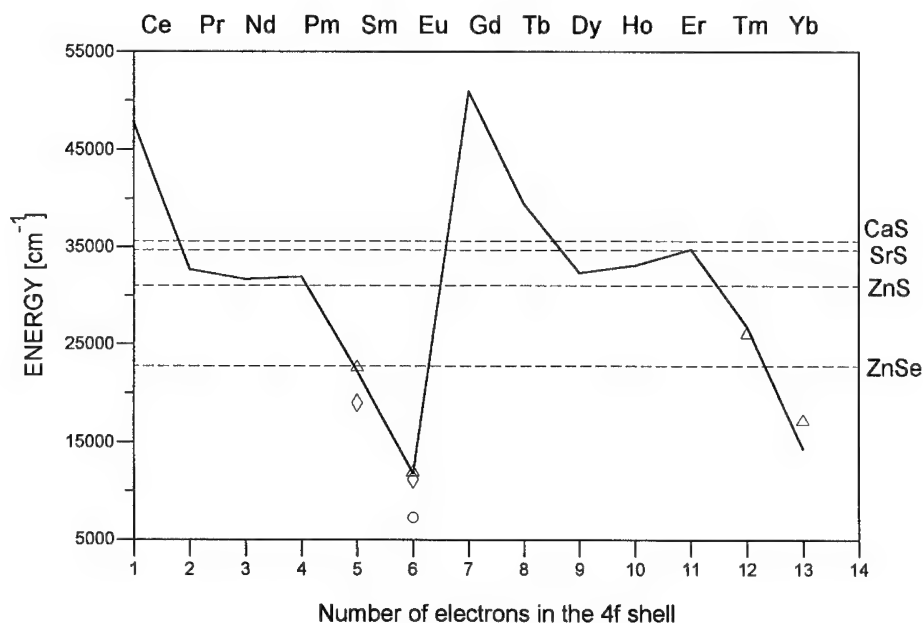


Fig. 3 Ionisation energies for  $3+$  to  $2+$  transitions of RE ions in wide band gap II-VI compounds. Solid line presents fit to the experimental results with the RESPET theory. Broken lines show band gaps of ZnSe, ZnS, SrS and CaS.

The observed gain in the EL luminance was surprisingly small. Instead of two to four orders in magnitude increase in the efficiency of the EL emission, as is predicted from the comparison of the impact excitation and impact ionisation cross - sections, a relatively small gain was observed [40]. Yoshida et al. showed that the efficiency of Pr PL in SrS:Pr,K is increased by factor  $10^2$  compared to that in ZnS:Pr,F [41] since the increased band gap of SrS allows the ionisation transition of Pr ion. However, the EL efficiency in SrS:Pr,K increases only 5 times compared to that of ZnS:Pr,F. Nearly all gain in the excitation efficiency is lost due to the ionisation of the excited state of the RE ion at high electric field conditions [35]. When the excited state is close to the continuum of the conduction or valence states, RE decay may be destabilised at increased temperatures or at high electric field, by field or thermal ionisation of the RE excited state [33,34,42,43]. Destructive role of the process was clearly evidenced experimentally by several groups [39,41] and is shown in Fig. 4 for Eu doped CaS.

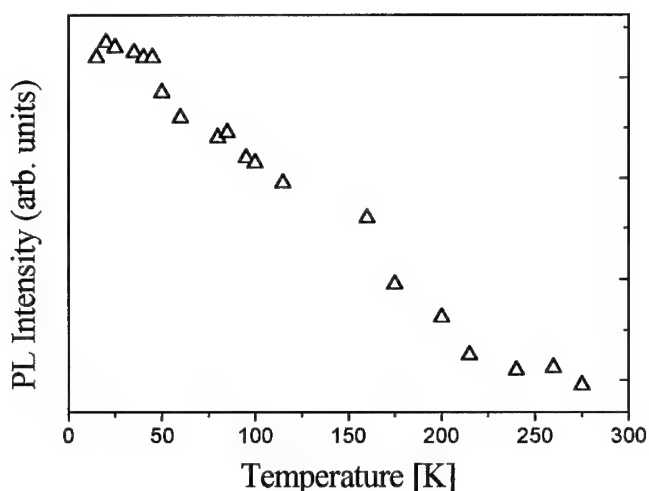


Fig. 4 Temperature dependence of the Eu photoluminescence in CaS:Eu

There are several reasons for the reduced gain in the luminance. Field ionisation mechanism is the most efficient process. However, carrier trapping rate by the ionised RE ions may also be field dependent and be fairly small at high electric fields, since the carrier is immediately swept from the ionised RE ion at strong electric field conditions. Consequently, the strongest EL should occur at lower electric fields and decrease in the intensity with rising field.

#### EXCITONIC MECHANISM OF RE EXCITATION

For low electric field EL or for PL and CL phosphors a new RE excitation mechanism can be important. Excitonic excitation mechanism was predicted for those of the RE ions which can

either change their charge state or can localise free carrier [35,44,45]. Formation of the so-called charge transfer state of the RE ion, consisting of the ion with an externally bound carrier, was suggested based on the indirect experimental results. Rich experimental evidence was then collected proving that such states may be quite common [45].

Carrier binding can be easily understood in the case of impurities which can change their charge state. Once the impurity is ionised it becomes charged in respect to the lattice sites and may attract a free carrier by a long range Coulomb potential. Such carrier may be trapped on an extended orbit forming the so-called charge transfer state of the RE ion. The charge transfer state of the RE ion consists thus of  $n-1$  electrons localised on the 4f shell of the RE ion and of one delocalised carrier (electron or hole) "externally" bound by a long range Coulomb attractive potential. For neutral (isoelectronic) impurities the carrier binding must be of a different origin and may be of identical nature to that responsible for the primary carrier binding in the case of excitons bound on isoelectronic centers [46]. The carrier is trapped by a short range potential caused either by a difference between the electronegativities of the impurity and the ion for which it substitutes and/or lattice distortion induced by the substitution. Core states polarisation induced by the trapped carrier and difference in spin-orbit interactions [47] can also contribute to the binding potential introducing a long range component to the attractive potential.

The short range binding potential of the ion may be either electron - or hole - attractive. A simple method for predicting the kind of the carrier binding potential was proposed by Robbins and Dean [48]. If an ion in its neutral charge state introduces an energy level into the band gap of the host material, i.e., it can change its charge state from the neutral to the positively charged in respect to the host atom, it is expected to have a short range hole attractive potential. The creation of the short range hole attractive potential may also occur for those RE ions which have only an unfilled atomic level within the band gap of the material. This is due to the higher order interactions admixing the ground state of the ion to the excited band gap state, i.e., the ground state of the neutral ion "partly enters" into the band gap. On the other hand, if only the negatively charged ion introduces an energy level into the band gap, the center may localise an electron by a short range attractive potential.

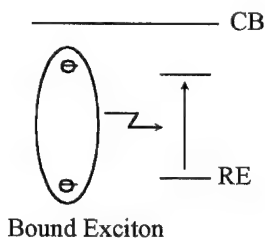


Fig. 5 Defect Auger recombination mechanism of the intra-shell excitation of RE ion by the energy transfer from the RE bound exciton.

Using the above model together with a knowledge of possible charge states of the ions we can predict that a hole binding may occur in the case of  $\text{Ce}^{3+}$ ,  $\text{Pr}^{3+}$ ,  $\text{Tb}^{3+}$  or  $\text{Eu}^{2+}$  ions and an electron binding e.g. for  $\text{Yb}^{3+}$  and  $\text{Eu}^{3+}$ . This is rather tentative model but already found some indirect experimental confirmation.

Possible recombination channels occurring after carrier binding by a RE ion are discussed in the Ref. 3. Quite complicated recombination paths are expected. The externally bound carrier can recombine with electron (hole) on the 4f shell of the RE ion with the recombination energy transferred to the 4f shell and used for 4f-4f excitation. Such RE excitation process is called the defect Auger recombination [48] (see Fig. 5) and is sometimes described in the literature as a nonradiative recombination of a localised bound exciton (LBE) state of the RE ion. The extremely high efficiency of the defect Auger recombination was verified experimentally for Ni ion in ZnS and CdS. Podlowski et al. [49] observed a totally nonradiative decay of a LBE for the  $\text{Ni}^{2+}$  ion in ZnS and CdS via the Auger type energy transfer mechanism.

A high efficiency of the defect Auger process is expected for those RE ions which have at least one of the excited 4f states quasi resonant with the charge transfer state. If the energy mismatch between LBE and 4f transitions is large, the efficiency of the Auger process is reduced and the radiative recombination of the localised BE becomes dominant. This was, for example, observed for the copper impurity in the ZnO lattice [50]. Energy transfer from the BE state to core states of the Cu ion would require dissipation (by phonon emission) of a large amount of the energy making this process inefficient. The unique situation was found for the Yb ion in ZnS. Because of the large energy mismatch between the LBE ( $[\text{Yb}^{2+}, h]$ ) and  $\text{Yb}^{3+}$  intra-shell transition the defect Auger recombination was of reduced efficiency and both LBE and 4f-4f transitions could be observed simultaneously [29].

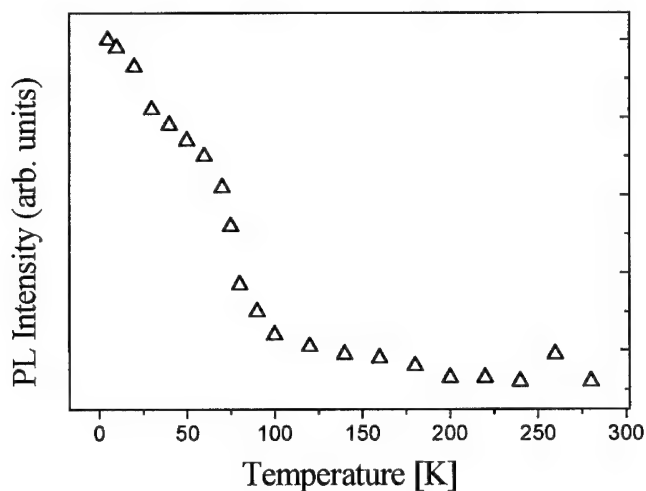


Fig. 6 Temperature dependence of the photoluminescence intensity in SrS:Ce

In some cases binding of a carrier by RE ion may be followed by localisation of a second carrier, which is analogous to the formation of the well known isoelectronic center bound exciton. This scenario is, however, less probable and will occur only if the lifetime of the charge transfer state is sufficiently long. The exciton binding and its indirect recombination was suggested for

$\text{Yb}^{3+}$  and  $\text{Er}^{3+}$  ions in the InP lattice [51,52,53]. In both these cases the  $2+$  charge state of the RE ion does not give rise to an energy level in the forbidden band gap of InP. Thus, the electron localisation on the charge transfer state could not be followed by the formation of the  $2+$  excited charge state of Yb and Er. Consequently, the favourable condition for exciton binding was realised.

#### SrS:Ce

Ce is presently the most studied RE ion due its efficient blue color EL emission. Ce doped SrS films are presently used in full color VGA-standard EL displays. Despite intensive research our knowledge of the Ce excitation mechanism is still limited. It is still disputed if Ce EL is excited by the impact excitation or by the impact ionisation ( $4+$  to  $3+$  transition) process.

We have already mentioned that a strong electric field dependence is expected for the impact ionisation mechanism of the RE excitation. Commercial EL displays operate under a pulsed excitation. For such displays electric field intensity increases at leading edge of the voltage pulse and then decreases at trailing edge of the pulse. By leading and trailing edge EL emission we mean here emission induced by front and edge of the voltage pulse applied to the active layer. For some EL structures a trailing edge emission, occurring at relatively low electric field, is few times more efficient than leading edge emission [54]. This is related to the field ionisation of electrons from excited states of ions or from carrier trap centers. Electrons trapped at shallow interface states during leading edge pulse are emitted and diffuse back to the active layer where they can recombine at ionised RE centers. Such difference in EL efficiency was not observed for Mn or Tb activated ZnS, i.e., when the impact excitation mechanism is responsible for EL excitation.

The difference between the leading and trailing edge EL was reported for SrS:Ce [54]. The above result suggested that Ce is ionised by collision with hot electrons. Also a strong temperature dependence of the PL intensity was observed, as shown in Fig. 6. These results suggested that Ce in SrS can be field or thermally ionised.

The data shown in Fig. 2 exclude the possibility of the  $3+$  to  $2+$  ionisation transition. Instead  $3+$  to  $4+$  process was suggested. The recent experimental results of Hüttel et al. [55] and the author group dispute this model of the EL excitation. For example, a strong electric field and temperature dependence of the PL (Fig. 6) and EL efficiency is not reflected by the temperature dependence of the emission decay time, which was expected in the case of field or thermal ionisation of the Ce excited state.

#### CONCLUSIONS

Excitation and deexcitation processes of RE ions in wide band gap II-VI compounds are presently understood for most of the RE ions. A real break through in emission efficiency was expected for those RE ions we can be ionised. However, the early expectations on the high efficiency of the impact ionisation mechanism of the EL excitation are still not confirmed by the experimental results. The main reason for lower gain in the EL efficiency relates to a high electric field present in the active layer of EL structures. Field ionisation rapidly shortens lifetime of the excited RE state via which ionised carrier is retrapped. In the result the intra-shell emission of the RE ion is deactivated. Also exciton binding mechanism (followed by the defect Auger recombination) of RE excitation is strongly deactivated in the presence of the electric field. However, processes such as RE ionisation or exciton binding may become important in EL structures working at low electric field conditions.

## REFERENCES

1. G. Destriau, *J. de Chimie Physique* **33**, 587 (1936).
2. T. Inoguchi, M. Takeda, Y. Kahikara, Y. Nakata and M. Yoshida, *Society for Information Display Intern. Symp. Dig.* 1974, p.86.
3. M. Godlewski and M. Leskelä, *Critical Reviews in Solid State and Materials Science* **19**, 199 (1994).
4. J. Schaffer and F. Williams, *Phys. Status Solidi* **38**, 657 (1970).
5. D.L. Dexter, *J. Chem. Phys.* **21**, 836 (1953).
6. W.W. Anderson, S. Razi and D.J. Walsh, *J. Chem. Phys.* **43**, 1153 (1965).
7. M.R. Brown, A.F.J. Cox, W.A. Shand and J.M. Williams, *Adv. in Quantum Electronics* **2**, 69 (1974).
8. R. Boyn, *Phys. Status Solidi (b)* **148**, 11 (1988).
9. D. Hommel, W. Busse, H.-E. Gumlich, D. Suisky, J. Röseler, K. Świątek and M. Godlewski, *J. Cryst. Growth* **101**, 393 (1990).
10. H. Kobayashi, S. Tanaka, H. Sasakura and Y. Hamakawa, *Jpn. J. Appl. Phys.* **13**, 1110 (1974).
11. D.C. Krupka, *J. Appl. Phys.* **43**, 476 (1972).
12. J.W. Allen, in *Electroluminescence*, Springer Proc. in Physics **38**, eds. S. Shionoya and H. Kobayashi (Springer, Berlin, 1989), p.10
13. J.W. Allen, *J. Luminescence* **48/49**, 18 (1991).
14. D.C. Krupka and M.M. Rochkind, *J. Appl. Phys.* **43**, 194 (1972).
15. D.C. Krupka and D.M. Mahoney, *J. Appl. Phys.* **43**, 2314 (1972).
16. K. Okamoto, T. Yoshimi and S. Miura, in *Electroluminescence*, Springer Proc. in Physics, vol. **38**, eds. S. Shionoya and H. Kobayashi (Springer, Berlin, 1989), p.139
17. T. Ogura, A. Mikami, K. Tanaka, K. Taniguchi, M. Yoshida and S. Nakajima, *Appl. Phys. Lett.* **48**, 1570 (1986).
18. Y. Charreire, A. Marbeuf, G. Tourillon, M. Leskelä, L. Niinistö, E. Nykänen, P. Soininen and O. Tolonen, *J. Electrochem. Soc.* **139**, 619 (1992).

- 
19. N.T. Gordon and J.W. Allen, Solid State Commun. **37**, 1441 (1981).
  20. A. Suchocki and J.M. Langer, Phys. Rev. **B39**, 7905 (1989).
  21. J.M. Langer, A. Suchocki, Le Van Hong, P. Ciepielewski and W. Walukiewicz, Physica B **117/118**, 152 (1983).
  22. J.M. Langer and Le Van Hong, J. Phys. **C17**, L923 (1984).
  23. P.B. Klein, J.E. Furneaux and R.L. Henry, Phys. Rev. **B34**, 8993 (1986).
  24. S. Tanaka, H. Yoshiyama, Y. Mikami, J. Nishiura, S. Ohshio, H. Deguchi and H. Kobayashi, Appl. Phys. Lett. **50**, 119 (1987).
  25. S. Tanaka, S. Ohshio, J. Nishiura, H. Kawakami, H. Yoshiyama and H. Kobayashi, Appl. Phys. Lett. **52**, 2102 (1988).
  26. R.S. Title, Phys. Rev. Lett. **3**, 273 (1959).
  27. M. Godlewski and D. Hommel, Phys. Status Solidi (a) **95**, 261 (1986).
  28. K. Świątek, M. Godlewski and D. Hommel, Phys. Rev. **B42**, 3628 (1990).
  29. H. Przybylińska, K. Świątek, A. Stapor, A. Suchocki and M. Godlewski, Phys. Rev. **B40**, 1748 (1989).
  30. K. Świątek, M. Godlewski and D. Hommel, Phys. Rev. **B43**, 9955 (1991).
  31. H. Zimmermann and R. Boyn, Phys. Status Solidi (b) **135**, 379 (1986).
  32. K. Świątek and M. Godlewski, J. Luminescence **53**, 406 (1992).
  33. M. Ando and Y.A. Ono, J. Appl. Phys. **68**, 3578 (1990).
  34. K. Świątek, M. Godlewski, D. Hommel, M. Leskelä, L. Niinistö, E. Nykänen, P. Soininen, and M. Tiitta, Acta Polytechn. Scand. Ser. Appl. Phys. **170**, 237 (1990).
  35. K. Świątek, A. Suchocki and M. Godlewski, Appl. Phys. Lett. **56**, 195 (1990).
  36. M. Godlewski, in Defect Engineering in Semiconductor Growth, Processing and Device Technology, Proc. MRS Spring Meeting, San Francisco, 1992, MRS Symp. Proc. vol. **262**, eds. S. Ashok, J. Chevallier, K. Sumino and E. Weber
  37. C.K. Jörgensen, Molecular Physics **5**, 3 (1962).
  38. S. Tanaka, H. Yoshiyama, Y. Mikami, J. Nishiura, S. Ohshio, H. Deguchi and H. Kobayashi, Appl. Phys. Lett. **50**, 119 (1987).

39. S. Tanaka, S. Ohshio, J. Nishiura, H. Kawakami, H. Yoshiyama and H. Kobayashi, Appl. Phys. Lett. **52**, 2102 (1988).
40. M. Yoshida, K. Tanaka, K. Taniguchi, T. Yamashita, Y. Kakihara, and T. Inoguchi, Society for Information Display Intern. Symp. Dig. 1984, p.251
41. M. Yoshida, K. Tanaka, K. Taniguchi, T. Yamashita, Y. Kakihara and T. Inoguchi, Society for Information Display Intern. Symp. Dig. 1980, p.106
42. M. Ando and Y.A. Ono, J. Appl. Phys. **69**, 7225 (1991).
43. K. Świątek, M. Godlewski, L. Niinistö and M. Leskelä, J. Appl. Phys. **74**, 3442 (1993).
44. M. Godlewski, K. Świątek, A. Suchocki and J.M. Langer, J. Luminescence **48/49**, 23 (1991).
45. M. Godlewski and K. Świątek, J. Crystal Growth **117**, 634 (1992).
46. J.J. Hopfield, D.G. Thomas and R.T. Lynch, Phys. Rev. Lett. **17**, 312 (1966).
47. J.W. Allen, J. Phys. **C4**, 1936 (1971).
48. D.J. Robbins and P.J. Dean, Adv. Phys. **27**, 499 (1978).
49. L. Podlowski, R. Heitz, A. Hoffmann and I. Broser, J. Luminescence **53**, 401 (1992).
50. R. Dingle, Phys. Rev. Lett. **23**, 579 (1969).
51. K. Thonke, K. Pressel, G. Bohnert, A. Stapor, J. Weber, M. Moser, A. Malassioti, A. Hangleiter and F. Scholz, Semicond. Sci. Technol. **5**, 1124 (1990).
52. B.J. Heijmink Liesert, M. Godlewski, A. Stapor, T. Gregorkiewicz, C.A.J. Ammerlaan, J. Weber, M. Moser and F. Scholz, Appl. Phys. Lett. **58**, 2237 (1991).
53. B. Lambert, A. Le Corre, Y. Toudic, C. Lhomer, G. Grandpierre and M. Gauneau, J. Phys.: Condense Matter **2**, 479 (1990).
54. K.O. Velthaus, R.H. Mauch, H.W. Shock, S. Tanaka, K. Yamada, K. Ohmi, and H. Kobayashi, in Electroluminescence, Proc. 6th Intern. Workshop on Electroluminescence, eds. V.P. Singh and J.C. McClure (Cinco Puntos Press, El Paso, 1992), p.187
55. B. Hüttl, U. Troppenz, K.O. Velthaus, C.R. Ronda and R.H. Mauch, J. Appl. Phys. **78**, 7282 (1985).



**Part IV**

**Electroluminescence and Integration**

## EXCITATION MECHANISMS AND LIGHT EMITTING DEVICE PERFORMANCES IN Er-DOPED CRYSTALLINE Si

F. PRIOLO<sup>(a)</sup>, S. COFFA<sup>(b)</sup>, G. FRANZO<sup>(b)</sup>, and A. POLMAN<sup>(c)</sup>

(a) *INFN and Dipartimento di Fisica dell'Università, Corso Italia 57, 95129 Catania (ITALY)*

(b) *CNR-IMETEM, Stradale Primosole 50, 95100 Catania (ITALY)*

(c) *FOM-AMOLF, Kruislaan 407, 1098 SJ Amsterdam (THE NETHERLANDS)*

### Abstract

In this paper the performances of room temperature operating light emitting diodes (LEDs), fabricated by Er ion implantation of crystalline silicon, are investigated in detail. It is shown that 1.54  $\mu\text{m}$  emission is observed under both forward and reverse bias operation, with a much higher intensity under reverse bias. The excitation mechanisms of  $\text{Er}^{3+}$  are demonstrated to be very different in the two cases: under forward bias Er is excited through the electron - hole recombination at an Er - related level, while under reverse bias impact excitation by hot carriers represents the excitation process. This last mechanism is shown to occur with a cross section of  $6 \times 10^{-17} \text{ cm}^2$  and population inversion of the excitable Er sites within the depletion region is demonstrated. The efficiency and limitations of this approach are also discussed.

### Introduction

The incorporation of Er in silicon has been recently recognized as a powerful method for the fabrication of Si-based optoelectronic devices [1-5]. In fact, Er in its  $3+$  state emits photons at 1.54  $\mu\text{m}$  as a result of an internal 4f shell transition between the  $^4\text{I}_{13/2}$  and the  $^4\text{I}_{15/2}$  states. This wavelength is strategic in the telecommunication technology since it falls in a window of minimum losses for the optical fibers. Erbium excitation can be achieved by direct photon absorption. However, when embedded in a silicon matrix, the excitation of  $\text{Er}^{3+}$  occurs electrically (i.e. through an electron-hole mediated process) and hence light emitting devices based on the Si:Er system are in principle feasible. Indeed, the first light emitting diode (LED) from Er-doped silicon was fabricated more than ten years ago by Ennen *et al.* [1]. This LED emitted strong 1.54  $\mu\text{m}$  electroluminescence (EL) at 77 K, but the signal was severely quenched with increasing temperature and no room temperature luminescence could be detected.

Since then a strong effort has been devoted both to the understanding of the Er:Si system [6-15] and to the improvement of device performances [2-5]. The Er-impurity (O, F, C, N) interaction has been recognized to play a crucial role in allowing the incorporation of Er at high concentrations [6-7], in providing Er with the proper chemical surrounding [8], in enhancing the luminescence [9-10], in reducing the luminescence temperature quenching [11], and in introducing new Er-related levels which are pathways for the transfer of energy from the electronic system of silicon to the erbium 4f shell [12-13]. This improved understanding has also allowed the fabrication of room temperature operating light emitting silicon diodes [2-5].

In this paper we will review our recent work on Er:Si LEDs. The device performances, the excitation mechanisms and the efficiency and limitations of this approach will be also discussed.

### LED Fabrication and Electrical Characteristics

We have fabricated  $p^+-n^+$  Si diodes by implanting different species into an epitaxial  $n$ -type ( $7 \Omega \text{ cm}$ ) layer grown on top of (100) oriented heavily  $n$ -type doped ( $10^{-2} \Omega \text{ cm}$ ) Si wafer. The  $p^+$  region of the device was formed by 40 keV B implantation to a dose of  $2 \times 10^{15}/\text{cm}^2$ , while part of the  $n^+$  region was produced by 2 MeV P implants to a dose of  $5 \times 10^{15}/\text{cm}^2$ . Six different Er implants in the energy range 0.5-5 MeV were then used to introduce an almost constant Er concentration of  $1 \times 10^{19}/\text{cm}^3$  in between the  $n^+$  and  $p^+$  regions.

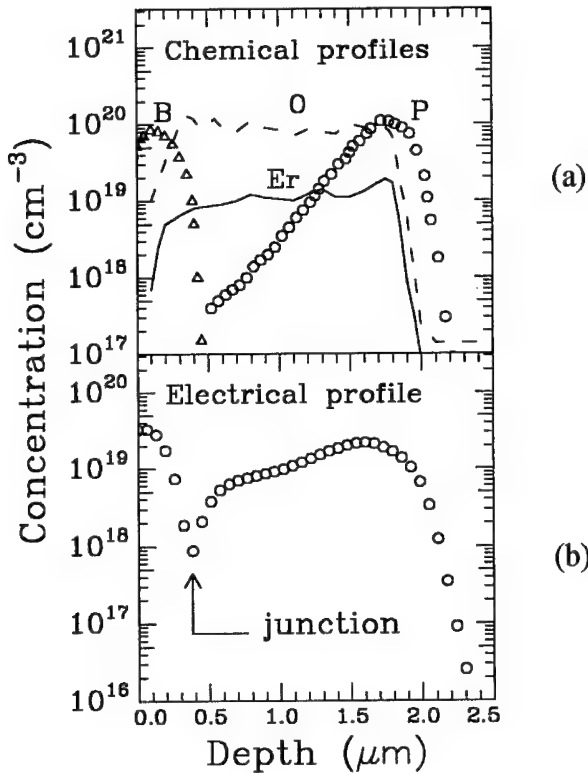


Fig. 1: Chemical profiles of the various implanted impurities introduced in the diode structure (a). The electrical profile is also reported (b).

Several different O implants in the energy range 0.15 - 1.4 MeV were subsequently performed to produce an almost constant O concentration of  $1 \times 10^{20}/\text{cm}^3$  in the Er - doped region, providing thus Er with the proper chemical surrounding. Since Er in presence of O shows a donor behavior [16], this region is of  $n^+$  type and, together with the P - doped region, forms the  $n^+$  side of the junction. All of these implants were performed at 77 K and produced a continuous amorphous layer extending from the surface to a depth of 2.3  $\mu\text{m}$ . After implantation, samples were annealed at 620°C for 3 h under  $\text{N}_2$  flux in order to induce the epitaxial recrystallization of the amorphous

layer. A further thermal treatment at 900 °C for 30 sec under N<sub>2</sub> flux was performed in order to electrically activate the implanted dopants. Finally, aluminum patterns were photolithographically defined on the samples allowing some open area for the exit of the light from the front of the device. Devices of several dimensions going from 0.25 cm<sup>2</sup> to 10<sup>-3</sup> cm<sup>2</sup> were realized in this way. The chemical profiles of the different implanted species are shown in Fig. 1a as measured by secondary ion mass spectroscopy. In Fig. 1b the electrical profile of the diode measured by spreading resistance is also reported, demonstrating the existence of a junction at a depth of about 0.4 μm.

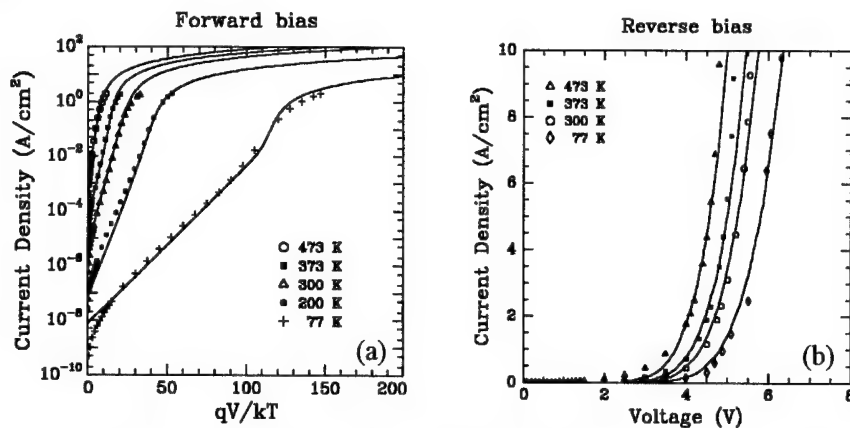


Fig.2: Current - voltage characteristics of the Er doped Si LEDs under both forward (a) and reverse (b) bias conditions.

The current density (J) - voltage (V) characteristics of this diode at different temperatures are shown in Fig. 2 under both forward (a) and reverse (b) bias conditions. Under forward bias the diode is in the recombination regime (described by  $J \propto \exp(qV/2kT)$ ) in the investigated temperature range (but at 77 K where the tunneling current plays a role), while at high current densities the current is limited by the series resistance. Indeed the continuous lines are fits to the data considering the recombination current and a series resistance of  $\sim 1 \Omega$ . Under reverse bias the device shows a breakdown voltage of  $\sim 5$  V which decreases by increasing temperature. The reverse temperature dependence of the breakdown voltage clearly demonstrates that the breakdown occurs by band to band tunneling (Zener effect). This is also expected due to the high doping level on both sides of the p - n junction (see Fig. 1). The continuous lines are simulations of the I - V characteristics assuming, in fact, breakdown by band to band tunneling.

We have also characterized our devices performing capacitance - voltage (C-V) measurements. These are reported in Fig. 3a where the linear dependence of  $1/C^3$  as a function of voltage clearly demonstrates that our junction can be treated as a linear gradient one with a carrier density gradient of  $1.06 \times 10^{24} \text{ cm}^{-4}$ . Data are presented for voltages below 3 V since the onset of the junction breakdown affects capacitance measurements. An analysis of these data allows to extract both the depletion region (Fig. 3b) and the maximum electric field (Fig. 3c) as a function of voltage. It is clearly seen that the depletion region is very small (40-60 nm) while the electric field in this region is extremely high ( $\sim 10^6 \text{ V/cm}$ ).

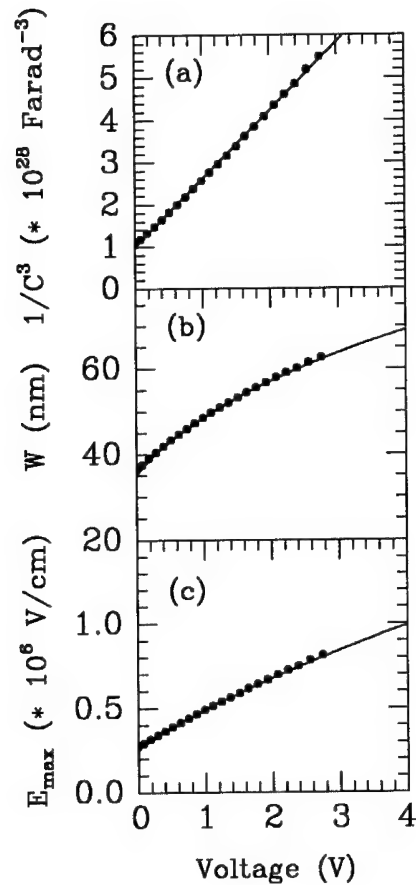


Fig. 3: Capacitance - voltage characteristics (a), depletion region width (b) and maximum electric field (c) of the Er - doped LEDs versus the reverse bias voltage.

### Electroluminescence Measurements

Electroluminescence measurements were performed by biasing the diode using a square wave with a frequency of 55 Hz. The EL signal was analyzed by a monochromator and detected by a liquid nitrogen cooled Ge detector. Spectra were recorded using a lock-in amplifier with the square wave as a reference.

From these diodes we have obtained light emission under both forward and reverse bias. Fig. 4a shows the EL spectrum obtained at room temperature (RT) under forward bias at a current density of  $2.5 \text{ A/cm}^2$ . The well defined structured spectrum of Er is observed on a flat background. Under reverse bias at breakdown ( $\sim 5\text{V}$ ), still at RT and with the same current

density passing through the device, a much higher signal is observed. This signal is about 12 times higher than its forward bias counterpart as shown in Fig. 4b. This well defined and intense Er peak sits on a very broad background which is essentially flat in the wavelength region where the germanium detector we used is sensitive (0.8-1.7  $\mu\text{m}$ ). Such a background was not observed in forward bias. This broad emission is known to occur in reverse biased junctions [17] and has been attributed to hot carrier transitions either as a consequence of bremsstrahlung or of intraband transitions [18]. As a matter of fact this spectrum is not confined to the infrared region but it also extends to the visible and a red glow is observable in the dark by the naked eye.

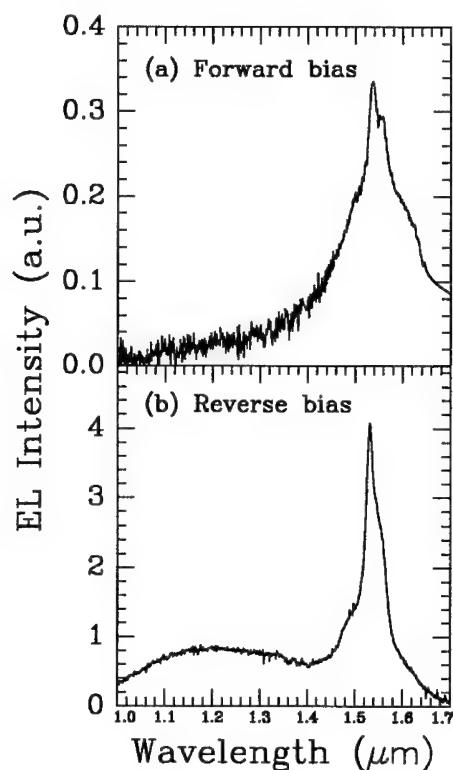


Fig. 4: Room temperature EL spectra under forward (a) and reverse (b) bias operation.

In order to understand the mechanisms underlying forward and reverse bias EL we have studied the EL temperature dependence in both cases. This is reported in Fig. 5. Under reverse bias the 1.54  $\mu\text{m}$  exhibits a different temperature dependence when compared to its forward bias counterpart. In fact, a decrease by only a factor of 4 is observed between 77 K and RT. In contrast, the EL intensity under forward bias decreases by a factor of 30 in the same temperature range in a similar fashion as the photoluminescence (PL) intensity measured on similar samples and also reported in Fig. 5. These results suggest that the same excitation mechanism is operative

in PL and forward bias EL. It has been proposed [19] that in PL  $\text{Er}^{3+}$  is excited through the recombination of an electron bound to an Er-related level in the Si bandgap with a hole in the valence band. We [12] have identified a donor level at 0.15 eV from the conduction band clearly related to Er-O complexes. The existence of this level in Er+O-doped Si samples, together with the enhanced luminescence associated with the presence of oxygen, suggests that this level might act as a pathway for the energy transfer. On the other hand, the larger efficiency of EL under reverse bias, and its different temperature dependence, suggest that a different mechanism might be operative. The clear evidence presented by the existence of hot carriers in the reverse biased diode supports the idea that Er excitation in this case is occurring through impact excitation.

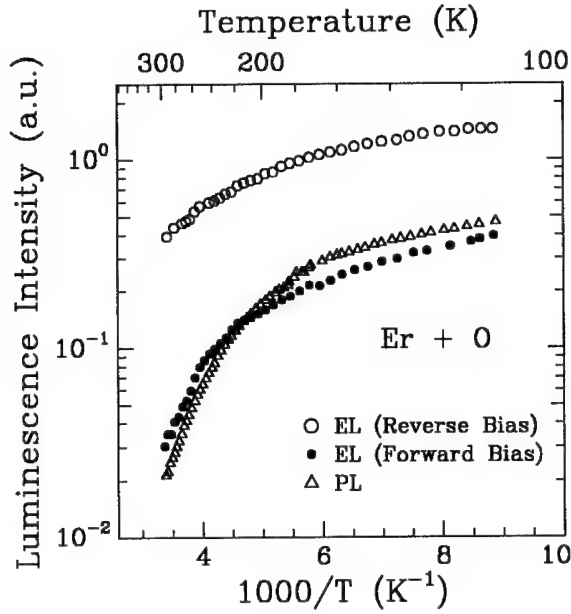


Fig. 5: Temperature dependence of the  $1.54 \mu\text{m}$  EL intensity under both forward and reverse bias operation at a current density of  $2.5 \text{ A/cm}^2$ . The photoluminescence temperature dependence is also reported for comparison.

#### Efficiency and Time Decay

The room temperature EL signal under reverse bias is rather intense. Information on the efficiency of impact excitation can be obtained by analyzing the rate equation governing the excited Er population:

$$\frac{dN_{\text{Er}}^*}{dt} = \sigma\phi(N_{\text{Er}} - N_{\text{Er}}^*) - \frac{N_{\text{Er}}^*}{\tau} \quad (1)$$

where  $N_{\text{Er}}^*$  is the concentration of excited Er,  $\sigma$  is the cross section for impact excitation,  $\phi$  is the electron flux,  $N_{\text{Er}}$  is the total excitable Er population and  $\tau$  is the lifetime of the excited state, taking into account both radiative and non-radiative processes. When the applied voltage

suddenly goes from zero bias to reverse bias in the breakdown regime,  $N_{Er}^*$  passes from zero to its steady state value with a transient described by the solution of eq.(1), i.e.:

$$N_{Er}^* = \frac{\sigma\tau\phi}{\sigma\tau\phi + 1} N_{Er} \left\{ 1 - \exp \left[ - \left( \sigma\phi + \frac{1}{\tau} \right) t \right] \right\} \quad (2)$$

Equation (2) describes an exponential increase of  $N_{Er}^*$  with a risetime equal to the reciprocal of  $\sigma\phi + \frac{1}{\tau}$ . As the EL intensity is proportional to  $\frac{N_{Er}^*}{\tau_{rad}}$  (where  $\tau_{rad}$  is the radiative lifetime), the EL should present a similar behavior as soon as the diode is switched on with an effective risetime  $\tau_{eff}$  given by  $\frac{1}{\tau_{eff}} = \sigma\phi + \frac{1}{\tau}$ . Hence increasing the current density the EL transient should be shorter and shorter, moreover a measurement of this risetime as a function of current density would provide information on both  $\sigma$  and  $\tau$ .

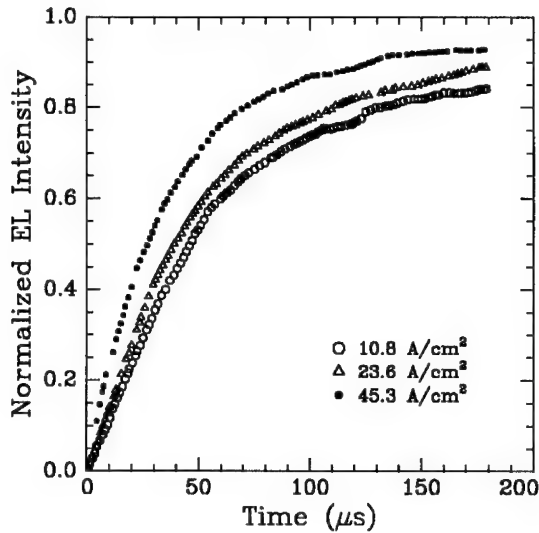


Fig. 6: Time dependence of the EL intensity after biasing the diode from 0 to  $\sim 5$  V under reverse bias in the breakdown regime. Measurements for different current densities through the device are reported.

We have performed such measurements at room temperature and the transients under reverse bias conditions are shown in Fig. 6 for the different current densities. As expected the risetime becomes shorter with increasing current density. The reciprocal of the risetime  $\frac{1}{\tau_{eff}}$  as a function

of the electron flux  $\phi$ , as obtained from an analysis of Fig. 6, is reported in Fig. 7. The intercept with the vertical axis provides information on the lifetime while the slope gives information on the cross section. From these measurements we obtain a lifetime at room temperature of  $\sim 100$   $\mu$ s and a cross section for impact excitation of  $\sim 6 \times 10^{-17}$   $\text{cm}^2$ . These numbers are extremely



important and they demonstrate that i) impact excitation is a very efficient way of exciting Er (more than 4 orders of magnitude more efficient than direct photon absorption which has a cross section of  $\sim 6 \times 10^{-21} \text{ cm}^2$  [20]), ii) the room temperature lifetime of the  $^4I_{13/2}$  excited state of  $\text{Er}^{3+}$  is about a tenth of its radiative lifetime ( $\sim 1 \text{ ms}$ ), demonstrating that in our samples non-radiative de-excitation at RT is only one order of magnitude more efficient than radiative processes.

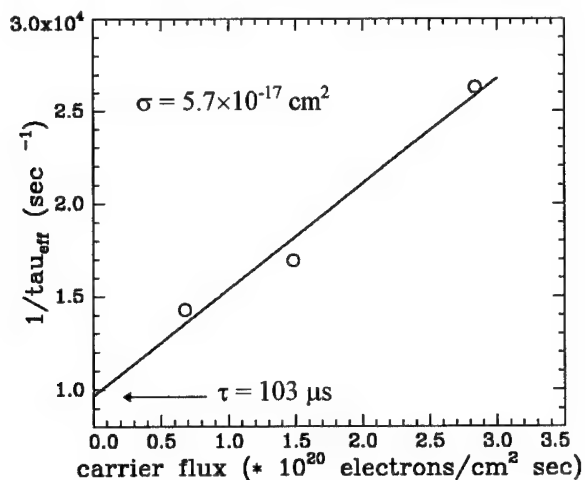


Fig. 7: Reciprocal risetime as extracted from the data in Fig. 6 versus carrier flux. The slope gives the cross section for impact excitation while the intercept with the vertical axis gives the room temperature  $\text{Er}^{3+}$  lifetime.

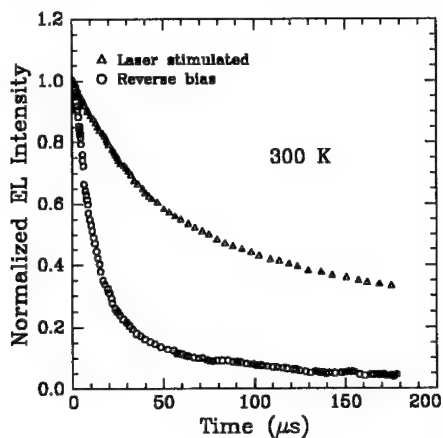


Fig. 8: Room temperature time-decay of the EL intensity on passing from reverse bias in the breakdown regime to 0 bias (circles) and upon biasing the diode with a constant reverse bias below breakdown and stimulating EL through laser irradiation (triangles).

In order to verify these findings we have measured directly the RT time decay of the EL intensity after pumping to steady state under reverse bias and switching off the diode. In contrast with the lifetime extracted from Fig. 7, in this case we have observed a lifetime of only  $\sim 15\mu\text{s}$  (see Fig. 8, circles), and indeed the actual value can also be much shorter since this corresponds to the time resolution of our system. This discrepancy can be understood by realizing that during pumping, with the diode under operation in reverse bias, the  $\text{Er}^{3+}$  ions are excited (and they de-excite) within the depletion region. However, when the diode is switched off the excited  $\text{Er}^{3+}$  ions find themselves within an  $n^+$  region. Hence the conditions are very different. In this latter case a fast non-radiative de-excitation through an Auger process with free carriers (or with carriers trapped in Er-related bandgap states) can occur, efficiently decreasing the lifetime. On the other hand, in the former case, the free carrier population is very small and bandgap states above the intrinsic level are empty, thus the above mentioned de-excitation routes cannot occur and the excited state can present a longer lifetime. It should be noted that this event is particularly fortunate since  $\text{Er}^{3+}$  presents a long lifetime during pumping (thus allowing for a high steady state excited population) while it has a short lifetime when switching off the diode (thus allowing for fast operation).

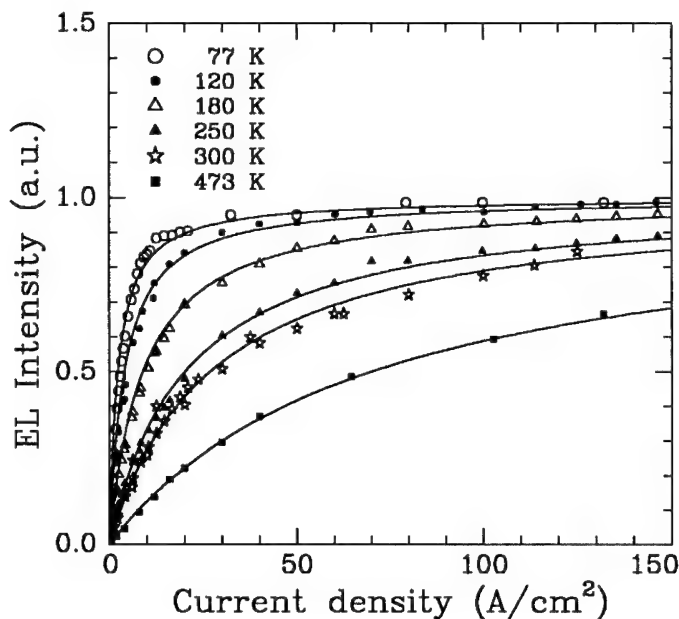


Fig. 9: Current density dependence of the EL intensity at different temperatures.

To verify the existence of a long lifetime within the depletion region we have also performed the following experiment. We have biased a diode by a constant reverse bias of  $\sim 3.5$  V (just below breakdown). The electric field in this condition is very high, however, no current is passing through the device and Er cannot be excited. We have then focused the light from an argon laser onto the diode in order to produce electron-hole pairs in the depletion region. These pairs are accelerated by the electric field and can excite Er by impact. Since the laser beam is chopped, the

excited state lifetime can be measured by recording the luminescence transient after shutting off the laser light. The result of such a measurement is reported also in Fig. 8 as triangles and shows a time decay of  $\sim 90 \mu\text{s}$ , in good agreement with the previous results.

As a result of the high cross section for impact excitation and of the long RT lifetime within the depletion region, Er is expected to be efficiently excited. We have therefore studied the increase of the EL intensity signal during reverse bias operation as a function of the current density. Data taken at different temperatures, in the range 77K to 473K, are reported in Fig. 9 for current densities up to  $150 \text{ A/cm}^2$ . At each temperature the EL yield first increases linearly with fluence and eventually saturates. The rate at which the EL increases before saturation decreases when the temperature is increased, but eventually the same saturation level is approached independently of temperature. These results indicate that at sufficiently high current densities all of the excitable Er sites are excited and hence population inversion of the excitable Er ions has been achieved. This is a further proof of the efficiency of impact excitation. Moreover, since the saturation value is independent of temperature, the density of excitable Er sites does not depend on temperature.

Data of Fig. 9 provide also an independent way of measuring the cross section for impact excitation. In fact, curves in Fig. 9 should have a functional shape given by the solution of eq.(1) under steady state conditions, i.e.:

$$N_{\text{Er}}^* = \frac{\sigma\tau\phi}{\sigma\tau\phi + 1} \quad (3)$$

and therefore they can be fitted by the use of a single parameter, namely  $\sigma\tau$ . The RT curve in Fig. 9 can be fitted with a  $\sigma\tau$  value of  $6 \times 10^{-21} \text{ cm}^2 \text{ sec}$ . Using the value of  $\tau$  obtained from Fig. 8 ( $90 \mu\text{sec}$ ), we obtain a value for  $\sigma$  of  $6.6 \times 10^{-17} \text{ cm}^2$ . This represents an independent way for obtaining  $\sigma$  and is in very good agreement with the cross section for impact excitation extracted from the data of Fig. 7.

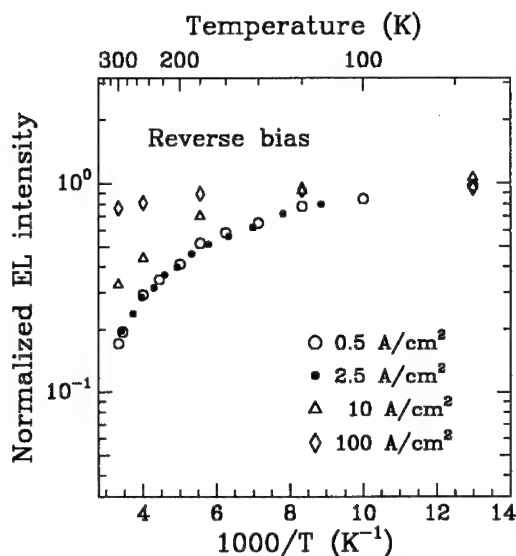


Fig. 10: Temperature dependence of the EL intensity under reverse bias conditions at different current densities. The data are normalized to the value at 77 K.

A further observation should be made. Data in Fig. 9, with an initial linear regime and a subsequent saturation, indicate that the temperature dependence of the EL intensity depends on the current density at which measurements are performed. This is clearly shown in Fig. 10 where we report the EL temperature dependence under reverse bias conditions and for four different current densities, namely 0.5, 10 and 100 A/cm<sup>2</sup>. As soon as the current density increases the temperature dependence becomes weaker and weaker. For instance, at 100 A/cm<sup>2</sup> the EL intensity decreases by only 30 % on going from 77 K to RT. It should be noted that this is only an effect of the saturation of the excitable sites and does not mean any way that excitation and de-excitation efficiencies are temperature independent. Therefore, when presenting temperature dependence data, it is always important to make sure that they are performed in a regime in which the EL vs current density is linear (as in the 0.5 and 2.5 A/cm<sup>2</sup> cases).

A question arises on what is the efficiency. By using a calibrated power meter we were able to measure a maximum internally emitted power of 1 μW and 10 μW under forward and reverse bias, respectively, at room temperature and at a current of 0.5 A. The internal quantum efficiency under reverse bias is of 6×10<sup>-5</sup> at 300 K. The maximum emitted power for a silicon LED is given by

$$P_{\max} = \frac{hc}{\lambda} \frac{N_{\text{Er}}}{\tau_{\text{rad}}} AW \quad (4)$$

where AW is the excitable volume (area times the depletion layer width). As  $hc/\lambda=0.8$  eV,  $A=0.05$  cm<sup>2</sup>, assuming  $\tau_{\text{rad}}=1$  msec, and using the measured value of  $P_{\max}$  we obtained:

$$N_{\text{Er}} W = 2 \times 10^{12} / \text{cm}^2$$

which gives the total number of excitable Er ions in the depletion region. On the other hand the total number of Er atoms in the depletion region is  $\sim 4 \times 10^{13} / \text{cm}^2$ . This implies that only 5% of the incorporated Er ions are excitable even by impact excitation. This is clearly a major limitation which severely reduces the maximum emitted power and the internal quantum efficiency. A possible explanation for the small fraction of excitable Er ions is the following. Band to band tunneling produces spatially separated electrons and holes in the vicinity of the central part of the depletion region where the electric field is at its maximum. Once generated, carriers are accelerated by the remaining field and eventually, when their energy is in excess of 0.8 eV they can excite Er. This occurs only in a thin region close to the end of the depletion region. Therefore the amount of excitable Er is much less than the total Er present in the depletion region. The small amount of excitable Er ions represents one of the major limiting steps towards higher luminescence. Further work should be aimed in reducing the efficiency of non-radiative processes and in increasing the excitable Er population.

## Acknowledgments

We wish to thank Aldo Spada, Natale Marino, Antonio Marino, Salvo Pannitteri and Nico Parasole for their continuous expert technical assistance during the different parts of the present work.

This work has been performed in the framework of the project SCOOP (Silicon-Compatible Optoelectronics) supported by the European Community.

Work at FOM was financially supported by NWO, STW and IOP Electro-optics.

## References

1. H. Ennen, G. Pomrenke, A. Axmann, W. Haydl and J. Schneider, Appl. Phys. Lett. 46, 381 (1985)
2. G. Franzò, F. Priolo, S. Coffa, A. Polman, and A. Carnera, Appl. Phys. Lett. 64, 2235 (1994)
3. B. Zheng, J. Michel, F.Y.G. Ren, L.C. Kimerling, D.C. Jacobson, and J.M. Poate, Appl. Phys. Lett. 64, 2842 (1994)
4. S. Coffa, F. Priolo, G. Franzò, A. Polman, S. Libertino, M. Saggio, and A. Carnera, Nucl. Instrum. Meth. B106, 386 (1995)
5. S. Lombardo, S.U. Campisano, G.N. van den Hoven, and A. Polman, J. Appl. Phys. 77, 6504 (1995)
6. S. Coffa, F. Priolo, G. Franzò, V. Bellani, A. Carnera, and C. Spinella, Phys. Rev. B48, 11782 (1993)
7. R. Serna, M. Lohmeier, P.M. Zagwijn, E. Vlieg, and A. Polman, Appl. Phys. Lett. 66, 1385 (1995)
8. D.L. Adler, D.C. Jacobson, D.J. Eaglesham, M.A. Marcus, J.L. Benton, J.M. Poate, and P.H. Citrin, Appl. Phys. Lett. 61, 2181 (1992)
9. P.N. Favenne, H. l'Haridon, D. Moutonnet, M. Salvi, and M. Gauneau, Jpn. J. Appl. Phys. 29, L524 (1990)
10. J. Michel, J.L. Benton, R.F. Ferrante, D.C. Jacobson, D.J. Eaglesham, E.A. Fitzgerald, Y.H. Xie, J.M. Poate, and L.C. Kimerling, J. Appl. Phys. 70, 2762 (1991)
11. S. Coffa, G. Franzò, F. Priolo, A. Polman, and R. Serna, Phys. Rev. B49, 16313 (1994)
12. S. Libertino, S. Coffa, G. Franzò, and F. Priolo, J. Appl. Phys. 78, 3867 (1995)
13. F. Priolo, G. Franzò, S. Coffa, A. Polman, S. Libertino, R. Barklie, and D. Carey, J. Appl. Phys. 78, 3874 (1995)
14. A. Polman, G.N. van den Hoven, J.S. Custer, J.H. Shin, R. Serna, and P.F.A. Alkemande, J. Appl. Phys. 77, 1256 (1995)
15. H. Przybylinska, G. Hendorfer, M. Bruckner, L. Palmetshofer, and W. Jantsch, Appl. Phys. Lett. 66, 490 (1995)
16. F. Priolo, S. Coffa, G. Franzò, C. Spinella, A. Carnera, and V. Bellani, J. Appl. Phys. 74, 4936 (1993)
17. A.G. Chynoweth and M.G. McKay, Phys. Rev. 106, 418 (1957)
18. W. Haecker, Phys. Status Solidi, A25, 301 (1974)
19. I.N. Yassievich and L.C. Kimerling, Semicond. Sci. Technol. 8, 718 (1993)
20. J.I. Pankove and R.J. Feuerstein, Mat. Res. Soc. Symp. Proc. 301, 287 (1993)

## ERBIUM DOPED SILICON FOR LIGHT EMITTING DEVICES

J. MICHEL, B. ZHENG, J. PALM, E. OUELLETTE, F. GAN, AND L. C. KIMERLING

Massachusetts Institute of Technology, Dept. of Materials Science and Engineering,  
Cambridge, MA 02139, [jurgen@jurgen.mit.edu](mailto:jurgen@jurgen.mit.edu)

### ABSTRACT

We report on the excitation and de-excitation processes of erbium implanted in silicon and the integration of Si:Er light emitting devices (LED) with standard CMOS technology. We find two de-excitation processes, an Auger process below 100 K and a phonon mediated energy backtransfer above 100 K. We present the first optical voice link with a silicon LED as the emitter. Optical transmission system performance with our LED is possible below 200 K.

### INTRODUCTION

In the past years, the development of silicon light emitters for optoelectronic applications have been the focus of extensive research. Erbium in silicon evolved as one of the most promising candidates for silicon light emission at room temperature. In 1983, Ennen et. al [1] demonstrated electroluminescence from erbium in silicon at 77 K. The next milestone towards room temperature luminescence was the observation that the Er luminescence is increased by more than two orders of magnitude in the presence of oxygen or other ligands [2,3]. Er and O co-implanted Si yielded the first room temperature photoluminescence (PL) of Er in Si [3] and soon afterwards room temperature electroluminescence (EL) [4,5] from LEDs.

During this progress it became obvious that a basic understanding of the excitation and deexcitation processes was needed. The excitation process is still not completely understood [6]. Furthermore, a backtransfer mechanism reduces the emission intensity by more than a factor of 100 at room temperature [2]. In the first part of this paper we will discuss our latest results on these important processes.

Since Er was introduced by ion implantation, an annealing step to remove lattice damage is necessary. The right annealing temperature and duration is critical for achieving optimum emission intensity. In order to integrate these devices with standard CMOS technology, a process flow that takes into account the thermal budget of the MOSFET devices and the LED has been developed. The second part of the paper deals with the issue of device integration and we will show that MOSFET drivers and LEDs can be fabricated on a single chip.

### EXCITATION AND DEEXCITATION PROCESSES

The excitation efficiency of erbium in silicon is controlled by different competing mechanisms. In Figure 1 these energy transfers are divided into four categories. After excess carrier generation excitons form due to the indirect band gap of silicon which results in a long carrier lifetime. Excitons then recombine in three different processes. The exciton-electron Auger recombination transfers the exciton energy to a free electron. Free and bound exciton radiative recombination is

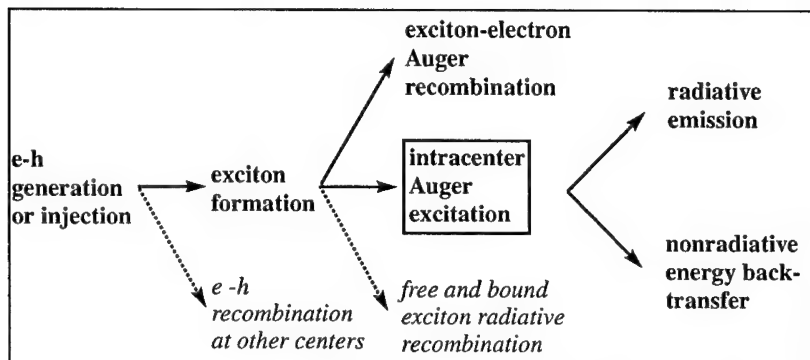


Figure 1. Energy flow of excitation and deexcitation processes in Si:Er

one recombination path for light emission from silicon. These exciton recombination processes compete with the intracenter Auger excitation which excites the lowest spin-orbit level,  $^4I_{15/2}$ , of the  $\text{Er}^{3+}$  4f manifold. A state in the gap acts as a gateway for energy flow to and from the Er 4f-shell but has little overlap with the 4f-manifold wavefunctions. A direct correlation between Si:Er-O emission intensity and donor state introduction has been observed [7]. Once the 4f manifold is excited, two processes can occur to relax the excitation. Radiative recombination leads to the  $1.54\text{ }\mu\text{m}$  emission, while the nonradiative backtransfer reduces the emission intensity. All processes before the erbium excitation, faster than the Er radiative recombination process, determine the pumping efficiency but do not influence the emission lifetime. For parallel processes after excitation, the fastest process dominates the emission lifetime. Therefore for a slow radiative process as is the case for excited erbium, a fast nonradiative backtransfer process will dominate the radiative lifetime of the emission. If there is no backtransfer process, any decrease in the radiative lifetime (increase in the photon emission rate) will increase the emission intensity.

A measurement of luminescence lifetime and corresponding luminescence intensity for temperatures below 100K is shown in Figure 2. Both curves show a decrease with increasing temperature, which indicates the

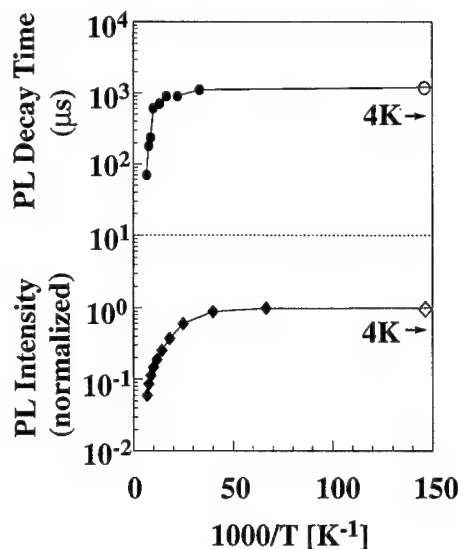
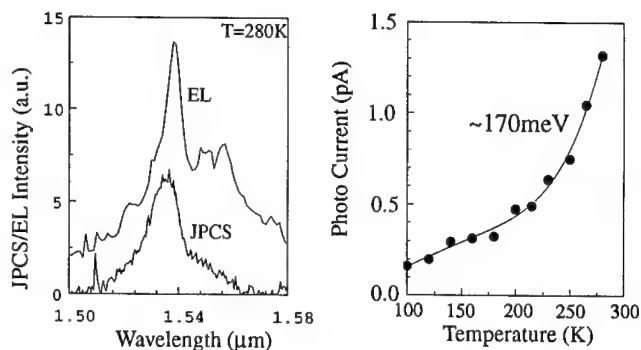


Figure 2. Dependency of PL Intensity and luminescence decay time on temperature

existence of a nonradiative energy backtransfer from the first excited state. Experiments on lifetime measurements of the emission dependence on the bias state of an electroluminescent device showed that with increasing forward bias the emission lifetime decreases [8]. During forward bias conditions, minority carriers are injected into the junction region. A reverse bias between injection pulses that depletes the junction

area always yielded an emission lifetime above 500  $\mu$ s, close to the observed Er lifetime of about 1 ms, while a forward bias decreased the emission lifetime to 70  $\mu$ s and smaller. These experiments confirm the existence of an Auger process at low temperature (< 100 K), where free conduction band electrons absorb the energy of the excited 4f manifold and, therefore, compete with the radiative process.

In the higher temperature regime (> 100K) energy backtransfer through phonon processes dominates [9]. Figure 3 shows the results of junction photocurrent spectroscopy (JPCS) on an Si:Er LED. The LED was used as a photodetector and the spectral response of the current was measured. In Fig 3 a) the JPCS response is compared with an electroluminescence spectrum of the LED. The comparison shows that the JPCS signal at 1.54  $\mu$ m originates from  $\text{Er}^{3+}$ . This photocurrent can only be observed if the energy of the excited 4f manifold can be transferred to the conduction band electrons. The spectral response clearly shows the existence of a backtransfer from the excited erbium where the energy is transferred to a valence band electron. The temperature dependence of the photocurrent at 1.54  $\mu$ m exhibits a temperature activated process with an activation energy of 170 meV (Fig. 3 b).



**Figure 3.** Junction photocurrent spectroscopy on a Si:Er LED. a) shows the JPCS spectrum compared to an EL spectrum from the same LED, b) shows the temperature behavior of the JPCS intensity.

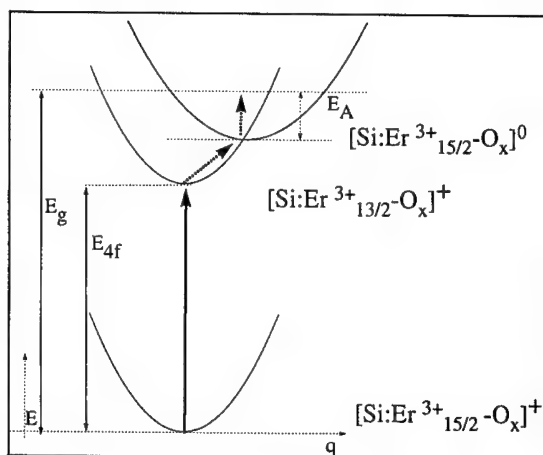


**Figure 4.** Configuration coordinate diagram of the excitation and de-excitation path at temperatures above 100K.



The excitation and deexcitation can be described by the configuration coordinate diagram in Figure 4.  $E_g$  is the silicon bandgap,  $E_{4f}$  the energy of the first excited state of the Er 4f manifold, and  $E_A$  is the ionization energy for the erbium related donor state [7].  $[\text{Si:Er}^{3+}_{z/2}\text{-O}_x]^{+/0}$  describes the Er-O complex with ground ( $z=15$ ) and excited ( $z=13$ ) 4f

manifold. + and 0 indicate the ionized and neutral state, respectively. After excitation of a 4f manifold by photon absorption the relaxation can occur radiatively by emitting light at  $1.54\text{ }\mu\text{m}$  or nonradiatively via an energy backtransfer. This nonradiative process occurs when the energy of the excited 4f manifold and an additional local phonon energy excite an electron resonantly to induce a transfer from the valence band to the erbium related donor state located about 160 meV below the conduction band [10]. The phonon energy necessary for this process is about 140 meV. Similar local phonon energies can be found in silicon, i.e. the  $9\text{ }\mu\text{m}$  absorption band due to a local vibrational mode of interstitial oxygen in silicon. The photocurrent is detected when the electron is thermalized. The measured activation energy (170 meV) of the JPCS temperature dependence indicates that the thermalization is the bottleneck for the backtransfer process. A similar model for ytterbium in InP was suggested by Taguchi et al. [11].

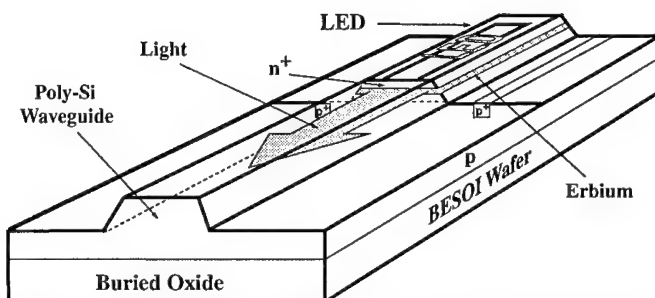


Figure 5. Integrated LED-waveguide design for edge emitting LED and multimode waveguide.

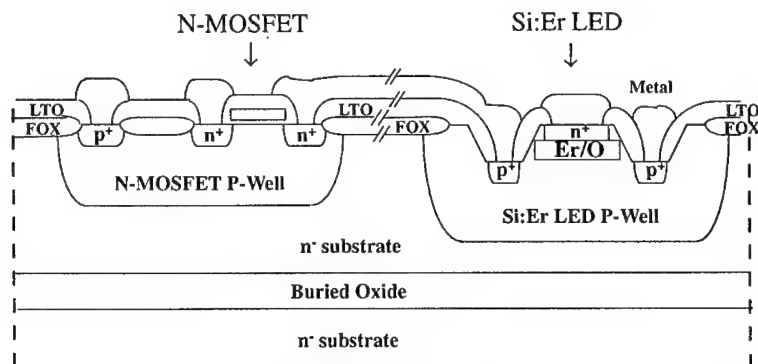


Figure 6. Process cross section of a LED - MOSFET integrated design fabricated due to CMOS design rules.

## LED INTEGRATION

Process incompatibility between Si CMOS and III-V semiconductors has been a major obstacle for the monolithic integration of Si electronics and compound semiconductor LEDs and other optoelectronic components. To demonstrate that Si:Er LEDs can be integrated with current Si VLSI technology, a circuit including a MOSFET driver in series with an Si:Er LED was processed in a CMOS process flow. For this purpose a twin-well CMOS baseline process was enhanced with additional processing steps to incorporate monolithic LED processing.

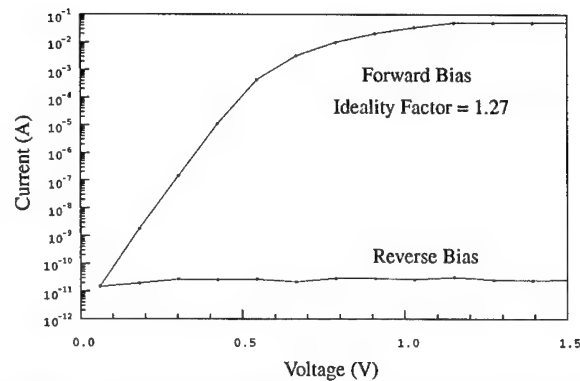


Figure 7. I-V characteristic of a Si:Er LED after CMOS processing.

As starting material we used BESOI (Bonded and Etched-back Silicon-On-Insulator) wafers in order to utilize the integrated LED/waveguide design, shown in Figure 5. In this design the light emitted from the Si:Er LED couples longitudinally into a silicon waveguide without the typical coupling losses. This design is possible because silicon is transparent at  $\lambda = 1.54 \mu\text{m}$ . The SOI wafer material provides a single crystalline silicon top layer with a thickness of about  $5 \mu\text{m}$ , which is necessary for the 4.5 MeV erbium implant and advantageous for waveguiding in an integrated waveguide structure. The large index difference between the crystalline silicon top-layer ( $n = 3.5$ ) and the buried oxide ( $n = 1.5$ ) provides light propagation with low loss. Simulations confirm that

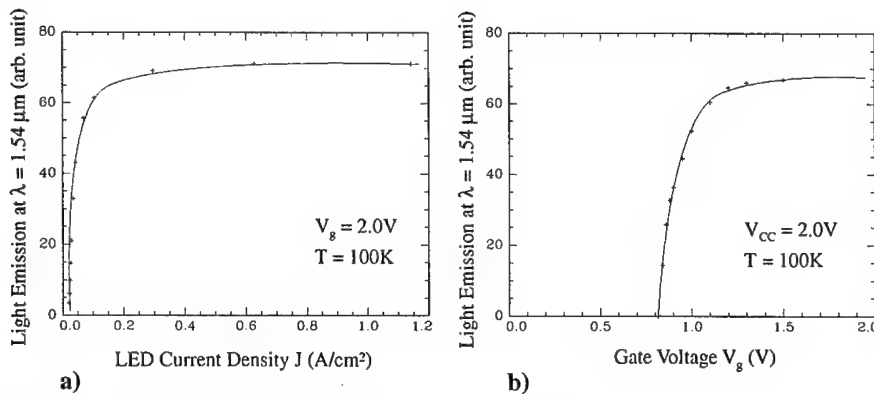


Figure 8. a) Er light emission intensity vs. drive current density. b) Modulation of Er light output by MOSFET gate voltage.

these structures can be used for multimode waveguiding.

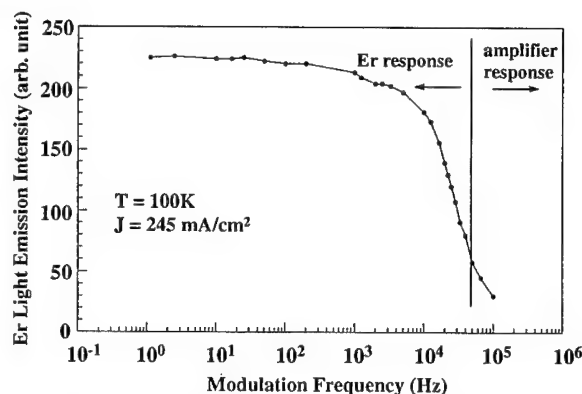
Standard 2 micron design rules were used to ensure chip functionality. Figure 6 shows a process cross section of the integrated devices. A p-well was chosen for the LED because of the enhanced light emission intensity of Er in p-type Si. The p-well depth for the N-MOSFET is 4  $\mu\text{m}$  with a boron concentration of  $5 \times 10^{16} \text{cm}^{-3}$  while the p-well depth for the LED is 5  $\mu\text{m}$  to accommodate the LED mesa structure. The boron concentration is  $1 \times 10^{16} \text{cm}^{-3}$ . The LED  $n^+$  emitter was formed by an arsenic implant. The LED areas were protected during MOS implants by photoresist. During the field oxidation the LED area was protected by a nitride. Er was implanted *after* the CMOS source/drain annealing to reduce the exposure of erbium to high temperatures which is detrimental to the luminescence intensity.

The I-V characteristic of a typical Si:Er LED is shown in Figure 7. An ideality factor of 1.27 was measured. The observed I-V characteristics of the integrated LED was similar to that of previously fabricated discrete Si:Er LEDs of p-type Cz material. The high leakage current is most likely due to residual implantation damage like dislocations, observed in the EL spectrum of some LEDs.

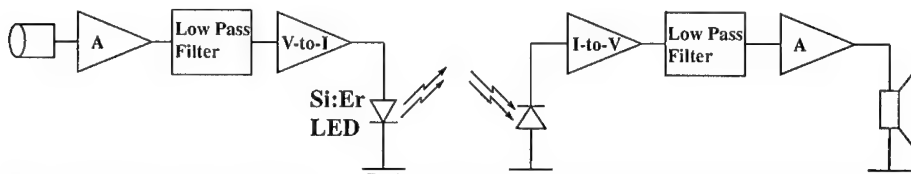
The I-V characteristic of a typical Si:Er LED is shown in Figure 7. An ideality factor of 1.27 was measured. The observed I-V characteristics of the integrated LED was similar to that of previously fabricated discrete Si:Er LEDs of p-type Cz material. The high leakage current is most likely due to residual implantation damage like dislocations, observed in the EL spectrum of some LEDs.

Figure 8 shows typical LED light emission intensity vs. current density and gate voltage, in a) and b), respectively. The LED reaches saturation at current densities below  $200 \text{mA/cm}^2$ . The switching behavior of the gate is shown in Fig. 8 b). The minimum switching voltage necessary to turn the LED on is 1.3 V. At that voltage, maximum light output is reached. Therefore the light emission can be efficiently modulated by varying the gate voltage around a threshold voltage of 0.8 V. Both figures show that MOSFET and Er doped Si LED are successfully integrated, with expected performance for an Si:Er LED at 100K.

The modulation speed of the LED is limited by the lifetime of the first excited state of  $\text{Er}^{3+}$ . At low temperatures this lifetime is about 1 ms. Palm et al. [8] showed that due to a nonradiative



**Figure 9.** Frequency response of a Si:Er LED. The amplifier response was limited to 20  $\mu\text{s}$ .



**Figure 10.** Optoelectronic infrared voice link utilizing surface-emitting Si:Er LED at variable temperatures for freespace signal transmission.

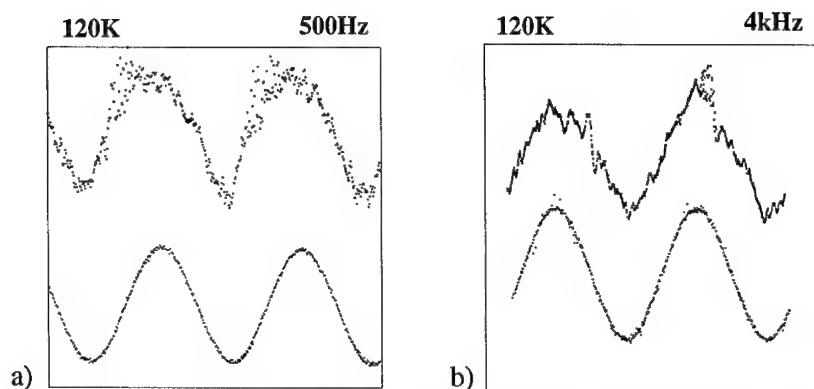


**Figure 11.** Optical transmission of a sine wave using a Si:Er LED. The lower sine wave shows the input signal, the output signal is shown in the upper trace. The signal was measured at 120K for 500 Hz (a) and 4 kHz (b).

backtransfer the radiative lifetime falls below 100  $\mu\text{s}$  at 100K. Therefore a modulation speed of 10 kHz should be attainable. The frequency response of the LED is shown in Figure 9. A fast liquid nitrogen cooled InGaAs detector was used for this measurement. The measurement system response time was limited by the current amplifier to 50 kHz. The amplifier response limit is indicated in the figure. As predicted we found a good response of the LED up to a modulation frequency of about 20 kHz.

A modulation frequency of 20 kHz allows optical voice transmission by our implementation of a cooled Si:Er LED as the emitter and an InGaAs detector as the receiver. Figure 10 shows a diagram of the setup. Transmitter and receiver electronics were assembled on separate bread-boards. The light from the LED was collimated and refocused by two lenses. Room light did not influence the transmission as a narrow optical band pass filter ( $\lambda = 1.54 \mu\text{m}$ , 30 nm bandwidth) was included in the optical path. The distance between lightsource and receiver was varied between 0.2 and 0.5 m. To demonstrate functionality, we used a standard amplitude modulation. Digital encoding and error determination and correction (EDC) of the voice signal will reduce the background noise significantly. The actual response of the system is shown in Figure 11. The signal trace was taken with a digital oscilloscope. A signal generator was used in place of the voice input source to supply a continuously variable frequency sine wave to the transmitter. Measurements were made of the output receiver response for two input frequencies, 500 Hz and 4 kHz. The resulting responses are shown in Fig. 11 a) and b), respectively. The output receiver noise is due to the large amplification on the detector side, the LED noise is not detectable. Voice transmissions are slightly distorted because of LED I-V non linearities. This non-ideality is visible in the deformation of the sine wave after free space transmission.

## CONCLUSIONS

We have shown that the nonradiative deexcitation of erbium involves two different processes depending on the temperature regime. Below 100 K an impurity-Auger process competes with the radiative recombination at  $\lambda = 1.54 \mu\text{m}$ . The efficiency of this process depends on the carrier concentration in the active region of an LED. By reducing minority carriers this backtransfer can be nearly completely suppressed. Above 100K we find a phonon mediated process as the dominating non radiative recombination process of the excited erbium 4f manifold. Both excitation and deexcitation of  $\text{Er}^{3+}$  can be explained by electron capture of a donor state, correlated with the optically active Er-O complex, and an additional phonon emission or absorption, respectively.

The integration of an Si:Er LED with standard CMOS technology was demonstrated. A MOSFET driver and Si:Er LED were fabricated on a single chip. The frequency response of the LED showed that the LED can be operated below 20 kHz. The functionality of this LED-driver circuit was demonstrated by realizing an optical voice link with optical transmission below 200K.

## ACKNOWLEDGEMENTS

We acknowledge partial support by ARPA, Rome Laboratories, and AFOSR under contract F19628-95-C-0049 and SRC under contract 94-SC-309.

## REFERENCES

- [1] H. Ennen, G. Pomrenke, A. Axmann, K. Eisele, W. Haydl, and J. Schneider, *Appl. Phys. Lett.* **46**, 381 (1985).
- [2] J. Michel, J.L. Benton, R.F. Ferrante, D.C. Jacobson, D.J. Eaglesham, E.A. Fitzgerald, Y.-H. Xie, J.M. Poate, and L.C. Kimerling, *J. Appl. Phys.* **70**, 2672 (1991)
- [3] P.N. Favennec, H. L'Haridon, D. Moutennet, M. Salvi, and M. Gauneau, *Jpn. J. Appl. Phys.* **29**, L524 (1990)
- [4] B. Zheng, J. Michel, F.Y.G. Ren, L.C. Kimerling, D.C. Jacobson and J.M. Poate, *Appl. Phys. Lett.* **64**, 2842 (1994)
- [5] G. Franzò, F. Priolo, S. Coffa, A. Polman, and A. Carnera, *Appl. Phys. Lett.* **64**, 2235 (1994)
- [6] I.N. Yassievich and L.C. Kimerling, *Semicond. Sci. Technol.* **7**, 1 (1993)
- [7] M. Morse, B. Zheng, J. Palm, X. Duan, and L.C. Kimerling, this volume
- [8] J. Palm, F. Gan, B. Zheng, J. Michel, and L.C. Kimerling, *Phys. Rev. B*, in press
- [9] J. Palm, to be published
- [10] S. Libertino, S. Coffa, G. Franzò, and F. Priolo, *J. Appl. Phys.* **78**, 3867 (1995)
- [11] A. Taguchi, K. Takahei, and J. Nakata, *Mat. Res. Soc. Symp. Proc. Vol.* **301**, 139 (1993)

## PHOTO- AND ELECTROLUMINESCENCE STUDY OF EXCITATION MECHANISM OF Er LUMINESCENCE IN a-Si:H(Er)

I.N.YASSIEVICH\*, O.B.GUSEV\*, M.S.BRESLER\*, W.FUHS\*\*,  
A.N.KUZNETSOV\*, V.F.MASTEROV\*\*\*, E.I.TERUKOV\*,  
B.P.ZAKHARCHENYA\*

\*A.F.Ioffe Physico-Technical Institute, Politekhnikeskaya 26, 194021 St.Petersburg,  
Russia, brems@solid.pti.spb.su

\*\*Hahn-Meitner Institut, Glienicke Str., Berlin, D-14109, Germany

\*\*\*St.Petersburg State Technical University, Politekhnikeskaya 29, 194251  
St.Petersburg, Russia

### ABSTRACT

Photo- and electroluminescence were studied in erbium-doped amorphous hydrogenated silicon films. A mechanism of excitation of erbium ions by defect-related Auger process is proposed which permits to explain consistently the whole set of our experimental results.

### INTRODUCTION

The idea to fabricate LEDs integrable into silicon electronics and emitting at the wavelength of 1.5  $\mu\text{m}$  corresponding to the absorption minimum of optical fibers attracted much attention to the luminescent properties of erbium-doped silicon [1]. Experiments showed that crystalline erbium-doped silicon (c-Si(Er)) suffers as an optical active medium from several drawbacks: the main are strong temperature quenching and a long radiative lifetime of erbium ions [2].

Recently we have demonstrated that the films of erbium-doped amorphous hydrogenated silicon (a-Si:H(Er)) prepared by cosputtering exhibit strong room-temperature photoluminescence and the lifetime of erbium ions in this material is considerably shortened by the effect of amorphous-matrix disorder [3].

Here we present results of more detailed studies of photoluminescence (PL) and the first observation of electroluminescence (EL) of a-Si:H(Er). The results of these studies gave a key to understanding of the excitation mechanism of erbium luminescence in amorphous matrix.

### EXPERIMENT

Erbium-doped amorphous silicon films were prepared by cosputtering applying magnetron-assisted silane decomposition (MASD) technique [4]. The concentration of erbium introduced was measured by Rutherford back scattering method and reached up to  $1 \times 10^{20} \text{ cm}^{-3}$ . For electroluminescent structures films of 0.5  $\mu\text{m}$  thickness were deposited on n-silicon substrates with concentration of donors of  $5 \times 10^{17} \text{ cm}^{-3}$ . Aluminium contacts were made to the amorphous film and to the n-type substrate. I-V characteristics of the EL structures had conventional diode type.

PL and EL spectra were analysed with a double grating spectrometer and detected by a nitrogen-cooled germanium photodetector. Excitation of PL was done by argon cw laser with the pumping power up to 100 mW. For EL studies excitation current pulses at 25 Hz were passed through the EL structure either in forward (plus on the amorphous film,

minus on the substrate) or in reverse direction. PL was measured in the temperature range 77-300K while EL at room temperature.

## RESULTS

PL-spectra of a-Si:H(Er) measured at 77K exhibit emission from both the  $\text{Er}^{3+}$  centers and the amorphous Si-matrix ( Fig. 1). The latter is seen as a broad band at 0.9 - 1.3 eV, which is believed to arise from radiative tunneling between localized band-tail states. The

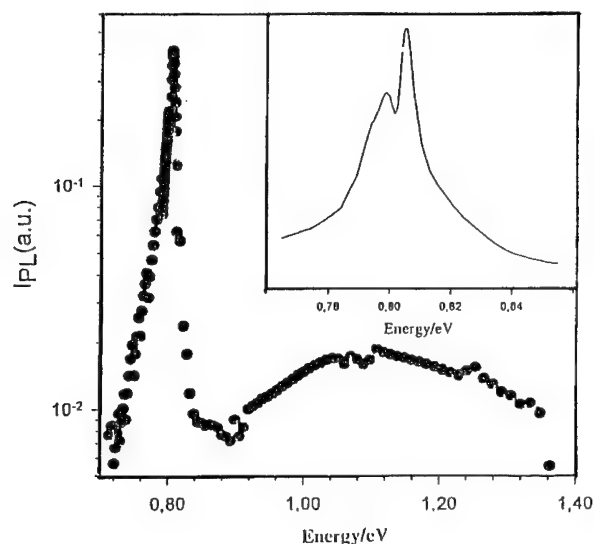


Fig.1  
Photoluminescence of  
a-Si:H(Er) at 77K

intrinsic emission is low and the band width is much larger than in a typical a-Si:H of good quality. The spectrum in Fig. 1 is dominated by strong Er- induced emission at 0.8 eV. There is no indication of defect-related emission which can be usually observed in a-Si:H of low quality at 0.8 - 0.9 eV. In our previous study where the amorphous film had been of minor quality this emission formed a broad background of the Er - photoluminescence [3]. At 300K the emission from the a-Si:H matrix is suppressed by temperature quenching and the remaining signal is entirely due to  $\text{Er}^{3+}$  ions (cf. the inset in Fig.1). Er- induced emission consists of two narrow lines at 0.806 eV and 0.798 eV which can be attributed to crystal field splitting of the ground state of the Er ions. The lines are broadened in comparison with the lines observed in erbium-implanted crystalline silicon pointing to an important role of disorder in amorphous matrix.

Our measurements of absorption in a-Si:H(Er) films show that significant absorption occurs at energies below 1.5 eV, where the absorption from deep defect states prevails. From the subgap absorption we inferred defect densities in the range  $5 \times 10^{17}$  to  $10^{18} \text{ cm}^{-3}$ .

Temperature dependences of intensity of PL for different optical transitions are displayed in Fig.2 (curve a - PL of erbium ions in a-Si:H(Er), curve b - PL of intrinsic emission of amorphous silicon in a-Si:H(Er), curve c - PL of erbium ions in erbium-doped crystalline silicon (c-Si(Er))).

In order to achieve high emission intensity in crystalline silicon the samples should be coimplanted with erbium and oxygen and optimization need extended high-temperature annealing [1]. In the case of a-Si:H the preparation is much simpler since high emission intensity does not require additional treatment of the films and high concentration of Er can be incorporated using the cosputtering technique. At low temperature ( $T < 100\text{K}$ ) the Er-induced emission is larger by 1.5 - 2 order of magnitude than that in optimized c-Si(Er,O). The Er concentration amounted to  $10^{20}\text{ cm}^{-3}$  and  $10^{17}\text{ cm}^{-3}$  in a-Si:H(Er) and

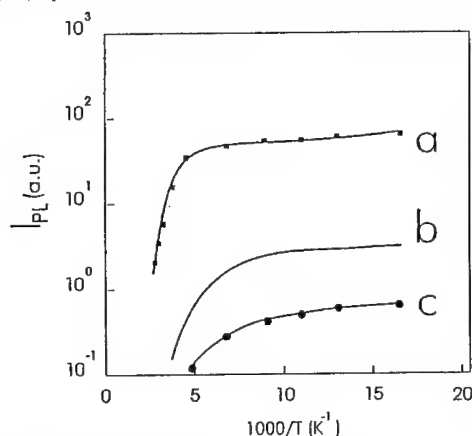


Fig. 2 Temperature dependence of PL of Er ions (curve a) and intrinsic band (curve b) for a-Si:H(Er) and Er ions for c-Si(Er) (curve c)

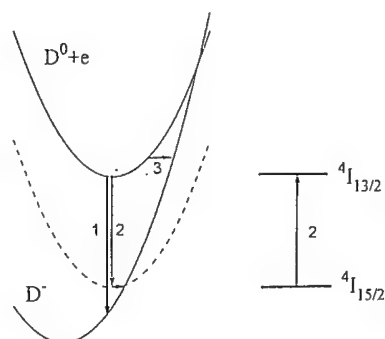


Fig.3 Configuration-coordinate diagram for  $e + D^0 \rightarrow D^-$  transition

c-Si(Er,O), respectively. The oxygen content in the c-Si(Er) sample was about  $10^{18}\text{ cm}^{-3}$ . Note that in crystalline silicon, the maximum of Er-luminescence intensity was realized with oxygen content larger by one order of magnitude than erbium concentration. In a-Si:H(Er) oxygen was not introduced deliberately but it is well known that such films contain oxygen on the order of  $10^{19}\text{ cm}^{-3}$  due to contamination.

The results presented in Figs.1,2 have been obtained in linear regime of pumping. It should be stressed that at sufficiently high pumping power PL of erbium ions is saturated which is well known for c-Si(Er) and was demonstrated by us for a-Si:H(Er). The saturation of Er-emission in a-Si:H(Er) samples takes place at much higher pumping level than in c-Si(Er,O) [3]. Saturation of erbium-ions luminescence is traditionally ascribed to a finite number of optical centers and comparatively long lifetime of the  $\text{Er}^{+3}$  ion in the  $4I_{13/2}$  excited state.

In saturation regime, there is no temperature dependence of  $I_{PL}$  in the region 77 - 300K. This fact indicates that the number of optically activated Er-centers and the radiative life time of the excited  $4I_{13/2}$  - state are independent of temperature. It is of great interest that the defect luminescence band has been distinctly detected in the saturation regime even at room temperature.

In the linear regime  $I_{PL}$  decreases only slightly at low temperature but is strongly quenched above about 200K. The slope of the temperature dependence suggests an activation energy of about 250 meV (curve a). This behavior is different from that of the optimized c-Si(Er,O) sample (curve c). In that case  $I_{PL}$  starts from a much lower level as outlined above and exhibits pronounced temperature quenching with the characteristic



energy of 20 meV at low temperature and the energy of 150 meV at higher temperatures. Here  $I_{PL}$  at room temperature is smaller by two orders of magnitude than that in the amorphous specimen. This behavior of c-Si(Er,O) is quite familiar and typical for an oxygen doped sample [1].

It is well known that the intrinsic band (curve b) is quenched strongly above about 60K when the carriers in the tail states become mobile due to thermally activated tunneling or are excited to the mobility edge which enhances non-radiative recombination through defect states.

Now we should like to discuss possible mechanisms of excitation of erbium ions in an amorphous matrix.

The energy transfer from electron states of the conduction band or electron states corresponding to localized levels in the forbidden gap to the strongly localized  $f$ -electron multiple states is produced by the Coulomb interaction. In amorphous matrix there are three possible ways of electronic excitation: impact ionization by mobile carriers, Auger-excitation in the recombination process of band electron-hole pairs, and Auger-process in which electron (or hole) is captured in a localized state in the forbidden gap.

The impact excitation needs a great number of mobile carriers with high energy and therefore is usually not efficient in the amorphous matrix.

In amorphous silicon there are long tails of band states with energies lower than the mobility threshold. Here the intrinsic luminescence is observed as a broad band with the center near 1.3 eV. Thus, one may suppose that the excitation of  $Er^{3+}$  ion to the second excitation state  $^4I_{11/2}$  from the ground state  $^4I_{15/2}$  (the transition energy is equal to 1.24 eV) could be induced by the Coulomb interaction in the process of recombination of electron-hole pairs located in the band tails. The process can be designated as the resonance band Auger excitation. If this process played an important role in amorphous silicon, we should observe similar temperature quenching for both  $Er^{3+}$  ion and intrinsic luminescence bands since both bands are produced by mobile thermalized electron-hole pairs. However, one can see that the temperature quenching of Er-luminescence starts only at  $T \geq 200K$ , when the intrinsic luminescence is already absent (see Fig.2).

Our experimental results have demonstrated that there is a great number of defect states in a-Si:H(Er) which is typical for a-Si:H. In a-Si:H(Er), the defect absorption band is observed in the range 1.0 - 1.1 eV. It is the energy range where defect absorption band is usually observed in a-Si:H doped by various impurities or in films of minor quality. The defect absorption band is traditionally associated with dangling bond D-defects. The band is connected with the optical transition from donor  $D^0$  states to the conduction band. It is accepted that in amorphous silicon there exist also  $D^-$  states originating from the ability of  $D^0$  defects to capture the second electron. The splitting between these states is of the order of 0.1-0.2 eV. The defect luminescence band is observed in the region 0.8 - 0.9 eV and is ascribed to the radiative transition  $e + D^0 \rightarrow D^-$ .  $D^-$  defects are also effective centers of nonradiative multiphonon recombination in a-Si:H due to strong electron-phonon coupling for electrons located in  $D^0$  and  $D^-$  states.

The energy that should be taken away in the transition  $e + D^0 \rightarrow D^-$  is close to the energy of transition  $^4I_{15/2} \rightarrow ^4I_{13/2}$  in the system of Er-ion  $f$ -electrons. As stated above, the introduction of erbium ions into the amorphous matrix is accompanied by formation of a great number of dangling bond defects with concentration  $\sim 10^{18} \text{ cm}^{-3}$ . Therefore, we can deduce that in a-Si:H(Er), practically all the defects should be associated with  $Er^{3+}$  ions. Thus, effective resonance excitation of the  $f$ -electrons may take place in the process of electron capture in  $D^0$ -state due to an Auger process. The absence of defect luminescence in a-Si:H(Er) in linear regime confirms the efficiency of this resonant defect-related Auger-excitation (DRAE) process. In saturation regime, when all  $Er^{3+}$  ions

occur in the excited  $4I_{13/2}$  state and, therefore, the Auger process is blocked, the defect luminescence appears and can be observed even at room temperature. This fact supports our Auger excitation model. It is not necessary to have the precise resonance since the excess energy on the order of the Franck-Condon shift (which is about 0,1 eV in a-Si:H) can be easily transformed to the system of local vibrations due to electron-phonon coupling.

The transitions involved are shown in the configuration-coordinate diagram of Fig.3. Besides radiative transition from  $e + D^0$  to  $D^-$ -state (transition 1), defect-related Auger-excitation (DRAE) (transition 2) and multiphonon (transition 3) nonradiative processes are presented in this diagram.

In the framework of our model of excitation it is easy to understand the difference in the temperature behavior of the Er-emission and the intrinsic emission of a-Si:H. It should be noted that in a-Si:H(Er) the basic channel of recombination is the nonradiative (multiphonon) recombination via  $D^-$  defects because the quantum yield of radiation is only about 2%. Since the carrier mobility is low in amorphous matrix, the recombination should be controlled by spatial diffusion of excess carriers. Thus, we deal here with so-called Langevin mechanism of nonradiative recombination in which the carrier transport in the vicinity of the defect is a "bottleneck" of the capture processes because the time of spatial redistribution of excess carriers is longer than the time of energy losses. In amorphous silicon with a great number of defects the mobility of holes is much lower than the mobility of electrons. So, we can think that electron-hole recombination is controlled by the rate of the hole capture by defects in  $D^0$  and/or  $D^-$  states.

Strong room-temperature erbium-ion electroluminescence was observed by us in erbium-doped amorphous silicon films. Erbium luminescence corresponding to a narrow line at  $1.54 \mu\text{m}$  (the energy of 805 meV) is observed only for the reverse bias when the

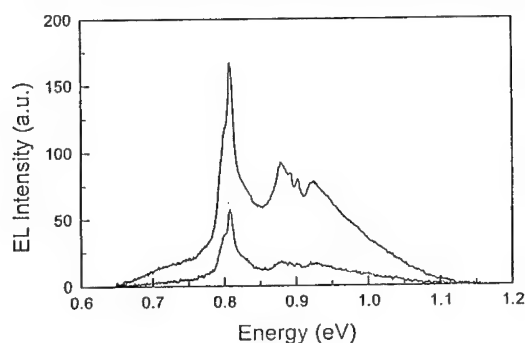


Fig. 4 EL spectra of a-Si:H(Er) with a reverse bias

excitation current through the structure exceeds the threshold value of  $\sim 5 \text{ mA}$  (the applied voltage is  $\sim 15 \text{ V}$ ). Spectra measured for two values of the excitation current at reverse bias are shown in Fig.4. Besides the narrow line corresponding to  $4I_{13/2} \rightarrow 4I_{15/2}$  transition in the f-shell of erbium ion a broad band at 0.8-0.9 eV can be seen. This broad band corresponds to defect-related luminescence of a-Si:H matrix as discussed above. Similar to the case of PL erbium luminescence exhibits a trend to saturation with the current increase.

In the case of forward bias no luminescence from erbium ions or defects is observed, but we detected free exciton line from crystalline silicon substrate (Fig.5). This fact demonstrates undoubtedly that free holes are injected into n-silicon substrate, i.e. the

current through the amorphous layer is carried by holes in this case. What is more remarkable, the holes moving through amorphous material excite neither erbium nor defect luminescence.

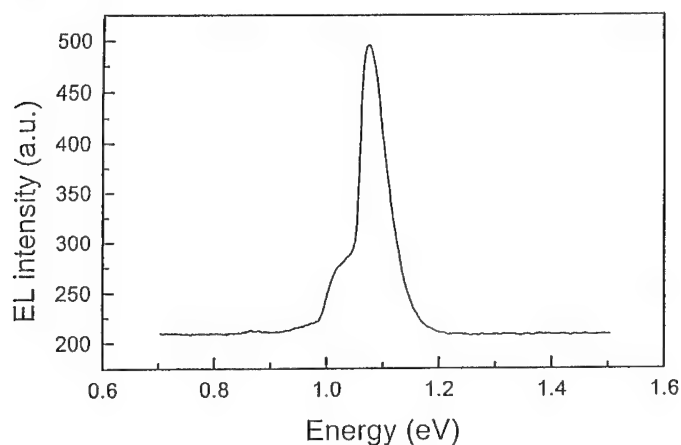


Fig.5 EL spectrum of photodiode structure with a forward bias

The aluminium contact to amorphous silicon operates usually as a holes injector. The Fermi level in the aluminium contact is situated below the defect level being in the middle of the forbidden gap of amorphous silicon. Due to high resistance of the amorphous film the potential drop is concentrated on the film itself. For the forward bias holes are injected from the contact due to thermostimulated tunneling and travel via amorphous layer until they arrive in the n-type crystalline silicon substrate and produce here luminescence caused by formation of free excitons in the crystalline material.

In the case of sufficiently high reverse bias electrons are injected by aluminium contact into the amorphous layer due to thermally activated tunneling. While moving in the amorphous layer the electrons excite erbium and defect-related luminescence. According to our dark-conductivity measurements the Fermi level in erbium-doped amorphous silicon at room temperature is slightly displaced upward from the middle of the gap, i.e. amorphous silicon doped by erbium is slightly n-type. In this case defects connected with the dangling bonds occur in  $D^0$  or  $D^-$  states. Since we have not observed defect-related luminescence at forward bias, we can deduce that no radiative capture of holes occurs to  $D^0$  or  $D^-$  centers. On the contrary, this emission band is observed when electrons are injected into amorphous silicon. Thus, our observations support traditional point of view that the broad emission band at 0.8-0.9 eV corresponds to processes of radiative capture of electrons from conduction band by neutral dangling bonds being described by a transition  $e + D^0 \rightarrow D^-$ .

The reverse transition  $D^- \rightarrow e + D^0$  which is necessary for continuous operation of LED is achieved due to thermal ionization enhanced by tunneling in high electric field ( $\sim 10^5$  V/cm) existing in the amorphous layer.

Recently room temperature PL in a-Si:H(Er) was observed also in the work [5]. PL [6] and EL [7] of  $Er^{3+}$  ions at room temperature were also studied in Er-doped SIPOS, material closely related to amorphous silicon.

## CONCLUSIONS

In conclusion, we have studied photo- and electroluminescence of erbium ions in erbium-doped amorphous silicon films. A mechanism of electronic excitation of erbium ions based on defect-related Auger excitation process is proposed and supported by experimental studies. Erbium-doped amorphous silicon can be regarded as a promising material for fabrication of LEDs compatible with the silicon electronics.

## ACKNOWLEDGEMENTS

This work was partly supported by Russian Foundation of Basic Research through grants 95-02-04163-a and 96-02-16931-a, by a grant 1-060/3 from Russian Ministry of Science, by AFOSR F49620-94-1-0390 grant, by INTAS grant No.93-1916 and by Volkswagen-Stiftung.

## REFERENCES

1. Rare Earth Doped Semiconductors, edited by G.S.Pomrenke, P.B.Klein, and D.W.Langer (Mater. Res. Soc. Proc. 301, Pittsburg, PA 1993).
2. S.Coffa, G.Franzo, F.Priolo, A.Polman, and R.Serna, Phys.Rev. B49, p.16,313 (1994).
3. M.S.Bresler, O.B.Gusev, V.Kh.Kudoyarova, A.N.Kuznetsov, P.E.Pak, E.I.Terukov, I.N.Yassievich, B.P.Zakharchenya, W.Fuhs, and A.Sturm, Appl.Phys.Lett. 67, p. 3,599 (1995).
4. V.Marakhonov, N.Rogachev, J.Ishkalov, J.Marakhonov, E.Terukov, and V.Chelnokov, J. Non-Cryst. Solids, 137&138, p. 817 (1991).
5. J.H.Shin, R.Serna, G.N.van den Hoven, A.Polman, W.G.J.H.M.van Sark, and A.M.Vredenberg. Appl.Phys.Lett. 68, p. 997 (1996).
6. S.Lombardo, S.U.Campisano, G.N.van den Hoven, A.Cacciato, and A.Polman, Appl.Phys.Lett. 63, p. 1,942 (1993).
7. S.Lombardo, S.U.Campisano, G.N.van den Hoven, and A.Polman, J.Appl.Phys.77, p. 6,504 (1995).

## ELECTROLUMINESCENCE OF ERBIUM IN OXYGEN DOPED SILICON

S. LOMBARDO \*, S. U. CAMPISANO \*, G. N. VAN DEN HOVEN \*\*, AND A. POLMAN \*\*

\*CNR-IMETEM, Stradale Primosole, 50, I95121 Catania, Italy, cnr@ct.infn.it

\*\*FOM-AMOLF, Kruislaan 407, 1098 SJ Amsterdam, The Netherlands

### ABSTRACT

It is demonstrated room-temperature electroluminescence at  $1.54\ \mu\text{m}$  in erbium-implanted oxygen doped silicon (27 at.% O), due to intra- $4f$  transitions of the  $\text{Er}^{3+}$ . The luminescence is electrically stimulated by biasing metal-(Si:O,Er)- $\text{p}^+$  silicon diodes. The 30 nm thick Si:O,Er films are amorphous layers deposited onto silicon substrates by chemical vapour deposition of  $\text{SiH}_4$  and  $\text{N}_2\text{O}$ , doped by ion implantation with Er to a concentration up to  $\approx 1.5\ \text{at.}\%$ , and annealed in a rapid thermal annealing furnace. The most intense electroluminescence is obtained in samples annealed at  $400\ ^\circ\text{C}$  in reverse bias under breakdown condition and it is attributed to impact excitation of erbium by hot carriers injected from the Si into the Si:O,Er layer. The electrical characteristics of the diode are studied in detail and related to the electroluminescence characteristics. A lower limit for the impact excitation cross-section of  $\approx 6 \times 10^{-16}\ \text{cm}^2$  is obtained.

### INTRODUCTION

The use of silicon-based semiconductors for integrated optoelectronics applications would allow to take advantage of the low material cost and of the large resources available in silicon device technology and manufacturing. Silicon doped with erbium shows sharp luminescence at  $1.54\ \mu\text{m}$ ,<sup>1</sup> a wavelength particularly relevant for fiber optics communications because it matches the transmission maximum in silica-based optical fibers. The luminescence is due to intra- $4f$  transitions in the  $\text{Er}^{3+}$  ion. However in pure silicon intense Er-related luminescence is observed only at low temperatures because there are problems related to the limited concentration of active Er in Si and to the strong luminescence quenching at increasing temperature. Since the co-doping with oxygen greatly enhances the luminescence intensity,<sup>2,3</sup> increasing the fraction of optically active  $\text{Er}^{3+}$  ions and reducing the luminescence quenching,<sup>4</sup> we have investigated the Er doping of heavily oxygen doped amorphous and polycrystalline silicon thin films deposited by chemical vapour deposition of  $\text{SiH}_4$  and  $\text{N}_2\text{O}$ .<sup>5,6,7</sup> The material is a solid mixture of silicon and silicon oxide phases usually indicated as semi-insulating polycrystalline silicon (SIPOS). For anneal temperatures below  $800\ ^\circ\text{C}$  the material is amorphous, while at higher temperatures SIPOS microstructure consists of silicon nano-grains surrounded by oxygen-rich  $\text{SiO}_x$  shells. Conductivity measurements as a function of temperature demonstrate the semiconducting nature of the material, which has resistivities ranging from  $10^6$  to  $10^9\ \Omega\ \text{cm}$  at room temperature.<sup>8</sup> The doping with B, P or As is very effective in reducing SIPOS resistivity which can be controlled in a way similar to that of polycrystalline silicon.<sup>9</sup> The combination of its high oxygen content and semiconducting properties makes SIPOS a very interesting candidate as host material for Er. Indeed, photoluminescence experiments on Er implanted SIPOS have shown intense room-temperature luminescence at  $1.54\ \mu\text{m}$  due to the  $^4I_{13/2} \rightarrow ^4I_{15/2}$  transition of the  $\text{Er}^{3+}$  ion.<sup>5</sup> Excitation curve measurements have shown that the luminescence is produced by a photocarrier mediated process and not, like in  $\text{SiO}_2$ , to the direct absorption of the pump light. The luminescence shows the highest internal quantum efficiencies ( $\approx 1 \times 10^{-3}$ ) in materials annealed at  $400\ ^\circ\text{C}$  and containing 30 at.% O and 10 at.% H.<sup>7</sup> In these materials the quenching of luminescence intensity is very low compared to Czochralski silicon or crystalline silicon containing 0.2 at.% O.<sup>4</sup> An-

other important difference with respect to crystalline silicon is that the photoluminescence decay lifetime is temperature independent between 77 and 300 K.<sup>7</sup>

In this paper we report the results of electroluminescence measurements performed at room temperature on erbium-implanted SIPOS containing 27 at.% O. The luminescence is due to intra-4f transitions of the  $\text{Er}^{3+}$  ion and is electrically stimulated by biasing metal-(Si:O,Er)- $\text{p}^+$  silicon diodes.

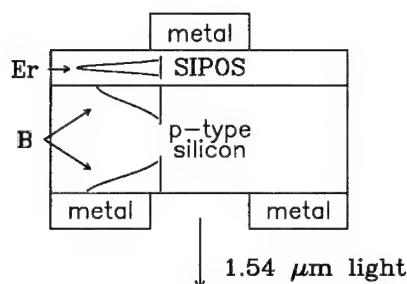


**Fig. 1.** Sketch of the device structure used for electroluminescence measurements.

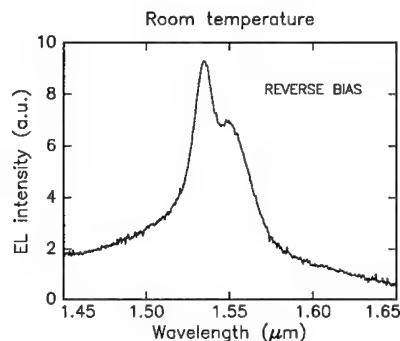


**Fig. 2.** Electroluminescence spectrum measured at room-temperature in SIPOS containing 27 at.% O, implanted with Er and annealed at 400 °C. The device is in reverse bias above breakdown, the pump current is 260 mA and the voltage is 20 V.

## EXPERIMENTAL

The metal-(Si:O,Er)- $\text{p}^+$  silicon diodes were fabricated as follows. Silicon wafers of 125 mm diameter, (100) oriented, polished on both sides, B-doped ( $10 - 20 \Omega \text{ cm}$ ) were implanted with 80 keV B at fluences of  $5 \times 10^{13}$  and  $2 \times 10^{15} \text{ cm}^{-2}$  on front and back side, respectively. For dopant activation, the samples were processed in a rapid thermal annealing (RTA) apparatus at 1000 °C for 5 minutes in a  $\text{N}_2$  ambient. After removal of the native oxide by dipping in a diluted HF solution, SIPOS was deposited by chemical vapor deposition of  $\text{SiH}_4$  and  $\text{N}_2\text{O}$  at 620 °C. The process resulted in 30 nm thick layers containing 27 at.% O. The samples were then implanted with 35 keV Er at an angle of 60° from the surface normal in order to confine all of the erbium inside the SIPOS layer; the doses were  $2.5$  or  $5 \times 10^{14} \text{ cm}^{-2}$ . At the highest fluence the Er peak concentration was  $\approx 1.6$  at.%, located at a depth of  $\approx 9$  nm, as evaluated by numerical simulations of the implantation process and confirmed by RBS.

After annealing in RTA for 5 minutes in a  $\text{N}_2$  ambient at a temperature between 400 and 1000 °C, Ti-Ni-Au metal contacts were deposited through a mask in an ultra high vacuum e-beam evaporator, defining a Burrus type geometry. A sketch of the structure is shown in Fig. 1. Due to the high resistivity of the SIPOS layer the current is confined in the cylindric volume under the contact on SIPOS and is then spread in the low resistivity silicon substrate. The infra-red light produced by biasing the device is collected from the back-side. Electroluminescence (EL) was studied by biasing the diodes between -35

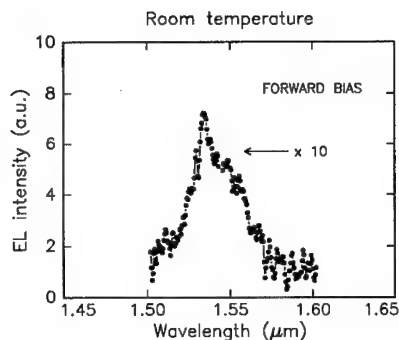


**Fig. 3.** Electroluminescence spectrum measured at room-temperature in SIPOS containing 27 at.% O, implanted with Er and annealed at 500 °C. The device is in forward bias, the pump current is 270 mA and the voltage is 13 V.

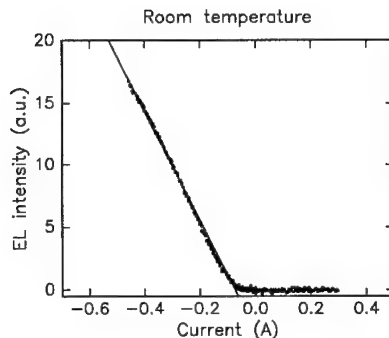


**Fig. 4.** EL intensity at 1.54 μm as a function of the pump current for the device described in the caption of Fig. 2.

and +15 V with the samples held at a temperature in the 200 – 400 K range. Diode polarization is assumed to be forward when the potential of the p-type silicon substrate is positive with respect to the metal contact on the SIPOS layer.

The electroluminescence signal was analyzed by a single-grating monochromator at a resolution of 6 nm, detected using a liquid-nitrogen cooled Ge detector and recorded with a lock-in amplifier. EL decay rate measurements were performed either by switching off or by step-decreasing to a lower level the pump current and monitoring the EL peak intensity as a function of time by recording the signals on a digitizing oscilloscope. The overall response-time of the system was below 30 μs.

## RESULTS AND DISCUSSION

Fig. 2 shows the electroluminescence signal observed at room temperature at –20 V bias with a current of 260 mA in a sample implanted with  $5 \times 10^{14}$  Er/cm<sup>2</sup> and annealed at 400 °C. The spectrum shown is similar to those observed in photoluminescence and it can clearly be attributed to the  $^4I_{13/2} \rightarrow ^4I_{15/2}$  transition of the Er<sup>3+</sup> ion. It is the sample implanted with  $5 \times 10^{14}$  cm<sup>-2</sup> and annealed at 400 °C in which the largest electroluminescence is observed and the data shown below refer to this device.

It is important to underline that strong luminescence is observed only in reverse bias when the device is fully in breakdown. An EL signal at 1.54 μm due to the Er<sup>3+</sup> ion is observed also in forward bias in devices annealed at 500 and 600 °C (Fig. 3), but the intensity measured at the largest current level ( $\approx 300$  mA) is approximately a factor of 10 smaller than the signal shown in Fig. 2.

Fig. 4 and Fig. 5 show, respectively, the electroluminescence intensity at 1.54 μm at room-temperature as a function of the current and I-V characteristics for the device annealed at 400 °C. In reverse bias the EL intensity (Fig. 4) increases linearly with current above a threshold of 75 mA, while it is at the noise level in forward bias. The almost perfect signal linearity in reverse bias occurs also when the EL intensity is plotted as a function of the voltage. This occurs because the intense luminescence is observed in the

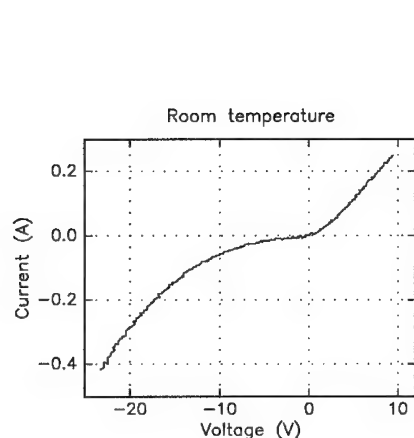


**Fig. 5.** I-V characteristics of the device described in the caption of Fig. 2.

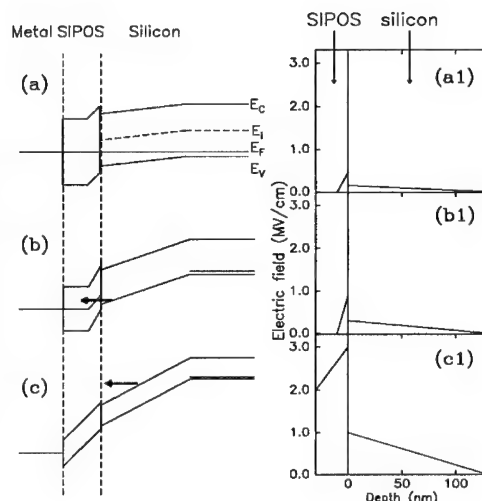


**Fig. 6.** Band diagrams of the metal-(SIPOS:Er)- $p^+$  Si structure at the thermal equilibrium (a) and in low (b) and high (c) reverse bias. On the right side are reported the corresponding field intensities versus depth.

linear region of the I-V characteristics; the threshold voltage for the onset of the EL is  $-14.5$  V.

The main features of the I-V characteristics (Fig. 5) are a large differential resistance between  $\approx -3$  and  $0$  V and nearly linear I-V characteristics at large positive and negative voltages, characterized by differential resistances of  $\approx 30$  and  $25 \Omega$ , respectively.

By increasing the temperature from 200 to 400 K, the threshold current, voltage, and slope of the EL signal versus current (not shown) shift slightly towards lower values, resulting in a very small quenching effect of the electroluminescence with temperature as also observed in photoluminescence.

In order to understand the origin of the luminescence we need to model the I-V characteristics of the device on the basis of the band structure of the metal-(SIPOS:Er)- $p^+$  silicon device. Capacitance-voltage and spreading resistance measurements<sup>6</sup> indicate that the band diagram at thermal equilibrium of the *metal-SIPOS- $p^+$  Si* structure is as shown in Fig. 6(a). In our device SIPOS has an amorphous microstructure and at low electric fields shows hopping conductivity. As sketched in Fig. 6(a), the mobility gap is larger than the crystalline Si forbidden gap as confirmed by the fact that the fundamental absorption edge of SIPOS occurs at a higher photon energy than that observed in amorphous silicon.

On the basis of Fig. 6(a) we can model the I-V characteristics of the device. In forward bias most of the voltage is applied across the SIPOS film because the metal-SIPOS and the SIPOS- $p^+$  Si junctions introduce negligible resistances, and thus the electrical characteristics are entirely due to the SIPOS layer. At low voltages carrier transport will occur by hopping while in large bias conditions it is due to tunneling of carriers moving through localized states up to several tenth of eV above the Fermi level, since large tunnel probabilities are expected in the presence of intense electric fields. In this conduction regime only a small fraction of the total current is due to electron-hole recombination and this may explain why small quantum efficiencies are obtained in the electroluminescence observed in forward bias (Fig. 3).



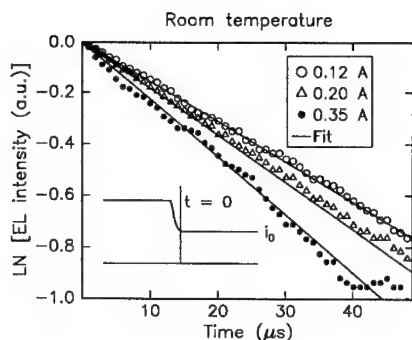


Fig. 7. EL decay transients.

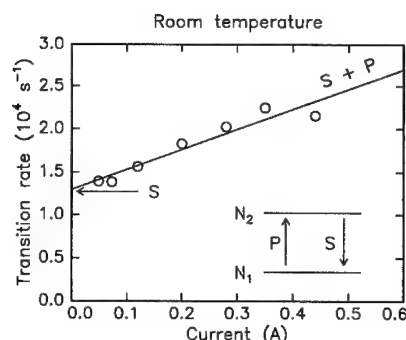


Fig. 8. EL decay rate as a function of pump current.

In reverse bias the situation is different: at low voltages the bias is almost entirely applied to the SIPOS- $p^+$  Si junction and not to the SIPOS layer, as sketched in Fig. 6(b); the current in this case is limited by the tunneling of valence band electrons of silicon towards free localized states in SIPOS of energies above the Fermi level (arrow in Fig. 6(b)). At large reverse bias the tunnel probability approaches unity and the voltage will be shared between the SIPOS film and the SIPOS- $p^+$  silicon junction, as shown in Fig. 6(c). At -14 V bias the field in the Si will reach a value of  $\approx 1 \times 10^6$  V/cm and this will cause a breakdown by the occurrence of a combination of avalanche and Zener mechanisms. In the  $p^+$  depletion layer under the SIPOS the breakdown produces a large density of hot electrons directed towards the Er doped SIPOS film. In these conditions the mechanism of  $Er^{3+}$  excitation is by impact with the hot electrons coming from the  $p^+$  silicon depletion layer. In fact, in breakdown conditions the carrier temperature is extremely high and can be estimated by solving the Boltzmann transport equation. According to estimates of the weights of the various mechanisms contributing to the breakdown current,<sup>6</sup> above the threshold, roughly half of the total current flowing in the SIPOS layer is given by hot electrons whose temperature is 0.65 eV. This implies that a significant fraction of hot electrons will have enough energy to excite the  $Er^{3+}$  ions (at least  $\approx 0.8$  eV). The occurrence of an impact excitation mechanism for the electroluminescence in reverse bias is supported by the weak temperature dependence of the phenomenon.

In order to determine the cross-section for impact excitation of  $Er^{3+}$  we have measured the transients of EL intensity at  $1.54 \mu m$  by switching the current source. An interesting behaviour is observed when the current is rapidly switched from a high level to a lower value. In this case, the EL signal rapidly decays to a new (lower) steady-state level. The transient of the EL to this second level is plotted in Fig. 7. It shows an exponential trend but the time constant depends on the second current level ( $i_0$ ): the time constant decreases with increasing currents.

Fig. 8 shows the EL decay rate (inverse of the time constant) versus the second current level determined from data as in Fig. 7. The decay rate increases with the current and the increase is almost linear. These results can be interpreted by a simple two level model: the  $Er^{3+}$  ions are divided into a group  $N_2$  excited to the  $^4I_{13/2}$  manifold and in a group  $N_1$  in the ground state ( $^4I_{15/2}$ ). The time derivative of  $N_2$  is given by

$$\frac{dN_2}{dt} = -SN_2 + P(N_0 - N_2) \quad (1)$$

where  $N_0$  is the total number of the  $Er^{3+}$  ions,  $S$  is the spontaneous emission rate ( $N_2 \rightarrow N_1$ ) and  $P$  the pump rate ( $N_1 \rightarrow N_2$ ). When the current is zero  $P$  is zero, because there is no excitation process. In this case, according to Eq. (1), by switching off the device, the transient EL signal will show an exponential decrease with time, with a rate equal to  $S$  independent on the initial current level. This effect has been experimentally confirmed.<sup>6</sup> On the other hand, when the current level is switched to a lower value  $i_0$  (Fig. 7)  $P$  is non zero and the transient will be characterized by a rate equal to  $(P + S)$ . Plotting the decay rate  $R$  as a function of  $i_0$  we observe a linear increase, as reported in Fig. 8. This fact implies that  $P$  is proportional to the hot carrier flux  $\Phi$ , and we assume that

$$P \approx \sigma \times \Phi \quad (2)$$

where  $\sigma$  is the impact excitation cross section.  $\Phi$  is the flux of high-energy electrons able to excite the Er and, as discussed before, is comparable to the total flux of carriers. Thus, by fitting the data of Fig. 8 assuming  $R = \sigma\Phi' + S$  with  $\Phi'$  equal to the total current density divided by  $q$ , we obtain an impact excitation cross section equal to  $6 \times 10^{-16} \text{ cm}^{-2}$ . This estimate represents a lower limit to the real value of  $\sigma$ , since the current density of hot electrons able to excite the Er is only a fraction of the total current density.

#### ACKNOWLEDGEMENTS

We wish to acknowledge the fruitful collaboration with Antonio Cacciato and Edwin Snoeks (FOM, Amsterdam). We wish also to thank Antonio Marino, Salvo Pannitteri, and Orazio Parasole for their expert technical support.

This work has been partially supported by GNSM-CNR. Work at FOM is part of the research program of FOM and is financially supported by NWO, IOP Electro-Optics and STW.

#### REFERENCES

1. H. Ennen, J. Schneider, G. Pomrenke and A. Axmann, Appl. Phys. Lett. **43**, 943 (1983).
2. P. N. Favenec, H. L'Haridon, D. Moutonnet, M. Salvi and M. Gauneau, Jpn. J. Appl. Phys. **29**, L521 (1990).
3. J. Michel, J. L. Benton, R. J. Ferrante, D. C. Jacobson, D. J. Eaglesham, E. A. Fitzgerald, Y. H. Xie, J. M. Poate and L. C. Kimerling, J. Appl. Phys. **70**, 2672 (1991).
4. S. Coffa, G. Franzò, F. Priolo, A. Polman and R. Serna, Phys. Rev. B **49**, 16313 (1994).
5. S. Lombardo, S. U. Campisano, G. N. van den Hoven, A. Cacciato and A. Polman, Appl. Phys. Lett. **63**, 1942 (1993).
6. S. Lombardo, S. U. Campisano, G. N. van den Hoven, and A. Polman, J. Appl. Phys. **77**, 6504 (1995).
7. G. N. van den Hoven, J. H. Shin, A. Polman, S. Lombardo, and S. U. Campisano, J. Appl. Phys **78**, 2642 (1995).
8. S. Lombardo, S. U. Campisano, and F. Baroetto, Phys. Rev. B **47**, 13561 (1993).
9. S. Lombardo, S. U. Campisano, and M. Nicotra, J. Appl. Phys. **75**, 345 (1994).

## 1.54 $\mu\text{m}$ PHOTOLUMINESCENCE AND ELECTROLUMINESCENCE IN ERBIUM IMPLANTED 6H SiC

M. YOGANATHAN<sup>a</sup>, W. J. CHOYKE<sup>a</sup>, R. P. DEVATY<sup>a</sup>, G. PENSL<sup>b</sup>, AND J. A. EDMOND<sup>c</sup>

<sup>a</sup>Department of Physics and Astronomy, University of Pittsburgh, Pittsburgh, PA 15260, e-mail: CHOYKE@POP.PITT.EDU

<sup>b</sup>Lehrstuhl Angewandte Physik, Universität Erlangen-Nürnberg, Staudtstrasse 7, D-91058, Erlangen, Germany

<sup>c</sup>Cree Research, Inc., 2810 Meridian Parkway, Durham, North Carolina 27713

### ABSTRACT

Photoluminescence in the neighborhood of 1.54  $\mu\text{m}$  due to the  $4I_{13/2} \rightarrow 4I_{15/2}$  transitions is observed from 2 K up to 520 K in erbium implanted 6H SiC. The integrated 1.54  $\mu\text{m}$  photoluminescence (PL) intensity is almost constant from 2 K up to about 400 K, with slight sample to sample variation. The shallow nitrogen donors play an important role in the excitation of the  $\text{Er}^{3+}$  centers. 1.54  $\mu\text{m}$  electroluminescence (EL) is observed in erbium implanted 6H SiC p-n junctions under forward bias conditions. The EL spectrum is identical to the PL spectrum.

### INTRODUCTION

The research interest in erbium doped semiconductors is growing rapidly [1] in recent years because of the 1.54  $\mu\text{m}$   $\text{Er}^{3+}$  emission that has applications in the fiber optics communication industry. While many erbium doped semiconductors have been studied to date, only a few show 300 K, 1.54  $\mu\text{m}$   $\text{Er}^{3+}$  emission. Favennec *et al.* [2] have observed that the quenching temperature associated with the integrated 1.54  $\mu\text{m}$  PL intensity increases with the bandgap of the host material up to 2.42 eV (CdS). This trend holds true for other wide bandgap materials. 300 K 1.54  $\mu\text{m}$  PL emission in erbium doped GaP [3], and erbium and oxygen coimplanted GaN [4, 5] and AlN [4] have been reported. Our studies on erbium implanted SiC polytypes 3C, 15R, 6H, and 4H [6, 7] show almost constant integrated PL intensity from 1.49  $\mu\text{m}$  to 1.64  $\mu\text{m}$  from 2 K up to 300 K in all polytypes within the experimental accuracy. The integrated PL intensity from 1.49  $\mu\text{m}$  to 1.64  $\mu\text{m}$  is almost constant up to about 400 K in 6H SiC: $\text{Er}^{3+}$ . Thus, devices operating at 300 K will be stable with respect to temperature fluctuations. In this paper, we report some important results from our PL and EL investigations of erbium implanted 6H SiC.

## EXPERIMENTAL

Single crystal epitaxial films of 6H SiC were grown on polished 6H SiC boule slice substrates either at Cree Research, Inc., Durham, North Carolina or at Westinghouse Science and Technology Center, Pittsburgh, PA. Film thicknesses range from 0.3  $\mu\text{m}$  to 12  $\mu\text{m}$ . The epi films are n-type (nitrogen doped) with carrier concentrations ranging from  $\sim 10^{15} \text{ cm}^{-3}$  to  $\sim 10^{18} \text{ cm}^{-3}$  (obtained from C-V and Hall measurements). Erbium ions are implanted at room temperature into epitaxial films at the University of Erlangen-Nürnberg, Erlangen, Germany. Implantations are performed at four energies from 40 keV to 1 MeV at fluences near  $10^{13} \text{ cm}^{-2}$  in order to obtain a flat implantation profile. The penetration depths of erbium in silicon carbide are about 180 Å and 2000 Å at 40 keV and 1 MeV, respectively. The samples are subsequently annealed at 1700°C in a pure Ar atmosphere in a closed CVD SiC crucible for half an hour. P-type 6H SiC epitaxial films were grown on some of the erbium implanted and annealed n-type films in order to fabricate erbium doped 6H SiC p-n junctions. Packaged infrared emitting diodes (IRED'S) with proprietary contacts were later made using these p-n junctions.

For the low resolution (20 Å) near infrared PL measurements, samples are excited with a 46 mW, 3250 Å, He-Cd laser and the spectra are measured from 2 K to 520 K using a 3/4 m monochromator (SPEX 1400) with a 600  $\mu\text{m}$  grating that is blazed at 1.6  $\mu\text{m}$  and a liquid nitrogen cooled Ge detector (North Coast EO-817L). A lockin detection system is used. An immersion type pumped liquid helium dewar is used for the 2 K measurements. Samples are immersed in liquid nitrogen for 77 K measurements. For room temperature and above, a special aluminum sample holder is used to mount the samples. An electric hot-plate is attached to this sample holder in order to vary the sample temperature. A chromel-alumel thermocouple is used to monitor the sample temperature. The laser beam is chopped in order to make sure that the thermal background from the hot sample surface is not detected at higher temperatures.

For the 2 K high resolution ( $0.3 \text{ cm}^{-1}$ ) 1.54  $\mu\text{m}$  PL measurements, samples are excited with a 20 mW, 3250 Å, He-Cd laser and the spectra are measured using an FTIR spectrometer (NICOLET-740) and a liquid nitrogen cooled Ge detector (North Coast EO-817S) with a response time of  $\sim 10 \mu\text{s}$ .

The electroluminescence spectra are measured under forward-bias conditions. The imaging and dispersive optics, and the detection systems are identical to the photoluminescence experimental setup.

## RESULTS AND DISCUSSION

### PHOTOLUMINESCENCE

Fig. 1 shows  $4I_{13/2} \rightarrow 4I_{15/2}$ , 1.54  $\mu\text{m}$  PL spectra of 6H SiC:Er<sup>3+</sup> at temperatures ranging from 2 K to 520 K. At 2 K, the initial state of the transitions is the lowest level of the first excited multiplet  $4I_{13/2}$ . The highest energy line B observed at 2 K is assumed to be due to the transition from the lowest level of  $4I_{13/2}$  to the lowest level of

the ground multiplet  $^4I_{15/2}$ . We see more than 10 sharp lines at 2 K with the strongest line A at  $15340 \text{ \AA} \pm 5 \text{ \AA}$ . At 77 K, we see five new lines C-G on the high energy side of the spectrum indicating transitions from the excited levels of the  $^4I_{13/2}$  multiplet. Note that G is the highest energy line even at 520 K. If G is due to a transition from the highest energy level of  $^4I_{13/2}$  to the lowest level of  $^4I_{15/2}$ , then the energy difference between the peaks B and G,  $\sim 14 \text{ meV}$  gives an estimate of the crystal field splitting between the lowest and the highest levels of  $^4I_{13/2}$  in 6H SiC:Er $^{3+}$ .

At high resolution, many of the lines shown in the 2K spectrum of Fig. 1 are further resolved into fine structures resulting in over 20 sharp lines as shown in Fig. 2. This spectrum was obtained using an FTIR spectrometer. The spectral resolution is  $0.3 \text{ cm}^{-1}$ . The possible local site symmetries of Er $^{3+}$  in 6H SiC are  $C_{3v}$  or lower. The  $^4I_{15/2}$  multiplet has eight crystal field split energy levels in  $C_{3v}$  or any lower symmetry. Thus, at 2 K we expect a maximum of 8 lines for a single Er $^{3+}$  center in 6H SiC:Er $^{3+}$  since the initial state of the transitions is the lowest energy level of  $^4I_{13/2}$ . Note that particular sharp lines (labeled 3, 9, 14, and 18) are accompanied by 13 meV side-bands (15, 16, 19, and 20). We believe that these side-bands are due to a localized vibrational excitation associated with a particular erbium center in 6H SiC. There are at least 11 sharp lines that are not accompanied by 13 meV side-bands. Thus, we believe that there is more than one type of erbium center in our samples.

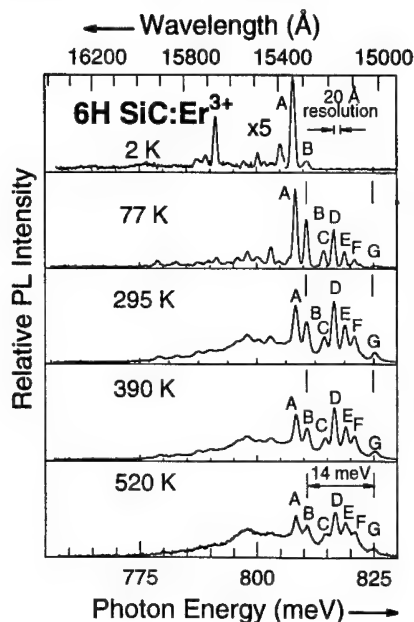


Fig. 1: PL spectra of 6H SiC:Er $^{3+}$ .

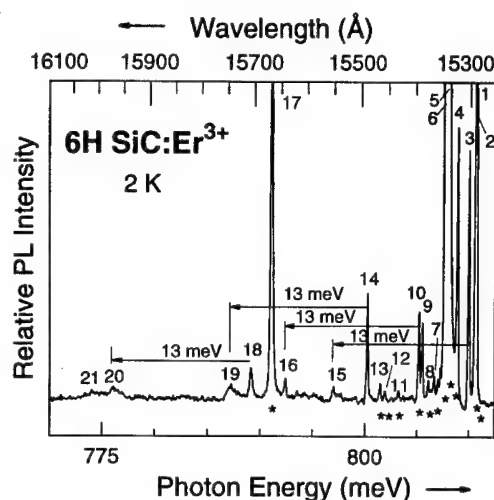


Fig. 2: 13 meV vibrational side-bands in the  $1.54 \mu\text{m}$  PL spectrum of 6H SiC:Er $^{3+}$  at 2 K. The peaks which do not show side-bands are indicated by stars at the bottom.

We observe a correlation between the shallow nitrogen donor concentration and the relative integrated 1.54  $\mu\text{m}$  PL emission intensity as shown in Fig. 3. The relative integrated intensity is obtained by measuring the area under the PL spectra over a wavelength range from 1.49  $\mu\text{m}$  to 1.64  $\mu\text{m}$ . The relative integrated intensity increases with the nitrogen concentration from the low  $10^{15}$  to the mid  $10^{17} \text{ cm}^{-3}$ . This correlation shows that the nitrogen donor plays an important role in the excitation of  $\text{Er}^{3+}$  in 6H SiC:Er $^{3+}$ . Further studies are required to obtain a detailed understanding.

Any practical use of erbium doped 6H SiC depends on the temperature dependence of the 1.54  $\mu\text{m}$  luminescence near room temperature. We have therefore studied the temperature dependence of the integrated 1.54  $\mu\text{m}$  PL intensity in a temperature range up to 500 K. Fig. 4 shows the normalized relative integrated 1.54  $\mu\text{m}$  PL intensity for samples with nitrogen donor concentrations  $\sim 5 \times 10^{17} \text{ cm}^{-3}$ ,  $\sim 6 \times 10^{15} \text{ cm}^{-3}$ , and  $\sim 1 \times 10^{15} \text{ cm}^{-3}$ . The relative integrated 1.54  $\mu\text{m}$  PL intensity of the lightly nitrogen doped samples is almost constant up to about 400 K whereas it is almost constant only up to about 350 K in the sample with  $\sim 5 \times 10^{17} \text{ cm}^{-3}$  nitrogen donor concentration. There is a peak just below 400 K in the lightly nitrogen doped samples.

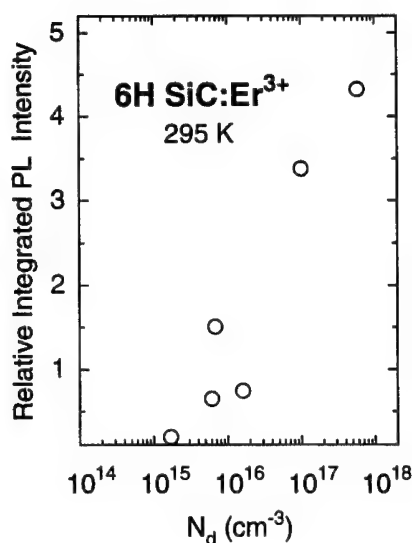


Fig. 3: Nitrogen donor concentration dependence of the 295 K 1.54  $\mu\text{m}$  integrated PL intensity in 6H SiC:Er $^{3+}$ .

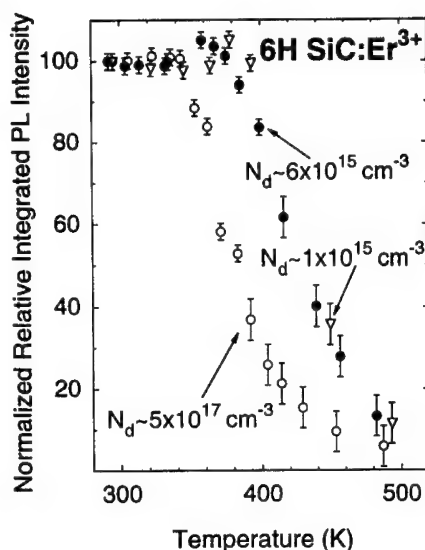


Fig. 4: Temperature dependence of the integrated 1.54  $\mu\text{m}$  PL emission in 6H SiC:Er $^{3+}$  samples with different nitrogen donor concentrations.

## ELECTROLUMINESCENCE

Excitation of the  $\text{Er}^{3+}$  ion by electrical means for optoelectronic device applications is a possible advantage of erbium doped semiconductors over glasses. We have observed room temperature  $1.54\ \mu\text{m}$  EL in erbium implanted 6H SiC p-n junctions under forward bias conditions. Fig. 5 shows a comparison of 295 K PL and EL spectra of a 6H SiC p-n junction. The spectra are essentially identical. This result shows that the same erbium centers are responsible for both EL and PL. The relative integrated  $1.54\ \mu\text{m}$  EL intensity shows sublinear current dependence as shown in Fig. 6. The  $1.54\ \mu\text{m}$  EL output does not increase significantly upon increasing the current above 20 mA. It is well known that at higher forward biases the recombination of injected minority carriers outside the depletion region becomes important. Thus, the fact that the erbium doping profile in our diodes is almost completely inside the depletion region is partly responsible for the saturation of the  $1.54\ \mu\text{m}$  EL at very low forward bias. The other possible factors responsible for this saturation effect are the limited number of  $\text{Er}^{3+}$  ions in our diodes and the long lifetime of the  $^4\text{I}_{13/2}$  multiplet.

We have observed the same correlation between the nitrogen donor concentration and the integrated  $1.54\ \mu\text{m}$  EL intensity that we observed in PL (Fig. 3).

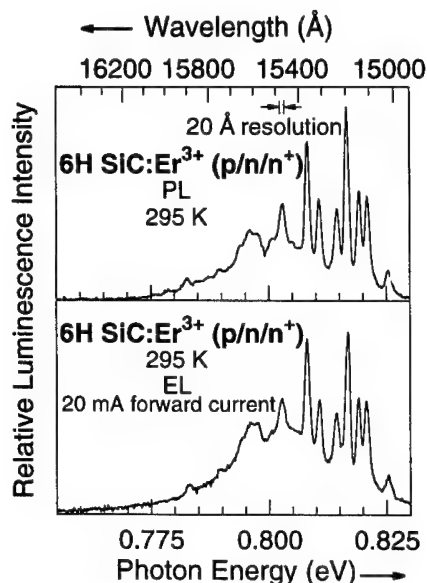


Fig. 5: Comparison of 295 K  $1.54\ \mu\text{m}$  PL and EL spectra of a 6H SiC: $\text{Er}^{3+}$  p-n junction.

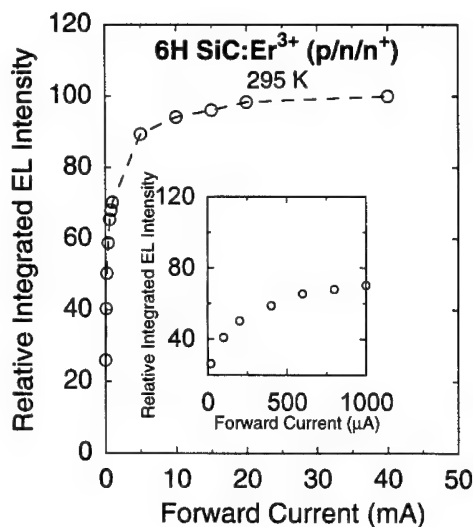


Fig. 6: Forward current dependence of the integrated  $1.54\ \mu\text{m}$  EL emission intensity in 6H SiC: $\text{Er}^{3+}$  at 295 K. The dashed line is drawn to guide the eye.

However, the forward current dependence of the normalized integrated emission intensity (Fig. 6) is almost identical for our diodes with different nitrogen donor concentrations. The 1.54  $\mu\text{m}$  EL is limited by the very narrow erbium doping profile in our diodes. We have estimated an external quantum efficiency (integrated 1.54  $\mu\text{m}$  EL output power / electrical input power) of about  $7.5 \times 10^{-6}$  at 10  $\mu\text{A}$  using a calibrated InGaAsP IRED. The external quantum efficiency decreases at higher forward currents. Our estimated value is comparable to the value reported for GaAs:Er<sup>3+</sup> [9]. This result shows that the observed low external quantum efficiency is characteristic of Er<sup>3+</sup> and not limited by the indirect bandgap of 6H SiC.

## CONCLUSIONS

We have studied the 1.54  $\mu\text{m}$  PL and EL properties of erbium implanted 6H SiC. The integrated 1.54  $\mu\text{m}$  PL intensity is almost constant up to about 400 K. Multiple Er<sup>3+</sup> centers are present in our erbium implanted 6H SiC samples. A 13 meV vibrational energy is associated with one of the erbium complexes in 6H SiC:Er<sup>3+</sup>. The integrated 1.54  $\mu\text{m}$  PL and EL intensities increase with the shallow nitrogen donor concentration from the low  $10^{15}$  to the mid  $10^{17} \text{ cm}^{-3}$ . This result shows that the shallow nitrogen donor is involved in the energy transfer to the Er<sup>3+</sup> ions in 6H SiC:Er<sup>3+</sup>. Increasing the erbium doping volume and an improved design of our diodes are further steps towards practical silicon carbide based 1.54  $\mu\text{m}$  optoelectronic devices.

## REFERENCES

1. Rare Earth Doped Semiconductors, edited by G. S. Pomrenke, P. B. Klein and D. W. Langer (Mater. Res. Soc. Symp. Proc. **301**, Pittsburgh, PA, 1993).
2. P. N. Favennec, H. L'Haridon, D. Moutonnet, M. Salvi, and M. Gauneau, *ibid*, pp. 181-193.
3. X. Z. Wang and B. W. Wessels, Appl. Phys. Lett., **67**, 518 (1995).
4. R. G. Wilson, R. N. Schwartz, C.R. Abernathy, S.J. Pearton, N. Newman, M. Rubin, T. Fu, and J.M. Zavada, Appl. Phys. Lett. **65**, 992 (1994).
5. C. H. Qiu, M. W. Leksono, J. I. Pankove, J. T. Trovik, R. J. Feuerstein, and F. Namavar, Appl. Phys. Lett. **66**, 562 (1995).
6. W. J. Choyke, R. P. Devaty, L. L. Clemen, M. Yoganathan, G. Pensl, and Ch. Hässler, Appl. Phys. Lett. **65**, 1668 (1994).
7. W. J. Choyke, R. P. Devaty, L. L. Clemen, M. F. MacMillan, M. Yoganathan, and G. Pensl, to be published in the proceedings of the International Conference on Silicon Carbide and Related Materials '95, Kyoto, Japan, Sept. 1995.
8. A. K. Alshawa, H. J. Lozykowski, T. Li, and I. Brown, Mat. Res. Soc. Symp. Proc. Vol. **301**, 281 (1993).
9. P. Galtier, T. Benyattou, J. P. Pocholle, M. N. Charasse, G. Guillot, and J. P. Hirtz, Inst. Phys. Conf. Ser. No **106**: Chapter 5, 327 (1989).



## 1.54 $\mu\text{m}$ ELECTROLUMINESCENCE FROM ERBIUM DOPED GALLIUM PHOSPHIDE DIODES

G.M. FORD\* and B.W. WESSELS

Department of Materials Science and Engineering and the Materials Research Center, Northwestern University, Evanston, Illinois 60208

### ABSTRACT

Er-doped GaP diodes that exhibit strong room temperature characteristic 4f-shell luminescence under forward bias have been fabricated. The output of the diode increases linearly with current for low current densities but eventually saturates. The radiative decay lifetime is 2.6 msec and is independent of current. It is proposed that the observed intensity dependence on excitation power results from saturation of the optically active  $\text{Er}^{3+}$  centers. Some diodes showed a superlinear dependence, with a threshold of about  $2 \text{ A/cm}^2$ .

### INTRODUCTION

Erbium doped semiconductors have long been studied for potential use as integrated optoelectronic devices for optical communications. Erbium-related electroluminescence (EL) has been reported in a wide variety of semiconductor hosts.<sup>1-3</sup> While the initial electroluminescent diodes exhibited appreciable thermal quenching, recently we have shown that strong room temperature electroluminescence can be obtained from Er-doped GaP diodes.<sup>4,5</sup> Under forward bias, the Er-related luminescence at 1.54 microns increased linearly with current density. However, at the highest current densities the EL saturated. The questions then arise as to what factors lead to saturation, and can the power output be further improved? Early studies indicated that Auger processes may be important in limiting the rare-earth luminescence efficiency.<sup>6,7</sup> Alternatively it has been proposed that saturation of the Er centers may result since they are present at relatively low concentrations and have long luminescence lifetimes.<sup>8,9</sup> In this paper we report on the electroluminescent properties of Er-doped GaP diodes. A model is presented to explain the observed room temperature EL intensity-current dependence.

### EXPERIMENTAL

Erbium doped gallium phosphide was grown on (100) GaP substrates at 700°C by atmospheric pressure metalorganic vapor phase epitaxy using trimethyl gallium, 10% phosphine in

---

\* email: g-ford@nwu.edu

hydrogen, and *tris*-tetramethylheptanedionate erbium as sources. The film was co-doped with the donor Se during growth to increase the net n-type carrier concentration to  $10^{18} \text{ cm}^{-3}$ . P-n junctions were formed by diffusing Zn using a  $\text{ZnP}_2$  source. Ohmic contacts were made by annealing In/Zn and In to the p- and n-sides of the junction, respectively. The diode area was nominally  $1.5 \text{ mm}^2$ .

To measure their electroluminescent properties, the diodes were biased by a pulse generator, typically at a frequency of 40 Hz and a duty cycle of 40%. The EL signal was dispersed through a Zeiss MM12 monochromator and focused onto a liquid nitrogen cooled North Coast Ge detector. EL transient decay curves were measured by signal averaging using a PAR model 1162 box car averager.

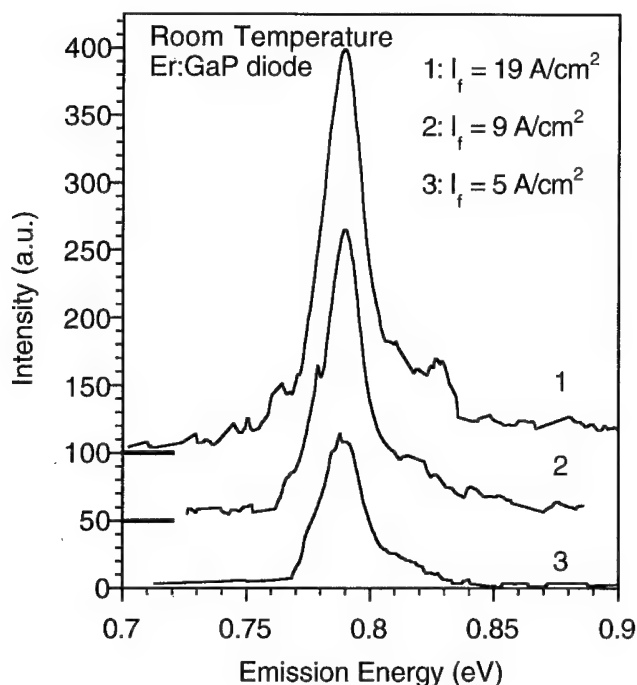


Figure 1: Forward bias spectra of Er:GaP diode at three different current densities. The spectra are instrumentally broadened.

## RESULTS

Figure 1 shows the electroluminescent spectra of an Er doped GaP p-n junction at three different current densities at room temperature. The strong emission near 0.80 eV (1.54  $\mu\text{m}$ ) is the  $^4I_{13/2}$  to  $^4I_{15/2}$  4f electron transition of the  $\text{Er}^{3+}$  ion. A weaker emission near 1.27 eV (0.98  $\mu\text{m}$ ) is also observed, and is due to the transition in  $\text{Er}^{3+}$  4f-shell from  $^4I_{11/2}$  to  $^4I_{15/2}$  states.

Figure 2 shows the peak emission intensity as a function of drive current for an Er:GaP diode under forward bias. Note at low excitation the EL intensity is linearly dependent on input power. As the power increases the intensity begins to saturate. For EL the intensity starts to saturate at current densities of the order of 10  $\text{A}/\text{cm}^2$ . The EL intensity curve could be fit to a semi-empirical expression given by:

$$I_{\text{out}} = \frac{AI_{\text{in}}}{1 + BI_{\text{in}}} \quad (1)$$

where A and B are constants and  $I_{\text{in}}$  is the excitation power. The curve in figure 2 is a best fit to

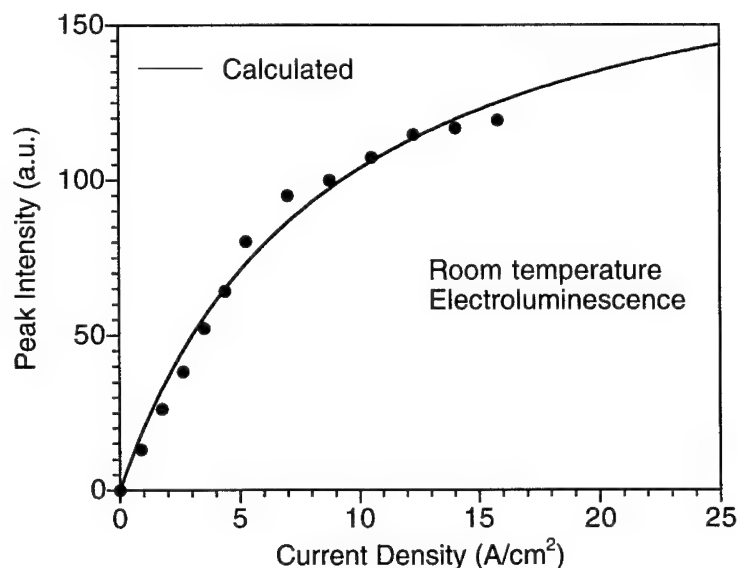


Figure 2: Current density versus peak intensity for a forward biased Er doped GaP diode. The curve is a best fit to equation (1).

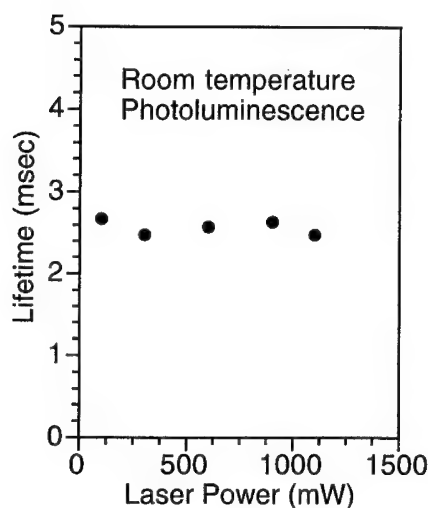


Figure 3a: Photoexcited luminescence lifetime versus laser pump power.

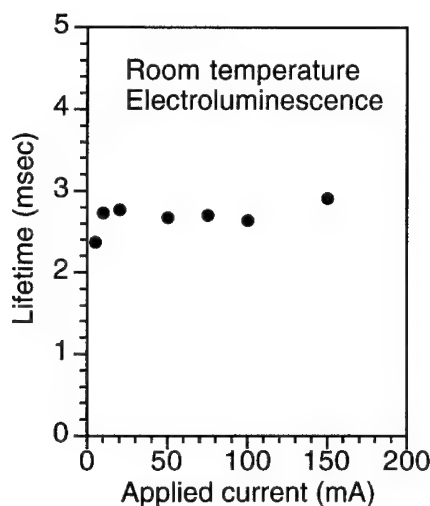


Figure 3b: Forward bias luminescence lifetime versus applied current.

this equation. It is noted that for  $BI_{in} \ll 1$  the emission power is linearly dependent on excitation power and for  $BI_{in} \gg 1$  the intensity is independent of excitation power.

To determine whether the saturation was due to changes in the efficiency of radiative relaxation, the lifetime was measured as a function of excitation power. The decay curve was a single exponential with a lifetime of 2.6 msec for both photoexcitation as well as forward bias injection. This luminescence lifetime is considerably longer than that previously measured for Er doped GaP,<sup>10</sup> indicating a highly efficient radiative de-excitation process. As can be seen from Figure 3a and 3b, the decay lifetime is independent of power, indicating that the intra-4f shell transition is unaffected by the presence of excess carriers. Thus it can be concluded that free carrier Auger processes are unimportant.

The observed dependence of the intensity and lifetime on excitation power is consistent with saturation of the optically active  $Er^{3+}$  centers. Indeed it is noted that equation (1) is similar in form to the expression derived by Serna et al. used to model Er emission saturation in silicon.<sup>9</sup> In their kinetic equation the luminescence decay lifetime was assumed to be a constant. It was also assumed that no back transfer processes were occurring at the highest excitation powers. These assumptions are certainly supported by the present luminescent decay data for the case of Er doped GaP.

While most of the previous data could be modeled by equation (1), some recent measurements on the EL intensity versus input power showed more complex behavior.

Figure 4 shows a plot of intensity versus current density for another series of erbium doped GaP diodes. Note the presence of a threshold near  $2 \text{ A/cm}^2$ . At current densities greater than this threshold the EL intensity rapidly increases and then saturates around  $10 \text{ A/cm}^2$ . The appearance of a threshold and superlinear increase in emission intensity is strongly suggestive of gain. Experiments are presently underway to determine whether or not stimulated emission is occurring.

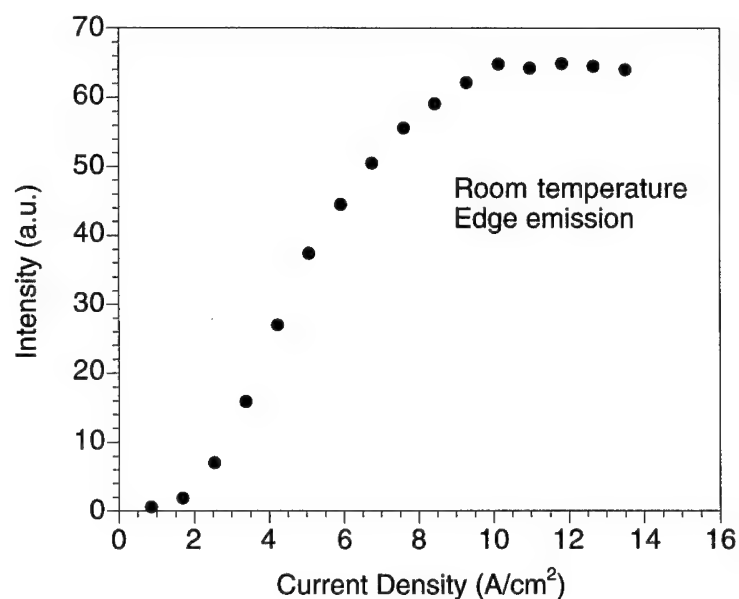


Figure 4: Forward bias  $1.54 \mu\text{m}$  emission intensity versus current density for the edge of an Er doped GaP diode.

## CONCLUSIONS

Strong room temperature electroluminescence at  $1.54 \mu\text{m}$  has been observed from forward biased Er doped GaP diodes. The EL intensity initially increases linearly with current density, but saturates at the highest levels. The observed intensity dependence was explained with a model whereby the radiative decay lifetime was independent of current density and the luminescence saturation resulted from a saturation of optically active  $\text{Er}^{3+}$  centers. Some diodes show a superlinear intensity dependence with a threshold of about  $2 \text{ A/cm}^2$ .

## ACKNOWLEDGEMENTS

This work was supported by the National Science Foundation (NSF) Ceramics and Electronic Materials Program under grant No. DMR-9302357. Extensive use of the measurement facility of the Materials Research Center at Northwestern University supported in part by the NSF under grant No. DMR-9120521 is acknowledged.

## REFERENCES

- <sup>1</sup>P. Whitney, K. Uwai, H. Nakagome, and K. Takahei, IEEE Trans. Elect. Dev. **35**, 2454 (1988).
- <sup>2</sup>H. Isshiki, H. Kobayashi, S. Yugo, T. Kimura, and T. Ikoma, Jpn. J. Appl. Phys. **30**, L225 (1991).
- <sup>3</sup>G. Franzo, F. Priolo, S. Coffa, A. Polman, and A. Carnera, Appl. Phys. Lett. **64**, 2235 (1994).
- <sup>4</sup>X. Z. Wang and B. W. Wessels, Appl. Phys. Lett. **65**, 584 (1994).
- <sup>5</sup>G. M. Ford and B. W. Wessels, Appl. Phys. Lett. **68**, 1126 (1996).
- <sup>6</sup>J. M. Langer, J. Luminescence **40&41**, 589 (1988).
- <sup>7</sup>K. Takahei and A. Taguchi, Mat. Science Forum, **83-87**, 641 (1992)
- <sup>8</sup>B. Zheng, J. Michel, F. Y. G. Ren, L. C. Kimerling, D. C. Jacobson, and J. M. Poate, Appl. Phys. Lett. **64**, 2842 - 2844 (1994).
- <sup>9</sup>R. Serna, J. H. Shin, M. Lohmeier, E. Vlieg, A. Polman, and P. F. A. Alkemade, J. Appl. Phys. **79**, 2658 (1996).
- <sup>10</sup>P. B. Klein and G. S. Pomrenke, Elec. Lett. **24**, 1502-1503 (1988).

## Neodymium-doped GaAs light-emitting diodes

S. J. Chang

Department of Electrical Engineering  
National Cheng Kung University  
Tainan 70101, Taiwan, Republic of China  
e-mail: sjchang@mail.ncku.edu.tw.

*Nd-doped semiconductor light-emitting diodes were fabricated by implanting Nd ions into a GaAs epi-layer. The fabricated GaAs:Nd diodes show good current-voltage characteristics with a typical reverse breakdown voltage between 8 and 12 V. By injecting minority carriers into the diodes, Nd<sup>3+</sup> related emissions were observed, at 77 K, in the 0.92, 1.11, and 1.3  $\mu$ m regions. These electroluminescence signals correspond to the transitions from Nd<sup>3+</sup> <sup>4</sup>F<sub>3/2</sub> state to the Nd<sup>3+</sup> <sup>4</sup>I<sub>9/2</sub>, <sup>4</sup>I<sub>11/2</sub>, and <sup>4</sup>I<sub>13/2</sub> states, respectively. The measured external quantum efficiency of the GaAs:Nd diodes at 77 K, was  $5 \times 10^{-7}$ .*

In recent years, there is increasing interest in doping rare-earth (RE) ions into III-V compound semiconductor hosts.<sup>1-5</sup> It is well known that RE ions have incompletely filled 4f shell electron orbitals. Due to the screening effects by the outer 5s<sup>2</sup> and 5p<sup>6</sup> electrons, the transitions between the partially filled RE 4f shell electrons will emit sharp and temperature stable luminescence that is insensitive to the surrounding host environment. On the other hand, III-V compound semiconductor devices are inexpensive, compact, and easy to fabricate. Thus, a combination of RE ion and III-V compound semiconductor is potentially useful as an optical source. In such a system, one can excite the RE ions easily through minority-carrier injection. Indeed, III-V:RE light-emitting diodes (LEDs) have already been reported.<sup>6-10</sup> However, most of the works on the RE-doped III-V compound semiconductor LEDs were focused on Er and Yb (e.g., InP:Yb,<sup>6</sup> GaAs:Er,<sup>7,8</sup> AlGaAs:Er,<sup>9</sup> and GaP:Er<sup>10</sup>). Nd-based III-V compound semiconductor LEDs have not been reported yet. Previously, the photoluminescence (PL) properties of Nd-doped GaAs and GaP either prepared by ion implantation<sup>11,12</sup> or grown by metalorganic chemical vapor deposition (MOCVD)<sup>13,14</sup> have been reported. It was found that Nd ions form many luminescence centers in the host GaAs and GaP, and some Nd centers in the MOCVD-grown GaP can still emit luminescence even at room temperature. The observation of Nd room-temperature luminescence is particularly interesting since Nd ions have been widely used in many laser applications (e.g., YAG:Nd laser) due to its four-level lasing scheme. A combination of Nd and III-V compound semiconductor host is thus promising

in providing us with a good RE-based LED. Also, Nd, rather than Er or Yb, seems to be the RE ion that one should choose to realize a feasible RE-doped III-V compound semiconductor laser. In this letter, we report the first study of the fabrication of Nd-doped GaAs LED.

In the experiment, n-type GaAs epitaxial layer was first grown on an n-type (100) GaAs substrate by MOCVD at 750°C. The electron concentration in the Si-doped GaAs epi-layer was  $1 \times 10^{17} \text{cm}^{-3}$ , and the thickness of the GaAs epi-layer was 3.5  $\mu\text{m}$ . Nd ions were subsequently implanted into the GaAs epi-layer at room temperature. The implantation energy was 4 MeV with a dose of  $5 \times 10^{13} \text{cm}^{-2}$ . After implantation, the samples were capped with a 200 nm of  $\text{SiO}_2$  and annealed at 850°C for 20 min in vacuum. After annealing, the  $\text{SiO}_2$  protective layer was removed by chemical etching. From secondary-ion mass spectroscopy (SIMS) measurement, the projected range ( $R_p$ ) and straggle ( $\Delta R_p$ ) of the implanted Nd ions were 1.1  $\mu\text{m}$  and 250 nm, respectively. At the projected range, the Nd concentration was  $8 \times 10^{17} \text{cm}^{-3}$ . For diode fabrication, p<sup>+</sup> layer of GaAs was made by Zn diffusion from the top surface at 600°C for 1.5 h using  $\text{ZnAs}_2$  as the Zn source.<sup>15</sup> After chemical etching to form the mesa structure of the diode with an area of  $1 \times 1 \text{mm}^2$ , Au/Zn and Au/Ge ohmic contacts were deposited respectively on the p-type layer and n-type layer. Figure 1 shows the current-voltage ( $I$ - $V$ ) characteristics of one of the GaAs:Nd diodes measured at 77 K. Typical reverse breakdown voltage was between 8 and 12 V. Electroluminescence (EL) spectra of the GaAs:Nd LEDs were also measured at 77 K. In EL measurement, the diodes were electrically excited by

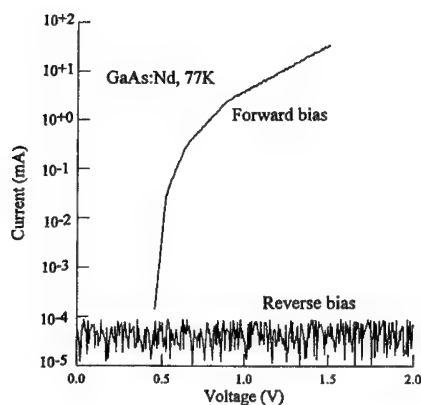


FIG. 1. The current-voltage ( $I$ - $V$ ) characteristics of a typical GaAs:Nd diode measured at 77K.



forward biasing the GaAs:Nd LEDs with pulses generated at frequency of 80 Hz and a duty cycle of 25. The emission spectra were monitored by a Spex monochromator, and a liquid-nitrogen-cooled germanium *p-i-n* photodiode was used for detection. Standard lock-in technology was used for signal analysis. Figure 2 (a) shows a typical EL spectrum of the GaAs:Nd LEDs measured at 77 K. The injection current was 50 mA. As shown in Fig. 2 (a), both band-gap emission related EL peaks centered at 0.84  $\mu\text{m}$ , and Nd<sup>3+</sup> intra-4*f*-shell transition related EL Peaks centered at 0.92, 1.11, and 1.3  $\mu\text{m}$  were observed. The EL peaks centered at 0.92  $\mu\text{m}$  was attributed to the Nd<sup>3+</sup>  $^4F_{3/2} \rightarrow ^4I_{11/2}$  transition. The EL peaks centered at 1.11 and 1.3  $\mu\text{m}$  was attributed to the Nd<sup>3+</sup>  $^4F_{3/2} \rightarrow ^4I_{13/2}$  and  $^4F_{3/2} \rightarrow ^4I_{15/2}$  transitions, respectively. The  $^4F_{3/2} \rightarrow ^4I_{11/2}$  transitions with the same amount of injection current, near 1.1  $\mu\text{m}$ , are displayed on an expanded wavelength scale in Fig. 2 (b). The integrated EL intensities of the Nd<sup>3+</sup> EL signal and the GaAs near band edge EL emission, measured at 77 K, as functions of the injected diode current are both shown in Fig. 3. As shown in Fig. 3, the Nd<sup>3+</sup> related EL intensity increased linearly in the low injection current region. At high injection current, the Nd<sup>3+</sup> emission intensity saturated probably due to the series resistance or due to the limited concentration of the Nd ions. Similar saturation behavior was observed in InP:Yb,<sup>6</sup> GaAs:Er,<sup>7,8</sup> and AlGaAs:Er<sup>9</sup> LEDs. However, no apparent saturation was observed for a GaP:Er EL device operated at an injection current density as

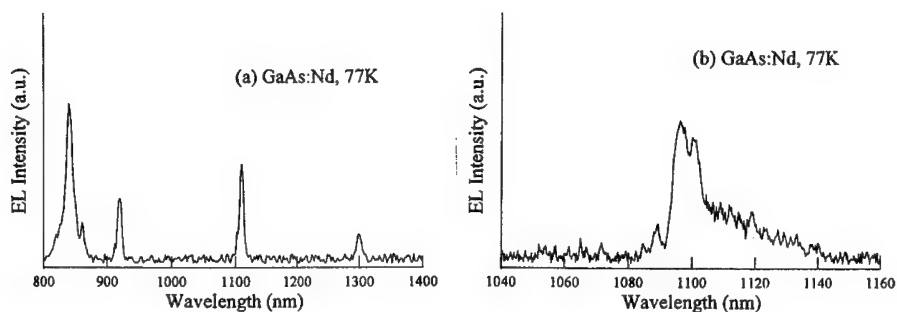


FIG. 2. (a) The full EL spectrum of a typical GaAs:Nd LED measured at 77K. (b) The EL spectrum in expanded wavelength scale for the Nd<sup>3+</sup>  $^4F_{3/2} \rightarrow ^4I_{11/2}$  transitions. The injection current was 50 mA for both figures.

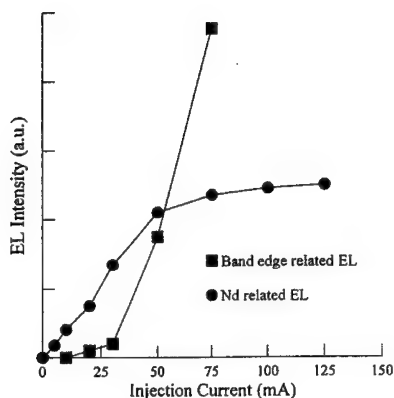


FIG.3. The integrated EL intensity of the  $\text{Nd}^{3+}$  and GaAs band edge emission as functions of the injected forward current measured at 77 K.

high as  $25 \text{ A/cm}^2$ .<sup>10</sup> In order to deduce quantitative information about the  $\text{Nd}^{3+}$  related emission, we compared the  $\text{Nd}^{3+}$  EL intensity with a standard GaAs LED. After correcting for the apparatus response due to monochromator and Ge detector, we estimated that the external quantum efficiency (including EL observed in 0.97, 1.11 and  $1.3 \mu\text{m}$  regions) of the GaAs:Nd, at 77 K in the low injection current region, is  $5 \times 10^{-7}$ . This value is close to the  $10^{-6}$  room-temperature external quantum efficiency of GaAs:Er<sup>8</sup> and AlGaAs:Er<sup>9</sup> LEDs. However, it is much smaller than the  $8 \times 10^{-4}$  external quantum efficiency for the InP:Yb LED measured at 77 K.<sup>6</sup> The low external quantum efficiency for the GaAs:Nd LED reported in this work is partially due to the large amount of damage and defects in the sample caused by ion implantation. To overcome this problem, one should use, instead of ion implantation, MOCVD or molecular beam epitaxy (MBE) to prepare the GaAs:Nd LEDs. By using MOCVD or MBE to incorporate Nd ions into GaAs, we should be able to reduce the number and defects and thus a larger efficiency can be expected.

In summary, Nd-doped GaAs LEDs were fabricated and the EL characteristics were studied. By injecting minority carriers into the diodes,  $\text{Nd}^{3+}$  related electroluminescence was observed, at 77 K, in the 0.92, 1.11, and  $1.3 \mu\text{m}$  regions which correspond to the transitions from the  $\text{Nd}^{3+} {}^4\text{F}_{3/2}$  state to the  $\text{Nd}^{3+} {}^4\text{I}_{9/2}$ ,  ${}^4\text{I}_{11/2}$ ,  ${}^4\text{I}_{13/2}$  states, respectively. The external quantum efficiency of the GaAs:Nd LED was  $5 \times 10^{-7}$ .

The authors would like to thank Dr. K. Takahei and Dr. A. Taguchi of NTT Basic Research Laboratories and Professor Y. K. Su of National Cheng Kung University for their helpful discussions. This work is supported by National Science Council under Contract No. NSC 82-0404-E-006-306-T.

- 1) K. Takahei and A. Taguchi, *Mater. Sci. Forum* **83-87**, 641 (1992).
- 2) H. Ennen and J. Schneider, *J. Electron. Mater.* **A 14**, 115 (1985).
- 3) W. Kober, J. Weber, A. Hangleiter, K. W. Benz, H. Ennen, And D. Muller, *J. Cryst. Growth* **79**, 741 (1986).
- 4) K. Takahei, P. S. Whitney, H. Nakagome, and K. Uwai, *J. Appl. Phys.* **65**, 1257 (1989).
- 5) V. F. Masterov and L. F. Zakhavronkov, *Sov. Phys. Semicond.* **24**, 383 (1990).
- 6) W. H. Haydl, H. D. Muller, H. Ennen, W. Kober, and K. W. Benz, *Appl. Phys. Lett.* **46**, 870 (1985).
- 7) P. Whitney, K. Uwai, H. Nakagome, and K. Takahei, *Lett.* **24**, 740 (1988).
- 8) P. B. Klein, F. G. Moore, and H. B. Dietrich, *Electron. Lett.* **26**, 1299 (1990).
- 9) P. Galtier, J. P. Pocholle, M. N. Charasse, B. de Cremoux, J. P. Hirtz, B. Groussin, T. Benyattou, and G. Guillot, *Appl. Phys. Lett.* **55**, 2105 (1989).
- 10) X. Z. Wang and B. W. Wessels, *Appl. Phys. Lett.* **65**, 584 (1994).
- 11) J. Wagner, H. Ennen, and H. D. Muller, *J. Appl. Phys.* **59**, 1202 (1986).
- 12) H. D. Muller, H. Ennen, J. Schneider, and A. Axmann, *J. Appl. Phys.* **59**, 2210 (1986).
- 13) H. Nakagome and K. Takahei, *Jpn. J. Appl. Phys.* **28**, L2098 (1989).
- 14) M. Taniguchi, H. Nakagome, and K. Takahei, *J. Lumin.* **52**, 251 (1992).
- 15) Y. Yamamoto and H. Kanbe, *Jpn. J. Appl. Phys.* **19**, 121 (1980).

## INCREASED REFRACTIVE INDICES IN RARE EARTH DOPED InP and In<sub>0.53</sub>Ga<sub>0.47</sub>As THIN FILMS

B.J.H. STADLER AND J.P. LORENZO

USAF Rome Laboratory, Optical Components Branch,  
Hanscom Air Force Base, MA 01731 USA  
stadler@maxwell.rl.plh.af.mil

### ABSTRACT

Rare earth (Gd, Eu, Er) doped InGaAs and InP layers were grown by liquid phase epitaxy (LPE). The refractive index of these layers was observed to increase with the addition of the rare earth ions. The observed increase could not be explained by changes in host composition as typically calculated from changes in lattice parameter. In fact, the refractive index was seen to increase (~0.25) by an order of magnitude more than would be expected by the change in the lattice parameter (~0.02). The increased refractive indices of InP layers due to Er-doping enabled waveguiding. These findings suggest that optically active waveguide devices can be fabricated from semiconducting hosts by simple rare earth doping.

### INTRODUCTION

Rare earth dopants have received much attention in optics due to their sharp 4f-intrashell emissions which are relatively independent of temperature and ligand field. The location of the erbium (Er) emission (1.54  $\mu\text{m}$ ) makes it especially interesting for applications in telecommunications because this wavelength corresponds to the point of lowest attenuation in optical fibers.

Er-doped glass fibers are commercially available for optical amplifiers, and rare earth doped oxide thin films are under intense study as optically active waveguides for use in telecommunication devices. For these materials, the rare earth dopant is often appreciated for its secondary effect of raising the index of the host in order to allow waveguiding within the doped region.<sup>1</sup> The raised index occurs because the electronic polarizability, and therefore the molar refractivity, of an ion is proportional to the cube of its radius.<sup>2</sup> Therefore, the addition of large rare earth ions increases the overall molar refractivity of the material.

Rare earth doped semiconductors have also been under intense study for their potential applications in optoelectronic integrated circuits (OEICs). The goal of this research field is to introduce the rare earth ions into a semiconductor host such that they can be activated electrically. This would enable well defined light emitting devices and laser diodes that would be ideal for source and amplifier materials for optical communication systems. Through OEIC technology, electronic control elements and photonic devices can be integrated on single chips for optimum size and system flexibility.

This work sought to demonstrate the benefits of rare earth dopants in semiconductors as waveguide definers as well as emission sources. Several InGaAs and InP layers were doped with rare earth ions, and characterization included examining the effects of the rare earth dopants on the refractive indices of the layers.

## EXPERIMENTAL

InP and InGaAs epitaxial layers were grown on undoped (100) InP and on semi-insulating Fe-doped (100) InP substrates by liquid phase epitaxy (LPE). Required amounts of InAs and GaAs were dissolved in indium melts to make the InGaAs layers, and separate indium melts were supersaturated with InP for growing the InP layers. Each melt was held at a saturation temperature (645°C) overnight in Pd-diffused H<sub>2</sub> before cooling. An InP substrate and a cover piece were then inserted, and the temperature was again raised to the saturation temperature for 30 min. The system was then cooled and held at an intermediate temperature (635°C) for 10 min. Finally, during a -1°C/min ramp, the melt was pulled over the substrate at the growth temperature (629-613°C). The film was grown for 30 sec to 40 min, depending on desired composition and thickness. To obtain doped films, the dopant element (Gd, Eu, or Er) was added (0.02 - 0.04 wt %) and the melt was again held at the saturation temperature overnight in H<sub>2</sub>.

A small region at the edge of each InGaAs film was preferentially etched with HNO<sub>3</sub> to allow the thickness profile to be measured. The lattice parameters of all the layers were measured via double-crystal x-ray diffraction (DCXRD) using the Cu K<sub>α</sub> line (1.5405 Å). Inductively-coupled plasma mass spectroscopy (ICPMS) was used to measure the average rare earth concentrations in some of the InGaAs films. The profile of the doping concentrations was measured by SIMS and was reported previously.<sup>3</sup>

Variable angle specular reflectance ( $\lambda = 2.0 - 10.0 \mu\text{m}$ ) was used to measure the interference fringes of the layers in a Fourier transform infrared (FTIR) spectrometer. The refractive index,  $n$ , was calculated using the following equation:

$$n = \left[ \left( \frac{\Delta m}{2t(\nu_1 - \nu_2)} \right)^2 + \sin^2 \theta \right]^{\frac{1}{2}} \quad \text{Eq.1}$$

where  $\Delta m$  is the number of fringes within a chosen frequency interval (for a consecutive max and min pair  $\Delta m = 1/2$ ),  $t$  is the thickness of the layer,  $(\nu_1 - \nu_2)$  is the chosen frequency interval, and  $\theta$  is the angle of incidence. For each sample, the fringes were measured at several angles on separate days in order to determine the accuracy of the calculated indices. Waveguiding was achieved by edge-coupling light from a 1.3  $\mu\text{m}$  laser into the films with a 20x objective lens. The output was imaged onto a CCD camera with a second 20x objective lens.

## RESULTS AND DISCUSSION

**InGaAs layers.** The InGaAs layers were approximately lattice-matched to the InP substrates, Fig. 1. The largest split between a layer peak and the substrate peak was 156.06 arcsec, which corresponds to a lattice mismatch of only 0.06%. In most semiconductors, an increase in lattice spacing causes a decrease in the band gap, and therefore an increase in the refractive index. An increase of 0.06% in lattice spacing typically increases the refractive index by only 0.02.<sup>4</sup> The change in lattice spacing was due to changing growth parameters, as reported previously,<sup>3</sup> and not due to the amount of rare earth that was incorporated into the films. This is also obvious from the lack of a trend in lattice spacing versus doping concentrations.

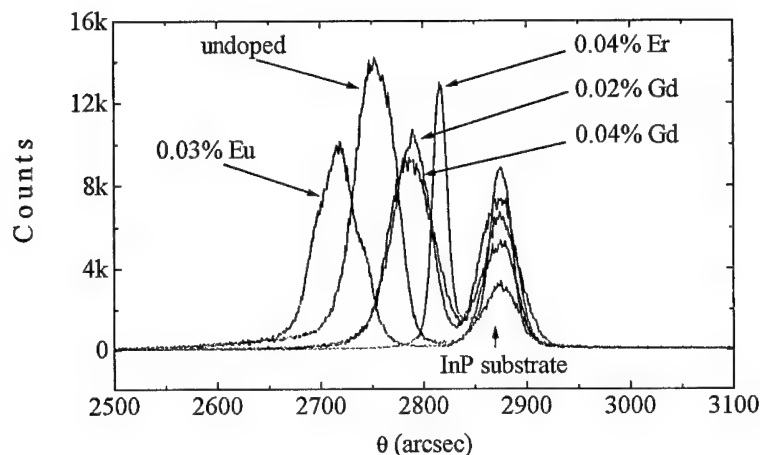


Fig. 1- Double crystal X-ray diffraction data of InGaAs layers on (100) InP. The amount of rare earth added to the melt is shown.

The rare earth concentration was measured by inductively-coupled plasma mass spectroscopy for some of the layers. When 0.04% Gd was added to the melt, the Gd concentration in the layer was found to be  $2.6 \times 10^{18} \text{ cm}^{-3}$ , and for the layer with 0.03% Eu added to the melt, the Eu concentration was found to be  $1.5 \times 10^{20} \text{ cm}^{-3}$ . The chemical profile of these dopants was measured by SIMS and was reported previously.<sup>3</sup> The Gd was distributed homogeneously through the InGaAs layers, but Eu, which was present at higher concentrations, was slightly segregated toward the interfaces.

The dispersion curves of the refractive indices are shown in Fig. 2. An increase in refractive index was observed as the amount of rare earth added to the melt was increased. The refractive index increases much more than can be explained by the small differences in the lattice parameters that were seen in Fig. 1. Rather, it seems that the increase is due to the large electronic polarizability of the rare earth dopants. The electronic polarizability, and therefore the molar refractivity, of an ion is proportional to the cube of its radius. Therefore, the addition of rare earth dopants ( $r > 1.0 \text{ \AA}$ ) in InGaAs ( $r_{\text{In}} = 0.81 \text{ \AA}$ ) leads to an increase in the overall molar refractivity of the material. Increased electronic polarizability is also the reason for adding large dopants to glass in order to form waveguides.<sup>2</sup>

The interference fringes were measured at several angles over a number of days in order to determine accuracy of the calculated indices, Fig. 3. Although there is a fair amount of noise in the calculated curves, the trend of increasing index with rare earth concentration remains. These results also agree with dispersion curves calculated for Er:InGaAs layers grown by MOCVD,<sup>5</sup> Fig. 4. The surfaces of these samples were smoother, which led to more accurate measurements of the fringes.

**Er-doped InP layers.** The rare earth-doped InP layers were lattice matched to the InP substrates, as can be seen from the sharp DCXRD InP peak (FWHM  $\sim 20$  arcsec), Fig. 5. The interference fringes were difficult to measure since the change in refractive index between the substrate and the layer was very small. With the InGaAs layers, the undoped host had a higher refractive index than the InP substrates, and this difference was merely enhanced by the rare earth doping. The InP films obviously had the same host as the substrate, so the interference fringes

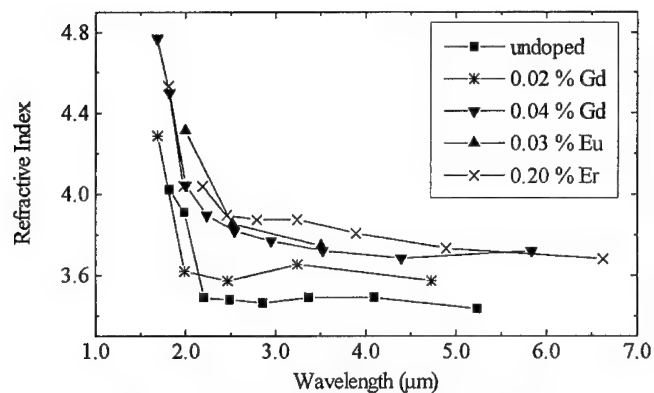


Fig. 2- Dispersion curves show that the refractive index increases with rare earth concentration.

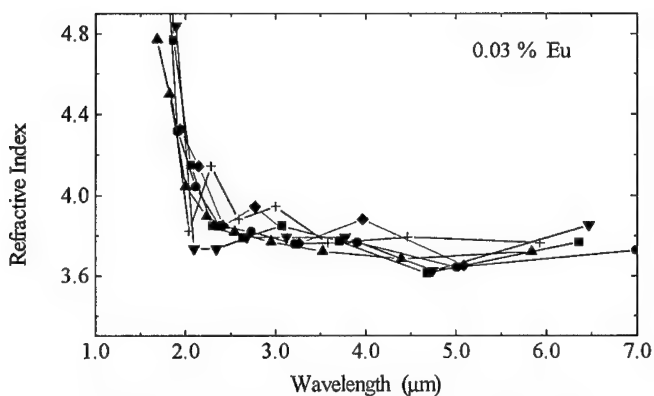


Fig. 3- Refractive index as calculated from interference fringes that were measured at various angles.

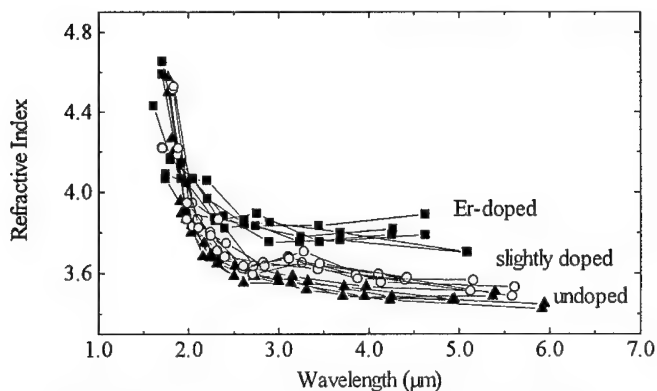


Fig. 4- Dispersion curves of Er:InGaAs layers grown by MOCVD. <sup>5</sup>

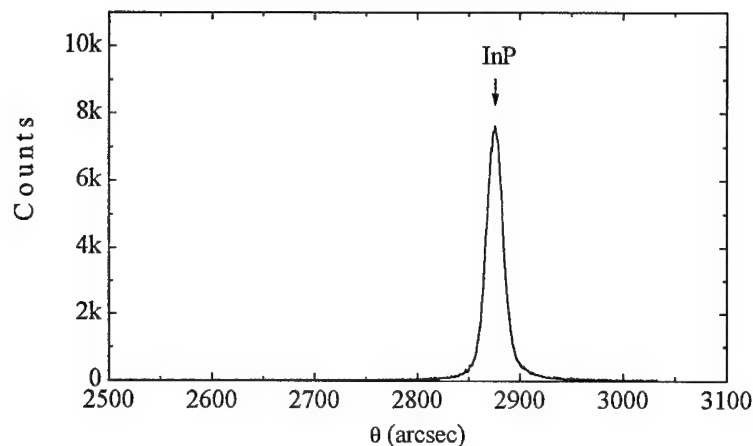


Fig. 5- The Er:InP films were lattice-matched to the (100) InP substrates. (FWHM  $\sim 20$  arcsec)

due to the increased index from doping alone were too slight to be measured confidently. However, waveguiding was achieved in these layers which indicates that the refractive index of the layers was indeed higher than that of the substrates, Fig. 6a. The figure shows the output of a planar waveguide of Er:InP. Since the optical confinement was only in the vertical direction, horizontal divergence of the beam causes the output to appear as a line. An optical micrograph of the output edge of the waveguide is also shown, Fig. 6b, in order to demonstrate the scale of the layer and the appearance of the edge. Applications of Er-doped InP could therefore include optically active waveguides, such as waveguide amplifiers.

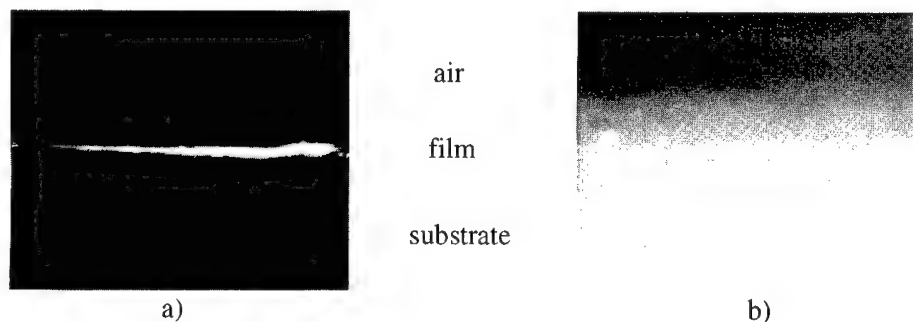


Fig. 6- a) Waveguiding was observed in Er:InP layers on InP substrates at  $1.3 \mu\text{m}$ . The waveguiding was viewed at the output edge; the beam divergence along the unconstrained dimension of the planar waveguide appears as a line.  
b) An optical micrograph of the edge of the layer is also shown.



## CONCLUSION

The refractive indices of InGaAs and InP were observed to increase with rare earth doping. The increase was more than an order of magnitude greater than could be attributed to the small differences in lattice parameter. This increase was observed in films made by LPE as well as MOCVD. The increased refractive index enabled waveguiding in Er:InP films that were grown on semi-insulating InP. Therefore, the potential applications for Er:InP can be expanded to include optically active waveguides, which can be a valuable addition to OEICs and fiber optic systems.

## ACKNOWLEDGMENTS

The authors would like to acknowledge the support of Ken Vaccaro, Andrew Davis, Helen Dauplaise, and Richard Soref through their helpful discussions and technical assistance. We would also like to dedicate this paper to Dr. Todd Crumbaker, whose enthusiasm for research and friendship will be missed by many.

## REFERENCES

- [1] S. Raoux, S. Anders, K.M. Yu, I.C. Ivanov, and I.G. Brown in Thin Films for Integrated Optics Applications, edited by B. Wessels, S. Marder, and D. Walba (Materials Research Society Proceedings **392**, Pittsburgh, PA, 1995) pp. 241-246.
- [2] W.D. Kingery, H.K. Bowen, D.R. Uhlmann, Introduction to Ceramics, (John Wiley & Sons, New York, 1976), p. 660.
- [3] B. Stadler, K. Vaccaro, A. Davis, H. Dauplaise, G. Ramseyer, E. Martin, L. Theodore, and J. Lorenzo, *Journal of Electronic Materials* **25** 709 (1996).
- [4] V. Swaminathan and A.T. Macrander, Materials Aspects of GaAs and InP Based Structures, (Prentice-Hall, Englewood Cliffs, 1991); H.C. Casey and M.B. Panish, *Heterostructure Lasers B*, (Academic Press, New York, 1978).
- [5] Undoped and Er-doped InGaAs layers provided by P. Bhattacharya of U. Michigan.

## AUTHOR INDEX

- Abernathy, C.R., 47, 193  
 Abstreiter, G., 15  
 Acciarri, M., 87  
 Adams, E., 57  
 Alexandrov, O.V., 125  
 Alves, E., 173  
 Ammerlaan, C.A.J., 161, 207  
 Andry, P.S., 57  
 Aoyagi, Yoshinobu, 143  
  
 Bennett, M.R., 29  
 Binetti, S., 87  
 Bray, K.L., 279  
 Bresler, M.S., 125, 325  
 Buchal, Ch., 15  
  
 Cai, Yongming, 93  
 Campisano, S.U., 239, 333  
 Chang, S.J., 131, 351  
 Choyke, W.J., 339  
 Christianen, P.C.M., 161  
 Coffa, S., 113, 305  
 Cremins-Costa, A.M., 137  
 Culp, T.D., 279  
 Custer, J.S., 21  
  
 Daly, S.E., 173  
 Dawson, P., 119  
 de Dood, M.J.A., 219  
 de Maat-Gersdorf, Ingrid, 161  
 Dejima, T., 149  
 Devaty, R.P., 339  
 Donder, S., 63  
 Dörnen, Achim, 179  
 Dravin, V.A., 187  
 Duan, X., 41  
  
 Edmond, J.A., 339  
 Emtsev, V.V., 125  
 Eryu, O., 75  
 Evans, J.H., 119  
  
 Feuerstein, Robert J., 199  
 Ford, G.M., 345  
 Franzo, G., 305  
 Freitag, K., 173  
 Fuhs, W., 325  
 Fujita, K., 155  
 Fujiwara, Y., 155  
  
 Gan, F., 317  
 Gelmi, I., 87  
 Gerchikov, L.G., 227  
 Gippius, A.A., 187  
 Godlewski, M., 291  
 Goldenberg, B., 69  
 Gombia, E., 113  
 Gong, Dawei, 93  
  
 Greenwald, A.C., 63  
 Gregorkiewicz, T., 161, 207  
 Gusev, O.B., 125, 325  
 Gwilliam, R., 173  
  
 Haase, Dieter, 179  
 Haegel, N.M., 63  
 Hartung, J., 119  
 Hengehold, R.L., 57, 69  
 Henry, M.O., 173  
 Hogg, R.A., 167, 267  
 Holzbrecher, H., 15  
 Hömmerich, U., 137, 193  
 Horiguchi, H., 81  
 Horikoshi, Y., 167  
 Hosokawa, I., 149  
 Huang, Daming, 93  
 Huda, M.Q., 119  
 Hunter, J., 57  
  
 Ichiki, S., 155  
 Iio, O., 75  
 Ikoma, T., 81, 149  
 Isshiki, Hideo, 143  
  
 Jafri, Z.H., 29  
 Jantsch, W., 101  
 Jeynes, C., 119  
 Just, O., 63  
  
 Kawamura, D., 155  
 Kik, P.G., 219  
 Kimerling, L.C., 41, 317  
 Kimura, T., 81, 149  
 Kinone, T., 81  
 Klein, P.B., 57  
 Komuro, Shuji, 143  
 Konnov, V.M., 187  
 Kuech, T.F., 279  
 Kuznetsov, A.N., 325  
  
 Lanzerstorfer, S., 101  
 Larikova, T.V., 187  
 Lavoie, M., 57  
 Leksono, Moeljanto W., 199  
 Libertino, S., 113  
 Linden, K.J., 63  
 Liu, Xiaohan, 93  
 Lohmeier, M., 21  
 Lombardo, S., 239, 333  
 Lorenzo, J.P., 357  
 Loyko, N.N., 187  
 Lozykowski, H.J., 285  
  
 Maan, J.C., 161  
 MacKenzie, J.D., 47, 193  
 Maruyama, Shinya, 143  
 Masterov, V.F., 227, 325

Matsubara, N., 155  
 Matsuoka, Morito, 3  
 Michel, J., 317  
 Minami, H., 75  
 Morse, M., 41  
 Mosca, R., 113  
  
 Nakashima, K., 75  
 Namavar, Fereydoon, 137, 199  
 Nayak, D.K., 131  
 Nishida, Y., 149  
  
 Ofuchi, H., 155  
 Ouellette, E., 317  
  
 Palm, J., 41, 317  
 Palmetshofer, L., 101  
 Pankove, Jacques I., 199  
 Peaker, A.R., 35, 119  
 Pearson, S.J., 47, 193  
 Pensl, Gerhard, 255, 339  
 Pizzini, S., 87  
 Polman, A., 21, 219, 239, 305, 333  
 Poloskin, D.S., 125  
 Pomrenke, G.S., 69  
 Priolo, F., 305  
 Przybylinska, H., 101  
  
 Qiu, Chang H., 199  
  
 Rees, Jr., W.S., 63  
 Reitinger, A., 15  
 Rutter, P., 35  
  
 Saha, U.K., 285  
 Saito, R., 81, 149  
 Scholes, A.P., 119  
 Schwartz, R.N., 47, 193  
 Sealy, B.J., 173  
 Sema, R., 21, 239  
 Shek, E.I., 125  
 Sheng, Chi, 93  
 Shin, Jung H., 219, 239  
 Shiraki, Y., 131  
 Shul, R.J., 47  
 Silkowski, E., 69  
 Singer, K.E., 29, 35  
  
 Skierbiszewski, C., 101  
 Soares, J.C., 173  
 Sobolev, N.A., 125, 207  
 Stadler, B.J.H., 357  
 Stievenard, D., 173  
 Stimmer, J., 15  
 Sugano, Takuo, 143  
  
 Tabuchi, M., 155  
 Taguchi, Akihito, 167, 179, 267  
 Takahei, Kenichiro, 167, 179, 267  
 Takeda, Y., 155  
 Taskin, T., 119  
 Terukov, E.I., 325  
 Tohno, Shun-ichi, 3  
 Torvik, John T., 199  
 Tsimperidis, I., 207  
  
 Ushakov, V.V., 187  
  
 van den Hoven, G.N., 239, 333  
 van Sark, W.G.J.H.M., 239  
 Varhue, W.J., 57  
 Vianden, R., 173  
 Vredenberg, A.M., 239  
  
 Wang, X.Z., 279  
 Wang, Xun, 93  
 Watanabe, M., 75  
 Wellmann, Peter, 255  
 Wessels, B.W., 247, 279, 345  
 White, R., 137  
 Widdershoven, F.P., 207  
 Wilson, R.G., 47, 193  
 Winnacker, Albrecht, 255  
 Wright, A.C., 29, 35  
 Wu, X., 137, 193  
  
 Yamada, N., 155  
 Yassievich, I.N., 325  
 Yeo, Y.K., 69  
 Yoganathan, M., 339  
  
 Zakharchenya, B.P., 325  
 Zavada, J.M., 47, 193  
 Zhao, Xinwei, 143  
 Zheng, B., 41, 317

## SUBJECT INDEX

- absorption edge, 143
- AlN:Er, 47
- amorphous Si:Er, 239, 325, 333
- Auger processes, 119, 285, 291, 325
- carrier lifetime, 113
- co-doping, 35, 81, 187, 219
- co-sputtering, 325
- CVD, 41
- diffusion, 81, 87, 125
- DLTS, 35, 113
- donor behavior, 41, 113, 317
- ECR, 57
- electrical properties, 87, 113, 187
- electrochemical incorporation, 143, 149
- electroluminescence, 15, 125, 247, 291, 305, 317, 325, 333, 339, 345, 351
- electroplating, 93
- Er-O interaction, 3, 15, 21, 63, 75, 81, 87, 113, 125, 167, 173, 179, 199, 227, 267, 333
- EXAFS, 155
- excitation mechanisms, 101, 125, 207, 219, 227, 239, 255, 267, 279, 291, 305, 317
- freespace signal transmission, 317
- GaAs:Er, 35, 63, 167, 173, 179, 267
- GaAs:Nd, 285, 351
- GaAs:Tm, 29
- GaAs:Yb, 187
- GaN:Er, 47, 69, 193, 199
- GaN:Nd, 69
- GaP:Er, 279, 345
- high resolution photoluminescence, 69, 75, 81, 101, 187, 267, 285, 339
- hydrogenated a-Si:Er, 239, 325, 333
- hydrostatic pressure, 101, 279
- II-VI semiconductors, 291
- impact excitation, 291, 305, 333
- InGaAs:Er, 357
- InGaAs:Eu, 357
- InGaAs:Gd, 357
- InGaAsP:Er, 255
- InGaAsP:Yb, 255
- InGaP:Er, 247
- InP:Er, 155, 357
- InP:Eu, 357
- InP:Gd, 357
- InP:Yb, 161, 207
- integration, 317
- ion beam epitaxy, 3
- ion implantation, 21, 41, 69, 101, 113, 119, 125, 131, 137, 173, 187, 199, 219, 239, 305, 317, 333, 339
- kinetic growth model, 21
- laser doping, 75
- lattice location, 173
- LED, 15, 247, 291, 305, 317, 325, 333, 339, 345, 351
- LPCVD, 239
- LPE, 255, 357
- luminescence lifetime, 119, 125, 137, 143, 149, 207, 219, 239, 255, 267, 305, 317, 333
- MBE, 15, 21, 29, 35, 179
- metal ion source, 3
- microwave excitation, 207
- MOCVD, 63, 69, 167, 267, 279, 285, 351
- modulation, 317
- MOMBE, 47, 193
- MOVPE, 179, 345
- OMVPE, 155
- optical anisotropy, 167
- PECVD, 57, 239
- PLE, 137, 143, 167, 267, 279
- polarization dependence, 167
- porous
  - Si:Er, 93, 137, 143, 149
  - Si:Yb, 149
- precipitation, 21, 29, 35, 87, 113, 173
- precursors, 41, 47, 57, 63
- pressure, 101, 279
- quenching, 81, 93, 101, 131, 137, 149, 207, 219, 227, 239, 247, 255, 267, 279, 291, 305, 317, 325, 339
- rate equations, 101, 137, 207, 219, 227, 247, 255, 285, 333
- refractive index, 357
- segregation, 3, 21
- self-organized growth, 29
- SiC:Er, 339
- Si:Er, 3, 15, 21, 41, 57, 75, 81, 87, 93, 101, 113, 119, 125, 207, 219, 227, 305, 317
- SiGe:Er, 131
- SIPOS, 333
- site symmetry, 101, 131, 155, 161, 167, 179, 267

solar cell, 219  
solid phase epitaxy, 21

TmAs, 29  
trapping, 21

UHV-CVD, 41

voice link, 317

waveguide, 317, 357

XPS, 75, 93  
X-ray CTR, 155  
X-ray diffraction, 57, 357

Zeeman splitting, 161, 179